AER/AGS Special Report 108

Alberta Energy Regulator

Petrographic Analysis of Selected Alberta Strata (Cardium, Viking, Banff, Exshaw, Duvernay, Slave Point)

AGS
ALBERTA GEOLOGICAL SURVEY

AER/AGS Special Report 108

Petrographic Analysis of Selected Alberta Strata (Cardium, Viking, Banff, Exshaw, Duvernay, Slave Point)

S.D.A. Anderson*, C.D. Rokosh, J.G. Pawlowicz

* Corresponding author

September 2017

©Her Majesty the Queen in Right of Alberta, 2017
ISBN 978-1-4601-1679-1

The Alberta Energy Regulator/Alberta Geological Survey (AER/AGS), its employees and contractors make no warranty, guarantee or representation, express or implied, or assume any legal liability regarding the correctness, accuracy, completeness or reliability of this publication. Any references to proprietary software and/or any use of proprietary data formats do not constitute endorsement by AER/AGS of any manufacturer's product.

If you use information from this publication in other publications or presentations, please acknowledge the AER/AGS. We recommend the following reference format:

Anderson, S.D.A, Rokosh, C.D., and Pawlowicz, J.G. (2017): Petrographic analysis of selected Alberta strata (Cardium, Viking, Banff, Exshaw, Duvernay, Slave Point); Alberta Energy Regulator, AER/AGS Special Report 107, 516 p.

Published September 2017 by:
Alberta Energy Regulator
Alberta Geological Survey
4th Floor, Twin Atria Building
4999 – 98th Avenue
Edmonton, AB T6B 2X3 Canada

Tel: 780.638.4491
Fax: 780.422.1459
E-mail: AGS-Info@aer.ca
Website: ags.aer.ca

Acknowledgements

This report includes data generated to support the AGS report “Summary of Alberta's shale- and siltstone-hosted hydrocarbon resource potential” (2012) and subsequent unconventional resource evaluations. Funding was provided in part by Alberta Energy. The authors thank B. Fildes and M. Grobe for their technical editing, comments and advice during the preparation of this release.

Abstract

This report presents petrographic analyses by Trican Geological Solutions Ltd. of thin sections prepared from 65 core samples from the Viking, Cardium, Banff, Exshaw, Duvernay, and Slave Point formations of Alberta. The thin sections were created to our specifications for very fine grained, transmitted-light microscopy.

The analysis and description of each thin section included visual estimations (in percent) of grain-size distribution, mineralogy, cement, allochem, opaque material, and organic material. Physical and biogenic primary and secondary sedimentary structures, fractures, and porosity were identified and described if present. General sample descriptions, rock classifications, and microphotographs are included for each sample.

1 Introduction

In 2012, the Alberta Geological Survey (AGS) published a report that determined the quantity and spatial extent of shale- and siltstone-hosted hydrocarbons (oil, gas, and natural gas liquids) in the province (Rokosh et al., 2012). The AGS is releasing client reports and digital data to disseminate knowledge from the project. These data and reports can be accessed from the AGS website (http://ags.aer.ca).

This report disseminates petrographic descriptions of thin sections from selected strata in Alberta.

2 Sample Locations and Descriptions

Table 1 lists the samples and sites examined in the study.

Table 1. Samples collected for petrographic analysis.

Sample_ID	UWI	Units	Depth	Lithology	Formation
11127	100/12-06-035-20W4/00	metre	1886.4	lime mudstone	Duvernay
11220	100/06-09-058-23W4/00	metre	731.9	silty shale	Viking
11221	100/16-23-058-24W4/00	metre	732.8	shale	Viking
11222	100/16-23-058-24W4/00	metre	736.4	shale	Viking
11224	100/07-29-056-20W4/00	metre	619.5	shale	Viking
11225	100/07-29-056-20W4/00	metre	625.5	shale	Viking
11226	100/07-29-056-20W4/00	metre	632.0	shale	Viking
11227	100/07-29-056-20W4/00	metre	636.6	shale	Viking
11228	100/07-29-056-20W4/00	metre	641.8	sandstone	Viking
13032	100/14-07-001-21W4/00	metre	1945.2	siltstone	Exshaw
13034	102/04-32-003-17W4/00	metre	1320.5	sandstone	Banff
13035	102/04-32-003-17W4/00	metre	1327.0	siltstone	Exshaw
13041	100/01-03-002-20W4/00	metre	1524.9	sandstone	Banff
13044	100/01-03-002-20W4/00	metre	1532.1	sandstone	Banff
13048	100/01-03-002-20W4/00	metre	1536.8	carbonate mudstone	Exshaw
13133	100/03-21-030-04W5/00	metre	2208.7	mudstone	Cardium
13135	100/03-21-030-04W5/00	metre	2220.0	sandstone	Cardium
13139	100/03-21-030-04W5/00	metre	2227.8	mudstone	Cardium
13144	102/14-25-039-05W5/00	metre	1803.9	sandstone	Cardium
13147	102/14-25-039-05W5/00	metre	1812.8	mudstone	Cardium
13174	100/16-25-055-20W4/00	metre	659.9	shale/siltstone	Viking
13175	100/16-25-055-20W4/00	metre	662.7	shale/siltstone	Viking
13177	100/16-25-055-20W4/00	metre	666.8	shale/siltstone	Viking
13178	100/16-25-055-20W4/00	metre	669.5	shale/siltstone	Viking
13181	100/16-25-055-20W4/00	metre	677.4	shale/sandstone	Viking
13182	100/16-25-055-20W4/00	metre	677.8	sandstone	Viking
13184	100/01-03-002-20W4/00	metre	1541.7	carbonate mudstone	Exshaw
13190	100/16-06-010-22W4/00	metre	1870.3	mudstone	Exshaw
13193	102/14-10-007-19W4/00	metre	1441.2	carbonate mudstone	Exshaw
13257	100/04-03-044-07W5/00	metre	1826.9	mudstone	Cardium
13258	100/04-03-044-07W5/00	metre	1828.1	sandstone	Cardium
13262	102/06-27-066-23W5/00	metre	1016.3	mudstone	Cardium
13283	100/04-18-060-20W5/00	metre	1607.3	sandstone	Cardium
13286	100/04-18-060-20W5/00	metre	1612.3	mudstone	Cardium

13403	100/06-12-048-11W5/00	metre	1773.8	mudstone	Cardium
13407	100/06-12-048-11W5/00	metre	1781.3	sandstone/mudstone	Cardium
13412	100/06-12-048-11W5/00	metre	1790.5	siltstone	Cardium
13413	100/06-12-048-11W5/00	metre	1791.7	mudstone	Blackstone
13420	100/03-07-048-08W5/00	metre	1650.2	sandstone/mudstone	Cardium
13425	100/06-07-047-04W5/00	metre	1442.9	sandstone	Cardium
13427	100/06-07-047-04W5/00	metre	1450.1	sandstone/mudstone	Cardium
13431	100/08-30-049-04W5/00	metre	1244.9	sandstone	Cardium
13432	100/08-30-049-04W5/00	metre	1247.2	mudstone	Cardium
13436	100/07-32-045-12W5/00	metre	2177.1	sandstone	Cardium
13437	100/07-32-045-12W5/00	metre	2180.2	sandstone/mudstone	Cardium
13438	100/07-32-045-12W5/00	metre	2181.7	mudstone	Cardium
13441	100/16-03-052-13W5/00	metre	1742.2	sandstone	Cardium
13442	100/16-03-052-13W5/00	metre	1743.2	sandstone/mudstone	Cardium
13443	100/05-17-049-08W5/00	metre	1505.3	mudstone	Cardium
13446	100/05-17-049-08W5/00	metre	1514.7	sandstone	Cardium
13448	100/05-17-049-08W5/00	metre	1521.5	sandstone/mudstone	Cardium
13451	100/12-08-088-08W5/00	feet	4275.7	limestone	Slave Point
13452	100/12-08-088-08W5/00	feet	4257.5	limestone	Slave Point
13455	100/12-08-088-08W5/00	feet	4233.5	limestone	Slave Point
13461	100/02-21-084-14W5/00	metre	1706.2	dolostone	Slave Point
13462	100/02-21-084-14W5/00	metre	1700.0	dolostone	Slave Point
13479	100/15-11-091-13W5/00	metre	1629.8	limestone	Slave Point
13818	102/10-07-077-04W5/00	metre	705.5	grainstone	Exshaw
13822	102/08-07-075-05W5/00	metre	1077.3	mudstone	Banff
15005	100/13-14-035-25W4/00	feet	7713.2	mudstone	Duvernay
15010	100/13-14-035-25W4/00	feet	7738.5	shale	Duvernay
15013	100/13-14-035-25W4/00	feet	7745.7	mudstone	Duvernay
15027	100/13-14-035-25W4/00	feet	7796.5	mudstone	Duvernay
15107	100/16-15-050-06W5/00	metre	1170.3	sandstone	Cardium
15109	100/16-15-050-06W5/00	metre	1177.1	mudstone	Cardium

References

Rokosh, C.D., Lyster, S., Anderson, S.D.A., Beaton, A.P., Berhane, H., Brazzoni, T., Chen, D., Cheng, Y., Mack, T., Pana, C. and Pawlowicz, J.G. (2012): Summary of Alberta's shale- and siltstone-hosted hydrocarbon resource potential; Energy Resources Conservation Board, ERCB/AGS Open File Report 2012-06, 327 p., URL < http://ags.aer.ca/publications/OFR_2012_06.html > [March 2017].



PETROGRAPHIC ANALYSIS REPORT

Alberta Energy Regulator
Various wells from the Viking, Cardium, Banff, Exshaw, Duvernay and Slave Point formations

Alberta Energy Regulator (AER)
4999-98 Avenue, Twin Atria Building, 4th Floor
Edmonton, Alberta T6B 2X3

Prepared for: John Pawlowicz, Dean Rokosh, Shar Anderson

Trican Geological Solutions

Trican Geological Solutions Ltd | 621 – 37th Avenue NE | Calgary, Alberta | Canada T2E 2M1 |P 403.250.5582
Geologicalsolutions.trican.ca

DISCLAIMER
Trican Well Service Ltd. ("**Trican**") retains the copyright to this document but the right to all content herein shall vest with the client for whom the document was prepared. This document shall only be used for the stated purpose. Trican does not make any representations, warranties or guarantees, express or implied, as to the accuracy or completeness of this document, its fitness for any particular purpose, or its usefulness in achieving any particular outcome or result from its use. Neither Trican nor any of its affiliates, nor their respective directors, officers, employees or agents shall be liable to any person for any loss, damage, injury, liability, cost or expense of any nature, including without limitation, incidental, special, direct or consequential damages arising out of or in connection with the use of the document.

© 2014 Trican Well Service Ltd.

Table of Contents

1. EXECUTIVE SUMMARY 7

2. METHODS AND SAMPLE DETAILS 8

2.1 Petrographic Analysis 8

3. VIKING FORMATION OVERVIEW 11

3.1 Summary 11

3.1.1 Core Samples: 11

3.1.2 Lithofacies, Groupings and Descriptions: 11

3.1.3 Sedimentary Structures & Bioturbation: 12

3.1.4 Diagenesis: 14

3.1.5 Organic Matter & Clays: 14

3.1.6 Porosity & Fracturing: 15

3.2 Results 17

3.2.1 100/06-09-058-23W4/00 Sample 11220 (731.90 m) 17

3.2.2 100/16-23-058-24W4/00 Sample 11221 (732.80 m) 24

3.2.3 100/16-058-24W4/00 Sample 11222 (736.40 m) 31

3.2.4 100/07-29-056-20W4/00 Sample 11224 (619.50 m) 38

3.2.5 100/07-29-056-20W4/00 Sample 11225 (625.50 m) 45

3.2.6 100/07-29-056-20W4/00 Sample 11226 (632.00 m) 52

3.2.7 100/07-29-056-20W4/00 Sample 11227 (636.60 m) 59

3.2.8 100/07-29-056-20W4/00 Sample 11228 (641.80 m) 66

3.2.9 100/16-25-055-20W4/00 Sample 13174 (659.90 m) 73

3.2.10 100/16-25-055-20W4/00 Sample 13175 (662.70 m) 80

3.2.11 100/16-25-055-20W4/00 Sample 13177 (666.80 m) 86

3.2.12 100/16-25-055-20W4/00 Sample 13178 (669.50 m) 93

3.2.13 100/16-25-055-20W4/00 Sample 13181 (677.40 m) 100

3.2.14 100/16-25-055-20W4/00 Sample 13182 (677.80 m) 108

4. CARDIUM FORMATION OVERVIEW 116

4.1 Summary 116

4.1.1 Core Samples: 116

4.1.2 Lithofacies, Groupings and Descriptions: 116

4.1.3 Sedimentary Structures & Bioturbation: 117

4.1.4 Diagenesis: 118

4.1.5 Organic Matter & Clays: 119

4.1.6 Porosity & Fracturing: 120

4.2 RESULTS 122

4.2.1 100/03-21-030-04W5/00 Sample 13133 (2208.70 m) 122

4.2.2 100/03-21-030-04W5/00 Sample 13135 (2220.00 m) 129

4.2.3 100/03-21-030-04W5/00 Sample 13139 (2227.80 m) 135
4.2.4 102/14-25-039-05W5/00 Sample 13144 (1803.90 m) 142
4.2.5 102/14-25-039-05W5/00 Sample 13147 (1812.80 m) 149
4.2.6 100/04-03-044-07W5/00 Sample 13257 (1826.90 m) 156
4.2.7 100/04-03-044-07W5/00 Sample 13258 (1828.10 m) 164
4.2.8 102/06-27-066-23W5/00 Sample 13262 (1016.30 m) 170
4.2.9 100/04-10-060-20W5/00 Sample 13283 (1607.30 m) 178
4.2.10 100/04-10-060-20W5/00 Sample 13286 (1612.30 m) 185
4.2.11 100/06-12-048-11W5/00 Sample 13403 (1773.80 m) 192
4.2.12 100/06-12-048-11W5/00 Sample 13407 (1781.30 m) 199
4.2.13 100/06-12-048-11W5/00 Sample 13412 (1790.50 m) 206
4.2.14 100/06-12-048-11W5/00 Sample 13413 (1791.70 m) 213
4.2.15 100/03-07-048-08W5/00 Sample 13420 (1650.20 m) 219
4.2.16 100/06-047-04W5/00 Sample 13425 (1442.90 m) 226
4.2.17 100/06-047-04W5/00 Sample 13427 (1450.10 m) 234
4.2.18 100/08-20-049-04W5/00 Sample 13431 (1244.90 m) 241
4.2.19 100/08-20-049-04W5/00 Sample 13432 (1247.20 m) 247
4.2.20 100/07-32-045-12W5/00 Sample 13436 (2177.10 m) 254
4.2.21 100/07-32-045-12W5/00 Sample 13437 (2180.20 m) 261
4.2.22 100/07-32-045-12W5/00 Sample 13438 (2181.70 m) 267
4.2.23 100/16-03-052-13W5/00 Sample 13441 (1742.20 m) 274
4.2.24 100/16-03-052-13W5/00 Sample 13442 (1743.20 m) 281
4.2.25 100/05-17-049-08W5/00 Sample 13443 (1505.30 m) 288
4.2.26 100/05-17-049-08W5/00 Sample 13446 (1514.70 m) 295
4.2.27 100/05-17-049-08W5/00 Sample 13448 (1521.50 m) 302
4.2.28 100/16-15-050-06W5/00 Sample 15107 (1170.30 m) 309
4.2.29 100/16-15-050-06W5/00 Sample 15109 (1177.10 m) 316

5. BANFF FORMATION OVERVIEW 323

5.1 Summary 323
5.1.1 Core Samples: 323
5.1.2 Lithofacies, groupings and descriptions: 323
5.1.3 Sedimentary Structures & Bioturbation: 324
5.1.4 Diagenesis: 325
5.1.5 Organic Matter & Clays: 326
5.1.6 Porosity & Fracturing: 327

5.2 Results 328
5.2.1 100/04-32-003-17W4/00 Sample 13034 (1320.50 m) 328
5.2.2 100/01-03-002-20W4/00 Sample 13041 (1524.90 m) 337
5.2.3 100/01-03-002-20W4/00 Sample 13044 (1532.10 m) 344

5.2.4 100/08-07-075-05W5/00 Sample 13822 (1022.30m) 351

6. EXSHAW FORMATION OVERVIEW 357

6.1 Summary 357
6.1.1 Core Samples: 357
6.1.2 Lithofacies, Groupings and Descriptions: 357
6.1.3 Sedimentary Structures & Bioturbation: 358
6.1.4 Diagenesis: 358
6.1.5 Organic Matter & Clays: 359
6.1.6 Porosity & Fracturing: 360

6.2 Results 361
6.2.1 100/14-07-001-21W4/00 Sample 13032 (1945.20 m) 361
6.2.2 100/04-32-003-17W4/00 Sample 13035 (1327.00 m) 367
6.2.3 100/01-03-002-20W4/00 Sample 13048 (1536.80 m) 374
6.2.4 100/01-03-022-20W4/00 Sample 13184 (1541.70 m) 381
6.2.5 100/16-06-010-22W4/00 Sample 13190 (1870.30 m) 388
6.2.6 102/14-10-007-19W4/00 Sample 13193 (1441.20 m) 395
6.2.7 102/10-077-04W5/00 Sample 13818 (705.50 m) 402

7. DUVERNAY FORMATION OVERVIEW 410

7.1 Summary 410
7.1.1 Core Samples: 410
7.1.2 Lithofacies, groupings and descriptions: 410
7.1.3 Sedimentary Structures & Bioturbation: 411
7.1.4 Diagenesis: 412
7.1.5 Organic Matter & Clays: 412
7.1.6 Bioclasts: 413
7.1.7 Porosity & Fracturing: 413

7.2 Results 415
7.2.1 100/12-08-035-20W4/00 Sample 11127 (1886.40 m) 415
7.2.2 100/13-14-035-25W4/00 Sample 15005 (7713.20 m) 425
7.2.3 100/13-14-035-25W4/00 Sample 15010 (7738.50 m) 434
7.2.4 100/13-14-035-25W4/00 Sample 15013 (7745.70 m) 442
7.2.5 100/13-14-035-25W4/00 Sample 15027 (7796.50 m) 451

8. SLAVE POINT FORMATION OVERVIEW 460

8.1 Summary 460
8.1.1 Core Samples: 460
8.1.2 Lithofacies, groupings and descriptions: 460
8.1.3 Sedimentary Structures & Bioturbation: 461
8.1.4 Diagenesis: 462
8.1.5 Organic Matter & Clays: 463

8.1.6 Bioclasts: 463
8.1.7 Porosity & Fracturing: 464
8.2 Results 465
8.2.1 100/12-08-088-08W5/00 Sample 13451 (4275.70 m) 465
8.2.2 100/12-08-088-08W5/00 Sample 13452 (4257.50 m) 474
8.2.3 100/12-08-088-08W5/00 Sample 13455 (4233.50 m) 483
8.2.4 100/02-21-084-14W5/00 Sample 13461 (1706.20 m) 491
8.2.5 100/02-21-084-14W5/00 Sample 13462 (1700.00 m) 499
8.2.6 100/15-11-091-13W5/00 Sample 13479 (1629.80 m) 507

1. EXECUTIVE SUMMARY

This report presents petrographic analyses of thin sections prepared from 65 core samples (taken from a variety of wells, see Table 1-A) from the Viking (n=12), Cardium (n=29), Banff (n=4), Exshaw (n=7), Duvernay (n=5), and Slave Point (n=6) formations of Alberta. Samples were obtained from the Alberta Energy Regular (AER) Core Research Centre. This study was commissioned by John Pawlowicz, Dean Rokosh and Shar Anderson (Alberta Geological Survey, Alberta Energy Regulator).

Each thin section analysis includes photomicrographs at a series of different magnifications highlighting observations of depositional and bioturbation structures, diagenetic features, clay and organic matter distributions, and the occurrence of porosity and fractures. Each analysis is accompanied by a summary table containing XRD mineralogical composition data, petrographic compositional data, observations of sedimentary features, a sample description, and a lithofacies classification. Classification diagrams, a core photograph, a thin section overview image and a series of high resolution photomicrographs are provided for every sample.

Well Location	Formation	Depth (m) (Sample ID)
100/06-09-058-23W4/00	Viking	731.9 (11220)
100/16-23-058-23W4/00	Viking	732.8 (11221), 736.4 (11222)
100/07-29-056-20W4/00	Viking	619.5 (11224), 625.5 (11225), 632.0 (11226), 636.6 (11227), 641.8 (11228)
100/16-25-055-20W4/00	Viking	659.9 (13174), 662.7 (13175), 666.8 (13177), 669.5 (13178), 677.4 (13181), 677.8 (13182)
100/03-21-030-04W5/00	Cardium	2208.7 (13133), 2220.0 (13135), 2227.8 (13139)
102/14-25-039-05W5/00	Cardium	1803.9 (13144), 1812.8 (13147)
100/04-03-044-07W5/00	Cardium	1826.9 (13257), 1828.1 (13258)
102/06-27-066-23W5/00	Cardium	1016.3 (13262)
100/04-18-060-20W5/00	Cardium	1607.3 (13283), 1612.3 (13286)
100/06-12-048-11W5/00	Cardium	1773.8 (13403), 1781.3 (13407), 1790.5 (13412), 1791.7 (13413)
100/03-07-048-08W5/00	Cardium	1650.2 (13420)
100/06-07-047-04W5/00	Cardium	1442.9 (13425), 1450.1 (13427)
100/08-30-049-04W5/00	Cardium	1244.9 (13431), 1247.2 (13432)
100/07-32-045-12W5/00	Cardium	2177.1 (13436), 2180.2 (13437), 2181.7 (13438)
100/16-03-052-13W5/00	Cardium	1742.2 (13441), 1743.2 (13442)
100/05-17-049-08W5/00	Cardium	1505.3 (13443), 1514.7 (13446), 1521.5 (13448)
100/16-15-050-06W5/00	Cardium	1170.3 (15107), 1177.1 (15109)
102/04-32-003-17W4/00	Banff	1320.5 (13034)
100/01-03-002-20W4/00	Banff	1524.9 (13041), 1532.1 (13044)
102/08-07-075-05W5/00	Banff	1077.3 (13822)
100/14-07-001-21W4/00	Exshaw	1945.2 (13032)
102/04-32-003-17W4/00	Exshaw	1327.0 (13035)
100/01-03-002-20W4/00	Exshaw	1536.8 (13048), 1541.7 (13184)
100/16-06-010-22W4/00	Exshaw	1870.3 (13190)
102/14-10-007-19W4/00	Exshaw	1441.2 (13193)
102/10-07-077-04W5/00	Exshaw	705.5 (13818)
100/12-06-035-20W4/00	Duvernay	1886.4 (11127)
100/13-14-035-25W4/00	Duvernay	7713.2 ft. (15005), 7738.5 ft. (15010), 7745.7 ft. (15013), 7796.5 ft. (15027)
100/12-08-088-08W5/00	Slave Point	4275.70 ft. (13451), 4257.45 ft. (13452), 4233.45 ft. (13455)
100/02-21-084-14W5/00	Slave Point	1706.2 (13461),1700.0 (13462)
100/15-11-091-13W5/00	Slave Point	1629.8 (13479)

Table 1-A: Well locations and sample information (formation, depth, sample ID).

2. Methods and Sample Details

2.1 PETROGRAPHIC ANALYSIS

A format ~30 µm thick polished thin section was made for each sample using rhodamine-B, a pink epoxy that fluoresces under UV illumination, highlighting porosity and fractures. Select thin sections were stained with a dual-stain (Alizarin Red S – the stain helps to differentiate carbonates, and affects them as follows: **calcite (pink- to red-brown), Fe-rich calcite (mauve to blue), dolomite (no stain), and Fe-rich dolomite (ankerite) (very pale blue, turquoise or greenish).** The thin sections were examined in transmitted light (PPL: plain; XPL: x-polarized; and UV: UV light) and photomicrographs were taken at various magnifications (40x, 100x, 200x and 400x) to document sample texture, porosity, organic matter occurrence, mineralogical composition and the nature of optically resolvable grains and matrix. An ***Olympus BX51*** research microscope with an EXFO (x-Cite Series 120Q) fluorescence illuminator (TRITC filter) was used for petrographic analysis. In some cases pertinent details are more visible at low or intermediate magnifications, and are noted as such.

Terminology for siliciclastic rocks is somewhat variable, but generally incorporates mudrocks (claystones, mudstones and siltstones) into the grab-bag term 'shale'. For petrographic purposes, the following general rules are applied. The term mudrock encompasses rocks composed of clay- and silt-sized detritus. The terms shale and claystone are used to describe rocks containing less than 33% silt-sized particles, and displaying a laminated (fissile) or non-laminated fabric, respectively. Rocks composed of between 33% and 66% silt-sized particles and displaying a laminated fabric are shales, whereas those with a massive fabric are mudstones. The term 'silty' is appended to the general terms if it appears there is close to 33% silt embedded in the matrix. Siltstones consist of less than 33% matrix. Grain size variations are variously ‘interlaminated’ or ‘interbedded’ (>1 cm thick) or simply ‘variable’. This report uses a grain size classification for clastic rocks (shales and sandstones) based on that of Folk (**Folk, R. L., 1954,** The distinction between grain size and mineral composition in sedimentary rocks. Journal of Geology, 62, 344-359).

Sandstones are commonly further divided based on their texture and framework mineralogy (see Figure 2-1, after **Tucker, M. E., 2001,** Sedimentary Petrology: An introduction to the origin of sedimentary rocks, Third Edition, Blackwell Science, Oxford, 262 pp). If the rocks are composed of grains only, they may be termed arenites. If the rocks contain more than 15% matrix, they are classified as wackes. Quartz arenite is applied to rocks with >95% quartz grains whereas arkosic arenite refers to an arenite with >25% feldspars (which must exceed the rock fragment component). The term litharenite is applied to a sandstone that contains >25% lithics (which must exceed the feldspar component). The terms subarkose and sublitharenite can also be used for samples that contain <25% but >5% feldspar and lithics, respectively, and contain higher volumes of feldspar (subarkose) or lithics (sublitharenite).

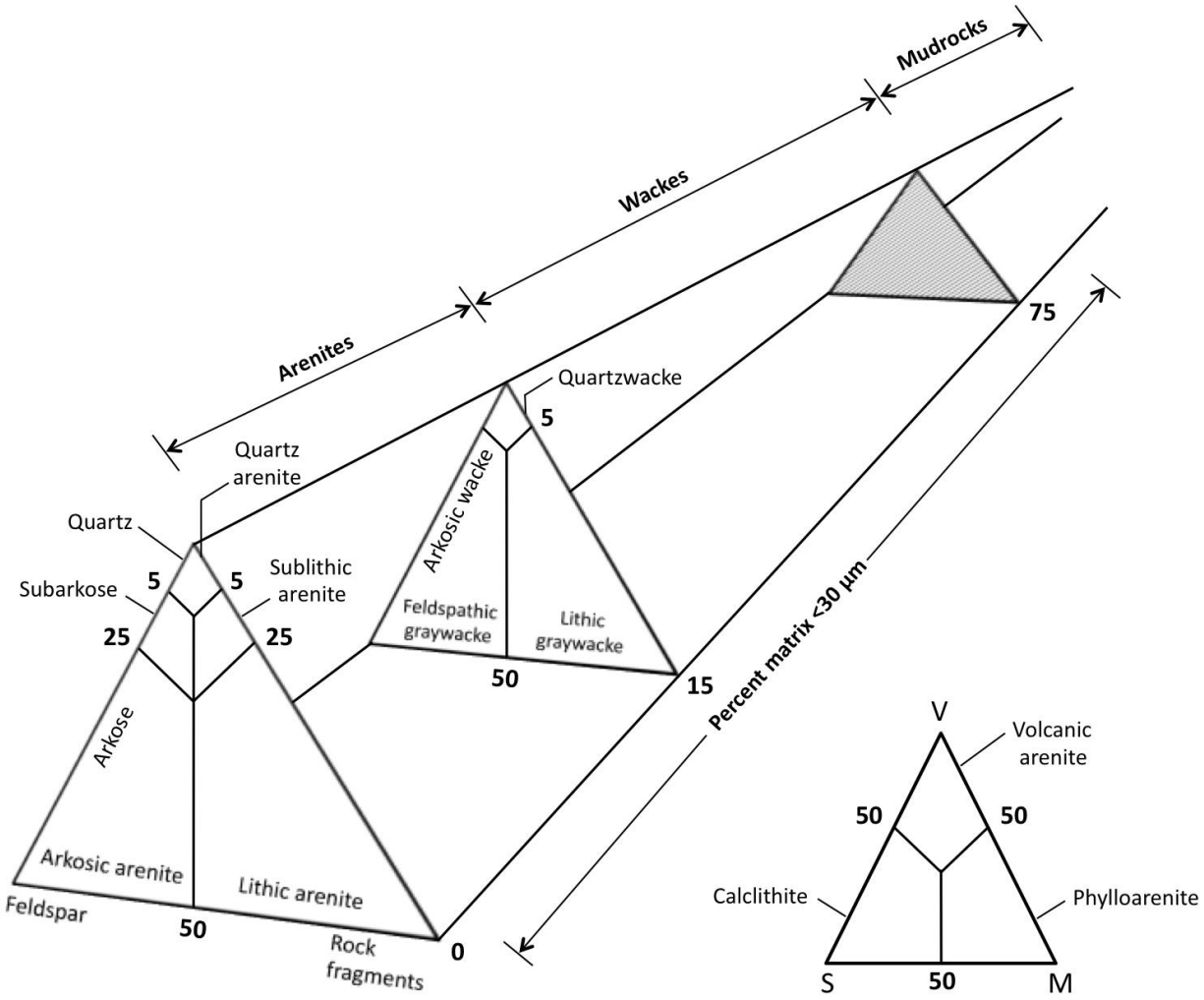


Fig. 2-1: Siliciclastic classification scheme (modified after Tucker, 2001).

Carbonate rocks (limestones and dolostones) are described based on the nature of their constituent allochems (fossils, ooids, pellets, intra- and extraclasts) and interstitial material (matrix). Classification schemes of Folk (1959, 1962) and Dunham (1962) are commonly applied to carbonate rocks. The classification of Folk (**Folk, R. L., 1959,** Practical petrographic classification of limestones, American Association of Petroleum Geologists Bulletin, 43, 1-38) subdivides limestones primarily on the basis of matrix content. Most limestones are classified as allochemical rocks if they contain over 10% allochems (carbonate 'grains'). Based on the percentage of interstitial material, the rocks may be further subdivided into two groups: sparry allochemical limestones (containing a sparry calcite cement) and microcrystalline allochemical limestone (containing microcrystalline calcite mud and micrite - calcareous particles less than about 5 µm in size). Further subdivision is based on allochem ratios (**Folk, R. L., 1962,** Spectral subdivision of limestone types, in Ham, W. E., (ed.), Classification of Carbonate Rocks - A symposium: American Association of Petroleum Geologists Memoir 1, 62-84). Rocks with appreciable matrix are termed micrites, whereas matrix-free rocks that contain sparry calcite cement are classified as sparites (Figure 2-2). The Folk classification scheme is best suited for thin section study.

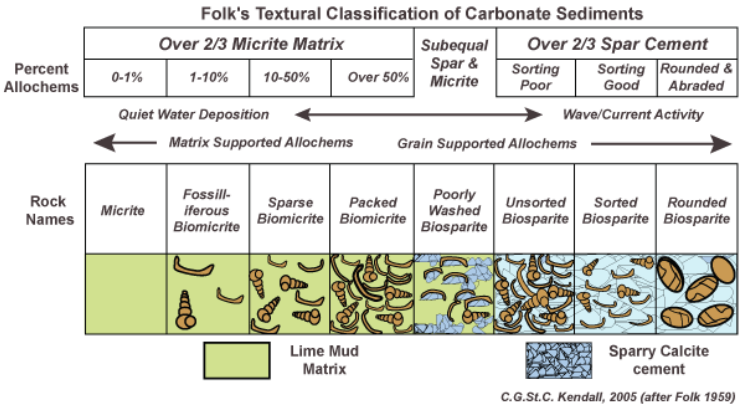


Fig. 2-2: Carbonate classification scheme (after Folk, 1959, 1962).

Whereas Folk's classification scheme is concerned with the abundance of matrix material and allochems, Dunham's classification (**Dunham, R. J., 1962,** Classification of carbonate rocks according to depositional texture. In: Ham, W. E. (ed.), Classification of Carbonate Rocks - A symposium: American Association of Petroleum Geologists Memoir 1, 108-121) and its modification by Embry and Klovan (**Embry, A. F., and Klovan, J. E., 1971,** A Late Devonian reef tract on Northeastern Banks Island, NWT: Bulletin of Canadian Petroleum Geology, 19, 730-781) is based on depositional texture (Figure 2-3).

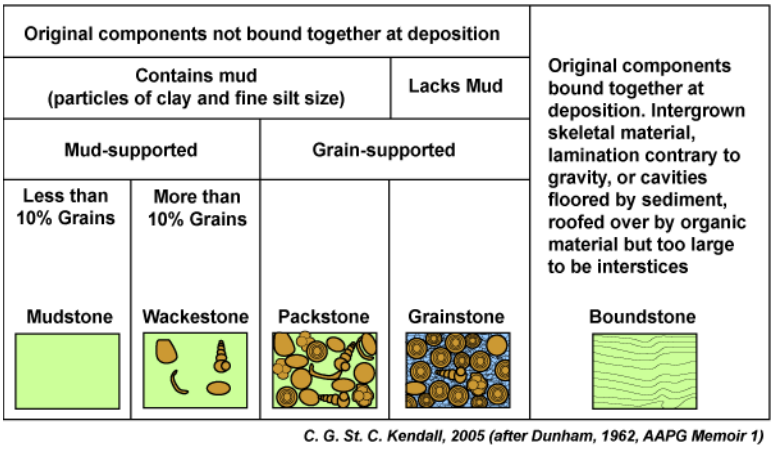


Fig. 2-3: Carbonate classification scheme (after Dunham, 1962).

3. Viking Formation Overview

This chapter presents a petrographic analysis of 14 core samples from the Viking Formation (see Table 3-A). Core samples were cut into small blocks and impregnated using rhodamine-B epoxy (pink) in order to identify porosity and fractures using UV fluorescence. Due to clay sensitivity issues, the majority of the samples were prepared without stains (with the exception of sample 13182, half-stained for carbonates). The following summary focuses on observations of rock compositional variability (i.e., lithofacies groupings), and provides photomicrographs of the most common depositional and bioturbation structures, diagenetic features, clay and organic matter distributions, and the occurrence of porosity and fractures. Several lithofacies were identified (Table 3-B) and the mineralogical XRD data for each lithofacies was averaged in order to determine common compositional parameters (Table 3-C).

3.1 SUMMARY

3.1.1 CORE SAMPLES:

Well Location	Depth m (Sample ID)
100/06-09-058-23W4/00	731.9 (11220)
100/16-23-058-23W4/00	732.8 (11221), 736.4 (11222)
100/07-29-056-20W4/00	619.5 (11224), 625.5 (11225), 632.0 (11226), 636.6 (11227), 641.8 (11228)
100/16-25-055-20W4/00	659.9 (13174), 662.7 (13175), 666.8 (13177), 669.5 (13178), 677.4 (13181), 677.8 (13182)

Table 3-A: Well locations and core sample depths.

3.1.2 LITHOFACIES, GROUPINGS AND DESCRIPTIONS:

Well Location	Lithofacies	Depth m (Sample ID)
100/06-09-058-23W4/00	1	731.9 (11220)
100/16-23-058-23W4/00	1	732.8 (11221)
100/16-23-058-23W4/00	2	732.8 (11222)
100/07-29-056-20W4/00	1	619.5 (11224), 625.5 (11225), 632.0 (11226), 636.6 (11227)
100/07-29-056-20W4/00	3	641.8 (11228)
100/16-25-055-20W4/00	1	659.9 (13174)
100/16-25-055-20W4/00	4	662.7 (13175), 666.8 (13177)
100/16-25-055-20W4/00	5	669.5 (13178), 677.4 (13181)
100/16-25-055-20W4/00	6	677.8 (13182)

Table 3-B: Lithofacies distribution by Well.

Lithofacies	Classification	Quartz/Chert %	Feldspar %	Clay/Mica %	Pyrite %
1	Claystone	45.4	4.4	48.7	1.6
2	Sandy mudstone	56.3	4.7	37.8	1.1
3	Muddy sandstone	84.1	6.9	8.7	0.4
4	Mudstone	61.1	5.4	32.8	1.0
5	Siltstone	64.9	7.4	27.1	0.9
6	Sandstone	90.9	4.8	3.9	0.3

Table 3-C: Average lithofacies composition, based on XRD data.

3.1.2.1 LITHOFACIES 1: CLAYSTONE

Samples 13174, 11224, 11225, 11226, 11227, 11221, and 11220 are classified as claystones. These samples contain 10-25% silt- and no more than 8% sand-sized grains. Clay material, which always forms distinct layers and laminae, accounts for 60-80% of the total composition.

3.1.2.2 LITHOFACIES 2: SANDY MUDSTONE

Sample 11222 is classified as a sandy mudstone. Clay (~50%) is more abundant than the combined silt- (~30%) and sand-sized (~10%) fractions of the sample, and forms distinct clay-rich layers and laminae. Quartz and chert comprise >85% of the silt- and sand-sized grains present in the sample.

3.1.2.3 LITHOFACIES 3: MUDDY SANDSTONE

Sample 11228 is classified as a muddy sandstone. Sand- and silt-sized grains (>90% quartz and chert) are the most abundant component of this sample, accounting for >70% of its composition. Clays comprise <20% of the composition of the sandstone, occurring predominantly in interbedded organic- and clay-rich horizons.

3.1.2.4 LITHOFACIES 4: MUDSTONE

Samples 13177 and 13175 are classified as mudstones. Both samples contain <10% sand-sized grains, and 30% or more clay (typically in distinct clay-rich layers). Silt-sized grains comprise >30% of both mudstones. Quartz and chert constitute >90% of the silt- and sand-sized grains in both samples.

3.1.2.5 LITHOFACIES 5: MUDDY SANDSTONE

Samples 13181 and 13178 are classified as siltstones. Both samples contain >60% silt-sized grains, of which >90% are composed of quartz and chert, and 4-5% are composed of feldspar. Sand-sized grains make up <10% of the composition of both rocks. Clays comprise ~20% of the composition of both siltstones, and occur in greatest abundance within distinct organic- and clay-rich layers.

3.1.2.6 LITHOFACIES 6: SANDSTONE

Sample 13182 is classified as a sublitharenite sandstone. Subrounded (common) to rounded (rare) coarse silt- to very coarse sand-sized quartz and chert grains comprise >90% of the rock. Clay is a minor component of the sample, accounting for ~2% of its mineralogical composition.

3.1.3 SEDIMENTARY STRUCTURES & BIOTURBATION:

Almost all of the samples examined consist predominately of organic- and clay-rich horizons with interbedded silty and sandy layers, lenses, and laminae. Many of the samples contain distinct burrow structures, as well as patches or lenses of mixed sediment and coarser-grained material that likely represent convoluted bioturbation features. Sample 13182 (sublitharenite sandstone) is an exception to this generalization, given that it contains <5% clay, and appears to lack both primary sedimentary structures and bioturbation features.

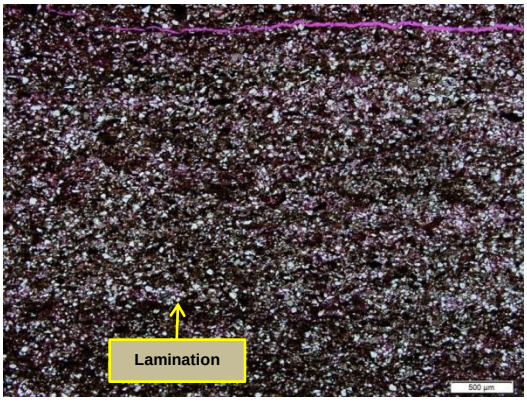


Fig. 3.1.3-1: Photomicrograph in PPL illustrating interbedded clay-rich and silty laminae present in a mudstone.

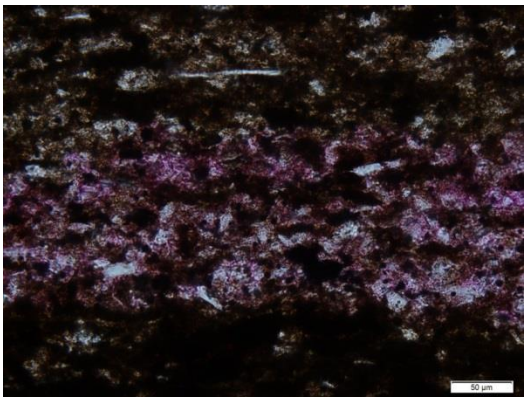


Fig. 3.1.3-2: Photomicrograph in PPL showing a thin silty lamination observed in a claystone. The porous lamination is surrounded by non-porous clay-rich bedding.

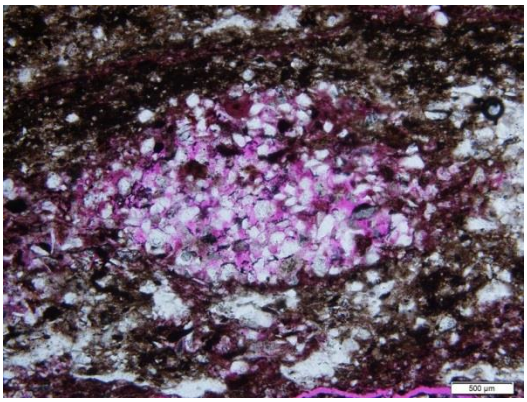


Fig. 3.1.3-3: Photomicrograph in PPL showing a possible *Planolites* burrow in a claystone. The burrow is surrounded by clay-rich matrix with few embedded detrital grains.

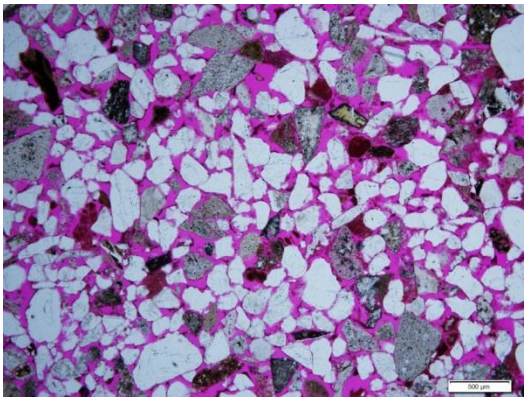


Fig. 3.1.3-4: Photomicrograph in PPL showing sample 13182, classified as a well-sorted sublitharenite sandstone.

3.1.4 DIAGENESIS:

Rare quartz overgrowth cements and secondary clays are the main diagenetic features observed in the samples. Quartz overgrowths occur in interbedded sandy layers and in burrow infills with minimal interstitial clay. These cements are never observed to completely fill pores, but do reduce pore connectivity. Secondary clays appear as pore-filling booklets (kaolinite – samples 11222 and 11224) and pore-bridging strands (sample 13182), both of which are restricted to sandy layers and burrow structures.

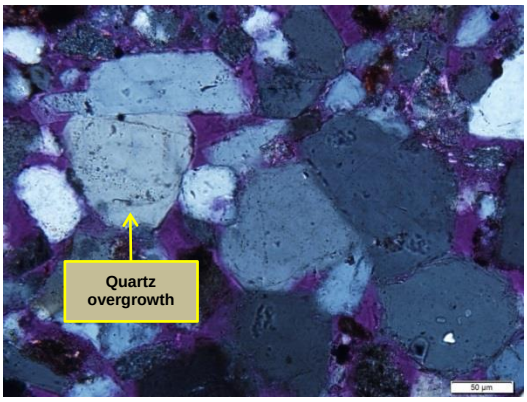


Fig. 3.1.4-1: Photomicrograph in XPL showing a silty/sandy lamination with minor quartz overgrowth cements.

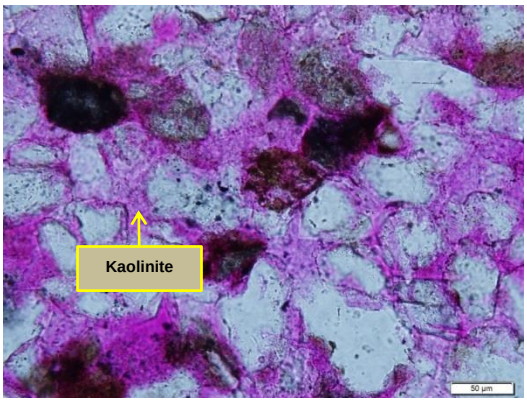


Fig. 3.1.4-2: Photomicrograph in PPL showing possible pore-filling kaolinite booklets present in a sandy burrow structure. Microporosity occurs in association with the clays, but much of the original porosity of the feature is occluded.

3.1.5 ORGANIC MATTER & CLAYS:

Clay and organic material typically occur in association in the samples, forming distinct dark-coloured layers and laminations. Organic matter is observed as finely dispersed particles and clumps, solid fragments, and bedding-parallel strands and streaks.

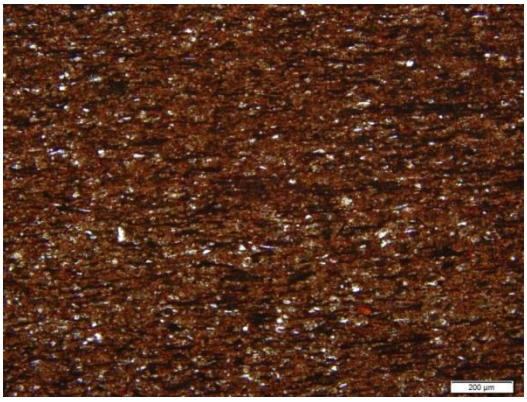


Fig. 3.1.5-1: Photomicrograph in PPL showing abundant bedding-parallel organic matter strands and streaks present in a claystone. Clay- to fine silt-size quartz and mica are also embedded within the clay-rich matrix.

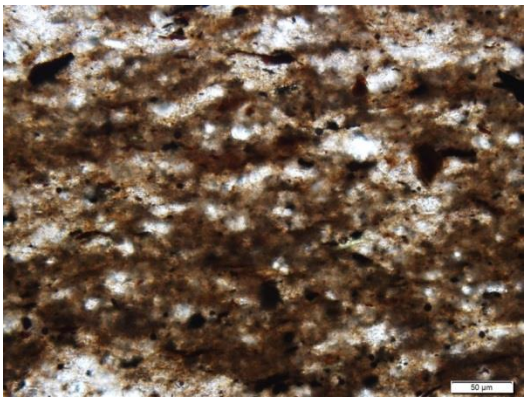


Fig. 3.1.5-2: Photomicrograph in PPL showing a clay-rich layer with associated fine bedding-parallel organic "wisps", flakes and blebs. Clay- to silt-size particles of quartz are also embedded in the clay-rich matrix.

3.1.6 POROSITY & FRACTURING:

Significant (>8%) intergranular porosity is typically restricted to clay-poor layers and laminae, and bioturbation structures with sandy infills. Some interbedded silty layers and laminae in particularly clay-rich samples contain laterally-discontinuous sections with minor (<5%) porosity. Epoxy-filled fractures and partings are abundant in the samples, especially in clay-rich layers, and occasionally split entire samples into smaller pieces. These fractures are likely artificial (due to sample cutting and polishing with water), and suggest that water-sensitive clay minerals are present in many of the samples.

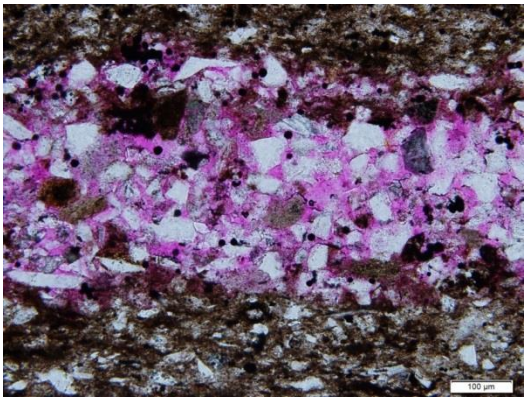


Fig. 3.1.6-1: Photomicrograph in PPL showing a silty/sandy lamination with up to 10% intergranular porosity (pink epoxy). Minor interstitial clay is observed in the lamination.

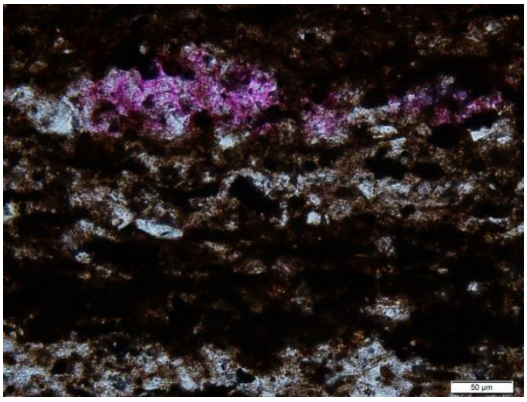


Fig. 3.1.6-2: Photomicrograph in PPL showing a laterally-discontinuous section of a silty lamination with <5% intergranular porosity. Abundant clay material surrounds the silty lamination.

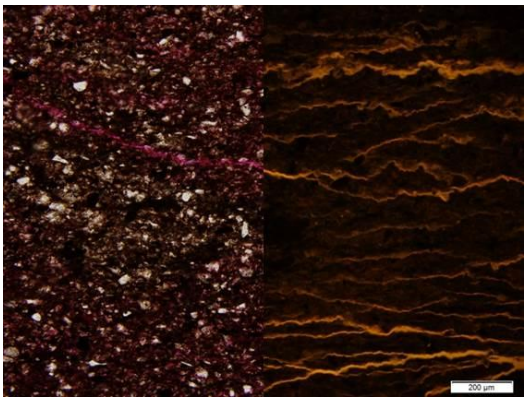


Fig. 3.1.6-3: Photomicrograph in (left half in PPL, right half in UV light) illustrating abundant thin epoxy-filled fractures in the clay-rich matrix of a mudstone. These fractures indicate that water-sensitive clays are abundant in the sample.

3.2 RESULTS

3.2.1 SAMPLE 11220

Sample ID	**11220**		
Sample type	**Core**	**UWI/Well**	**100/06-09-058-23W4/00**
Strat. Unit	**Viking Formation**	**Depth**	**731.85 m**

XRD/SRA results

Quartz (%)	Fsp (%)	Cb (%)	Clays (%)	Pyrite (%)
37.9	3.3	0	57.2	1.7

Composition (*in order of abundance*)

Grain size	%	Variety (%)	Variety (%)	Variety (%)	Variety (%)
sand	8	Quartz/chert (96)	Feldspar (4)		
silt	21	Quartz/chert (96)	Feldspar (3)	Mica (1)	
clay	65	Clay mins (100)			
Cement	<1	Quartz (100)			
Bioclasts	1	Phosphatic (100)			
Organics	3	Amorphous (100)			
Opaques	2	Pyrite (100)			
	100				

*Intensively altered to clay minerals

^ Including bitumen

Sedimentary structures

Primary	Clay-rich horizons with thinly interbedded silt (common) to fine sand (rare) beds and lenses.
Biogenic	Heavy bioturbation, including *Planolites* and possible *Zoophycos* burrows.

Fractures	10-500 µm thick partings and fractures occur throughout entire sample.
Porosity	Clay-rich layers are non-porous, with the exception of sandy infills present in *Planolites* burrows (~8-10% porosity). Interbedded silty layers and lenses have discontinuous patches of low porosity (<5%). Interbedded sandy layers have 10-15% intergranular porosity, some of which may be artificial. A large bioturbation feature observed near the center of the sample shows up to 10% intergranular porosity.

Description

Heavily bioturbated claystone with thin silt (common) to fine sand (rare) beds and lenses. Interbedded silty layers and lenses contain subrounded to subangular very fine silt- to fine sand-sized (average grain size is coarse silt) detrital quartz (18-25%), chert (5-8%), feldspar (<6%), and mica (<4%). These layers have discontinuous patches of low porosity (<5%), occurring within clusters of detrital grains. Interbedded sandy layers are comprised of subrounded to subangular very fine silt- to fine sand-sized (average grain size is coarse silt) detrital quartz (55-65%), chert (8-10%), feldspar (2 4%), and mica (<1%). These layers have 10-15% intergranular porosity, some of which may be artificial (created during sample preparation).

Thin Section Quality

Poor.

Rock Classification

Claystone.

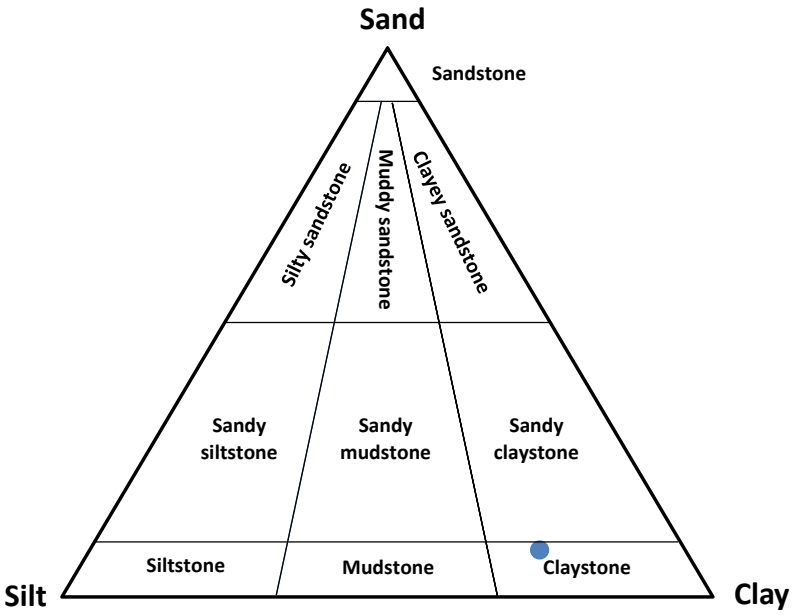


Fig. 3-1: Ternary plot showing the grain size composition of the sample based on the Wentworth scale (after Folk, 1954). Sample 11220 is classified as a claystone.



Fig. 3-2: Core photograph of sample 11220 from the Viking Formation, well 100/06-09-058-23W4/00 (depth 731.85 m). The thin section prepared from this sample was cut from the area marked with an X. The sample was received with no way up-direction. Scale is in mm.

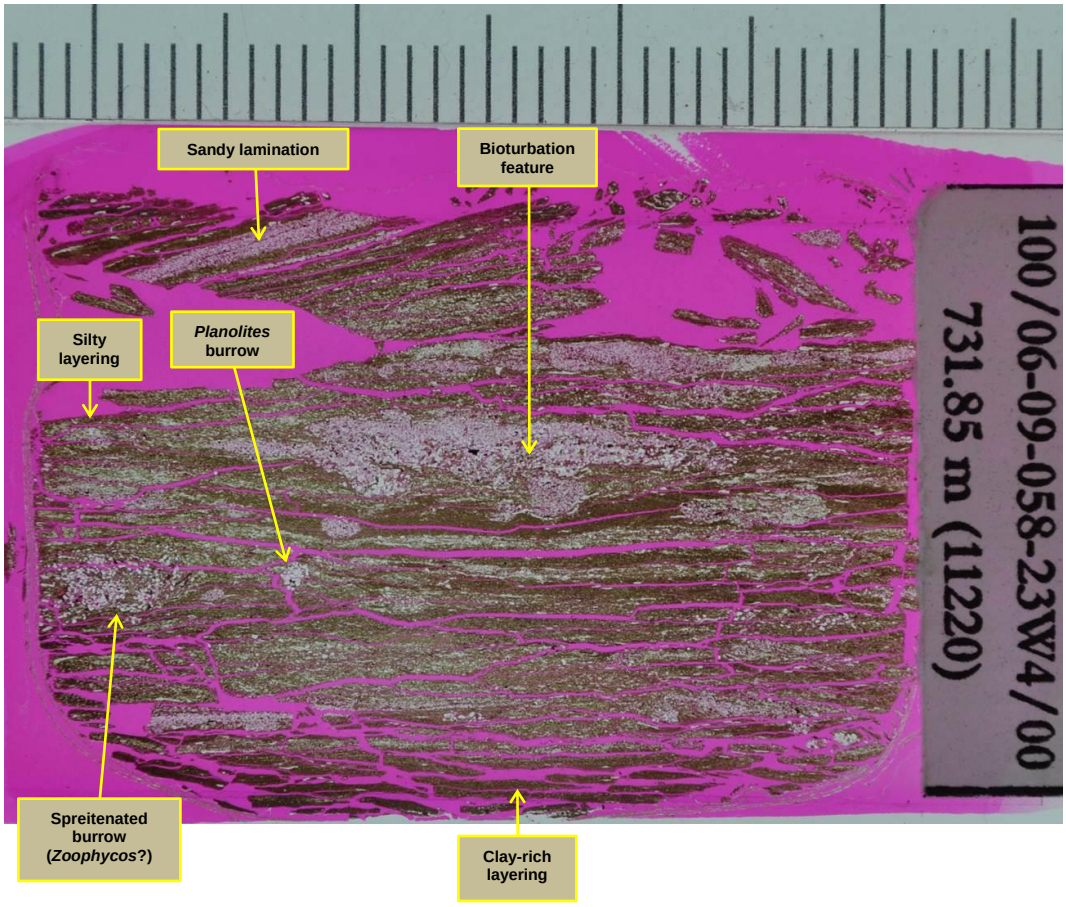


Fig. 3-3: Thin section photograph of sample 11220 from the Viking Formation, well 100/06-09-058-23W4/00 (depth 731.85 m). The sample is a heavily bioturbated claystone with thin silt (common) to fine sand (rare) beds and lenses. Burrow structures are observed throughout the silty and clay-rich layers of the sample, and include* Planolites *(circular burrows with sandy infills) and possible* Zoophycos *burrows (subhorizontal spreitenated burrow). A large bioturbation feature containing coarser grains than the surrounding layers is present near the centre of the sample. The abundance of partings and fractures in this sample suggests that it contains abundant water-sensitive clay minerals. Scale is in mm.

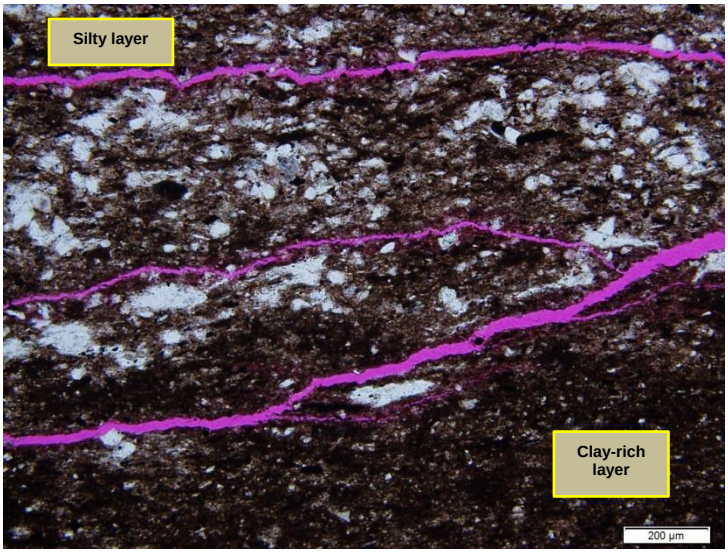


Fig. 3-4: Photomicrograph in PPL showing an overview of silty and clay-rich layers present in the claystone. Light-coloured minerals consist of quartz and chert, with some white patches due to plucking or removal of grains and clays during thin section preparation. Abundant artificial fractures (pink epoxy) occur at both bedding parallel and oblique angles, and are also the result of sample preparation (due to the presence of swelling clay minerals). Angled fractures may indicate that the sample is not strongly stratified

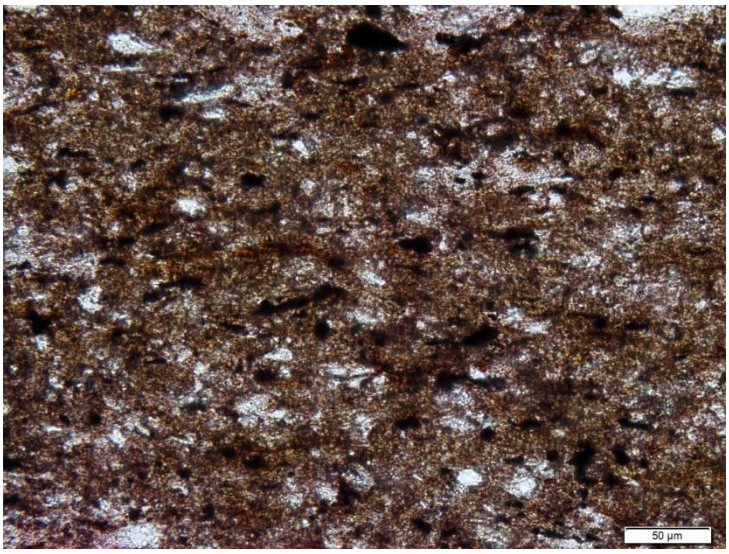


Fig. 3-5: Photomicrograph in PPL showing detail of a clay-rich layer. Pyrite (opaque) and disseminated, bedding-parallel organic matter are common in these layers. Light colored grains embedded in the clay-rich matrix include clay- to fine silt-size quartz, chert, and feldspar. Clays are estimated at ~65% of the total composition.

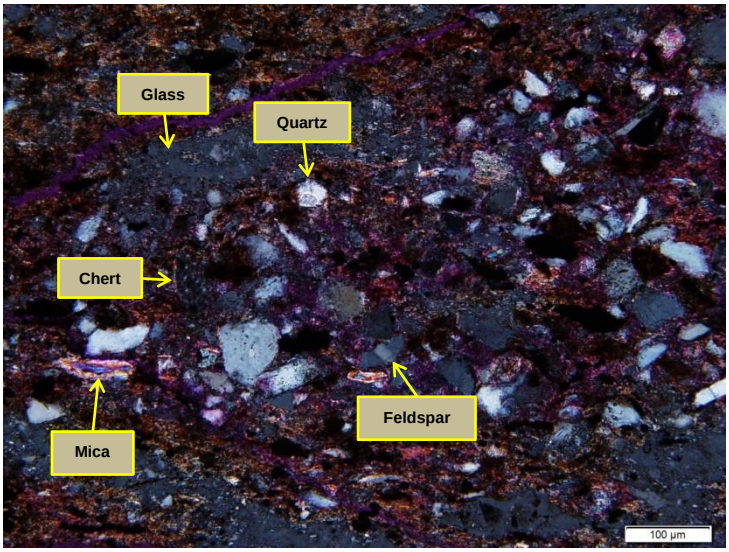


Fig. 3-6: Photomicrograph in XPL showing subangular (rare) to subrounded (common), very fine silt- to very fine sand-sized (average grain size is coarse silt) detrital quartz (18-25%), chert (5-8%), feldspar (<6%), and mica (<4%) present in a silty layer. Exposed thin section glass (dull blue-grey colour) is common in this sample.

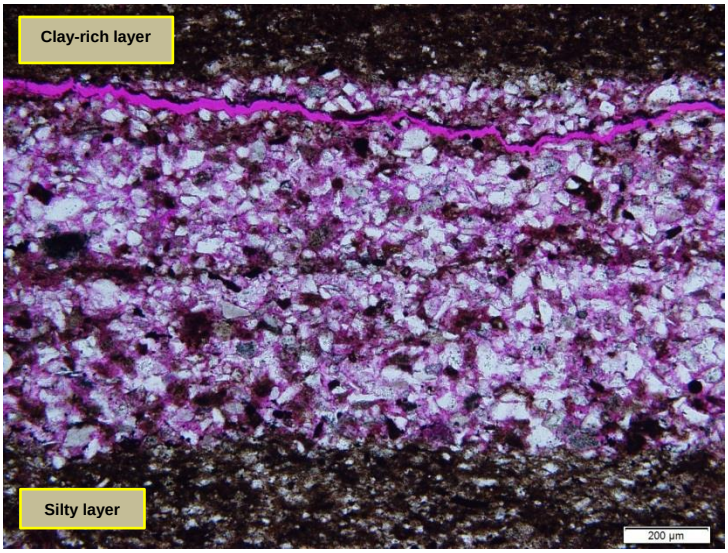


Fig. 3-7: Photomicrograph in PPL showing a porous, interbedded sandy lamination bound between clay-rich and silty layers. These laminae have ~10-15% intergranular porosity (pink epoxy), some of which may be artificial (caused by sample preparation).

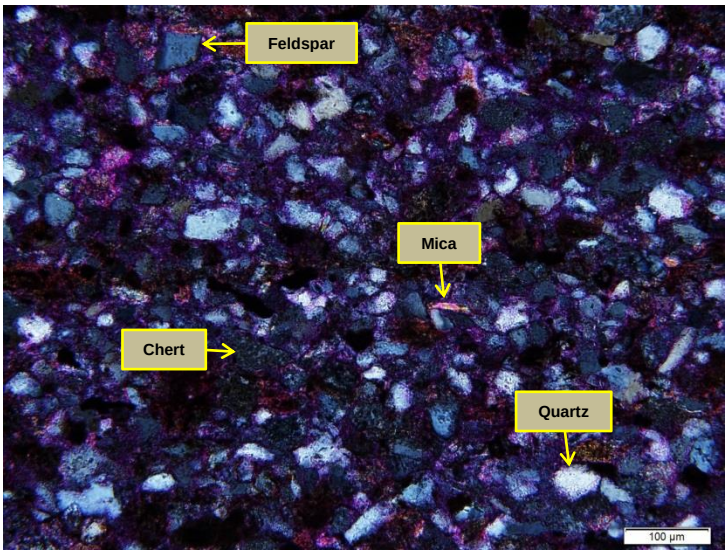


Fig. 3-8: Photomicrograph in XPL showing subangular (rare) to subrounded (common), very fine silt- to very fine sand-sized (average grain size is coarse silt) detrital quartz (55-65%), chert (8-10%), feldspar (2-4%), and mica (<1%) present in an interbedded sandy lamination.

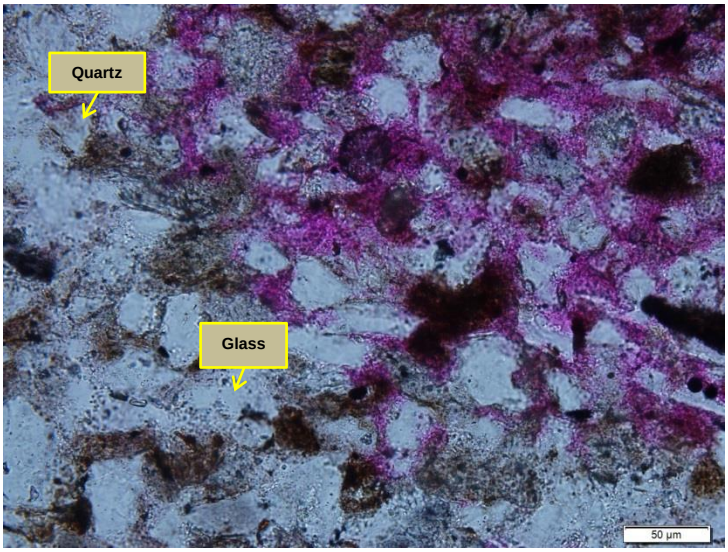


Fig. 3-9: Photomicrograph in PPL showing detail of intergranular porosity in an interbedded sandy lamination. The right side of the image has ~10-15% intergranular porosity (visible as pink epoxy) but the left side shows no porosity with exposed thin section glass between detrital grains. Exposed glass indicates removal of material (most likely clay matrix) during sample polishing, whereas the pink epoxy represents removal immediately after cutting (the sample was likely cut using water). The image shows a single, laterally continuous lamination and the partial epoxy infill represents an artifact of sample preparation (removal of material during preparation).

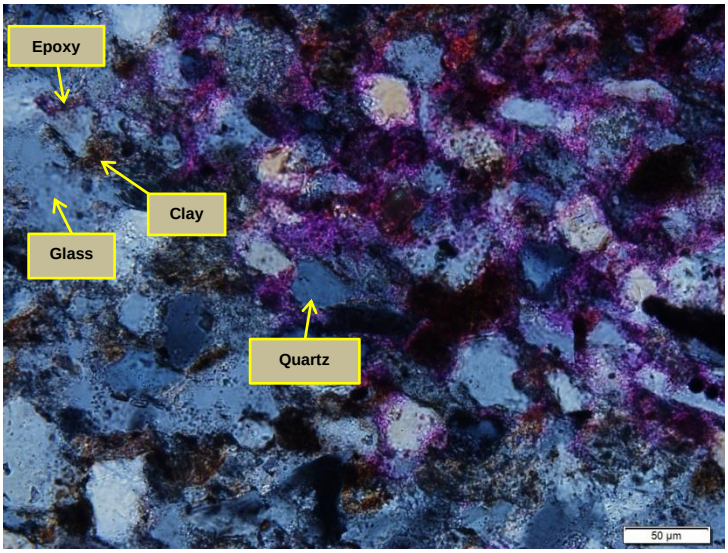


Fig. 3-10: Photomicrograph of Figure 3-9 in XPL showing detail of epoxy and glass in the sandy lamination. Quartz is more easily distinguished from thin section glass under cross-polarised light.

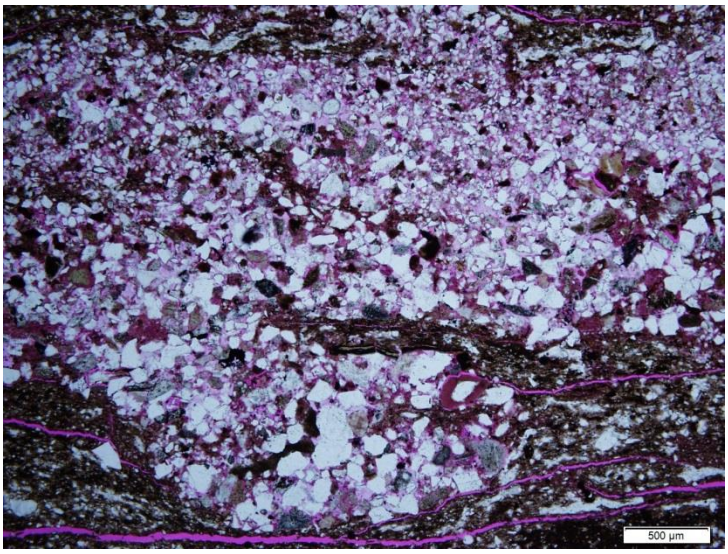


Fig. 3-11: Photomicrograph in PPL showing an overview of a massive bioturbation feature observed near the center of the sample (see location in Figure 3-3). This feature contains coarser grains than the surrounding layers and is composed of very fine silt- to medium sand-sized detrital quartz (65-75%), chert (6-8%), and feldspar (4-6%), as well as clays and opaque material. Up to an estimated 10% intergranular porosity is observed within this feature. Both kaolinite and quartz overgrowths are observed in the feature.

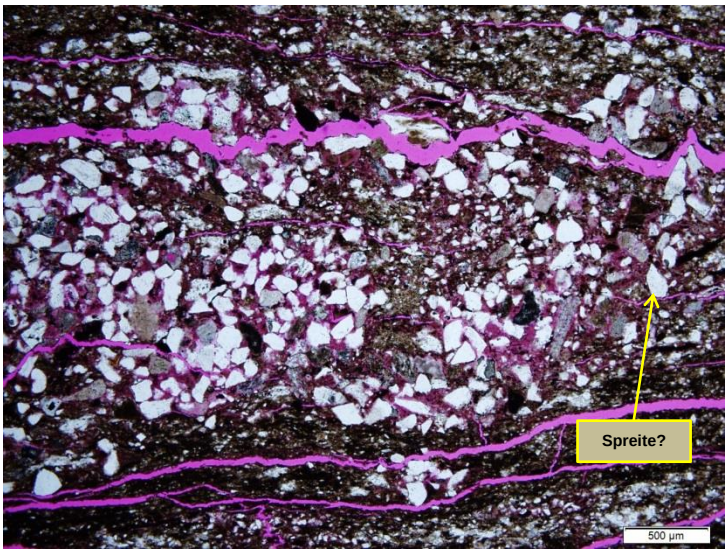


Fig. 3-12: Photomicrograph in PPL showing a possible spreitenated burrow (*Zoophycos*?) observed in a predominately silty section of the sample (see location in Fig. 3-3). Grains up to medium sand-size are present in the burrow, which shows distinct mixing features (convoluted bedding). Spreiten are u-shaped laminae (vertically oriented, and defined by quartz, chert, and feldspar grains in this example) produced by deposit feeding organisms.

3.2.2 SAMPLE 11221

Sample ID	**11221**		
Sample type	**Core**	**UWI/Well**	**100/16-23-058-24W4/00**
Strat. Unit	**Viking Formation**	**Depth**	**732.80 m**

XRD/SRA results

Quartz (%)	Fsp (%)	Cb (%)	Clays (%)	Pyrite (%)
38	2.6	0	58.6	0.8

Composition (*in order of abundance*)

Grain size	%	Variety (%)	Variety (%)	Variety (%)	Variety (%)
sand	6	Quartz/chert (95)	Feldspar (5)		
silt	25	Quartz/chert (96)	Mica (3)	Feldspar (1)	
clay	62	Clay mins (100)			
Cement	0				
Bioclasts	1	Phosphatic (100)			
Organics	5	Amorphous (100)			
Opaques	1	Pyrite (100)			
	100				

*Intensively altered to clay minerals

^ Including bitumen

Sedimentary structures

Primary	Silty and clay-rich layers and laminae, with interbedded sandy lenses.
Biogenic	Some sandy lenses may be biogenic.

Fractures	Common epoxy-filled fractures and partings.
Porosity	Discontinuous patches with up to 4% intergranular porosity occur in silty layers. Interbedded sandy lenses have up to 10% intergranular porosity. Both types of porosity may be largely artificial.

Description

Claystone with silty and clay-rich layers and laminae, and interbedded sandy lenses. Silty layers contain fine silt- to very fine sand-sized (average grain size is medium silt) detrital quartz (20-30%), chert (5-8%), mica (<5%), and feldspar (<2%). Interbedded sandy lenses are comprised of subangular to subrounded very fine silt- to fine sand-sized (average grain size is very fine sand) detrital quartz (50-60%), chert (8-12%), feldspar (<5%), and mica (<2%).

Thin Section Quality

Poor.

Rock Classification

Claystone.

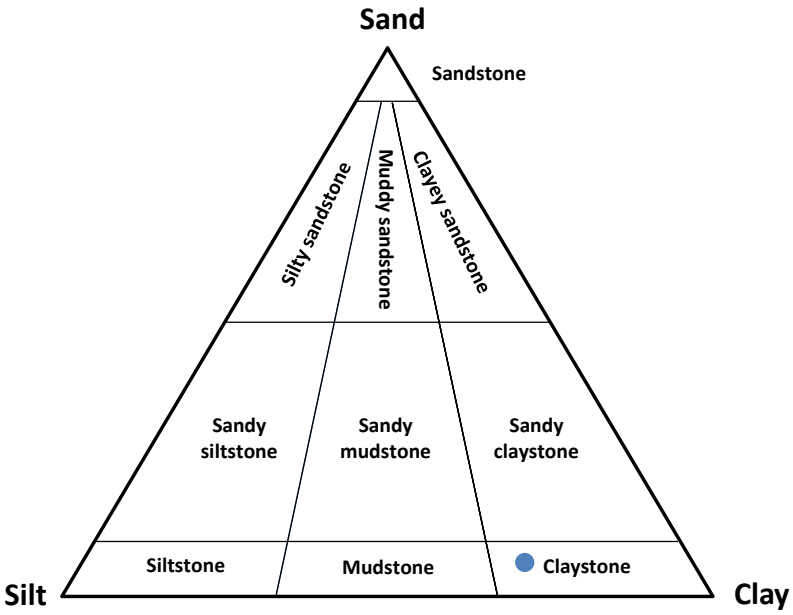


Fig. 3-13: Ternary plot showing the grain size composition of the sample based on the Wentworth scale (after Folk, 1954). Sample 11221 is classified as a claystone.



Fig. 3-14: Core photograph of sample 11221 from the Viking Formation, well 100/16-23-058-24W4/00 (depth 732.80 m). The thin section prepared from this sample was cut from the area outlined with black marker. The sample was received with no way-up direction. Scale is in mm.

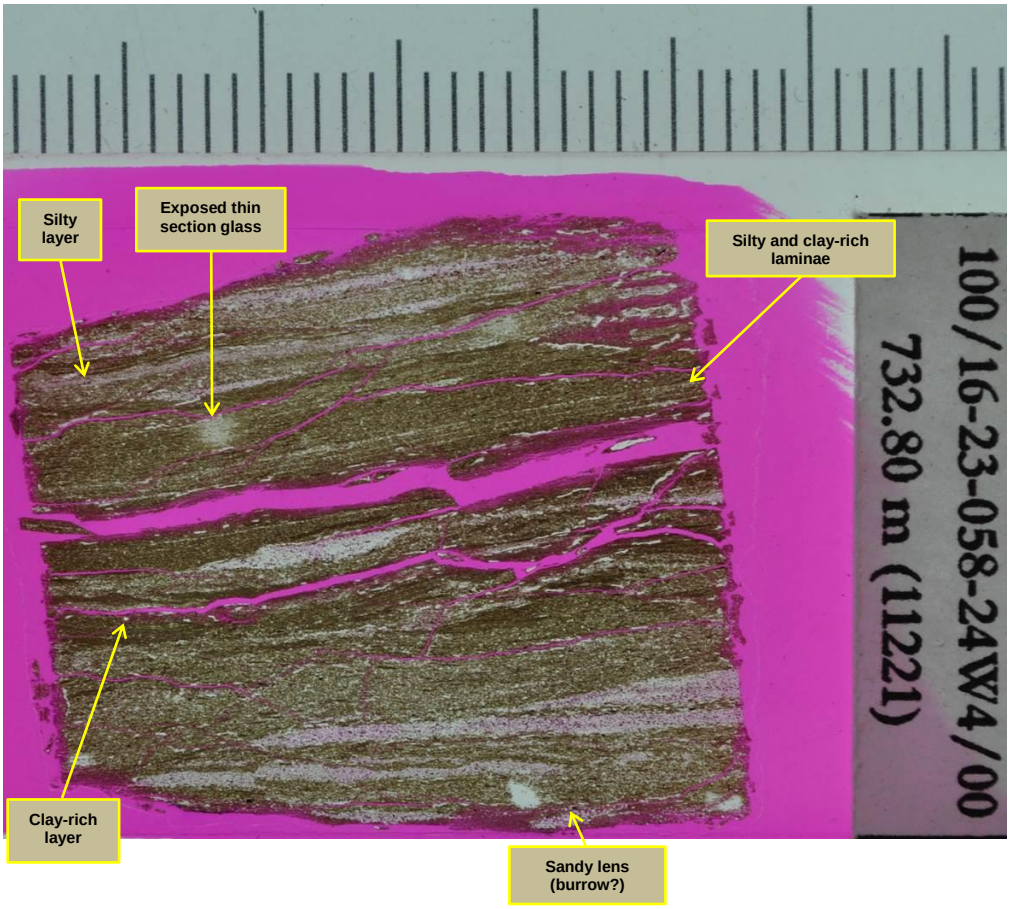


Fig. 3-15: Thin section photograph of sample 11221 from the Viking Formation, well 100/16-23-058-24W4/00 (depth 732.80 m). The sample is a claystone with silty and clay-rich layers and laminae, and interbedded sandy lenses (possibly related to bioturbation, or oblique sections through discontinuous sandy layers). Abundant artificial fractures (pink epoxy – mostly subparallel to bedding) indicate the presence of swelling clays. Scale is in mm. Note: way-up direction was not indicated and is difficult to identify, and therefore may differ from the orientation shown.

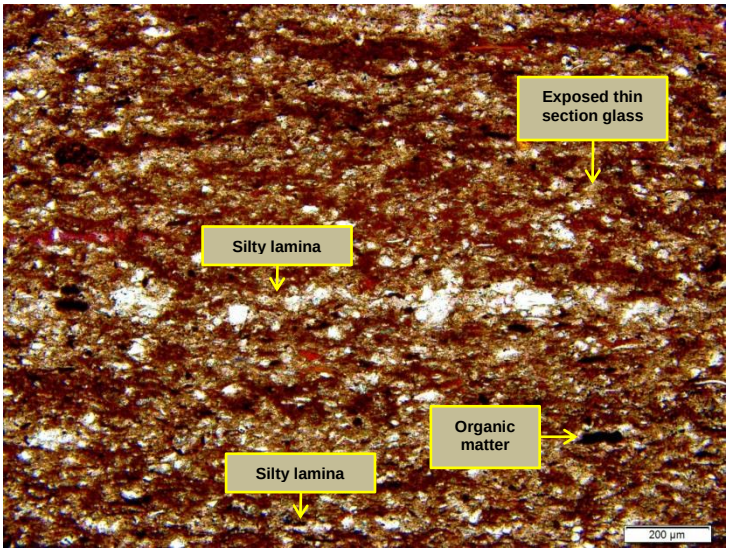


Fig. 3-16: Photomicrograph in HDR (high dynamic range) PPL showing a clay-rich layer with interbedded silty laminae. Much of the sample is dominated by clays, estimated at ~60-65% of the total composition. The interbedded silty laminae contain more angular to subrounded quartz and chert grains and fewer mica lathes than the surrounding clay-rich matrix. Significant material appears to have been removed from the sample (exposed thin section glass – light yellow color) during cutting and polishing, indicating that swelling clays may be present.

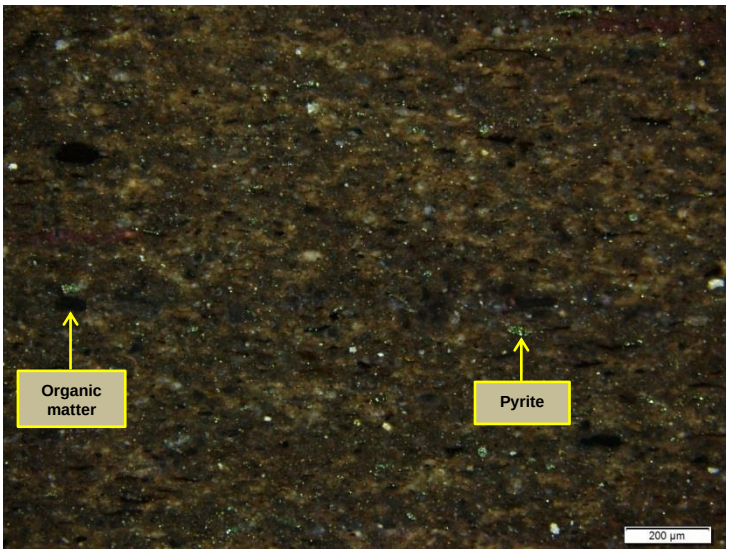


Fig. 3-17: Photomicrograph in reflected light showing finely dispersed opaque material (mostly organic matter and pyrite) observed in a clay-rich layer (same field of view as Figure 3-16). Organic matter particles comprise ~5% of the sample, with pyrite (gold colour) estimated at ~1% of the total composition.

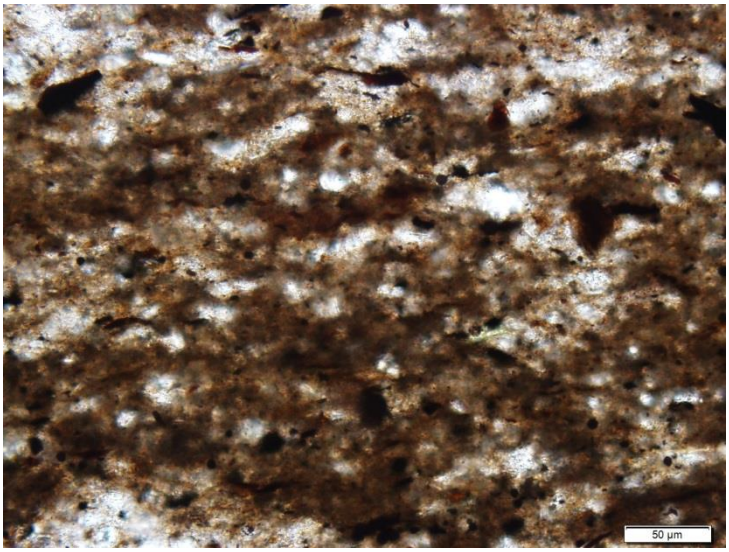


Fig. 3-18: Photomicrograph in PPL showing detail of a clay-rich layer with associated fine bedding-parallel organic “wisps”, flakes and blebs. Clay- to silt-size particles of quartz are also embedded in the clay-rich matrix.

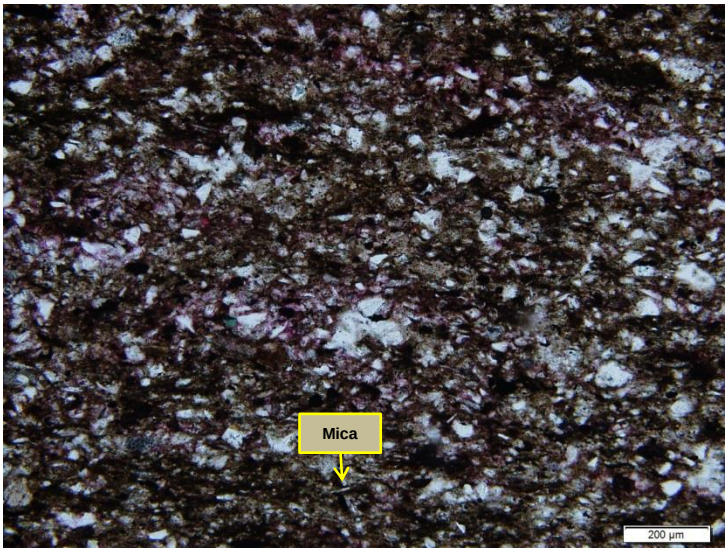


Fig. 3-19: Photomicrograph in PPL showing a silty layer. These layers show discontinuous patches with up to 4% intergranular porosity, which may be artificial, possibly resulting from removal of water-sensitive clay minerals during sample preparation. Light-coloured minerals consist of quartz (predominant), chert, feldspar and mica with the darker patches consisting of clays and opaque material (pyrite, organics).

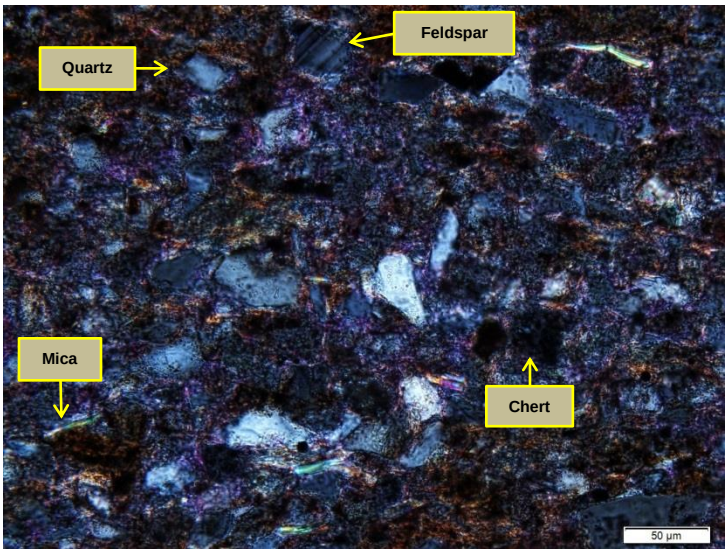


Fig. 3-20: Photomicrograph in XPL showing fine silt- to very fine sand-sized (average grain size is medium silt) detrital quartz (20-30%), chert (5-8%), mica (<5%), and feldspar (<2%) present in a silty lamination. Note polysynthetic twinning associated with some feldspars.

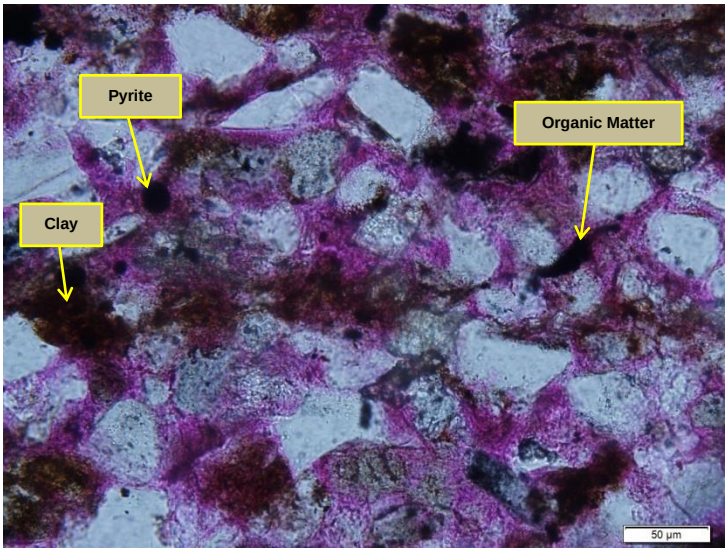


Fig. 3-21: Photomicrograph in PPL showing a sandy lens. These features have up to 10% intergranular porosity, some of which may be artificial, due to removal of clays during sample preparation. Note patchy clays draping around grains and filling some intergranular space. Finely disseminated pyrite and some organic matter are also observed.

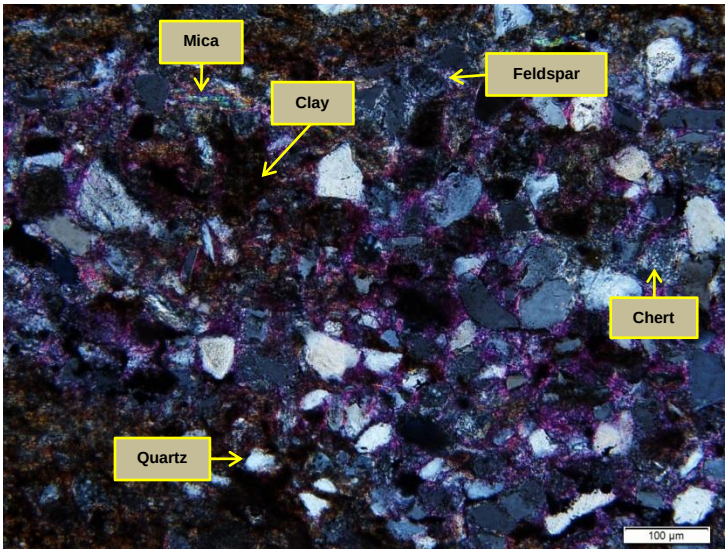


Fig. 3-22: Photomicrograph in XPL showing subangular to subrounded very fine silt- to fine sand-sized (average grain size is very fine sand) detrital quartz (50-60%), chert (8-12%), feldspar (<5%), and mica (<2%) present in a sandy lens.

3.2.3 SAMPLE 11222

Sample ID	**11222**		
Sample type	**Core**	**UWI/Well**	**100/16-23-058-24W4/00**
Strat. Unit	**Viking Formation**	**Depth**	**736.40 m**

XRD/SRA results

Quartz (%)	Fsp (%)	Cb (%)	Clays (%)	Pyrite (%)
56.3	4.7	0	37.8	1.1

Composition (*in order of abundance*)

Grain size	%	Variety (%)	Variety (%)	Variety (%)	Variety (%)
sand	10	Quartz/chert (90)	Feldspar (10)	Mica (<1)	
silt	30	Quartz/chert (88)	Feldspar (8)	Mica (2)	
clay	50	Clay mins (100)			
Cement	4	Quartz (100)			
Bioclasts	1	Phosphatic (100)			
Organics	4	Amorphous (100)			
Opaques	1	Pyrite (100)			
	100				

*Intensively altered to clay minerals

^ Including bitumen

Sedimentary structures

Primary	The sample consists of a lower silty layer with occasional clay-rich and silty laminae, and an upper clay-rich layer with rare silty laminae.
Biogenic	Common bioturbation features, including *Planolites* and possible *Zoophycos* burrows.

Fractures	Numerous thin (4-36 μm) epoxy-filled fractures occur throughout the sample, particularly in the upper clay-rich layer.
Porosity	Up to 5% intergranular porosity in possible *Planolites* burrows, discontinuous clusters of detrital grains with limited interstitial clay, and some silty laminae.

Description

Heavily bioturbated sandy mudstone with silty and clay-rich layers and laminations. The sample consists of a lower silty layer and an upper clay-rich layer. The silty layer contains some alternating silty and clay-rich laminae, and is comprised of subrounded (common) to subangular (rare) very fine silt- to fine sand-sized (average grain size is coarse silt) detrital quartz (35-50%), chert (8-12%), feldspar (<4%), and mica (<2%). The clay-rich layer contains rare silty laminae, and is comprised of subrounded very fine silt to fine sand-sized detrital quartz (10-15%), chert (6-8%), feldspar (<5%), and mica (<2%).

Thin Section Quality

Moderate.

Rock Classification

Sandy mudstone.

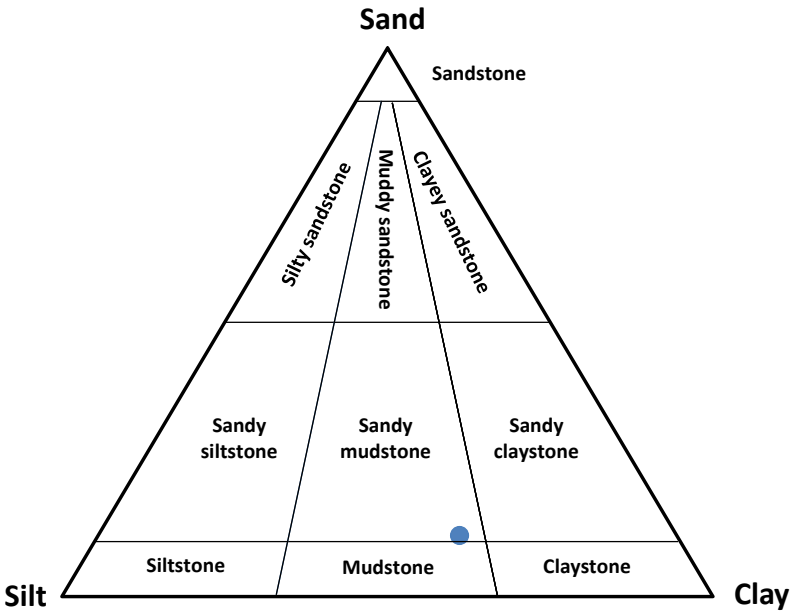


Fig. 3-23: Ternary plot showing the grain size composition of the sample based on the Wentworth scale (after Folk, 1954). Sample 11222 is classified as a sandy mudstone.

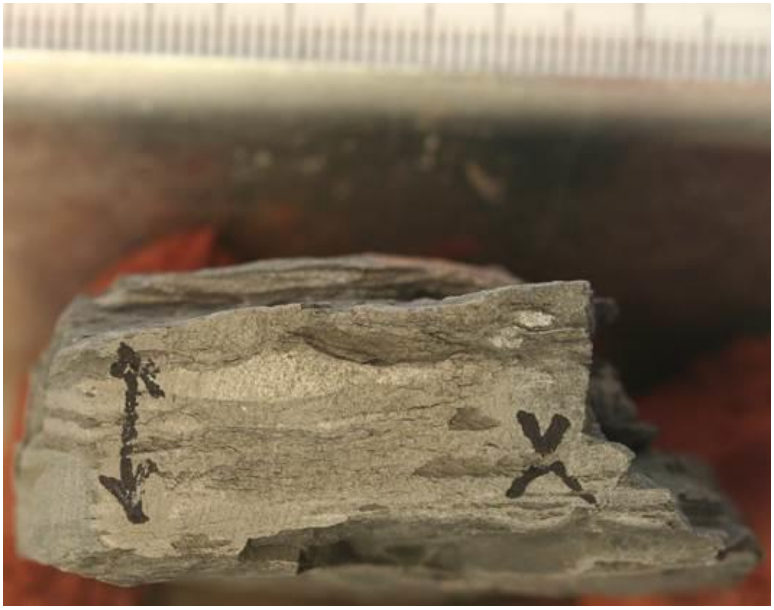


Fig. 3-24: Core photograph of sample 11222 from the Viking Formation, well 100/16-23-058-24W4/00 (depth 736.4 m). The thin section prepared from this sample was cut from the area marked with an X. The sample was received with no up-direction and the plucking of sample material may indicate the presence of swelling clays. Scale is in mm.

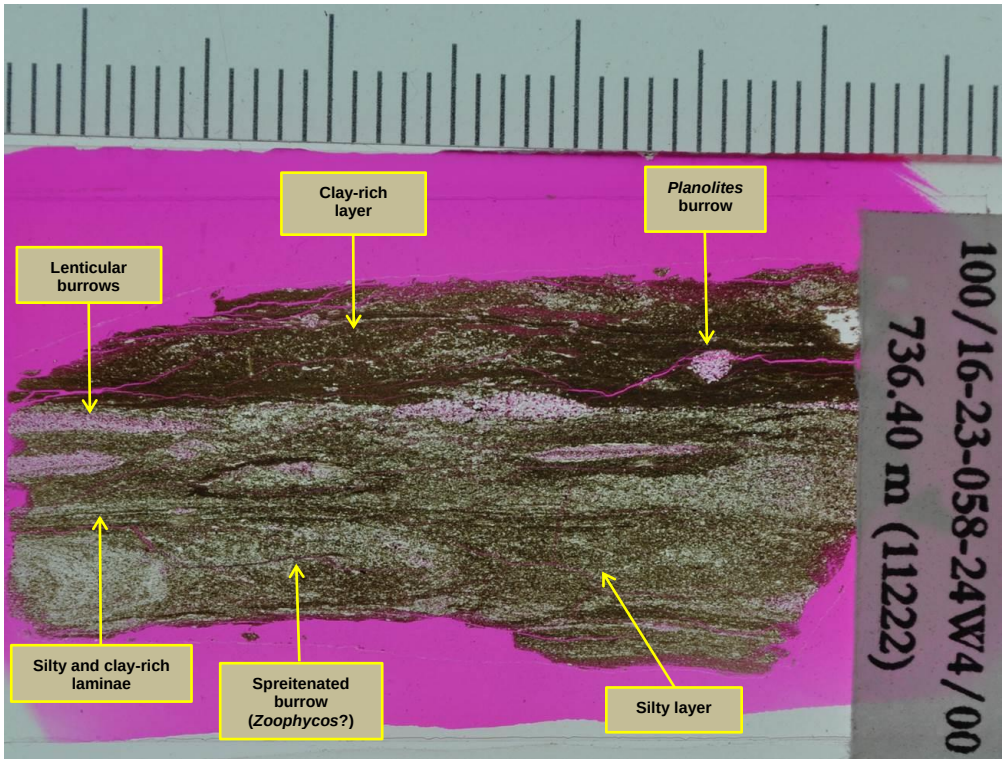


Fig. 3-25: Thin section photograph of sample 11222 from the Viking Formation, well 100/16-23-058-24W4/00 (depth 736.4 m). The sample is a heavily bioturbated sandy mudstone with distinct clay-rich and silty layers and laminations. At least three different bioturbation features are visible in this sample, including* Planolites *burrows (circular pockets of well sorted coarse silt- and very fine sand-sized grains within the upper clay-rich layer), a possible* Zoophycos *burrow (subhorizontal spreitenated burrow in the lower silty layer), and lenticular burrows consisting of well sorted coarse silt- to very fine sand-sized grains (possibly transverse sections through* Planolites *burrows). Scale is in mm. Note that the depositional way up was not indicated on this sample, and may differ from the orientation shown in the above image.

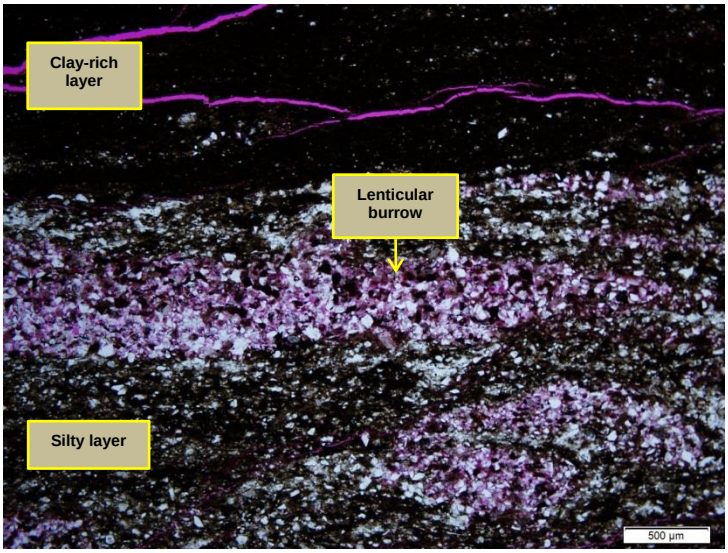


Fig. 3-26: Photomicrograph in PPL showing a sharply defined contact between the upper clay-rich layer and lower silty layer observed in the sample. The depositional up direction is not indicated on the sample, and may therefore differ from the orientation shown in this image. Several lenticular burrow structures, possibly transverse sections through *Planolites* burrows, are present in the silty layer.

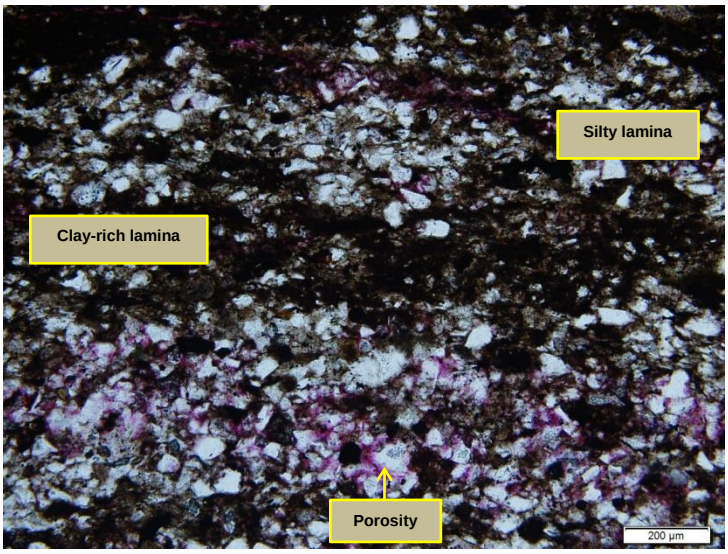


Fig. 3-27: Photomicrograph in PPL showing clay-rich and silty laminae present above a porous section of the lower silty layer. Although much of the layer is non-porous, discontinuous clusters of detrital grains with up to 5% intergranular porosity are present. Few undisturbed, continuous laminae are observed in this heavily bioturbated sample.

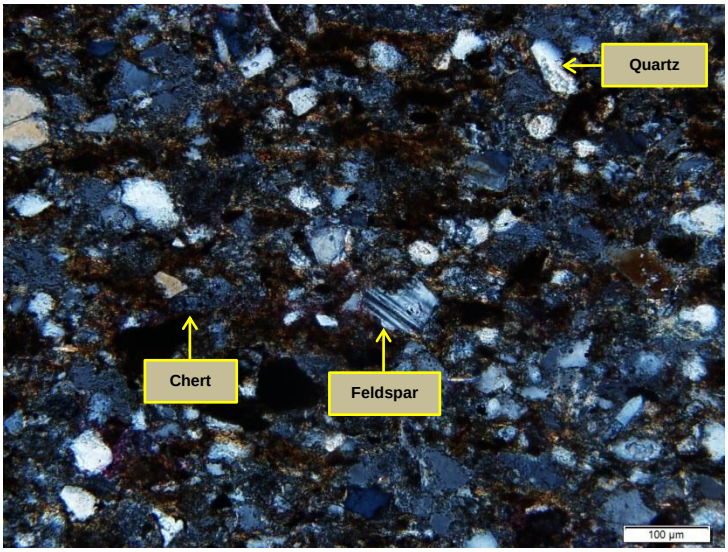


Fig. 3-28: Photomicrograph in XPL showing subangular to subrounded, very fine silt- to fine sand-sized (average grain size range is coarse silt) detrital quartz (35-50%), chert (8-12%), feldspar (<4%), and mica (<2%) present in the lower silty layer. Chert grains are composed of microcrystalline quartz. Note polysynthetic twinning associated with some feldspars (albite).

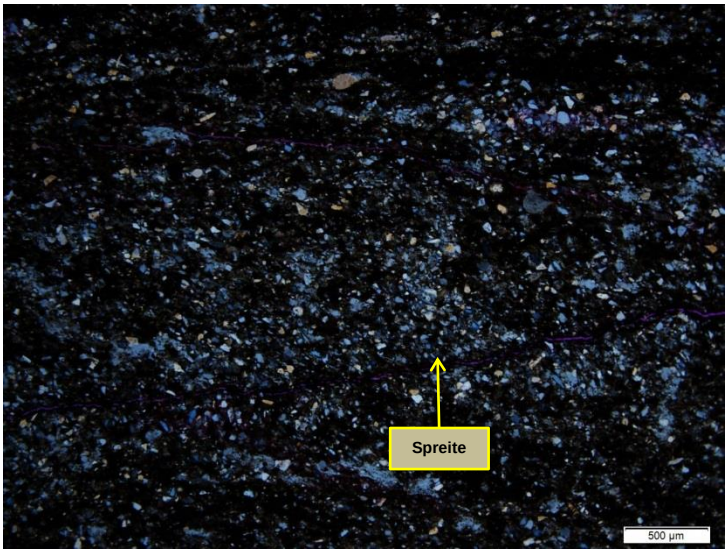


Fig. 3-29: Photomicrograph in XPL showing detail of a possible spreitenated burrow (*Zoophycos*?) burrow present in the lower silty layer (see location in Figure 3-25). Spreiten are repeated u-shaped laminations produced by deposit feeding organisms, and are visible in this example as vertically-oriented laminae comprised of detrital quartz grains.

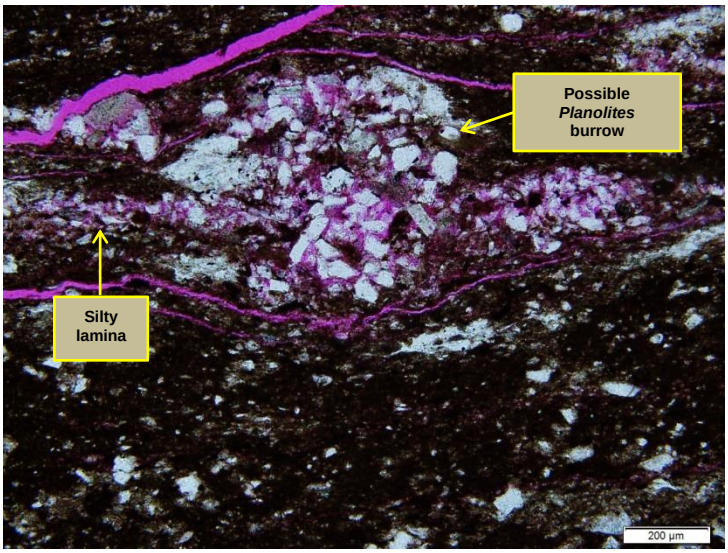


Fig. 3-30: Photomicrograph in PPL showing part of the upper clay-rich layer. Numerous epoxy-filled fractures occur in this horizon, possibly resulting from damage during cutting and polishing of the sample (water sensitive clays?). The majority of the layer is non-porous, with the exception of rare thin silty laminae and lenses, and occasional isolated clusters of silt- and sand-sized detrital grains (possible *Planolites* burrows), all of which have up to 5% intergranular porosity.

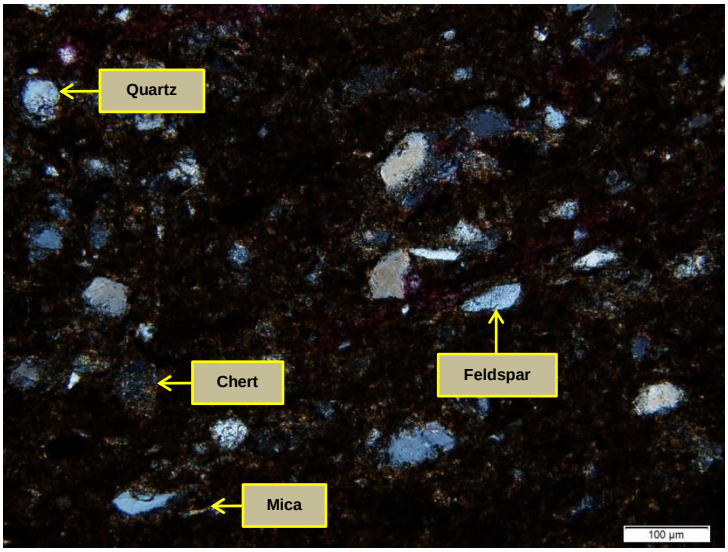


Fig. 3-31: Photomicrograph in XPL showing subrounded very fine silt- to very fine sand-sized detrital quartz (10-15%), chert (6-8%), feldspar (<5%), and mica (<2%) observed in the upper clay-rich layer.

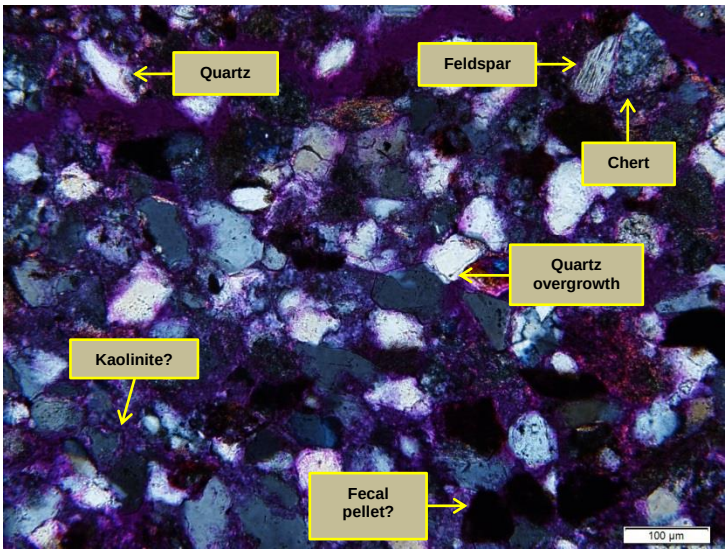


Fig. 3-32: Photomicrograph in XPL showing detail of a *Planolites* burrow. These burrows are comprised of subangular (common) to subrounded (rare) fine silt- to fine sand-sized detrital quartz/chert (60-75%) and feldspar (<5%) grains, as well as amorphous solid organic matter (<5%). Rounded organic matter particles may be fecal pellets deposited by burrowing organisms. These burrows contain quartz overgrowth cements, and have up to 5% intergranular porosity.

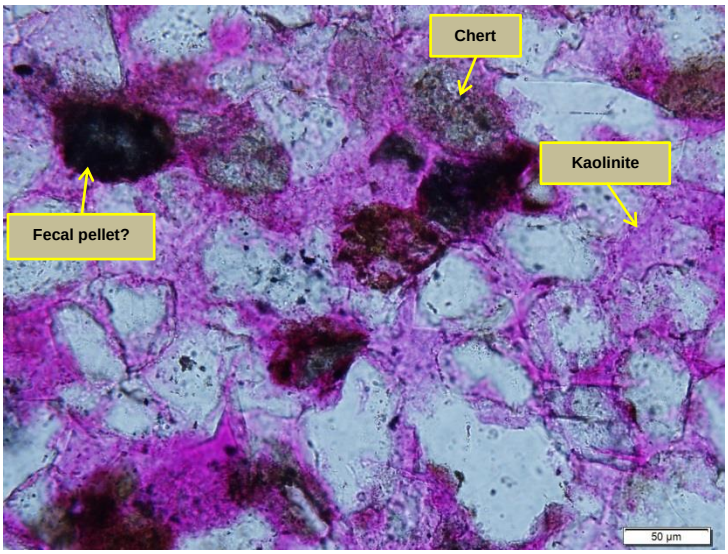


Fig. 3-33: Photomicrograph in PPL showing detail of a *Planolites* burrow (same as shown in Figure 3-30). Some pores appear to be filled with possible kaolinite booklets, which are associated with microporosity.

3.2.4 SAMPLE 11224

Sample ID	**11224**		
Sample type	**Core**	**UWI/Well**	**100/07-29-056-20W4/00**
Strat. Unit	**Viking Formation**	**Depth**	**619.50 m**

XRD/SRA results

Quartz (%)	Fsp (%)	Cb (%)	Clays (%)	Pyrite (%)
49.8	6.7	0	42	1.6

Composition (*in order of abundance*)

Grain size	%	Variety (%)	Variety (%)	Variety (%)	Variety (%)
sand	5	Quartz/chert (90)	Feldspar (7)	Mica (3)	
silt	25	Quartz/chert (90)	Feldspar (5)	Mica (5)	
clay	59	Clay mins (100)			
Cement	4	Quartz (100)			
Bioclasts	2	Phosphatic (100)			
Organics	4	Amorphous (100)			
Opaques	1	Pyrite (100)			
	100				

*Intensively altered to clay minerals

^ Including bitumen

Sedimentary structures

Primary	Interbedded clay-rich, silty, and sandy layers.
Biogenic	At least two possible bioturbation features.

Fractures	Common thin (10-20 μm) epoxy-filled fractures in clay-rich layers.
Porosity	Sandy layers have up to 15% intergranular porosity. Rare, laterally discontinuous sections with up to 5% porosity occur in silty layers.

Description

Bioturbated claystone with interbedded sandy and silty layers. Clay-rich layers contain subangular to subrounded very fine silt- to fine sand-sized (average grain size is medium silt) detrital quartz, chert, mica, and feldspar grains. Silty layers are comprised of very fine silt- to fine sand-sized (average grain size is coarse silt) detrital quartz (65-75%), chert (6-10%), mica (<5%), and feldspar (<3%). Sandy layers are comprised of subangular to subrounded fine silt- to fine sand-sized (average grain size is very fine sand) detrital quartz (35-45%), chert (15-20%), feldspar (<8%), and mica (<2%).

Thin Section Quality

Good.

Rock Classification

Claystone.

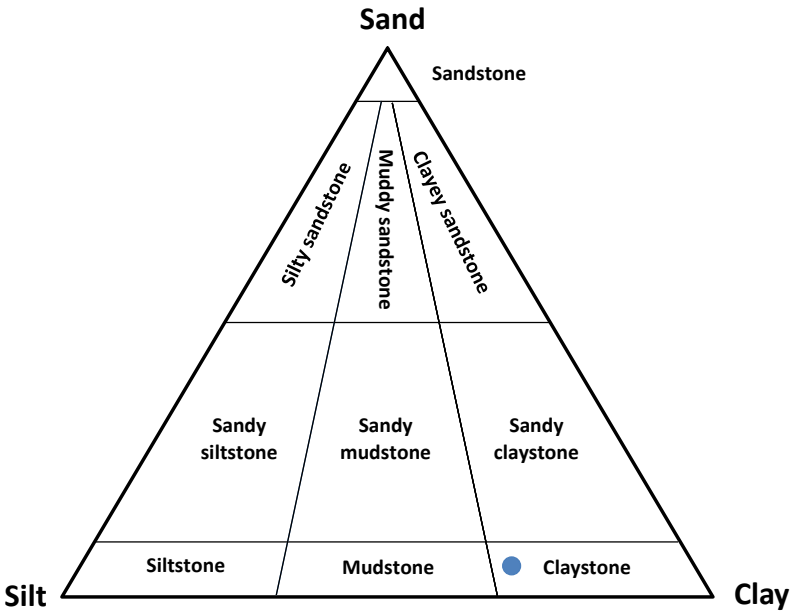


Fig. 3-34: Ternary plot showing the grain size composition of the sample based on the Wentworth scale (after Folk, 1954). Sample 11224 is classified as a claystone.



Fig. 3-35: Core photograph of sample 11224 from the Viking Formation, well 100/07-29-056-20W4/00 (depth 619.50 m). The thin section prepared from this sample was cut from the area marked with an X. The sample was received with no up-direction. Scale is in mm.

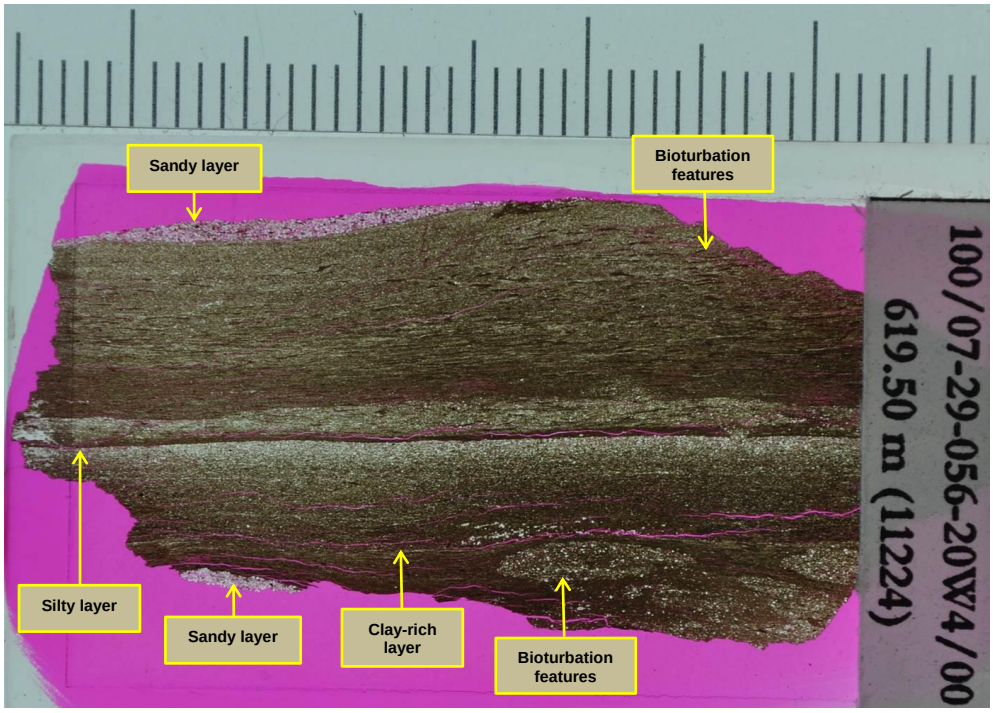


Fig. 3-36: Thin section photograph of sample 11224 from the Viking Formation, well 100/07-29-056-20W4/00 (depth 619.50 m). The sample is a bioturbated claystone with interbedded sandy and silty layers (lenses). The abundant artificial fractures (pink-epoxy) indicate the presence of swelling clays in this sample. Scale is in mm. Note: way-up direction was not indicated and is difficult to identify, and therefore may differ from the orientation shown.

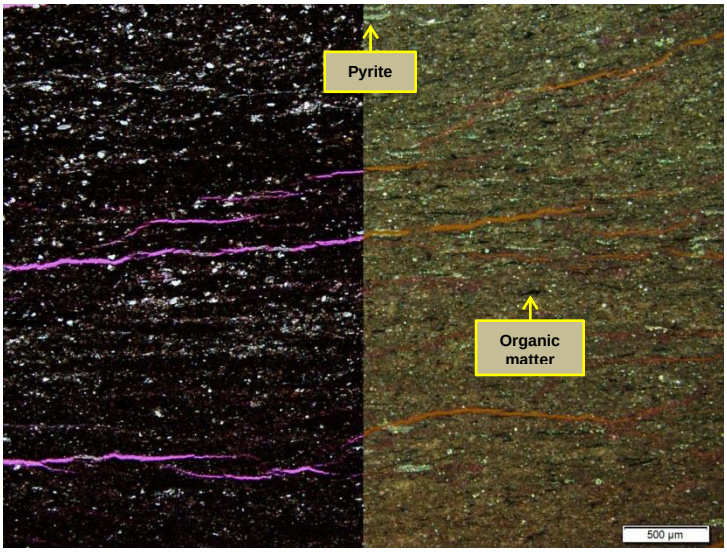


Fig. 3-37: Photomicrograph (left half in PPL, right half in reflected light) showing an overview of the lowermost clay-rich layer observed in this claystone. This layer contains abundant dispersed quartz and mica grains, as well as common bedding parallel pyrite (replaced organic matter?) and organic matter particles. Clays are estimated at ~60% of the total composition. The common epoxy-filled fractures are artificial and indicate the presence of swelling clays in the matrix.

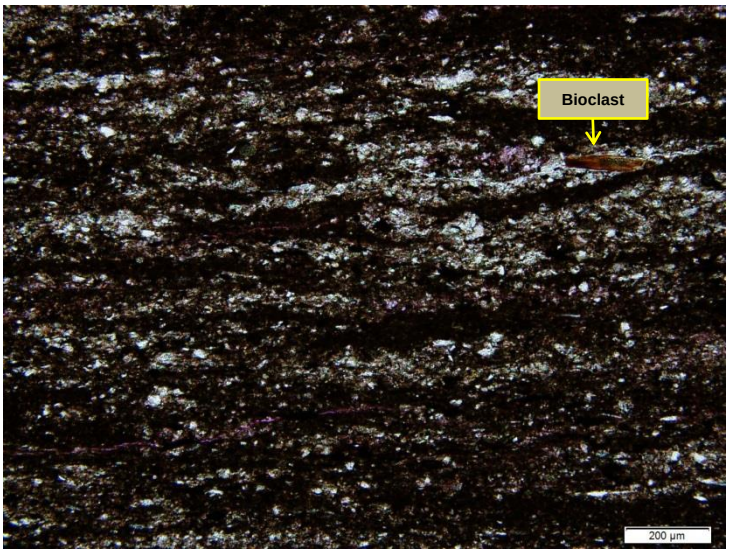


Fig. 3-38: Photomicrograph in PPL of the uppermost clay-rich layer, which contains common elongate, occasionally sinuous bioturbation features. Phosphatic bioclasts (fish bones?) are observed in all of the layers in this sample. The light-coloured minerals consist mostly of quartz with the darker material consisting of clays, organic matter and pyrite.

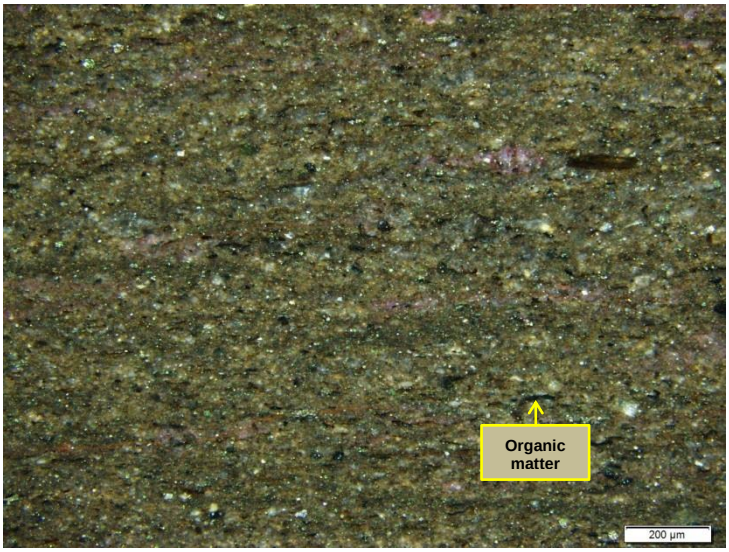


Fig. 3-39: Photomicrograph of Figure 3-38 in reflected light illustrating relatively few bedding-parallel organic matter particles and some pyrite (gold colour).

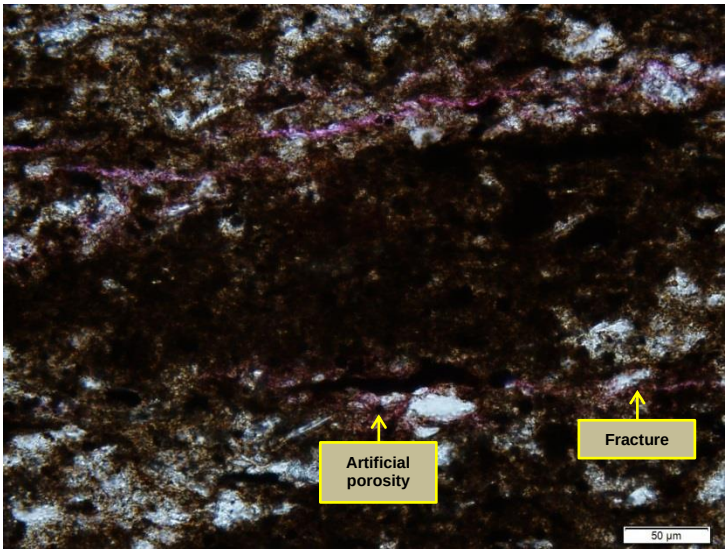


Fig. 3-40: Photomicrograph in PPL showing a clay-rich layer. These layers show rare instances of epoxy "bleeding" around grain edges (artificial porosity) in association with artificial fractures.

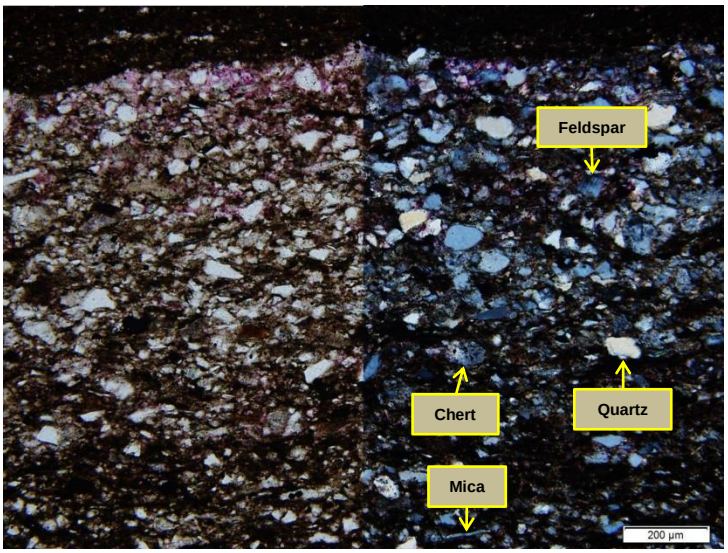


Fig. 3-41: Photomicrograph (left half in PPL, right half in XPL) showing subangular very fine silt- to fine sand-sized (average grain size is coarse silt) detrital quartz (65-75%), chert (6-10%), mica (<5%), and feldspar (<3%) present in a silty layer.

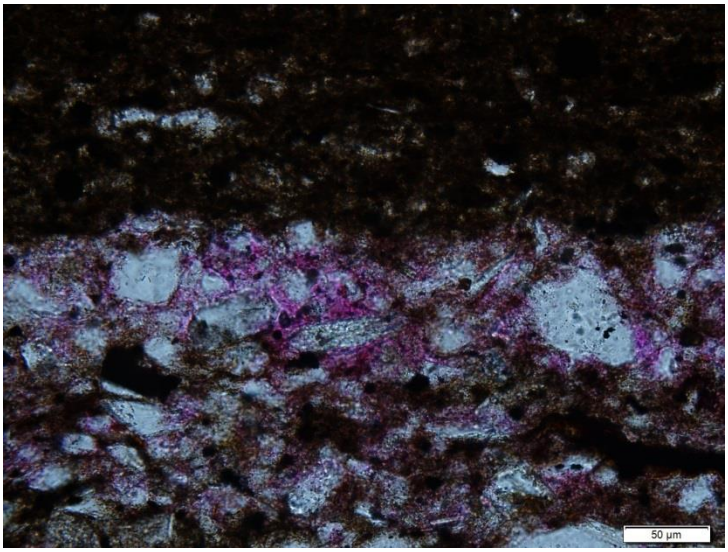


Fig. 3-42: Photomicrograph in PPL showing a discontinuous silty lens with up to 5% intergranular porosity (pink epoxy). The silty layers in this sample generally have no visible porosity.

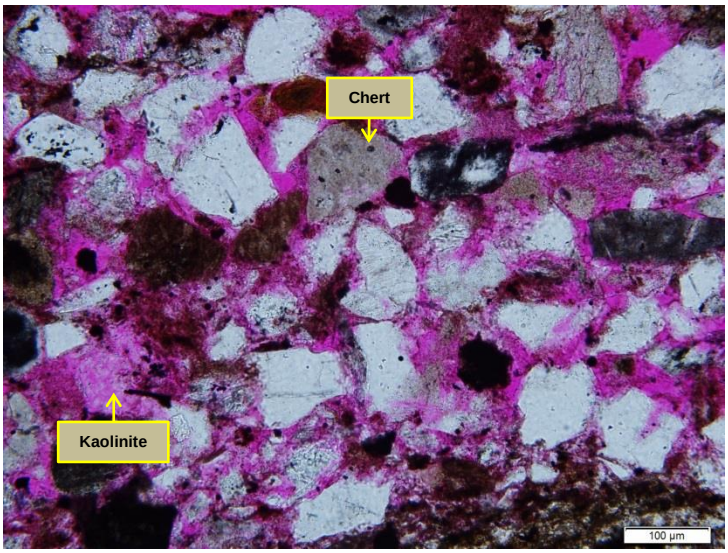


Fig. 3-43: Photomicrograph in PPL showing part of a sandy layer with up to 15% intergranular porosity. Pore-lining clays and pore-filling kaolinite booklets are observed between some grains in these layers. The true porosity in the sandy lenses and layers may be much lower than shown, as part of the intergranular material may have been removed during preparation (removal of water sensitive clays during cutting with water).

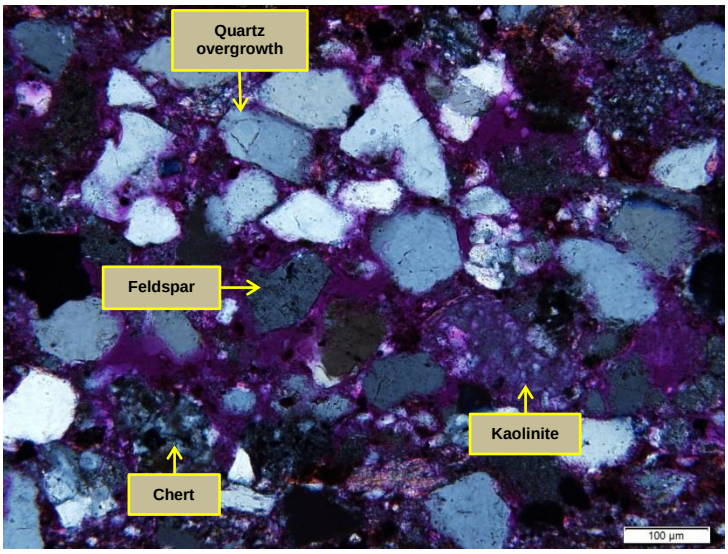


Fig. 3-44: Photomicrograph in XPL showing a sandy layer containing subangular to subrounded fine silt- to fine sand-sized (average grain size is very fine sand) detrital quartz (35-45%), chert (15-20%), and feldspar (<8%). Some of the quartz grains present in these layers show overgrowths.

3.2.5 SAMPLE 11225

Sample ID	**11225**		
Sample type	**Core**	**UWI/Well**	**100/07-29-056-20W4/00**
Strat. Unit	**Viking Formation**	**Depth**	**625.50 m**

XRD/SRA results

Quartz (%)	Fsp (%)	Cb (%)	Clays (%)	Pyrite (%)
42.3	5.6	0	50.5	2.5

Composition (*in order of abundance*)

Grain size	%	Variety (%)	Variety (%)	Variety (%)	Variety (%)
sand	0				
silt	11	Quartz/chert (85)	Mica (15)		
clay	66	Clay mins (100)			
Cement	0				
Bioclasts	<1	Phosphatic (100)			
Organics	18	Amorphous (100)			
Opaques	5	Pyrite (100)			
	100				

*Intensively altered to clay minerals

^ Including bitumen

Sedimentary structures

Primary	Clay-rich horizons with interbedded thin silty laminae.
Biogenic	None apparent.

Fractures	Common small (<10 µm) epoxy-filled fractures.
Porosity	Rare sections of some silty laminae with <5% intergranular porosity.

Description

Organic-rich claystone with interbedded thin silty layers. The majority of the rock consists of clay-rich horizons with abundant bedding-parallel organic matter particles. Thin (20-230 µm thickness), interbedded silty laminae contain very fine to medium silt-sized detrital quartz/chert (85-95%) and mica (2-5%). These laminae are generally non porous, with the exception of rare, laterally discontinuous patches of sediment with <5% intergranular porosity.

Thin Section Quality

Moderate.

Rock Classification

Claystone.

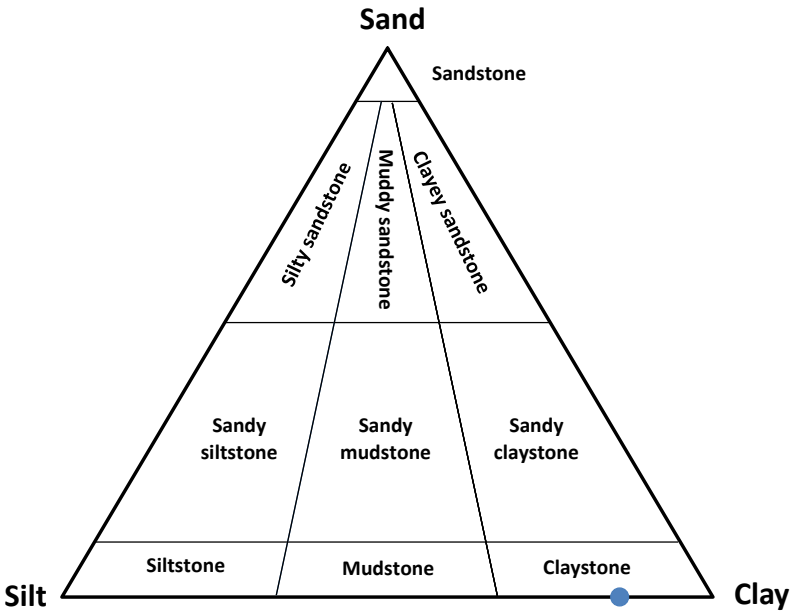


Fig. 3-45: Ternary plot showing the grain size composition of the sample based on the Wentworth scale (after Folk, 1954). Sample 11225 is classified as a claystone.



Fig. 3-46: Core photograph of sample 11225 from the Viking Formation, well 100/07-29-056-20W4/00 (depth 632.00 m). The thin section prepared from this sample was cut from the area marked with an X. The sample was received with no way up-direction. Scale is in mm.

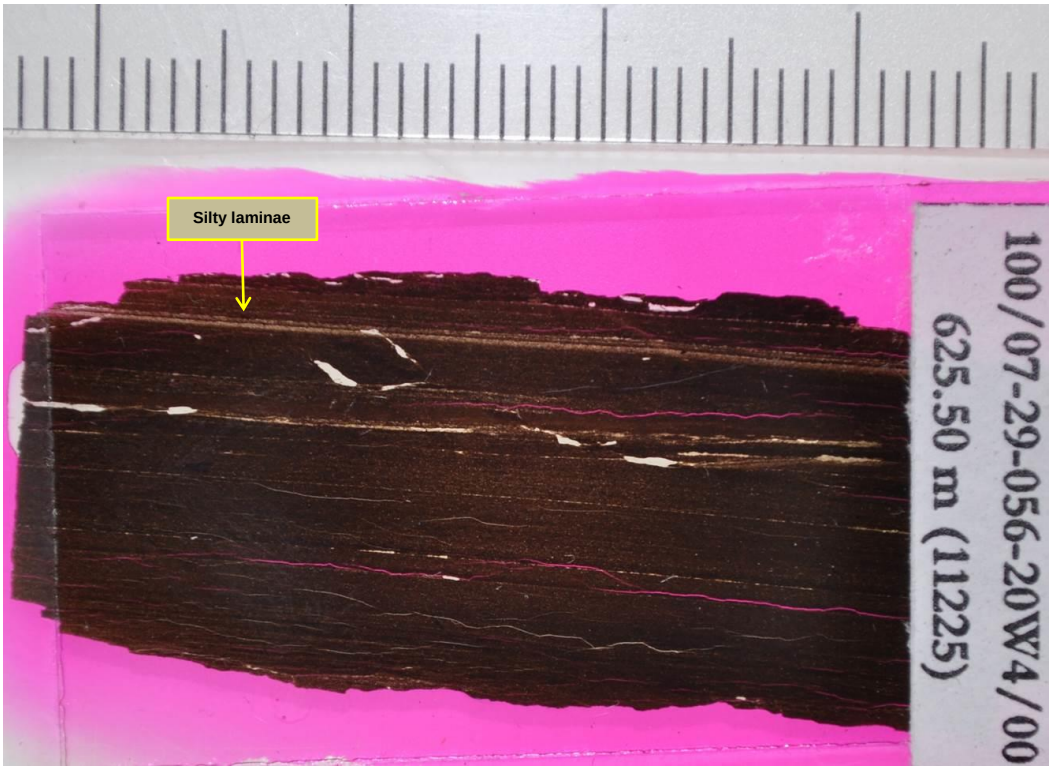


Fig. 3-47: Thin section photograph of sample 11225 from the Viking Formation, well 100/07-29-056-20W4/00 (depth 625.50 m). The sample is an organic-rich claystone with interbedded thin silty laminae. Scale is in mm. Note: way-up direction was not positively identified in this sample and may differ from the orientation shown.

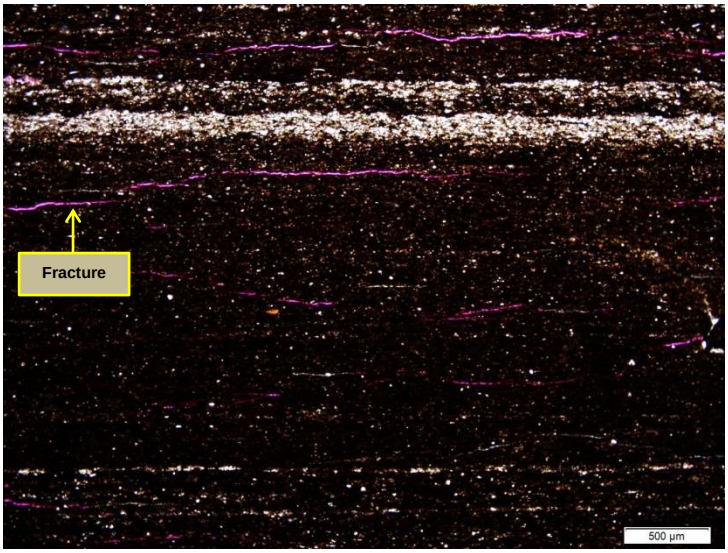


Fig. 3-48: Photomicrograph in PPL showing an overview of the finely laminated claystone and few interbedded silty laminae. Clay-sized material constitutes ~66% of the sample. Note numerous epoxy-filled fractures, oriented sub-parallel to bedding, which are all artificial.

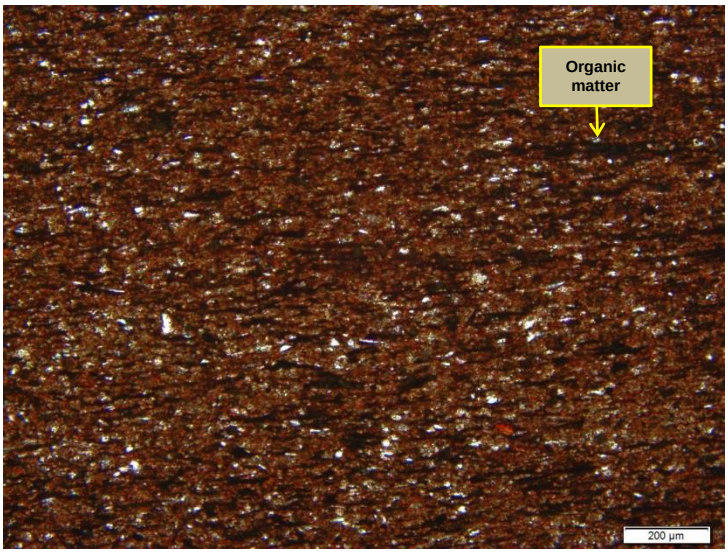


Fig. 3-49: Photomicrograph in HDR (high dynamic range) PPL showing abundant (~18% of the sample composition) bedding-parallel organic matter. Clay- to fine silt-size quartz and mica are also embedded within the clay-rich matrix.

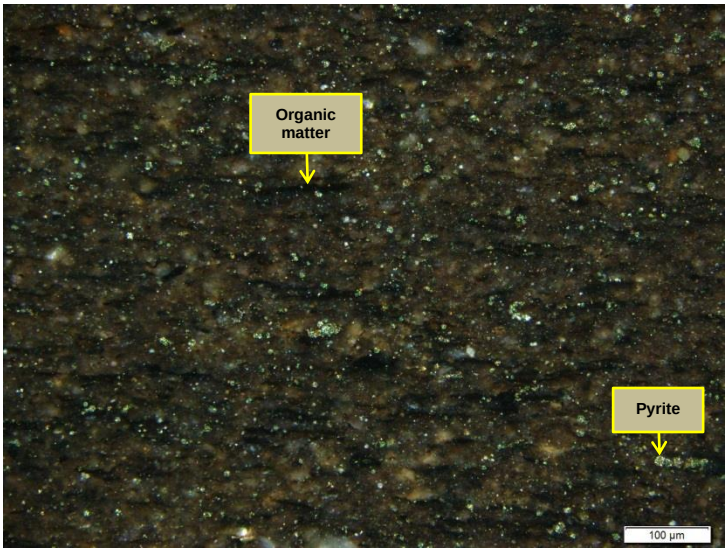


Fig. 3-50: Photomicrograph in reflected light showing detail of bedding-parallel organic matter “strands” and finely dispersed pyrite (gold colour; mostly framboidal). Pyrite comprises ~5% of the rock.

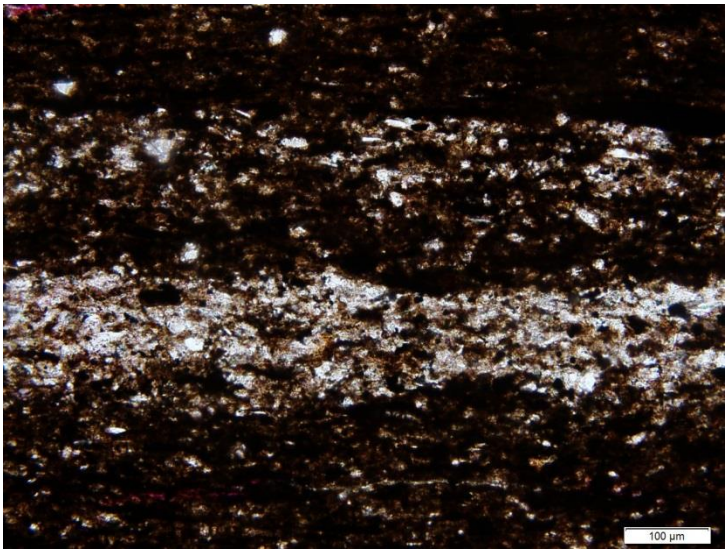


Fig. 3-51: Photomicrograph in PPL detailing some of the interbedded silty laminae (20-230 µm thick). These laminae are a relatively minor component of this organic- and clay-rich sample. Numerous sub-spherical clusters and pockets of opaque material may be derived from fecal remains.

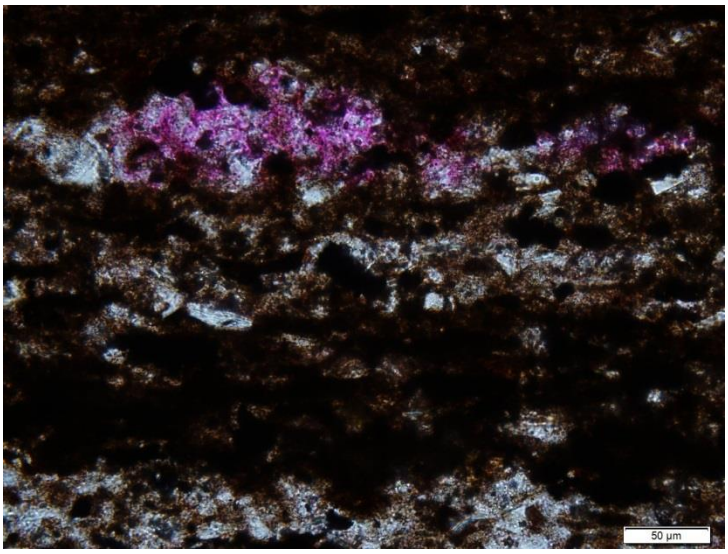


Fig. 3-52: Photomicrograph in PPL showing a rare, laterally discontinuous section of an interbedded silty lamination with <5% intergranular porosity (pink epoxy).

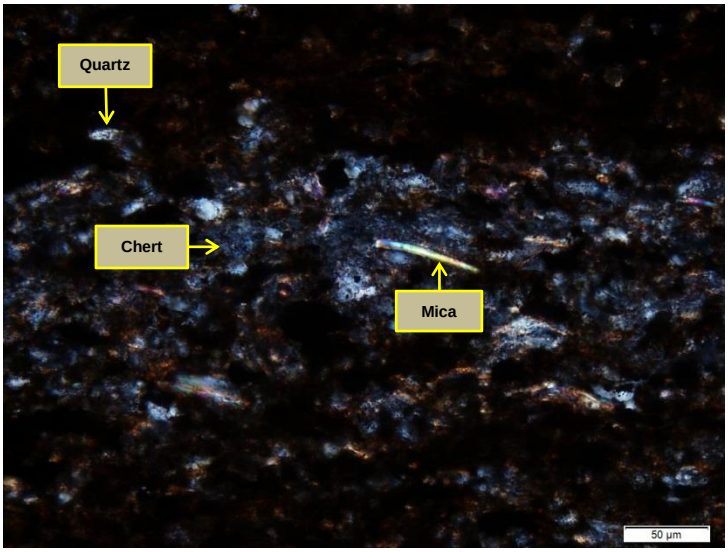


Fig. 3-53: Photomicrograph in XPL showing very fine to medium silt-sized detrital quartz/chert (85-95%) and mica (2-5%) observed in a silty lamination. The small size and tight packing of these grains makes distinguishing individual particles difficult.

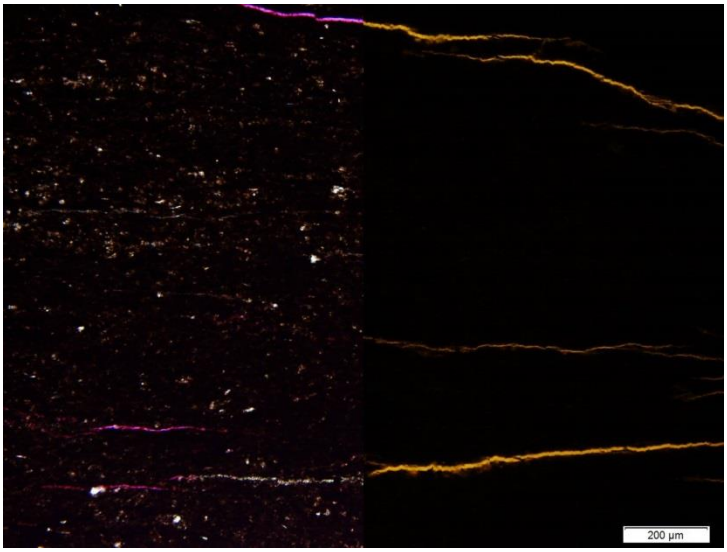


Fig. 3-54: Photomicrograph (left half in PPL, right half in UV light) showing artificial fractures in this sample. All fractures appear sub-parallel to bedding and are artificial, due both to unloading and sample recovery as well as sample preparation (cutting at core repository). Smaller fractures, such as that shown in the middle of this image, are not visible under transmitted light. These fractures are likely the result of swelling clay minerals present in the sample.

3.2.6 SAMPLE 11226

Sample ID	**11226**		
Sample type	**Core**	**UWI/Well**	**100/07-29-056-20W4/00**
Strat. Unit	**Viking Formation**	**Depth**	**632.00 m**

XRD/SRA results

Quartz (%)	Fsp (%)	Cb (%)	Clays (%)	Pyrite (%)
45.8	5.3	0	46.8	2.1

Composition (*in order of abundance*)

Grain size	%	Variety (%)	Variety (%)	Variety (%)	Variety (%)
sand	2	Quartz/chert (100)			
silt	22	Quartz/chert (90)	Mica (6)	Feldspar (4)	
clay	70	Clay mins (100)			
Cement	<1	Quartz (100)			
Bioclasts	<1	Phosphatic (100)			
Organics	4	Amorphous (100)			
Opaques	2	Pyrite (100)			
	100				

*Intensively altered to clay minerals

^ Including bitumen

Sedimentary structures

Primary	Clay-rich horizons with interbedded thin silty laminae.
Biogenic	None apparent.

Fractures	Numerous epoxy-filled fractures and partings.
Porosity	Interbedded thin silty laminae have up to 10% intergranular porosity.

Description

Claystone with thin interbedded silty laminae. Clay-rich layers contain very fine silt- to very fine sand-sized detrital quartz (8-12%), chert (6-8%), mica (<6%), and feldspar (<2%). Silty laminae are comprised of very fine silt- to very fine sand-sized (average grain size is medium silt) detrital quartz (70-80%), chert (5-8%), feldspar (<5%), and mica (<2%).

Thin Section Quality

Poor.

Rock Classification

Claystone.

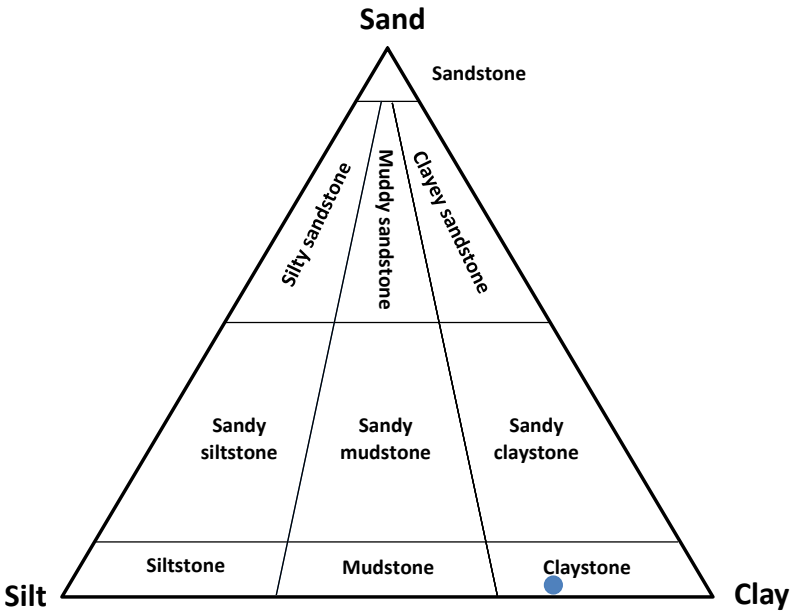


Fig. 3-55: Ternary plot showing the grain size composition of the sample based on the Wentworth scale (after Folk, 1954). Sample 11226 is classified as a claystone.

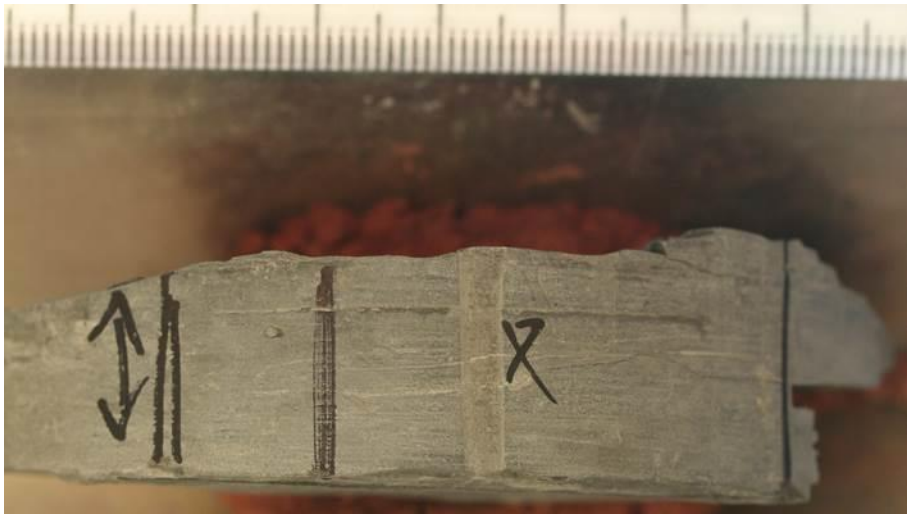


Fig. 3-56: Core photograph of sample 11226 from the Viking Formation, well 100/07-29-056-20W4/00 (depth 632.00 m). The thin section prepared from this sample was cut from the area marked with an X. The sample was received with no up-direction. Scale is in mm.

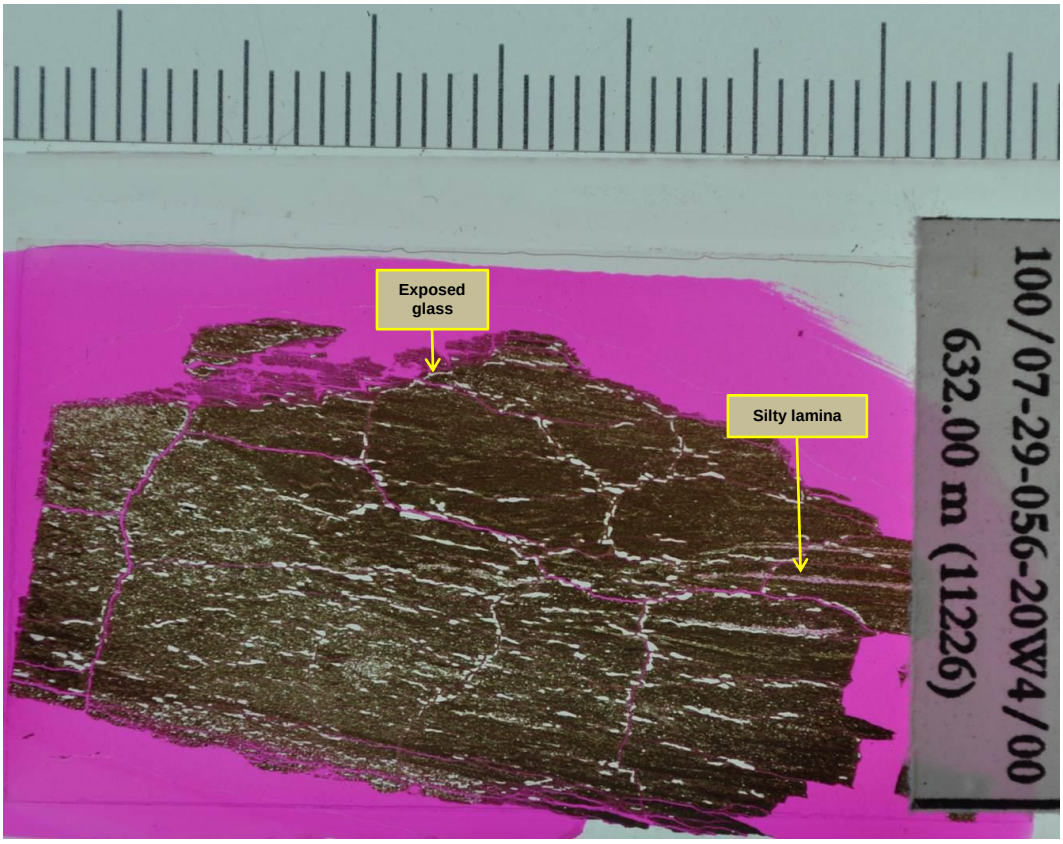


Fig. 3-57: Thin section photograph of sample 11226 from the Viking Formation, well 100/07-29-056-20W4/00 (depth 632.00 m). The sample is a claystone with interbedded thin silty laminae. Extensive patches of removed sample (exposed glass) as well as several artificial partings are observed. Scale is in mm. Note: way-up direction was not indicated and is difficult to identify, and therefore may differ from the orientation shown.

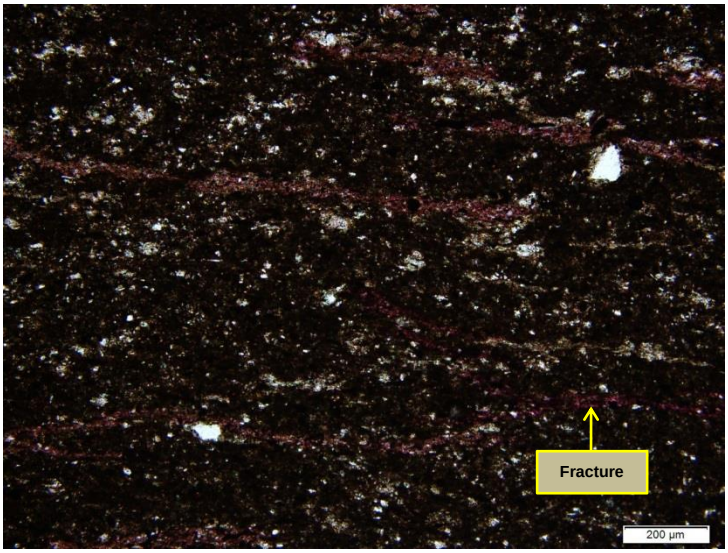


Fig. 3-58: Photomicrograph in PPL showing the fine-grained nature of this claystone. Clay-sized particles constitute ~70% of the sample, and include quartz and chert (light-coloured). Some quartz grains are up to coarse silt-size and are embedded within the matrix. Numerous bedding-parallel and cross-cutting fractures (epoxy-filled, likely artificial) are observed.

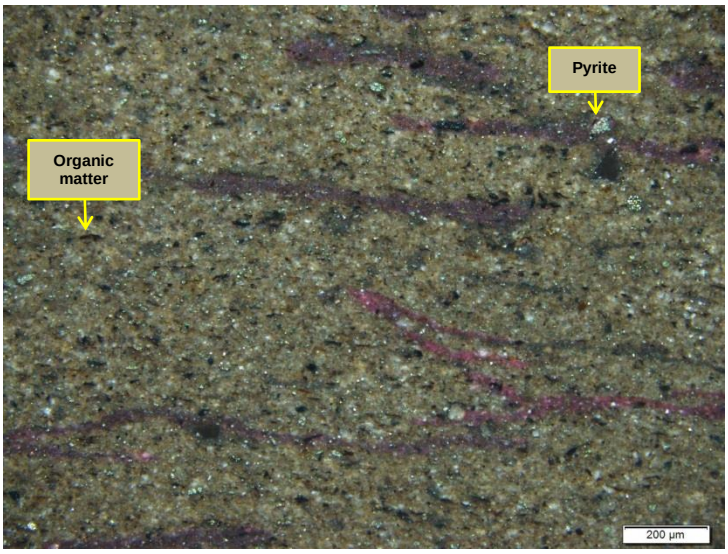


Fig. 3-59: Photomicrograph in reflected light showing finely dispersed pyrite (gold colour) and bedding-parallel organic matter (black) observed in the clay-rich matrix (same field of view as Figure 3-58). The sample contains ~4% organic matter and ~2% pyrite.

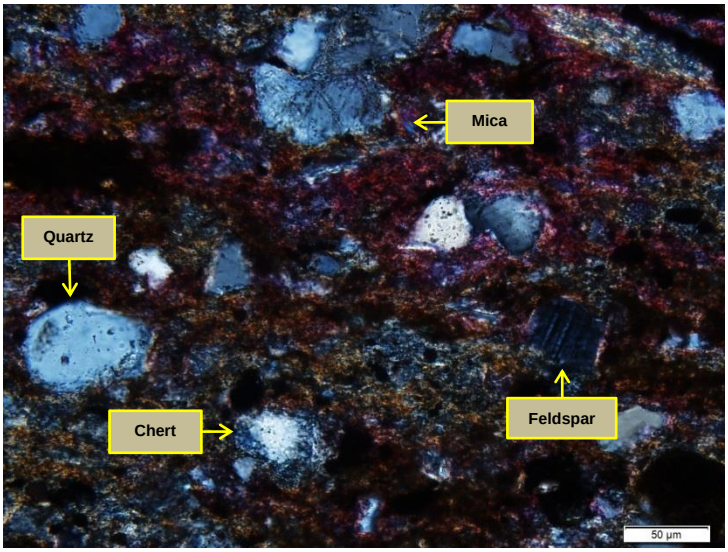


Fig. 3-60: Photomicrograph in XPL showing very fine silt- to very fine sand-sized detrital quartz (8-12%), chert (6-8%), mica (<6%), and feldspar (<2%) embedded in the organic- and clay-rich matrix. Some quartz grains exhibit overgrowths.

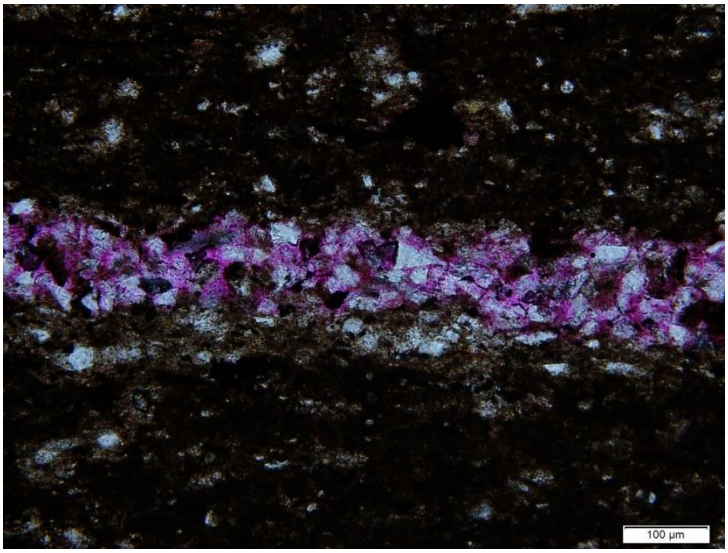


Fig. 3-61: Photomicrograph in PPL showing a bedding-parallel silty lamination. These laminae have up to 10% intergranular porosity (pink epoxy). A total of 4 such laminae are observed in the sample, ranging from ~50-150 µm in thickness.

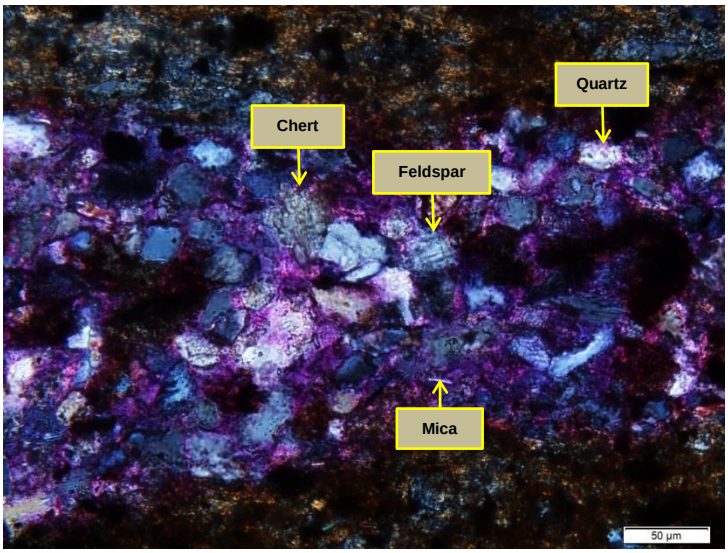


Fig. 3-62: Photomicrograph in XPL showing very fine silt- to very fine sand-sized (average grain size is medium silt) detrital quartz (70-80%), chert (5-8%), feldspar (<5%), and mica (<2%) observed in a silty lamination. Opaques observed within the silty lamination include clays, organic matter and pyrite.

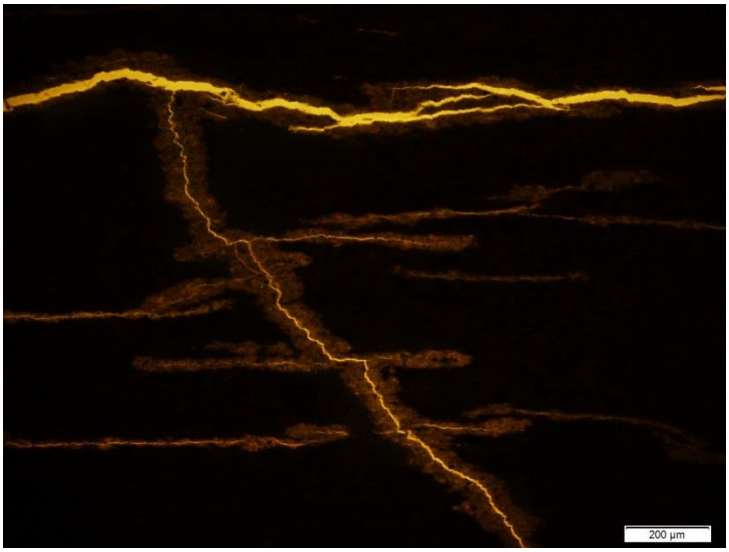


Fig. 3-63: Photomicrograph in UV light showing common bedding-parallel and cross-cutting fractures. These fractures may have been created or “enhanced” during sample preparation.

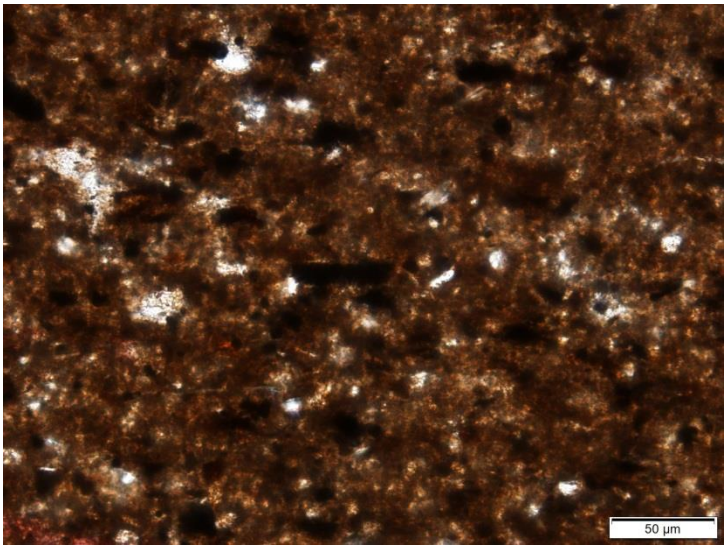


Fig. 3-64: Photomicrograph in PPL detailing the clay-rich matrix, which includes embedded finely dispersed clay- to fine silt-size quartz. Opaque material observed in the matrix includes pyrite and organic matter.

3.2.7 SAMPLE 11227

Sample ID	**11227**		
Sample type	**Core**	**UWI/Well**	**100/07-29-056-20W4/00**
Strat. Unit	**Viking Formation**	**Depth**	**636.55 m**

XRD/SRA results

Quartz (%)	Fsp (%)	Cb (%)	Clays (%)	Pyrite (%)
61.8	3.7	0	34	0.6

Composition (*in order of abundance*)

Grain size	%	Variety (%)	Variety (%)	Variety (%)	Variety (%)
sand	5	Quartz/chert (100)			
silt	10	Quartz/chert (95)	Mica (3)	Feldspar (2)	
clay	80	Clay mins (100)			
Cement	0				
Bioclasts	<1	Phosphatic (100)			
Organics	5	Amorphous (100)			
Opaques	<1	Pyrite (100)			
	100				

*Intensively altered to clay minerals

^ Including bitumen

Sedimentary structures

Primary	Clay-rich layers with interbedded thin sandy laminae and lenses.
Biogenic	One possible *Planolites* burrow.

Fractures	Common thin (5-40 μm) epoxy-filled fractures.
Porosity	Up to 10% intergranular porosity in sandy laminae and lenses. Up to 15% porosity in possible *Planolites* burrow.

Description

Claystone with interbedded sandy laminae and lenses. Clay-rich layers contain very fine silt- to very fine sand-sized (average grain size is coarse silt) detrital quartz (5-12%), chert (5-8%), mica (<5%), and feldspar (<3%). Sandy laminae and lenses are comprised of very fine silt- to very fine sand-sized (average grain size is coarse silt) detrital quartz (50-60%), chert (8-10%), feldspar (<5%), and mica (<2%).

Thin Section Quality

Poor.

Rock Classification

Claystone.

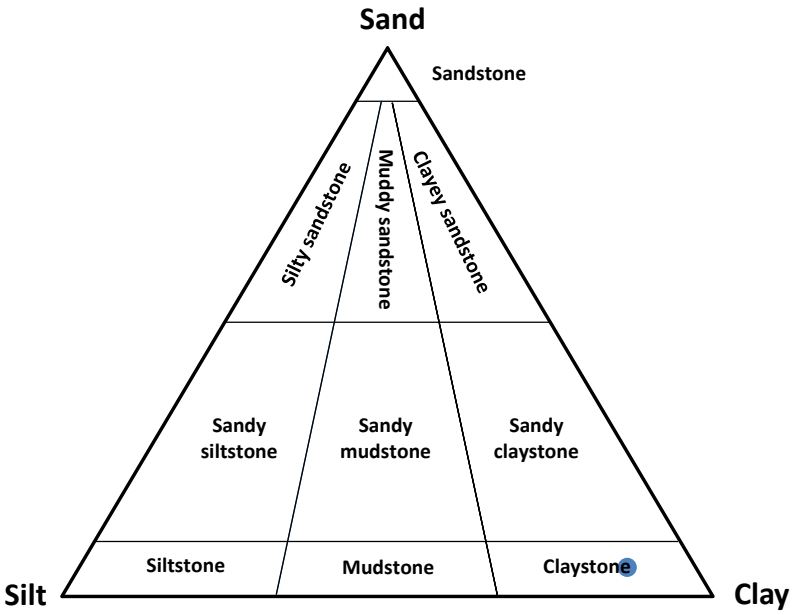


Fig. 3-65: Ternary plot showing the grain size composition of the sample based on the Wentworth scale (after Folk, 1954). Sample 11227 is classified as a claystone.



Fig. 3-66: Core photograph of sample 11227 from the Viking Formation, well 100/07-29-056-20W4/00 (depth 636.55 m). The thin section prepared from this sample was cut from the area marked with an X. The sample was received with no way up-direction. Scale is in mm.

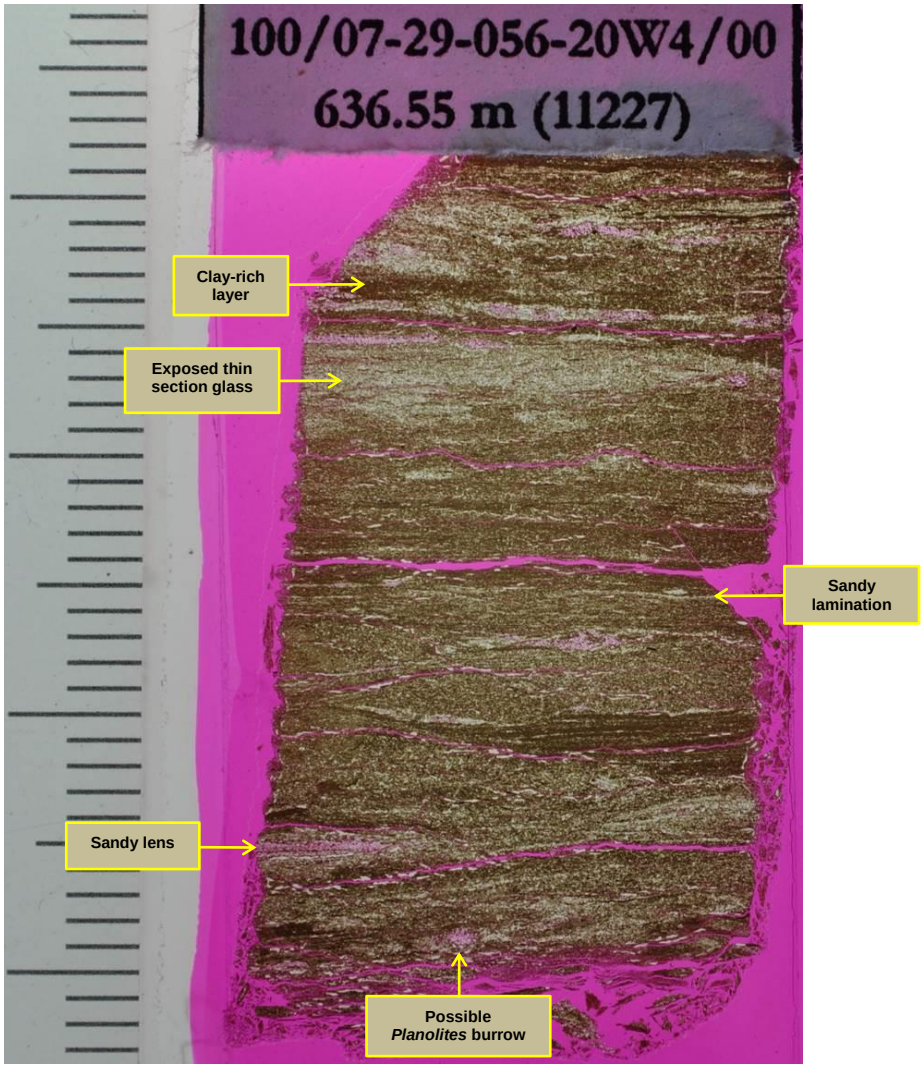


Fig. 3-67: Thin section photograph of sample 11227 from the Viking Formation, Well 100/07-29-056-20W4/00 (depth 636.55 m). The sample is a claystone with interbedded sandy laminae and lenses. Exposed glass is abundant in this thin section, indicating significant removal of clays (water-sensitive clay minerals?) and detrital grains during sample preparation. Much of what appears to be detrital grains or cement in the above image is in fact exposed thin section glass. Artificial partings are common. Scale is in mm. Note: way-up direction was not indicated and is difficult to identify, and therefore may differ from the orientation shown.

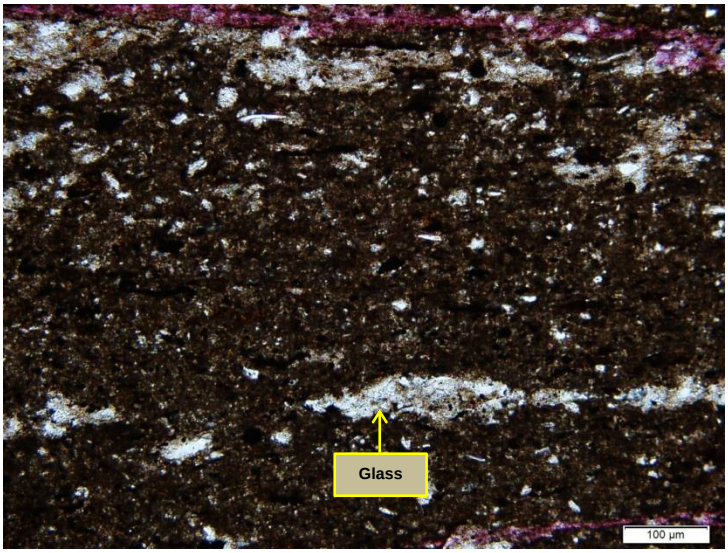


Fig. 3-68: Photomicrograph in PPL detailing a clay-rich layer observed in the sample, which is classified as a claystone. Argillaceous layers dominate the composition with numerous coarser-grained laminae and lenses observed (see Figure 3-71). Exposed thin section glass is common throughout the sample, particularly in clay-rich layers, indicating removal of clays (water sensitive clay minerals?) and detrital grains during cutting and polishing.

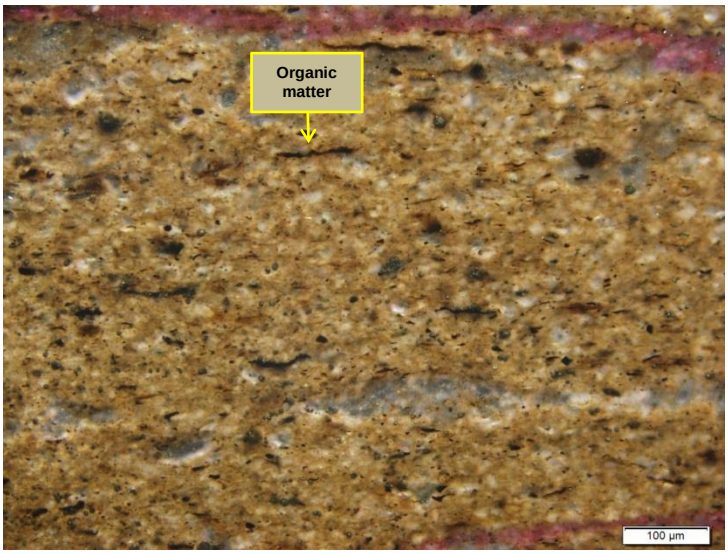


Fig. 3-69: Photomicrograph in reflected light showing a clay-rich layer observed in the sample (same field of view as Figure 3-68). Thin, bedding-parallel strands, flakes and clusters of organic matter are common in these laminae, and comprise ~5% of the sample.

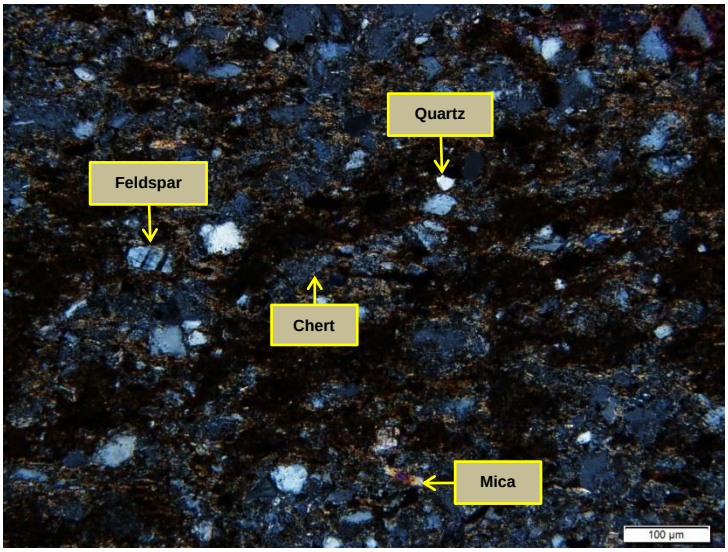


Fig. 3-70: Photomicrograph in XPL showing very fine silt- to very fine sand-sized (average grain size is coarse silt) detrital quartz (5-12%), chert (5-8%), mica (<5%), and feldspar (<3%) observed in a clay-rich layer.

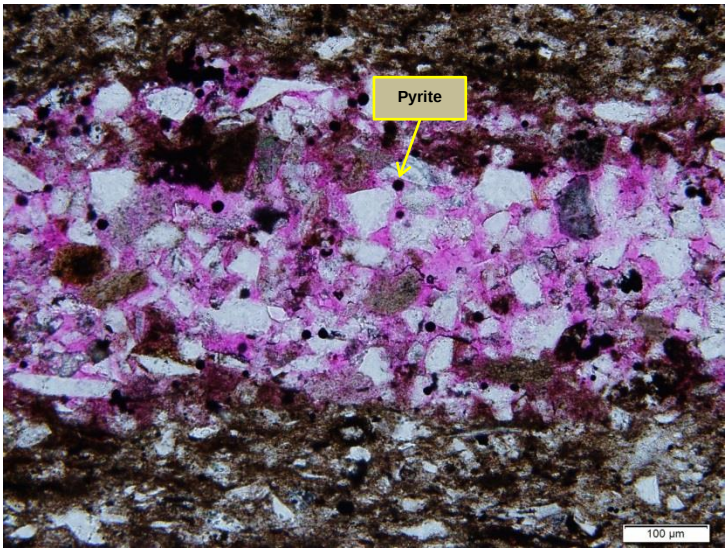


Fig. 3-71: Photomicrograph in PPL showing a rare silty/sandy lamination observed in the sample. Porosity (up to 10%, pink epoxy) is common within these laminae. Grains range from silt- to very fine sand-sized (average grain size is coarse silt) and include detrital quartz (50-60%), chert (8-10%), feldspar (<5%), and mica (<2%). Note numerous pyrite framboids (opaque) distributed within the lamination.

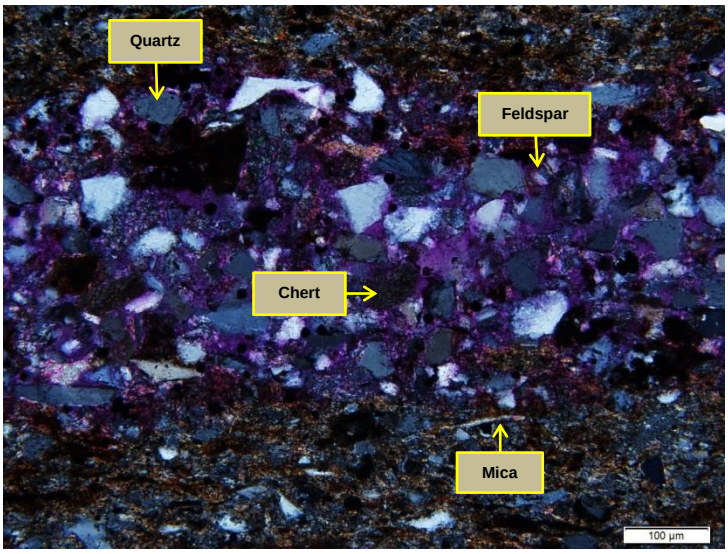


Fig. 3-72: Photomicrograph in XPL showing very fine silt- to very fine sand-sized (average grain size is coarse silt) detrital quartz (50-60%), chert (8-10%), feldspar (<5%), and mica (<2%) observed in a sandy lamination (same field of view as Figure 3-71).

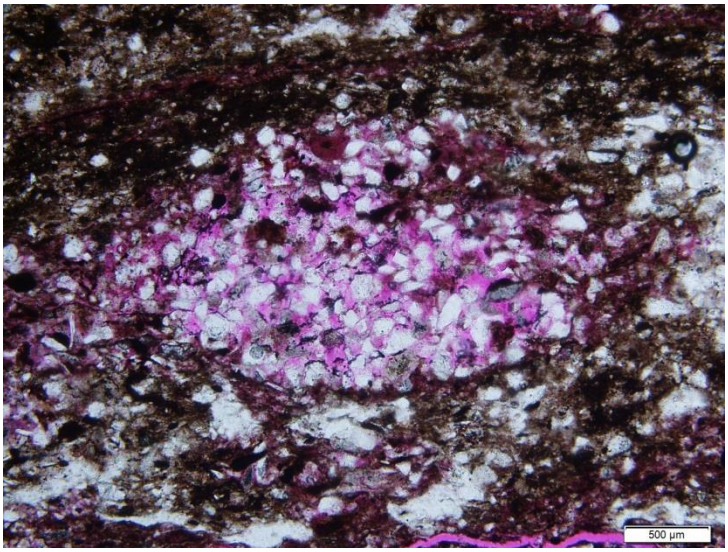


Fig. 3-73: Photomicrograph in PPL showing a possible *Planolites* burrow observed in the sample. This lenticular feature is coarser-grained than the interbedded sandy lenses and laminae observed in the sample, and has ~15% intergranular porosity.

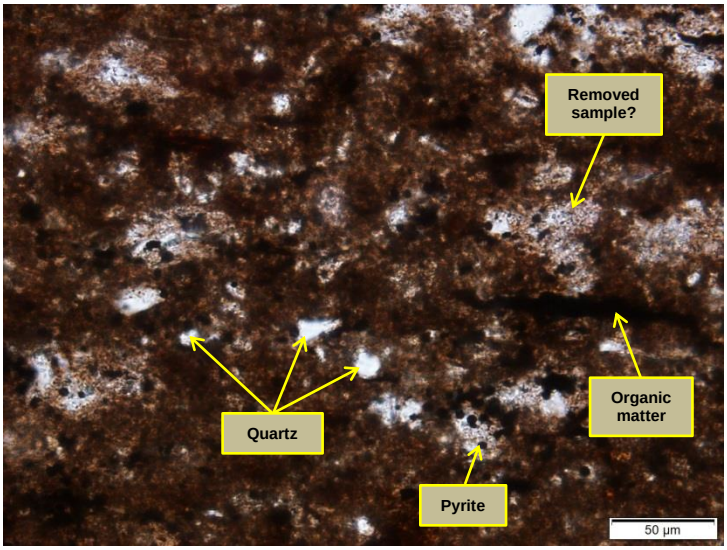


Fig. 3-74: Photomicrograph in PPL detailing the clay-rich matrix, which includes clay- to silt-size quartz, numerous pyrite framboids (<5 µm in size) and organic matter distributed in short, lenticular streaks or strands. Parts of the sample where the colours are light (patchy) may have been removed during sample preparation.

3.2.8 SAMPLE 11228

Sample ID	**11228**		
Sample type	**Core**	**UWI/Well**	**100/07-29-056-20W4/00**
Strat. Unit	**Viking Formation**	**Depth**	**641.75 m**

XRD/SRA results

Quartz (%)	Fsp (%)	Cb (%)	Clays (%)	Pyrite (%)
84.1	6.9	0	8.7	0.4

Composition (*in order of abundance*)

Grain size	%	Variety (%)	Variety (%)	Variety (%)	Variety (%)
sand	50	Quartz/chert (90)	Feldspar (10)	Mica (<1)	
silt	22	Quartz/chert (100)			
clay	16	Clay mins (100)			
Cement	4	Quartz (100)			
Bioclasts	1	Phosphatic (100)			
Organics	5	Amorphous (100)			
Opaques	2	Pyrite (100)			
	100				

*Intensively altered to clay minerals

^ Including bitumen

Sedimentary structures

Primary	Interbedded sandy and organic/clay-rich layers.
Biogenic	Possible bioturbation features.

Fractures	Thin (20-100 μm thickness) epoxy-filled fractures occur in clay-rich layers.
Porosity	Up to 25% porosity in sandy layers. Up to 5% porosity in clay rich layers, typically occurring within clusters of fine to medium sand-sized quartz grains.

Description

Muddy sandstone with interbedded sandy and organic/clay-rich layers. Sandy layers contain subrounded (common) to subangular (rare) very fine silt- to coarse sand-sized (average grain size is very fine sand) detrital quartz (55-65%), chert (10-15%), feldspar (<5%), and mica (<1%). These layers have up to 25% porosity, with little interstitial clay, and many point contacts between grains. Organic- and clay-rich layers contain subrounded (common) to subangular (rare) very fine silt- to coarse sand-sized (average grain size is fine sand) detrital quartz (15-20%), chert (6-8%), feldspar (<5%), and mica (<1%). These layers have up to 5% porosity, with the highest porosity occurring within clusters of fine to medium sand-sized quartz grains.

Thin Section Quality

Good.

Rock Classification

Muddy sandstone.

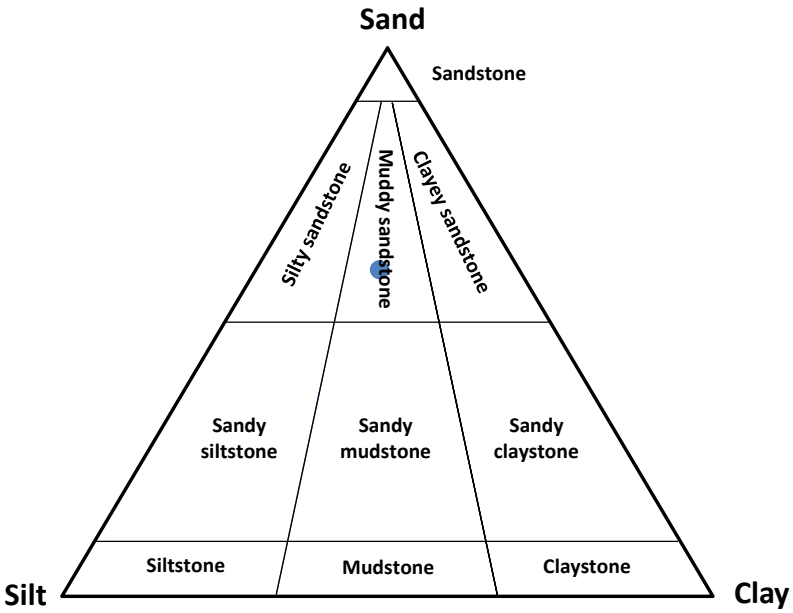


Fig. 3-75: Ternary plot showing the grain size composition of the sample based on the Wentworth scale (after Folk, 1954). Sample 11228 is classified as a muddy sandstone.

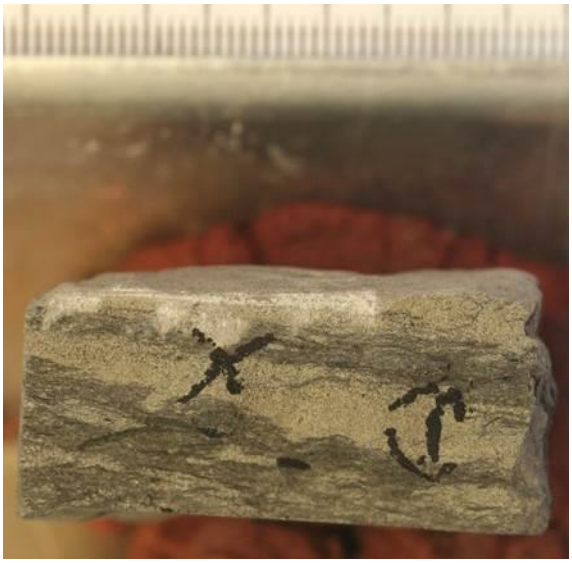


Fig. 3-76: Core photograph of sample 11228 from the Viking Formation, well 100/07-29-056-20W4/00 (depth 641.75 m). The thin section prepared from this sample was cut from the area marked with an X. The sample was received with no way up-direction. Scale is in mm.

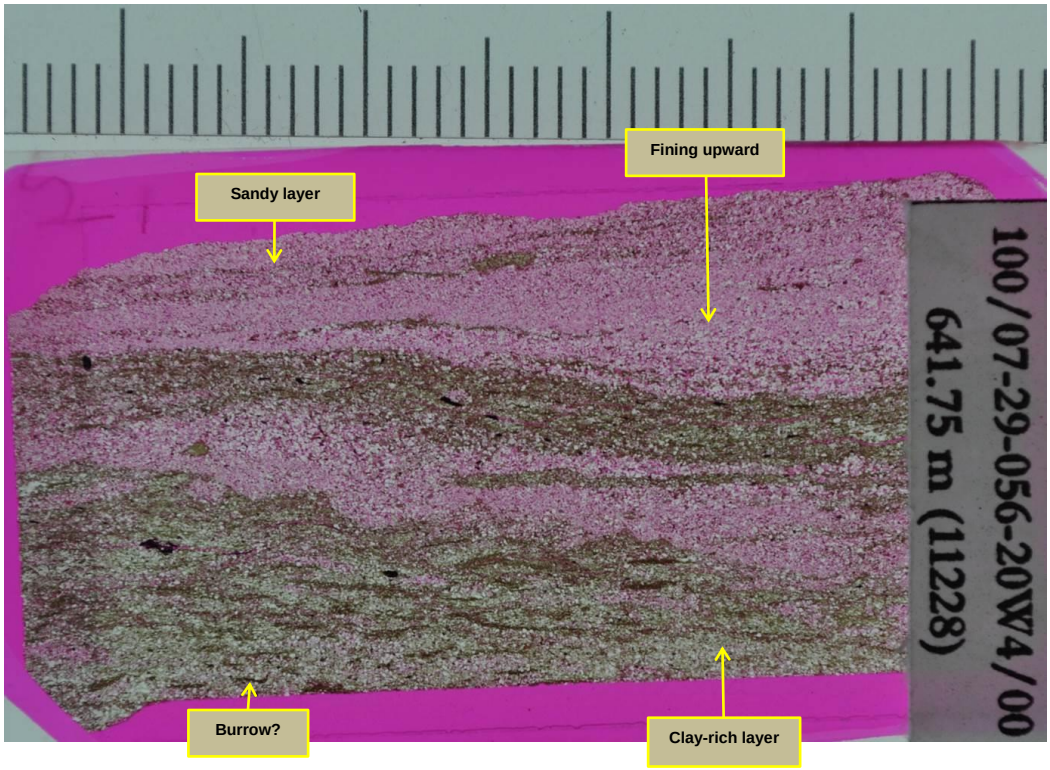


Fig. 3-77: Thin section photograph of sample 11228 from the Viking Formation, well 100/07-29-056-20W4/00 (depth 641.75 m). The sample is a muddy sandstone with wavy/rippled, interbedded sandy and organic/clay-rich layers. Scale is in mm. Note: way-up direction was interpreted based on sedimentary structures.

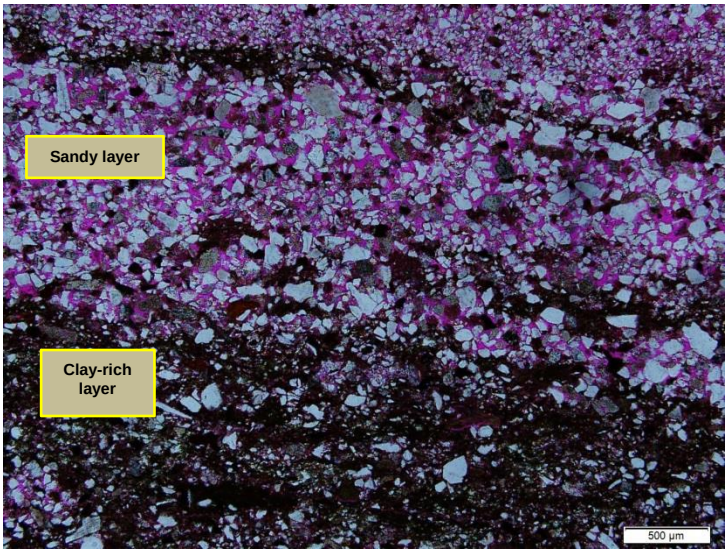


Fig. 3-78: Photomicrograph in PPL showing interbedded sandy and clay-rich layers observed in the muddy sandstone. Light-coloured minerals consist mostly of quartz, with chert, mica and feldspars also present. The darker laminations are clay-rich with embedded silt- to sand-size grains, organic matter and pyrite.

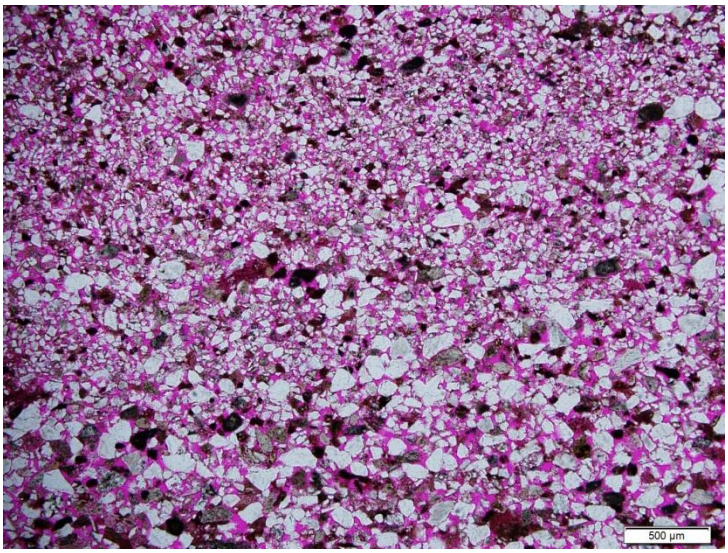


Fig. 3-79: Photomicrograph in PPL showing a fining-upward depositional sequence observed in a sandy layer (see Figure 3-77 for location within sample). No sharp boundaries are apparent within the sequence, which contains a mixture of both coarser (up to 191 µm) and finer (<15 µm) grains (of similar particle composition).

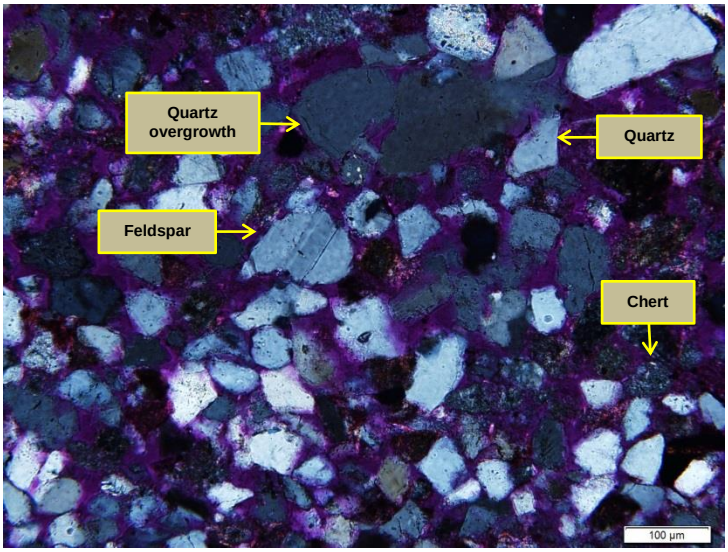


Fig. 3-80: Photomicrograph in XPL showing very fine silt- to fine sand-sized (average grain size is very fine sand) detrital quartz (55-65%), chert (10-15%), and feldspar (<5%) observed in a sandy layer.

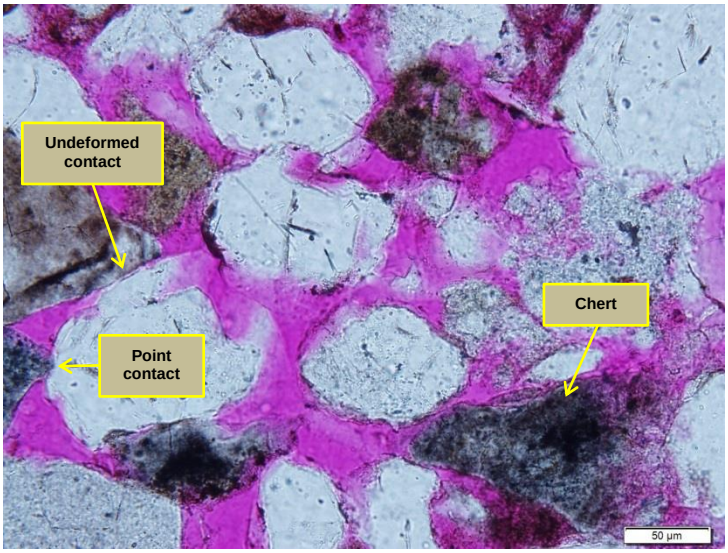


Fig. 3-81: Photomicrograph in PPL showing part of a sandy layer with up to 25% porosity. Detailed analysis of the thin section billet and hand sample shows that some of the porosity (pink epoxy) is artificial (due to sample preparation). Point contacts and undeformed flat contacts are common, indicating minor post-depositional sediment compaction during burial. Darker grains in the image represent chert.

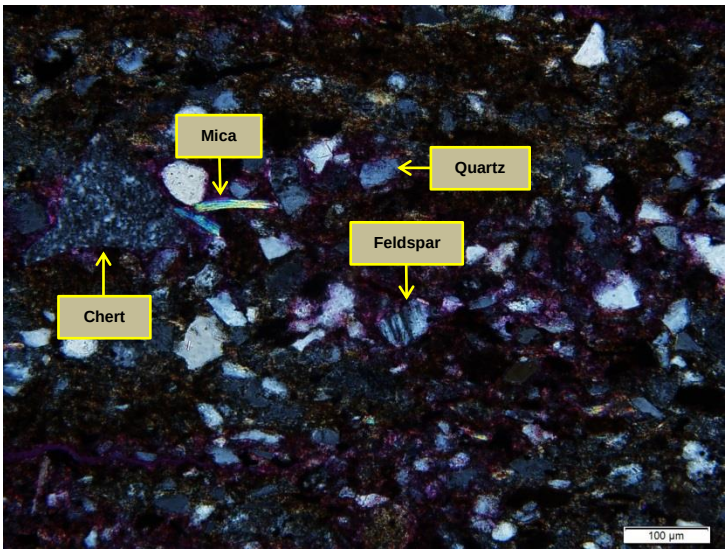


Fig. 3-82: Photomicrograph in XPL showing very fine silt- to fine sand-sized detrital quartz (15-20%), chert (6-8%), feldspar (<5%), and mica (<1%) observed in a clay-rich layer. Note a mica lathe oriented parallel to bedding.

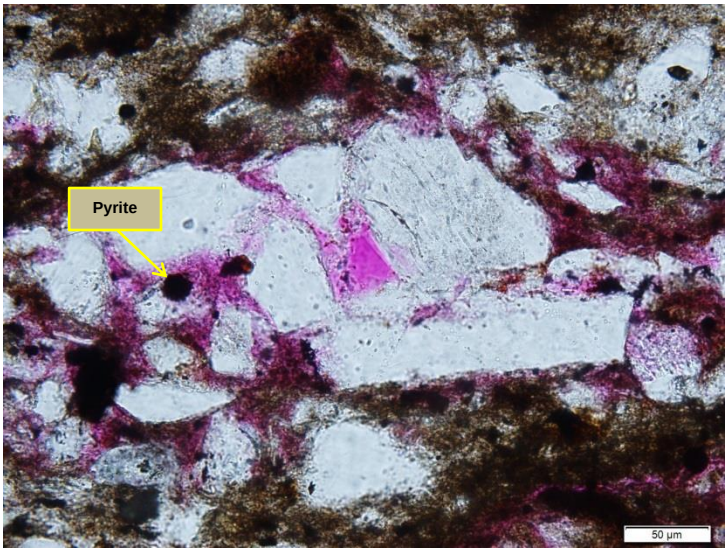


Fig. 3-83: Photomicrograph in PPL showing a cluster of fine to medium sand-sized quartz grains present in an organic- and clay-rich layer. These clusters have up to ~5% porosity (the highest porosity observed in organic- and clay-rich layers). Most of this porosity is possibly artificial (removal of material when cutting with water prior to epoxy impregnation?). Note finely disseminated pyrite.

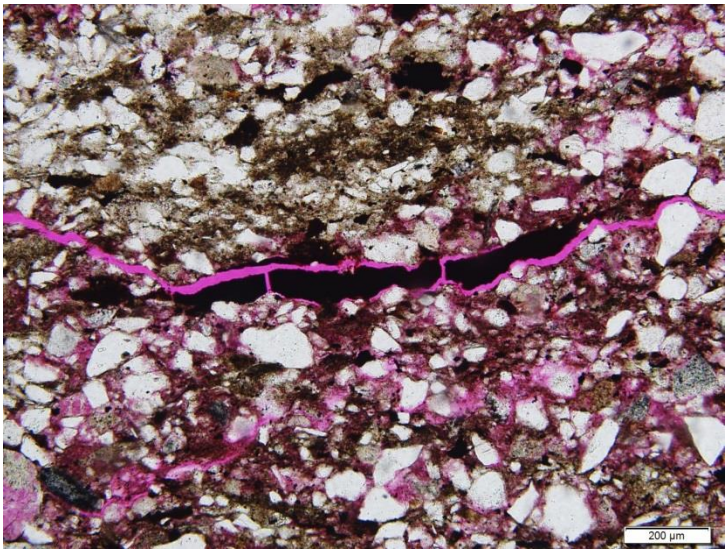


Fig. 3-84: Photomicrograph in PPL showing fragments of solid amorphous organic matter (opaque) within an open artificial fracture (filled with pink epoxy). Organic matter occurs as both solid and finely dispersed particles (associated with clays) in the sample.

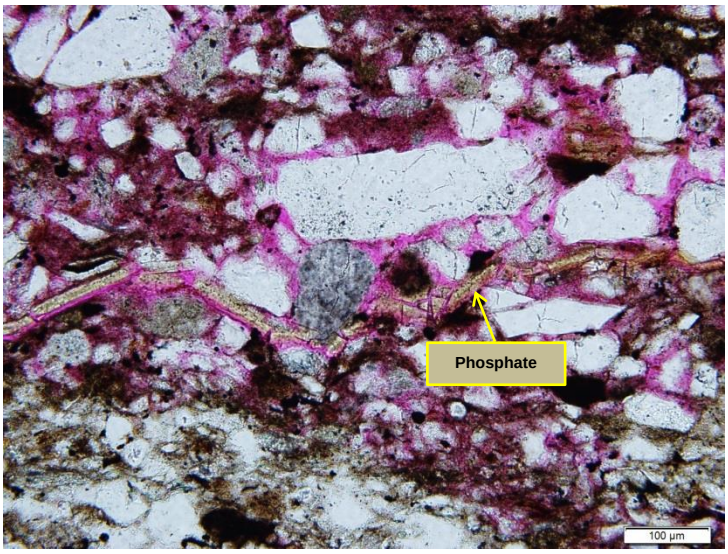


Fig. 3-85: Photomicrograph in PPL showing fragmented phosphatic material (fish bone?) concentrated along an epoxy-filled micro-fracture (potentially artificial). Phosphatic material occurs only in organic- and clay-rich layers, and accounts for ~1% of the sample.

3.2.9 SAMPLE 13174

Sample ID	**13174**		
Sample type	**Core**	**UWI/Well**	**100/16-25-055-20W4/00**
Strat. Unit	**Viking Formation**	**Depth**	**659.93 m**

XRD/SRA results

Quartz (%)	Fsp (%)	Cb (%)	Clays (%)	Pyrite (%)
41.9	4.3	0	51.6	2.1

Composition (*in order of abundance*)

Grain size	%	Variety (%)	Variety (%)	Variety (%)	Variety (%)
sand	0				
silt	20	Quartz/chert (90)	Mica (10)	Feldspar (<1)	
clay	63	Clay mins (100)			
Cement	0				
Bioclasts	0				
Organics	12	Amorphous (100)			
Opaques	5	Pyrite (100)			
	100				

*Intensively altered to clay minerals

^ Including bitumen

Sedimentary structures

Primary	The sample consists largely of finely laminated clay-rich bedding, with some interbedded silty laminae.
Biogenic	None apparent.

Fractures	Numerous epoxy-filled fractures and partings.
Porosity	Some thin silty laminae have up to 2% intergranular porosity.

Description

Organic-rich claystone with interbedded silty laminae. Bedding-parallel organic matter comprises ~12% of both clay-rich and silty laminae. Clay-rich layers, comprising >85% of the sample, contain minor (<5%) detrial quartz and mica grains. Interbedded silty laminae are comprised of very fine to coarse silt-sized (average grain size is medium silt) detrital quartz (15-20%), chert (<5%), mica (<5%), and feldspar (<1%).

Thin Section Quality

Poor.

Rock Classification

Claystone.

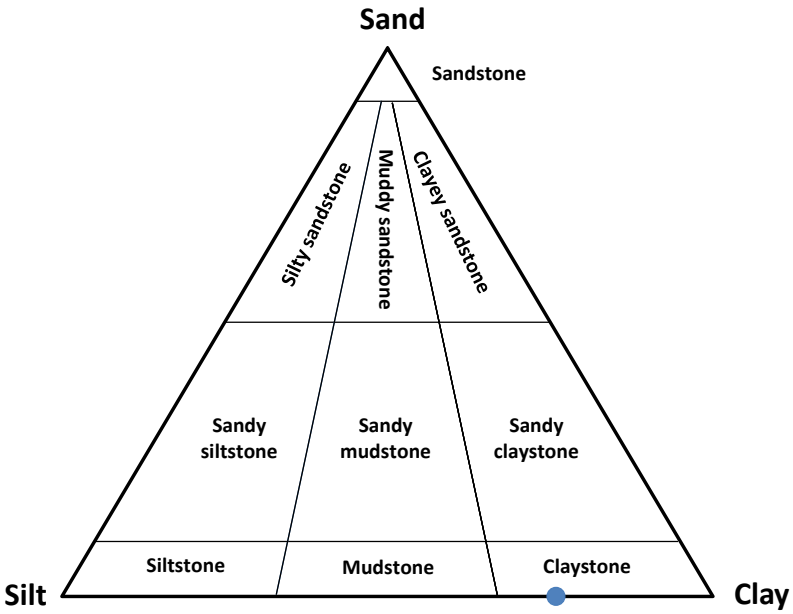


Fig. 3-86: Ternary plot showing the grain size composition of the sample based on the Wentworth scale (after Folk, 1954). Sample 13174 is classified as a claystone.

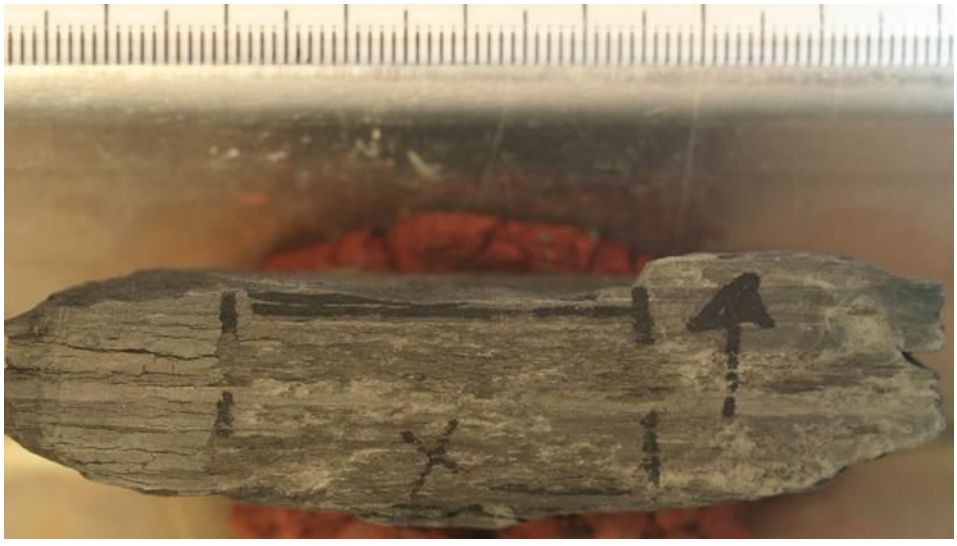


Fig. 3-87: Core photograph of sample 13174 from the Viking Formation, well 100/16-25-055-20W4/00 (depth 659.93 m). The thin section prepared from this sample was cut from the area marked with an X. The arrow indicates stratigraphic up-direction. Scale is in mm.

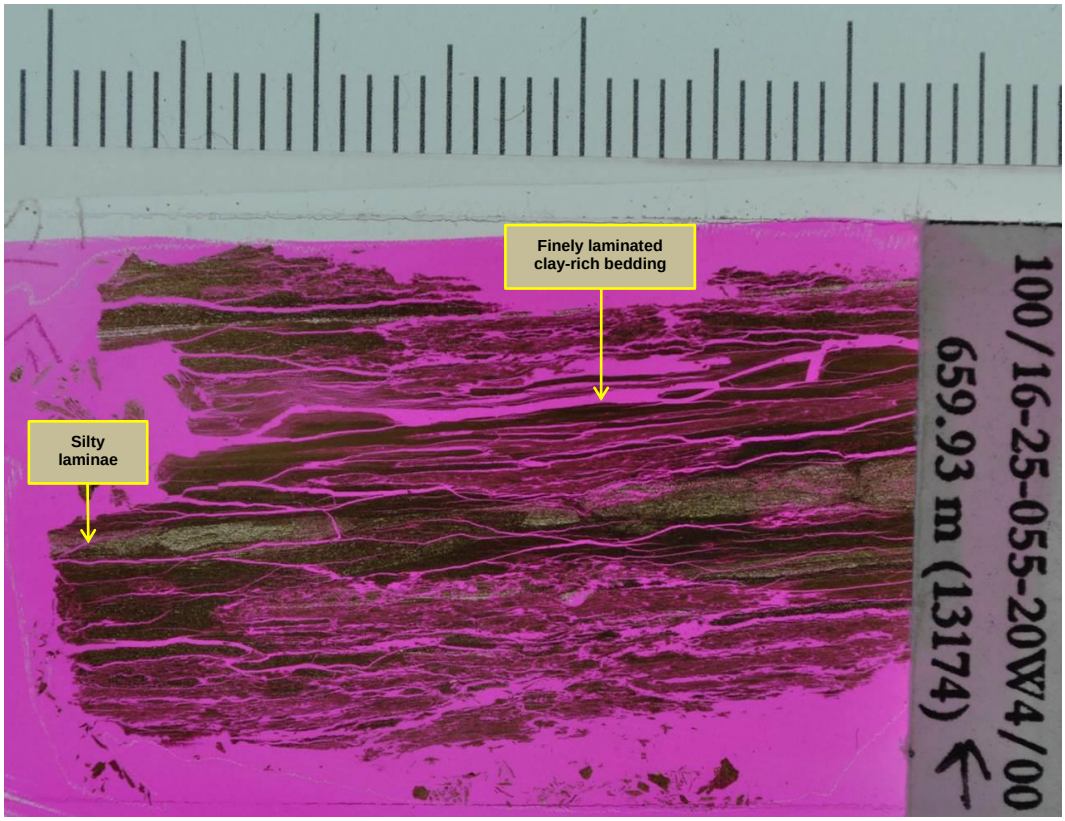


Fig. 3-88: Thin section photograph of sample 13174 from the Viking Formation, well 100/16-25-055-20W4/00 (depth 659.93 m). The sample is an organic-rich claystone with interbedded silty laminations. Pervasive artificial fracturing indicates that water-sensitive clay minerals are present in the sample. Scale is in mm. Note: very poor thin section quality, with abundant plucking and splitting due to water-sensitive clay minerals.

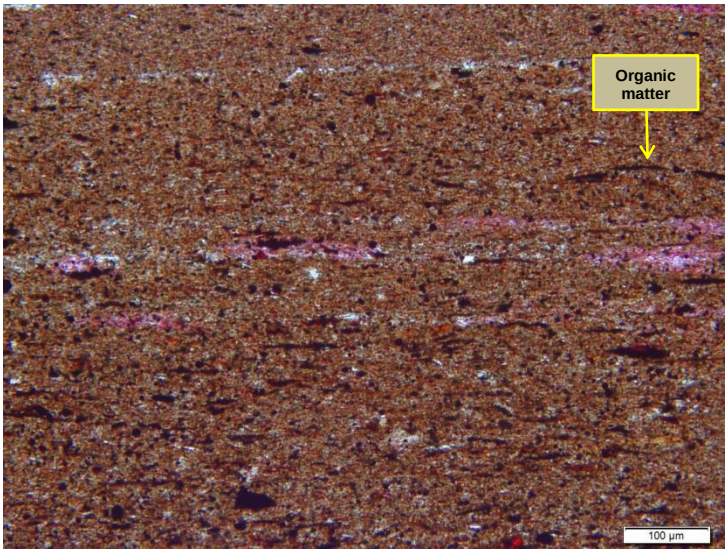


Fig. 3-89: Photomicrograph in HDR (high dynamic range) PPL showing the sample, which is classified as an organic-rich claystone. Numerous bedding-parallel organic matter strands are observed. Organic matter is common in both clay-rich bedding and silty laminae, accounting for ~12% of the total sample composition. Total clay content in the sample is estimated at ~63%.

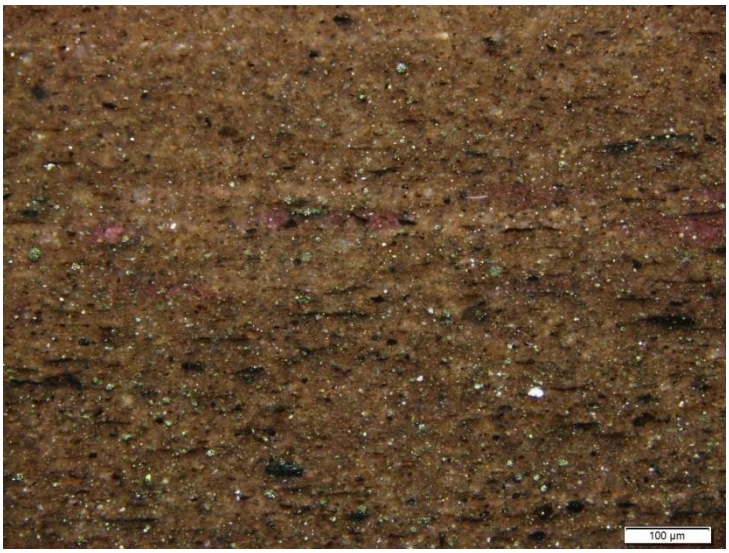


Fig. 3-90: Photomicrograph in reflected light showing the abundant bedding-parallel organic matter strands (same field of view as Figure 3-89) as well as common finely dispersed pyrite (gold colour; estimated at ~5% of total sample composition).

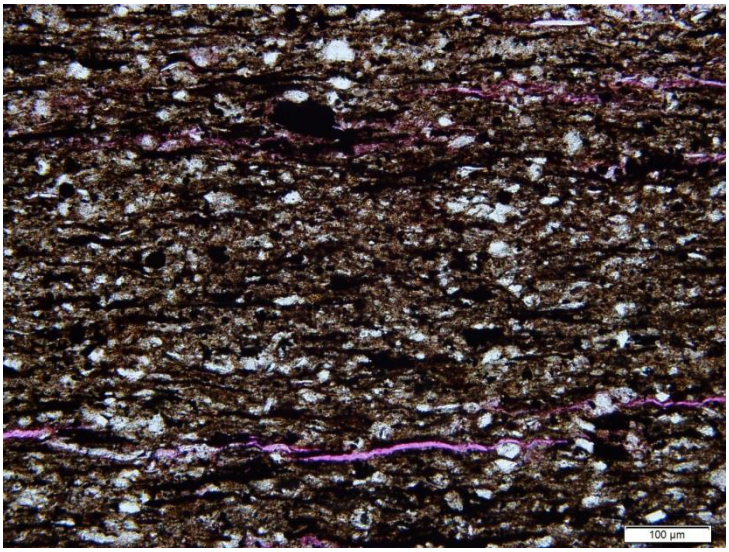


Fig. 3-91: Photomicrograph in PPL showing a silty lamination observed in the sample, which contains abundant clay and organic matter with clay to silt-size quartz (light-coloured) embedded in the matrix. These laminae tend to have very little observable porosity. Note several artificial fractures filled with pink epoxy.

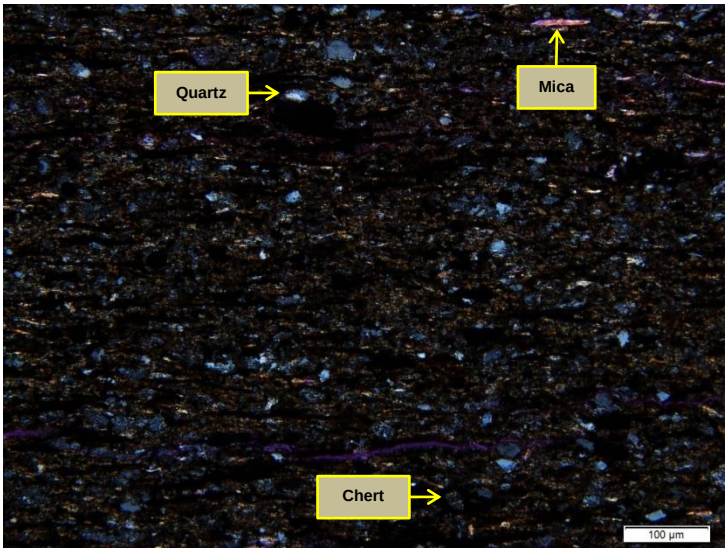


Fig. 3-92: Photomicrograph in XPL (same field of view as Figure 3-91) illustrating that these layers are comprised of very fine to coarse silt-sized (average grain size is medium silt) detrital quartz (15-20%), chert (<5%), mica (<5%), and feldspar (<1%). Note that mica lathes predominantly have bedding-parallel orientations.

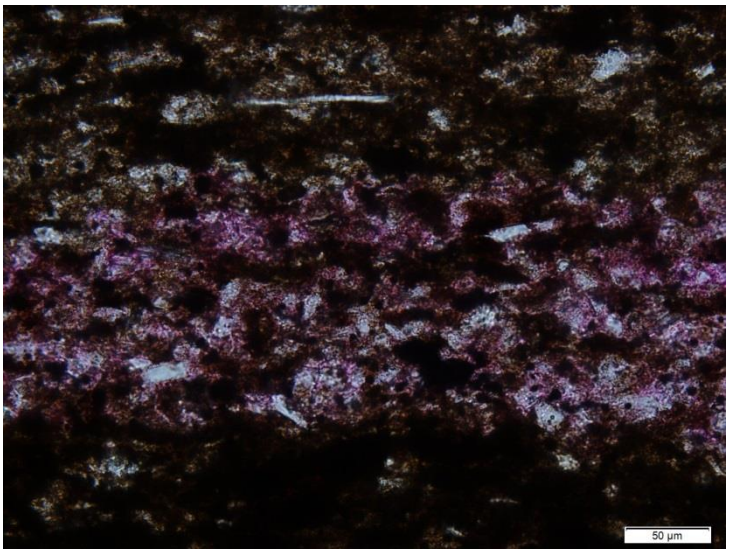


Fig. 3-93: Photomicrograph in PPL showing a thin silty lamination observed in the sample. These horizons have up to 2% intergranular porosity (pink epoxy), with some interstitial clay impeding pore connectivity. Opaque material in the image consists of clays, organic matter and pyrite.

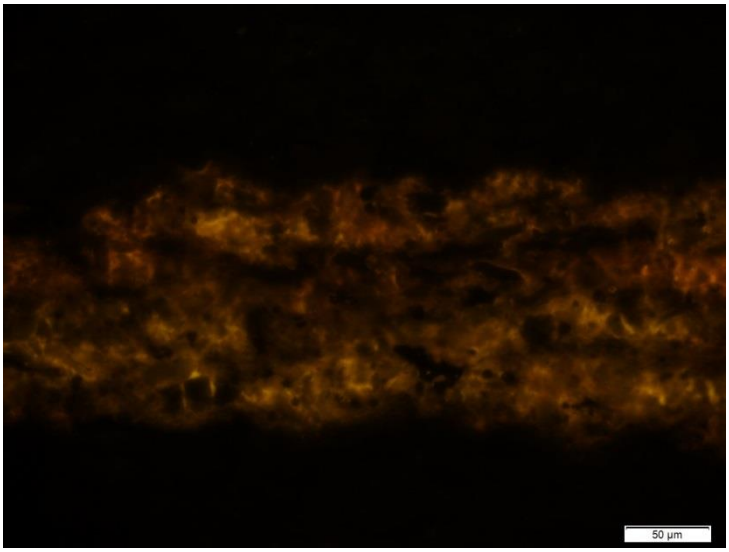


Fig. 3-94: Photomicrograph showing Figure 3-93 in UV light. Bright yellow colours correspond to “cleaner”, more open pores. Much of the porosity observed in these horizons may be microporosity, visible due to epoxy “bleeding” through clays and organic matter.

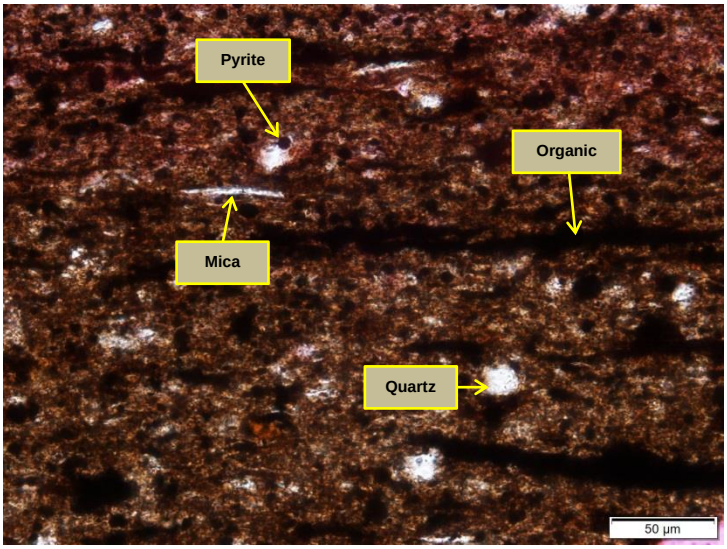


Fig. 3-95: Photomicrograph in PPL detailing the clay matrix (brown, dark-brown), which includes embedded clay- to silt-size quartz and mica (light-coloured grains) as well as several opaque streaks, flakes and blebs of organic matter. Finely disseminated pyrite framboids are also observed.

3.2.10 SAMPLE 13175

Sample ID	**13175**		
Sample type	**Core**	**UWI/Well**	**100/16-25-055-20W4/00**
Strat. Unit	**Viking Formation**	**Depth**	**662.70 m**

XRD/SRA results

Quartz (%)	Fsp (%)	Cb (%)	Clays (%)	Pyrite (%)
61.8	6.4	0	31.2	0.7

Composition (*in order of abundance*)

Grain size	%	Variety (%)	Variety (%)	Variety (%)	Variety (%)
sand	5	Quartz/chert (100)			
silt	38	Quartz/chert (94)	Feldspar (5)	Mica (1)	
clay	50	Clay mins (100)			
Cement	0				
Bioclasts	0				
Organics	6	Amorphous (100)			
Opaques	1	Pyrite (100)			
	100				

*Intensively altered to clay minerals

^ Including bitumen

Sedimentary structures

Primary	Interbedded clay-rich and silty bedding.
Biogenic	Bioturbation appears to have obscured some original bedding.

Fractures	Common epoxy-filled fractures and partings.
Porosity	Silty layers have up to 5% intergranular porosity, often occurring in discontinuous sections or patches.

Description

Bioturbated mudstone with interbedded clay-rich and silty bedding. Clay-rich layers are comprised of fine silt to very fine sand-sized (average grain size is coarse silt) detrital quartz/chert (15-25%), feldspar (<4%), and mica (<1%). Silty layers are comprised of fine silt to very fine sand-sized (average grain size is coarse silt) detrital quartz/chert (25-55%), feldspar (<6%), and mica (<1%).

Thin Section Quality

Poor.

Rock Classification

Mudstone.

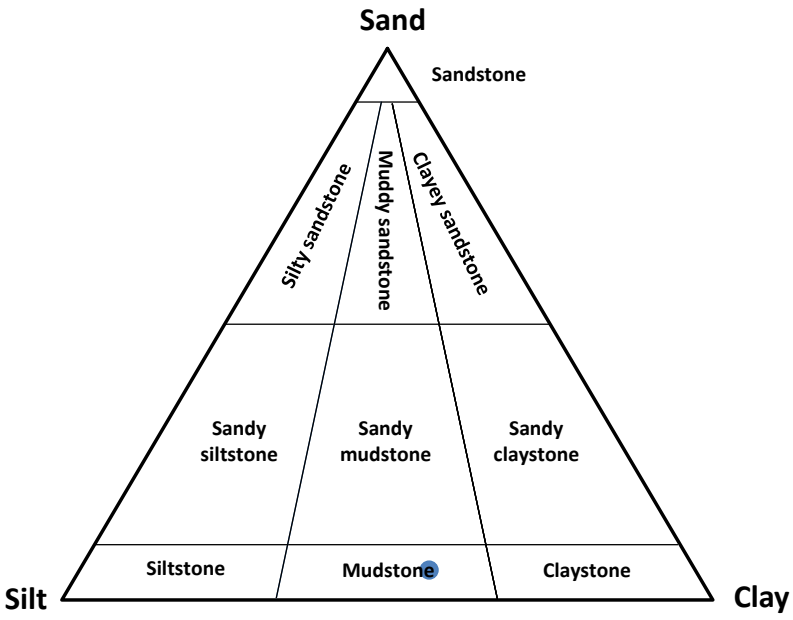


Fig. 3-96: Ternary plot showing the grain size composition of the sample based on the Wentworth scale (after Folk, 1954). Sample 13175 is classified as a mudstone.



Fig. 3-97: Core photograph of sample 13175 from the Viking Formation, well 100/16-25-055-20W4/00 (depth 662.70 m). The thin section prepared from this sample was cut from the area marked with an X. The sample was received with no way up-direction. The mudcake on the cut surface indicates that abundant water-sensitive clay minerals are present within this sample. Scale is in mm.

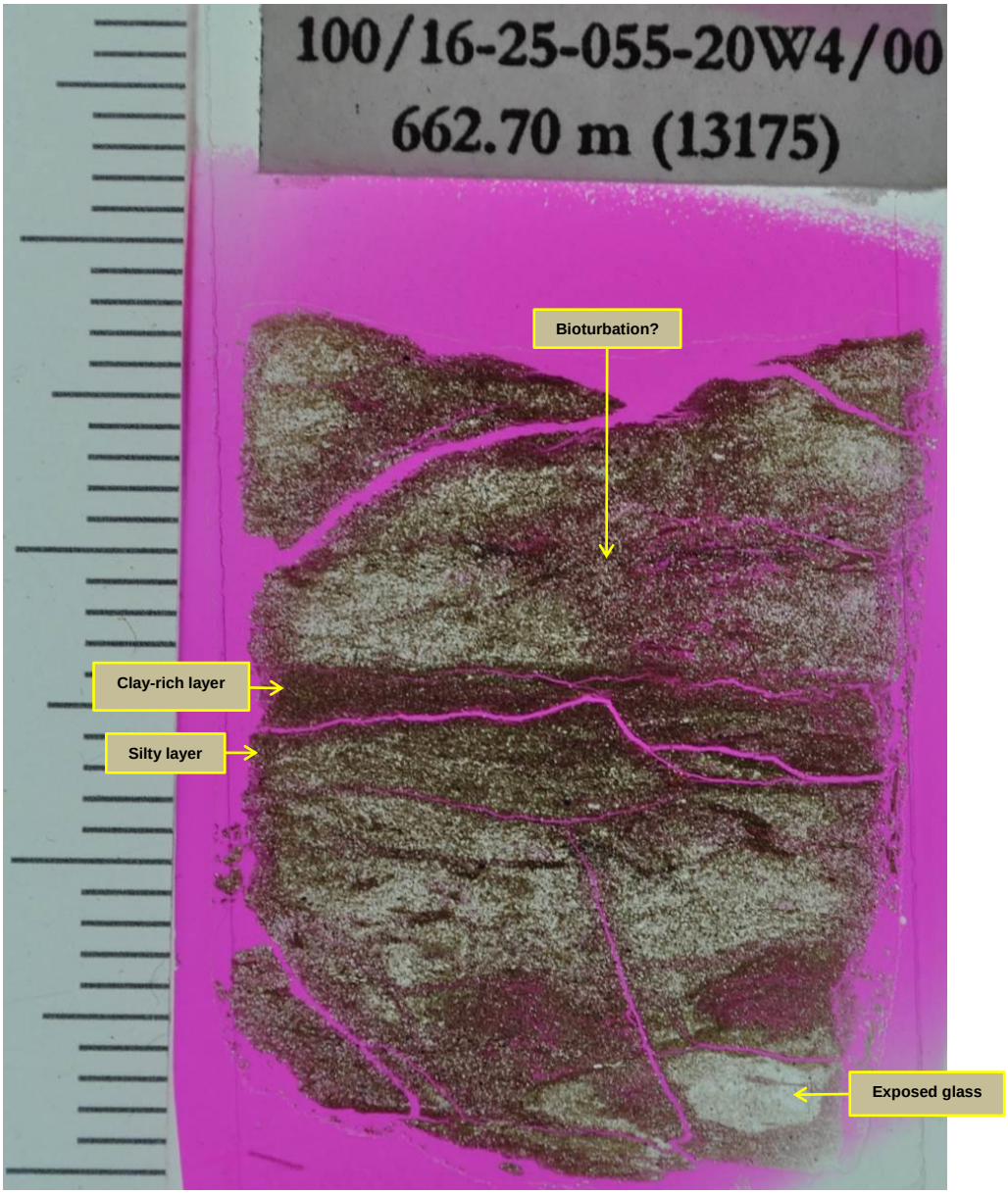


Fig. 3-98: Thin section photograph of sample 13175 from the Viking Formation, well 100/16-25-055-20W4/00 (depth 662.70 m). The sample is a bioturbated mudstone with interbedded clay-rich and silty layers and laminae. Several artificial partings and areas of exposed glass are observed (caused by material removal due to the presence of water-sensitive clays). Scale is in mm. Note: way-up direction was not indicated and is difficult to identify, and therefore may differ from the orientation shown.

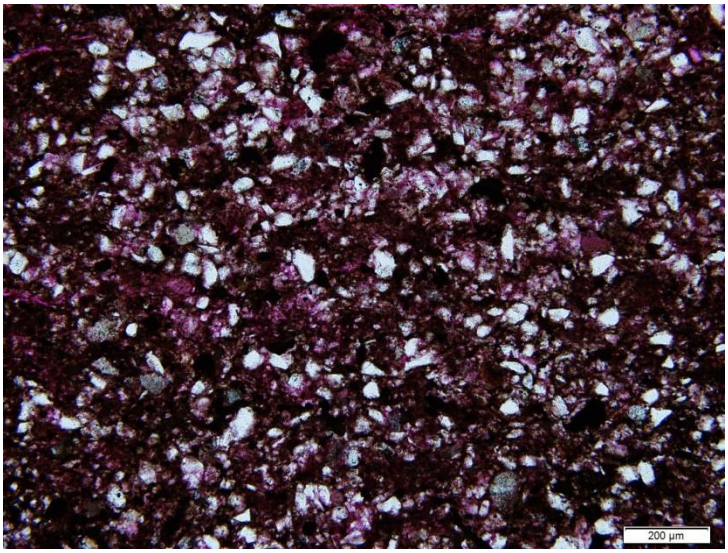


Fig. 3-99: Photomicrograph in PPL showing a silty layer observed in the mudstone. These layers have up to ~5% intergranular porosity (pink epoxy), often occurring in discontinuous sections or patches. Light coloured minerals include quartz (predominant), chert, feldspars and mica. Darker patches are more clay-rich, with finer grained particles and opaque material (pyrite, organic matter).

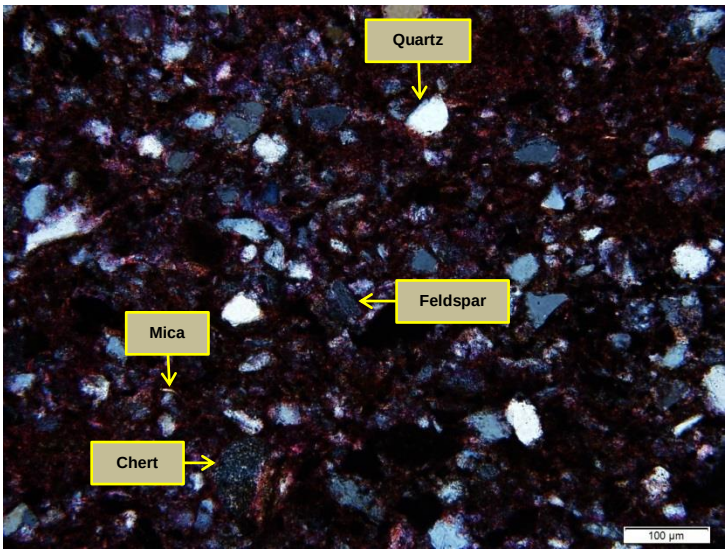


Fig. 3-100: Photomicrograph in XPL showing fine silt- to very fine sand-sized (average grain size is coarse silt) detrital quartz/chert (25-55%), feldspar (<6%), and mica (<1%) in a silty layer.

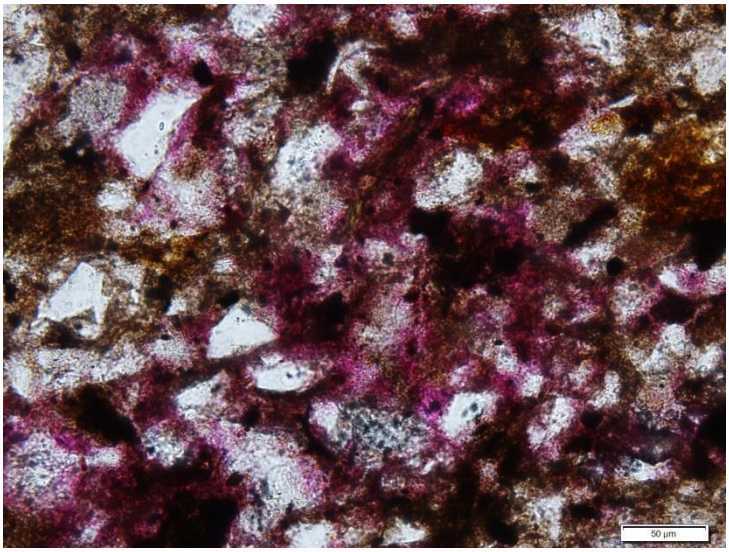


Fig. 3-101: Photomicrograph in PPL illustrating a porous section of a silty layer. Grain size and shape are similar in both porous and non-porous sections of these layers, with elevated porosity associated with a reduction in clay. Opaque material in the image includes finely disseminated pyrite and organic matter.

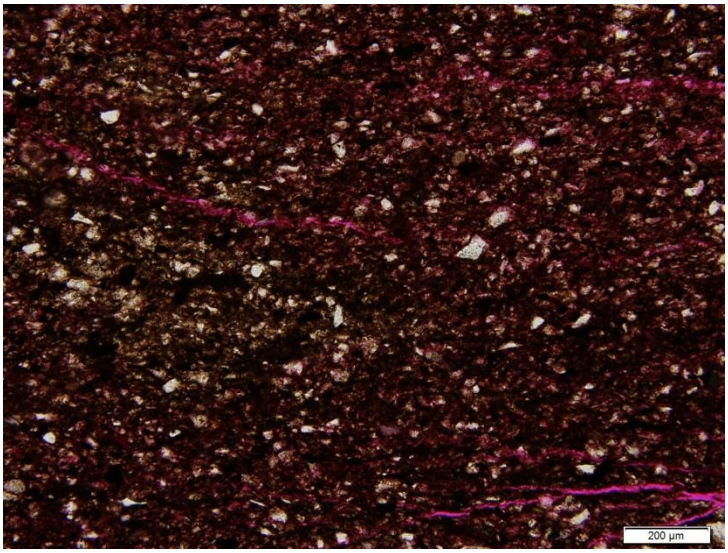


Fig. 3-102: Photomicrograph in PPL showing a clay-rich layer, which exhibits a lower abundance of detrital grains compared to the silty layer shown in Figure 3-99.

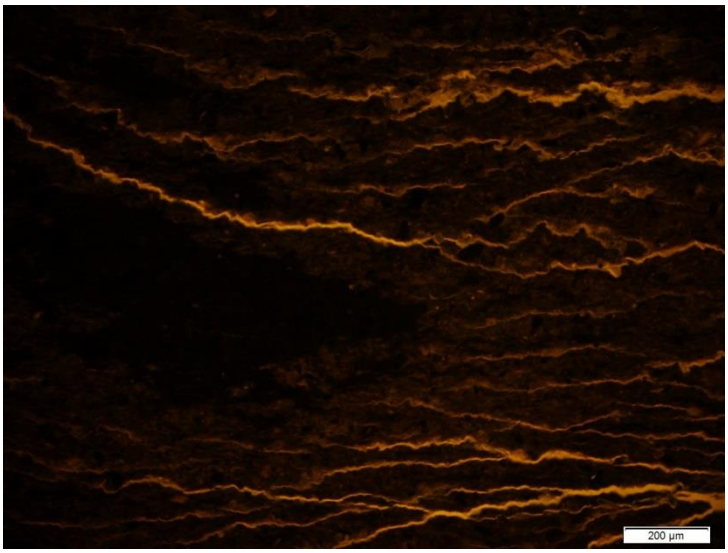


Fig. 3-103: Photomicrograph of Figure 3-102 in UV light showing common thin fractures. These fractures are likely artificial, and suggest that water-sensitive clay minerals are present in the sample.

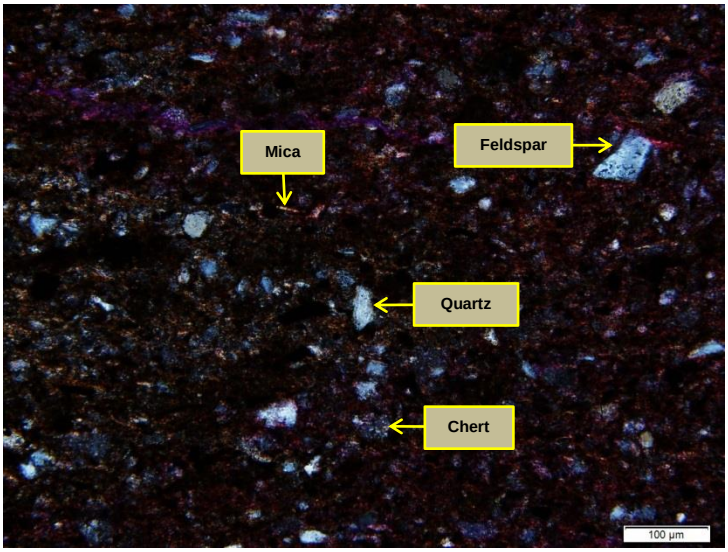


Fig. 3-104: Photomicrograph in XPL showing fine silt- to very fine sand-sized (average grain size is coarse silt) detrital quartz/chert (15-25%), feldspar (<4%), and mica (<1%) observed in a clay-rich layer.

3.2.11 SAMPLE 13177

Sample ID	**13177**		
Sample type	**Core**	**UWI/Well**	**100/16-25-055-20W4/00**
Strat. Unit	**Viking Formation**	**Depth**	**666.81 m**

XRD/SRA results

Quartz (%)	Fsp (%)	Cb (%)	Clays (%)	Pyrite (%)
60.3	6	0	34.4	1.2

Composition (*in order of abundance*)

Grain size	%	Variety (%)	Variety (%)	Variety (%)	Variety (%)
sand	4	Quartz/chert (92)	Feldspar (8)		
silt	60	Quartz/chert (93)	Feldspar (5)	Mica (2)	
clay	30	Clay mins (100)			
Cement	<1	Quartz (100)			
Bioclasts	<1	Phosphatic (100)			
Organics	5	Amorphous (100)			
Opaques	1	Pyrite (100)			
	100				

*Intensively altered to clay minerals

^ Including bitumen

Sedimentary structures

Primary	Interbedded clay-rich, silty, and sandy layers and laminae.
Biogenic	Possible burrow structures.

Fractures	Numerous 14-70 µm epoxy-filled fractures and partings.
Porosity	Up to 8% porosity in silty laminae, and ~15-25% porosity in sandy laminae and burrow structures. Clay-rich layers have <2% porosity.

Description

Bioturbated mudstone with interbedded clay-rich, silty, and sandy layers and laminae. Clay-rich layers are comprised of fine silt to very fine sand-sized (average medium silt-sized) detrital quartz, chert, feldspar, and mica occurring within a dark-colored clay matrix. Silty laminae are comprised of fine silt to very fine sand-sized (average coarse silt-sized) detrital grains of the same composition, occurring with less clay matrix, and up to 8% intergranular porosity. Sandy laminae are comprised of medium silt to fine sand-sized detrital quartz, chert, and feldspar, and have ~15-25% intergranular porosity.

Thin Section Quality

Moderate.

Rock Classification

Mudstone.

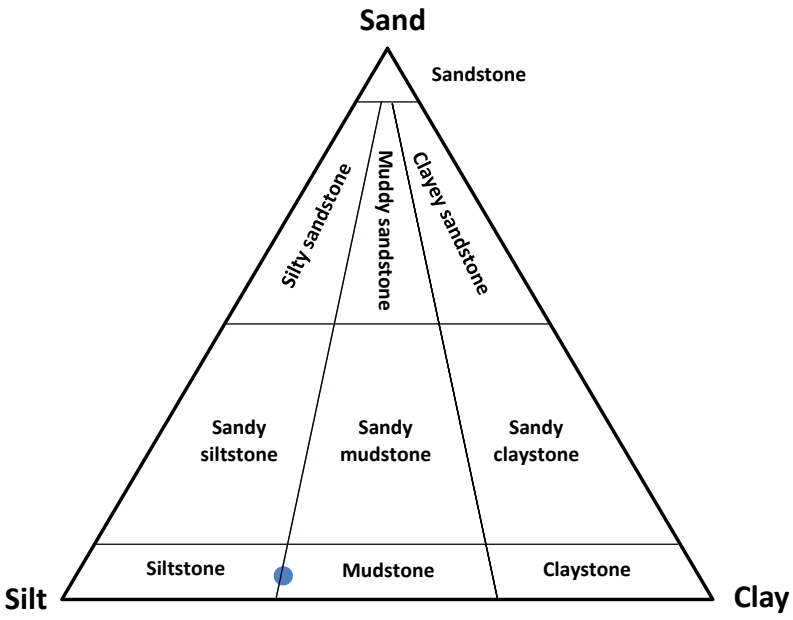


Fig. 3-105: Ternary plot showing the grain size composition of the sample based on the Wentworth scale (after Folk, 1954). Sample 13177 is classified as a mudstone, verging on siltstone classification.

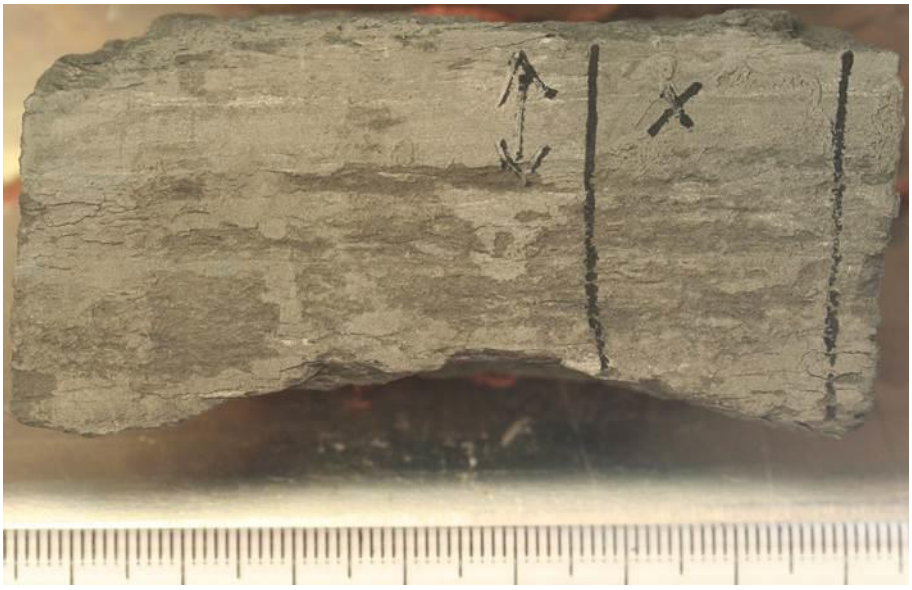


Fig. 3-106: Core photograph of sample 13177 from the Viking Formation, well 100/16-25-055-20W4/00 (depth 666.81 m). The thin section prepared from this sample was cut from the area marked with an X. The sample was received with no way up-direction. Note the draping mud on the surface, which indicates that swelling clay material is present in this sample. Scale is in mm.

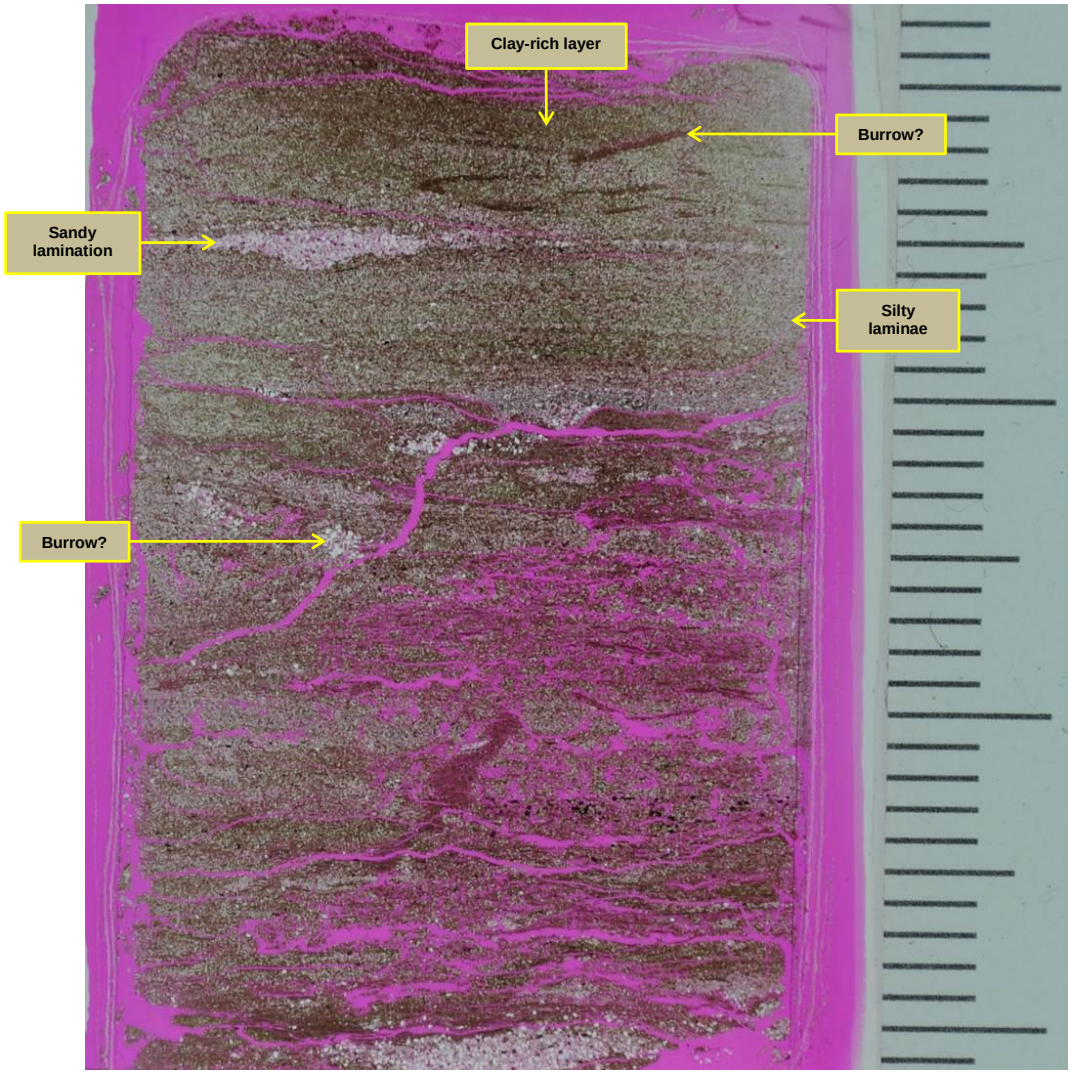


Fig. 3-107: Thin section photograph of sample 13177 from the Viking Formation, well 100/16-25-055-20W4/00 (depth 666.81 m). The sample is a bioturbated mudstone with interbedded clay-rich, silty, and sandy layers and laminae. Numerous epoxy-filled fractures and partings occur throughout the sample, caused by thin section preparation (due to the presence of water-sensitive clay minerals). Scale is in mm. Note: way-up direction was not indicated and is difficult to identify, and therefore may differ from the orientation shown.

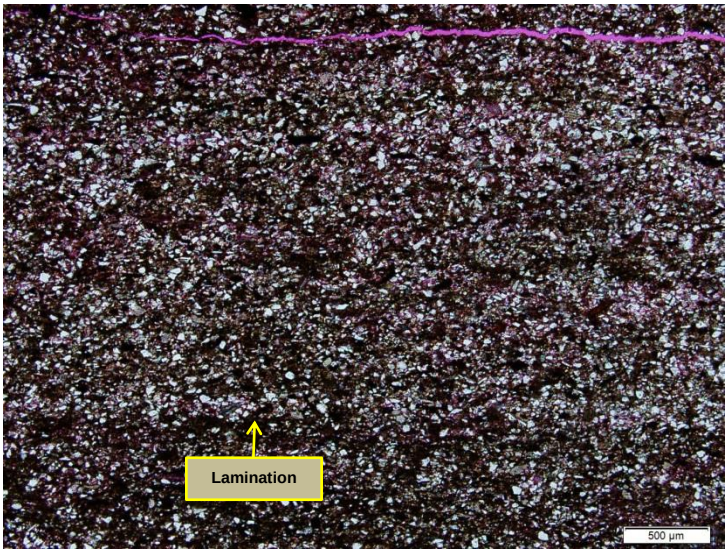


Fig. 3-108: Photomicrograph in PPL showing an overview of the mudstone (verging on siltstone classification, see Figure 3-105). The sample largely consists of interbedded clay-rich layering and silty laminae. Light-coloured minerals consist of quartz (predominant), chert, feldspar and mica. Darker patches and laminations consist of opaque material (clays, pyrite and organics). An artificial fracture (filled with pink epoxy) is observed at the top of the image.

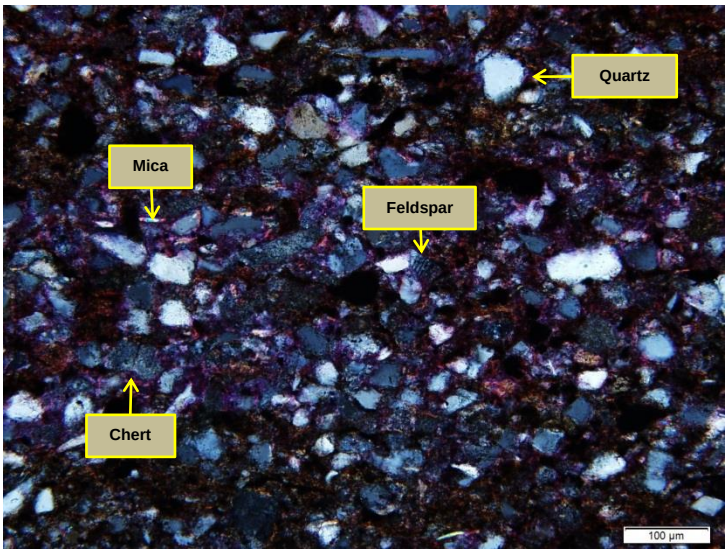


Fig. 3-109: Photomicrograph in XPL showing fine silt- to very fine sand-sized (average coarse silt-sized) detrital quartz (30-45%), chert (8-12%), feldspar (1-5%), and mica (<2%) in a silty lamination.

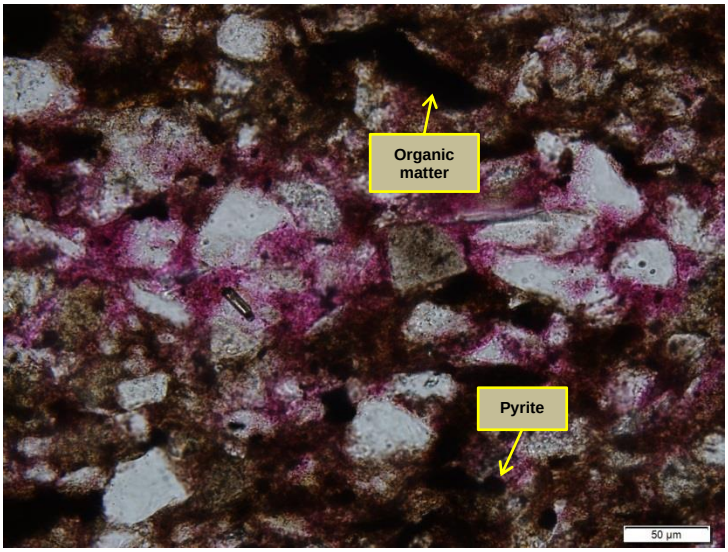


Fig. 3-110: Fig. 6: Photomicrograph in PPL showing a porous section of a silty lamination, which has up to ~8% intergranular porosity (filled with pink epoxy). The opaque material consists of organic matter, clays and pyrite.

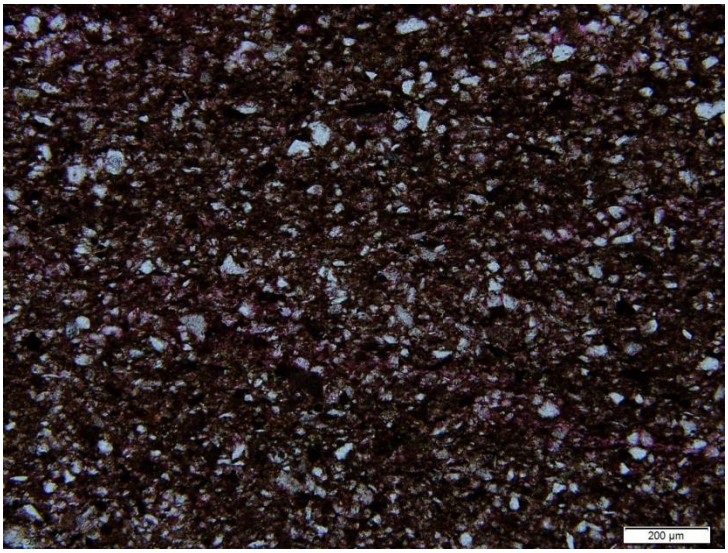


Fig. 3-111: Photomicrograph in PPL illustrating a clay-rich layer. These layers have <2% intergranular porosity. Abundant silt-size grains (light-coloured) are embedded within the clay-rich matrix.

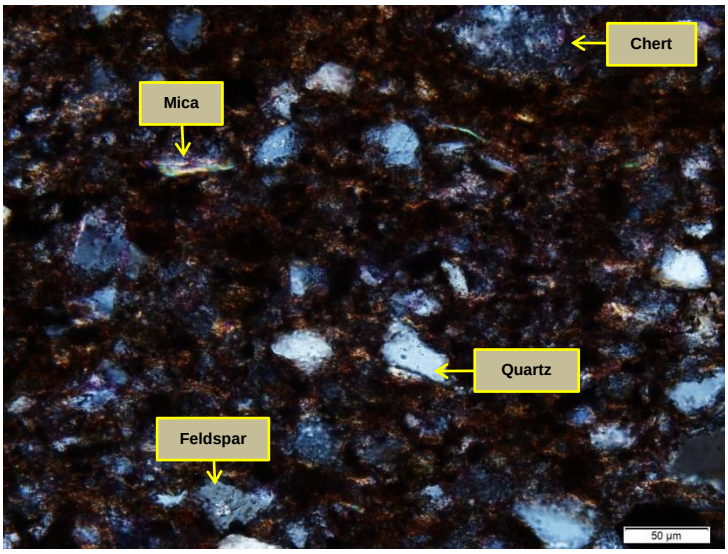


Fig. 3-112: Photomicrograph in XPL showing fine silt- to very fine sand-sized (average medium silt-sized) detrital quartz (15-35%), chert (5-8%), feldspar (1-5%), and mica (<2%) in a clay-rich layer.

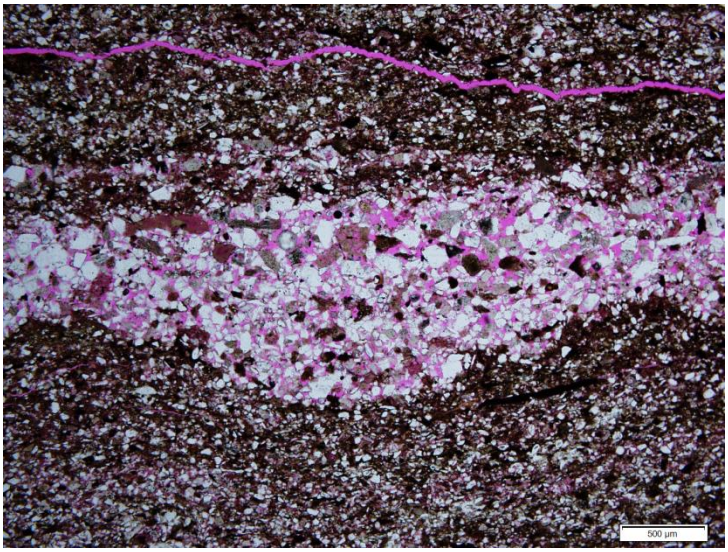


Fig. 3-113: Photomicrograph in PPL showing a silty/sandy lamination (~1.2 mm thick) interbedded between fine silty laminae in the top half of the sample. Several porous silty/sandy lenses and patches are observed, with ~15-25% intergranular porosity (pink epoxy). Abundant solid organic fragments are also present, some of which are >0.5 mm in length.

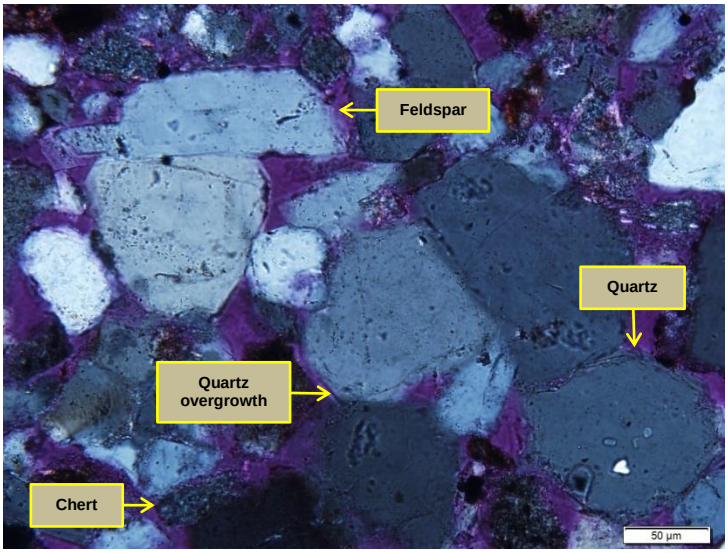


Fig. 3-114: Photomicrograph in XPL showing medium silt to fine sand-sized detrital quartz, chert, and feldspar observed in a silty/sandy lamination. Minor (<1%) quartz overgrowths are observed in these features.

3.2.12 SAMPLE 13178

Sample ID	**13178**		
Sample type	**Core**	**UWI/Well**	**100/16-25-055-20W4/00**
Strat. Unit	**Viking Formation**	**Depth**	**669.47 m**

XRD/SRA results

Quartz (%)	Fsp (%)	Cb (%)	Clays (%)	Pyrite (%)
62.1	6	0	31.2	0.8

Composition (*in order of abundance*)

Grain size	%	Variety (%)	Variety (%)	Variety (%)	Variety (%)
sand	4	Quartz/chert (91)	Feldspar (8)	Mica (1)	
silt	70	Quartz/chert (95)	Feldspar (4)	Mica (1)	
clay	20	Clay mins (100)			
Cement	<1	Quartz (100)			
Bioclasts	1	Phosphatic (100)			
Organics	4	Amorphous (99)	Plant material (1)		
Opaques	1	Pyrite (100)			
	100				

*Intensively altered to clay minerals

^ Including bitumen

Sedimentary structures

Primary	Alternating clay-rich and finely laminated silty bedding.
Biogenic	Possible burrow structures.

Fractures	Numerous 6-40 µm epoxy-filled fractures, particularly in clay-rich layers.
Porosity	Up to 10% intergranular porosity in finely laminated silty layers and possible burrow structures. <3% porosity in clay-rich layers.

Description

Clay-rich siltstone with alternating clay-rich and finely laminated silty bedding. Within clay-rich layers, very fine silt to very fine sand-sized (average medium silt-sized) detrital quartz, chert, feldspar, and mica occur within a dark-colored clay matrix. In finely laminated silty layers, very fine silt to very fine sand-sized (average coarse silt-sized) detrital quartz, chert, and feldspar occur with less clay matrix.

Thin Section Quality

Good.

Rock Classification

Siltstone.

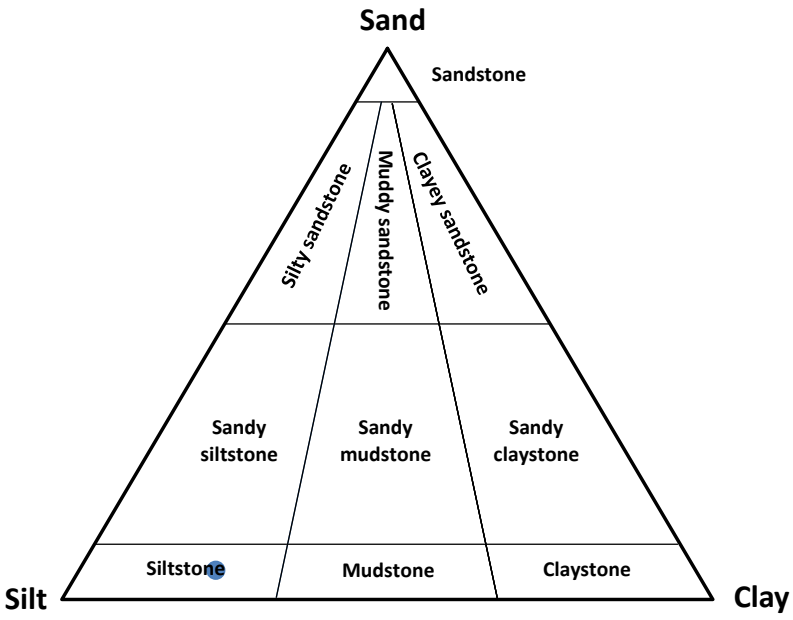


Fig. 3-115: Ternary plot showing the grain size composition of the sample based on the Wentworth scale (after Folk, 1954). Sample 13178 is classified as a siltstone.



Fig. 3-116: Core photograph of sample 13178 from the Viking Formation, well 100/16-25-055-20W4/00 (depth 669.74 m). The thin section prepared from this sample was cut from the area marked with an X. The sample was received with no way up-direction. Scale is in mm.

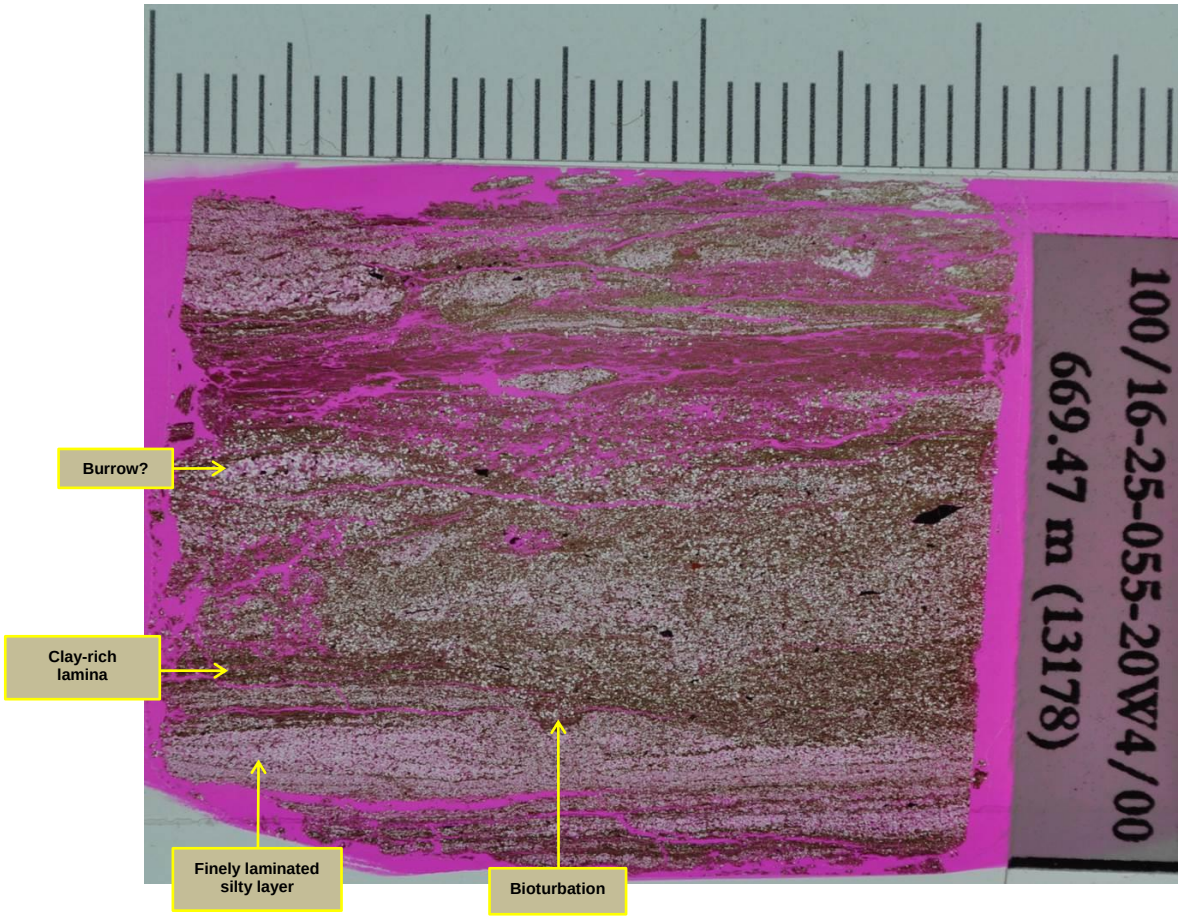


Fig. 3-117: Thin section photograph of sample 13178 from the Viking Formation, well 100/16-25-055-20W4/00 (depth 669.74 m). The sample is a bioturbated organic- and clay-rich siltstone with interbedded finely laminated silty layers. Abundant artificial partings are observed and are due to the presence of water-sensitive clays. Scale is in mm. Note: way-up direction was not indicated and is difficult to identify, and therefore may differ from the orientation shown.

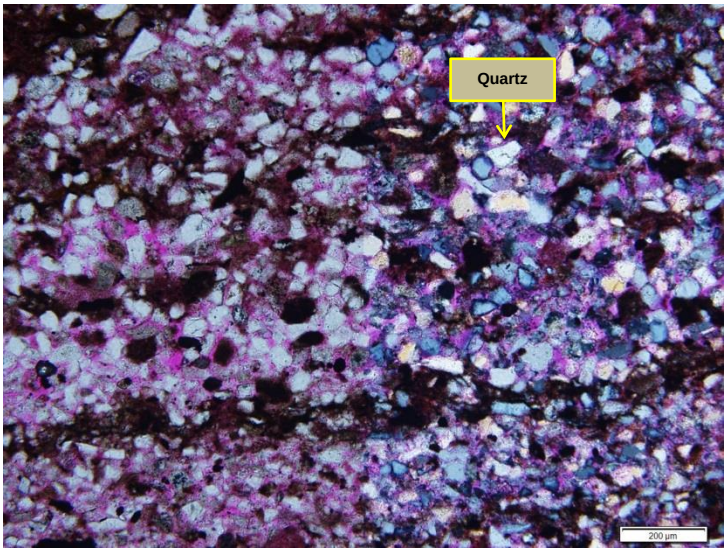


Fig. 3-118: Photomicrograph (left half in PPL, right half in XPL) showing a finely laminated silty layer. Note the abundance of detrital quartz grains (50-55%; majority of light-coloured minerals) and small amounts of clay in the horizon. These layers have up to ~15% intergranular porosity (pink epoxy). Darker material consists of clays, pyrite and organic matter.

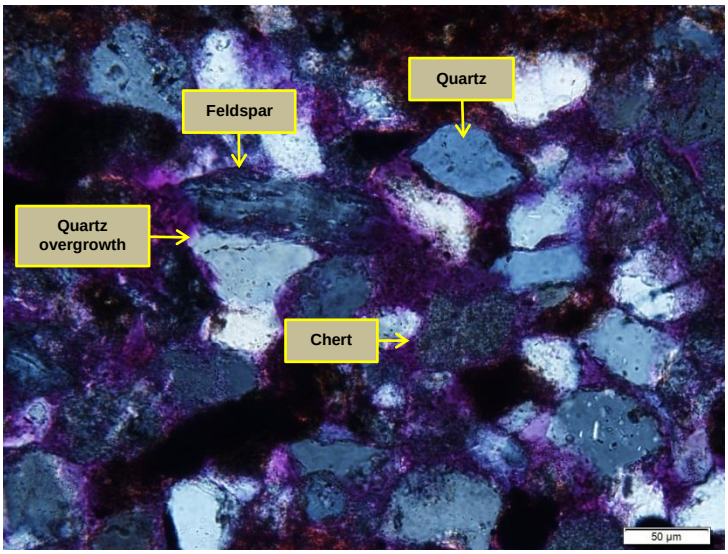


Fig. 3-119: Photomicrograph in XPL showing very fine silt- to very fine sand-sized (average grain size is coarse silt) detrital quartz (50-55%), chert (10-15%), and feldspar (<5%) present in a finely laminated silty layer. Minor (<1%) quartz overgrowths are observed in these horizons.

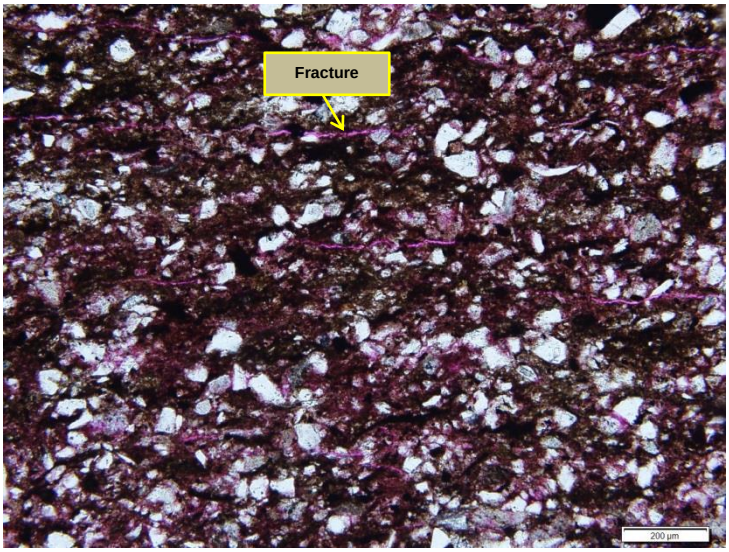


Fig. 3-120: Photomicrograph in PPL illustrating an organic- and clay-rich layer observed in the sample. Clays are estimated at ~20% of the total composition. These layers lack strongly defined laminations or bedding features. Note several artificial fractures filled with pink epoxy.

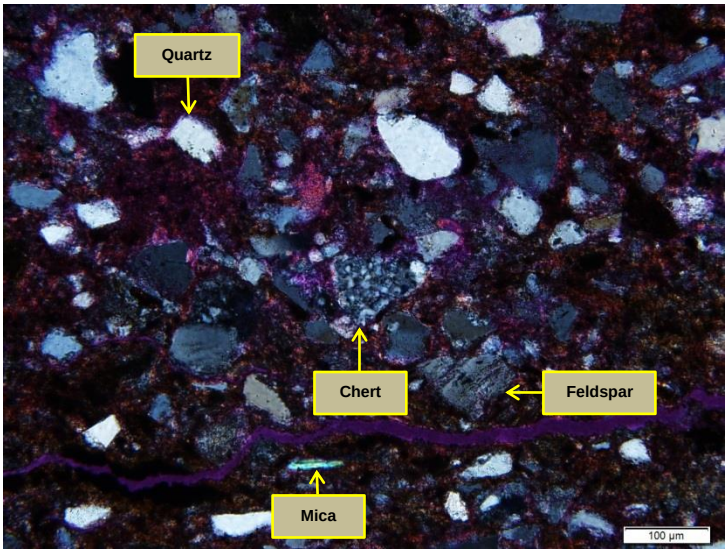


Fig. 3-121: Photomicrograph in XPL showing very fine silt- to very fine sand-sized (average grain size is medium silt) detrital quartz (25-30%), chert (8-12%), feldspar (2-4%), and mica (<2%) in a clay-rich lamination. These layers have <3% intergranular porosity.

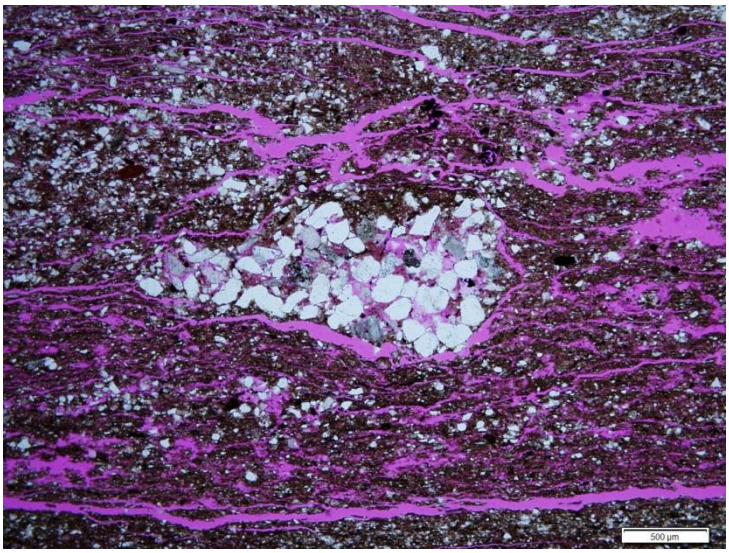


Fig. 3-122: Photomicrograph in PPL showing a lens of medium silt- to fine sand-sized detrital grains, possibly representing a burrow structure. These features have the coarsest grain size (fine sand) observed in the sample. Abundant epoxy-filled fractures and partings occur throughout and are the result of water-sensitive clay minerals (removed or swelled during sample preparation, i.e. cutting with water prior to epoxy impregnation).

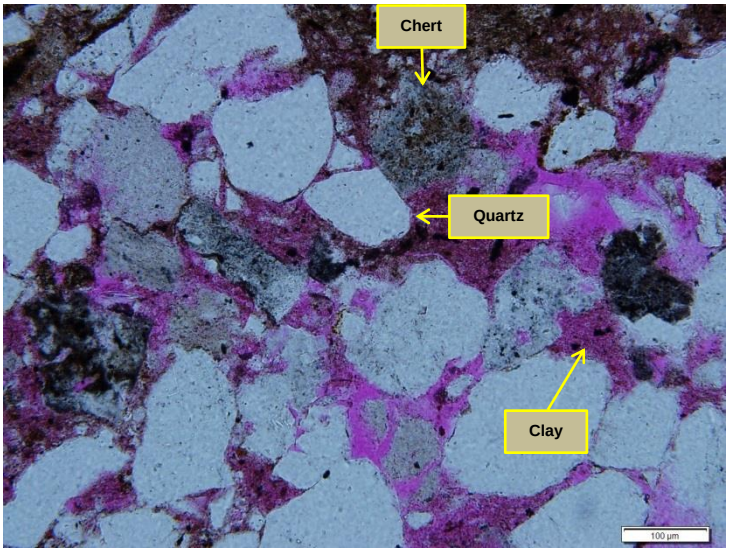


Fig. 3-123: Photomicrograph in PPL showing detrital quartz (50-60%) and chert (8-10%) present in the possible burrow structure shown in Figure 3-122. These features have up to 10% intergranular porosity (pink epoxy). Occasional chert grains exhibit a more “dirty” surface compared to quartz and feldspars. Note some finely disseminated clay material in the open pores.

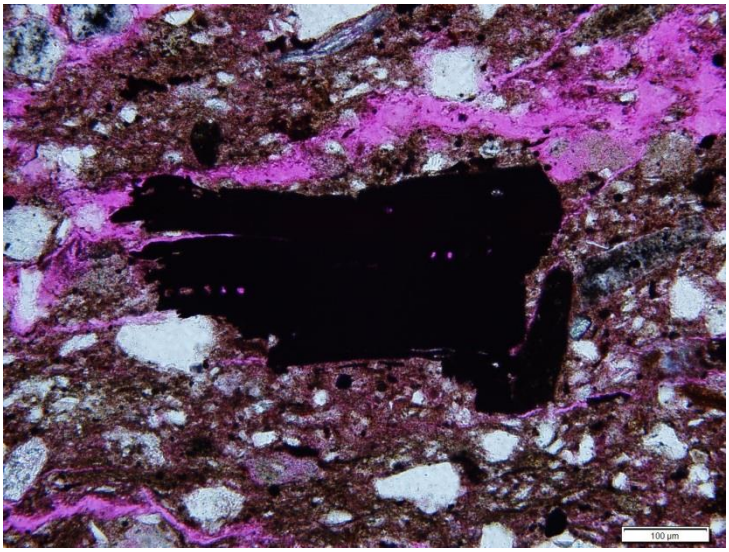


Fig. 3-124: Photomicrograph in PPL showing a solid organic fragment (opaque), present in a clay-rich layer, which exhibits partially preserved plant cell structure. Other opaques may include pyrite idiomorphs. Some quartz grains embedded in the clay-rich matrix are up to ~120 µm in size.

3.2.13 SAMPLE 13181

Sample ID	**13181**		
Sample type	**Core**	**UWI/Well**	**100/16-25-055-20W4/00**
Strat. Unit	**Viking Formation**	**Depth**	**677.4 m**

XRD/SRA results

Quartz (%)	Fsp (%)	Cb (%)	Clays (%)	Pyrite (%)
67.6	8.7	0	22.9	1

Composition (*in order of abundance*)

Grain size	%	Variety (%)	Variety (%)	Variety (%)	Variety (%)
sand	8	Quartz/chert (87)	Feldspar (8)	Mica (5)	
silt	65	Quartz/chert (93)	Feldspar (5)	Mica (2)	
clay	20	Clay mins (100)			
Cement	0				
Bioclasts	1	Phosphatic (100)			
Organics	5	Amorphous (100)			
Opaques	1	Pyrite (100)			
	100				

*Intensively altered to clay minerals

^ Including bitumen

Sedimentary structures

Primary	Interbedded clay-rich layers and silty lenses.
Biogenic	Possible *Planolites* burrow structures.

Fractures	Thin (2-20 µm) epoxy filled fractures occur throughout the sample, particularly in clay-rich layers.
Porosity	Up to 15% intergranular porosity in silty lenses and burrow structures. Negligible porosity (<5%) in clay-rich layers.

Description

Bioturbated clay-rich siltstone with interbedded silty lenses. Clay- and organic-rich layers contain medium silt- to fine sand-sized (average grain size is coarse silt) detrital quartz, chert, feldspar, and mica. Interbedded silty lenses contain medium silt- to medium sand-sized (average grain size is coarse silt) detrital quartz, chert, feldspar, and mica, and lower abundances of clays and organics. Burrow structures of different sizes occur throughout the sample, with infills showing grain sizes ranging from medium silt to medium sand.

Thin Section Quality

Poor. Apparent plucking/removal of clays and detrital grains.

Rock Classification

Siltstone.

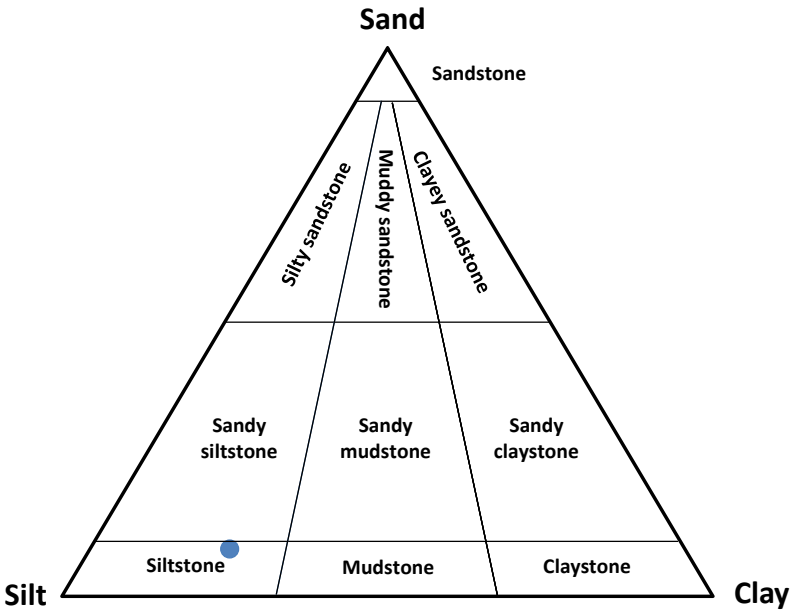


Fig. 3-125: Ternary plot showing the grain size composition of the sample based on the Wentworth scale (after Folk, 1954). Sample 13181 is classified as a siltstone.

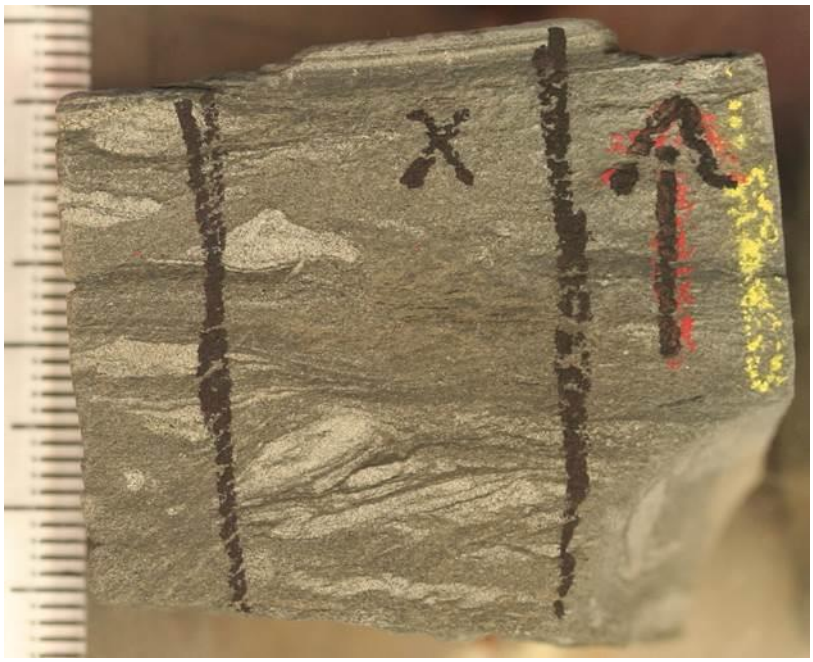


Fig. 3-126: Core photograph of sample 13181 from the Viking Formation, well 100/16-25-055-20W4/00 (depth 677.4 m). The thin section prepared from this sample was cut from the area marked with an X. The arrow indicates stratigraphic up-direction. Scale is in mm.

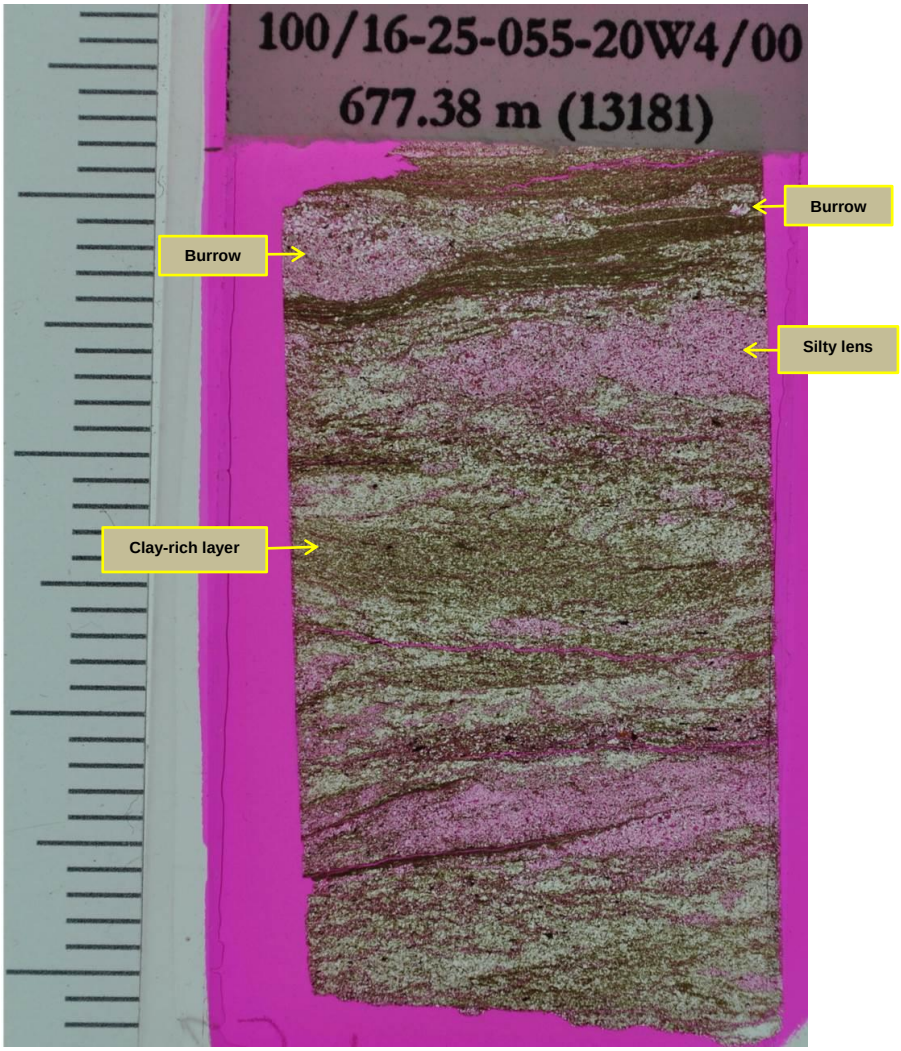


Fig. 3-127: Thin section photograph of sample 13181 from the Viking Formation, well 100/16-25-055-20W4/00 (depth 677.4 m). The sample is a bioturbated clay-rich siltstone with interbedded silty lenses. Burrow structures of different sizes, possibly including the trace fossil* Planolites*, occur within the sample. Scale is in mm. Note: way-up direction was not indicated and is difficult to identify, and therefore may differ from the orientation shown.

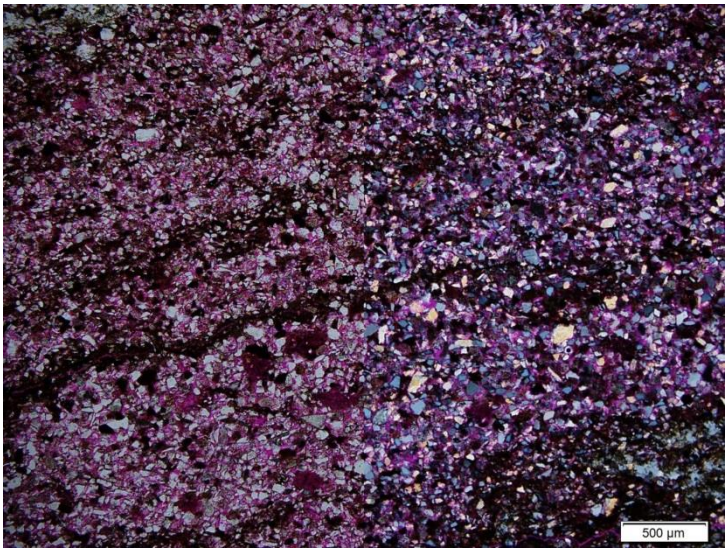


Fig. 3-128: Photomicrograph (left half in PPL, right half in XPL) showing an overview of a silty lens. These lenses are comprised of medium silt- to medium sand-sized grains, with an average grain size of coarse silt, and have up to 15% intergranular porosity. Organic- and clay-rich lenses and bedding-parallel laminae are also present.

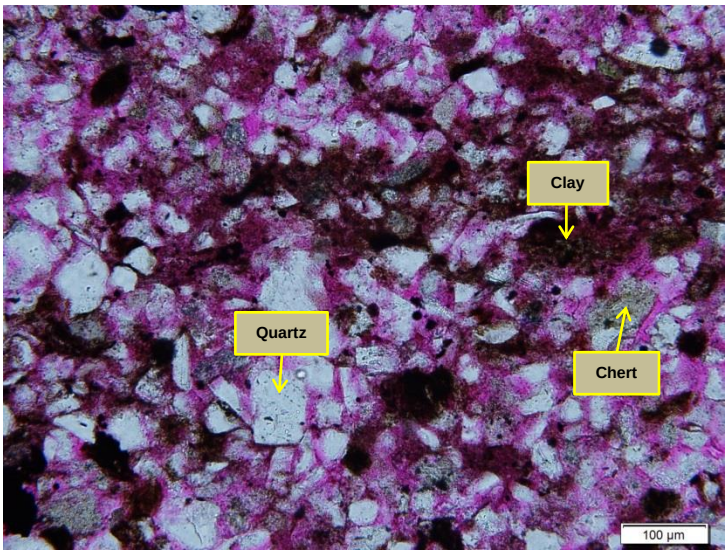


Fig. 3-129: Photomicrograph in PPL of well sorted angular to subrounded sediment within a silty lens. Variable amounts of clay (5-15%), organics (~5%), and pyrite (~1%) are present between the detrital grains. A large amount of pink epoxy highlights open pore space, some or most of which may be attributed to sample preparation (removal of matrix during cutting with water).

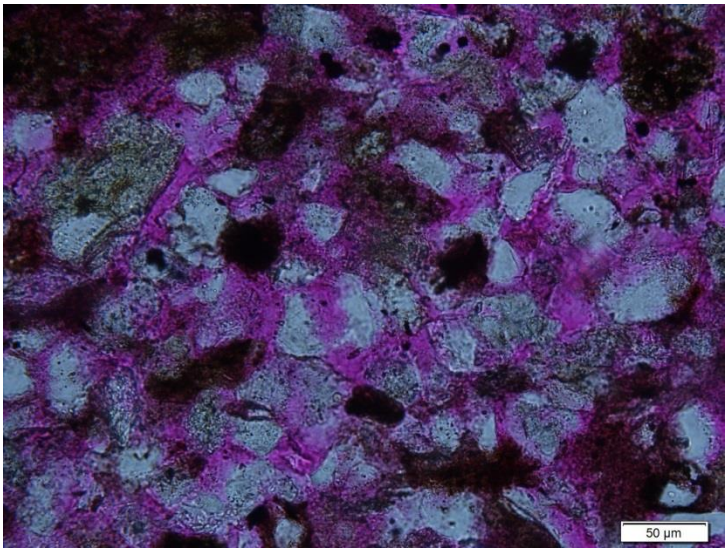


Fig. 3-130: Photomicrograph in PPL showing well sorted, angular to subrounded detrital quartz (50-70%) and chert (8-12%) observed in a silty lens.

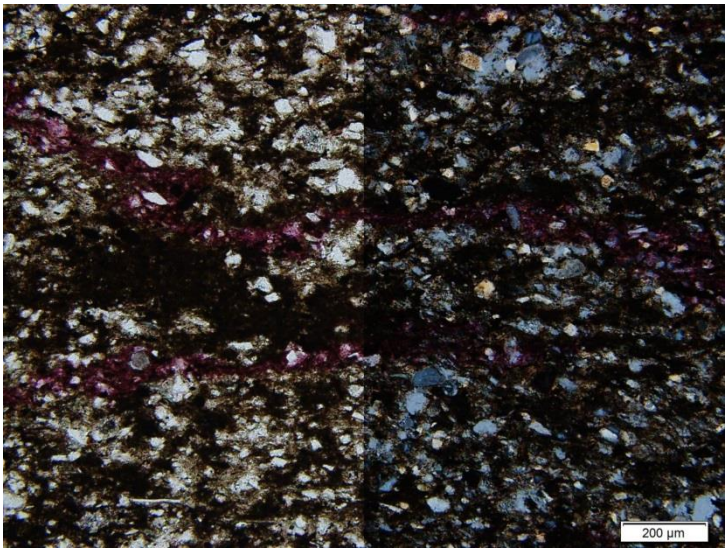


Fig. 3-131: Photomicrograph (left half in PPL, right half in XPL) of an organic- and clay-rich layer containing medium silt- to fine sand-sized (average grain size is coarse silt) detrital quartz (20-25%), chert (5-8%), feldspar (2-5%), and mica (<2%). These layers contain 50-60% clay, and have <5% intergranular porosity.

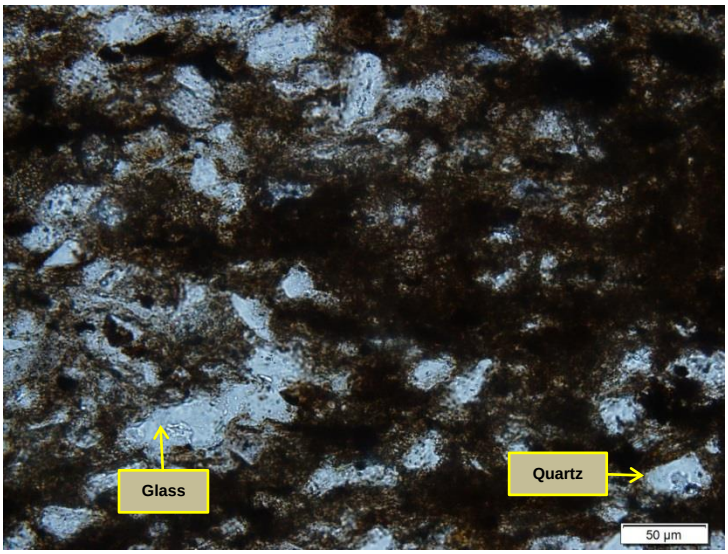


Fig. 3-132: Photomicrograph in PPL showing part of an organic- and clay-rich layer containing fine to coarse silt-sized quartz and chert grains, abundant clay matrix, and little/no intergranular porosity. Exposed thin section glass (likely resulting from sample preparation) is abundant in some parts of the sample (see Figure 3-137).

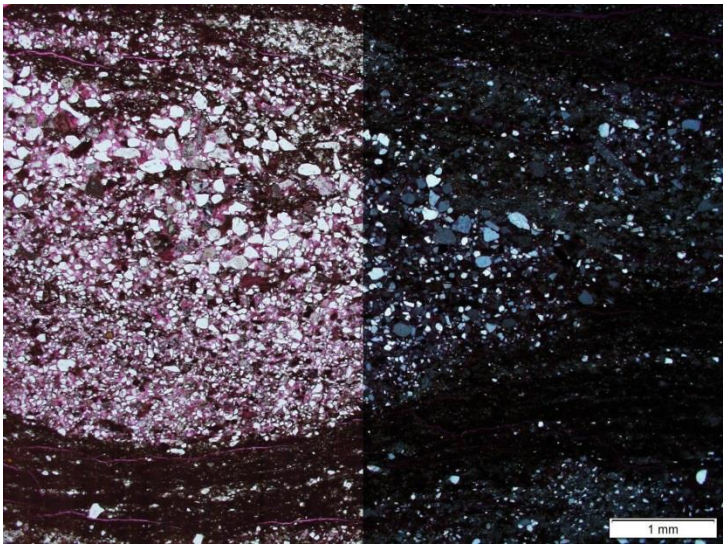


Fig. 3-133: Photomicrograph (left side in PPL, right side in XPL) showing a possible *Planolites* burrow structure. Note the distinct grading within the silt-sand lens and organic/clay patches dispersed throughout. The lenticular deposit is embedded in organic- and clay-rich laminae that have abundant artificial epoxy-filled fractures (swelling clays present?).

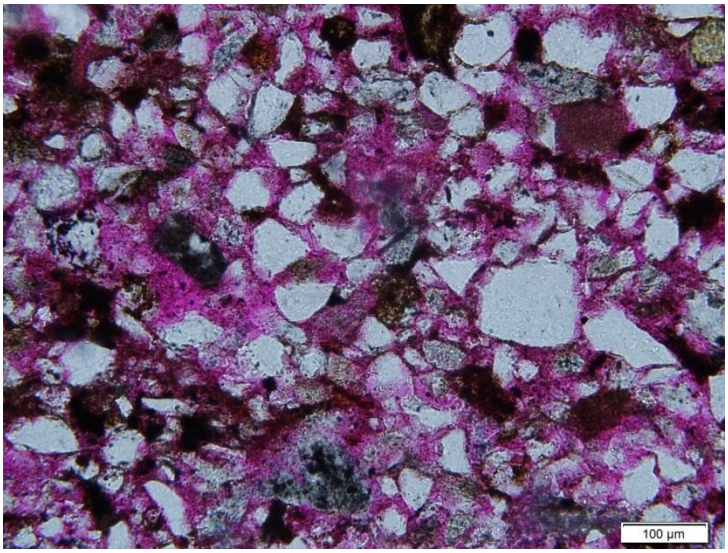


Fig. 3-134: Photomicrograph in PPL showing angular to subrounded medium silt- to medium sand-sized quartz (50-60%), chert (8-10%), and feldspar (5-8%) grains infilling a burrow structure. These structures have up to ~15% intergranular porosity (pink epoxy).



Fig. 3-135: Photomicrograph in PPL showing an amorphous solid organic fragment. Pink epoxy surrounding the fragment possibly represents plucked clay material removed during sample preparation. The organic fragment contains an epoxy-filled fracture, and a hairline fracture (right side). A phosphatic bioclast fragment is present below the organic particle.

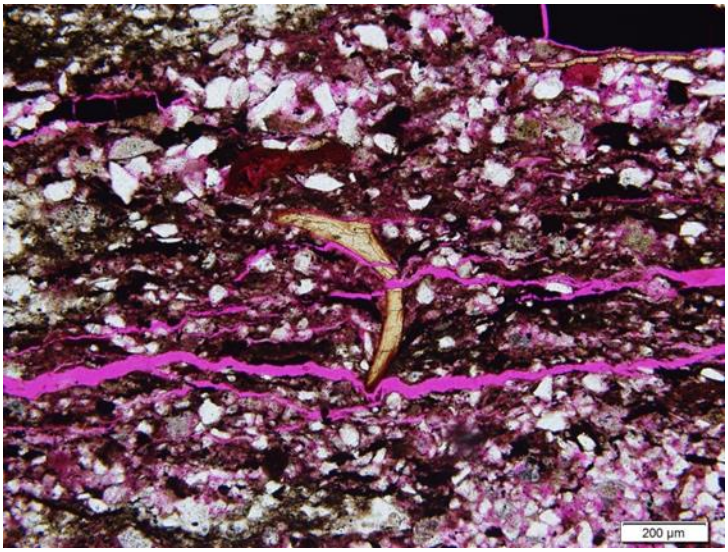


Fig. 3-136: Photomicrograph in PPL showing a rare (~1%) phosphatic bioclast (fish bone?) present within an organic- and clay-rich layer. Several opaque clusters, some pyrite and some solid organic matter, are also present in the layer.

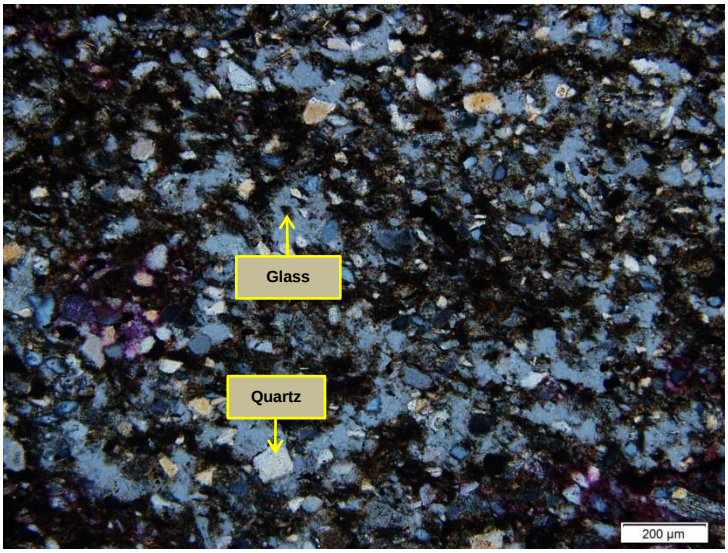


Fig. 3-137: Photomicrograph in PPL showing sample damage, possibly caused by the presence of swelling clays. Plucking of grains during rock cutting and thin section polishing leaves glass material exposed, as is frequently seen in this sample. Examining Figure 3-127, some layers appear to be quartz-rich (in comparison to darker, brown-colored, clay-rich layers), but actually lack epoxy infiltration (i.e., intergranular porosity) between detrital grains, as seen in other layers in the sample. This likely indicates removal of water-sensitive clay and/or other detrital minerals during sample preparation.

3.2.14 SAMPLE 13182

Sample ID	**13182**		
Sample type	**Core**	**UWI/Well**	**100/16-25-055-20W4/00**
Strat. Unit	**Viking Formation**	**Depth**	**677.77 m**

XRD/SRA results

Quartz (%)	Fsp (%)	Cb (%)	Clays (%)	Pyrite (%)
90.9	4.8	0	3.9	0.3

Composition (*in order of abundance*)

Grain size	%	Variety (%)	Variety (%)	Variety (%)	Variety (%)
sand	90	Quartz/chert (98)	Feldspar (1)	Mica (1)	
silt	6	Quartz/chert (100)			
clay	2	Clay mins (100)			
Cement	1	Quartz (100)			
Bioclasts	0				
Organics	1	Amorphous (100)			
Opaques	0				
	100				

*Intensively altered to clay minerals

^ Including bitumen

Sedimentary structures

Primary	None apparent.
Biogenic	None apparent.

Fractures	None apparent.
Porosity	Up to ~25% intergranular porosity. <15% porosity only in an isolated, non-porous clay streak.

Description

Sublitharenite composed predominately of subrounded (common) to rounded (rare) coarse silt- to very coarse sand-sized quartz and chert grains. Most of the sample has ~15-25% intergranular porosity, with the exception of a non-porous clay streak accounting for ~2% of total sample composition. Pore-bridging clay minerals and euhedral quartz overgrowths occur throughout the sample, but never completely eliminate intergranular pore space. Both point contacts and deformed grain contacts are observed in the sample, suggesting low to moderate post-burial sediment compaction.

Thin Section Quality

Good, 1/2 carbonate stained.

Rock Classification

Sublitharenite.

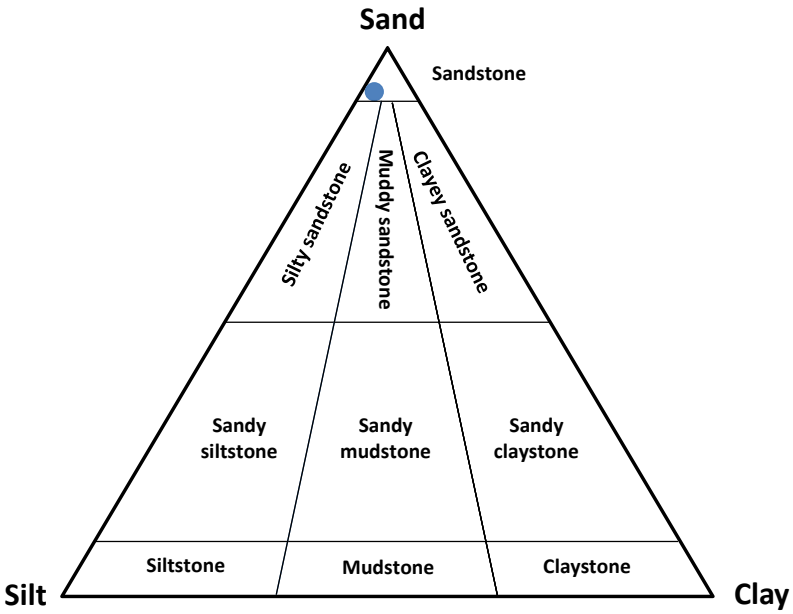


Fig. 3-138: Ternary plot showing the grain size composition of the sample based on the Wentworth scale (after Folk, 1954). Sample 13182 is classified as a sandstone.

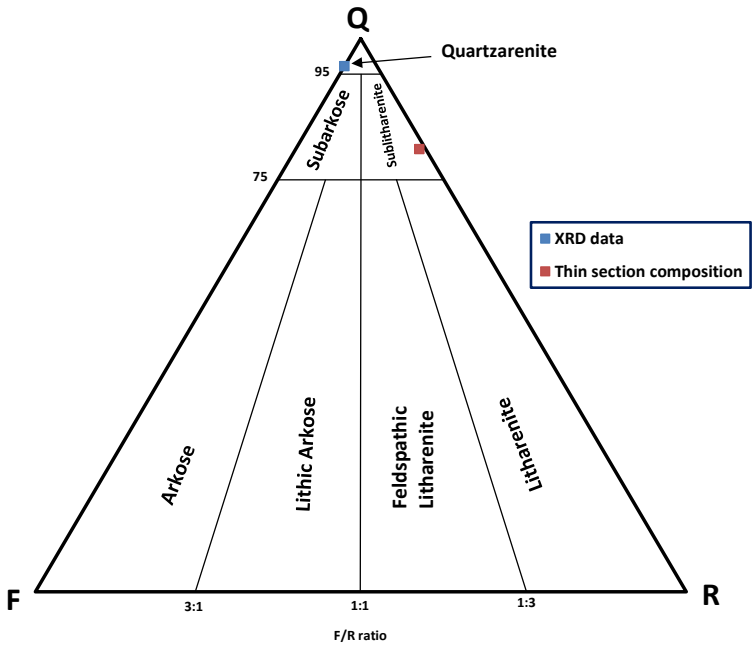


Fig. 3-139: Ternary plot showing the relative abundance of different grain compositions within the sample (after Folk, 1968). Sample 13182 is classified as a sublitharenite (note that XRD analysis cannot distinguish between quartz and chert).

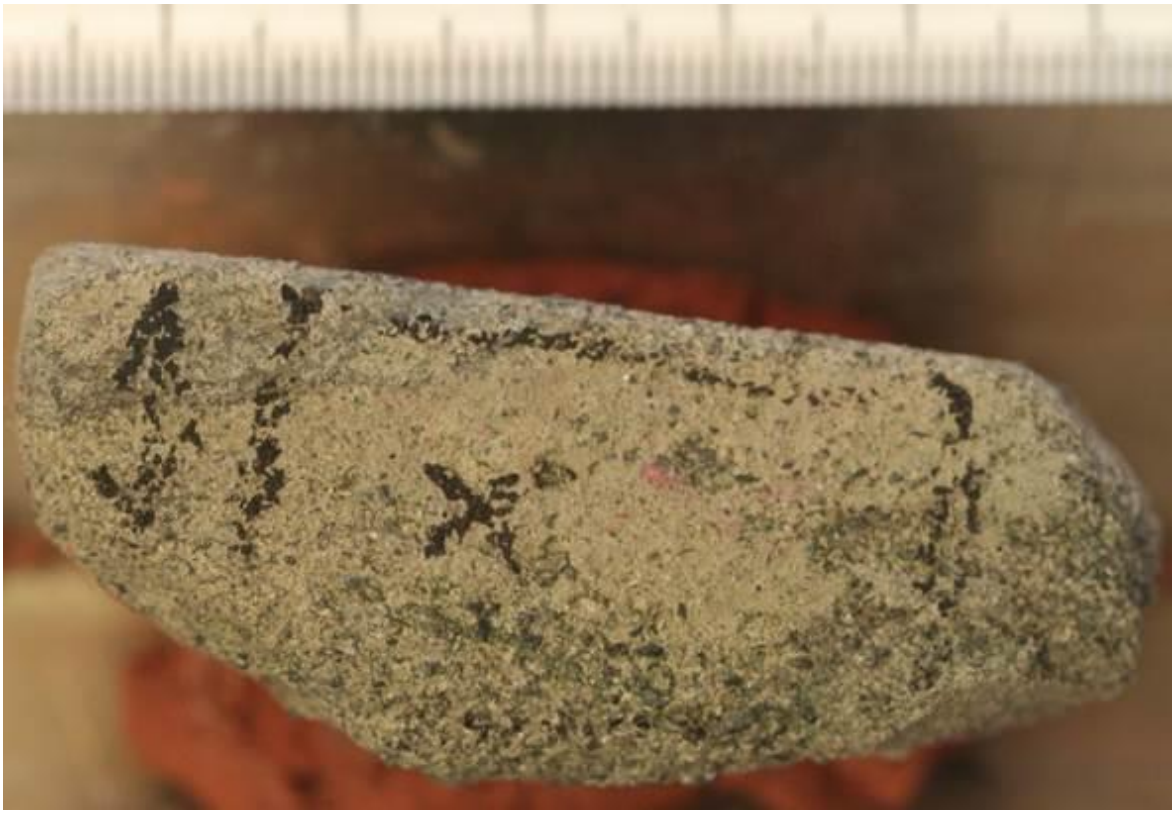


Fig. 3-140: Core photograph of sample 13182 from the Viking Formation, well 100/16-25-055-20W4/00 (depth 677.8 m). The thin section prepared from this sample was cut from the area marked with an X. The sample was received with no up-direction. Scale is in mm.

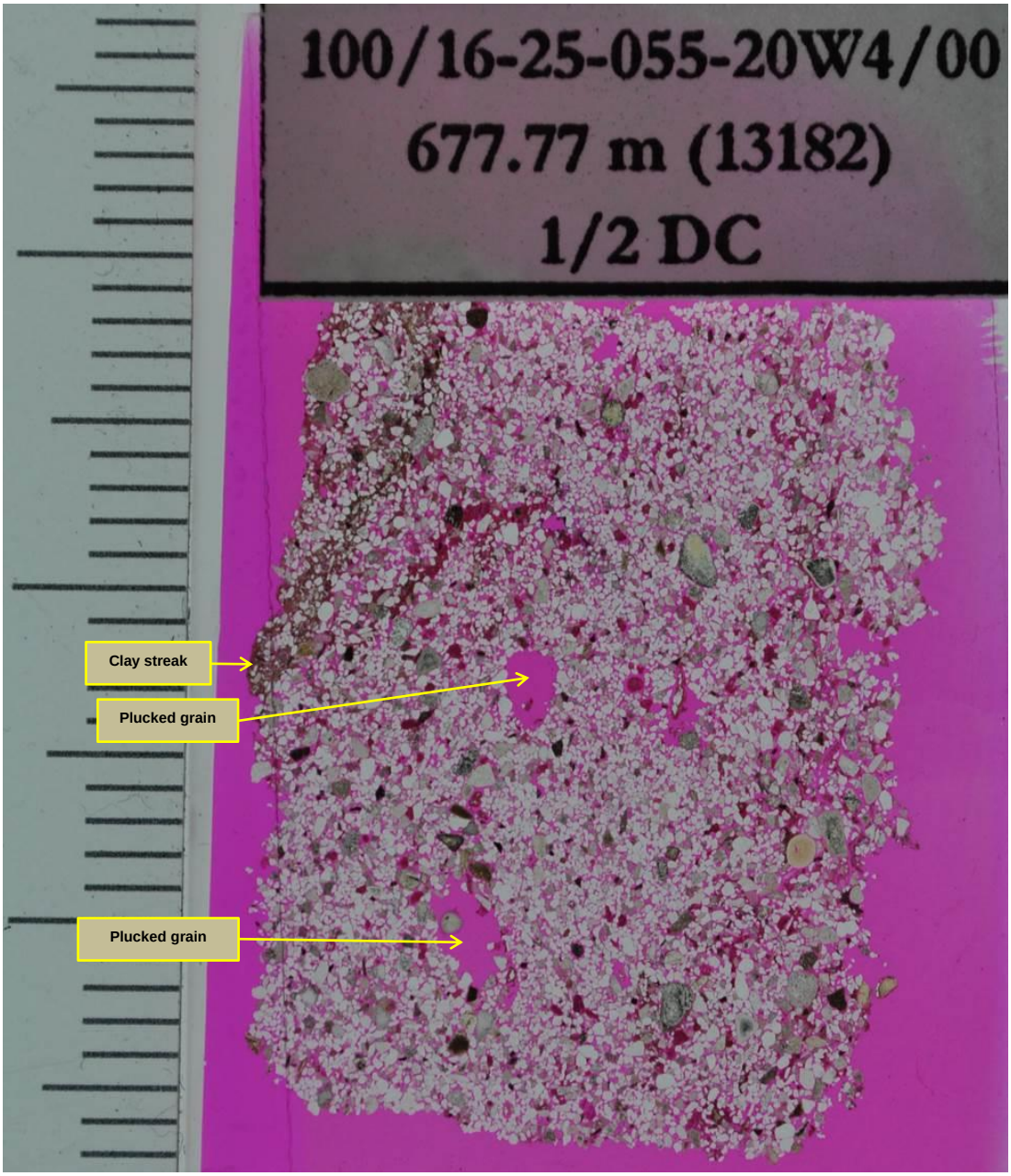


Fig. 3-141: Thin section photograph of sample 13182 from the Viking Formation, well 100/16-25-055-20W4/00 (depth 677.77 m). The sample is a sublitharenite composed predominately of subrounded (common) to rounded (rare), coarse silt- to very coarse sand-sized quartz and chert grains. The two large pores indicated in the above image represent grains plucked from the sample during thin section preparation. Scale is in mm. Note: way-up direction was not indicated and is difficult to identify, and therefore may differ from the orientation shown.

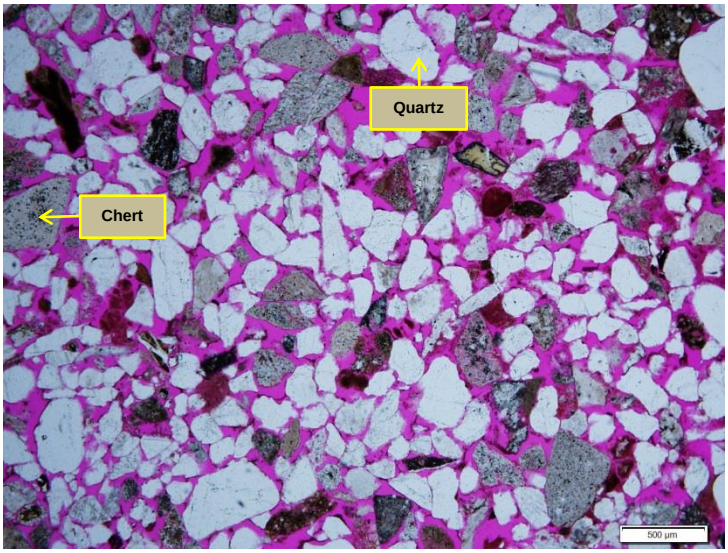


Fig. 3-142: Photomicrograph in PPL showing the sample, classified as a moderately sorted sublitharenite sandstone. The rock framework composition is predominantly coarse silt- to very coarse sand-sized quartz (70-80%) and chert (20-30%) grains. Note abundant porosity highlighted by pink epoxy.

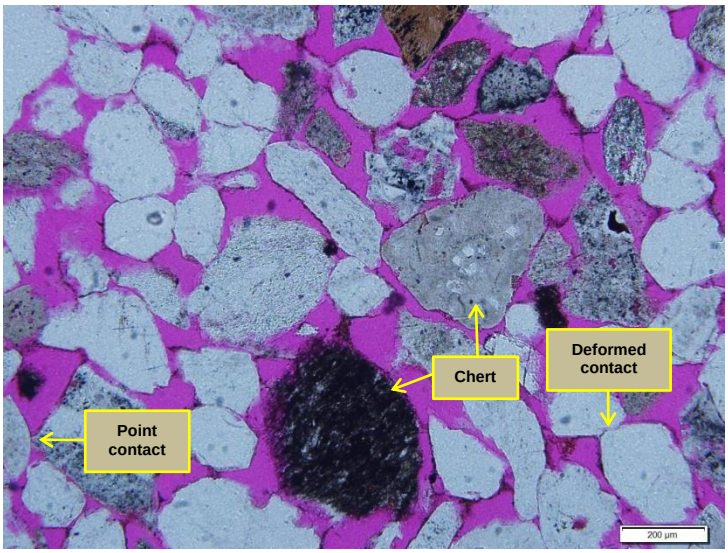


Fig. 3-143: Photomicrograph in PPL showing point contacts and deformed grain contacts present in the sandstone. Most chert grains show a “dirty” surface with numerous inclusions and coatings, which helps to distinguish them from quartz in PPL. Note abundant intergranular porosity, which is estimated at 25%. It is difficult to determine if some of the open porosity is due to removal of material during sample preparation (cutting).

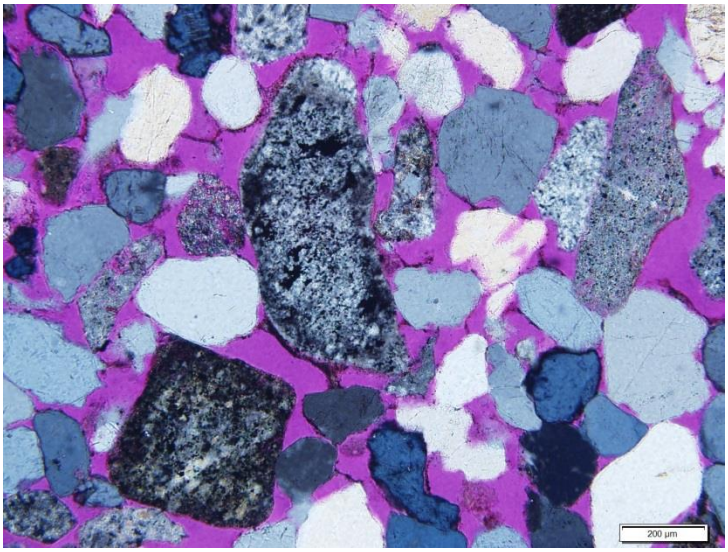


Fig. 3-144: Photomicrograph in XPL showing the abundance of monocrystalline quartz (~96% of quartz grains present in the sample) and cryptocrystalline chert in the sandstone. Only two non-cryptocrystalline, radiolarian chert grains were observed in the sample (see Figure 3-149).

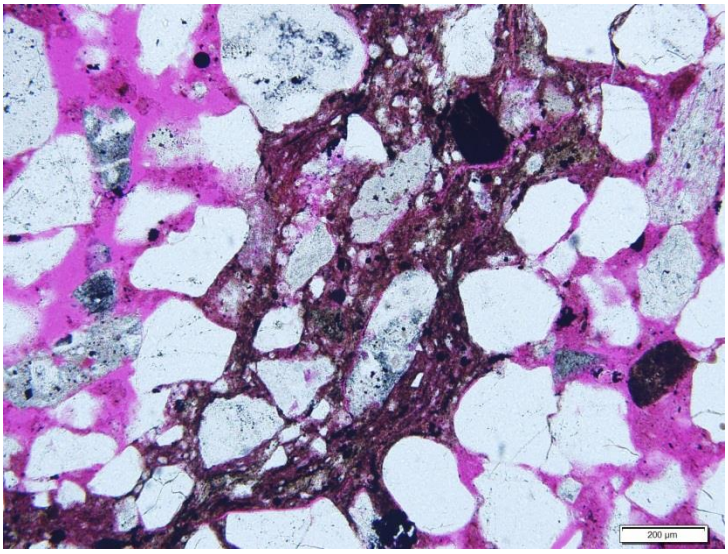


Fig. 3-145: Photomicrograph in PPL showing an isolated clay streak observed in the sandstone (~2% of sample composition). Fine silt-size particles and opaque material (pyrite and organics) are observed embedded in the clay streak.

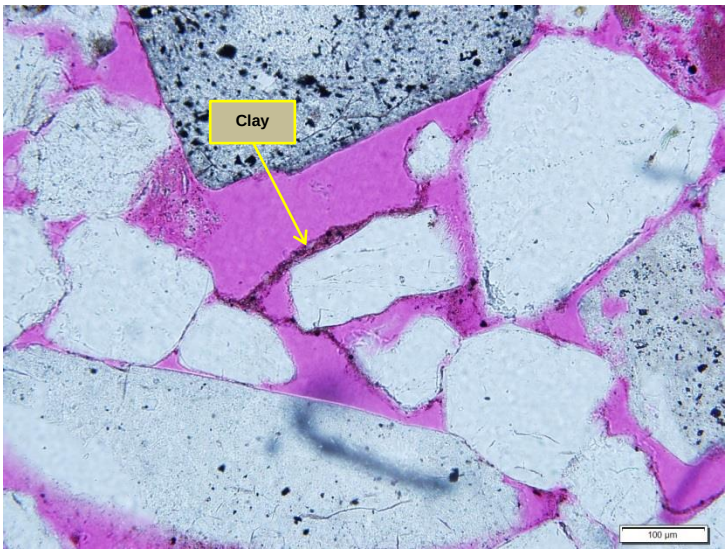


Fig. 3-146: Photomicrograph in PPL detailing pore-bridging secondary clay. This type of clay mineralization is common throughout the entire sample, and reduces pore connectivity.

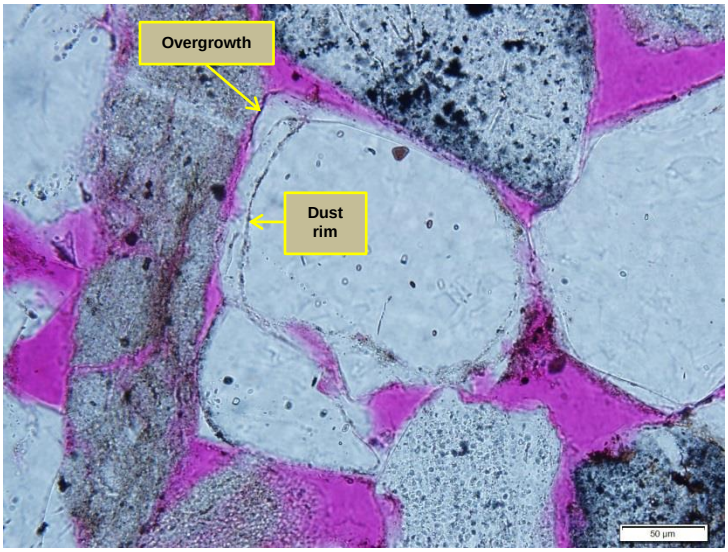


Fig. 3-147: Photomicrograph in PPL showing euhedral secondary quartz overgrowths, which can be distinguished from detrital grains by a dust rim. Quartz overgrowths occur throughout the entire sample, but are never observed to completely fill intergranular pores.

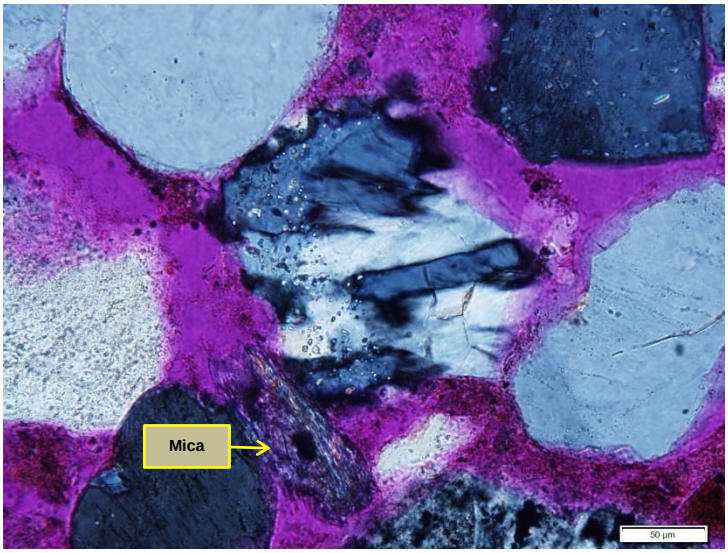


Fig. 3-148: Photomicrograph in XPL showing a polycrystalline quartz grain present in the sample. Polycrystalline quartz accounts for ~4% of the quartz grains observed. Note rare mica fragment (~1% of sample composition).

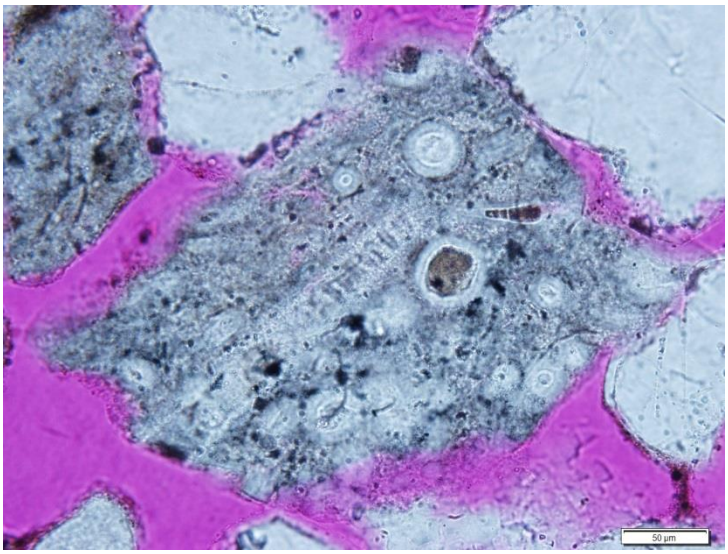


Fig. 3-149: Photomicrograph in PPL illustrating a radiolarian chert grain present in the sample. Only two radiolarian chert fragments are observed.

4. Cardium Formation Overview

This chapter presents a petrographic analysis of 13 wells of the Cardium Formation (see Table 4-A). Core samples were impregnated using rhodamine-B epoxy (pink) in order to allow identification of porosity and fractures using UV fluorescence microscopy. Due to clay sensitivity issues, the majority of the samples were prepared without staining solutions (with the exception of samples 13258 and 15107, half-stained for carbonates). The following summary focuses on observations of compositional variability (i.e., lithofacies groupings) with illustrations of the most common depositional and bioturbation structures, diagenetic features, clay and organic matter distributions, and observations about porosity and fractures. A total of 5 distinct lithofacies were identified (Table 4-B) and the mineralogical XRD data for each lithofacies was averaged in order to determine common compositional parameters (Table 4-C).

4.1 SUMMARY

4.1.1 CORE SAMPLES:

Well Location	Depth m (Sample ID)
100/03-21-030-04W5/00	2208.7 (13133), 2220.0 (13135), 2227.8 (13139)
102/14-25-039-05W5/00	1803.9 (13144), 1812.8 (13147)
100/04-03-044-07W5/00	1826.9 (13257), 1828.1 (13258)
102/06-27-066-23W5/00	1016.3 (13262)
100/04-18-060-20W5/00	1607.3 (13283), 1612.3 (13286)
100/06-12-048-11W5/00	1773.8 (13403), 1781.3 (13407), 1790.5 (13412), 1791.7 (13413)
100/03-07-048-08W5/00	1650.2 (13420)
100/06-07-047-04W5/00	1442.9 (13425), 1450.1 (13427)
100/08-30-049-04W5/00	1244.9 (13431), 1247.2 (13432)
100/07-32-045-12W5/00	2177.1 (13436), 2180.2 (13437), 2181.7 (13438)
100/16-03-052-13W5/00	1742.2 (13441), 1743.2 (13442)
100/05-17-049-08W5/00	1505.3 (13443), 1514.7 (13446), 1521.5 (13448)
100/16-15-050-06W5/00	1170.3 (15107), 1177.1 (15109)

Table 4-A: Well locations and core sample depths.

4.1.2 LITHOFACIES, GROUPINGS AND DESCRIPTIONS:

Well Location	Lithofacies	Depth m (Sample ID)
100/03-21-030-04W5/00	2	2208.7 (13133)
100/03-21-030-04W5/00	4	2220.0 (13135)
100/03-21-030-04W5/00	3	2227.8 (13139)
102/14-25-039-05W5/00	2	1803.9 (13144)
102/14-25-039-05W5/00	4	1812.8 (13147)
100/04-03-044-07W5/00	2	1826.9 (13257)
100/04-03-044-07W5/00	5	1828.1 (13258)
102/06-27-066-23W5/00	1	1016.3 (13262)
100/04-18-060-20W5/00	4	1607.3 (13283)
100/04-18-060-20W5/00	5	1612.3 (13286)
100/06-12-048-11W5/00	2	1773.8 (13403), 1790.5 (13412), 1791.7 (13413)
100/06-12-048-11W5/00	5	1781.3 (13407)
100/03-07-048-08W5/00	5	1650.2 (13420)
100/06-07-047-04W5/00	5	1442.9 (13425)
100/06-07-047-04W5/00	2	1450.1 (13427)
100/08-30-049-04W5/00	4	1244.9 (13431)
100/08-30-049-04W5/00	1	1247.2 (13432)
100/07-32-045-12W5/00	2	2177.1 (13436), 2180.2 (13437), 2181.7 (13438)
100/16-03-052-13W5/00	5	1742.2 (13441), 1743.2 (13442)
100/05-17-049-08W5/00	2	1505.3 (13443)
100/05-17-049-08W5/00	5	1514.7 (13446), 1521.5 (13448)
100/16-15-050-06W5/00	4	1170.3 (15107)
100/16-15-050-06W5/00	2	1177.1 (15109)

Table 4-B: Lithofacies distribution by Well.

Lithofacies	Classification	Quartz/Chert %	Feldspar %	Clay/Mica %	Pyrite %
1	Sandy claystone	52.95	4.45	39.55	0.25
2	Sandy mudstone	62.01	4.23	32.12	0.69
3	Mudstone	64.70	4.80	29.00	0.50
4	Clayey sandstone	73.26	2.80	22.72	0.76
5	Muddy sandstone	73.52	3.27	22.51	0.61

Table 4-C: Average lithofacies composition, based on XRD data.

4.1.2.1 LITHOFACIES 1: SANDY CLAYSTONE

Samples 13262 and 13432 are classified as sandy claystones. Both samples contain >40% clay, >25% sand, and <20% silt. Quartz and chert comprise at least 90% of the silt- and sand-sized grains present in both rocks.

4.1.2.2 LITHOFACIES 2: SANDY MUDSTONE

Samples 13133, 13144, 13257, 13403, 13412, 13413, 13427, 13436, 13437, 13438, 13443, and 15109 are classified as sandy mudstones. These rocks show the greatest variation in grain size of all the samples examined. All samples contain at least 25% clay material and 20-40% silt-sized grains. Sand-sized grains show the greatest compositional range, accounting for 11-43% of these rocks.

4.1.2.3 LITHOFACIES 3: MUDSTONE

Sample 13139 is classified as a mudstone. Silt-sized particles, of which >95% are quartz and chert, account for >50% of the sample. Clay comprises ~30% of the sample, with sand-sized particles accounting for <10% of the total composition.

4.1.2.4 LITHOFACIES 4: CLAYEY SANDSTONE

Samples 13135, 13147, 13283, 13431, and 15107 are classified as clayey sandstones. All of these samples contain >45% sand-, at least 20% clay-, and 8-12% silt-sized particles. Quartz and chert account for >90% of the sand- and silt-sized fractions.

4.1.2.5 LITHOFACIES 5: MUDDY SANDSTONE

Samples 13258, 13286, 13407, 13420, 13425, 13441, 13442, 13446, and 13448 are classified as muddy sandstones. These samples contain no more than 25% clay, and 8-20% silt-sized grains. Sand-sized particles are the most abundant in these rocks, accounting for 47-81% of the total composition.

4.1.3 SEDIMENTARY STRUCTURES & BIOTURBATION:

Many of the samples examined lack depositional structures and consist of unstratified (well-mixed) clay-rich and sandy sediments. This fabric results from bioturbation, post-depositional sediment mixing, rapid deposition, or some combination thereof. The mixing has also resulted in patchy porosity, where porosity is mostly confined to areas of clay-poor sediment.

Finely laminated beds, often partially disturbed or mixed (bioturbation?), are common in the samples. These horizons are typically made up of silt-sized grains and clays (as well as clay-associated organic

matter). Porous sandy layers (not shown – see Figures 4.1.4-1, 4.1.5-2, and 4.1.6-1) also occur in these rocks, but are less abundant than finely laminated clay-rich and silty beds.

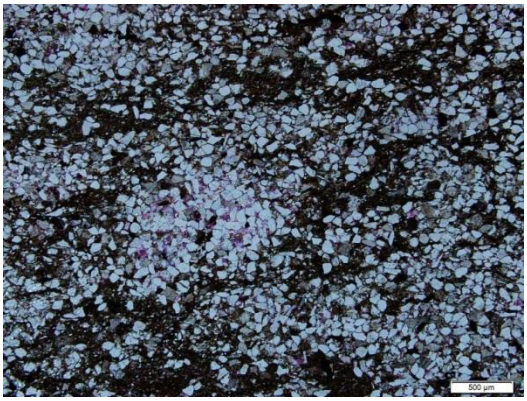


Fig. 4.1.3-1: Photomicrograph in PPL showing patches of porous and non-porous sandy sediment present in an unstratified muddy sandstone. Porosity (highlighted by pink epoxy) occurs where interstitial clays or clay patches are absent.

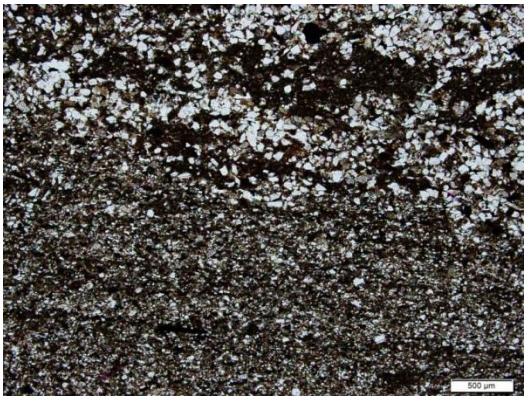


Fig. 4.1.3-2: Photomicrograph in PPL highlighting an interval of finely laminated (silty) clay-rich bedding observed in a largely unstratified muddy sandstone. Mixed clay-rich sand overlies the finely laminated layer.

4.1.4 DIAGENESIS:

Quartz overgrowths are the most common diagenetic feature observed in the samples and are typically found in porous sandy layers. Quartz overgrowths appear to be an important control on permeability in samples that have sandy layers or abundant sand content. Although overgrowths are rarely observed to completely cement sandy layers in the samples, they often significantly reduce original porosity and pore connectivity.

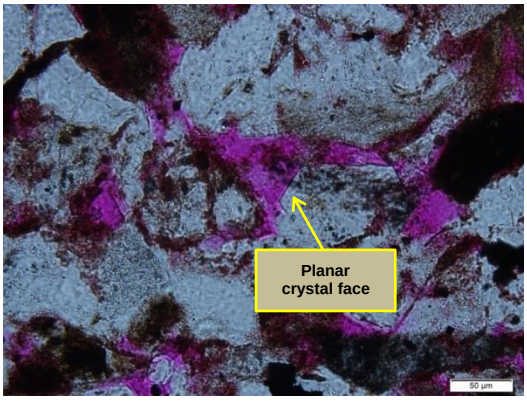


Fig. 4.1.4-1: Photomicrograph in PPL illustrating a partially cemented sandy layer. Overgrowths are sometimes difficult to distinguish from original grain edges, particularly on grains with faint outlines, but are readily apparent where overgrowths show planar (euhedral) crystal faces.

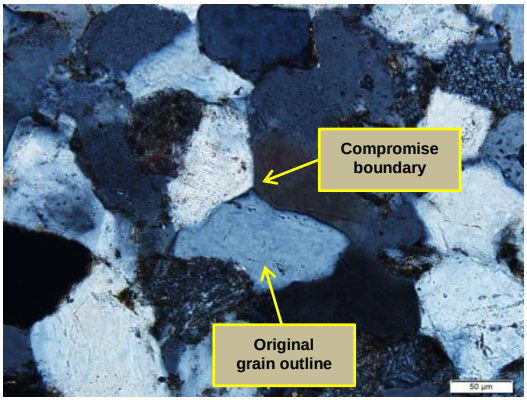


Fig. 4.1.4-2: Photomicrograph in PPL illustrating a completely cemented sandy bed. Compromise boundaries occur where overgrowth cements from three detrital grains terminate against each other in a triple junction, completely filling intergranular pore space.

4.1.5 ORGANIC MATTER & CLAYS:

Clays and organic matter typically occur together in the samples. Bedding-parallel organic matter strands are commonly observed with clay in samples that have distinct clay-rich layers and laminae, whereas finely-dispersed organics and pyrite typically occur together with clays in samples that have unstratified or convoluted fabrics. Clay rims or clay material enveloping detrital grains are occasionally observed in samples with distinct sandy layers. These clays generally have a minor detrimental impact on porosity and pore connectivity compared to clays in more thoroughly mixed or bioturbated samples.

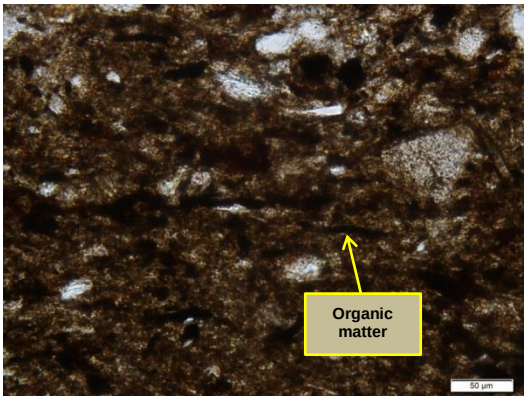


Fig. 4.1.5-1: Photomicrograph in PPL showing a finely laminated clay-rich bed present in a sandy mudstone. Organic matter occurs in wisps, strands, and streaks, most of which are bedding-parallel.

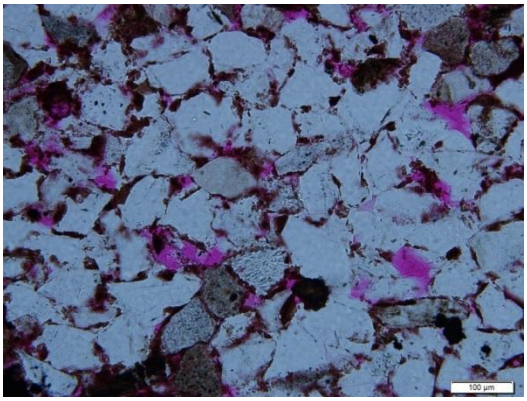


Fig. 4.1.5-2: Photomicrograph in PPL showing detrital grains (mostly quartz and chert) with clay mineral “coatings” observed in a muddy sandstone.

4.1.6 POROSITY & FRACTURING:

Significant porosity is typically observed in clay-poor sandy layers, burrow structures with sandy infills, and in patches of sand and silt with minimal clay. Microporosity is occasionally observed in clay-rich layers with common embedded detrital grains. This porosity may be artificial, due to thin section epoxy "bleeding" through clay mineral sheets and around the edges of detrital grains. Epoxy-filled fractures and partings are common in the samples, particularly in clay-rich layers and laminae. These fractures are likely artificial (due to sample cutting and polishing with water), and suggest that water-sensitive clay minerals are present in many of the samples.

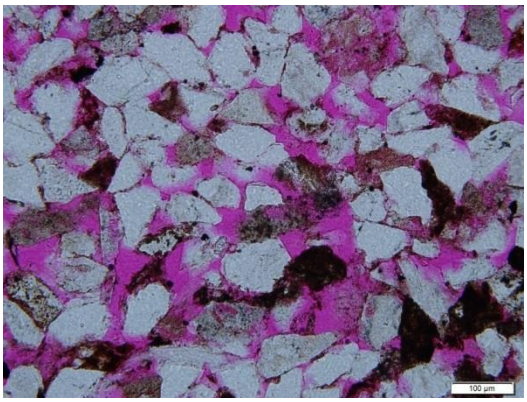


Fig. 4.1.6-1: Photomicrograph in PPL illustrating intergranular porosity (pink epoxy) within a clay-poor sandy layer. Some of this porosity may be artificial in instances where interstitial clay is common within pores.

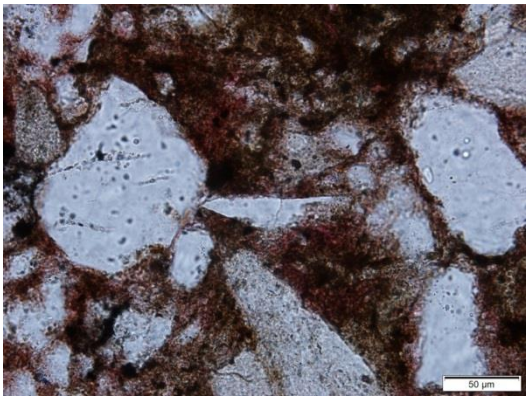


Fig. 4.1.6-2: Photomicrograph in PPL showing patchy microporosity observed in the matrix of a clayey sandstone. Note detrital quartz and chert grains embedded in the clay-rich matrix.

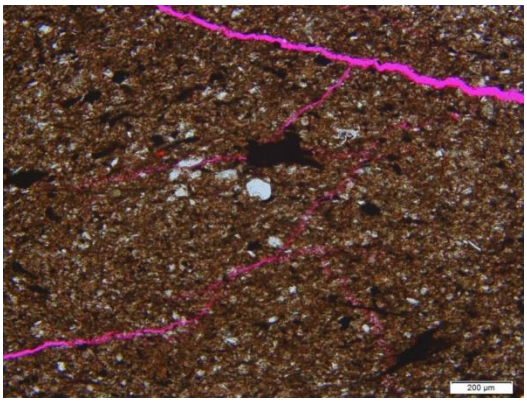


Fig. 4.1.6-3: Photomicrograph in PPL of a clay-rich horizon with common artificial fractures (filled with pink epoxy).

4.2 RESULTS

4.2.1 SAMPLE 13133

Sample ID	**13133**		
Sample type	**Core**	**UWI/Well**	**100/03-21-30-04W5/00**
Strat. Unit	**Cardium Formation**	**Depth**	**2208.65 m**

XRD/SRA results

Quartz (%)	Fsp (%)	Cb (%)	Clays (%)	Pyrite (%)
60.8	5.5	0.3	32.4	1

Composition (*in order of abundance*)

Grain size	%	Variety (%)	Variety (%)	Variety (%)	Variety (%)
sand	24	Quartz/chert (95)	Mica (3)	Feldspar (<4)	
silt	40	Quartz/chert (97)	Mica (3)		
clay	30	Clay mins (100)			
Cement	<1	Quartz (100)			
Bioclasts	0				
Organics	4	Amorphous (100)			
Opaques	2	Pyrite (100)			
	100				

*Intensively altered to clay minerals

^ Including bitumen

Sedimentary structures

Primary	Rare thin, discontinuous (reworked?) clay-rich and sandy laminae.
Biogenic	Appears heavily reworked.

Fractures	Common thin epoxy-filled fractures. Likely artificial.
Porosity	Rare, discontinuous microporosity. Largely non-porous.

Description

Bioturbated sandy mudstone comprised of subangular (common) to subrounded (rare) very fine silt- to very fine sand-sized (average grain size is coarse silt) detrital quartz (20-50%), chert (5-10%), mica (1-5%), and feldspar (1-2%). The sample largely appears to be unstratified, with the exception of two small sections of thin, discontinuous (reworked?) clay-rich and sandy laminae. Much of the rock is non-porous, with the exception of rare microporosity observed around isolated grain edges and in restricted clay-rich patches.

Thin Section Quality

Good.

Rock Classification

Sandy mudstone.

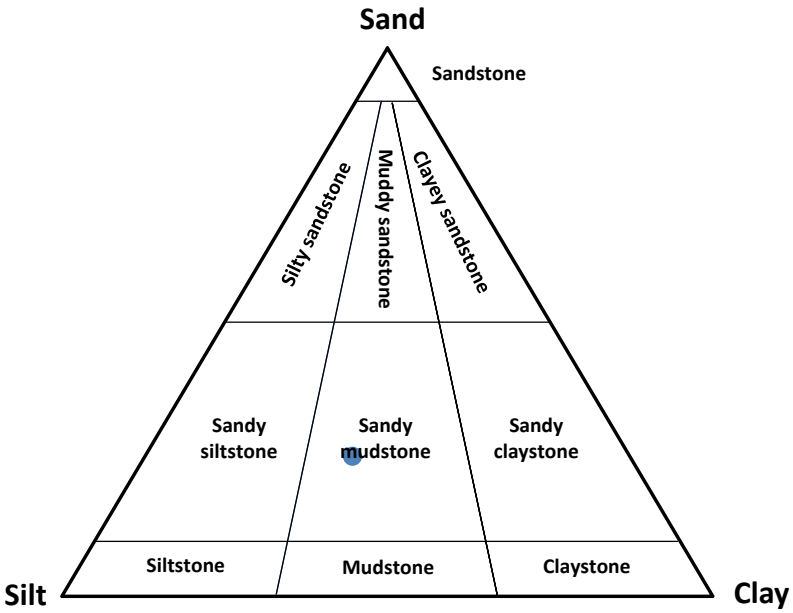


Fig. 4-1: Ternary plot showing the grain size composition of the sample based on the Wentworth scale (after Folk, 1954). Sample 13133 is classified as a sandy mudstone.



Fig. 4-2: Core photograph of sample 13133 from the Cardium Formation, well 100/03-21-30-04W5/00 (depth 2208.65 m). The thin section prepared from this sample was cut from the area marked with an X. The arrow indicates stratigraphic up-direction. Scale is in mm.

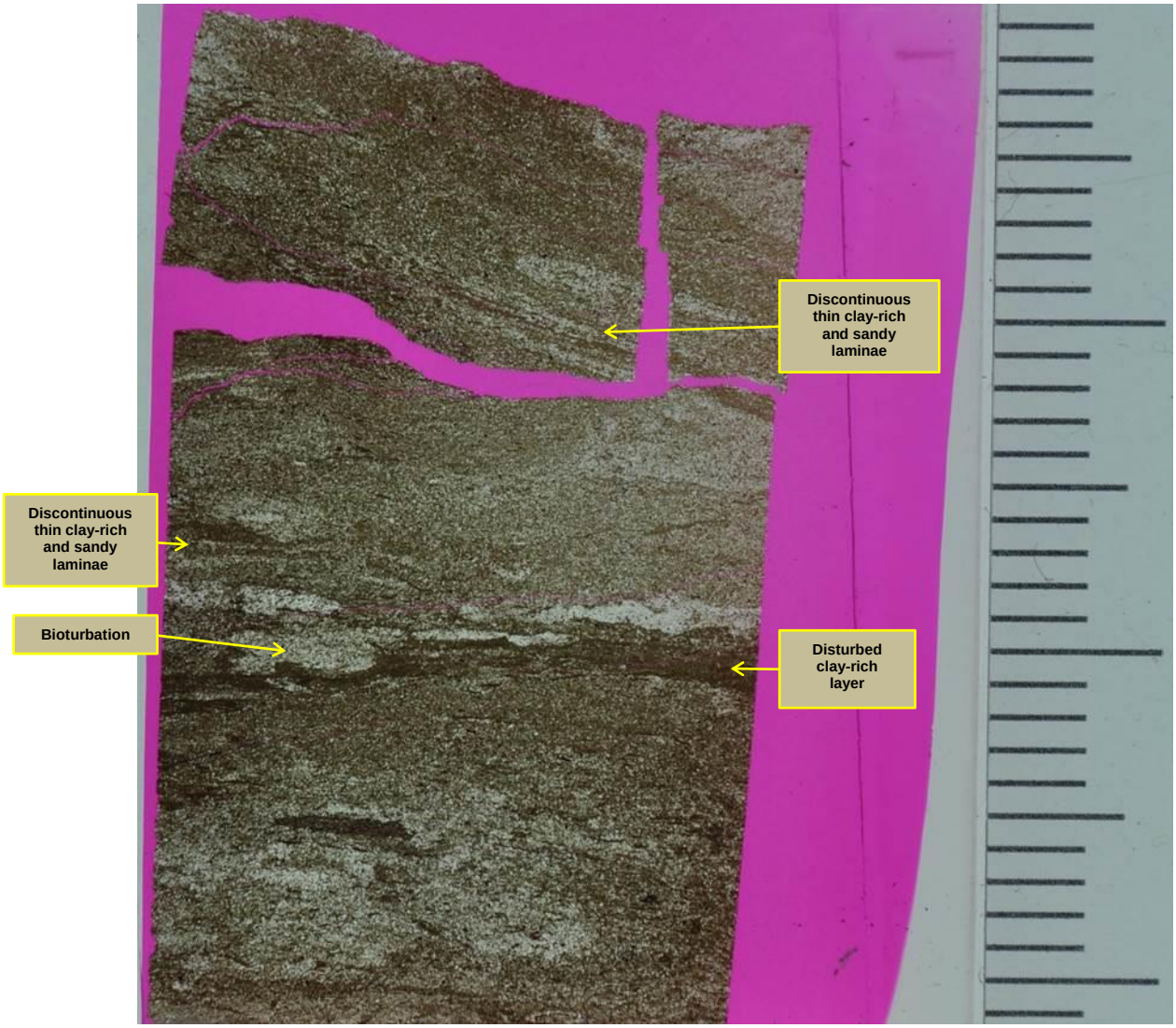


Fig. 4-3: Thin section photograph of sample 13133 from the Cardium Formation, well 100/03-21-30-04W5/00 (depth 2208.65 m). The sample is a bioturbated sandy mudstone with both parallel and slightly angular bedding. Some of the sediment layers appear convoluted likely due to bioturbation activity. Few (discontinuous) clay-rich and silty/sandy laminae are visible. Scale is in mm.

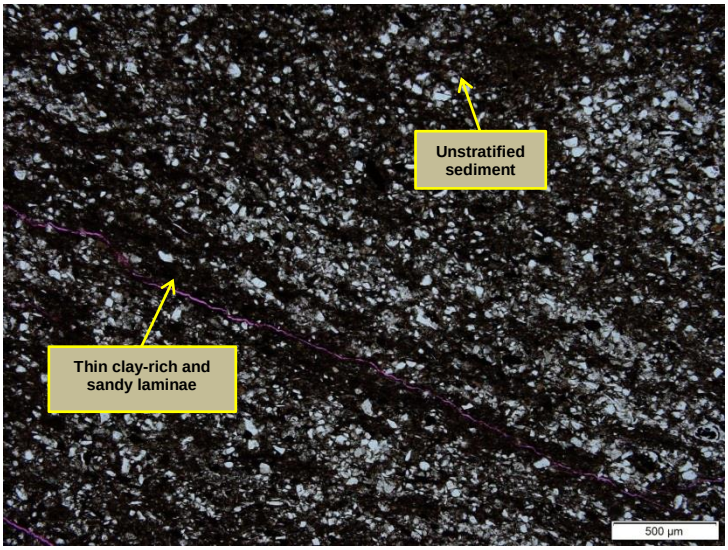


Fig. 4-4: Photomicrograph in PPL showing an overview of the silty mudstone where some thinly bedded to laminated layers are present (angular bedding). Much of the sample shows signs of bioturbation (feeding trails, etc) which resulted in unstratified or mixed sediment; however, rare discontinuous clay-rich and silt-rich (minor very fine-sand) laminae are observed, possibly representing minimally reworked or partially preserved remnants of original bedforms. An artifical fracture filled with pink epoxy is present within the finer-grained material.

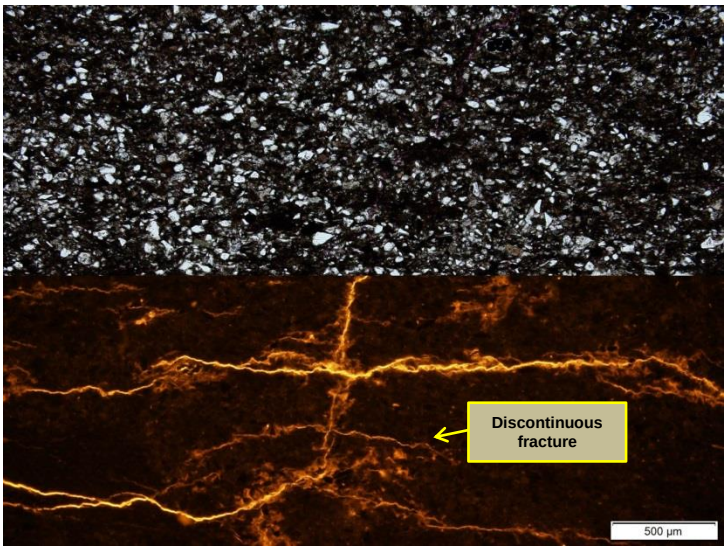


Fig. 4-5: Photomicrograph (upper half in PPL, lower half in UV light) showing common thin horizontal and vertical fractures observed in the mudstone. These fractures are often not visible in transmitted light, and may be artificial or enhanced during thin section preparation. Numerous discontinuous fractures are observed to emanate from larger partings that occur in the rock.

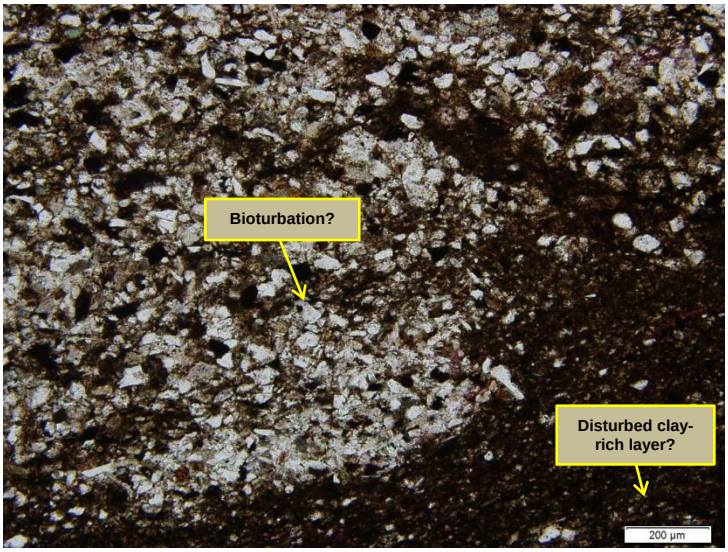


Fig. 4-6: Photomicrograph in PPL showing a possible bioturbation feature observed in the mudstone. The silt-rich lenticular feature embedded in the clay-rich layer may be part of a burrow that disturbed the original continuity of the horizon.

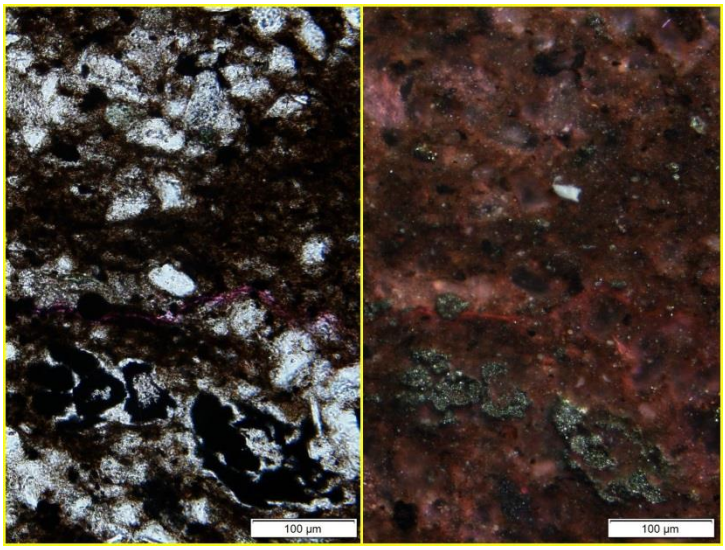


Fig. 4-7: Photomicrograph (left side in PPL, right side in reflected light; same field of view) showing finely dispersed and framboidal pyrite (gold colour in reflected light) present in the mudstone. Pyrite accounts for ~2% of the total composition but appears concentrated in patches and therefore may partly be derived from fecal remains.

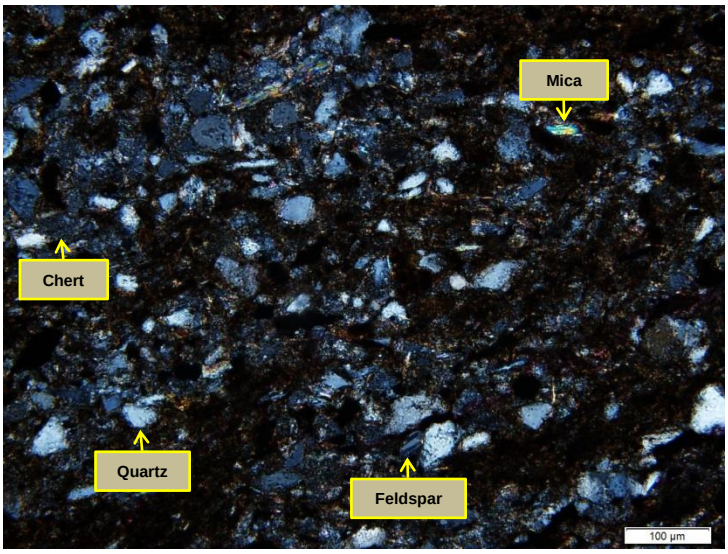


Fig. 4-8: Photomicrograph in XPL showing a typical example of subangular (common) to subrounded (rare), very fine silt- to very fine sand-sized (average grain size is coarse silt) detrital quartz (20-50%), chert (5-10%), mica (1-5%), and feldspar (1-2%). The remainder of the sample is composed of opaques and clay material.

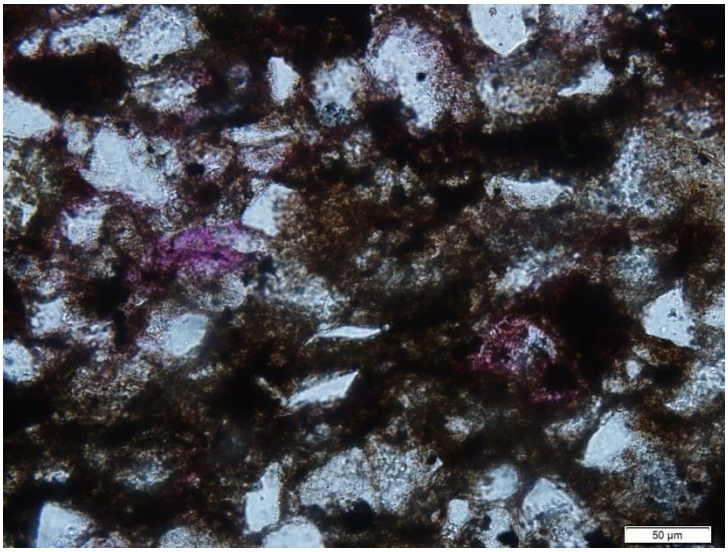


Fig. 4-9: Photomicrograph in PPL showing an example of rare microporosity. Much of the microporosity occurs around isolated grain edges and within restricted patches of clay.

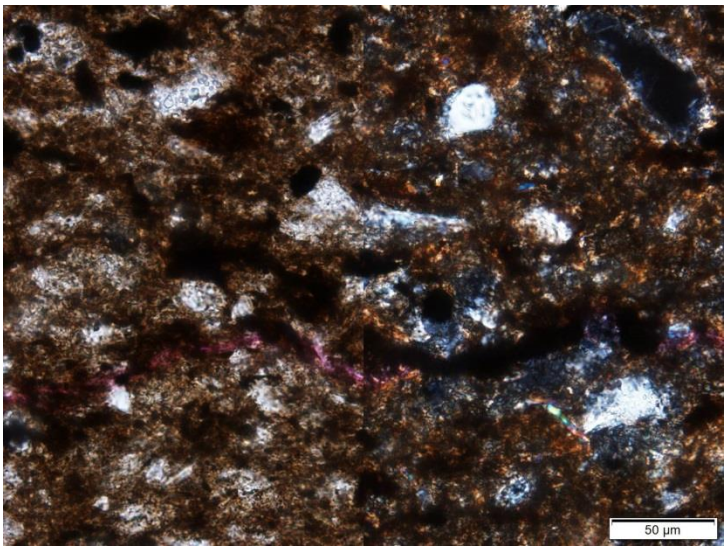


Fig. 4-10: Photomicrograph in PPL (left) an XPL (right) illustrating silt-size quartz and chert grains embedded within the clay-rich matrix (brownish). Clays reach ~30% of the total composition. Pyrite can also occur within short streaks or “trails” associated with organic matter. Note rare mica lathes (high birefringence in XPL) and some organic material.

4.2.2 SAMPLE 13135

Sample ID	**13135**		
Sample type	**Core**	**UWI/Well**	**100/03-21-30-04W5/00**
Strat. Unit	**Cardium Formation**	**Depth**	**2219.95 m**

XRD/SRA results

Quartz (%)	Fsp (%)	Cb (%)	Clays (%)	Pyrite (%)
76	3.8	0.4	19.4	0.4

Composition (*in order of abundance*)

Grain size	%	Variety (%)	Variety (%)	Variety (%)	Variety (%)
sand	63	Quartz/chert (94)	Feldspar (4)	Mica (2)	
silt	10	Quartz/chert (99)	Mica (1)		
clay	20	Clay mins (100)			
Cement	5	Quartz (100)			
Bioclasts	<1	Foraminifera (100)			
Organics	2	Amorphous (100)			
Opaques	<1	Pyrite (100)			
	100				

*Intensively altered to clay minerals

^ Including bitumen

Sedimentary structures

Primary	None apparent.
Biogenic	Appears heavily bioturbated.

Fractures	Common thin epoxy-filled fractures. Likely artificial.
Porosity	Discontinuous microporosity in areas of the rock with abundant clay matrix.

Description

Bioturbated clayey sandstone comprised of subangular (common) to subrounded (rare) very fine silt- to fine sand-sized (average grain size is very fine sand) detrital quartz (30-60%), chert (6-18%), feldspar (1-3%), and mica (1-2%). The rock does not show any primary sedimentary structures, suggesting that the original sediment may have been heavily reworked.

Thin Section Quality

Fair. Some exposed thin section glass.

Rock Classification

Clayey sandstone.

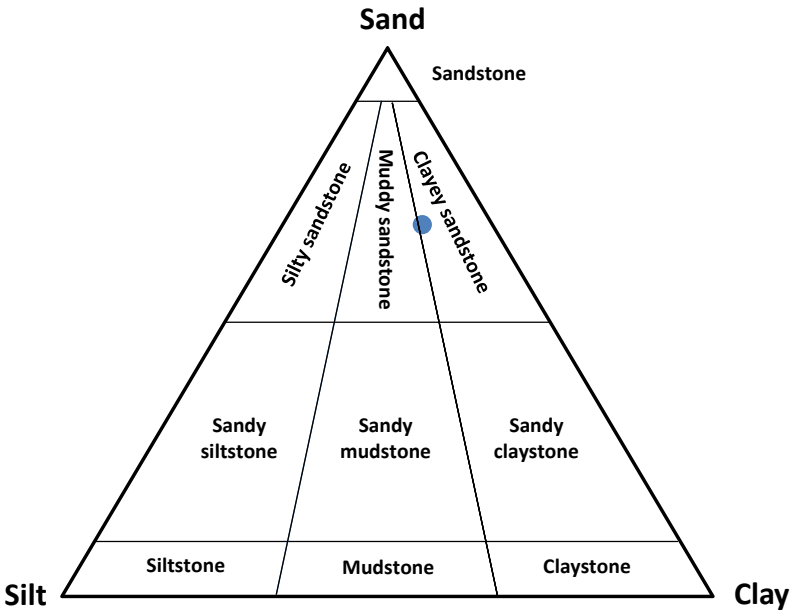


Fig. 4-11: Ternary plot showing the grain size composition of the sample based on the Wentworth scale (after Folk, 1954). Sample 13135 is classified as a clayey sandstone.



Fig. 4-12: Core photograph of sample 13135 from the Cardium Formation, well 100/03-21-30-04W5/00 (depth 2219.95 m). The thin section prepared from this sample was cut from the area outlined in black marker. The arrow indicates stratigraphic up-direction. Scale is in mm.



Fig. 4-13: Thin section photograph of sample 13135 from the Cardium Formation, well 100/03-21-30-04W5/00 (depth 2219.95 m). The sample is a bioturbated clayey sandstone. The sample lacks bedding features but sediment disturbance indicates that the original sediment has been heavily reworked by burrowing organisms. Scale is in mm.

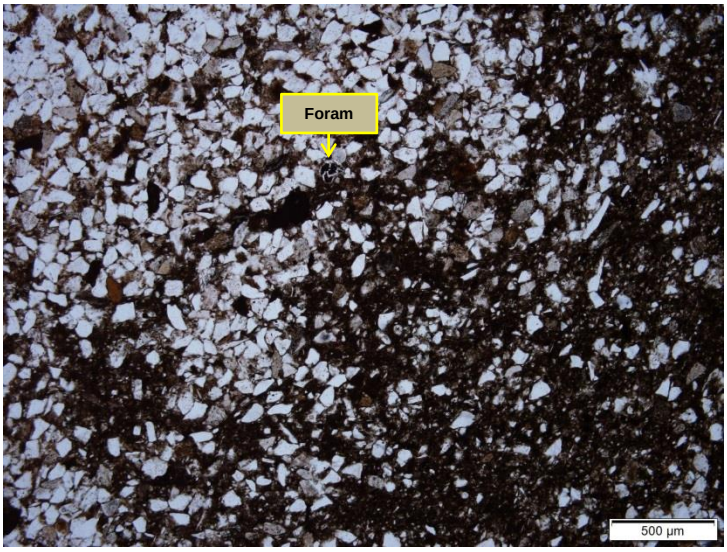


Fig. 4-14: Photomicrograph in PPL showing an overview of the sample, classified as a clayey sandstone. Abundant very fine to fine sand-sized quartz and feldspar grains are observed with patches of clay-rich material. The sample lacks primary sedimentary structures. The patchy nature of unstratified areas of sand-rich (light-coloured) and clay-rich (dark-coloured) sediment indicates strong sediment mixing. A single foraminiferan test is observed in the sample.

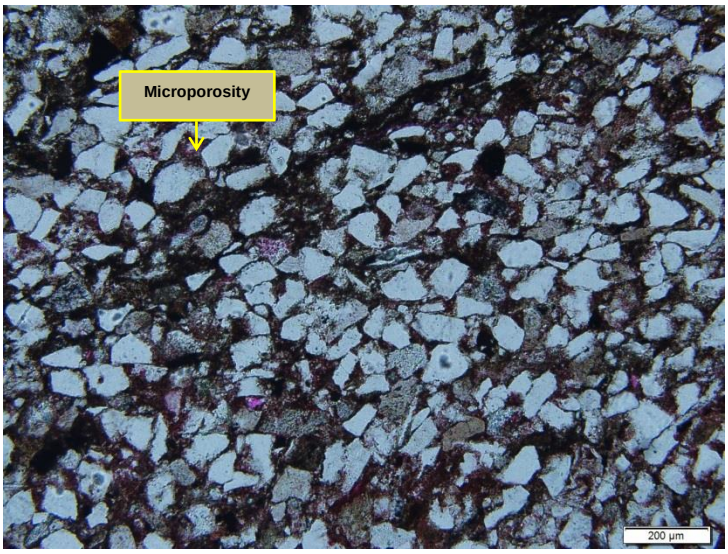


Fig. 4-15: Photomicrograph in PPL showing relative abundances of sand- (~63%), silt- (~10%), and clay-sized (~20%) particles. Subangular fine sand-sized grains are the most abundant. Patchy microporosity is observed in areas of the sample with abundant clay matrix.

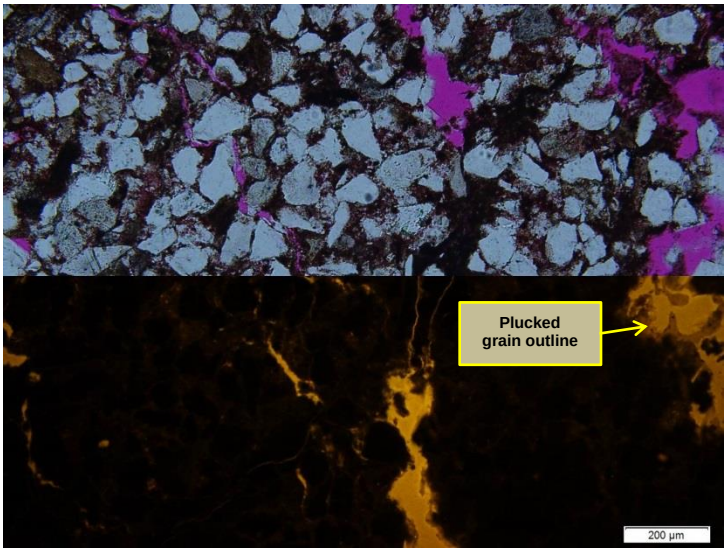


Fig. 4-16: Photomicrograph (upper half in PPL, lower half in UV light) showing epoxy-filled (pink) fractures and outlines of plucked grains. These features are likely artificial byproducts of sample preparation, and suggest that water-sensitive clay minerals may be present.

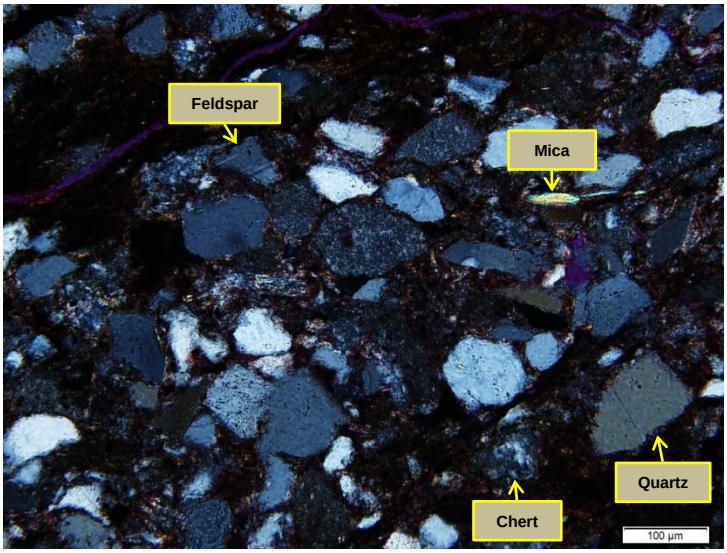


Fig. 4-17: Photomicrograph in XPL showing subangular (common) to subrounded (rare) very fine silt- to fine sand-sized (average grain size is very fine sand) detrital quartz (30-60%), chert (6-18%), feldspar (1-3%), and mica (1-2%) within the argillaceous matrix. Some feldspars exhibit polysynthetic twinning. Chert grains are composed of microcrystalline quartz.

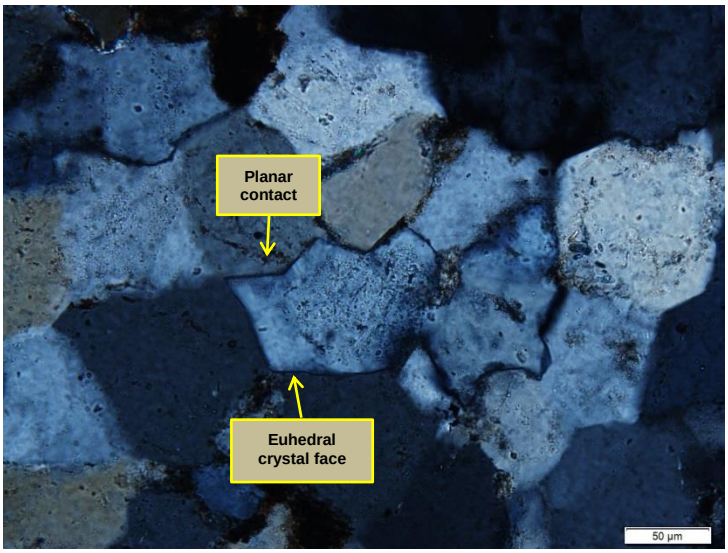


Fig. 4-18: Photomicrograph in XPL showing a patch where tight grain-grain contacts are present. Pervasive quartz overgrowth and quartz cementation is observed. Although dust rims are only faintly visible on the quartz particles, planar contacts between euhedral crystal faces are characteristic of overgrowth cements. Quartz cement accounts for ~5% of the total composition.

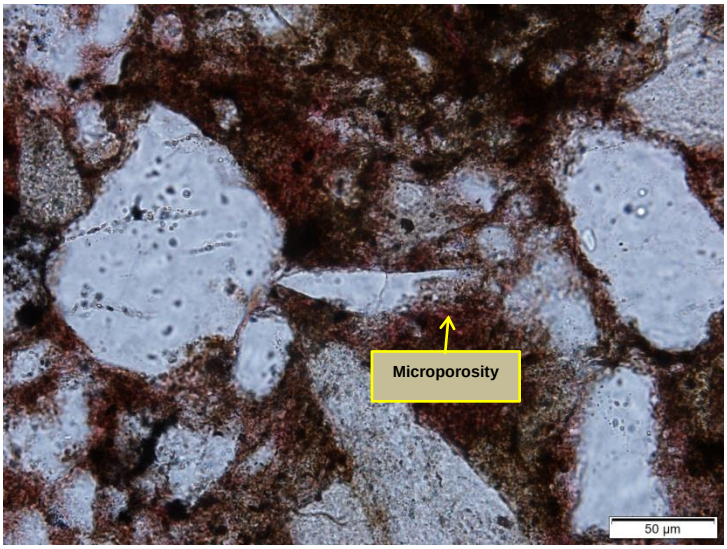


Fig. 4-19: Photomicrograph in PPL showing details of patchy microporosity (filled with pink epoxy) observed within the clay-rich matrix. Some of this porosity may be artificial, caused by epoxy “bleeding” through patches of clay and around grain edges.

4.2.3 SAMPLE 13139

Sample ID	**13139**		
Sample type	**Core**	**UWI/Well**	**100/03-21-30-04W5/00**
Strat. Unit	**Cardium Formation**	**Depth**	**2227.8 m**

XRD/SRA results

Quartz (%)	Fsp (%)	Cb (%)	Clays (%)	Pyrite (%)
64.7	4.8	1	29	0.5

Composition (*in order of abundance*)

Grain size	%	Variety (%)	Variety (%)	Variety (%)	Variety (%)
sand	8	Quartz/chert (100)			
silt	58	Quartz/chert (97)	Mica (3)		
clay	30	Clay mins (100)			
Cement	0				
Bioclasts	<1	Foraminifera (100)			
Organics	4	Amorphous (100)			
Opaques	<1	Pyrite (100)			
	100				

*Intensively altered to clay minerals

^ Including bitumen

Sedimentary structures

Primary	None apparent.
Biogenic	Appears reworked.

Fractures	Common thin epoxy-filled fractures. Likely artificial.
Porosity	None apparent.

Description

Bioturbated mudstone comprised of subangular (common) to subrounded (rare) very fine silt- to very fine sand-sized (average grain size is coarse silt) detrital quartz (25-50%), chert (5-8%), and mica (1 2%). The texture of this apparently unstratified rock is characterized by amorphous areas of clay- and silt-rich sediment. Several clay-rich lenses that may be burrow structures are observed in the mudstone.

Thin Section Quality

Fair. The thin section was broken during preparation and is glued together with an additional glass plate.

Rock Classification

Mudstone.

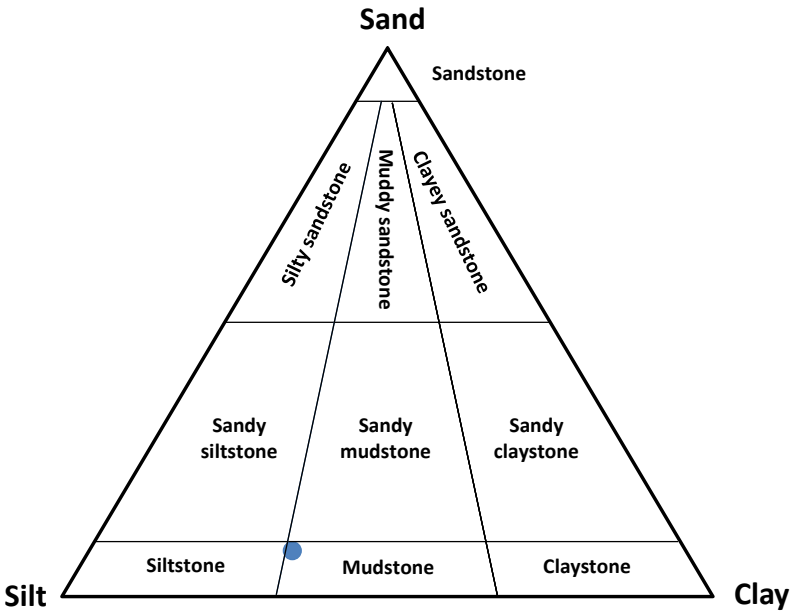


Fig. 4-20: Ternary plot showing the grain size composition of the sample based on the Wentworth scale (after Folk, 1954). Sample 13139 is classified as a mudstone.

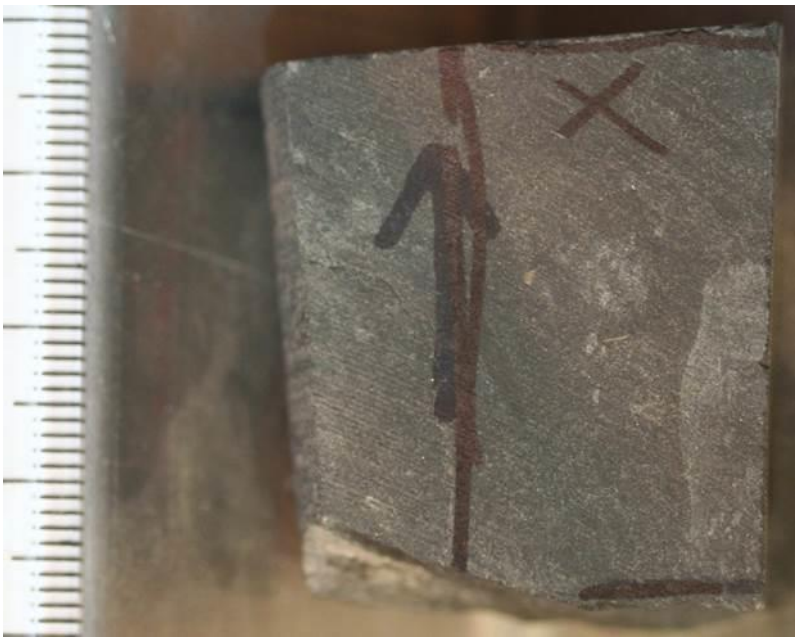


Fig. 4-21: Core photograph of sample 13139 from the Cardium Formation, well 100/03-21-30-04W5/00 (depth 2227.80 m). The thin section prepared from this sample was cut from the area outlined in black marker. The arrow indicates stratigraphic up-direction. Scale is in mm.

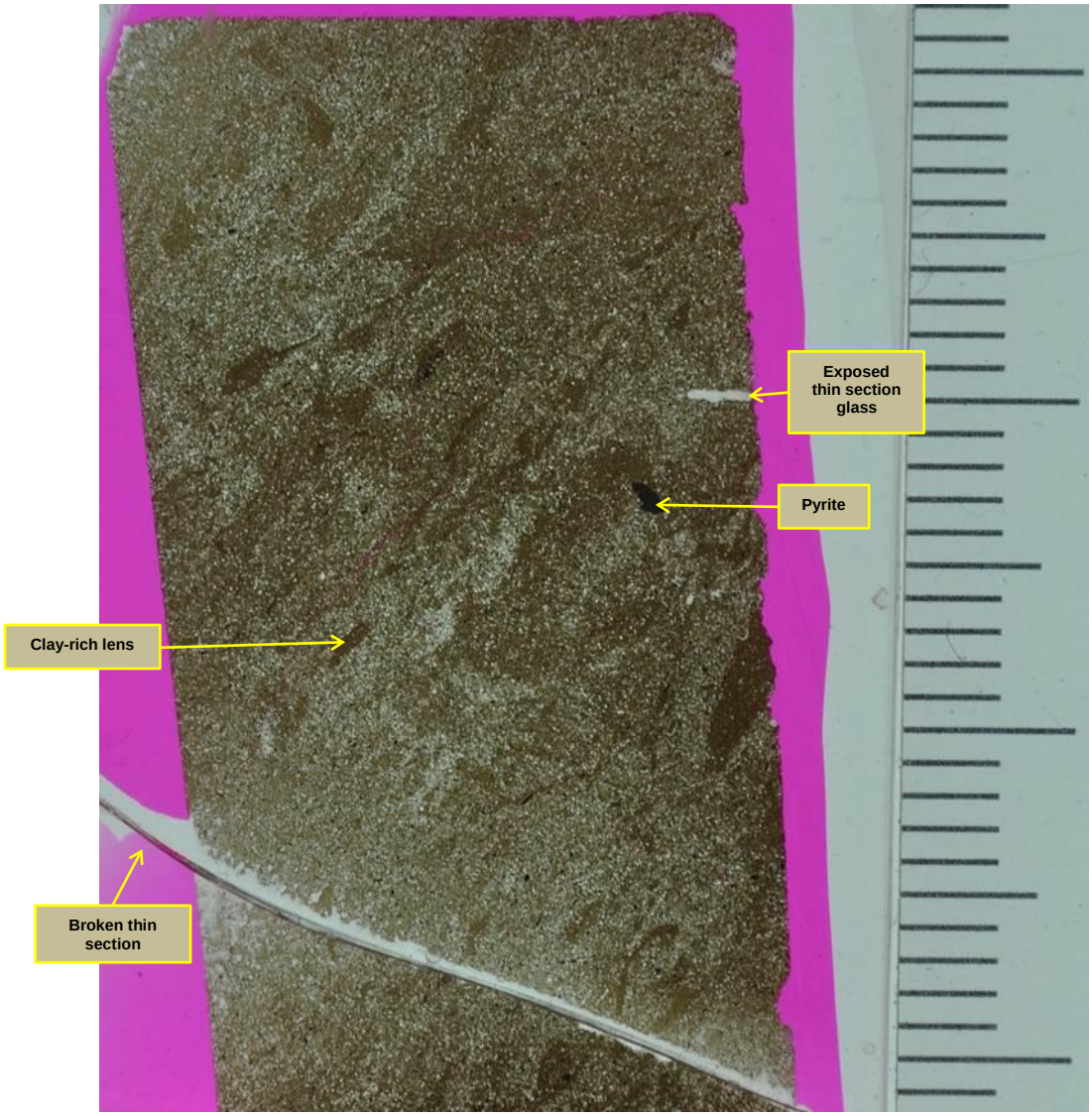


Fig. 4-22: Thin section photograph of sample 13139 from the Cardium Formation, well 100/03-21-30-04W5/00 (depth 2227.8 m). The sample is a heavily bioturbated mudstone. This sample lacks primary sedimentary structures, but contains several clay-rich wisps, lenses and convoluted patches that indicate marked sediment mixing, most of which is due to bioturbation (burrow structures). Scale is in mm.

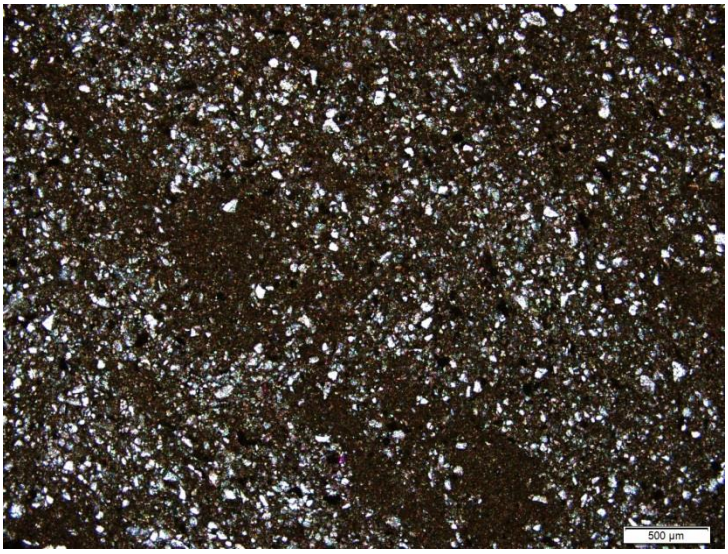


Fig. 4-23: Photomicrograph in PPL showing an overview of the mudstone. The sample is unstratified with irregularly-shaped patches of clay-rich and silt-rich sediment. Some very fine sand-size grains are also present. The lack of primary sedimentary structures is due to heavy sediment mixing (bioturbation).

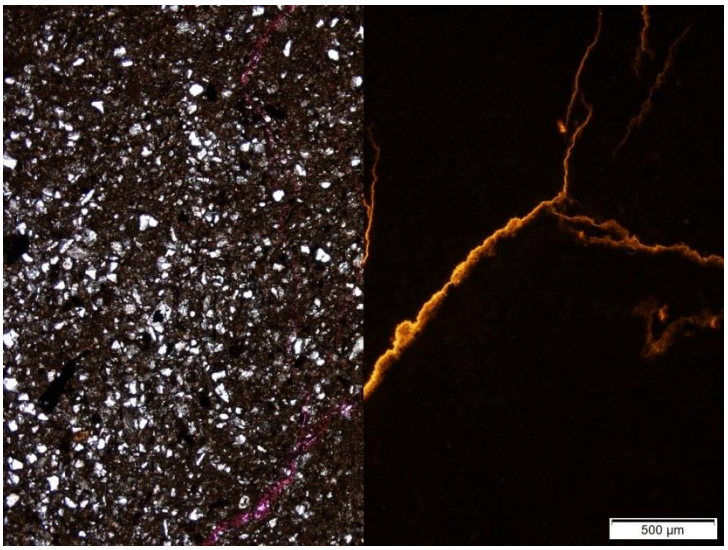


Fig. 4-24: Photomicrograph (left half in PPL, right half in UV light) showing an epoxy-filled fracture, likely created (artificial) or enhanced during thin section preparation.

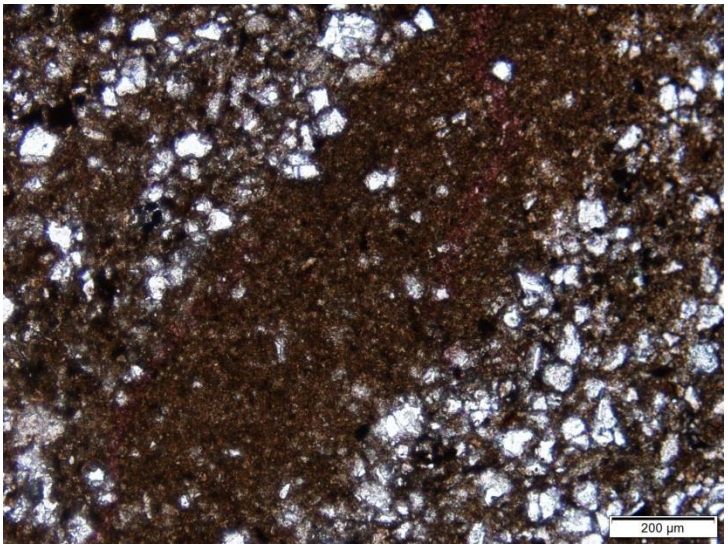


Fig. 4-25: Photomicrograph in PPL illustrating one of several clay lenses (possible burrow structures?) observed in the sample. These clay-rich lenticular and patchy features contain fewer detrital grains and less organic matter than the surrounding sediment.

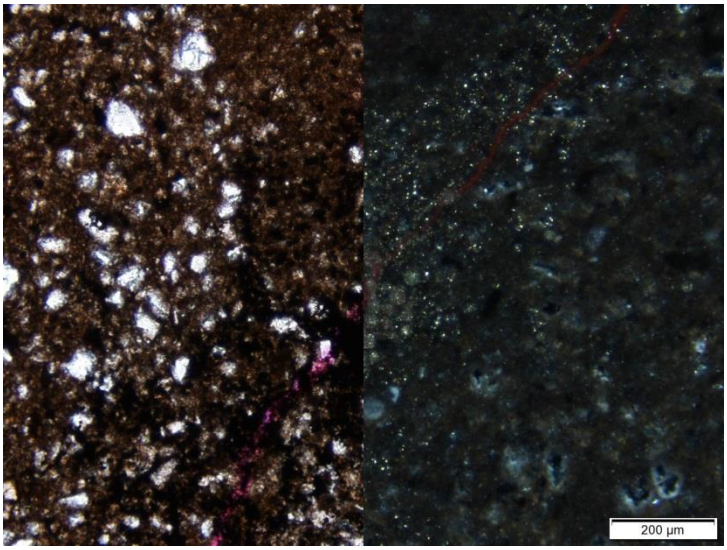


Fig. 4-26: Photomicrograph (left half in PPL, right half in reflected light) showing pyrite mineralization (gold colour in reflected light) concentrated within a fine-grained clay-rich sediment package. An epoxy-filled fracture (artificial) is observed cutting across this feature.

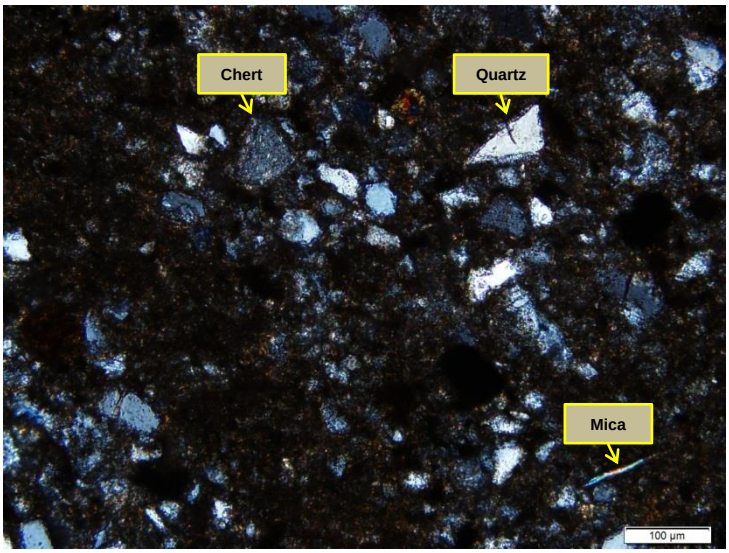


Fig. 4-27: Photomicrograph in XPL showing a typical example of subangular (common) to subrounded (rare) very fine silt- to very fine sand-sized (average grain size is coarse silt) detrital quartz (25-50%), chert (5-8%), and mica (1-2%). The muscovite lathes are randomly oriented and have high birefringent colours. The very fine sand grain shows a thin rim of quartz overgrowth.

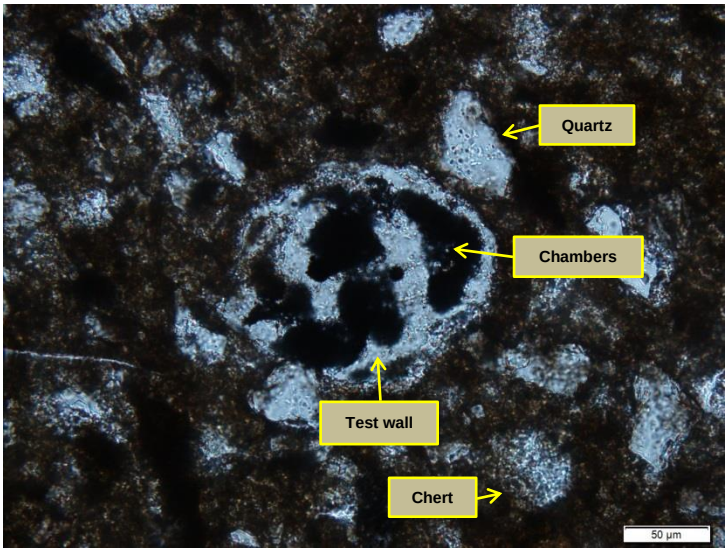


Fig. 4-28: Photomicrograph in PPL showing a rare (4 total) milioline foraminiferan observed in the mudstone. The wall of this imperforate test is composed of microcrystalline quartz (recrystallized) and the chambers are filled with opaques (i.e. pyrite). Subangular coarse silt-size quartz and chert grains are present in the clay-rich sediment surrounding the microfossil.

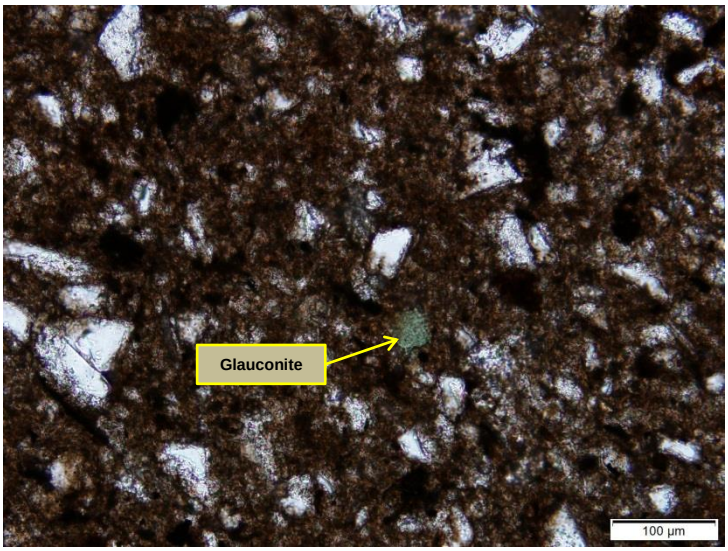


Fig. 4-29: Photomicrograph in PPL detailing the fine-grained, argillaceous matrix. Total clay content is estimated at ~30% (average). Very fine-silt to rare sand-sized grains are observed embedded within the matrix. Some organic matter (estimated at ~4%) is also associated with the clay-rich matrix. Note rare glauconite grain (green colour).

4.2.4 SAMPLE 13144

Sample ID	**13144**		
Sample type	**Core**	**UWI/Well**	**102/14-25-039-05W5/00**
Strat. Unit	**Cardium Formation**	**Depth**	**1803.89 m**

XRD/SRA results

Quartz (%)	Fsp (%)	Cb (%)	Clays (%)	Pyrite (%)
61.5	4.4	0.5	32.6	1

Composition (*in order of abundance*)

Grain size	%	Variety (%)	Variety (%)	Variety (%)	Variety (%)
sand	33	Quartz/chert (90)	Mica (6)	Feldspar (<4)	
silt	26	Quartz/chert (97)	Mica (3)		
clay	33	Clay mins (100)			
Cement	<1	Quartz (100)			
Bioclasts	0				
Organics	8	Amorphous (100)			
Opaques	<1	Pyrite (100)			
	100				

*Intensively altered to clay minerals

^ Including bitumen

Sedimentary structures

Primary	Finely laminated sandy and clay-rich bedding.
Biogenic	Heavy bioturbation, including possible *Planolites* burrows.

Fractures	Occasional thin epoxy-filled fractures. Likely artificial.
Porosity	Minor (~5%) intergranular porosity associated with a single burrow structure.

Description

Heavily bioturbated sandy mudstone comprised of subangular (common) to subrounded (rare) very fine silt- to fine sand-sized (average grain size very fine sand) detrital quartz (40-55%), chert (10-15%), mica (1-5%), and feldspar (<4%). Whereas the lower half of the rock appears to be pervasively bioturbated, with no primary sedimentary structures visible, the upper half shows finely laminated clay-rich and sandy bedding with occasional burrow features.

Thin Section Quality

Moderate. Some exposed thin section glass.

Rock Classification

Sandy mudstone.

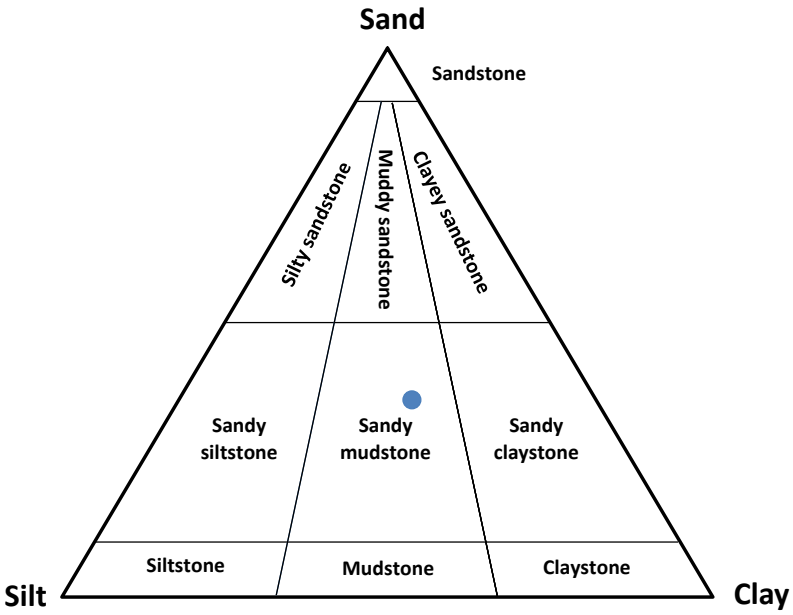


Fig. 4-30: Ternary plot showing the grain size composition of the sample based on the Wentworth scale (after Folk, 1954). Sample 13144 is classified as a sandy mudstone.

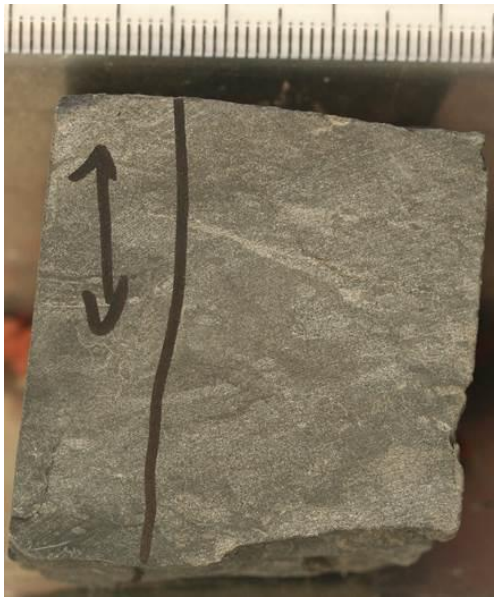


Fig. 4-31: Core photograph of sample 13144 from the Cardium Formation, well 102/14-25-039-05W5/00 (depth 1803.89 m). The thin section prepared from this sample was cut from the area outlined in black marker. Sediment composition varies from muddy (lower left) to very fine sandy (lenticular light-coloured streak in the centre) and original bedding structures are destroyed due to heavy mixing (i.e. bioturbation). The sample was received with no up direction but has been placed according to orientation interpretations based on the thin section. Scale is in mm.

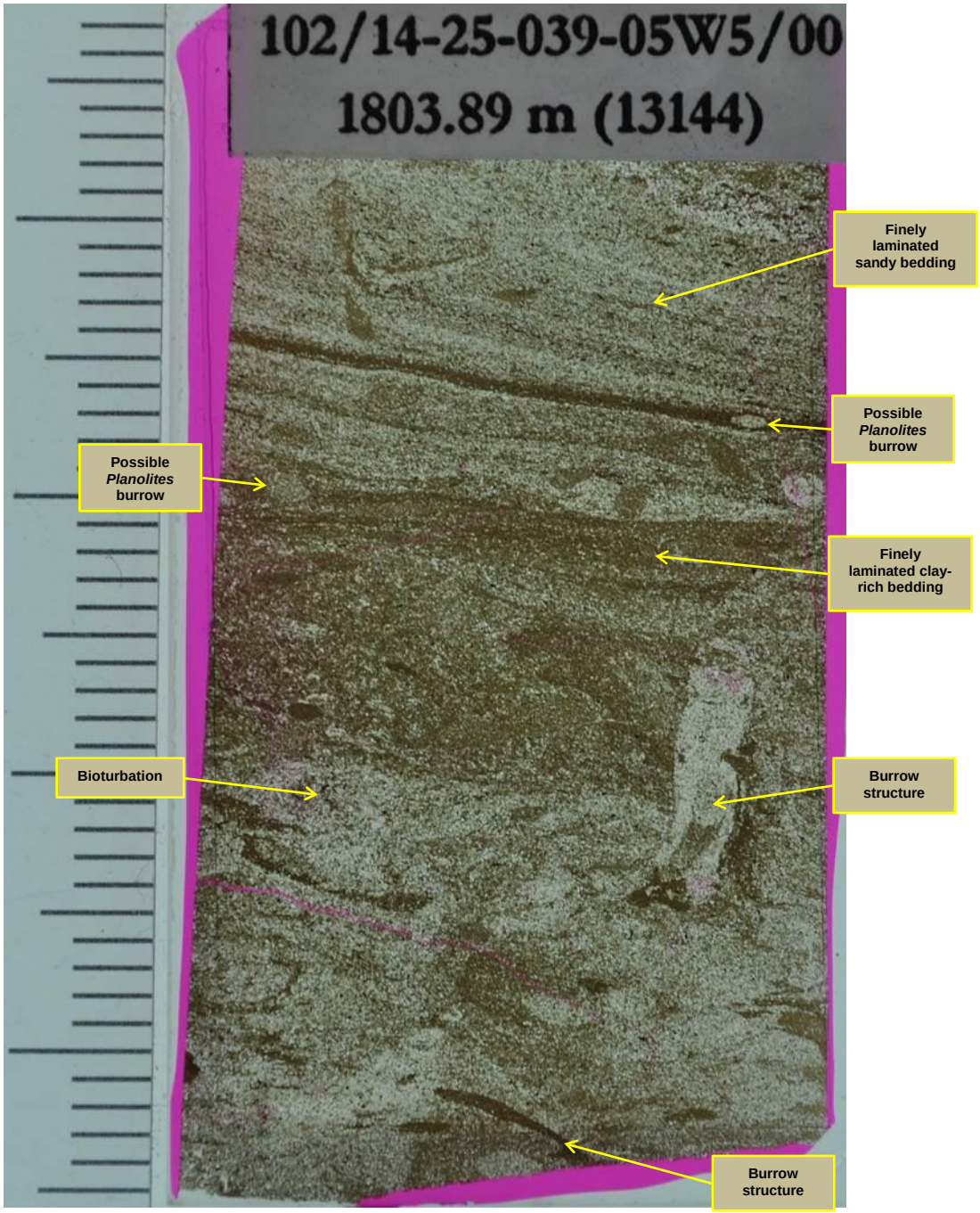


Fig. 4-32: Thin section photograph of sample 13144 from the Cardium Formation, well 102/14-25-039-05W5/00 (depth 1803.89 m). The sample is a heavily bioturbated sandy mudstone with finely-laminated sandy and clay-rich bedding. The lower (as shown) half of the sample is completely mixed (by burrowing organisms), with no primary sedimentary structures visible. The depositional way up was not indicated on the received sample but was determined based on sedimentary structures. Scale is in mm.

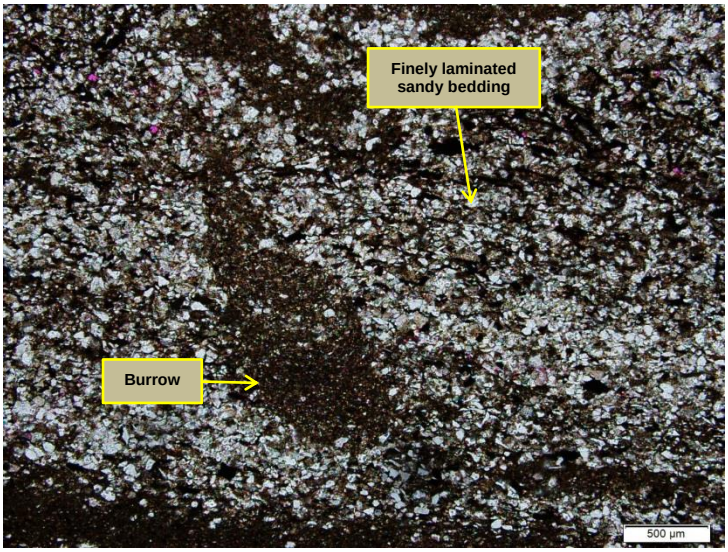


Fig. 4-33: Photomicrograph in PPL showing an overview from the upper half of the sample illustrating thinly laminated medium to coarse silt- and very fine sand-sized particles with some clay matrix. Sub-vertical elongate clay-rich patches represent infilled burrow structures. Despite the bioturbation activity, original bedding structures are easily recognized in this upper part of the sample, whereas bedding structures in the lower part of the sample are absent due to heavy sediment mixing.

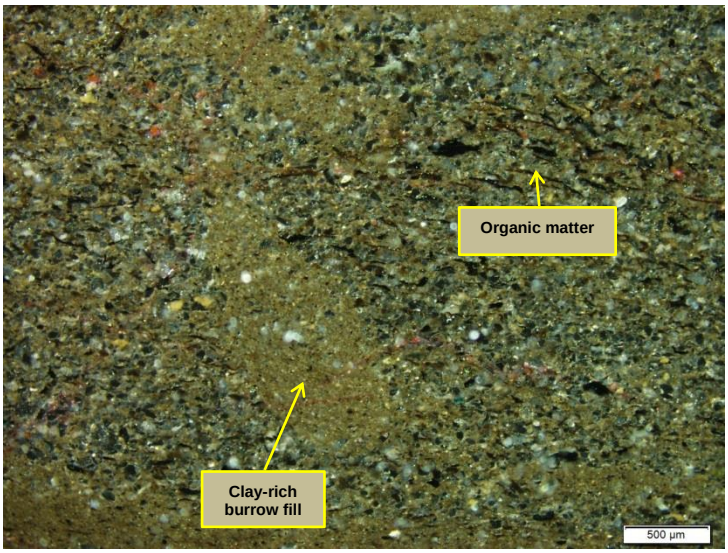


Fig. 4-34: Photomicrograph in reflected light showing bedding-parallel organic matter (opaques) and biogenic sediment sorting (same field of view as Figure 4-33). Strands and wisps of solid organic matter are common in the silty-sandy laminae and are mostly oriented parallel or sub-parallel along the bedding plane. Within the burrowing structures, organics are rare or absent (mostly pyrite), especially in the well-sorted, clay-rich or silty (possible *Planolites* burrows, see Figure 4-32) infills.

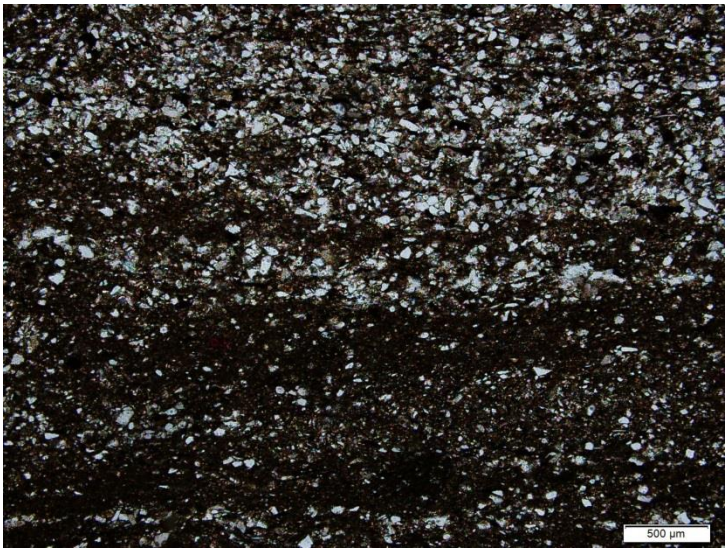


Fig. 4-35: Photomicrograph in PPL showing another overview of the upper part of the sample illustrating undisturbed fine clay-rich and silty laminae. Clay abundance in the fine-grained opaque-rich laminae is ~40-60%, but much lower in the silt-rich laminae. On average, clay-sized particles comprise ~30-35% of the sample, with sand- and silt-sized particles accounting for ~33% and ~26%, respectively.

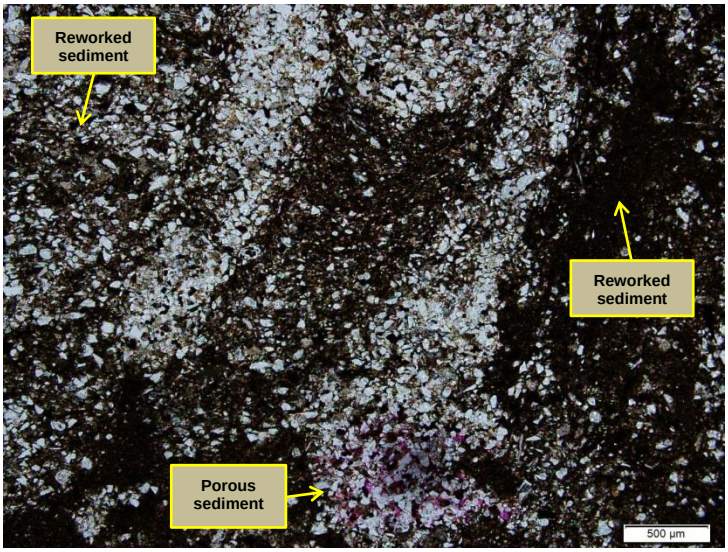


Fig. 4-36: Photomicrograph in PPL showing a sub-vertically-oriented burrowing structure observed within the lower half of the sample. Reworked fine-grained and opaque-rich sediments surround the burrow, suggesting that this portion of the rock has been pervasively bioturbated. A patch of porous sediment is visible near the bottom of the burrow (a similar porous feature also occurs near the top of the burrow).

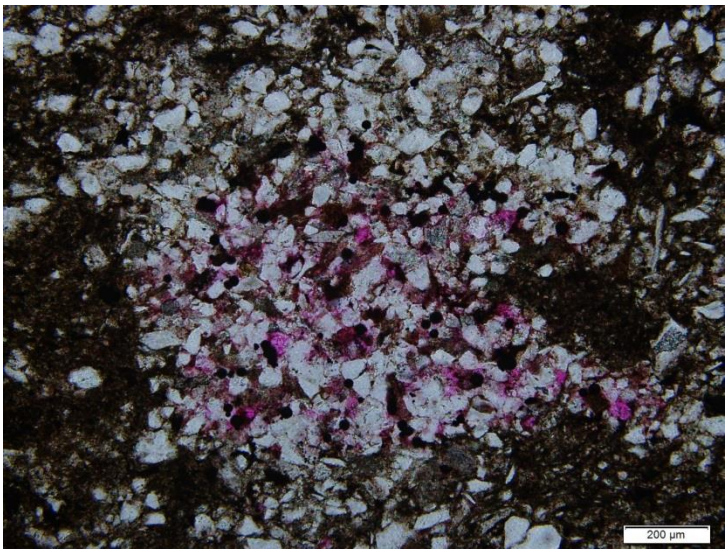


Fig. 4-37: Photomicrograph in PPL detailing the patch of porous sediment shown in Figure 4-36. The patch has much lower clay content and ~5% intergranular porosity, in contrast to the remainder of the sediments where clays are common and porosity is very low.

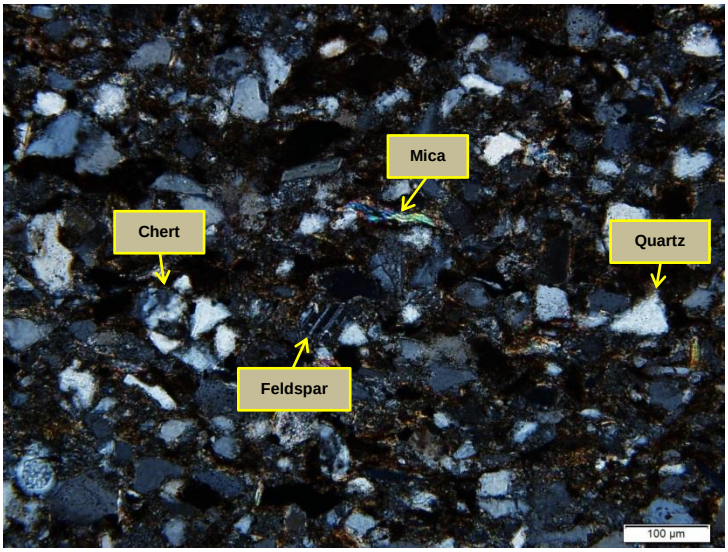


Fig. 4-38: Photomicrograph in XPL showing subangular (common) to subrounded (rare) very fine silt- to fine sand-sized (average grain size is very fine sand) detrital quartz (40-55%), chert (10-15%), mica (1-5%), and feldspar (<4%) observed in a finely laminated silty/sandy bed. Note a mica lathe (high birefringent colours), bent due to sediment compaction, and an albite grain with polysynthetic twinning in the centre of the image.

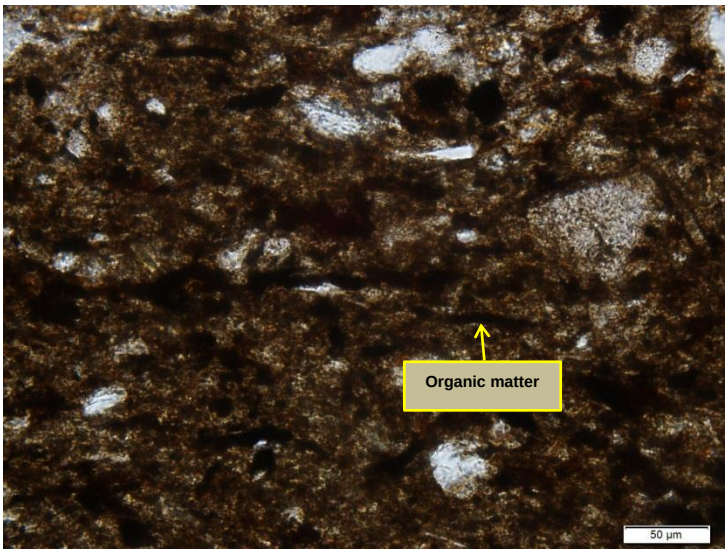


Fig. 4-39: Photomicrograph in PPL detailing a finely laminated clay-rich bed present in the upper half of the sample. Organic matter occurs in wisps, strands, or streaks (mostly bedding-parallel), and comprises ~8% of the finely laminated clay-rich and silty/sandy beds.

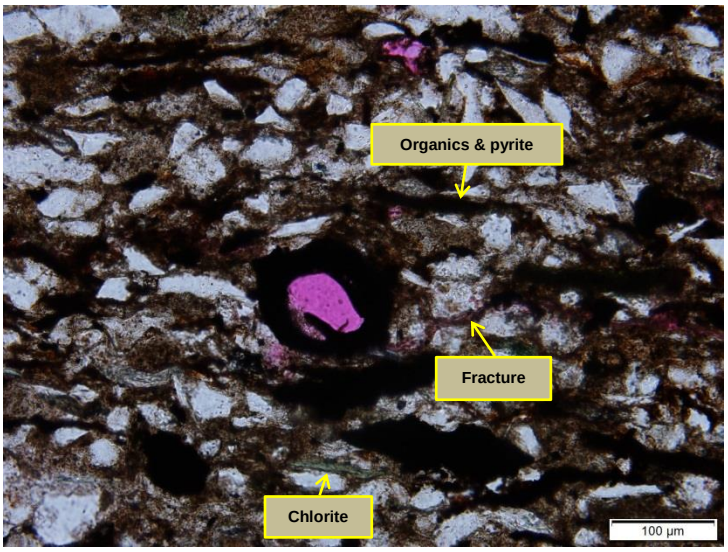


Fig. 4-40: Photomicrograph in PPL detailing silt to sand size grains (light-coloured) embedded within the argillaceous matrix. The center of the image shows an oversized pore (pink-epoxy) rimmed with pyrite, which possibly represents a former microfossil. Several smaller pores and a thin micro-fracture are also observed. Organic matter and pyrite occur as numerous short, lenticular streaks. A rare detrital chlorite grain (green colour) is also present.

4.2.5 SAMPLE 13147

Sample ID	**13147**		
Sample type	**Core**	**UWI/Well**	**102/14-25-039-05W5/00**
Strat. Unit	**Cardium Formation**	**Depth**	**1812.84 m**

XRD/SRA results

Quartz (%)	Fsp (%)	Cb (%)	Clays (%)	Pyrite (%)
68.6	3.6	0.9	26.4	0.5

Composition (*in order of abundance*)

Grain size	%	Variety (%)	Variety (%)	Variety (%)	Variety (%)
sand	48	Quartz/chert (98)	Mica (2)	Feldspar (<2)	
silt	12	Quartz/chert (95)	Mica (5)		
clay	30	Clay mins (100)			
Cement	4	Quartz (100)			
Bioclasts	0				
Organics	6	Amorphous (100)			
Opaques	<1	Pyrite (100)			
	100				

*Intensively altered to clay minerals

^ Including bitumen

Sedimentary structures

Primary	Alternating clay-rich and sandy layers present near top of sample.
Biogenic	Apparent heavy bioturbation, including a possible *Teichichnus* burrow.

Fractures	Occasional thin (4-30 μm thickness) epoxy-filled fractures. Likely artificial.
Porosity	<5% porosity, restricted to sandy layers present near top of sample.

Description

Bioturbated clayey sandstone comprised of subangular (common) to subrounded (rare) very fine silt- to very fine sand-sized (average grain size is very fine sand) detrital quartz (20-70%), chert (5-12%), mica (2-5%), and feldspar (<3%). Much of the sandstone is apparently unstratified, consisting primarily of sand-sized grains suspended within an organic-rich clay matrix. Interbedded clay-rich and sandy layers comprise the upper 1/3 of the sample. Minor (<5%) porosity is observed in the sandy layers present near the top of the sample.

Thin Section Quality

Fair. Some exposed thin section glass.

Rock Classification

Clayey sandstone.

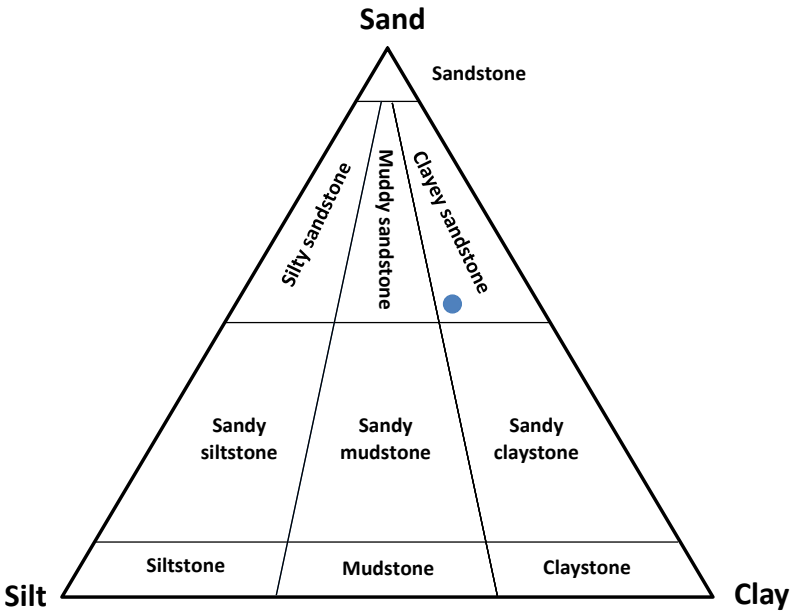


Fig. 4-41: Ternary plot showing the grain size composition of the sample based on the Wentworth scale (after Folk, 1954). Sample 13147 is classified as a clayey sandstone.

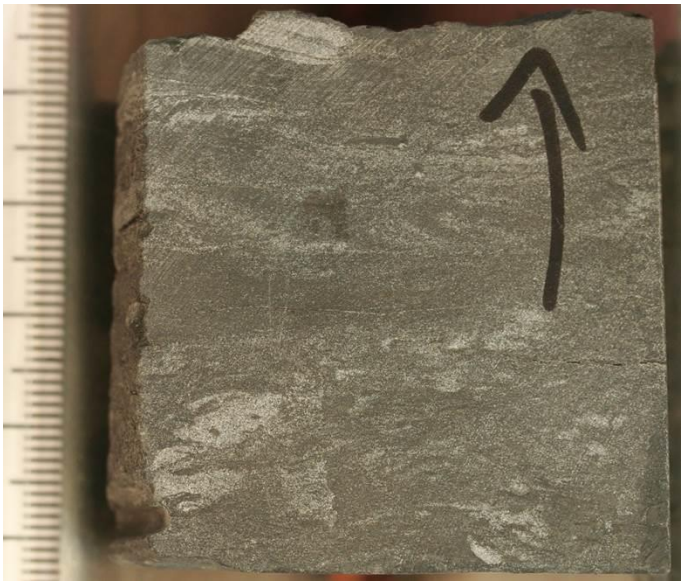


Fig. 4-42: Core photograph of sample 13147 from the Cardium Formation, well 102/14-25-039-05W5/00 (depth 1812.84 m). The depositional way up direction is indicated by the arrow. Scale is mm.

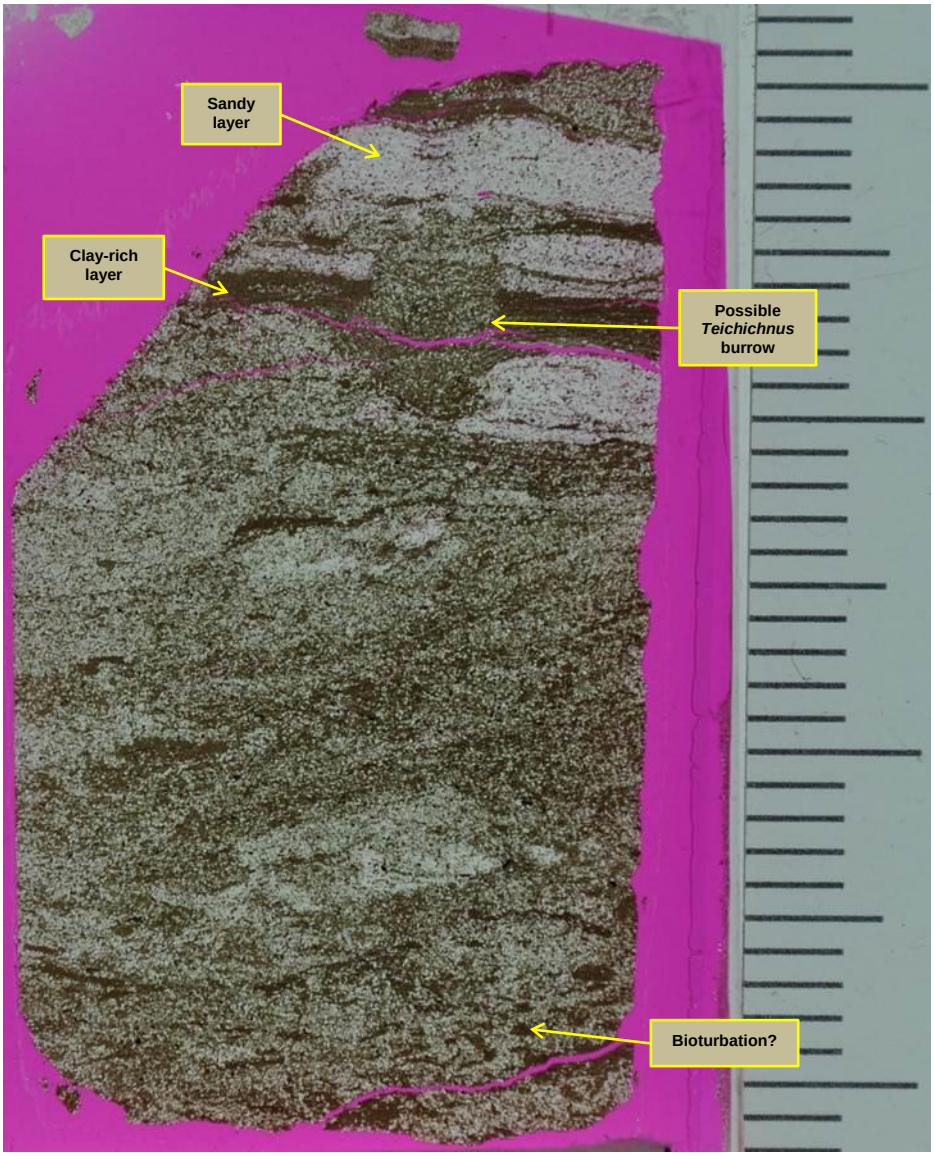


Fig. 4-43: Thin section photograph of sample 13147 from the Cardium Formation, well 102/14-25-039-05W5/00 (depth 1812.84 m). The sample is a bioturbated clayey sandstone. The lower 2/3 of the sample lacks distinct primary sedimentary structures with clay-rich and covoluted sandy patches possibly indicating heavy post-depositional sediment mixing, most of which is due to bioturbation. The upper part of the sample consists of interbedded clay-rich and sandy layers, cross-cut by a possible* Teichichnus *burrow. Scale is in mm.

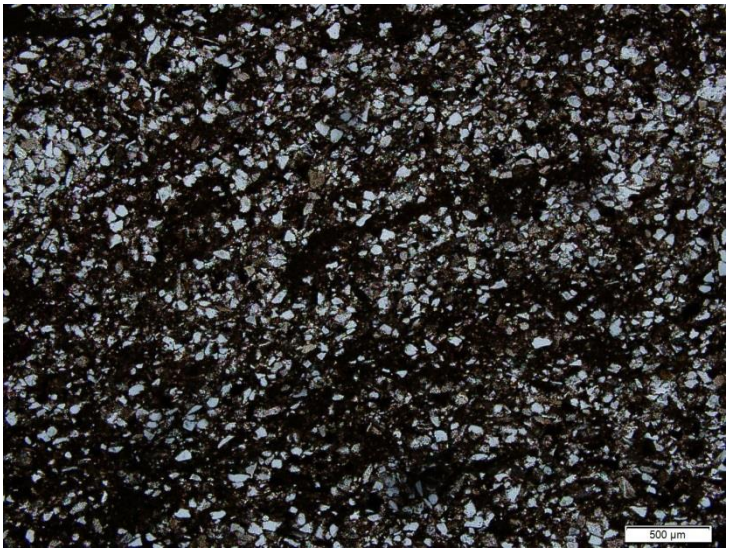


Fig. 4-44: Photomicrograph in PPL showing an overview of the clayey sandstone. The majority of the sample consists of fine silt- to very fine sand-sized grains (light-coloured) within an argillaceous matrix. The lower 2/3 of this sample lacks distinct primary sedimentary structures and has been bioturbated heavily (see opaque distribution pattern), with some subtle vertical and horizontal mixing features observed.

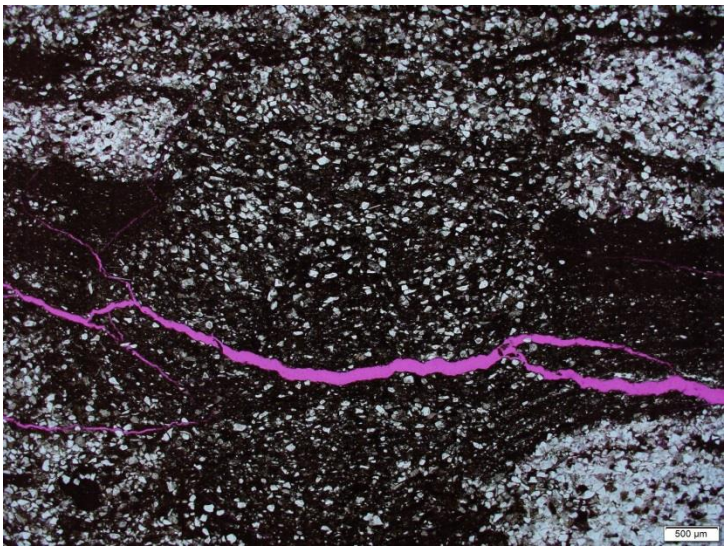


Fig. 4-45: Photomicrograph in PPL showing the possible *Teichichnus* burrow present near the top of the sample (see Figure 4-43). The burrow structure cross-cuts interbedded sandy and clay-rich layers, producing an argillaceous sandstone texture typical of much of the sample (see Figure 4-44). Note an artificial fracture filled with pink epoxy.

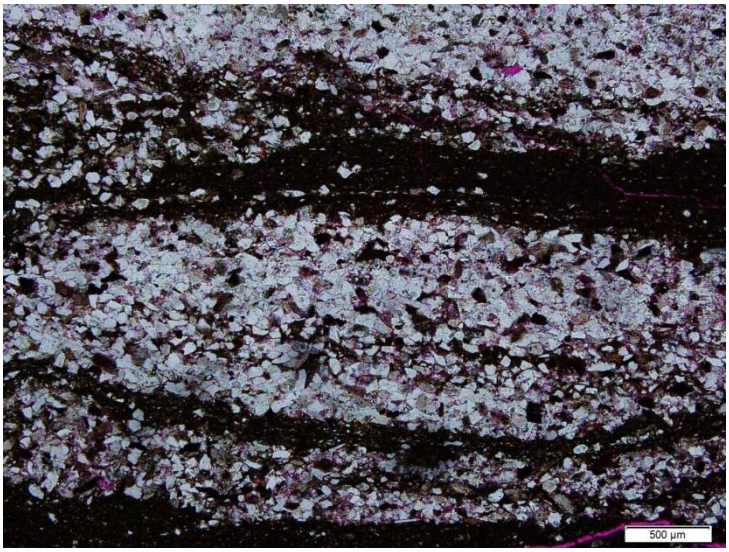


Fig. 4-46: Photomicrograph in PPL showing an overview of interbedded thin clay-rich and sandy layers present near the top of the sample. With the exception of a possible *Teichichnus* burrow, these layers show little evidence of bioturbation.

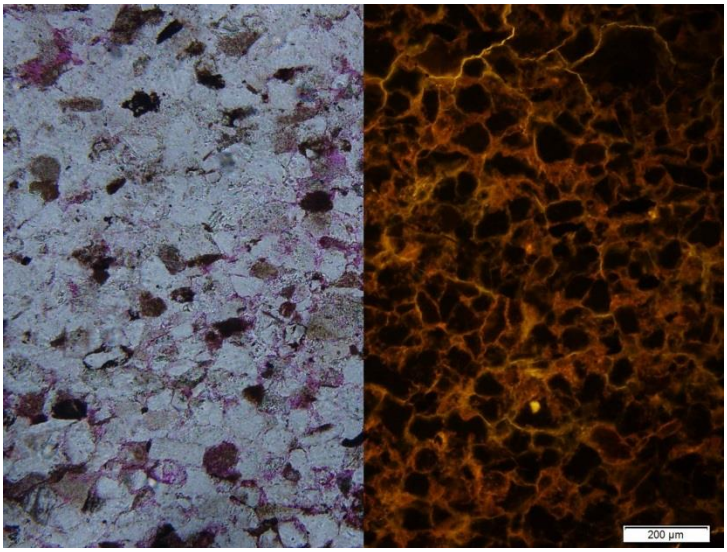


Fig. 4-47: Photomicrograph (left half in PPL, right half in UV light) showing minor (<5%) porosity observed in sandy layers present near the top of the sample (see Figure 4-46). These layers are the only porous features observed in the sample. The UV image reveals possible thin, porous rims around the grains.

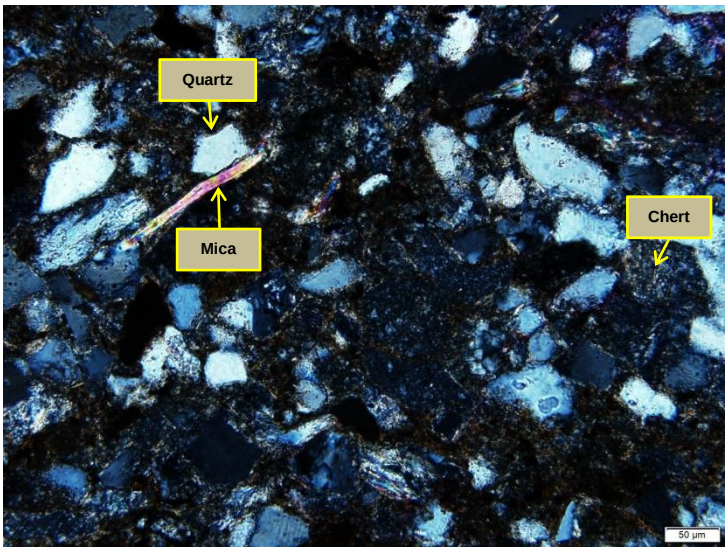


Fig. 4-48: Photomicrograph in XPL showing subangular (common) to subrounded (rare) very fine silt- to very fine sand-sized (average grain size is very fine sand) detrital quartz (20-70%), chert (5-12%), and mica (2-5%). Chert grains are composed predominantly of microquartz. Note mica lathes (up to ~165 µm in length) exhibiting high birefringent colours.

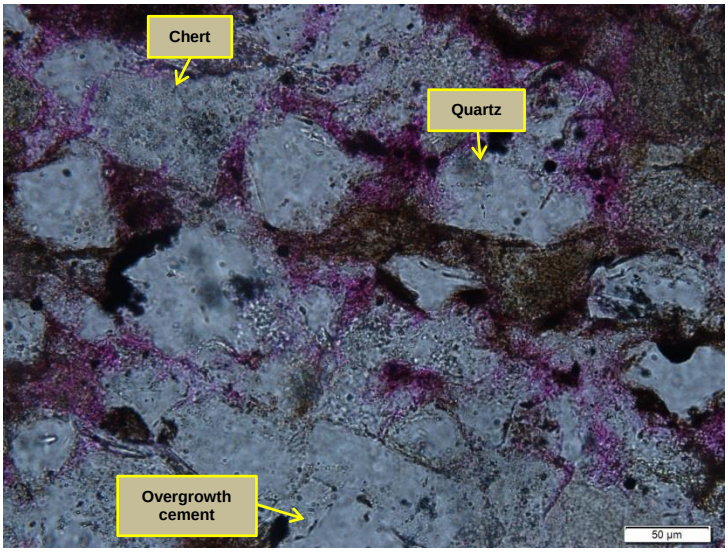


Fig. 4-49: Photomicrograph in PPL showing quartz overgrowths observed in a sandy lamination present near the top of the sample. Quartz cementation appears to have significantly reduced porosity and pore connectivity in these layers. Quartz overgrowths are typically identified by a subtle dust rim around the detrital grain. Note minor (<5%) intergranular porosity (filled with pink epoxy).

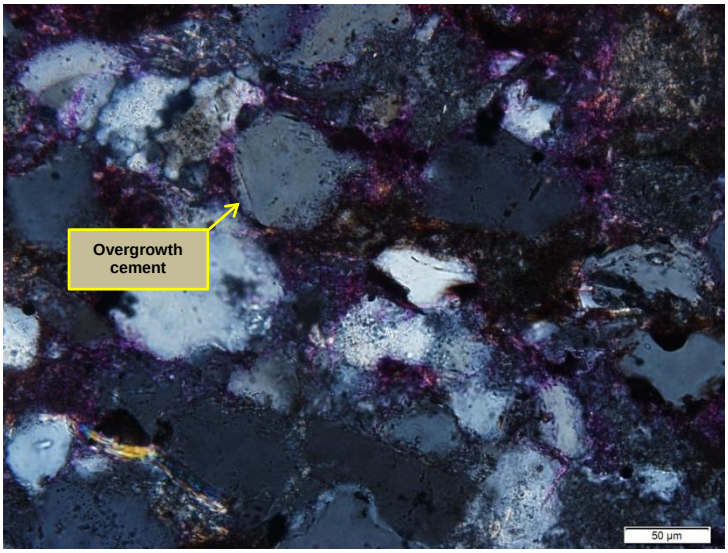


Fig. 4-50: Photomicrograph of Figure 4-49 in XPL showing detrital quartz with overgrowth rims. Some quartz cement forms irregular shapes. Quartz cement comprises ~4% of the sample.

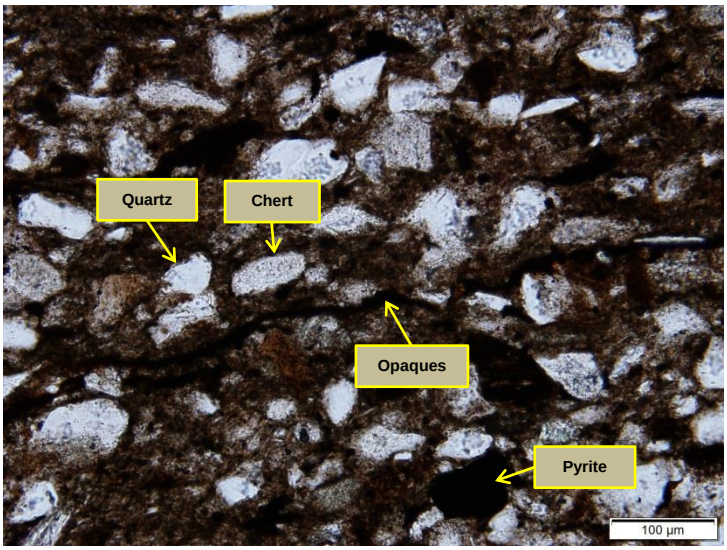


Fig. 4-51: Photomicrograph detailing a clay-rich portion of the sample. Total clay content in the sample is estimated at ~30%. Clays are typically associated with organic matter and finely disseminated pyrite. Clay-sized particles of quartz may be present within the matrix, but are difficult to identify. Note opaques (organic matter and pyrite) forming clusters and thin streaks or “trails”, which possibly represent former fecal remains.

4.2.6 SAMPLE 13257

Sample ID	**13257**		
Sample type	**Core**	**UWI/Well**	**100/04-03-044-07W5/00**
Strat. Unit	**Cardium Formation**	**Depth**	**1826.90 m**

XRD/SRA results

Quartz (%)	Fsp (%)	Cb (%)	Clays (%)	Pyrite (%)
61.7	5.5	2.0 (Siderite)	30.5	0.4

Composition (*in order of abundance*)

Grain size	%	Variety (%)	Variety (%)	Variety (%)	Variety (%)
sand	35	Quartz/chert (93)	Feldspar (4)	Mica (3)	
silt	26	Quartz/chert (96)	Mica (3)	Feldspar (1)	
clay	30	Clay mins (100)			
Cement	4	Siderite (100)			
Bioclasts	0				
Organics	5	Amorphous (100)			
Opaques	< 1	Pyrite (100)			
	100				

*Intensively altered to clay minerals

^ Including bitumen

Sedimentary structures

Primary	Interbedded sandy and silty layers. Apparent fining-upward micro-cycles are visible in some layers, and inclined laminae are present in one sandy layer.
Biogenic	Heavy bioturbation including possible *Helminthopsis*, *Teichichnus*, and *Planolites* burrows.

Fractures	Occasional thin (6-24 μm thickness) epoxy-filled fractures. Likely artificial.
Porosity	The lowermost (interpreted), sandy layer has 2-8% intergranular porosity. The overlying, fining-upward silty layer is non-porous. The uppermost, fining-upward sandy layer has discontinuous patches of 2-5% porosity near its base, and is non-porous through its increasingly clay-rich middle and upper sections.

Description

Heavily bioturbated sandy mudstone with interbedded sandy and silty layers. The lowermost (interpreted), sandy layer contains subangular fine silt- to fine sand-sized (average grain size range is coarse silt to very fine sand) detrital quartz (70-80%), feldspar (2-6%), and mica (1-5%). This layer has 2-8% intergranular porosity. The overlying, fining-upward silty layer contains subangular (common) to subrounded (rare) very fine silt- to very fine sand-sized (average grain size is medium silt) detrital quartz (25-40%), mica (3-5%), and feldspar (1-3%). The uppermost, fining-upward sandy layer contains subrounded (common) to subangular (rare) very fine silt- to fine sand-sized detrital quartz (30-80%), feldspar (3-5%), and mica (1-5%). This layer has discontinuous sandy patches near its base with 2-5% intergranular porosity, and contains some siderite cement.

Thin Section Quality

Good. Occasional epoxy-filled fractures, and rare exposed thin section glass.

Rock Classification

Sandy mudstone.

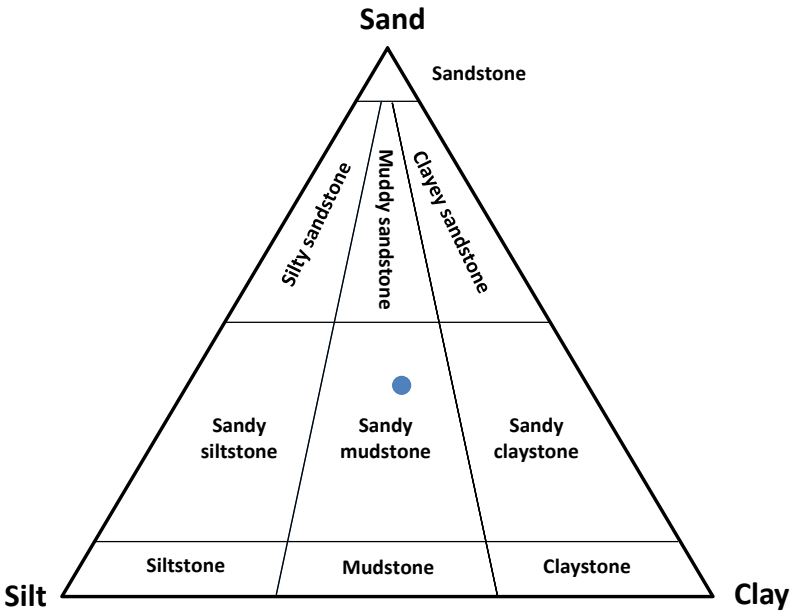


Fig. 4-52: Ternary plot showing the grain size composition of the sample based on the Wentworth scale (after Folk, 1954). Sample 13257 is classified as a sandy mudstone.

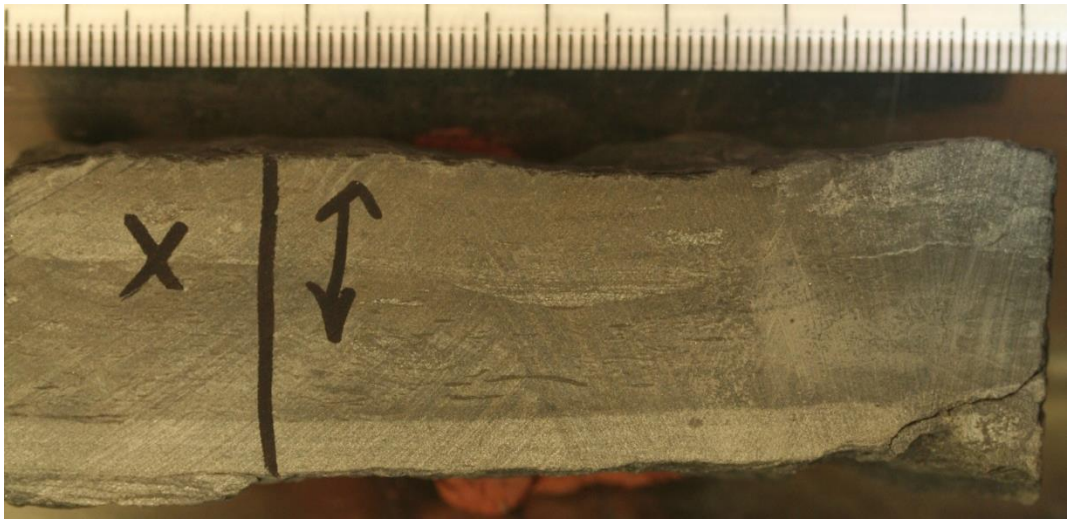


Fig. 4-53: Core photograph of sample 13257 from the Cardium Formation, well 100/04-03-044-07W5/00 (depth 1826.90 m). The thin section prepared from this sample was cut from the area marked with an X. Scale is in mm.

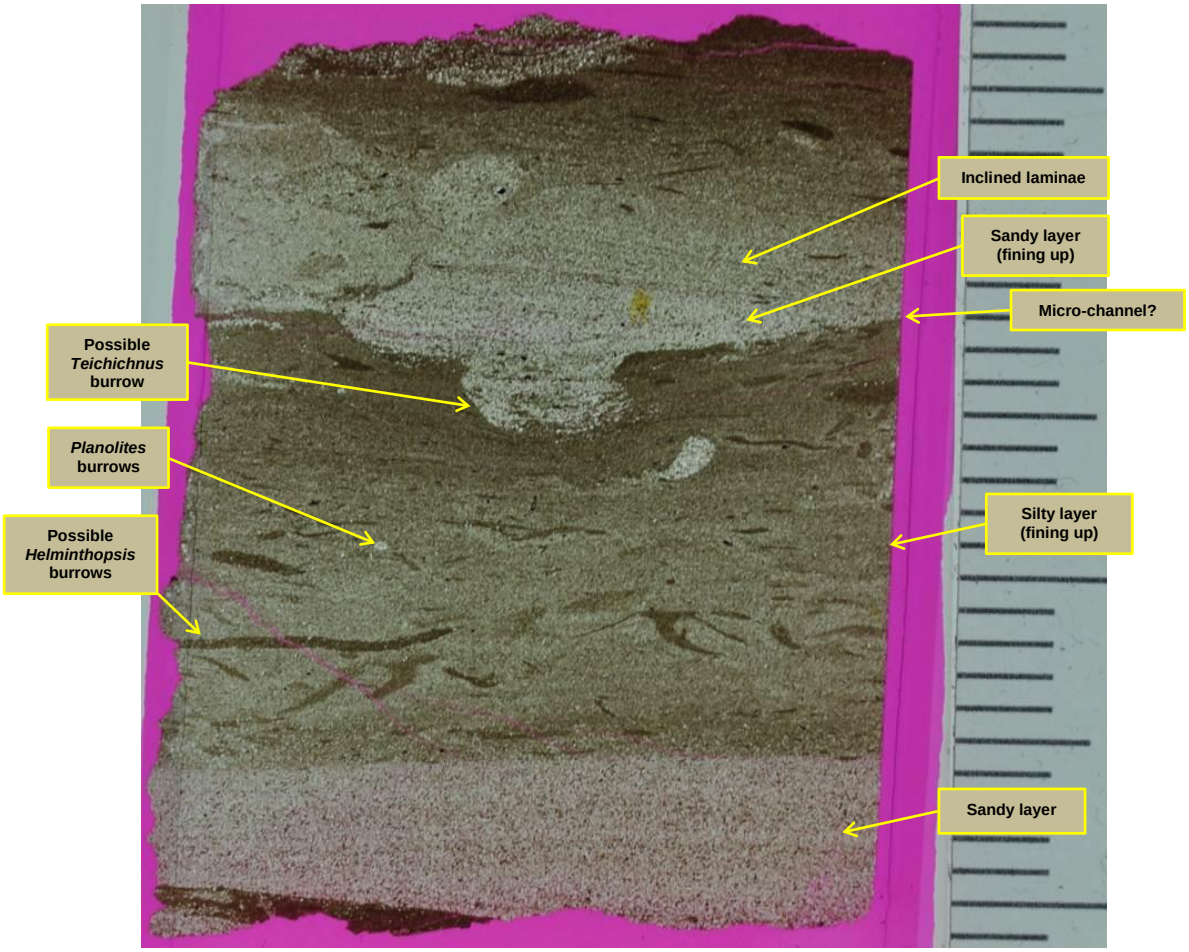


Fig. 4-54: Thin section photograph of sample 13257 from the Cardium Formation, well 100/04-03-044-07W5/00 (depth 1826.90 m). The sample is a heavily bioturbated sandy mudstone with interbedded sandy and silty layers. The lowermost (as shown), sandy layer does not show evidence of bioturbation, and shares a sharply defined contact with the overlying heavily bioturbated silty layer. At least two different bioturbation features (possible* Helminthopsis *burrows, elongate, occasionally sinuous patches of clay with few detrital grains, and* Planolites *burrows, circular pockets of well sorted sand-sized grains) are observed. The sandy and silty layers display apparent fining-upward micro-cycles (rapid deposition?). Note that the depositional way up was not indicated on this sample but inferred based on sedimentary structures. Scale is in mm.

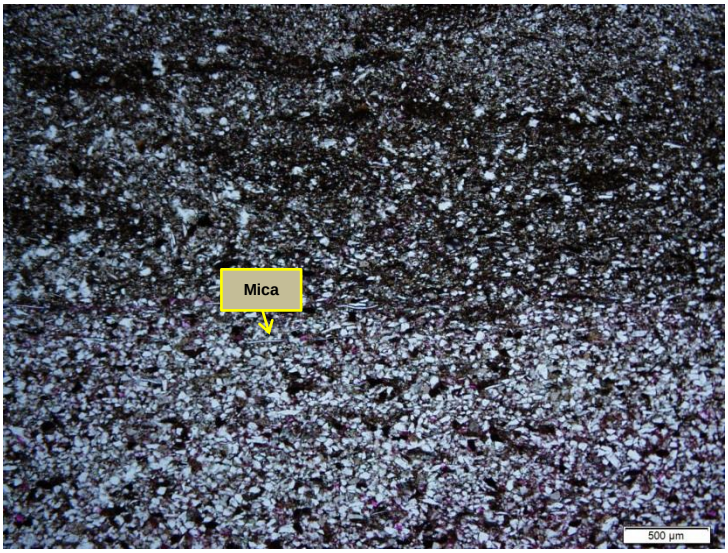


Fig. 4-55: Photomicrograph in PPL showing an overview of the sample, classified as a sandy mudstone. The image illustrates a contact separating the lowermost, silty/sandy layer of the sample from the overlying bioturbated, finer-grained, clay-rich silty layer. Light-coloured minerals consist of quartz, chert, feldspar and mica with the darker laminae and patches consisting mostly of clay material. Note abundant bedding-parallel mica lathes present near the contact.

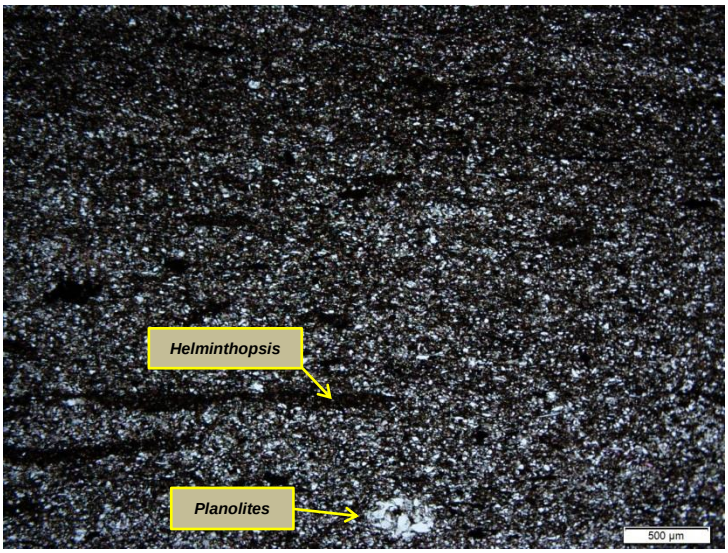


Fig. 4-56: Photomicrograph in PPL illustrating an apparent fining-upward micro-cycle in the bioturbated silty layer, with several possible burrowing features also observed.

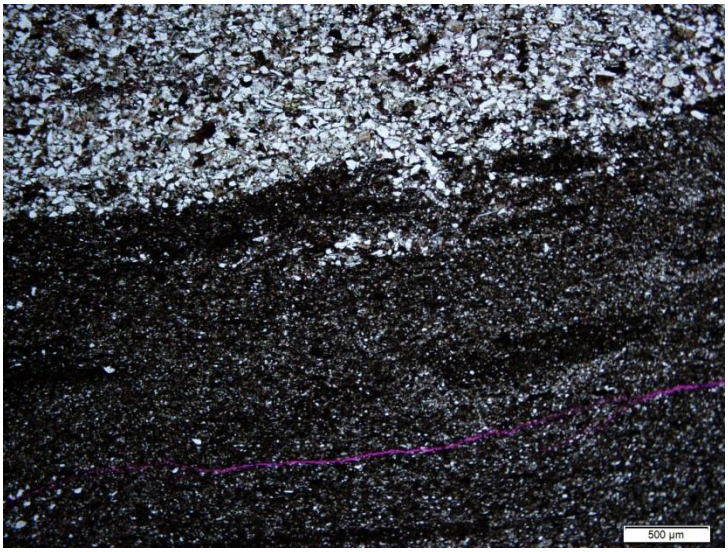


Fig. 4-57: Photomicrograph in PPL showing an overview of the sharp u-shaped (erosional?) contact separating the bioturbated clay-rich silty layer from the overlying, coarser-grained, silty/sandy layer. A possible *Teichichnus* burrow occurs at the interface of these heavily bioturbated layers (see Figure 4-54). Note an artificial fracture filled with pink epoxy along the bottom half of the image.

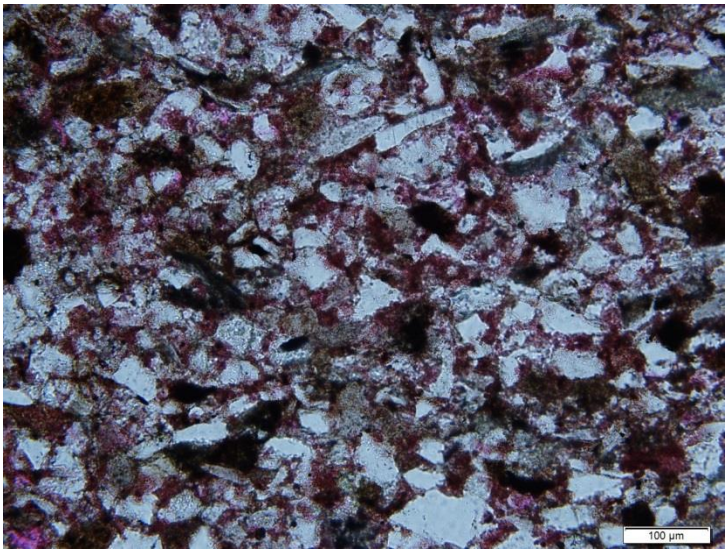


Fig. 4-58: Photomicrograph in PPL showing detail of the lowermost, sandy layer. This layer contains subangular fine silt- to fine sand-sized (average grain size range is coarse silt to very fine sand) detrital quartz/chert (70-80%), feldspar (2-6%), and mica (1-5%). Intergranular porosity is estimated at 2-8%.

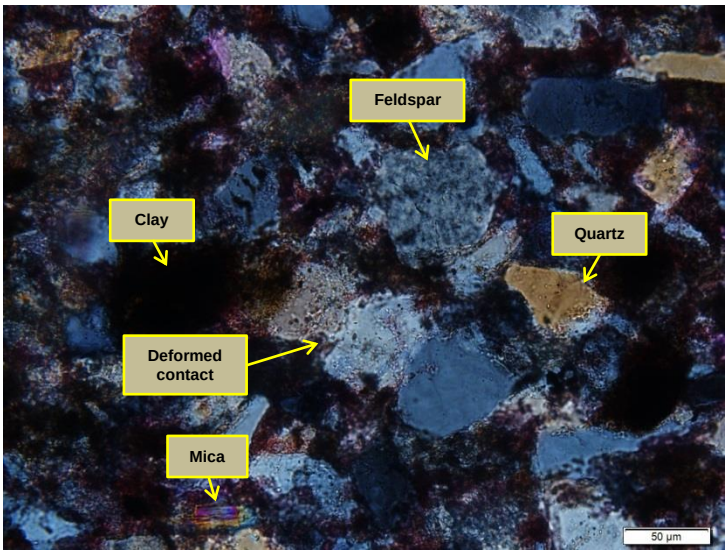


Fig. 4-59: Photomicrograph in XPL detailing grain contacts in the lowermost, sandy layer. Deformed grain contacts indicate that moderate to high post-depositional sediment compaction occurred during burial.

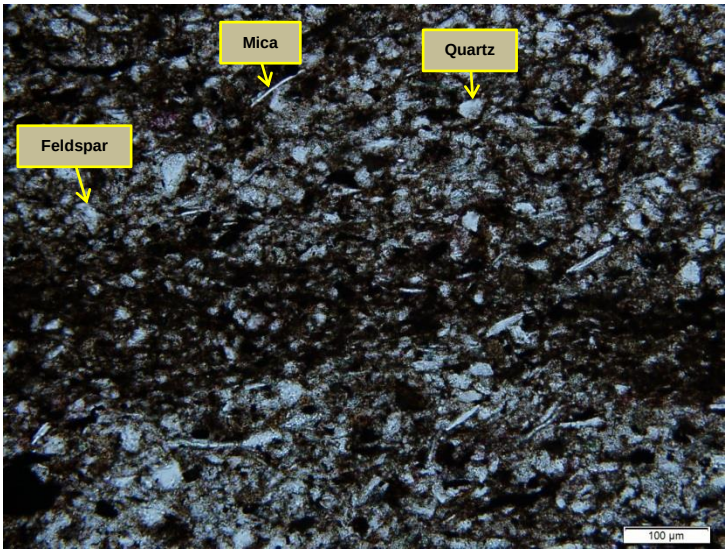


Fig. 4-60: Photomicrograph in PPL detailing the fining-upward clay-rich silty layer. This non-porous layer contains subangular (common) to subrounded (rare) very fine silt- to very fine sand-sized (average grain size is medium silt) detrital quartz/chert (25-40%), mica (3-5%), and feldspar (1-3%). Sub-spherical clusters or pockets of opaque material likely represent fecal remains.

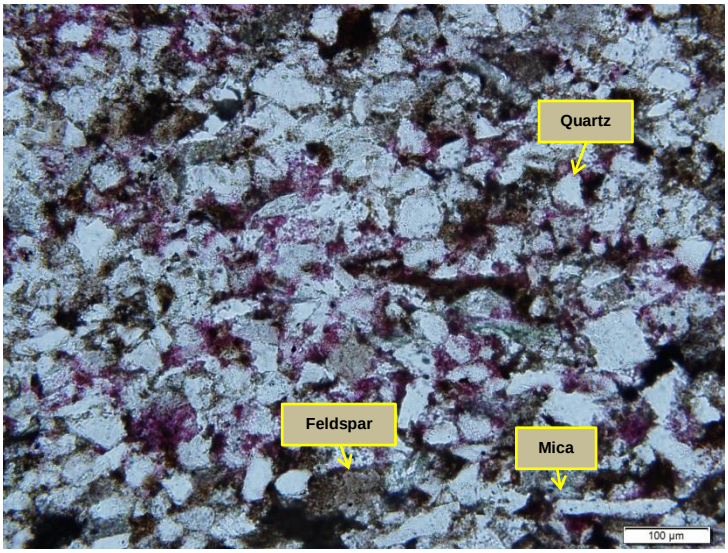


Fig. 4-61: Photomicrograph in PPL detailing the uppermost, sandy layer. This layer contains subrounded (common) to subangular (rare) very fine silt- to fine sand-sized detrital quartz (30-80%), feldspar (3-5%), and mica (1-5%). Discontinuous patches of intergranular porosity (pink-epoxy) estimated at ~2-5% are observed near the base of the layer (shown in this image).

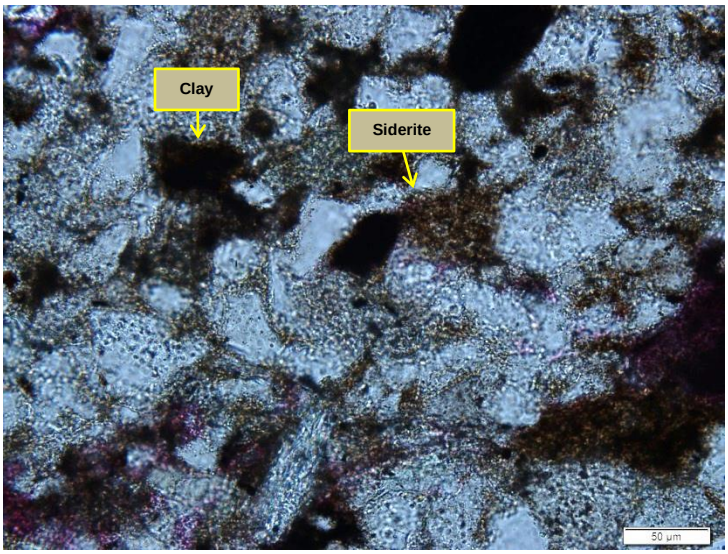


Fig. 4-62: Photomicrograph in PPL illustrating microcrystalline siderite cement in the uppermost, sandy layer. Siderite cement occurs only in the coarser, basal section of this fining-upward layer. Note minor intergranular porosity (pink epoxy).

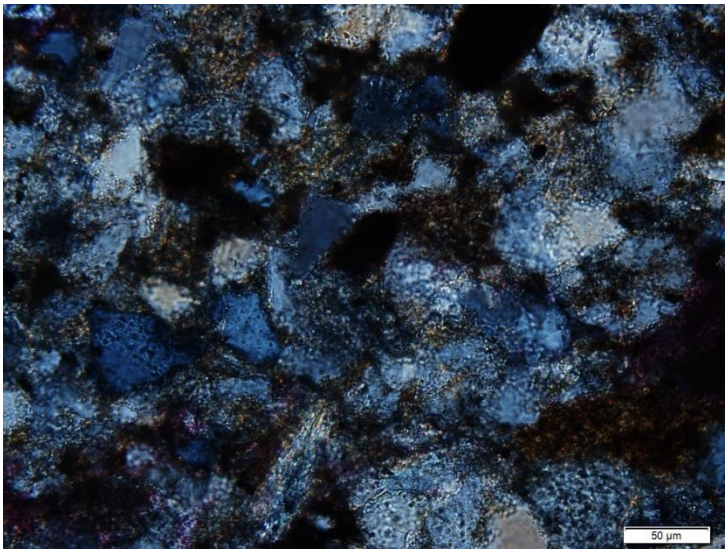


Fig. 4-63: Photomicrograph in XPL showing details of siderite cement in the uppermost, sandy layer (same view as shown in Figure 4-62). Siderite crystals have high birefringence under cross-polarized light. Siderite in the sample also occasionally forms microcrystalline grains.

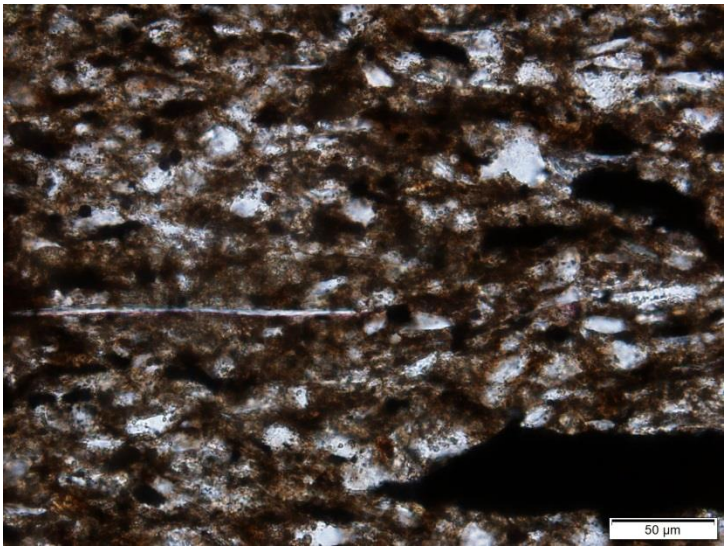


Fig. 4-64: Photomicrograph in PPL illustrating a clay-rich silty layer, which contains fine to medium silt-size quartz (predominant), chert and feldspar. Several mica lathes (up to 172 µm) are observed and are generally oriented parallel to bedding. Mica grains within these beds often exhibit random orientations (elevated depositional energy or biological activity?). Note numerous organic fragments, which are also associated with pyrite.

4.2.7 SAMPLE 13258

Sample ID	**13258**		
Sample type	**Core**	**UWI/Well**	**100/04-03-044-07W5/00**
Strat. Unit	**Cardium Formation**	**Depth**	**1828.05 m**

XRD/SRA results

Quartz (%)	Fsp (%)	Cb (%)	Clays (%)	Pyrite (%)
86.4	3.3	0	9.7	0.6

Composition (*in order of abundance*)

Grain size	%	Variety (%)	Variety (%)	Variety (%)	Variety (%)
sand	81	Quartz/chert (97)	Mica (2)	Feldspar (1)	
silt	8	Quartz/chert (100)			
clay	6	Clay mins (100)			
Cement	5	Quartz (100)			
Bioclasts	0				
Organics	<1	Amorphous (100)			
Opaques	<1	Pyrite (100)			
	100				

*Intensively altered to clay minerals

^ Including bitumen

Sedimentary structures

Primary	Possible faint clay-rich laminae.
Biogenic	None visible.

Fractures	Rare thin (10 μm thickness) epoxy-filled fractures.
Porosity	5-10% intergranular porosity.

Description

Muddy sandstone with rare clay-rich laminae. The sample consists of subangular to subrounded fine silt- to fine sand-sized (average grain size is very fine sand) detrital quartz (70-80%), chert (8-12%), mica (<2%), and feldspar (<1%), with 5-10% intergranular porosity. Clay (pore-filling and grain enveloping) and quartz cements reduce pore connectivity throughout the sandsone.

Thin Section Quality

Good.

Rock Classification

Muddy sandstone.

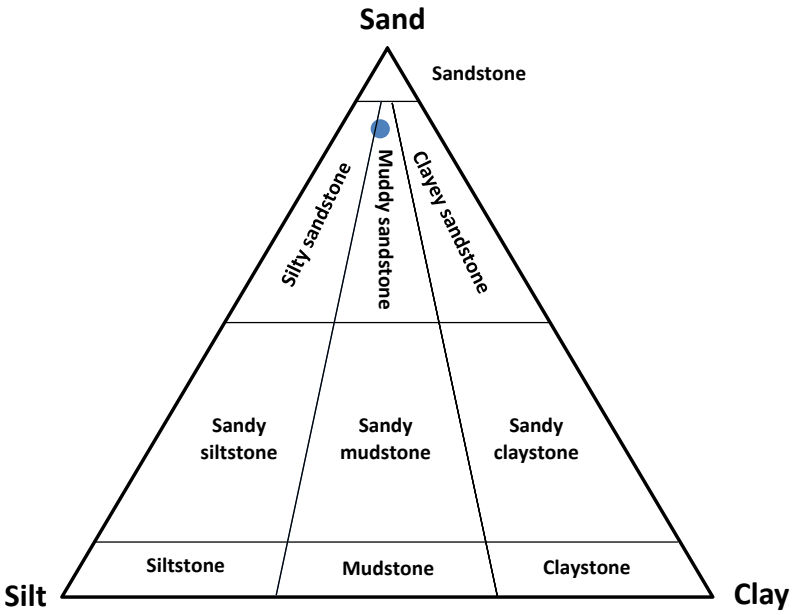


Fig. 4-65: Ternary plot showing the grain size composition of the sample based on the Wentworth scale (after Folk, 1954). Sample 13258 is classified as a muddy sandstone.

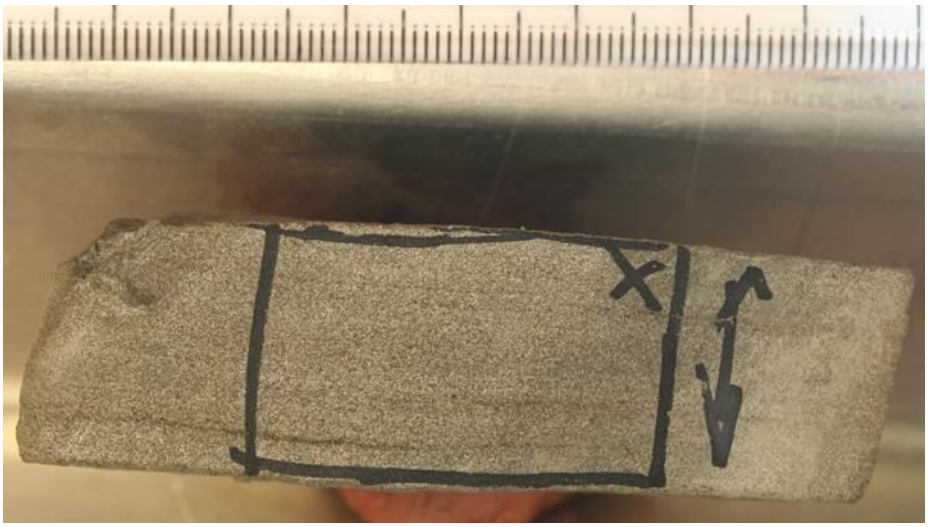


Fig. 4-66: Core photograph of sample 13258 from the Cardium Formation, well 100/04-03-044-07W5/00 (depth 1828.05 m). The thin section prepared from this sample was cut from the area marked with an X. Scale is in mm.

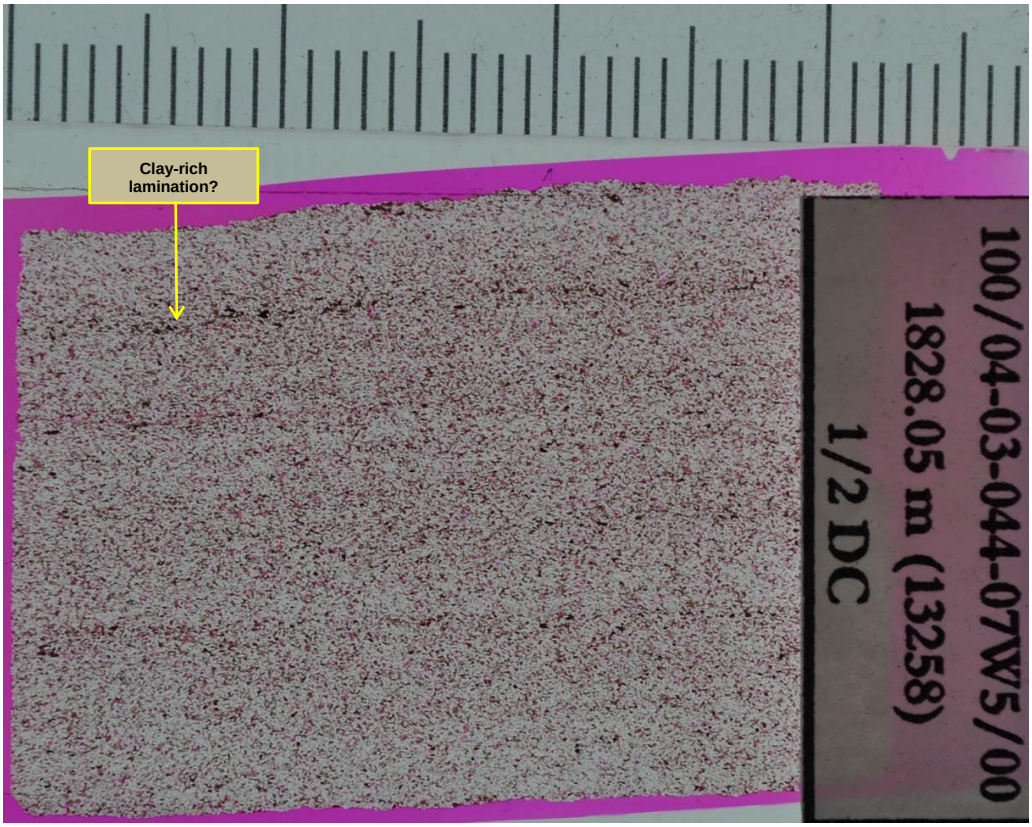


Fig. 4-67: Thin section photograph of sample 13258 from the Cardium Formation, well 100/04-03-044-07W5/00 (depth 1828.05 m). The sample is a muddy sandstone with rare clay-rich laminations.

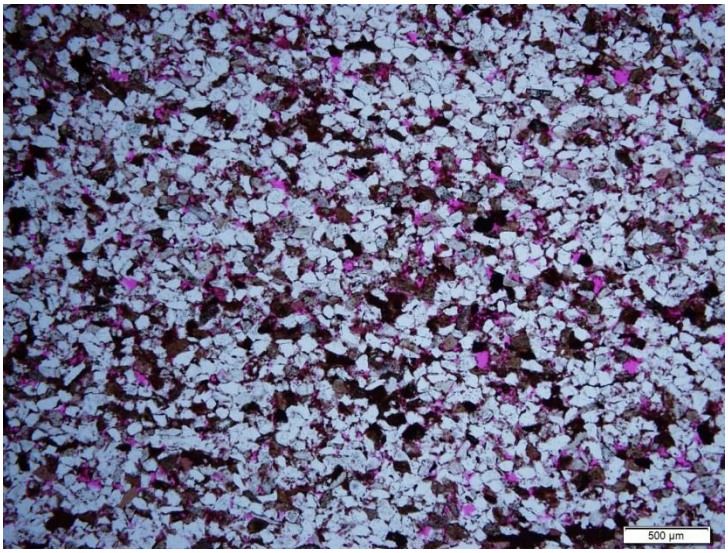


Fig. 4-68: Photomicrograph in PPL showing an overview of the sandstone. Although faint bedding parallel laminae are visible in Figure 4-67 (including a few opaque-rich laminae), no primary depositional features are observed in thin section.

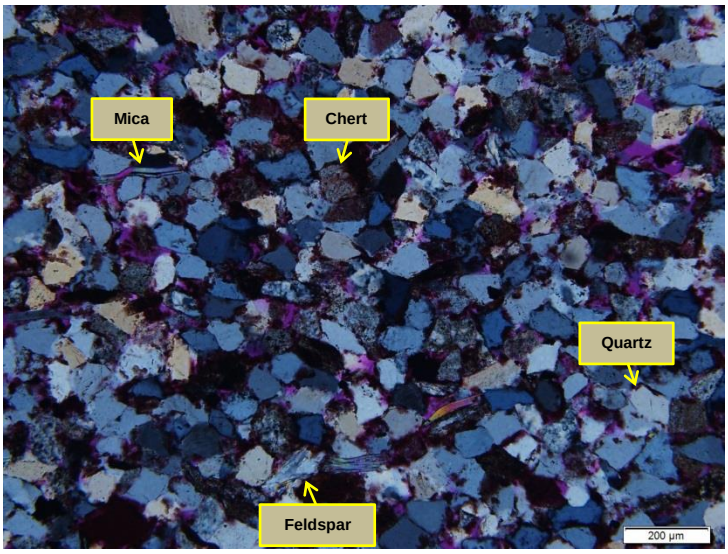


Fig. 4-69: Photomicrograph in XPL showing subangular to subrounded fine silt- to fine sand-sized (average grain size is very fine sand) detrital quartz (70-80%), chert (8-12%), mica (<2%), and feldspar (<1%). Feldspar grains are often observed to be partially altered (illite/mica) in this sandstone.

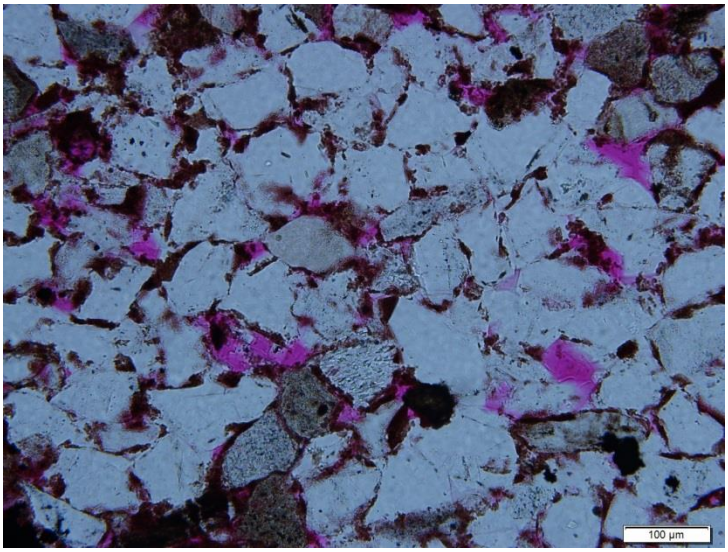


Fig. 4-70: Photomicrograph in PPL showing detrital grains with clay mineral “coatings” (draping around grains). Clay minerals comprise 2-6% of this sandstone, and occur more frequently around the edges of detrital grains than within intergranular pores. Clusters of framboidal pyrite (black) are also observed.

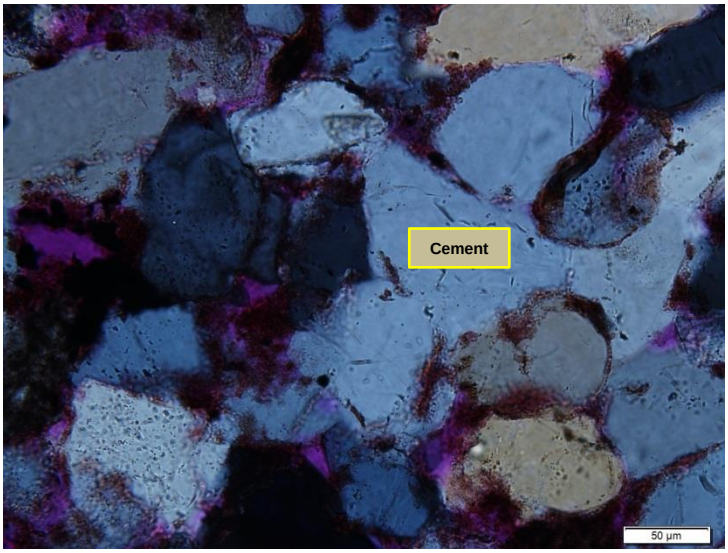


Fig. 4-71: Photomicrograph in XPL showing pore-filling quartz cement observed in the sample. Quartz cements and clays (both grain enveloping and pore-filling) reduce both intergranular porosity and pore connectivity in this sandstone.

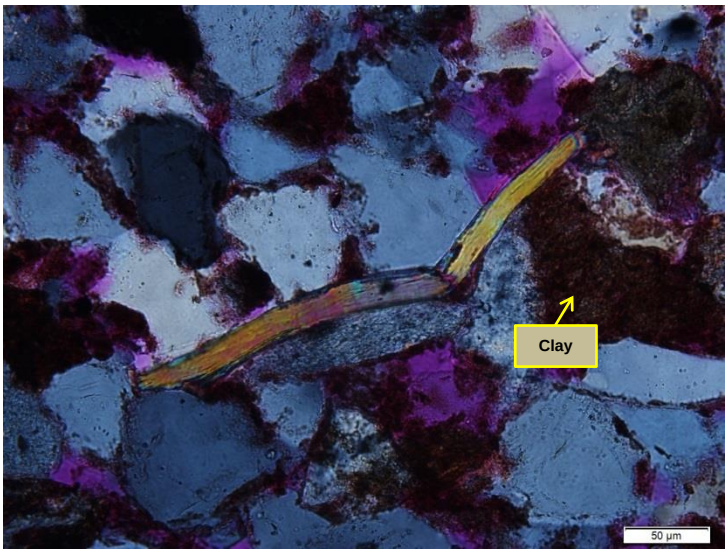


Fig. 4-72: Photomicrograph in XPL showing a bent mica grain observed in the sample. Deformed mica and tight grain-grain contacts indicate that moderate to high post-depositional sediment compaction occurred during burial. Some pore-filling clay (e.g. right side of image) clusters occupy space between detrital grains.

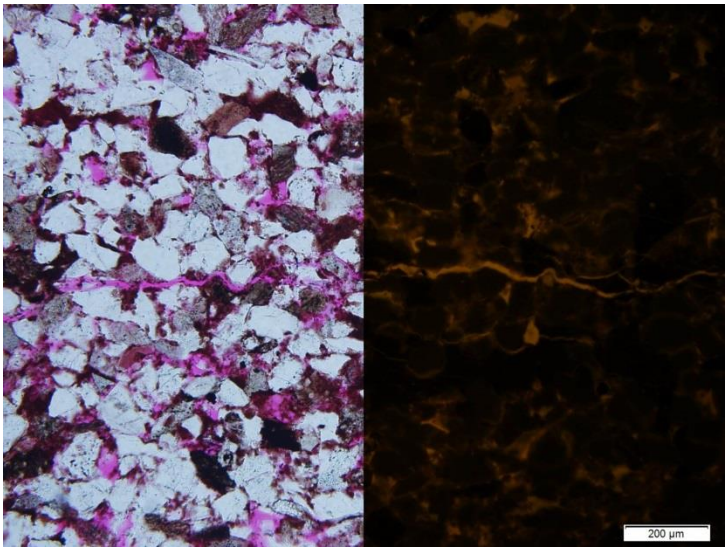


Fig. 4-73: Photomicrograph (left half in PPL, right half in UV light) showing a thin (10 µm thickness) epoxy-filled fracture observed in the sample. Fractures are rare in this sandstone, and may be artificial (created during sample preparation).

4.2.8 SAMPLE 13262

Sample ID	**13262**		
Sample type	**Core**	**UWI/Well**	**102/06-27-066-23W5/00**
Strat. Unit	**Cardium Formation**	**Depth**	**1016.32 m**

XRD/SRA results

Quartz (%)	Fsp (%)	Cb (%)	Clays (%)	Pyrite (%)
51.4	5.3	4.1	39	0.2

Composition (*in order of abundance*)

Grain size	%	Variety (%)	Variety (%)	Variety (%)	Variety (%)
sand	30	Quartz/chert (90)	Mica (6)	Feldspar (<5)	
silt	15	Quartz/chert (97)	Mica (3)		
clay	45	Clay mins (100)			
Cement	4	Quartz (100)			
Bioclasts	0				
Organics	6	Amorphous (100)			
Opaques	<1	Pyrite (100)			
	100				

*Intensively altered to clay minerals

^ Including bitumen

Sedimentary structures

Primary	Finely laminated clay-rich sandy bedding, a single mm-scale sandy bed, and a bioturbated clay-rich sandy layer comprise the lower part of the sample. The middle portion of the sample is made up of finely laminated clay-rich bedding. Finely laminated silty bedding and a thinner overlying section of finely laminated clay-rich bedding occur at the top of the sample.
Biogenic	Possible burrow structures occur in finely laminated clay-rich bedding. A layer comprised of bioturbated sediment occurs near the base of the sample.

Fractures	Common thin epoxy-filled fractures. Likely artificial.
Porosity	Porosity occurs within sandy burrow features (~5%) and layers of the sandy sequence occuring at the base of the sample. Within the lower sandy sequence, minor (<2%) intergranular porosity is observed in both the finely laminated clay-rich sandy bedding and bioturbated clay-rich sandy layer, whereas the mm-scale sandy bed has ~5% intergranular porosity.

Description

Bioturbated sandy claystone comprised of subrounded (common) to angular (rare) very fine silt- to fine sand-sized (average grain size is coarse silt) detrital quartz (25-60%), chert (4-12%), mica (2-6%), and feldspar (<5%). The majority of the sample is made up of non-porous finely laminated clay-rich bedding, present in both the middle and upper sections of the rock. The lower section of the rock, comprised of a sequence of sandy layers, contains the only porous horizons in the sample.

Thin Section Quality

Moderate.

Rock Classification

Sandy claystone.

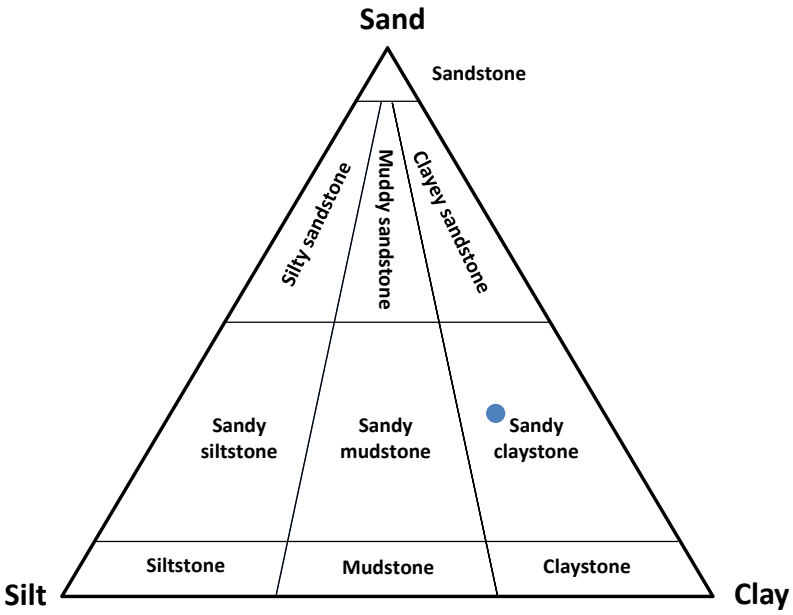


Fig. 4-74: Ternary plot showing the grain size composition of the sample based on the Wentworth scale (after Folk, 1954). Sample 13262 is classified as a sandy claystone.

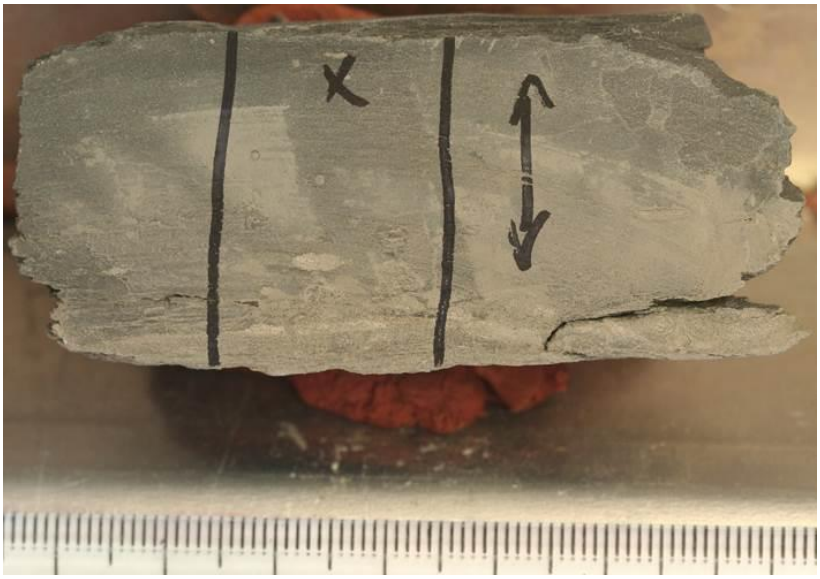


Fig. 4-75: Core photograph of sample 13262 from the Cardium Formation, well 102/06-27-066-23W5/00 (depth 1016.32 m). The thin section prepared from this sample was cut from the area marked with an X. Scale is in mm. Comment: the sample was received with no up direction. Direction was NOT positively identified and hence the way up is described as shown in the image.

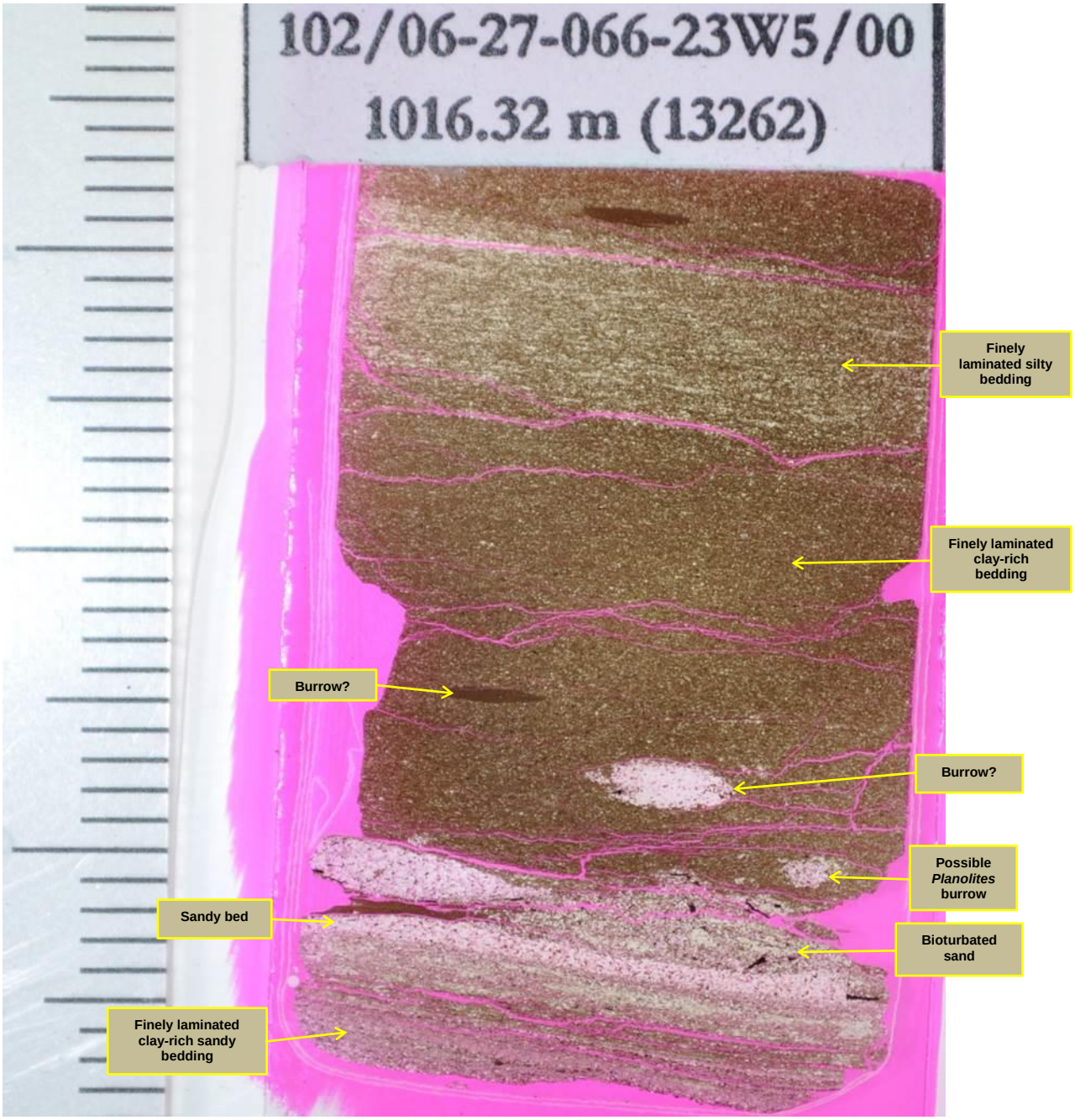


Fig. 4-76: Thin section photograph of sample 13262 from the Cardium Formation, well 102/06-27-066-23W5/00 (depth 1016.32 m). The sample is a bioturbated sandy claystone. Sandy laminae/layers occur at the bottom of the image, overlain by a package of finely-laminated, clay-rich sediment that comprises approximately half of the sample. Finely laminated silty bedding and an overlying section of finer-grained clay-rich bedding are present at the top of the image. Scale is in mm. Caution: way-up was not provided and may not be as shown in image.

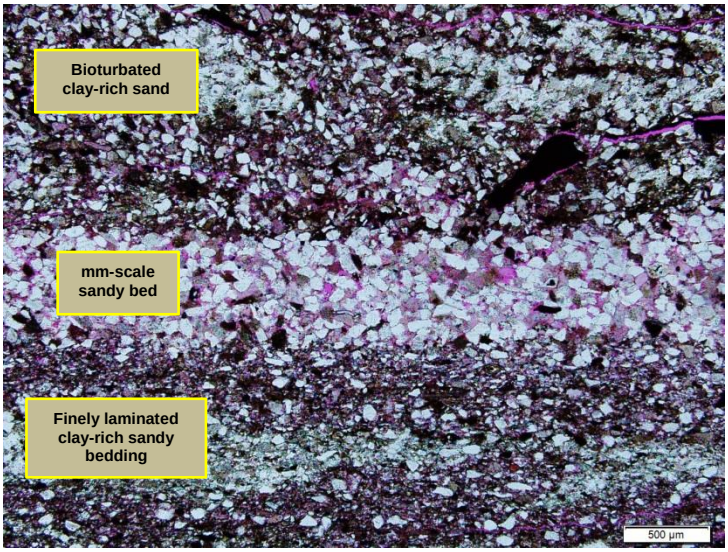


Fig. 4-77: Photomicrograph in PPL showing finely laminated and bioturbated clay-rich silty/sandy layering interbedded with a porous, coarser grained (up to 180 µm; predominantly very fine-sand) sandy bed (lower part of the sample).

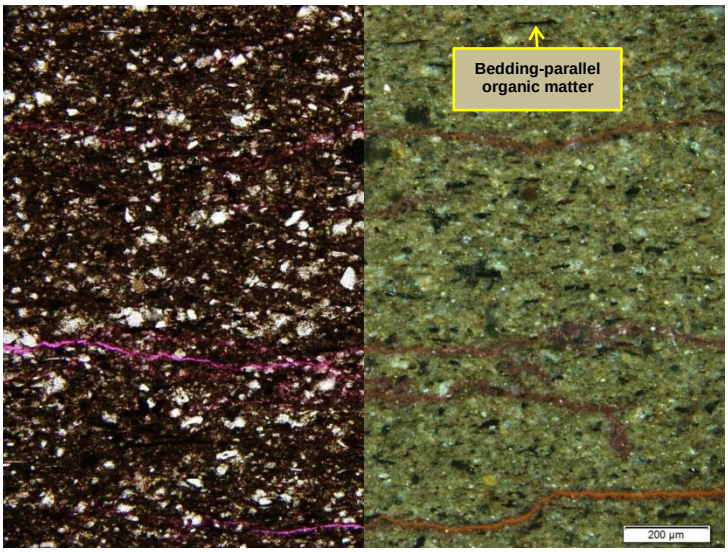


Fig. 4-78: Photomicrograph (left half in PPL, right half in reflected light) showing finely laminated clay-rich layering observed in the middle portion of the sample. Strands of bedding-parallel organics are abundant (~6%) within this area of the sample.

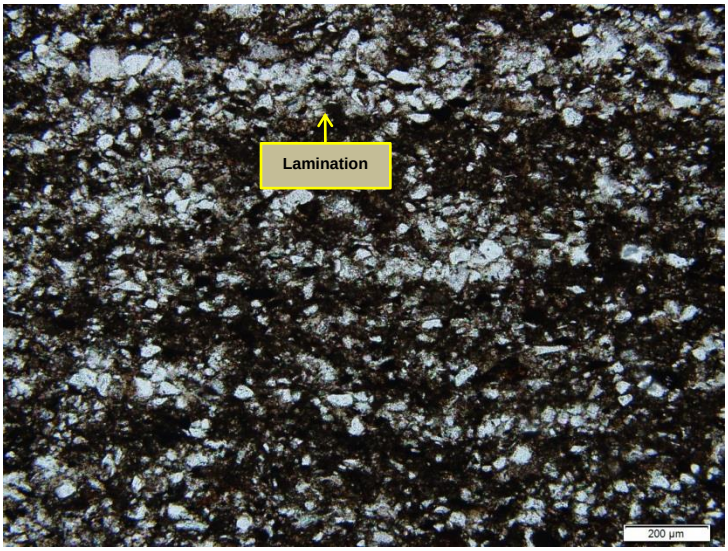


Fig. 4-79: Photomicrograph in PPL showing thin silty laminae and short, discontinuous lenses of silt-size particles interbedded with finer-grained, opaque-rich material (clays, organics and pyrite) in the upper portion of the sample. Very fine silt- to very fine sand-sized detrital quartz and chert grains define the laminae.

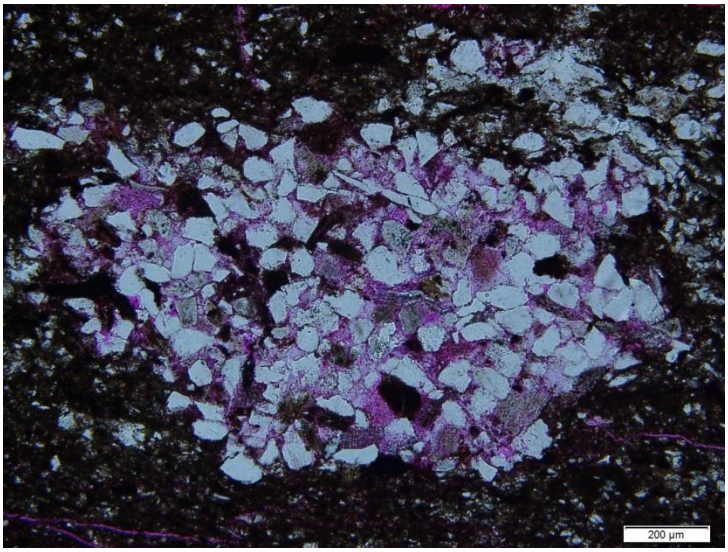


Fig. 4-80: Photomicrograph in PPL showing a possible *Planolites* burrow (~1.5 mm in size) observed within the middle section of the sample. This and other sandy burrowing features present in the sample have ~5% intergranular porosity.

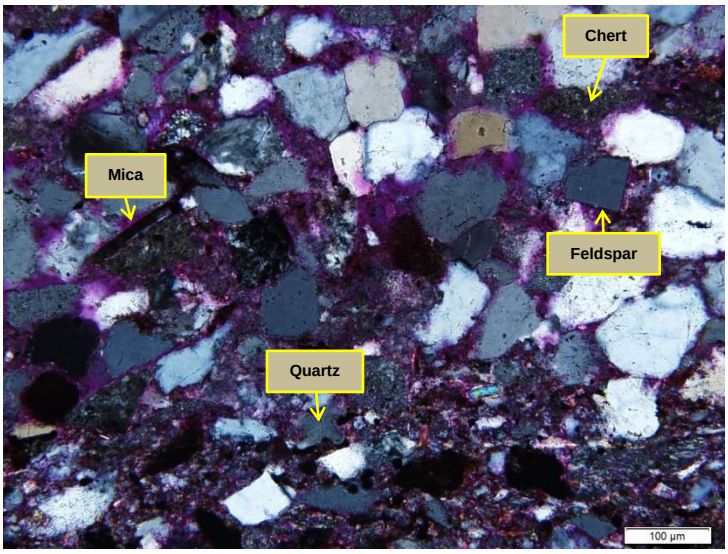


Fig. 4-81: Photomicrograph in XPL showing subrounded (common) to angular (rare) very fine silt- to fine sand-sized (average grain size is coarse silt) detrital quartz (25-60%), chert (4-12%), mica (1-6%), and feldspar (<5%) observed in the claystone.

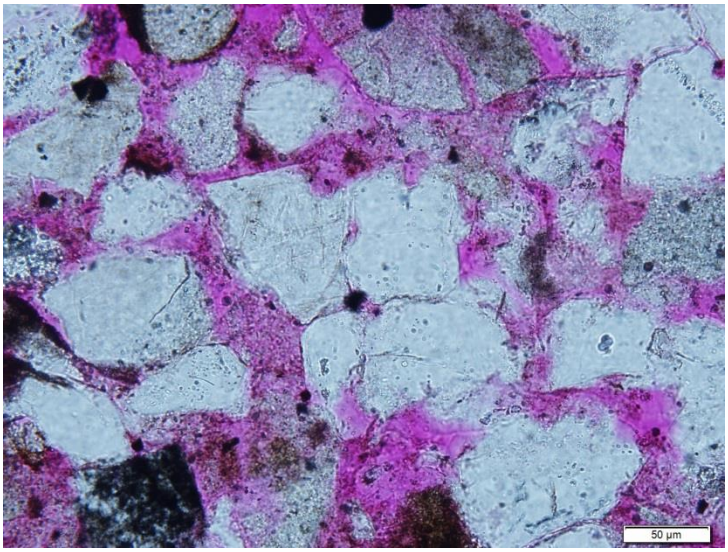


Fig. 4-82: Photomicrograph in PPL of the sandy bed illustrated in Figure 4-77, which shows intergranular porosity filled with pink epoxy. Some clay material can be observed partially occluding pore space. This layer has ~5% intergranular porosity.

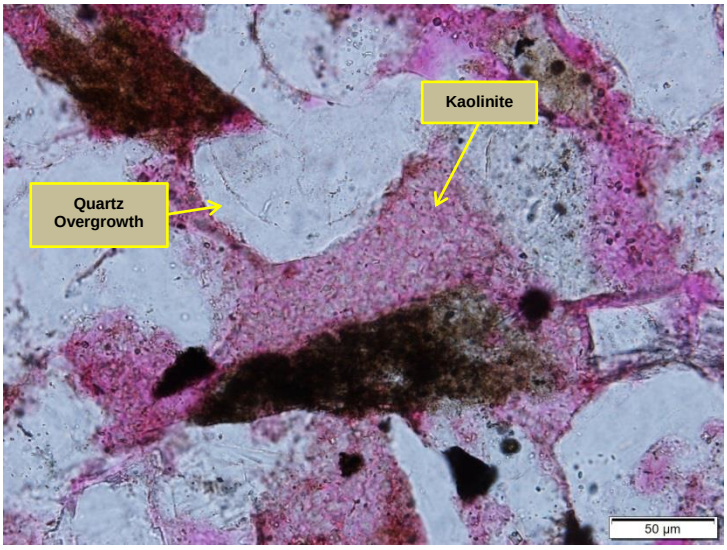


Fig. 4-83: Photomicrograph in PPL illustrating pore-filling kaolinite booklets and associated microporosity observed in the mm-scale sandy bed present near the base of the sample. Some detrital quartz grains exhibiting quartz overgrowths are also observed in the bed.

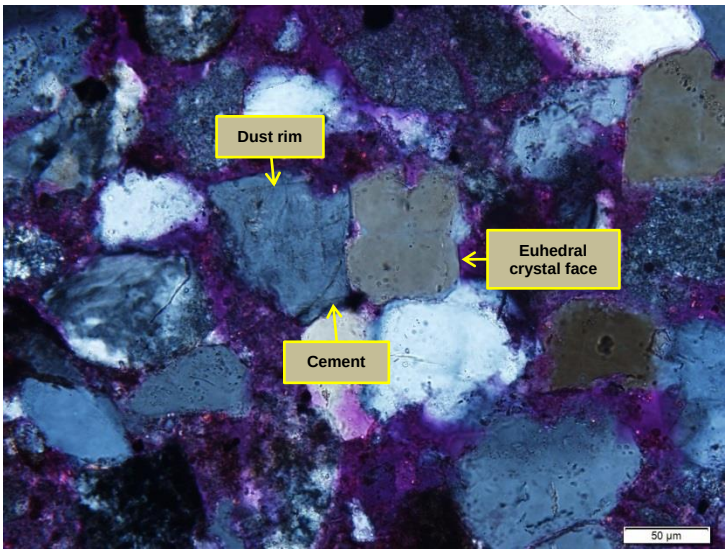


Fig. 4-84: Photomicrograph in XPL showing quartz overgrowth cementation observed in the mm-scale sandy bed present near the base of the sample (same field of view as Figure 4-82).

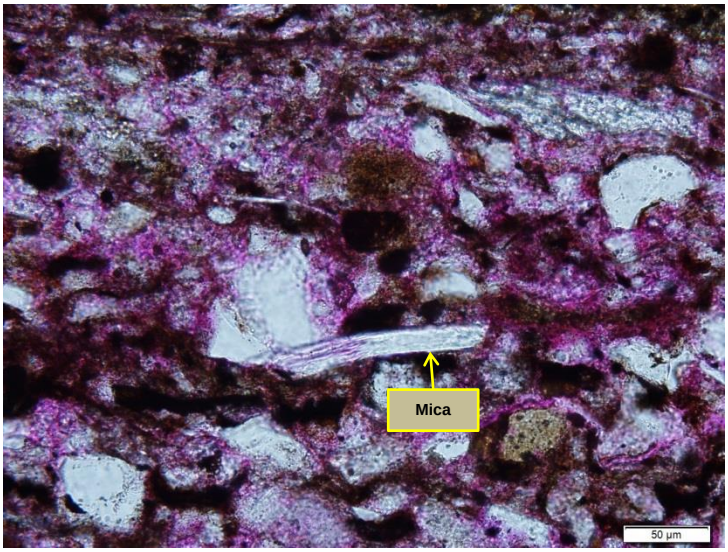


Fig. 4-85: Photomicrograph in PPL showing minor (<2%) intergranular porosity observed in the finely laminated clay-rich sandy bedding present at the base of the sample. Note several mica lathes.

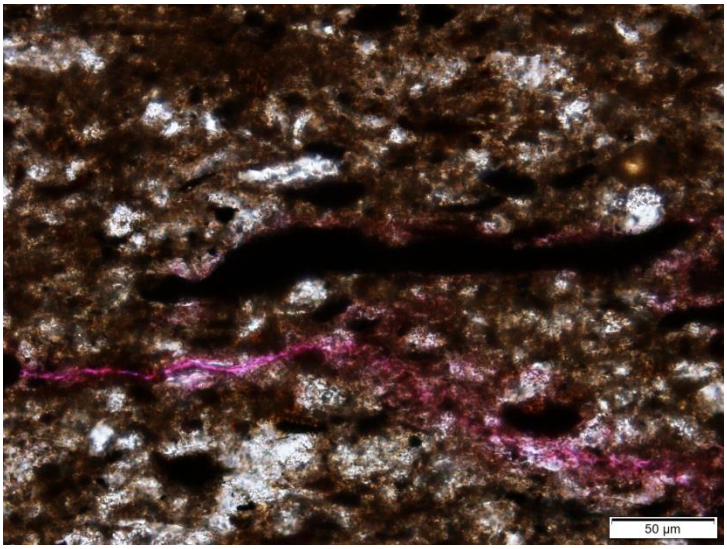


Fig. 4-86: Photomicrograph in PPL detailing the clay-rich bedding present near the middle of the sample, which contains fine silt-size particles of quartz along with some flakes, specks and short, lenticular streaks of opaque material. Opaques include organic matter and pyrite. Total clay content is estimated at ~45% of the total composition. Note several micro-fractures (filled with pink epoxy), which are likely artificial or “enhanced”.

4.2.9 SAMPLE 13283

Sample ID	**13283**		
Sample type	**Core**	**UWI/Well**	**100/04-18-060-20W5/00**
Strat. Unit	**Cardium Formation**	**Depth**	**1607.30 m**

XRD/SRA results

Quartz (%)	Fsp (%)	Cb (%)	Clays (%)	Pyrite (%)
75.4	1.3	1	20.3	2.1

Composition (*in order of abundance*)

Grain size	%	Variety (%)	Variety (%)	Variety (%)	Variety (%)
sand	50	Quartz/chert (99)	Mica (1)	Feldspar (<1)	
silt	10	Quartz/chert (96)	Mica (4)		
clay	25	Clay mins (100)			
Cement	8	Quartz (100)			
Bioclasts	0				
Organics	5	Amorphous (100)			
Opaques	2	Pyrite (100)			
	100				

*Intensively altered to clay minerals

^ Including bitumen

Sedimentary structures

Primary	Interbedded clay-rich and sandy layers, with possible micro-channel structures.
Biogenic	None apparent.

Fractures	Occasional thin (4-45 µm thickness) epoxy-filled fractures and partings, particularly in clay-rich layers. Likely artificial.
Porosity	5-10% porosity in sandy layers. Clay-rich layers are non-porous.

Description

Clayey sandstone comprised of angular (common) to subrounded (rare) fine silt- to fine sand-sized (average grain size is very fine sand) detrital quartz (70-80%), chert (8-12%), mica (1-5%), and feldspar (<1%). Sharp contacts separate the interbedded clay-rich and sandy layers present in the sandstone. 5-10% porosity is observed in the sandy layers, which are cemented by quartz and chert, whereas the clay-rich layers are non-porous.

Thin Section Quality

Good.

Rock Classification

Clayey sandstone.

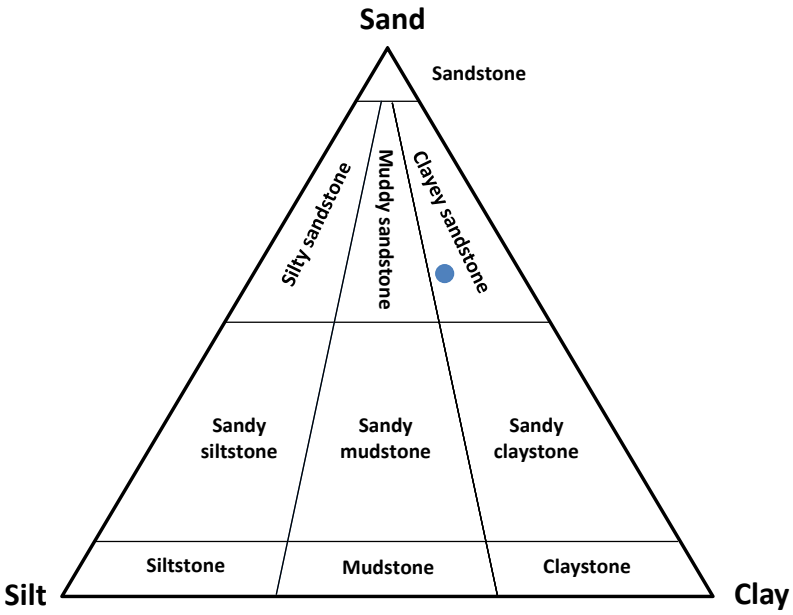


Fig. 4-87: Ternary plot showing the grain size composition of the sample based on the Wentworth scale (after Folk, 1954). Sample 13283 is classified as a clayey sandstone.

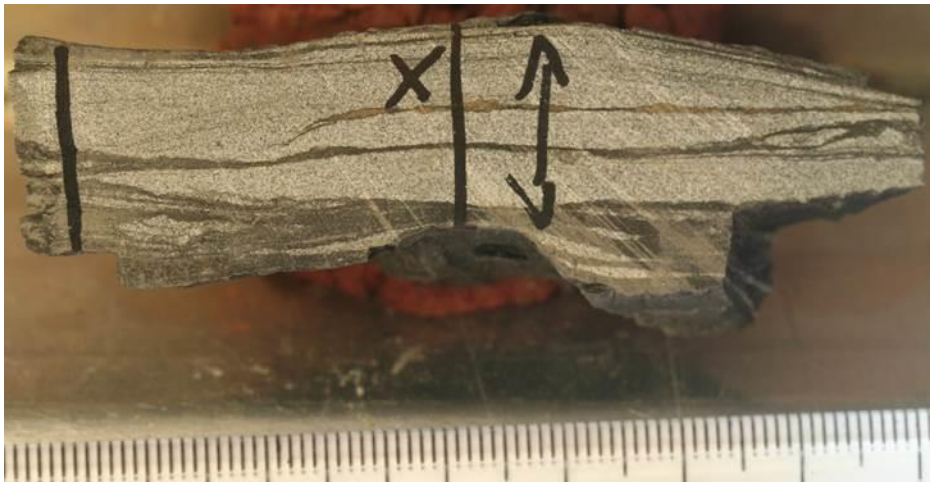


Fig. 4-88: Core photograph of sample 13283 from the Cardium Formation, well 100/04-18-060-20W5/00 (depth 1607.30 m). The thin section prepared from this sample was cut from the area marked with an X. The sample was received with no top orientation. Scale is in mm.

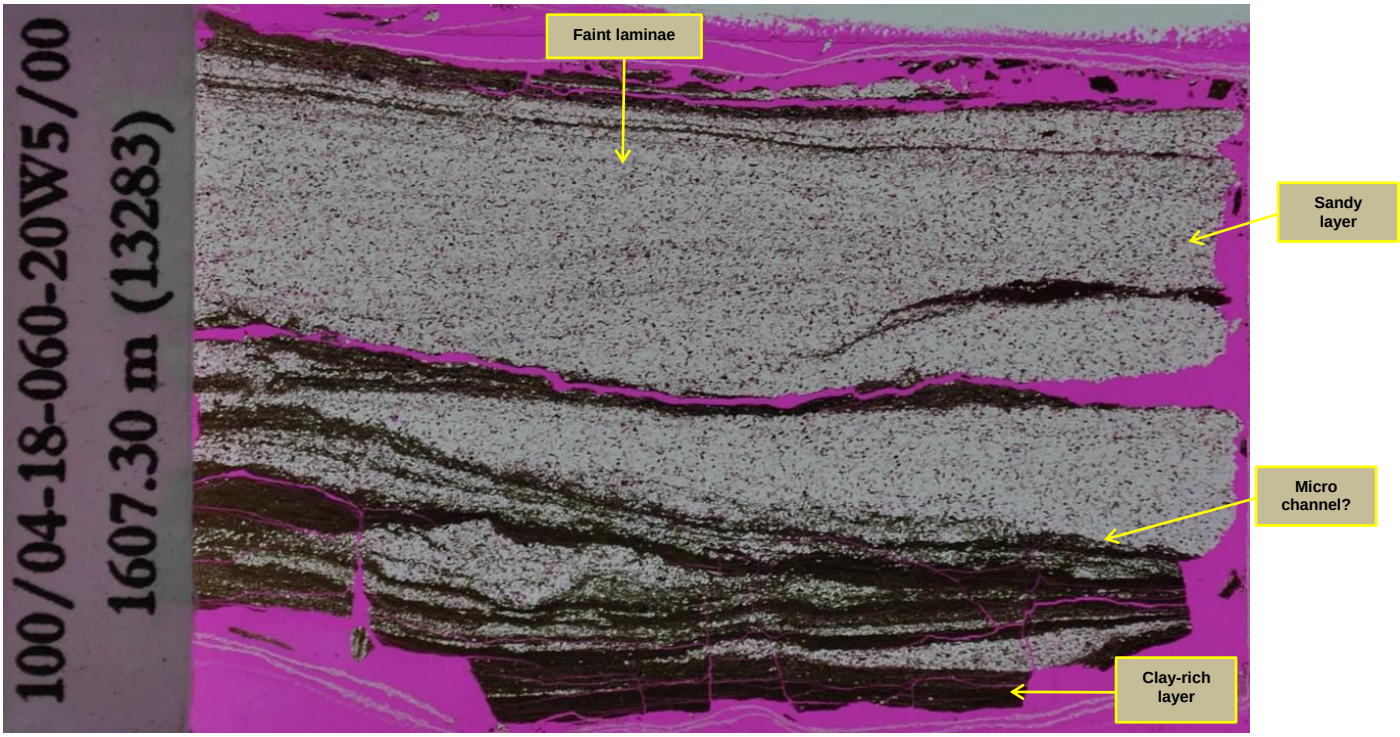


Fig. 4-89: Thin section photograph of sample 13283 from the Cardium Formation, well 100/04-18-060-20W5/00 (depth 1607.30 m). The sample is an interbedded clayey sandstone. Sharp contacts separate the sandy layers and interbedded organic/clay-rich laminae and lenses. Some wavy and ripple-like features are observed along the bases of the sandy layers. The lower part of the sample shows occasional thin silty lenses. Faint cross- and parallel laminae are observed in the uppermost (as shown) sandy layer. The depositional way up was not indicated on this sample, and has been inferred from the bedding structure. Scale is mm.

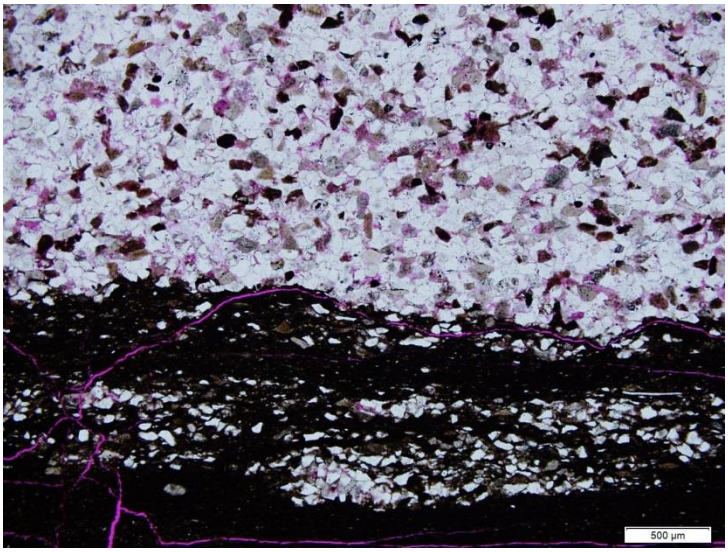


Fig. 4-90: Photomicrograph in PPL showing an overview of the interbedded sandstone. Much of the sample consists of sandy packages interbedded with organic/clay-rich laminae. Sharp contacts separate these layers. Some discontinuous silty lenses are present within the clay-rich laminae. Note several artificial fractures in the lower half of the image (filled with pink epoxy).

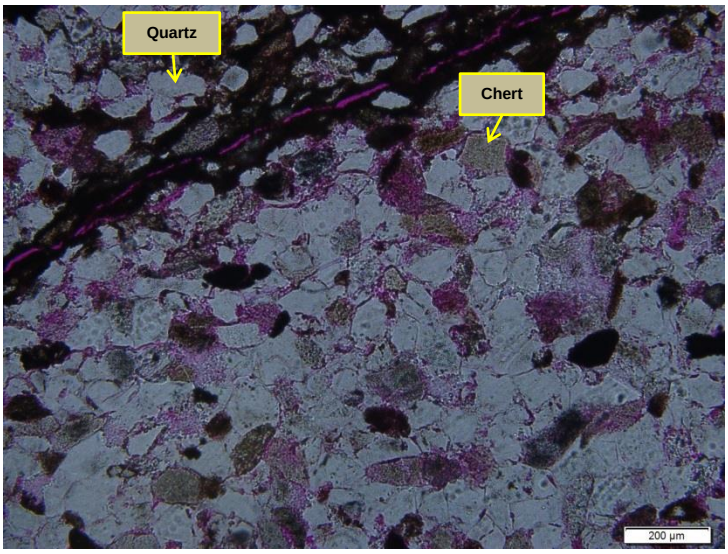


Fig. 4-91: Photomicrograph in PPL showing angular (common) to subrounded (rare) fine silt- to fine sand-sized (average grain size is very fine sand) detrital quartz (70-80%) and chert (8-12%). Chert grains appear more dusty or “dirty” in PPL. The upper left coner of the image shows a thin, opaque streak that contains a micro-fracture (pink epoxy).

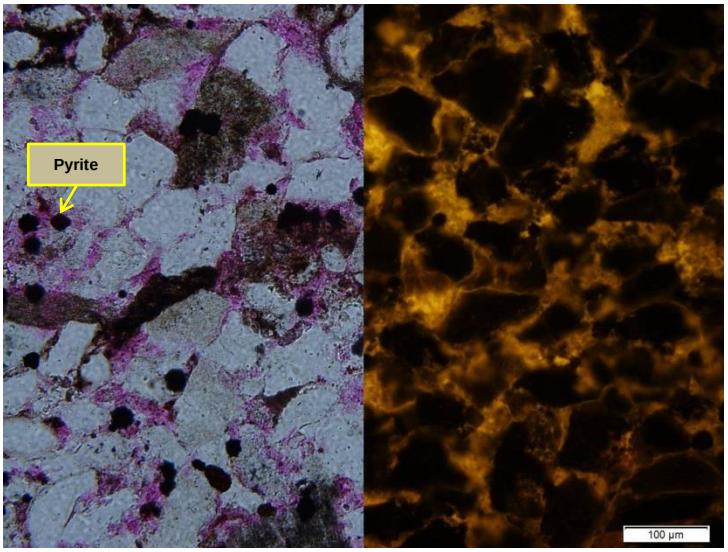


Fig. 4-92: Photomicrograph (left half in PPL, right half in UV light) showing 5-10% estimated intergranular porosity (pink epoxy) observed in a sandy layer. These layers comprise ~75% of the sandstone. Note several pyrite framboids within the pore space.

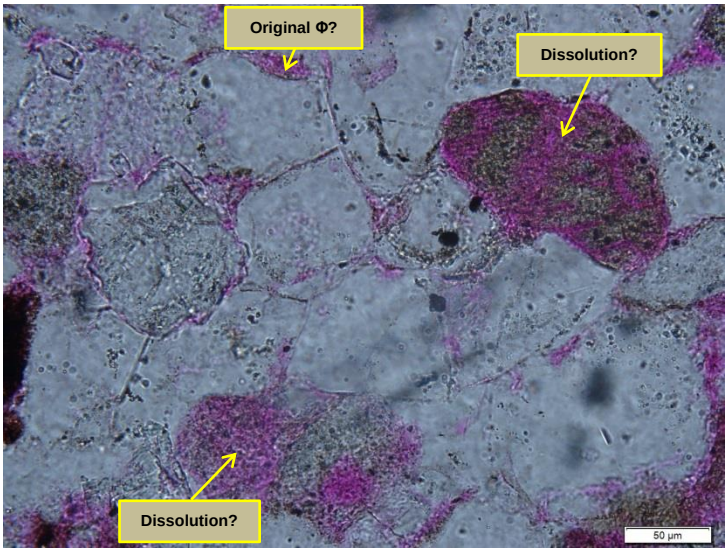


Fig. 4-93: Photomicrograph in PPL detailing porosity within a sandy layer. The porosity observed in these layers appears to include a combination of intergranular porosity and secondary porosity (microporosity) created by partial dissolution of detrital chert grains.

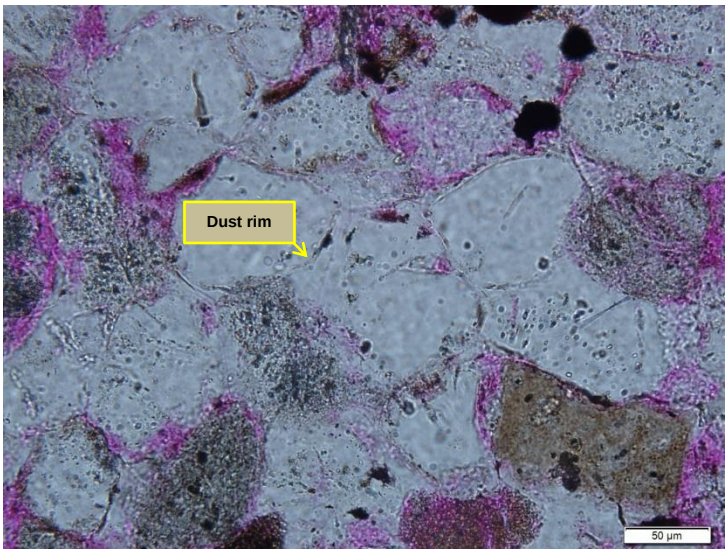


Fig. 4-94: Photomicrograph in PPL showing numerous quartz overgrowth cements observed in a sandy layer. Original quartz grain boundaries are highlighted by subtle dust rims.

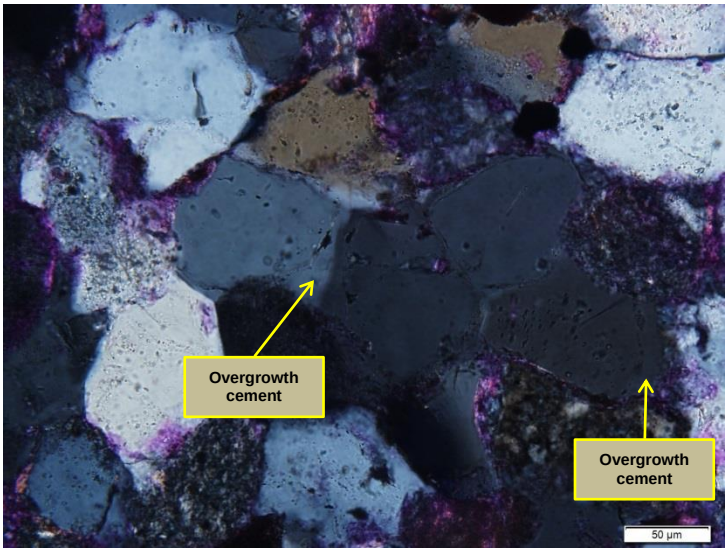


Fig. 4-95: Photomicrograph in XPL showing common quartz overgrowth cements observed in a sandy layer (same field of view as shown in Figure 4-94). Overgrowth cements occur on both quartz and chert grains, and appear to significantly reduce pore connectivity in the sandstone.

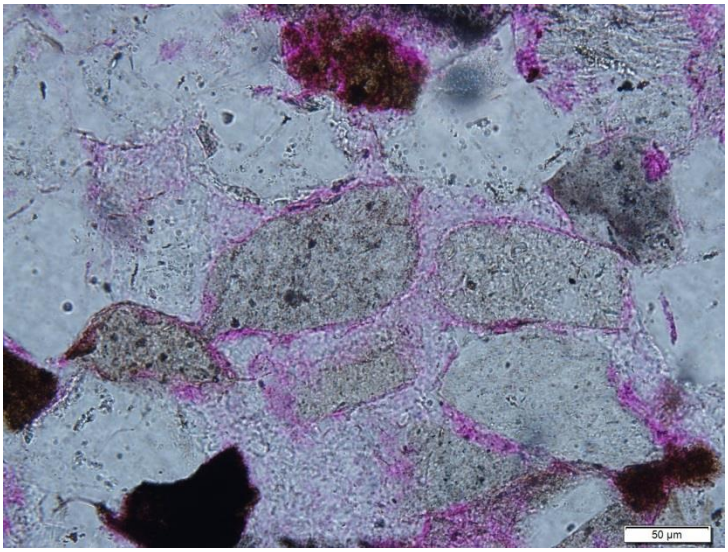


Fig. 4-96: Photomicrograph in PPL showing pore-filling kaolinite observed in a sandy layer.

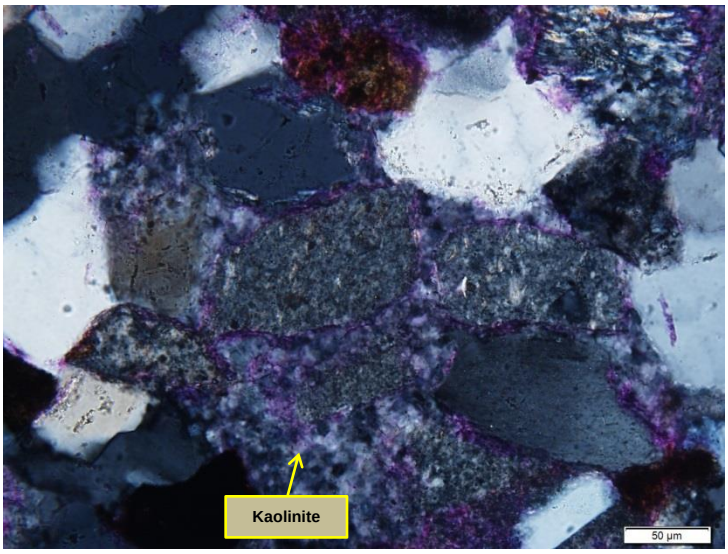


Fig. 4-97: Photomicrograph in XPL showing pore-filling kaolinite observed in a sandy layer (same field of view as shown in Figure 4-96). Areas of the sample that contain kaolinite show more complete filling of pore space than those dominated by quartz overgrowth cements.

4.2.10 SAMPLE 13286

Sample ID	**13286**		
Sample type	**Core**	**UWI/Well**	**100/04-18-060-20W5/00**
Strat. Unit	**Cardium Formation**	**Depth**	**1612.25 m**

XRD/SRA results

Quartz (%)	Fsp (%)	Cb (%)	Clays (%)	Pyrite (%)
78.1	1.4	0.3	20	0.3

Composition (*in order of abundance*)

Grain size	%	Variety (%)	Variety (%)	Variety (%)	Variety (%)
sand	47	Quartz/chert (98)	Mica (2)	Feldspar (<1)	
silt	20	Quartz/chert (96)	Mica (4)		
clay	25	Clay mins (100)			
Cement	5	Quartz (95)	Chert (5)		
Bioclasts	0				
Organics	3	Amorphous (100)			
Opaques	<1	Pyrite (100)			
	100				

*Intensively altered to clay minerals

^ Including bitumen

Sedimentary structures

Primary	None apparent (heavily bioturbated).
Biogenic	Pervasive bioturbation.

Fractures	Occasional thin (10-77 µm thickness) epoxy-filled fractures. Likely artificial.
Porosity	2-5% porosity in clay-poor sections.

Description

Heavily bioturbated muddy sandstone comprised of subangular (common) to subrounded (rare) fine silt- to medium sand-sized detrital quartz (75-85%), chert (12-18%), mica (1-5%), and feldspar (<1%). 2-5% porosity is observed in clay-poor sections of the sandstone, which are cemented by quartz and chert.

Thin Section Quality

Good. Some exposed thin section glass.

Rock Classification

Muddy sandstone.

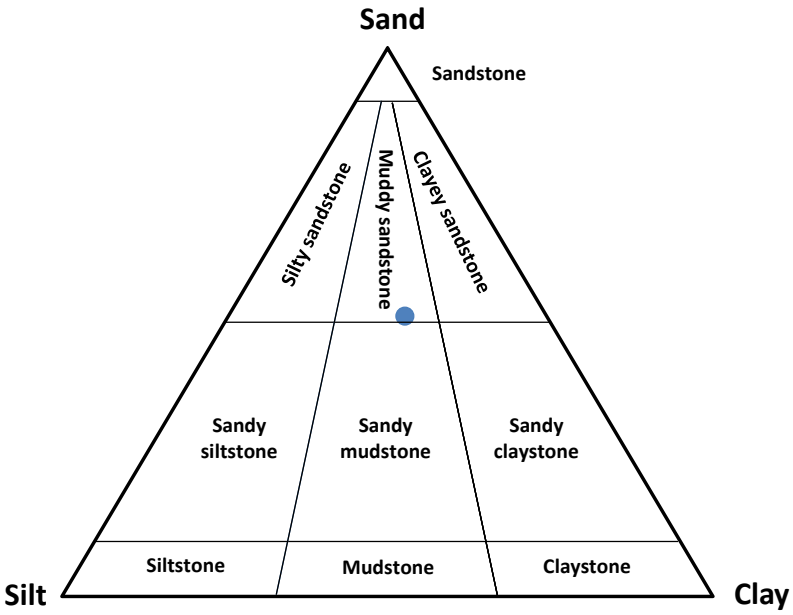


Fig. 4-98:Ternary plot showing the grain size composition of the sample based on the Wentworth scale (after Folk, 1954). Sample 13286 is classified as a muddy sandstone.

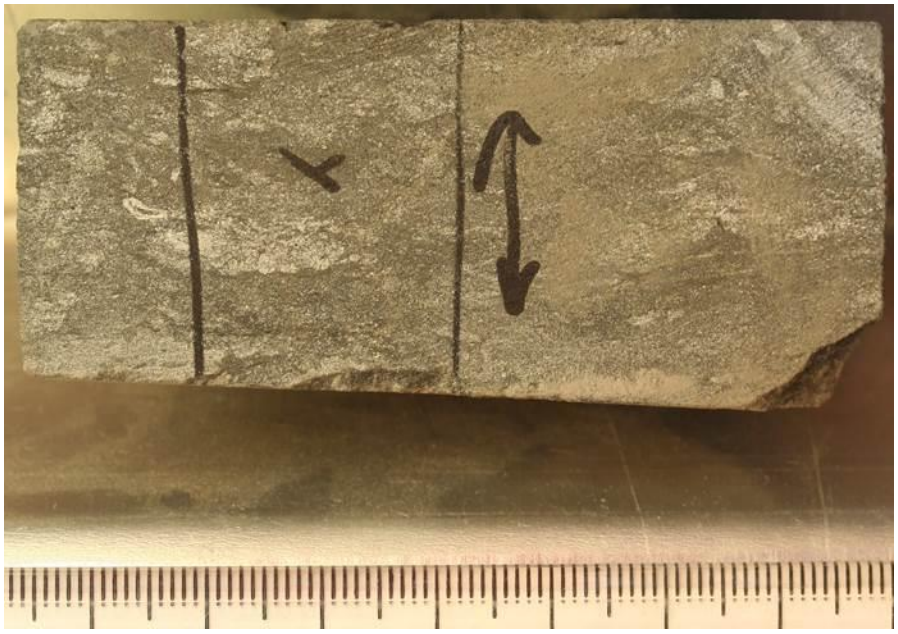


Fig. 4-99: Core photograph of sample 13286 from the Cardium Formation, well 100/04-18-060-20W5/00 (depth 1612.25 m). The thin section prepared from this sample was cut from the area marked with an X. The sample was received with no top orientation. Scale is mm.

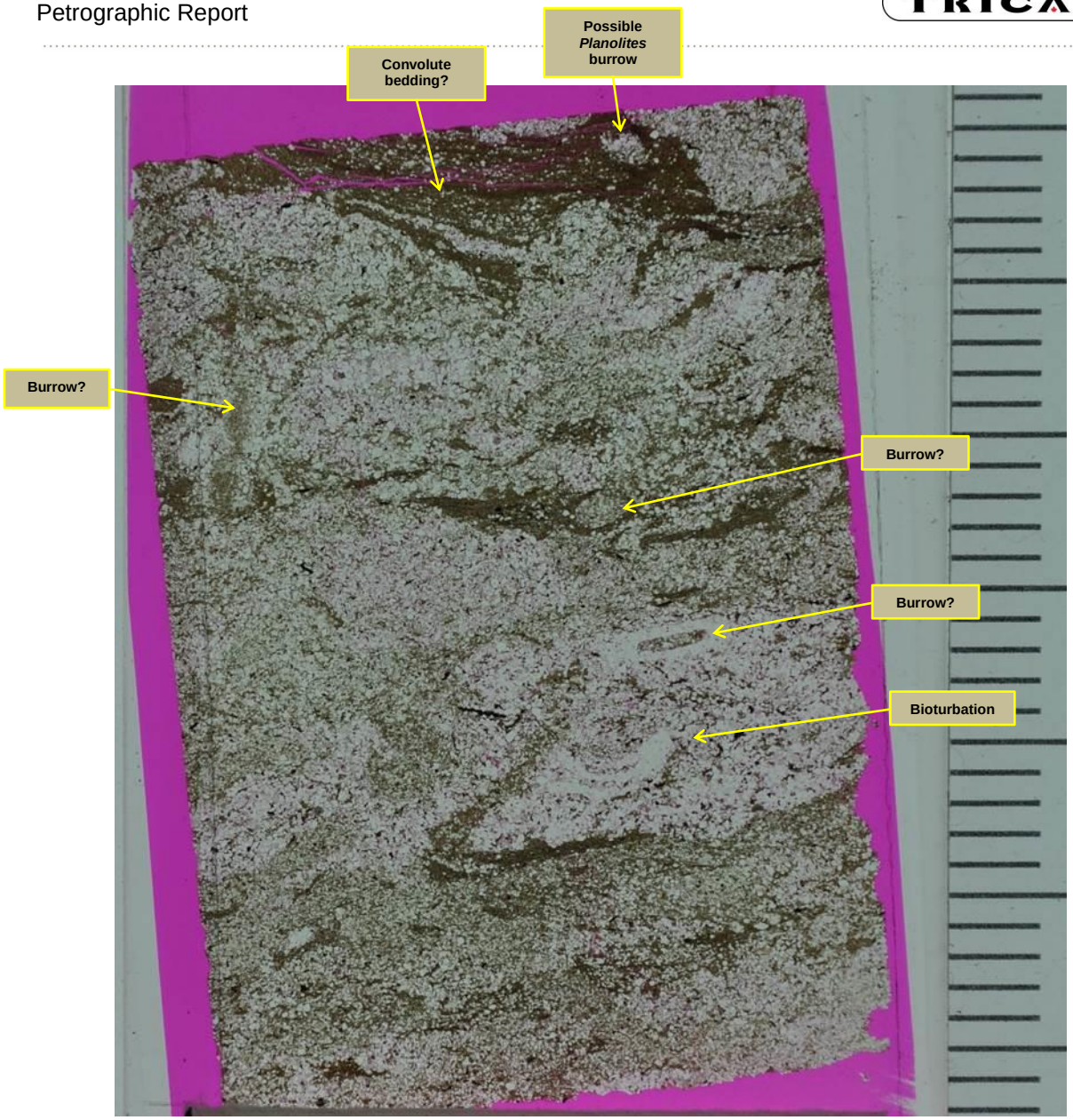


Fig. 4-100: Thin section photograph of sample 13286 from the Cardium Formation, well 100/04-18-060-20W5/00 (depth 1612.25 m). The sample is a heavily bioturbated muddy sandstone. The sample lacks distinct bedding-parallel sedimentary structures, with several clay-rich wisps and convolute patches indicating that the original sediment was pervasively reworked by burrowing organisms. Scale is in mm. Comment: orientation of sample was not established.

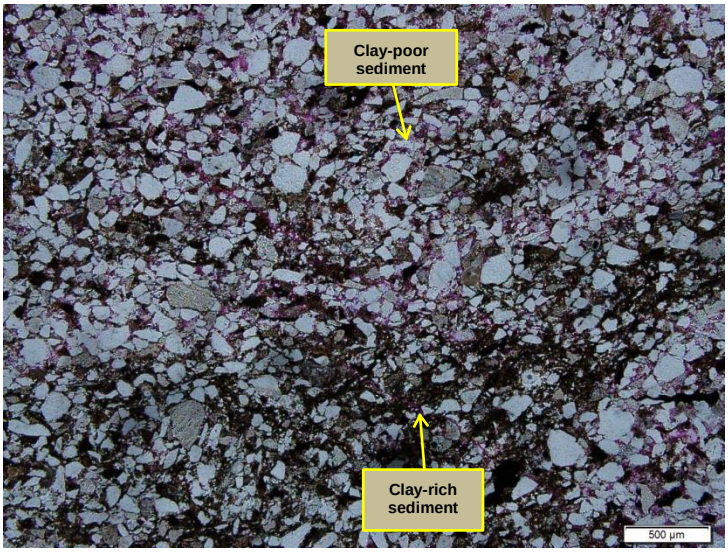


Fig. 4-101: Photomicrograph in PPL showing an overview of the heavily bioturbated muddy sandstone. Clay-rich patches are common and are associated with reduced porosity. The majority of the sample lacks distinct primary sedimentary structures, suggesting that the original sediment was pervasively bioturbated after deposition.



Fig. 4-102: Photomicrograph in PPL showing possible convolute bedding with clay-rich lenses and patches observed near the top of the sample (see location in Figure 4-100). Note porosity (pink epoxy) within the coarser-grained sediment patch.

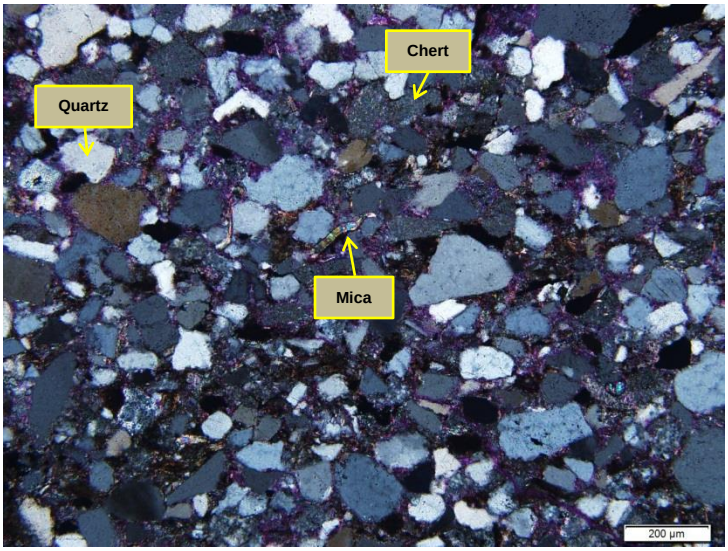


Fig. 4-103: Photomicrograph in XPL showing subangular (common) to subrounded (rare) fine silt- to medium sand-sized detrital quartz (75-85%), chert (12-18%), and mica (1-5%) observed in the sandstone.

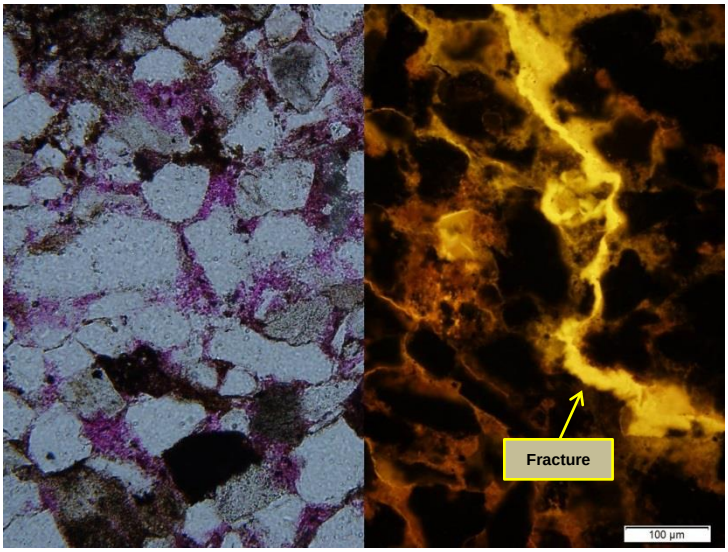


Fig. 4-104: Photomicrograph (left half in PPL, right half in UV light) showing ~5% intergranular porosity (filled with pink epoxy) observed in a clay-poor section of the sample. Fractures are occasionally observed in porous sections of this rock, and may have artificially enhanced the amount of porosity observed.

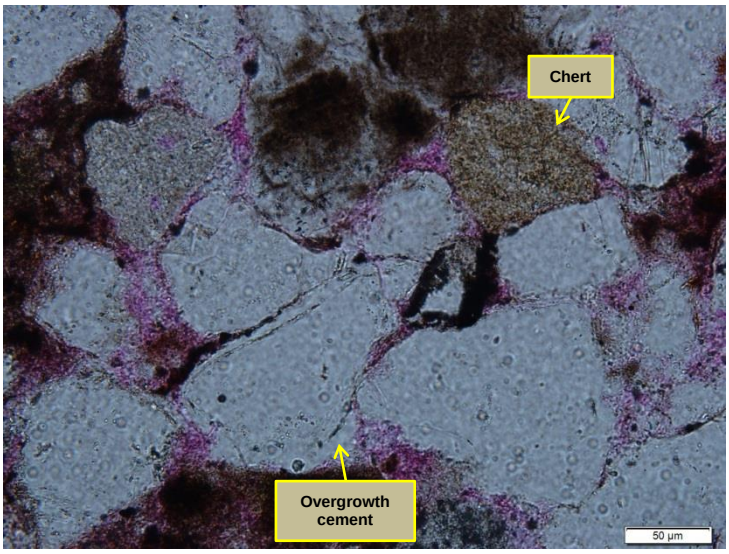


Fig. 4-105: Photomicrograph in PPL illustrating quartz overgrowths observed cementing detrital grains. Quartz overgrowths account for ~95% of the cement present in the sample.

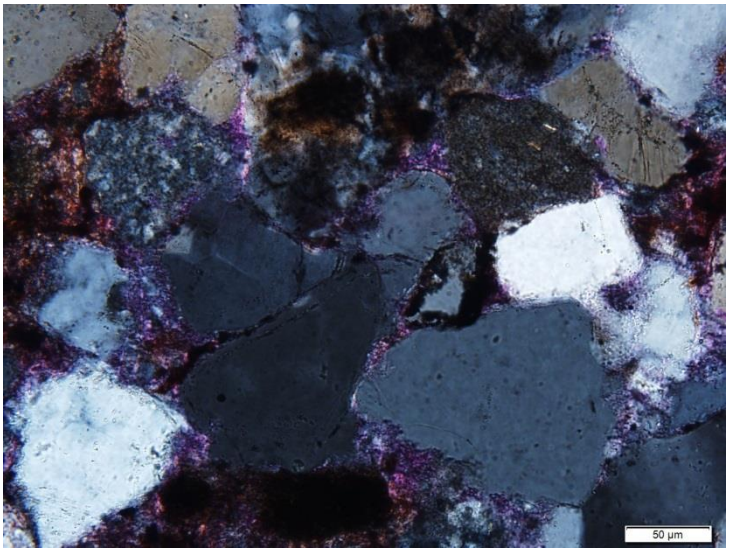


Fig. 4-106: Photomicrograph in XPL showing an example of quartz overgrowth cements (same field of view as Figure 4-105). These overgrowths fill pores and form bridges between grains, significantly reducing pore connectivity in some parts of the sample.

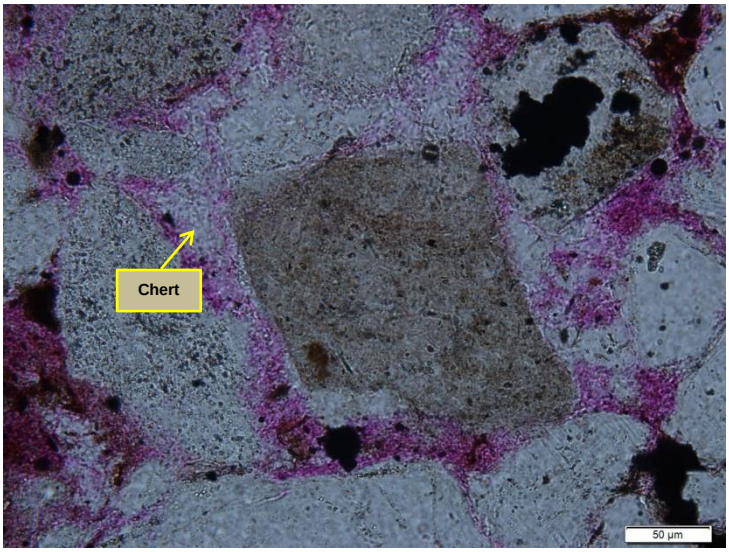


Fig. 4-107: Photomicrograph in PPL showing an example of microcrystalline quartz cement, which accounts for ~5% of the cement present in the sample. Some clay material is likely present in the pore system.

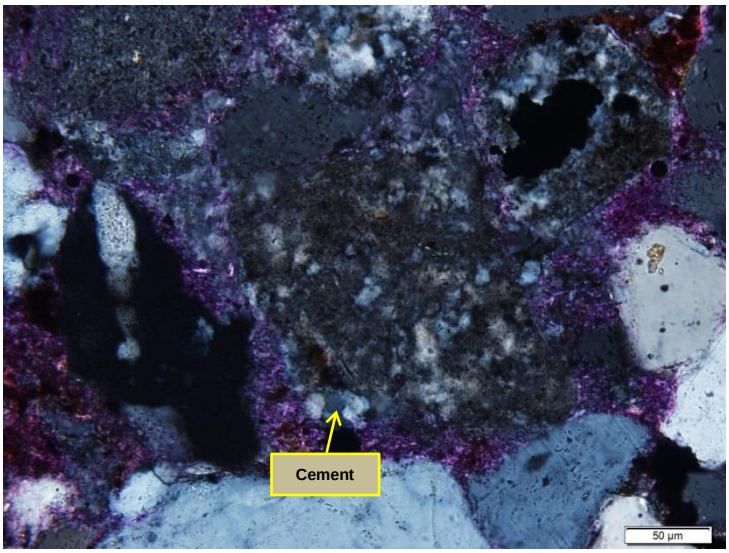


Fig. 4-108: Photomicrograph in XPL showing an example of microcrystalline quartz cement (same field of view as Figure 4-107). The detrital chert shows darker grey colours than the cements.

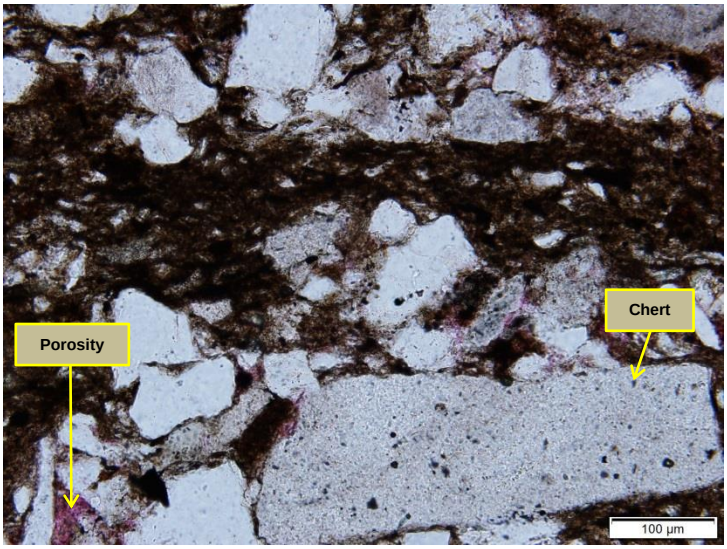


Fig. 4-109: Photomicrograph in PPL showing a clay-rich streak observed at the top of the sample. Fine silt- to medium sand-sized grains (a chert grain in the image reaches ~440 µm in size) are embedded in the clay-rich layer. Organic matter and finely disseminated pyrite are associated with clay material. Note minor intergranular porosity (pink epoxy).

4.2.11 SAMPLE 13403

Sample ID	**13403**		
Sample type	**Core**	**UWI/Well**	**100/06-12-048-11W5/00**
Strat. Unit	**Cardium Formation**	**Depth**	**1773.75 m**

XRD/SRA results

Quartz (%)	Fsp (%)	Cb (%)	Clays (%)	Pyrite (%)
51.1	3.5	0.1	43.8	1.6

Composition (*in order of abundance*)

Grain size	%	Variety (%)	Variety (%)	Variety (%)	Variety (%)
sand	11	Quartz/chert (90)	Mica (6)	Feldspar (<5)	
silt	28	Quartz/chert (97)	Mica (3)		
clay	45	Clay mins (100)			
Cement	6	Quartz (100)			
Bioclasts	<1	Foraminifera (100)			
Organics	8	Amorphous (100)			
Opaques	2	Pyrite (100)			
	100				

*Intensively altered to clay minerals

^ Including bitumen

Sedimentary structures

Primary	The upper half of the sample shows a sequence consisting of (in stratigraphic order): thinly interbedded clay-rich and silty laminae, cross-bedded sand, finely laminated silty bedding, and finely laminated clay-rich bedding.
Biogenic	The lower half of the sample appears partially reworked, with some discontinuous (remnant?) finely laminated clay-rich bedding visible.

Fractures	Common epoxy-filled fractures. Likely artificial.
Porosity	None apparent.

Description

Sandy mudstone comprised of subangular (common) to subrounded (rare) very fine silt- to very fine sand-sized detrital quartz (20-40%), chert (5-12%), mica (1-5%), and feldspar (1-2%). The lower half of the rock appears heavily bioturbated, with only a small, discontinuous section of finely laminated clay-rich bedding visible. The upper half of the rock shows a depositional sequence consisting of thinly interbedded clay-rich and silty laminae, cross-bedded sand, finely laminated silty bedding, and finely laminated clay-rich bedding.

Thin Section Quality

Good.

Rock Classification

Sandy mudstone.

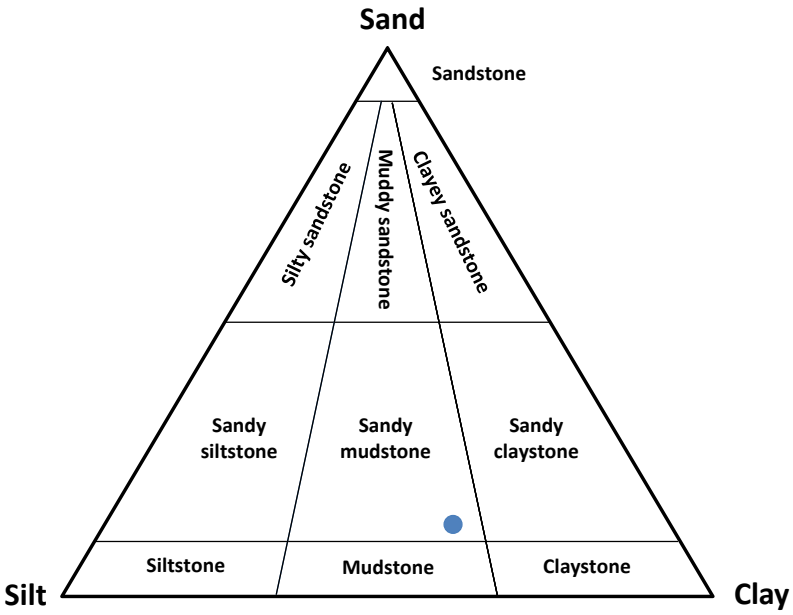


Fig. 4-110: Ternary plot showing the grain size composition of the sample based on the Wentworth scale (after Folk, 1954). Sample 13403 is classified as a sandy mudstone.



Fig. 4-111: Core photograph of sample 13403 from the Cardium Formation, well 100/06-12-048-11W5/00 (depth 1773.75 m). The thin section prepared from this sample was cut from the area marked with an X. The sample was received with no up direction. Scale is in mm.

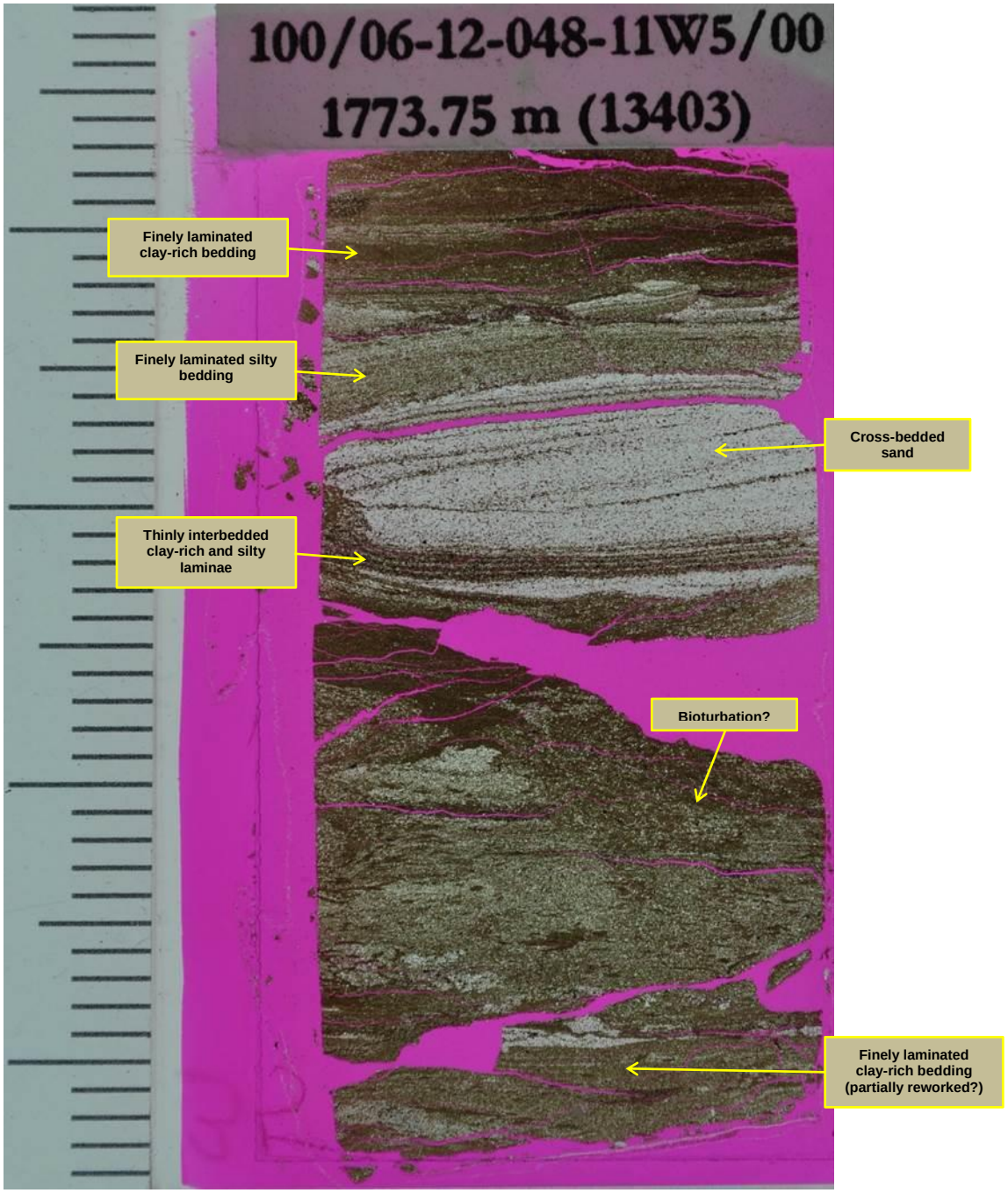


Fig. 4-112: Thin section photograph of sample 13403 from the Cardium Formation, well 100/06-12-048-11W5/00 (depth 1773.75 m). The sample is a sandy mudstone. The lower half of the sample appears heavily bioturbated, and shows discontinuous (remnant?) finely laminated clay-rich bedding. The upper half of the sample contains a depositional sequence consisting of thinly interbedded clay-rich and silty laminae, cross-bedded sand, finely laminated silty and finely laminated clay-rich sediments. Note that the up direction was not indicated on this sample, but was interpreted based on sedimentary structures. Scale is in mm.

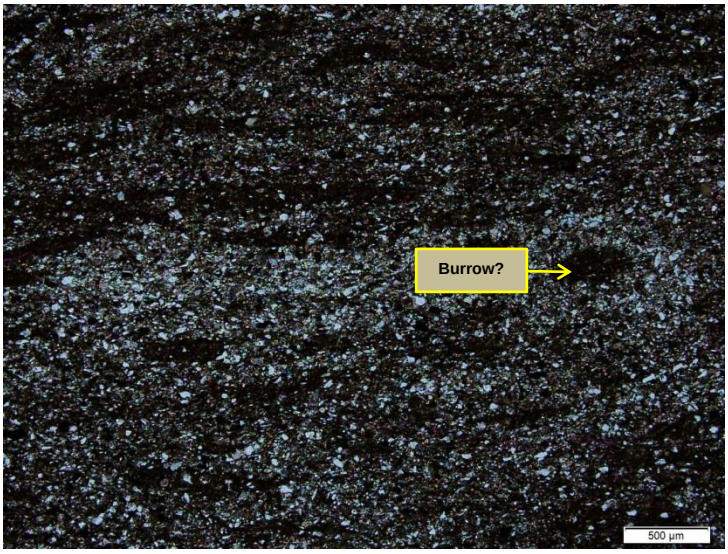


Fig. 4-113: Photomicrograph in PPL showing an overview image of the lower, heavily bioturbated section of the sandy mudstone. Discontinuous laminae are observed in this part of the thin section (see Figure 4-112), but are difficult to identify under the microscope.



Fig. 4-114: Photomicrograph in PPL showing thinly interbedded clay-rich and silty laminae observed in the upper half of the sample. Finer-grained, silt-size particles are observed within the clay-rich laminae. Note several artificial fractures filled with pink epoxy.

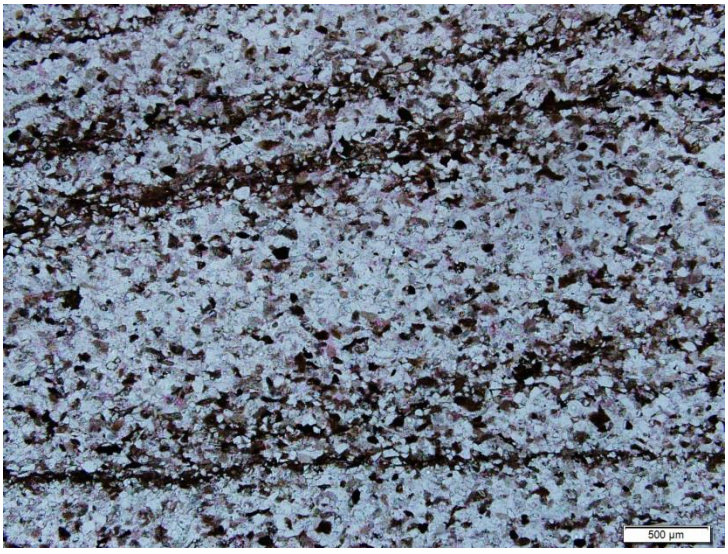


Fig. 4-115: Photomicrograph in PPL showing a cross-bedded sand (upper half of sample) with thin, interbedded opaque-rich laminae. This layer and other sand-rich layers show pervasive quartz cementation, with rare visible intergranular porosity.

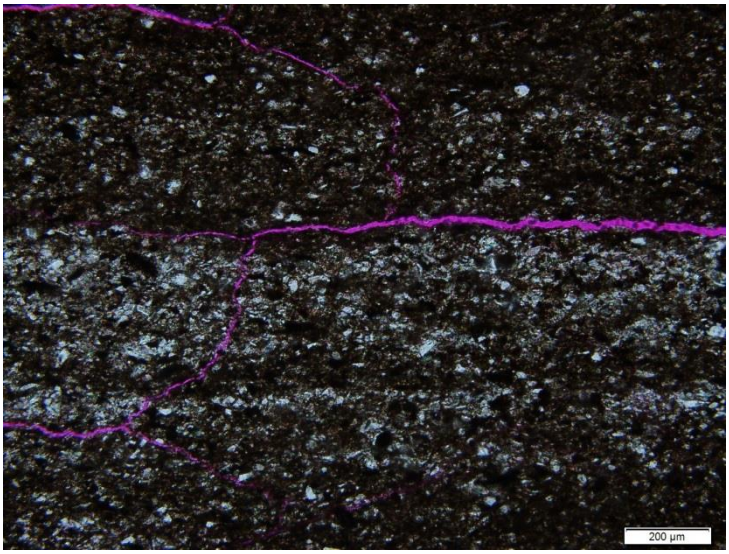


Fig. 4-116: Photomicrograph in PPL showing finely laminated silty and clay-rich bedding observed in the upper half of the sample. Clay patches within the silty laminae are likely due to bioturbation. Note artificial fracturing (pink epoxy).

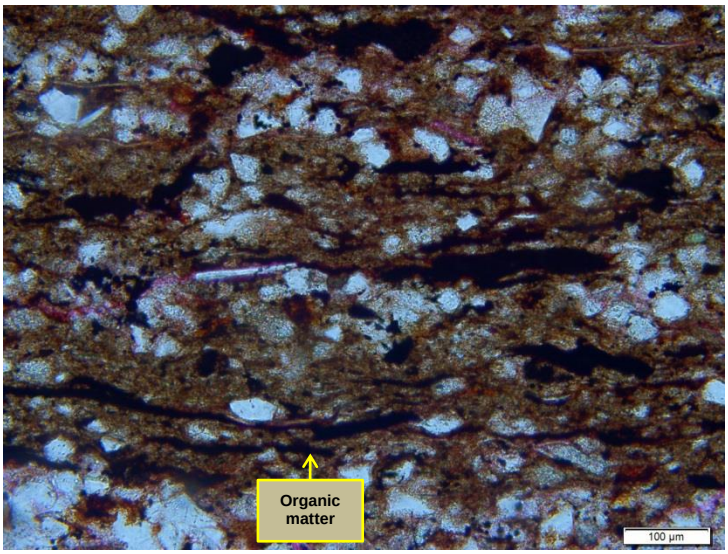


Fig. 4-117: Photomicrograph in PPL detailing the thinly interbedded clay-rich and silty bedding shown in Figure 4-114. Strands of bedding-parallel organic matter are abundant in these layers. Organic matter comprises ~8% of the total composition. Some finely disseminated pyrite framboids and idiomorphs are also observed.

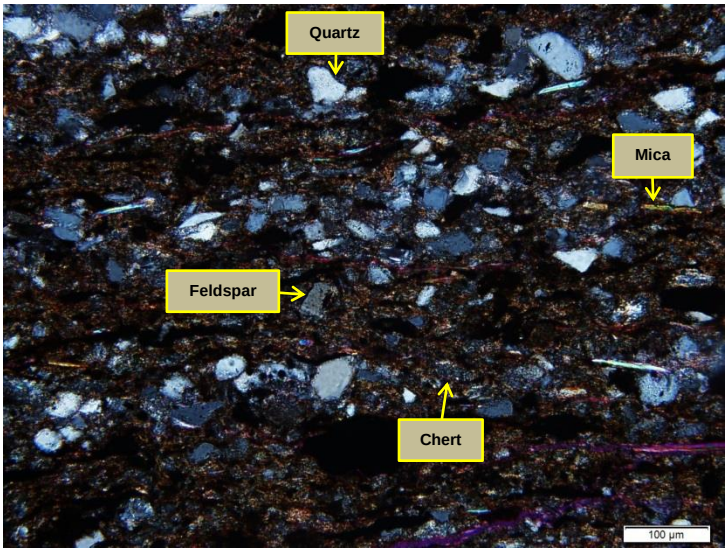


Fig. 4-118: Photomicrograph in XPL showing subangular (common) to subrounded (rare) very fine silt- to very fine sand-sized detrital quartz (20-40%), chert (5-12%), mica (1-5%), and feldspar (1-2%) embedded within the clay-rich matrix. Most mica lathes are oriented parallel to bedding and have high birefringent colours.

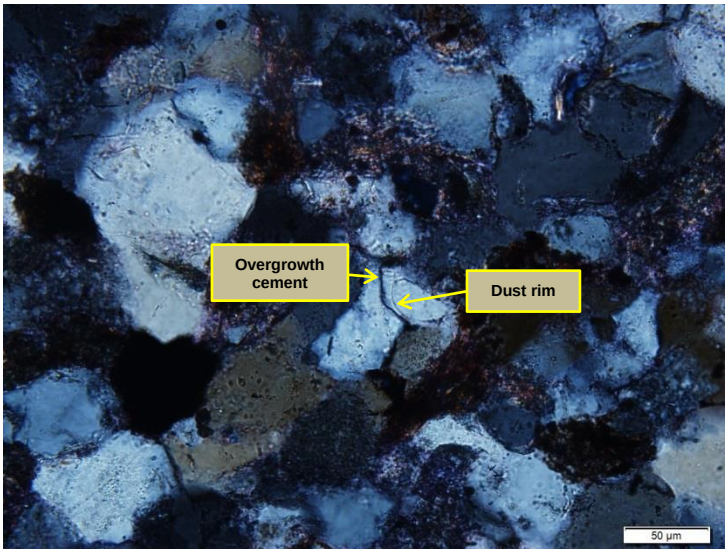


Fig. 4-119: Photomicrograph in XPL illustrating quartz overgrowth cementation observed in the cross-bedded sand shown in Figure 4-115. Intergranular porosity is rare (see Figure 4-121) within this layer due to pervasive cementation of the detrital constituents (quartz, chert, feldspar).

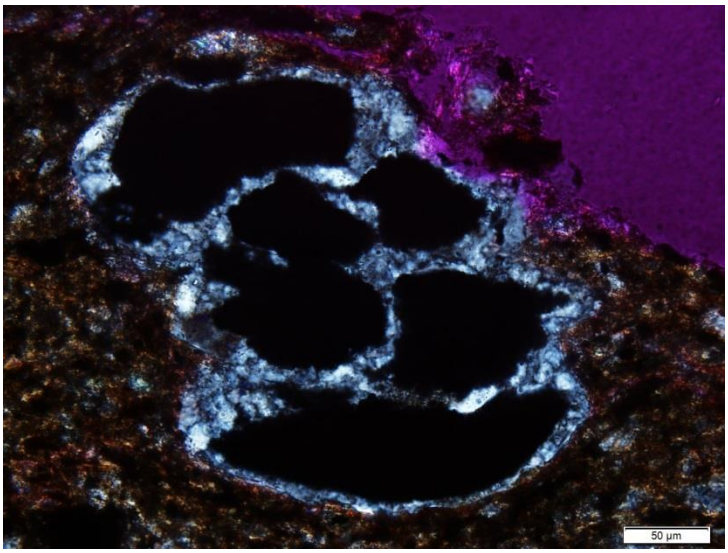


Fig. 4-120: Photomicrograph in XPL of a foram test observed near the top of the sample. The test wall is composed of microcrystalline quartz (recrystallized, ~315 µm in size) and the chambers are filled with pyrite.

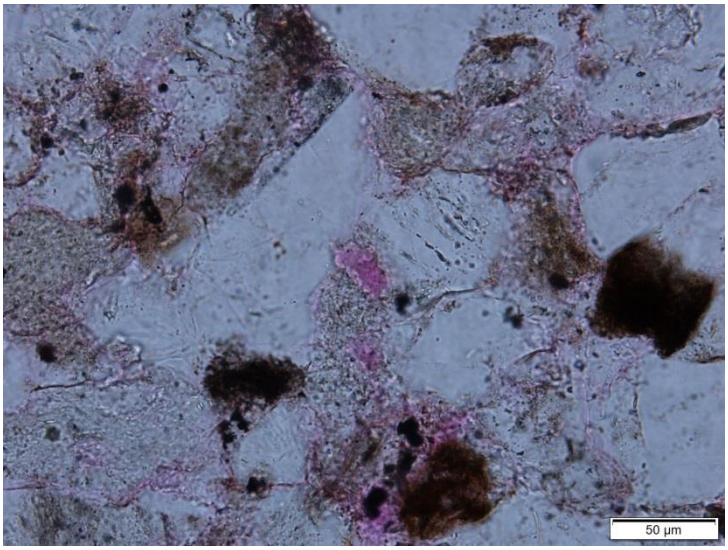


Fig. 4-121: Photomicrograph in PPL illustrating rare intergranular porosity (pink epoxy) in the cross-bedded sand layer. Quartz cementation and compaction are the primary controls on porosity and permeability in the sample.

4.2.12 SAMPLE 13407

Sample ID	**13407**		
Sample type	**Core**	**UWI/Well**	**100/06-12-048-11W5/00**
Strat. Unit	**Cardium Formation**	**Depth**	**1781.31 m**

XRD/SRA results

Quartz (%)	Fsp (%)	Cb (%)	Clays (%)	Pyrite (%)
69.4	3.8	0.1	26	0.7

Composition (*in order of abundance*)

Grain size	%	Variety (%)	Variety (%)	Variety (%)	Variety (%)
sand	60	Quartz/chert (94)	Feldspar (<5)	Mica (3)	
silt	12	Quartz/chert (98)	Mica (2)		
clay	20	Clay mins (100)			
Cement	6	Quartz (100)			
Bioclasts	0				
Organics	1	Amorphous (100)			
Opaques	1	Pyrite (100)			
	100				

*Intensively altered to clay minerals

^ Including bitumen

Sedimentary structures

Primary	Appears unstratified, possibly reflecting pervasive bioturbation.
Biogenic	Appears heavily reworked.

Fractures	Common thin epoxy-filled fractures. Likely artificial.
Porosity	2-8% intergranular porosity is observed in pockets of clay-poor sand.

Description

Bioturbated muddy sandstone comprised of subangular (common) to subrounded (rare) very fine silt to fine sand-sized (average grain size is very fine sand) detrital quartz (30-60%), chert (10-18%), feldspar (1-5%), and mica (1-3%). No primary sedimentary structures are visible in this apparently unstratified rock. Patches of porous, clay-poor, and non-porous, clay-rich, sandy sediment characterize the texture of the rock.

Thin Section Quality

Good.

Rock Classification

Muddy sandstone.

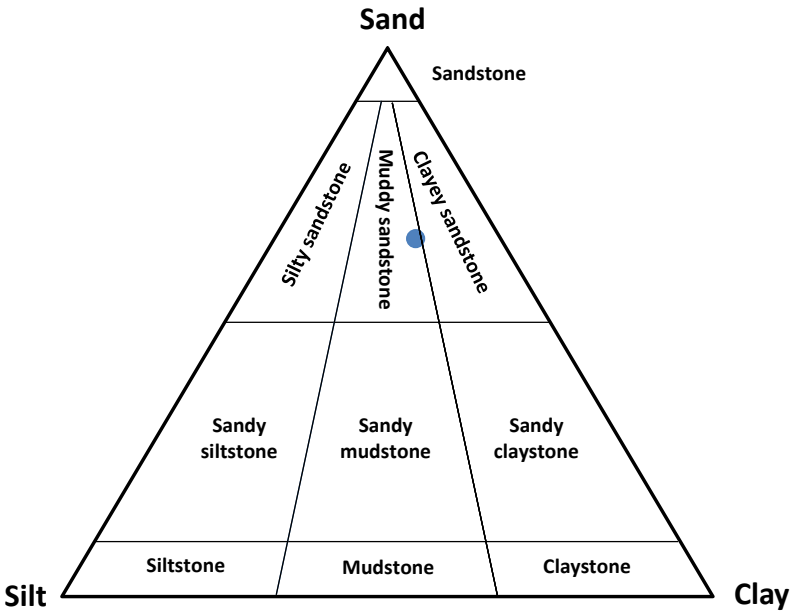


Fig. 4-122: Ternary plot showing the grain size composition of the sample based on the Wentworth scale (after Folk, 1954). Sample 13407 is classified as a muddy sandstone.

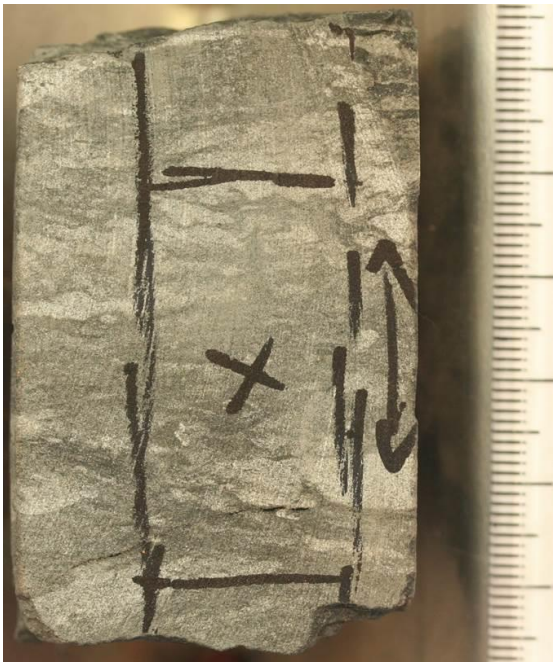


Fig. 4-123: Core photograph of sample 13407 from the Cardium Formation, well 100/06-12-048-11W5/00 (depth 1781.31 m). The thin section prepared from this sample was cut from the area marked with an X. The sample was received with no up direction. Scale is in mm.



Fig. 4-124: Thin section photograph of sample 13407 from the Cardium Formation, well 100/06-12-048-11W5/00 (depth 1781.31 m). The sample is a bioturbated muddy sandstone. The sample lacks distinct primary sedimentary strucutres, possibly indicating heavy sediment mixing or reworking by burrowing organisms. Scale is in mm.

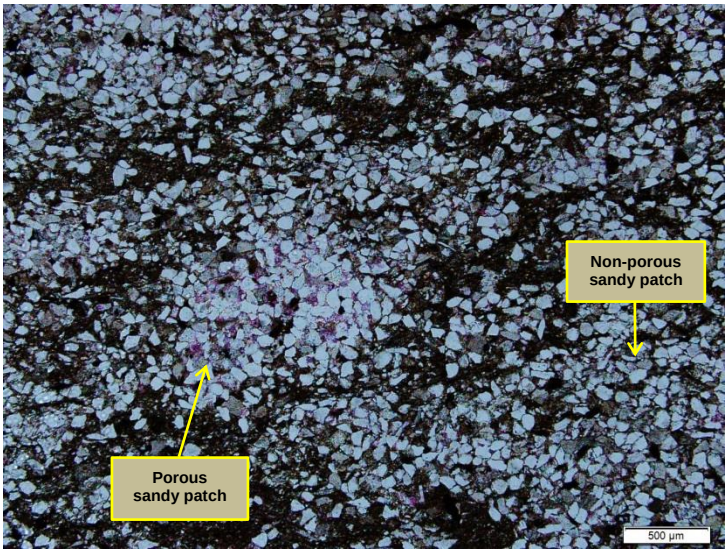


Fig. 4-125: Photomicrograph in PPL showing an overview of the muddy sandstone. The sample lacks primary sedimentary structures, likely due to sediment mixing or pervasive bioturbation. Patches of porous and non-porous sandy sediment characterize the texture, with porosity occurring where interstitial clays or clay patches are minor or absent.

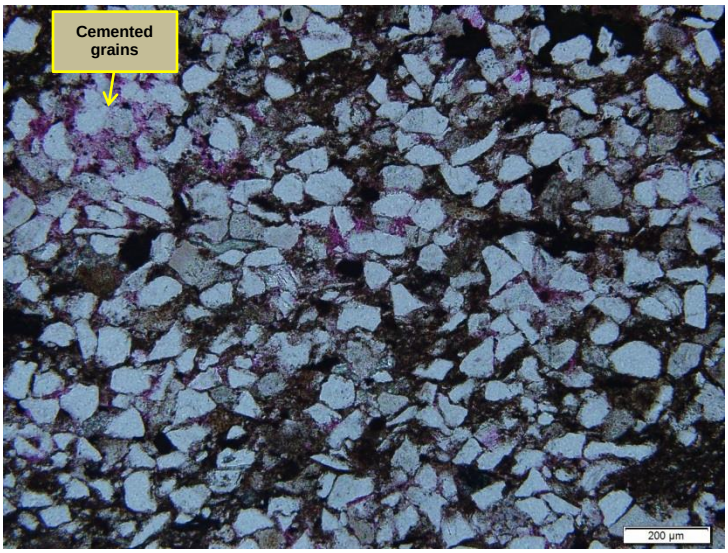


Fig. 4-126: Photomicrograph in PPL showing a mostly clay-rich area of the sample. Clay appears to be the dominant control on the occurrence and distribution of porosity. Some cemented grains are observed within the patch of porous sand.

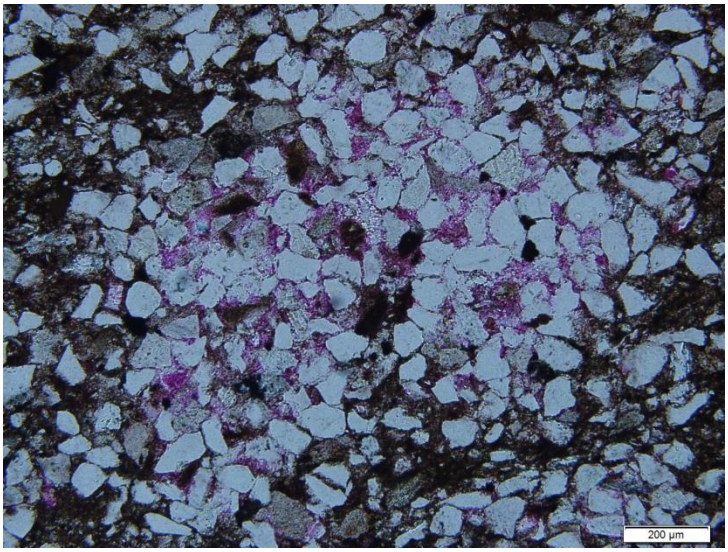


Fig. 4-127: Photomicrograph in PPL showing a patch of predominantly sand-sized sediment with 2-8% estimated intergranular porosity (filled with pink epoxy).

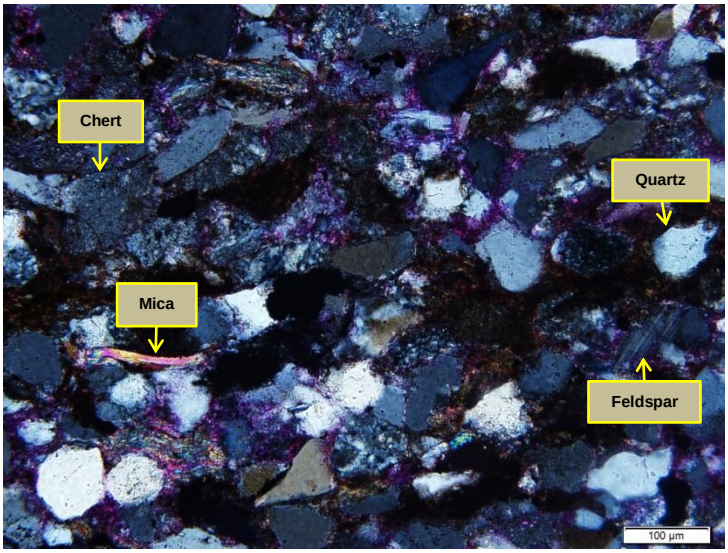


Fig. 4-128: Photomicrograph in XPL showing subangular (common) to subrounded (rare) very fine silt- to fine sand-sized (average grain size is very fine sand) detrital quartz (30-60%), chert (10-18%), feldspar (1-5%), and mica (1-3%). Micas have high birefringent colours in XPL. Note polysynthetic twinning associated with some feldspars.

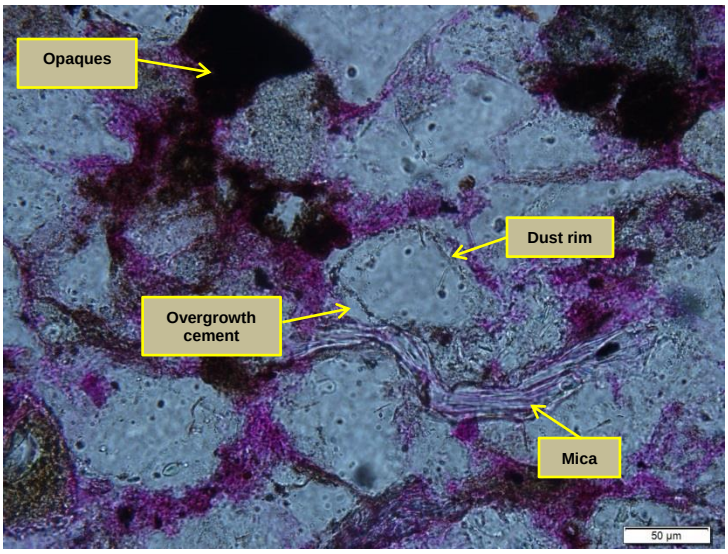


Fig. 4-129: Photomicrograph in PPL detailing quartz overgrowth cementation observed in a patch of porous sand. Whereas the distribution of interstitial clay appears to be the main control on the occurrence and distribution of porosity in this rock, the extent of quartz overgrowth cementation appears to control permeability within areas of porous, clay-poor sediment. Opaque material is also observed within the pore system. Dust rims seperate the detrital grains from the quartz overgrowths. Note a mica lathe bent due to grain compaction.

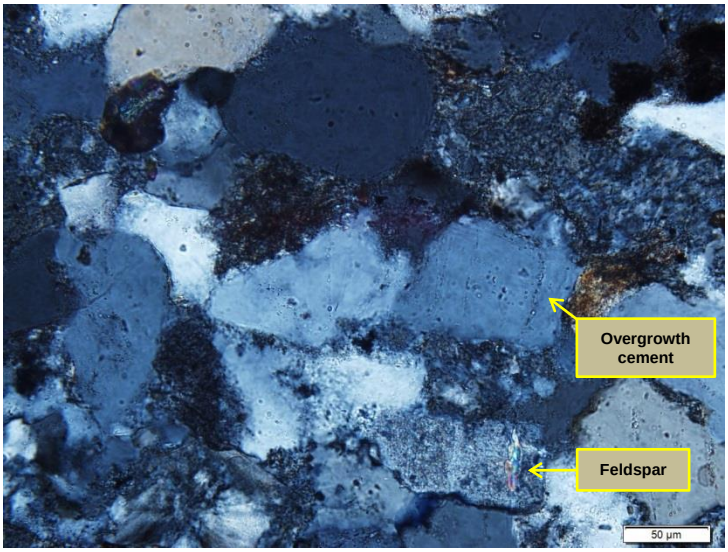


Fig. 4-130: Photomicrograph in XPL showing a completely cemented (clay-poor, and non-porous) area of the sample. Some feldspars can be distinguished from quartz due to a “dirty” appearance and numerous inclusions. Note quartz overgrowths.

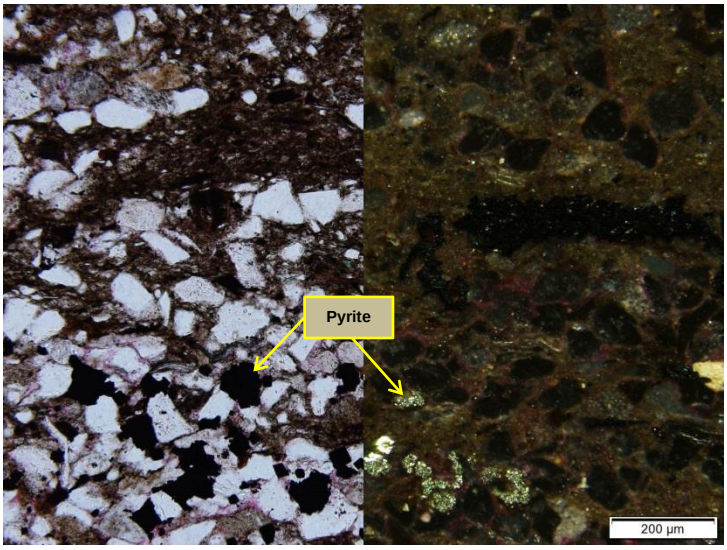


Fig. 4-131: Photomicrograph in PPL (left) and reflected light (right) illustrating clay-rich patches and laminae, as well as numerous pyrite idiomorphs (gold colour in reflected light) forming clusters, within the sandstone. Note minor intergranular porosity (pink epoxy).

4.2.13 SAMPLE 13412

Sample ID	**13412**		
Sample type	**Core**	**UWI/Well**	**100/06-12-048-11W5/00**
Strat. Unit	**Cardium Formation**	**Depth**	**1790.50 m**

XRD/SRA results

Quartz (%)	Fsp (%)	Cb (%)	Clays (%)	Pyrite (%)
63.7	2.9	3.1	29.9	0.3

Composition (*in order of abundance*)

Grain size	%	Variety (%)	Variety (%)	Variety (%)	Variety (%)
sand	27	Quart/chert (94)	Mica (5)	Feldspar (<2)	
silt	40	Quart/chert (98)	Mica (2)		
clay	25	Clay mins (100)			
Cement	2	Quartz (100)			
Bioclasts	0				
Organics	5	Amorphous (100)			
Opaques	1	Pyrite (100)			
	100				

*Intensively altered to clay minerals

^ Including bitumen

Sedimentary structures

Primary	Partially reworked sandy and clayey bedding is visible near the base of the sample. The upper part of the sample appears unstratified, possibly indicating pervasive bioturbation.
Biogenic	Appears heavily reworked.

Fractures	Common thin epoxy-filled fractures. Likely artificial.
Porosity	Minor (<2%) intergranular porosity occurs in a sandy layer near the base of the sample.

Description

Heavily bioturbated sandy mudstone comprised of subangular to subrounded very fine silt- to fine sand-sized (average gain size is coarse silt) detrital quartz (40-55%), chert (10-18%), mica (1-5%), and feldspar (<3%). Much of the rock appears unstratified, possibly indicating heavy post-depositional sediment reworking by burrowing organisms. Partially reworked sandy and clay-rich bedding is visible near the base of the sample.

Thin Section Quality

Poor. Abundant exposed thin section glass.

Rock Classification

Sandy mudstone.

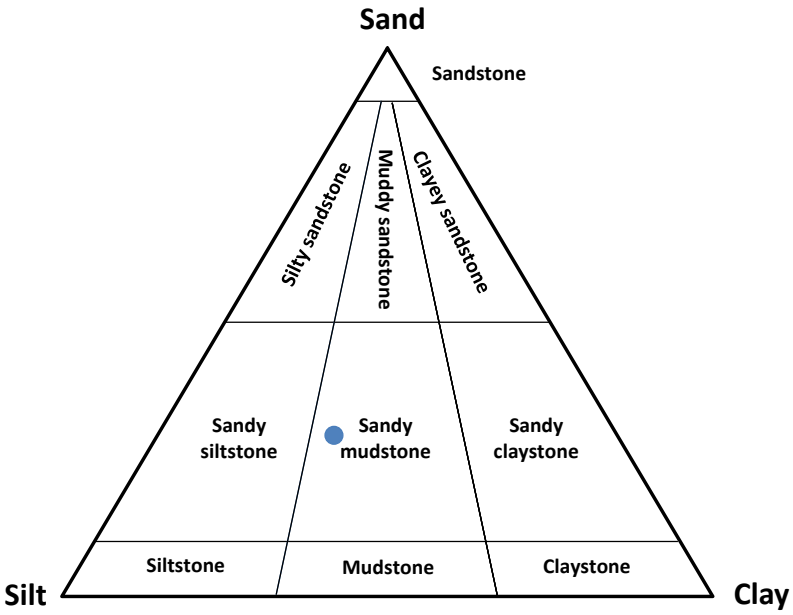


Fig. 4-132: Ternary plot showing the grain size composition of the sample based on the Wentworth scale (after Folk, 1954). Sample 13412 is classified as a sandy mudstone.

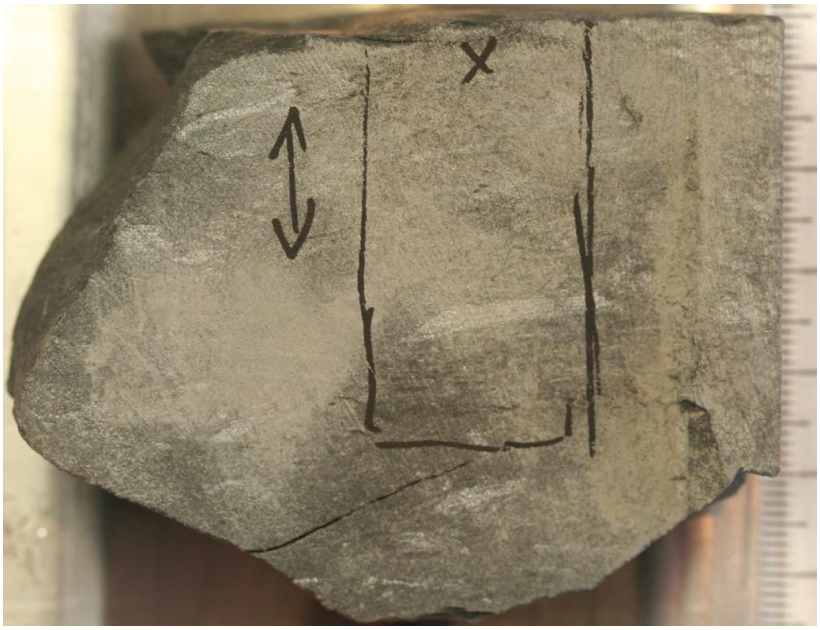


Fig. 4-133: Core photograph of sample 13412 from the Cardium Formation, well 100/06-12-048-11W5/00 (depth 1790.50 m). The thin section prepared from this sample was cut from the area marked with an X. The sample was received with no up direction. Scale is in mm.

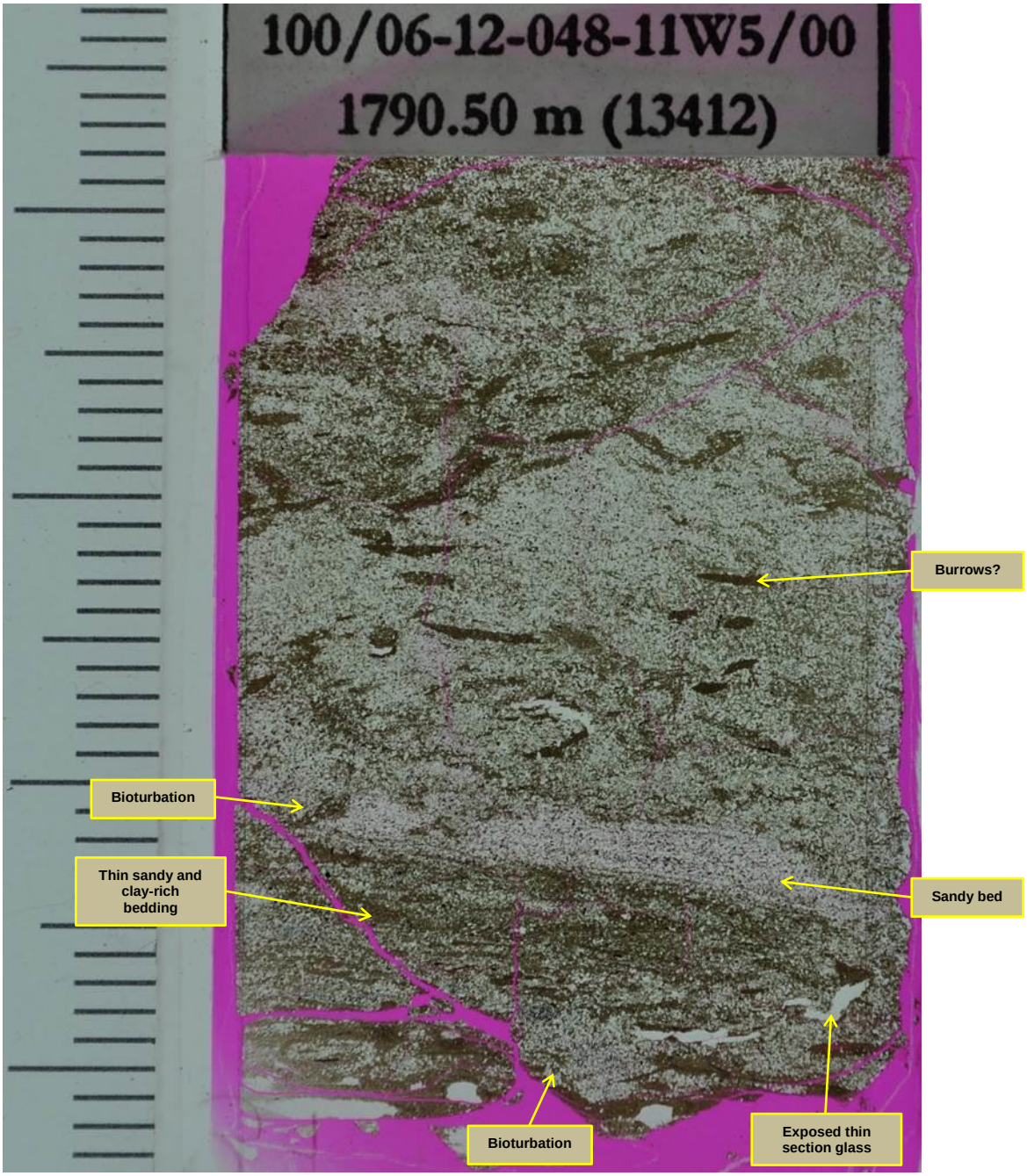


Fig. 4-134: Thin section photograph of sample 13412 from the Cardium Formation, well 100/06-12-048-11W5/00 (depth 1790.50 m). The sample is a heavily bioturbated sandy mudstone. Partially disturbed clay-rich and sandy bedding are observed towards the base of the image, whereas the upper part appears to be unstratified, possibly indicating pervasive bioturbation or sediment mixing. Scale is in mm. Note: Up-direction was not indicated and is difficult to positively identify.

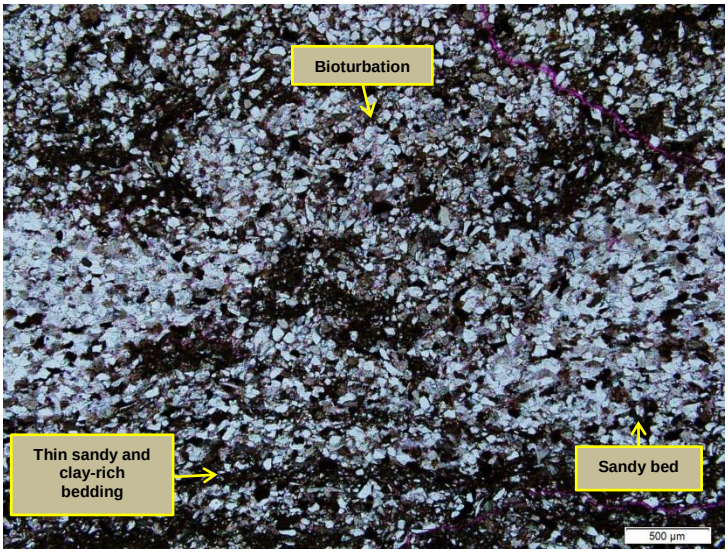


Fig. 4-135: Photomicrograph in PPL showing an overview of the sandy mudstone. Much of the upper section of the sample lacks bedding features, and is heavily bioturbated or mixed with abundant clay-rich patches and thin streaks. The sandy bed shown in the middle of this image (see location in Figure 4-134) is partially reworked, with bioturbation disturbing the original continuity of the layer.

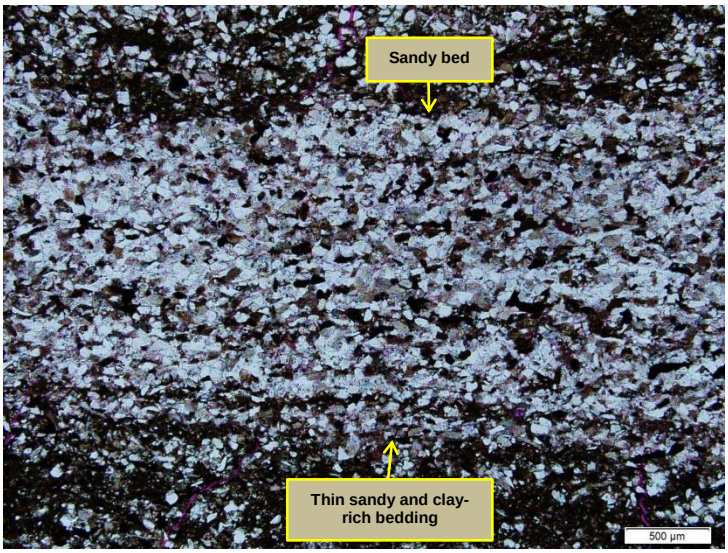


Fig. 4-136: Photomicrograph in PPL showing an undisturbed sandy layer bound between clay-rich bedding near the base of the sample.

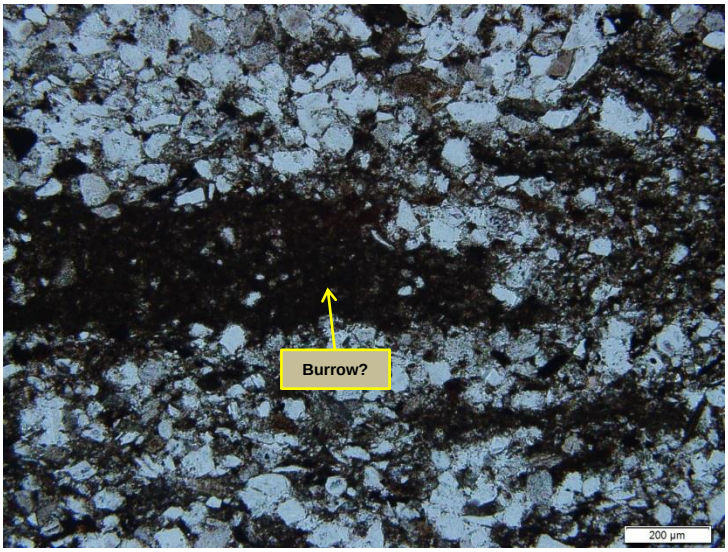


Fig. 4-137: Photomicrograph in PPL detailing the unstratified upper section of the sample. No primary sedimentary structures are apparent, but clay rich patches and lenses intermixed with sandy sediments are common due to burrowing and bioturbation.

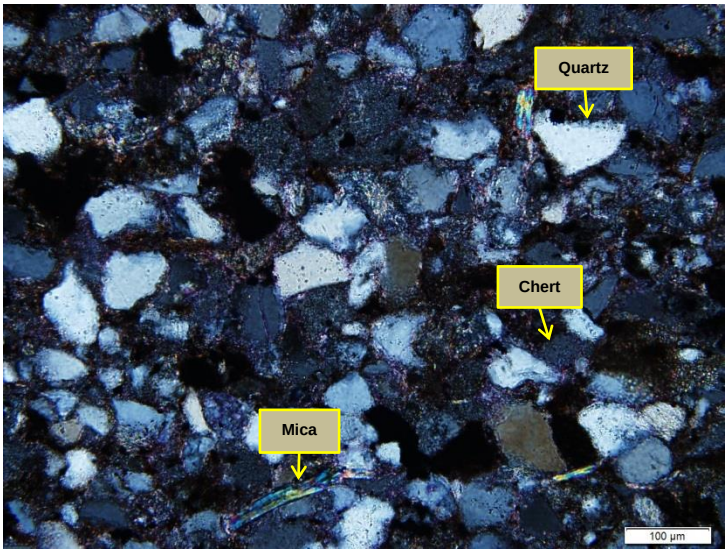


Fig. 4-138: Photomicrograph in XPL showing subangular to subrounded, very fine silt- to fine sand-sized (average gain size is coarse silt) detrital quartz (40-55%), chert (10-18%) and mica (1-5%). Note several mica lathes with random orientations and high birefringent colours.

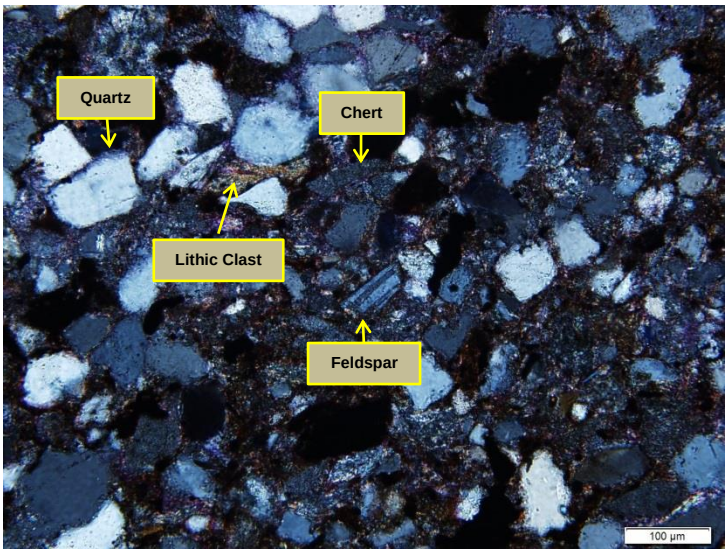


Fig. 4-139: Photomicrograph in XPL showing rare (<3%) detrital feldspar. The feldspar in the center of the image exhibits polysynthetic twinning. Most chert grains are of the microcrystalline variety. Note a compacted lithic clast.

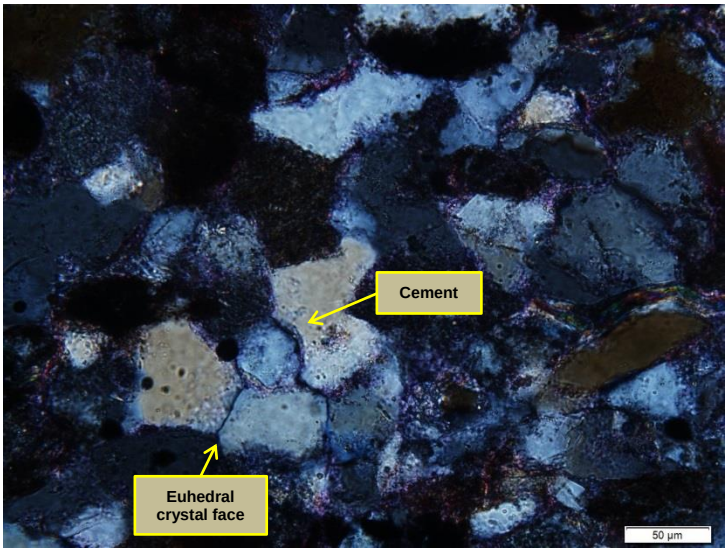


Fig. 4-140: Photomicrograph in XPL showing quartz overgrowths observed in the partially reworked sandy layer present near the base of the sample. Overgrowth cements are visible where euhedral (planar) crystal faces terminate against one another, and where grains appear “encased” by cement.

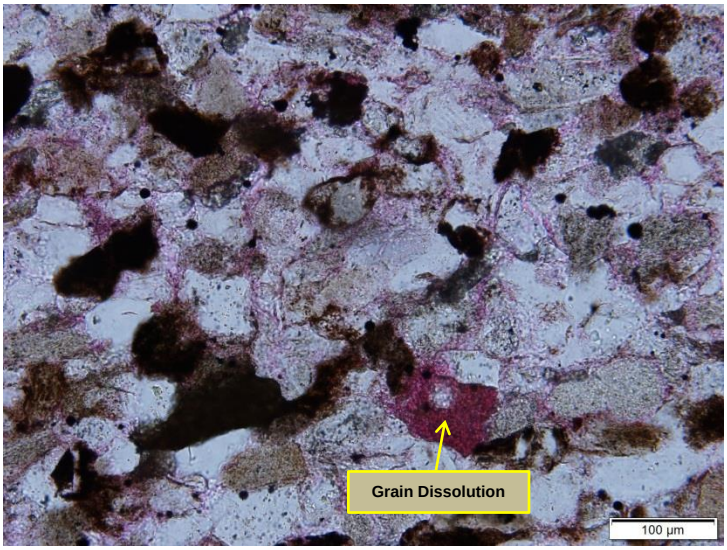


Fig. 4-141: Photomicrograph in PPL illustrating intergranular porosity (pink epoxy) present within the sandy layer near the base of the sample. Some pores occur around cements and grain boundaries. Some secondary porosity is also present due to partial grain dissolution. Note softer grains (chert, lithic clasts) that have been deformed due to compaction.

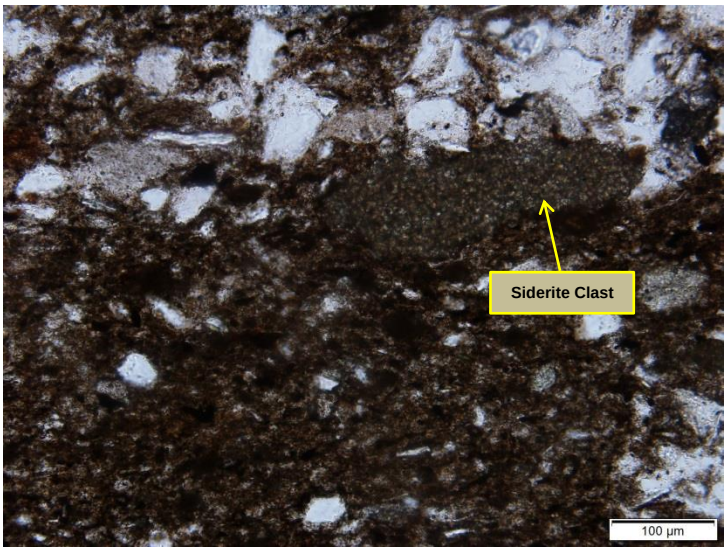


Fig. 4-142: Photomicrograph in PPL illustrating a clay-rich area present near the top of the sample. Some fine silt-size grains of quartz and chert are embedded within the clay rich matrix, which also includes organics and pyrite. Note a lenticular clast composed of microcrystalline siderite.

4.2.14 SAMPLE 13413

Sample ID	**13413**		
Sample type	**Core**	**UWI/Well**	**100/06-12-048-11W5/00**
Strat. Unit	**Cardium Formation**	**Depth**	**1791.70 m**

XRD/SRA results

Quartz (%)	Fsp (%)	Cb (%)	Clays (%)	Pyrite (%)
60.4	2.3	0	37	0.3

Composition (*in order of abundance*)

Grain size	%	Variety (%)	Variety (%)	Variety (%)	Variety (%)
sand	24	Quartz/chert (97)	Mica (2)	Feldspar (1)	
silt	35	Quartz/chert (99)	Mica (1)		
clay	35	Clay mins (100)			
Cement	<1	Quartz (100)			
Bioclasts	0				
Organics	6	Amorphous (100)			
Opaques	<1	Pyrite (100)			
	100				

*Intensively altered to clay minerals

^ Including bitumen

Sedimentary structures

Primary	Possible remnants of interbedded clay-rich and sandy laminae. Original bedding is difficult to recognize due to heavy bioturbation.
Biogenic	Appears heavily reworked.

Fractures	Rare thin epoxy-filled fractures. Likely artificial.
Porosity	None apparent.

Description

Heavily bioturbated sandy mudstone comprised of subangular (common) to subrounded (rare) very fine silt- to fine sand-sized (average grain size is coarse silt) detrital quartz (30-45%), chert (6-10%), mica (1-3%), and feldspar (<2%). The rock is largely composed of and unstratified, clay-rich sandy sediment. A small, apparently less bioturbated, area of possible interbedded clay-rich and sandy laminae is present near the base of the sample.

Thin Section Quality

Good.

Rock Classification

Sandy mudstone.

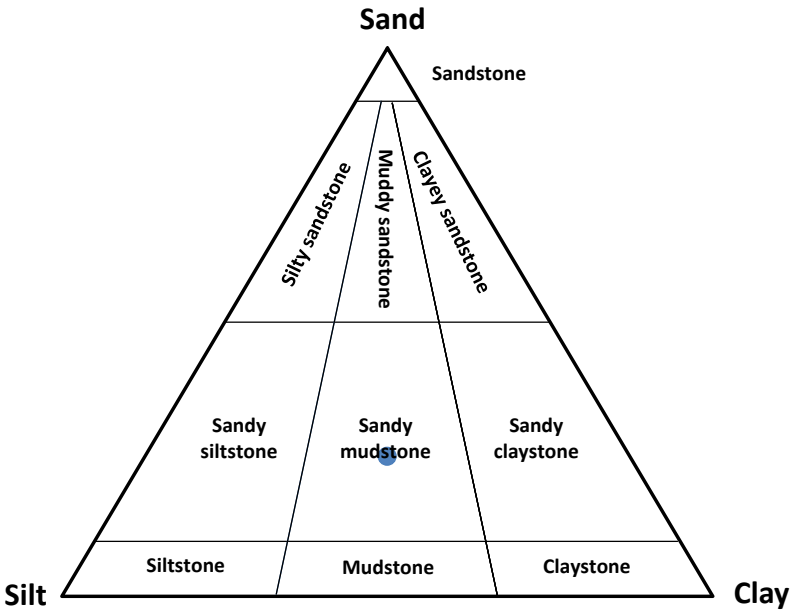


Fig. 4-143: Ternary plot showing the grain size composition of the sample based on the Wentworth scale (after Folk, 1954). Sample 13413 is classified as a sandy mudstone.



Fig. 4-144: Core photograph of sample 13413 from the Cardium Formation, well 100/06-12-048-11W5/00 (depth 1791.70 m). The thin section prepared from this sample was cut from the area marked with an X. The sample was received with no up direction. Scale is in mm.

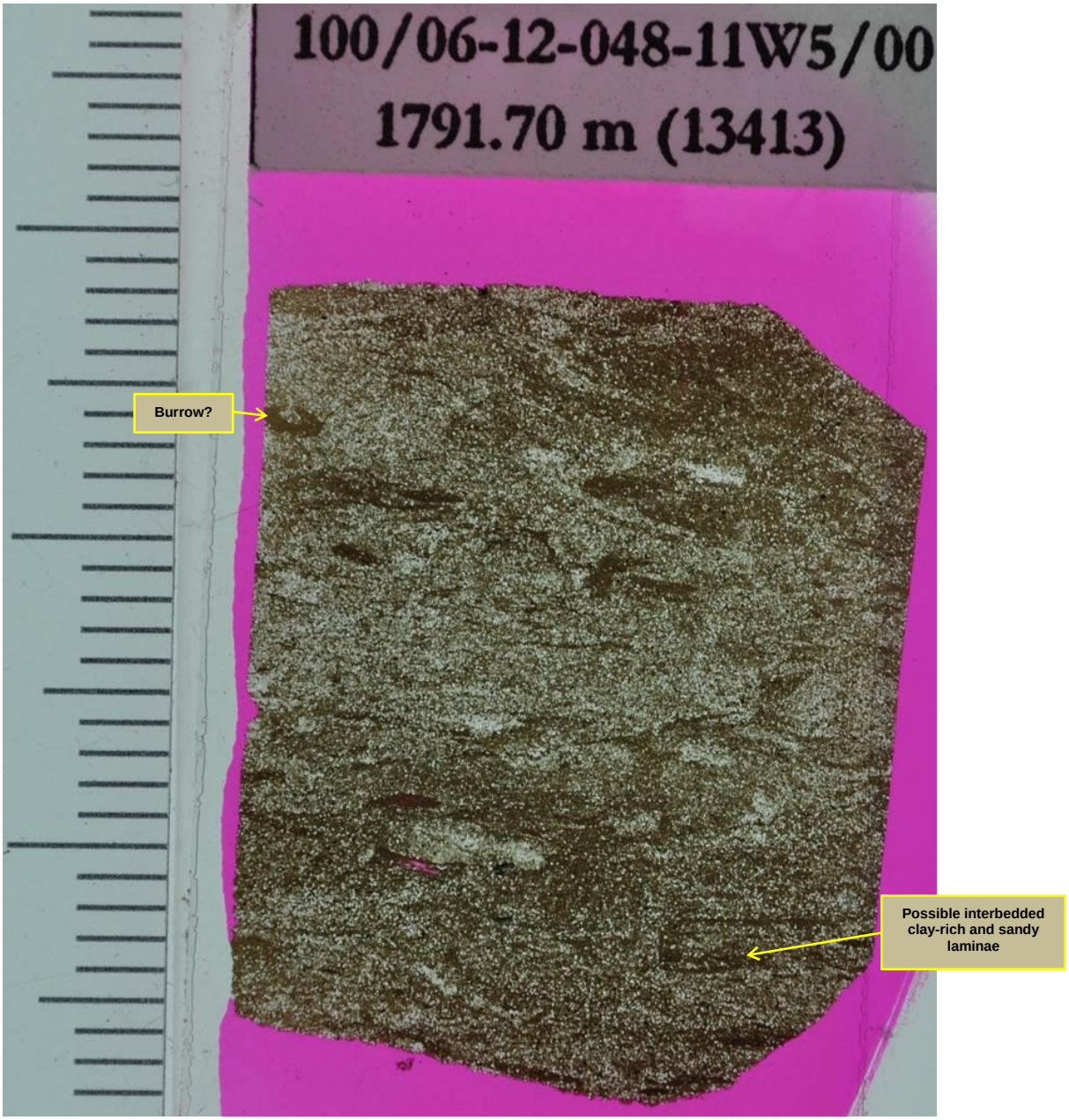


Fig. 4-145: Thin section photograph of sample 13413 from the Cardium Formation, well 100/06-12-048-11W5/00 (depth 1791.70 m). The sample is a heavily bioturbated sandy mudstone. Although apparent remnants of thinly interbedded clay-rich and sandy laminae are observed, the majority of the sample lacks bedding parallel structures due to heavy reworking or mixing. Scale is in mm. Note: Up-direction was not positively identified.

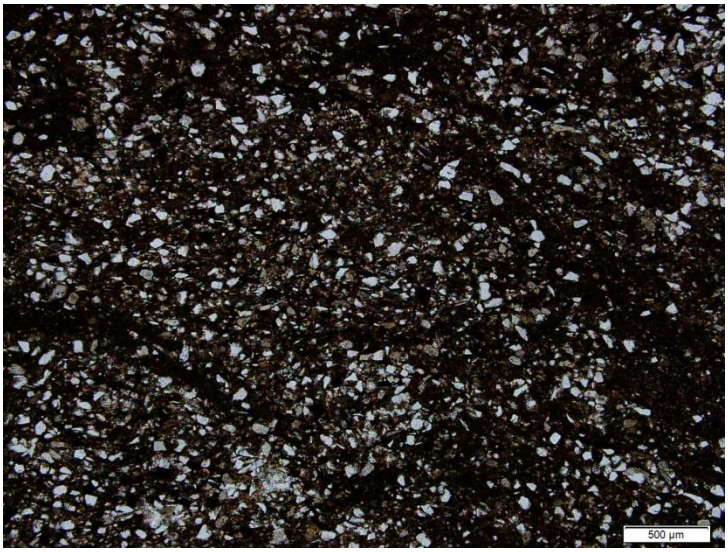


Fig. 4-146: Photomicrograph in PPL showing an overview of the sandy mudstone. The sample is largely comprised of an unstratified, clay-rich silty/sandy sediment. Light-coloured minerals consist of quartz, chert and feldspar. Note subtle vertical and horizontal traces or "trails" of opaque material likely due to burrowing activity.

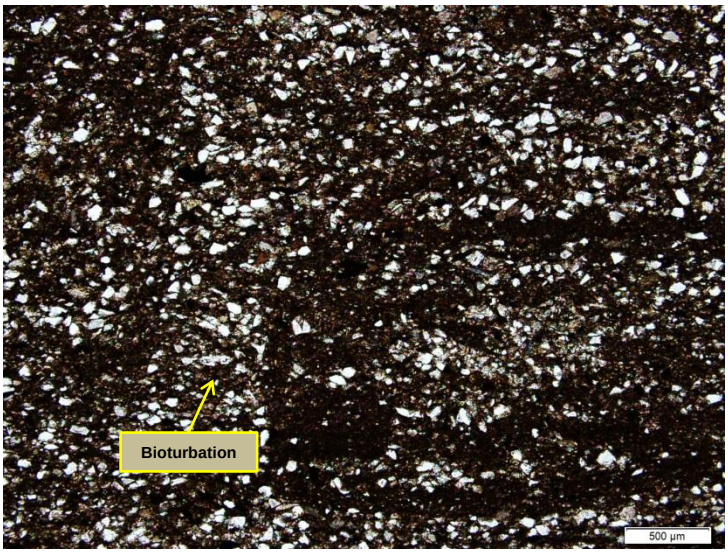


Fig. 4-147: Photomicrograph in PPL showing apparent remnants of interbedded clay-rich and sandy laminae (right side of image) present near the base of the sample. Bioturbation and possible burrowing activity have disturbed much of the original continuity of the laminae.

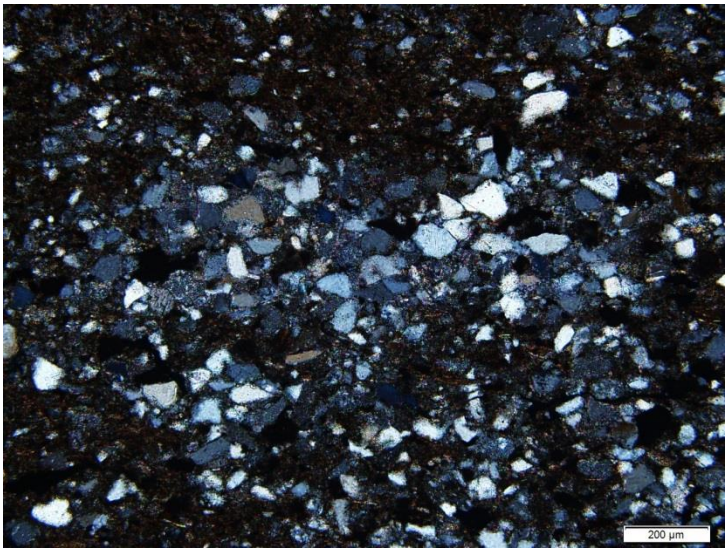


Fig. 4-148: Photomicrograph in XPL showing one of several clusters of coarse silt- to very fine sand-sized grains present in the sample. These features likely represent burrow structures (*Planolites*?) produced by deposit feeding organisms.

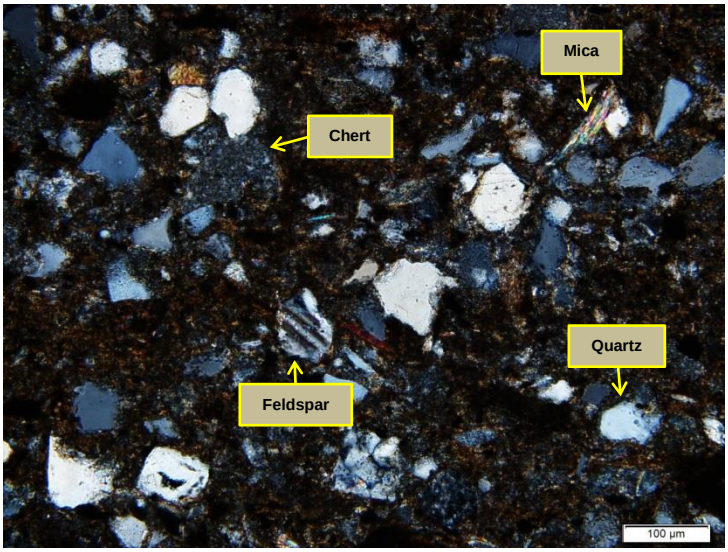


Fig. 4-149: Photomicrograph in XPL showing subangular (common) to subrounded (rare) very fine silt- to fine sand-sized (average grain size is coarse silt) detrital quartz (30-45%), chert (6-10%), mica (1-3%), and feldspar (<2%). Note polysynthetic twinning associated with feldspar.

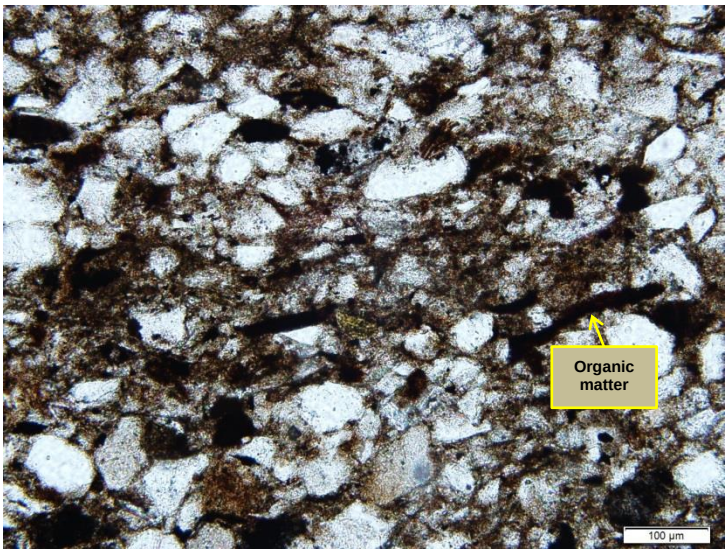


Fig. 4-150: Photomicrograph in PPL showing detail of the unstratified, clay-rich sandy sediment that constitutes the majority of the sample. This sediment is comprised of ~24% sand-, ~35% silt-, and ~35% clay-sized particles. Organic matter accounts for ~6% of the rock.

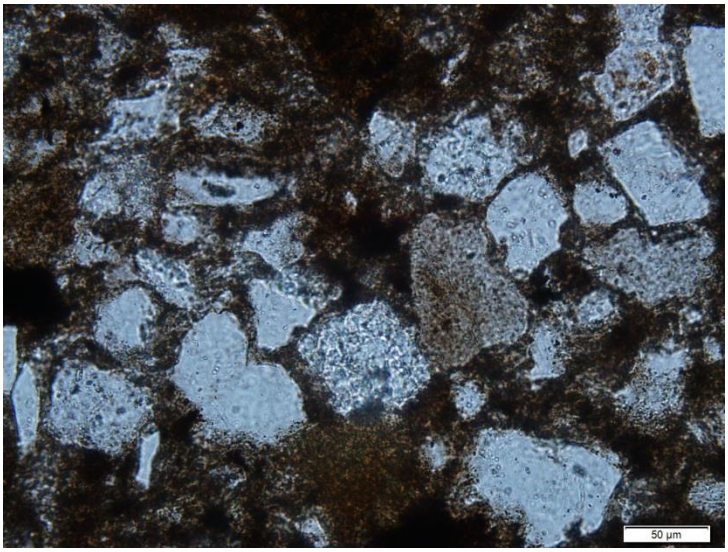


Fig. 4-151: Photomicrograph in PPL showing a typical example of uncemented detrital quartz and chert grains embedded within the clay-rich matrix. Some clay-size particles of quartz are likely present in matrix. The abundance of clay may have precluded secondary quartz cementation.

4.2.15 SAMPLE 13420

Sample ID	**13420**		
Sample type	**Core**	**UWI/Well**	**100/03-07-048-08W5/00**
Strat. Unit	**Cardium Formation**	**Depth**	**1650.16 m**

XRD/SRA results

Quartz (%)	Fsp (%)	Cb (%)	Clays (%)	Pyrite (%)
71.8	3.7	0	24.4	0.2

Composition (*in order of abundance*)

Grain size	%	Variety (%)	Variety (%)	Variety (%)	Variety (%)
sand	55	Quartz/chert (94)	Mica (4)	Feldspar (2)	
silt	20	Quartz/chert (98)	Mica (2)		
clay	20	Clay mins (100)			
Cement	<1	Quartz (100)			
Bioclasts	0				
Organics	5	Amorphous (100)			
Opaques	<1	Pyrite (100)			
	100				

*Intensively altered to clay minerals

^ Including bitumen

Sedimentary structures

Primary	A small area of finely laminated clay-rich bedding is visible near the base of the sample. The majority of the rock appears unstratified, possibly reflecting pervasive bioturbation.
Biogenic	The sample appears heavily reworked, and contains at least one possible *Planolites* burrow.

Fractures	Occasional epoxy-filled fractures and partings. Likely artificial.
Porosity	1-5% intergranular porosity occurs intermittently within discontinuous patches of sandy sediment, some of which may be possible burrow structures.

Description

Heavily bioturbated muddy sandstone comprised of subrounded (common) to angular (rare) very fine silt- to fine sand-sized (average grain size is very fine sand) detrital quartz (30-60%), chert (10-15%), mica (1-6%), and feldspar (<3%). The majority of the sample consists of apparently unstratified (pervasively bioturbated?) clay-rich sand. Intermittent patches of this sediment, including possible burrow structures, have 1-5% porosity, which may partly be an artificial byproduct of sample preparation. A small area of finely laminated clay-rich bedding (stringers of bedding-parallel organic matter define some laminae) occurs near the base of the sandstone, and may be the only undisturbed component of the rock.

Thin Section Quality

Good.

Rock Classification

Muddy sandstone.

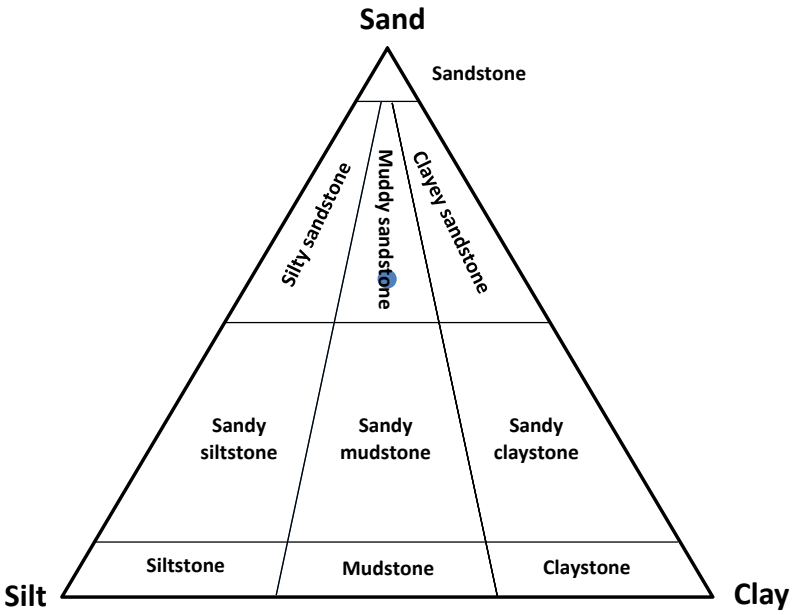


Fig. 4-152: Ternary plot showing the grain size composition of the sample based on the Wentworth scale (after Folk, 1954). Sample 13420 is classified as a muddy sandstone.

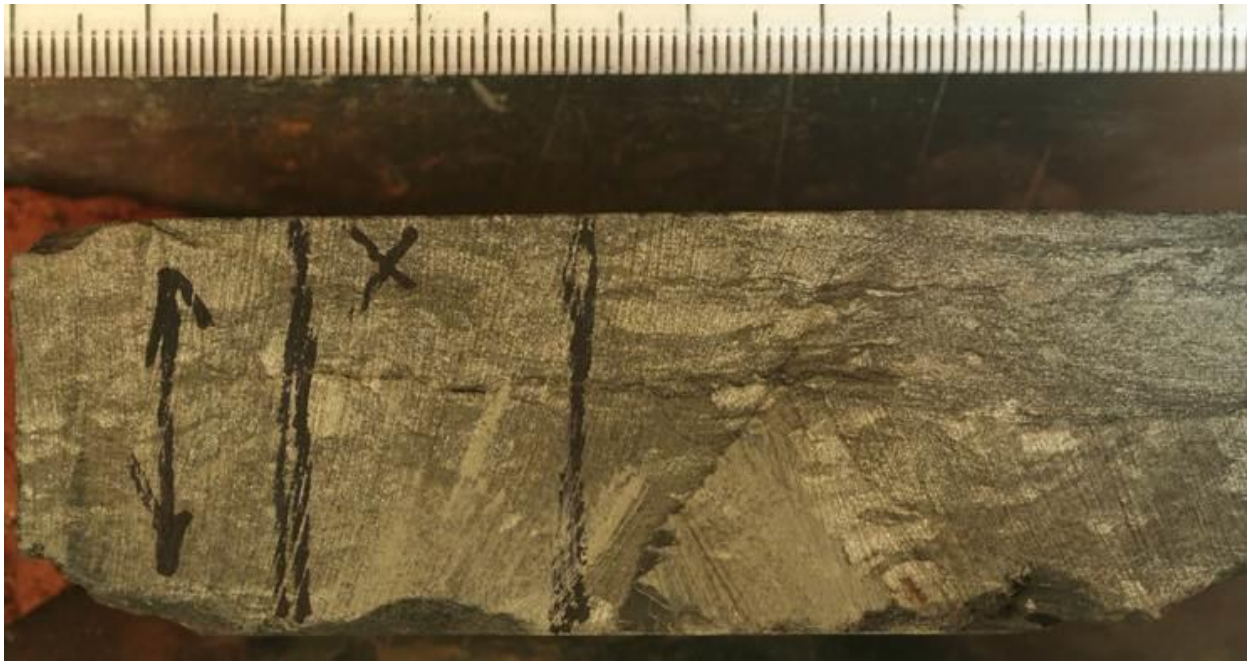


Fig. 4-153: Core photograph of sample 13420 from the Cardium Formation, well 100/03-07-048-08W5/00 (depth 1650.16 m). The thin section prepared from this sample was cut from the area marked with an X. The sample was received with no up direction but is oriented based on sedimentary structures. Scale is in mm.

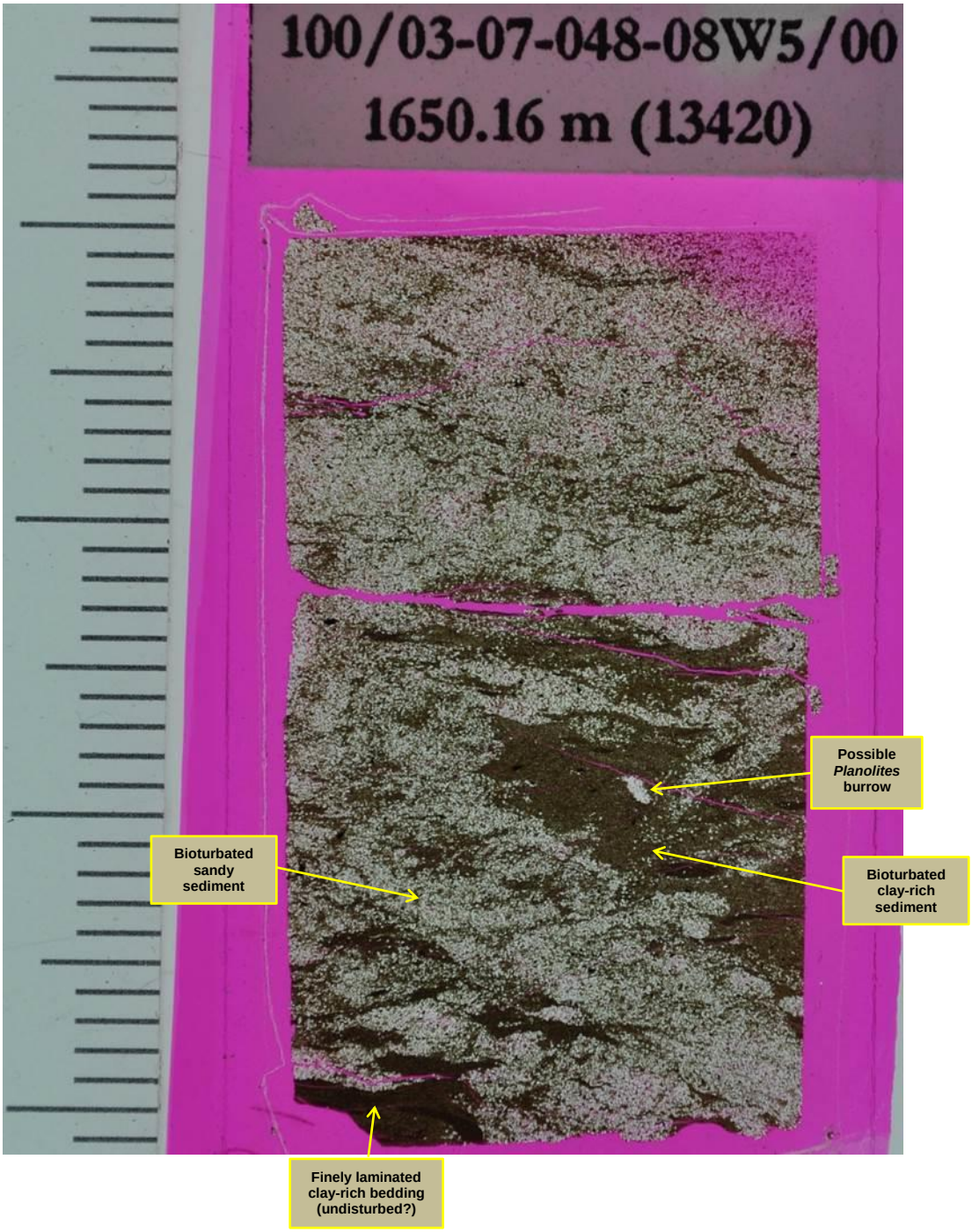


Fig. 4-154: Thin section photograph of sample 13420 from the Cardium Formation, well 100/03-07-048-08W5/00 (depth 1650.16 m). The sample is a heavily bioturbated muddy sandstone. The majority of the sample consists of unstratified clay-rich sand, with rare discontinuous laminae or lenses. Scale is in mm.

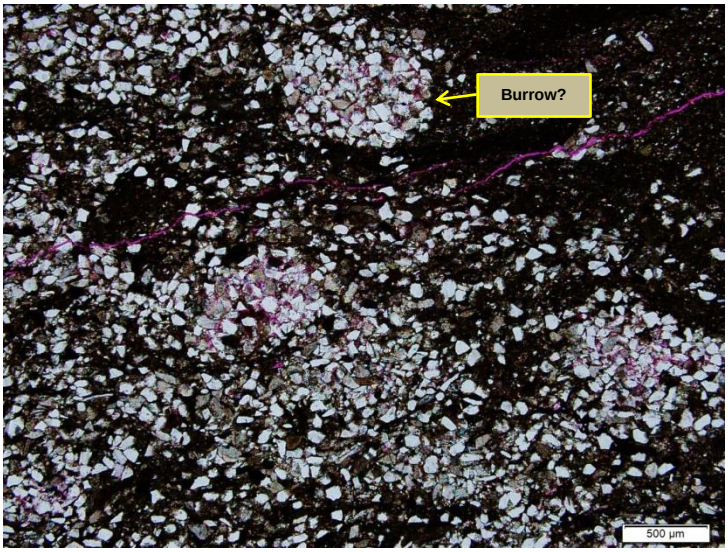


Fig. 4-155: Photomicrograph in PPL showing an overview of the clayey sandstone. Clay-rich sand constitutes the majority of the sample, which is heavily bioturbated. Clays occur between grains or form patches and lenses. Note a burrowing feature infilled with sandy constituents.



Fig. 4-156: Photomicrograph in PPL illustrating patches of porous sediment. Porosity (filled with pink epoxy) occurs discontinuously in this sample (sometimes due to plucked grains), and is primarily observed within areas of clay-poor sand and within possible burrow structures.

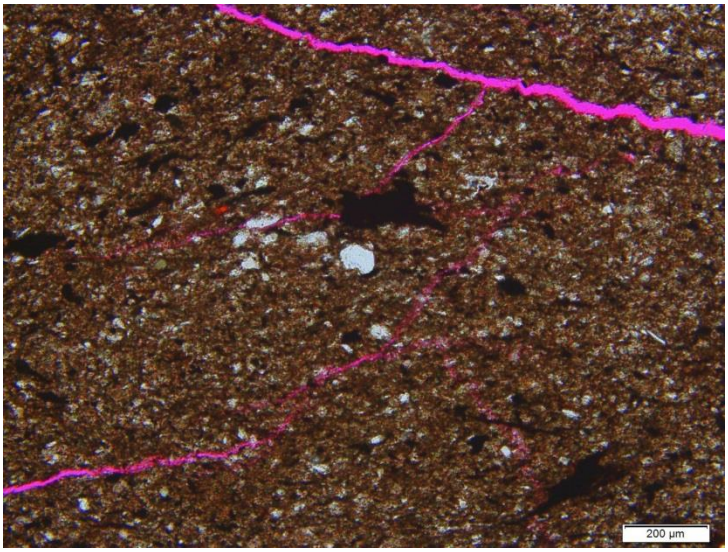


Fig. 4-157: Photomicrograph in PPL showing an area of bioturbated clay-rich sediment (see location in Figure 4-154). Like the clay-rich sand that comprises the majority of the sample, this sediment also lacks bedding features. Clays are estimated at ~20% of the total sample composition. Some clay- to fine silt-sized particles (quartz) are embedded within the clay matrix. Note several artificial fractures filled with pink epoxy.

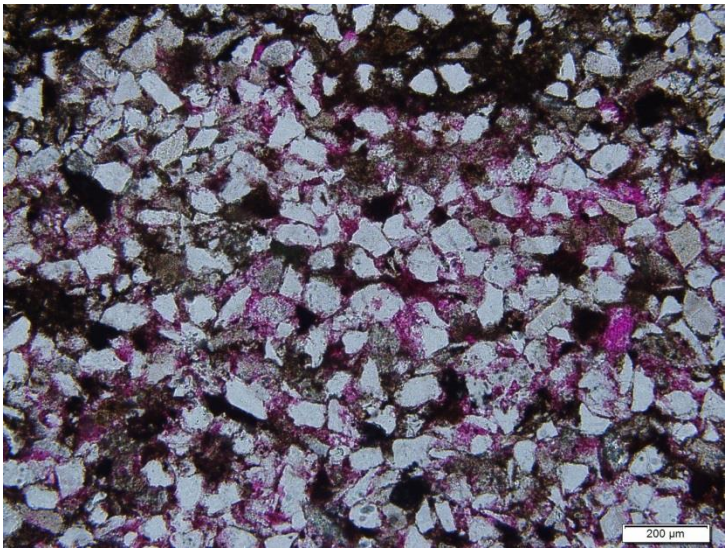


Fig. 4-158: Photomicrograph in PPL showing ~5% intergranular porosity (pink epoxy) occurring within a patch of sandy sediment. Light-coloured minerals are primarily quartz and chert, with the darker patches consisting of clays, organic matter and pyrite.

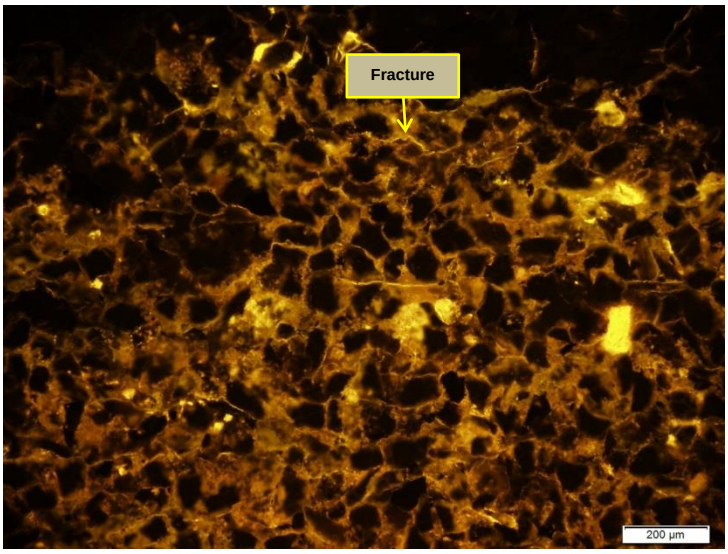


Fig. 4-159: Photomicrograph in UV light showing intergranular porosity within a patch of sandy sediment (same field of view as Figure 4-158). Thin fractures are apparent in UV light, suggesting that some of the observed porosity may have been artificially enhanced during sample preparation.

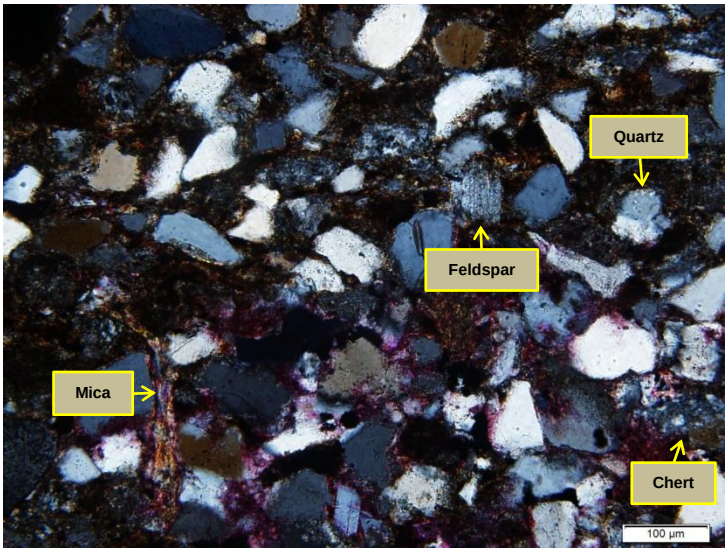


Fig. 4-160: Photomicrograph in XPL showing subrounded (common) to angular (rare) very fine silt- to fine sand-sized (average grain size is very fine sand) detrital quartz (30-60%), chert (10-15%), mica (1-6%), and feldspar (<3%) observed in the sandstone. Some feldspars appear degraded as well as exhibiting subtle polysynthetic twinning. Note a degraded muscovite lathe, which is vertically oriented and has high birefringent colours.

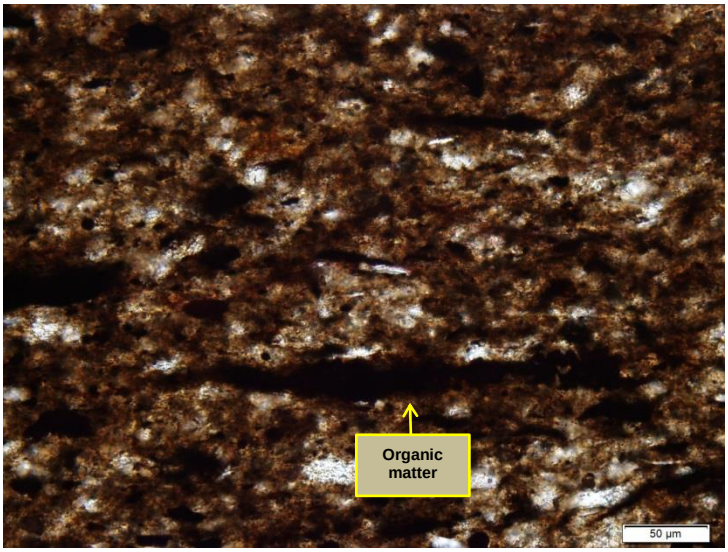


Fig. 4-161: Photomicrograph in PPL illustrating part of a finely laminated clay-rich layer near the base of the sample (see location in Figure 4-154). Stringers of bedding-parallel organic matter (opaque) are common within this area of the sample. Some finely disseminated pyrite is also observed.

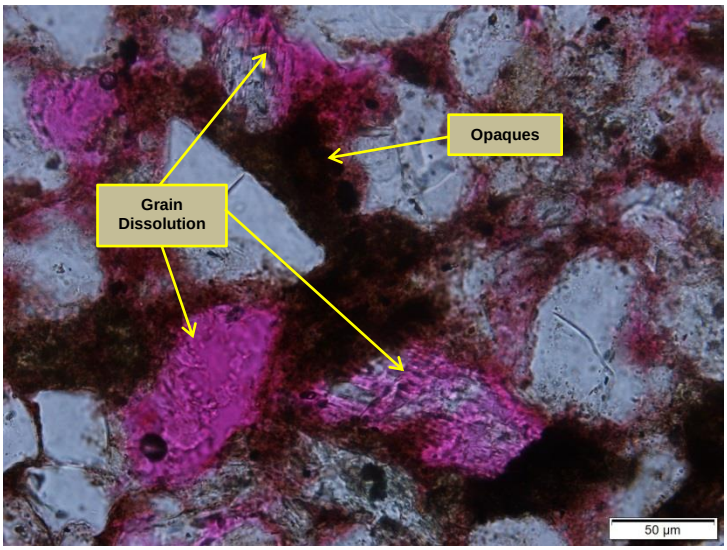


Fig. 4-162: Photomicrograph in PPL detailing secondary porosity associated with partial to near complete grain dissolution (likely feldspar). Note opaque material (clays, organics, pyrite) between grains.

4.2.16 SAMPLE 13425

Sample ID	**13425**		
Sample type	**Core**	**UWI/Well**	**100/06-07-047-04W5/00**
Strat. Unit	**Cardium Formation**	**Depth**	**1442.92 m**

XRD/SRA results

Quartz (%)	Fsp (%)	Cb (%)	Clays (%)	Pyrite (%)
70.8	3.6	0	24.2	1.4

Composition (*in order of abundance*)

Grain size	%	Variety (%)	Variety (%)	Variety (%)	Variety (%)
sand	50	Quartz/chert (97)	Mica (2)	Feldspar (1)	
silt	19	Quartz/chert (99)	Mica (1)		
clay	22	Clay mins (100)			
Cement	3	Quartz (100)			
Bioclasts	0				
Organics	4	Amorphous (100)			
Opaques	2	Pyrite (100)			
	100				

*Intensively altered to clay minerals

^ Including bitumen

Sedimentary structures

Primary	Finely laminated clay-rich bedding is visible near the base of the sample.
Biogenic	At least one possible burrow feature within finely laminated clay-rich bedding.

Fractures	Occasional thin epoxy-filled fractures. Likely artificial.
Porosity	1-4% intergranular porosity is observed in a partially cemented sandy lens present near the top of the sample.

Description

Muddy sandstone comprised of subrounded (common) to subangular (rare) very fine silt- to fine sand-sized (average grain size is very fine sand) detrital quartz (30-50%), chert (8-15%), mica (1-4%), and feldspar (<2%). A thin sequence of finely laminated clay-rich bedding occurs near the base of the sample, and is overlain by unstratified clay-rich sand that forms the majority of the rock. Two sandy lenses occur near the top of sample, one which is completely cemented, and one with 1-4% intergranular porosity.

Thin Section Quality

Poor. Exposed thin section glass is common.

Rock Classification

Muddy sandstone.

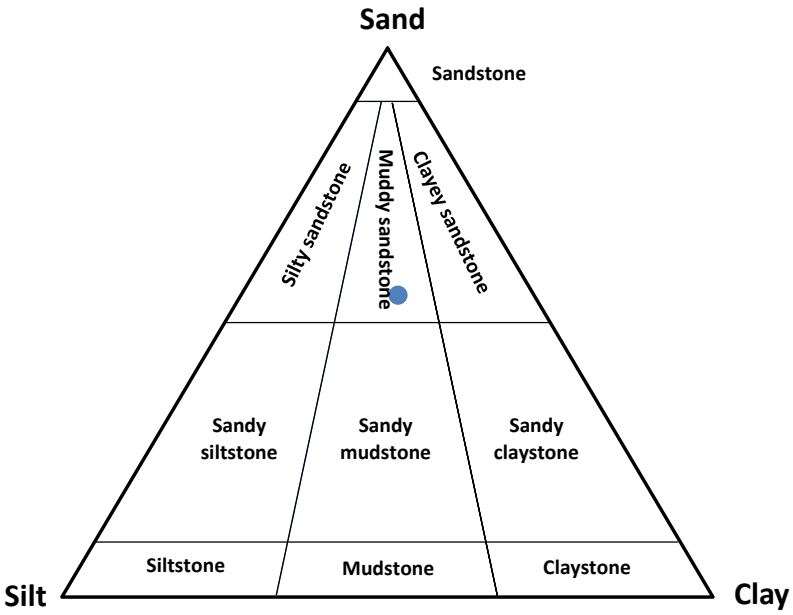


Fig. 4-163: Ternary plot showing the grain size composition of the sample based on the Wentworth scale (after Folk, 1954). Sample 13425 is classified as a muddy sandstone.



Fig. 4-164: Core photograph of sample 13425 from the Cardium Formation, well 100/06-07-047-04W5/00 (depth 1442.92m). The thin section prepared from this sample was cut from the area marked with an X. The sample was received with no up direction. Scale is in mm.

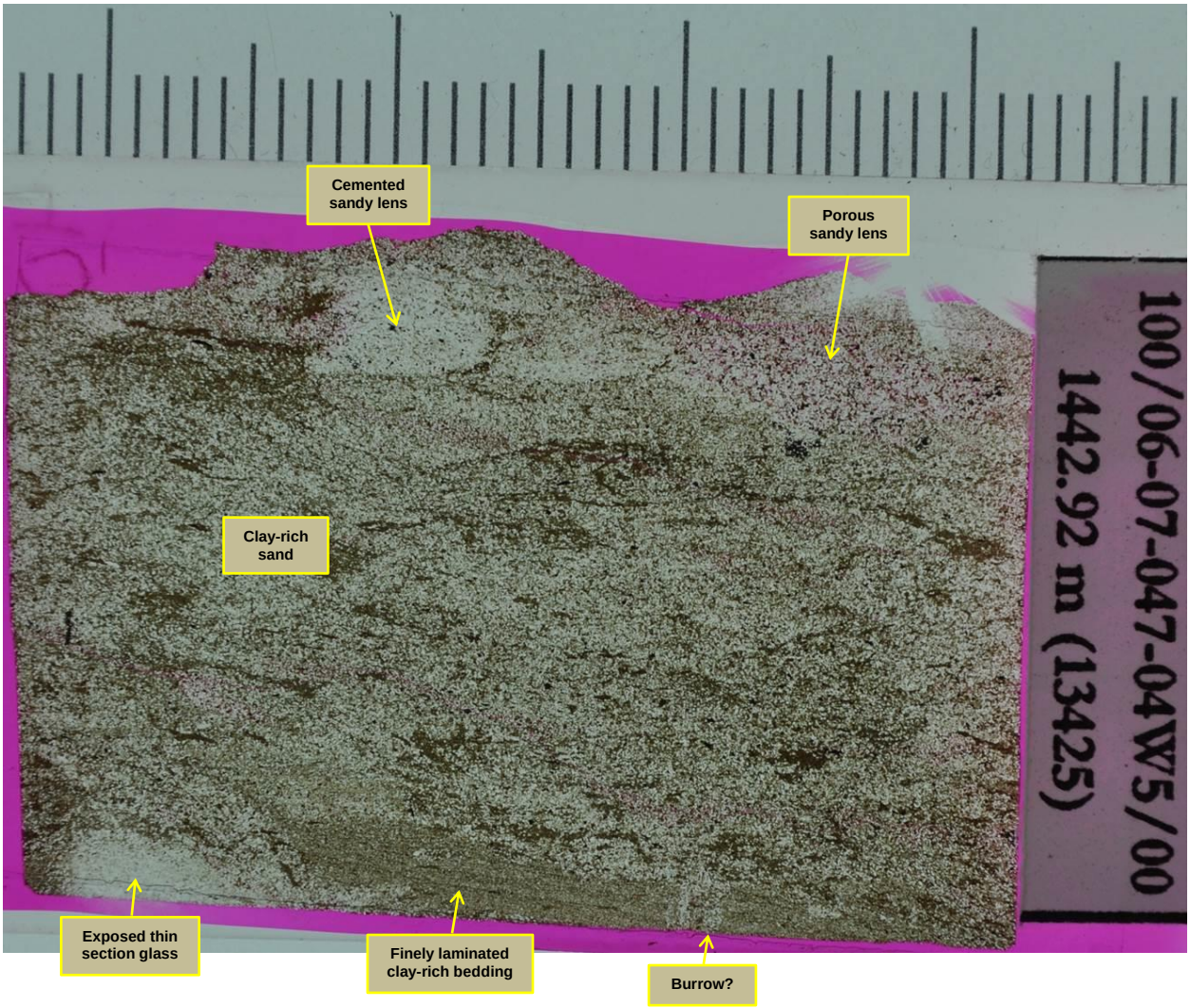


Fig. 4-165: Thin section photograph of sample 13425 from the Cardium Formation, well 100/06-07-047-04W5/00 (depth 1442.92m). The sample is a muddy sandstone. A thin sequence of finely laminated clay-rich bedding is visible near the base of the image and is overlain by unstratified, bioturbated, clay-rich sand, which forms the majority of the sample. Clays form patches or thin wisps in the sandy portion. Sandy lenses, one of which is completely cemented, and another with 1-4% (estimated) intergranular porosity, occur near the top of the image. Scale is in mm.

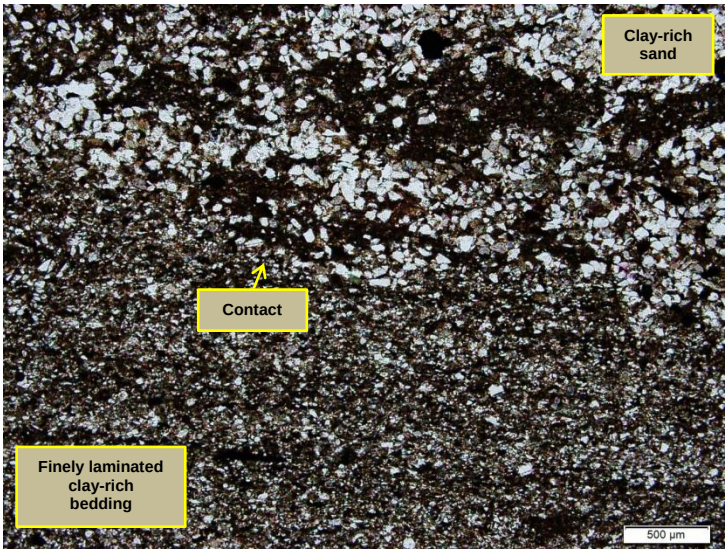


Fig. 4-166: Photomicrograph in PPL showing an overview of finely laminated (silty) clay-rich bedding near the base of the sample, which is classified as a muddy sandstone. The overlying clay-rich sand constitutes the majority of the sample.

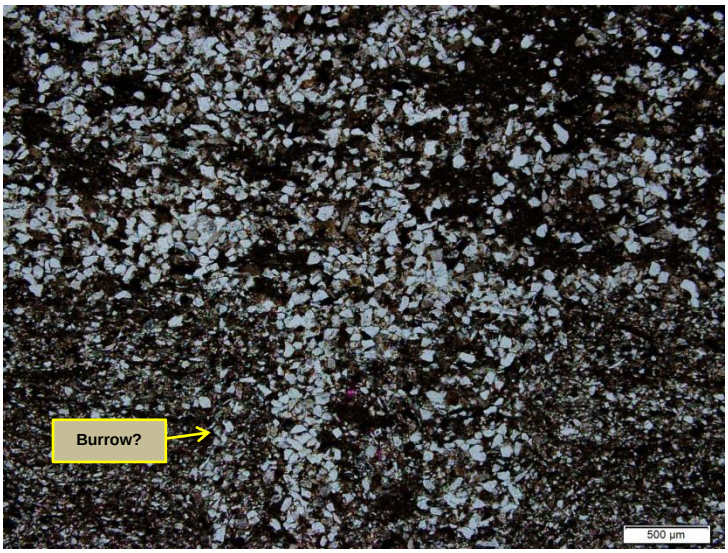


Fig. 4-167: Photomicrograph in PPL showing a possible burrowing structure observed cutting vertically into the finely laminated clay-rich bedding present near the base of the sandstone. Note numerous opaque (darker) patches within the upper sandy layer, likely due to bioturbation. Light coloured minerals consist of quartz, chert, mica and feldspar.

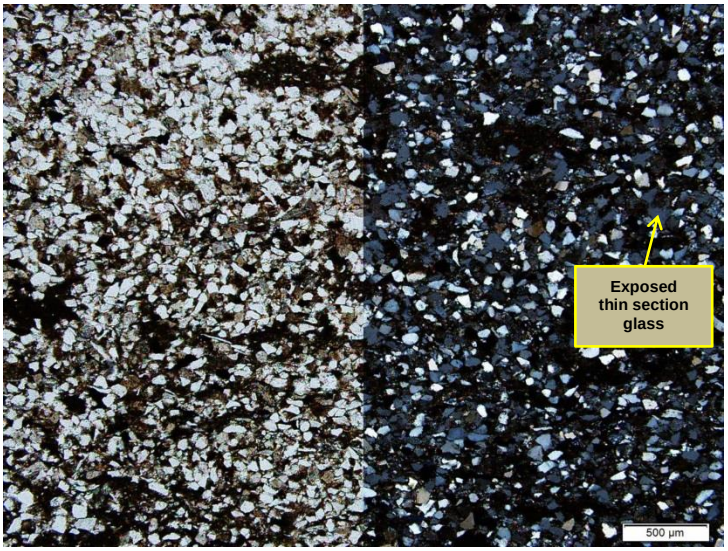


Fig. 4-168: Photomicrograph (left half in PPL, right half in XPL) showing an overview image of the clay-rich sand that makes up the majority of the sample. Exposed thin section glass is prevalent in this sample, indicating that clays and/or detrital grains were removed during sample preparation.

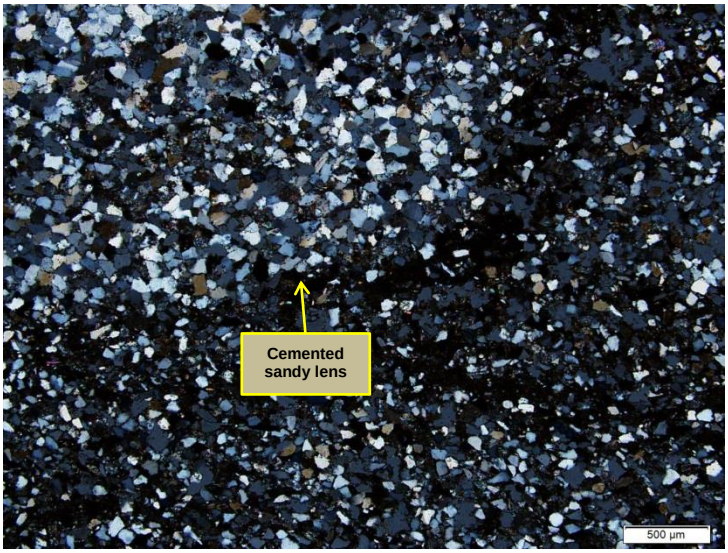


Fig. 4-169: Photomicrograph in XPL showing a well-cemented sandy lens observed near the top of the sample (see location in Figure 4-165).

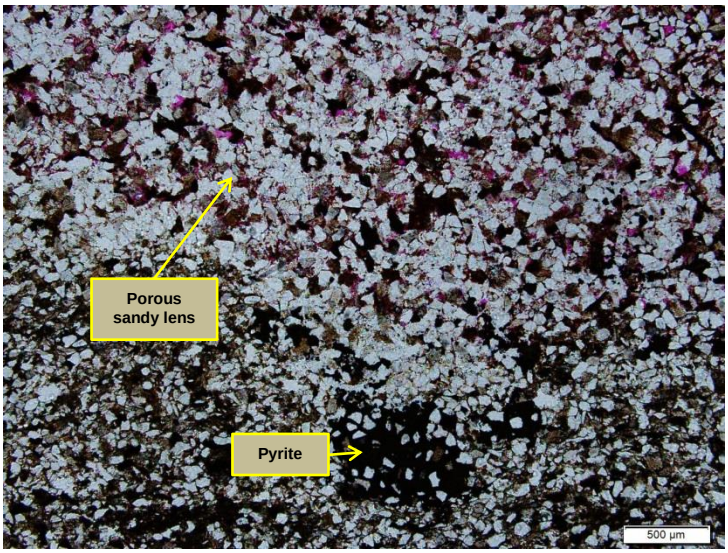


Fig. 4-170: Photomicrograph in PPL showing a porous sandy lens observed near the top of the sample (see location in Figure 4-165). Porosity is infilled with pink epoxy. Note a patch of pyrite mineralization with embedded silt-size quartz at the bottom of the image.

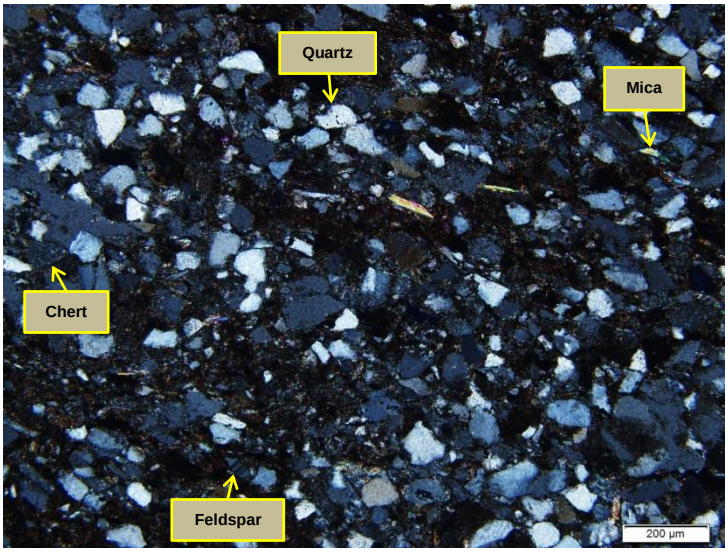


Fig. 4-171: Photomicrograph in XPL showing subrounded (common) to subangular (rare) very fine silt- to fine sand-sized (average grain size is very fine sand) detrital quartz (30-50%), chert (8-15%), mica (1-4%), and feldspar (<2%). Some feldspars exhibit polysynthetic twinning.

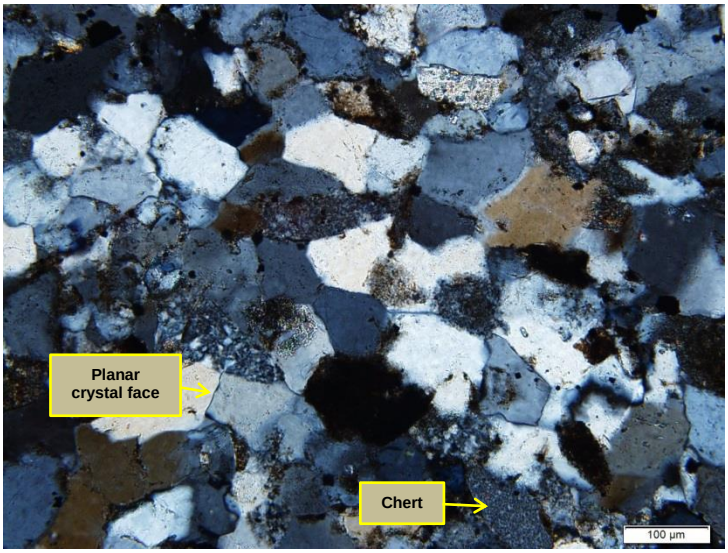


Fig. 4-172: Photomicrograph in XPL detailing the cemented sandy lens shown in Figure 4-169. Planar crystal faces are visible where quartz overgrowth cements from adjacent grains interlock and terminate against one another. Note chert grains composed of microcrystalline quartz.

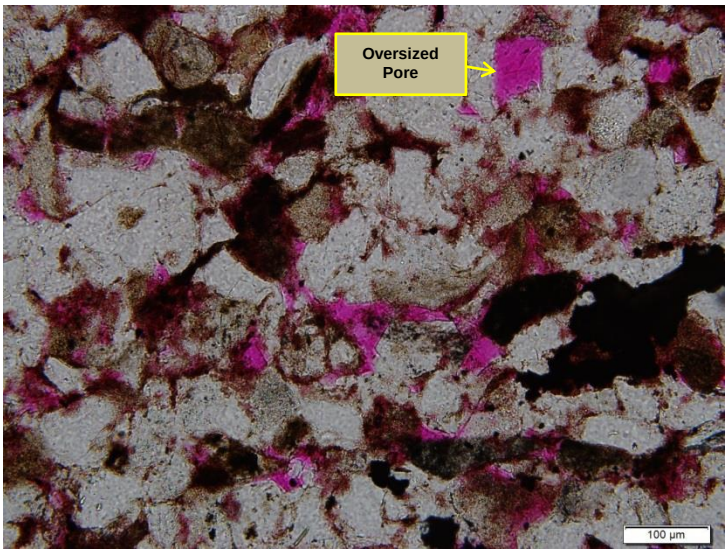


Fig. 4-173: Photomicrograph in PPL showing 1-4% (estimated) intergranular porosity (pink epoxy) observed in the sandy lens shown in Figure 4-170. Clay and organic material is observed partially filling and lining pore space. Some oversized pores are likely the result of grain dissolution.

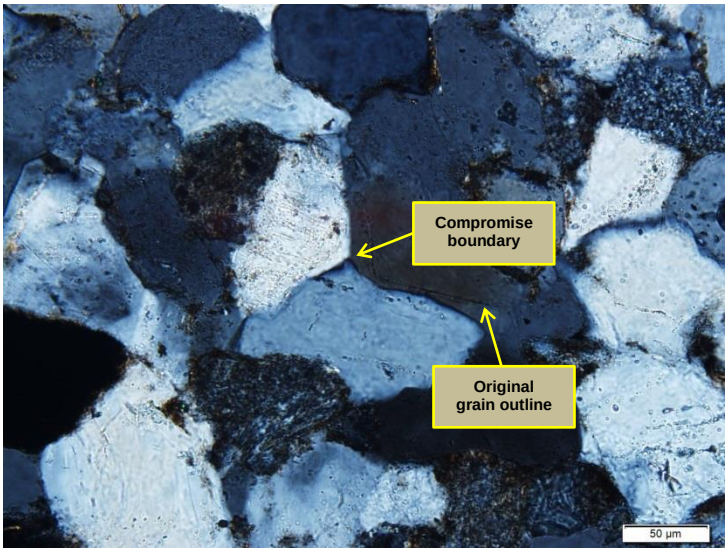


Fig. 4-174: Photomicrograph in XPL illustrating the cemented sandy lens shown in Figures 4-169 and 4-172. Compromise boundaries occur where overgrowth cements from three detrital grains terminate against each other in a triple junction. Most quartz overgrowths can be identified by a dust rim around the detrital grain.

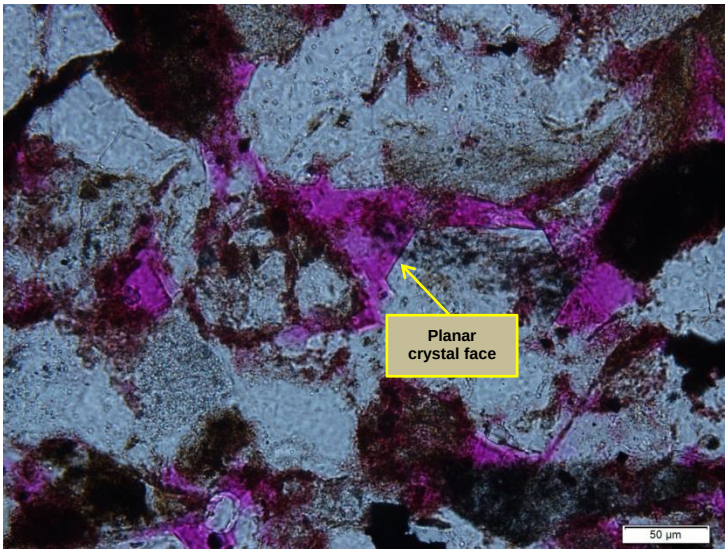


Fig. 4-175: Photomicrograph in PPL detailing the porous sandy lens shown in Figures 4-170 and 4-173. Quartz overgrowth cements are visible as planar crystal faces partially filling intergranular pore space (pink epoxy). Note clay material (dark-brown) and organics in the pore system.

4.2.17 SAMPLE 13427

Sample ID	**13427**		
Sample type	**Core**	**UWI/Well**	**100/06-07-047-04W5/00**
Strat. Unit	**Cardium Formation**	**Depth**	**1450.13 m**

XRD/SRA results

Quartz (%)	Fsp (%)	Cb (%)	Clays (%)	Pyrite (%)
62.4	3.7	0.5	33.2	0.3

Composition (*in order of abundance*)

Grain size	%	Variety (%)	Variety (%)	Variety (%)	Variety (%)
sand	35	Quartz/chert (96)	Mica (3)	Feldspar (<2)	
silt	35	Quartz/chert (94)	Mica (6)		
clay	25	Clay mins (100)			
Cement	<1	Quartz (100)			
Bioclasts	0				
Organics	5	Amorphous (100)			
Opaques	<1	Pyrite (100)			
	100				

*Intensively altered to clay minerals

^ Including bitumen

Sedimentary structures

Primary	Possible finely laminated clay-rich bedding.
Biogenic	None apparent (abundant exposed glass makes identification difficult).

Fractures	Rare thin epoxy-filled fractures. Likely artificial.
Porosity	None apparent.

Description

Sandy mudstone comprised of subrounded (common) to subangular (rare) very fine silt- to fine sand sized (average grain size is coarse silt) detrital quartz (35-50%), chert (10-15%), mica (1-4%), and feldspar (<1%). The rock appears to have been badly damaged during thin section preparation, with substantial exposed thin section glass visible in all areas of the sample. Aside from a small area of possible finely laminated clay-rich bedding, no identifiable sedimentary structures remain visible. It is likely that the true compositional abundances for this sample differ from those given here, with the abundance of clay minerals, in particular, probably being higher in the actual rock.

Thin Section Quality

Very poor. Exposed thin section glass is more prevalent than detrital mineral grains in some areas.

Rock Classification

Sandy mudstone.

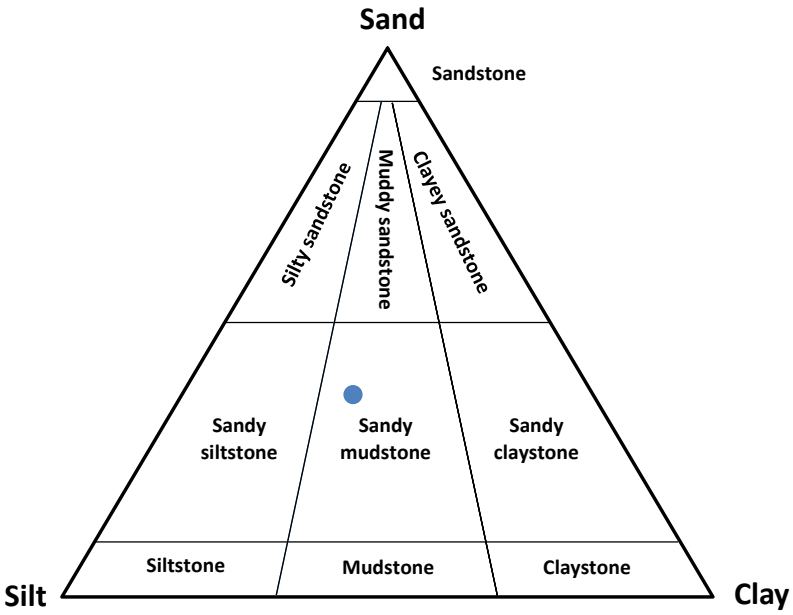


Fig. 4-176: Ternary plot showing the grain size composition of the sample based on the Wentworth scale (after Folk, 1954). Sample 13427 is classified as a sandy mudstone.



Fig. 4-177: Core photograph of sample 13427 from the Cardium Formation, well 100/06-07-047-04W5/00 (depth 1450.13 m). The thin section prepared from this sample was cut from the area marked with an X. The sample was received with no up direction. Scale is in mm.

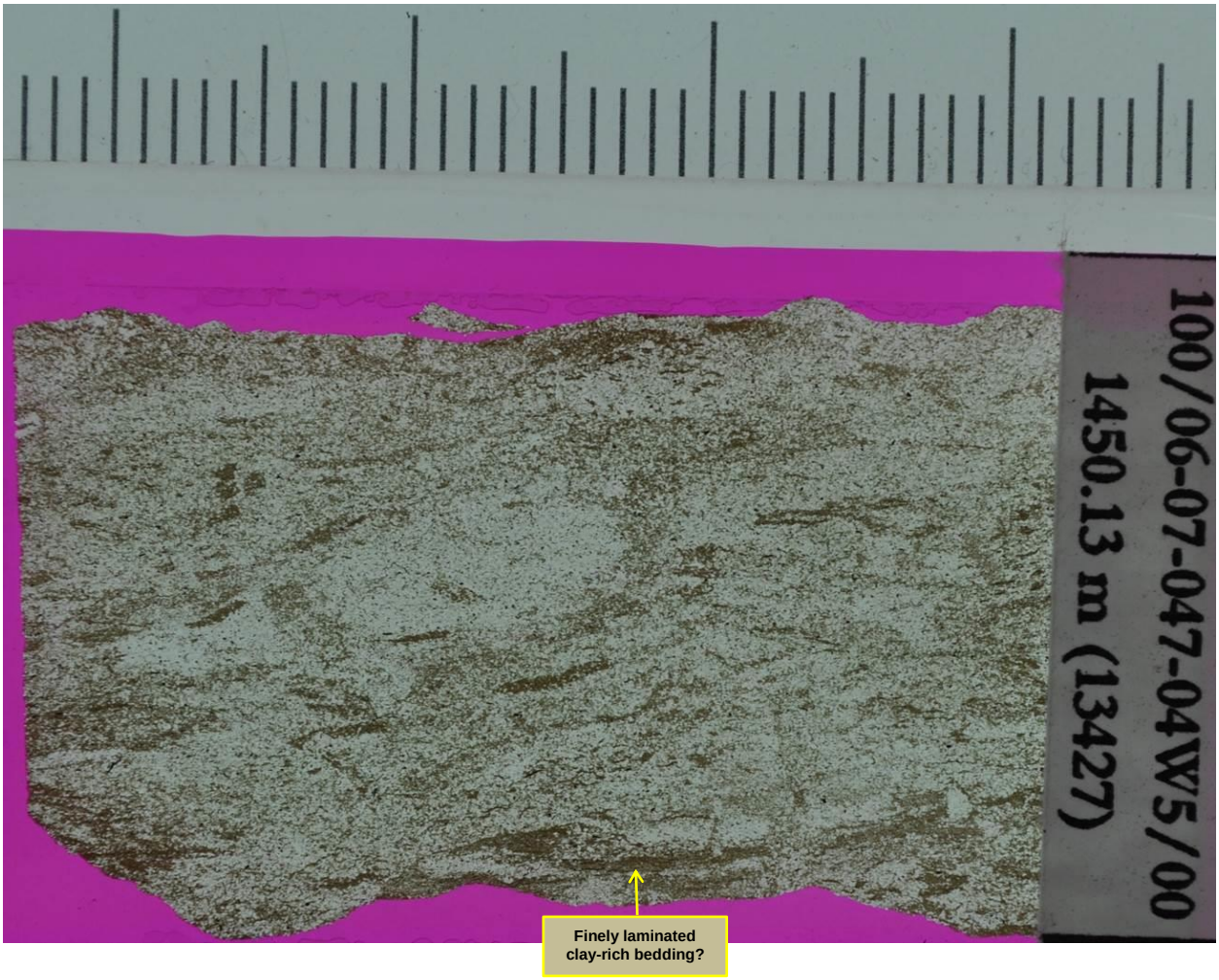


Fig. 4-178: Thin section photograph of sample 13427 from the Cardium Formation, well 100/06-07-047-04W5/00 (depth 1450.13 m). The sample is a bioturbated sandy mudstone with common clay-rich patches, wisps, lenses and possible burrowing features. Abundant exposed thin section glass (representing material plucked during sample preparation) is observed in this sample, indicating that water-sensitive clay minerals may be present. Scale is in mm.

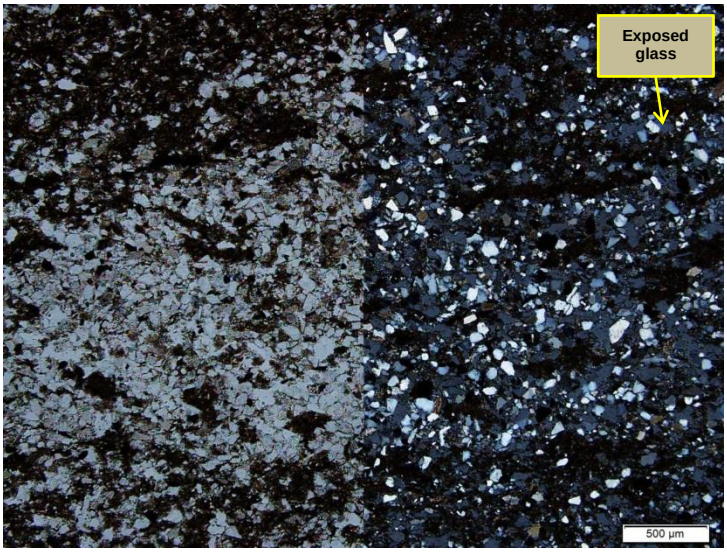


Fig. 4-179: Photomicrograph (left half in PPL, right half in XPL) showing an overview image of the sandy mudstone. Much of the original detail of the sample is lost due to issues of thin section preparation. Exposed thin section glass (dull blue-gray color) is abundant and is left when material is removed from the sample during sample cutting (can appear similar to quartz).

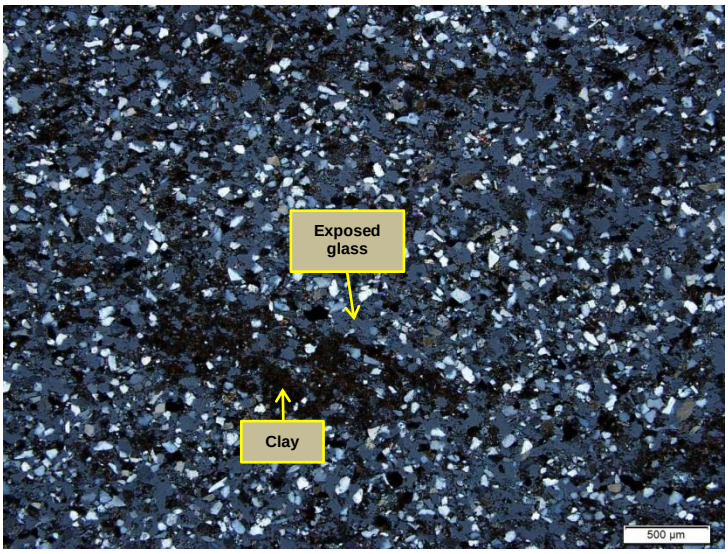


Fig. 4-180: Photomicrograph in XPL showing abundant exposed thin section glass with few dispersed detrital mineral grains. Despite the large amount of material that has been removed from the sample, an isolated patch of clay matrix remains present, suggesting that clays may have occupied some of the space currently visible as exposed glass.

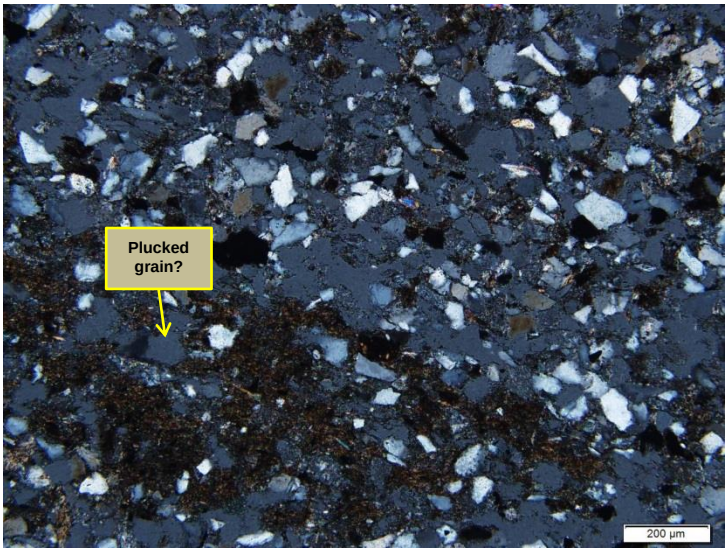


Fig. 4-181: Photomicrograph in XPL detailing the patch of clay matrix shown in Figure 4-180. Some areas of exposed thin section glass observed in the sample have subrounded or subangular outlines that may represent removal of detrital grains of the same shape.

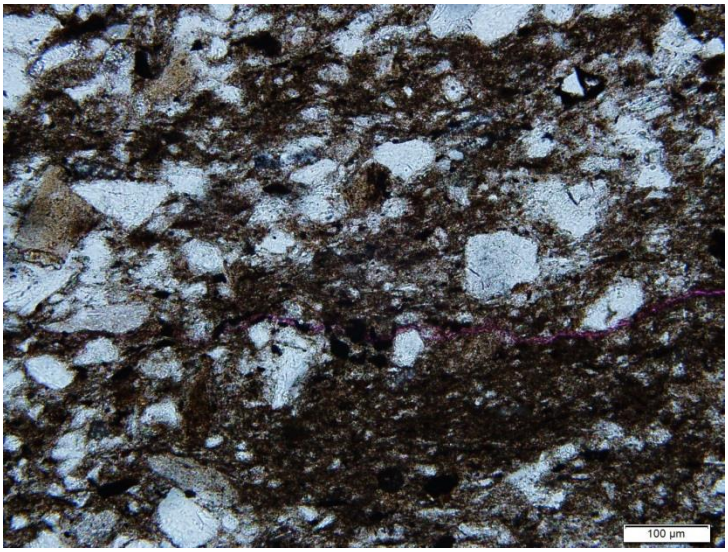


Fig. 4-182: Photomicrograph in PPL showing a small area of the mudstone with minimal sample-preparation damage. This part of the sample contains >25% clay, suggesting that clays may constitute a large portion of the material removed from other parts of the sample. Note a thin micro-fracture filled with pink epoxy.

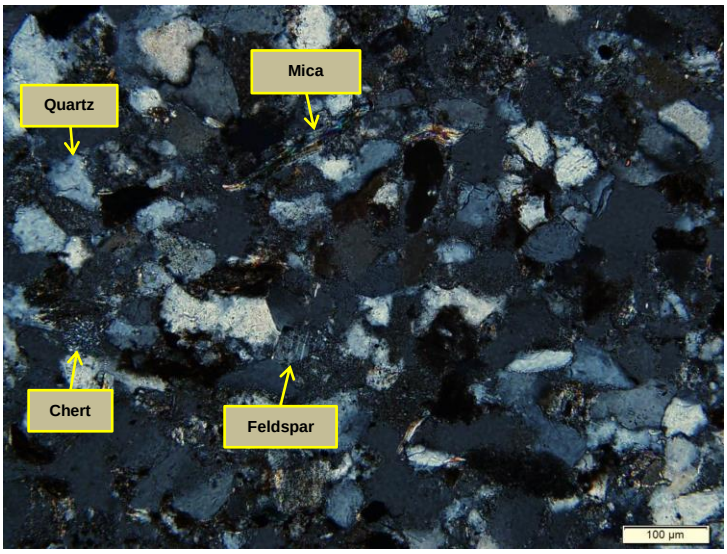


Fig. 4-183: Photomicrograph in XPL showing subrounded (common) to subangular (rare) very fine silt- to fine sand-sized (average grain size is coarse silt) detrital quartz (35-50%), chert (10-15%), mica (1-4%) and feldspar (<1%) observed in the sample.

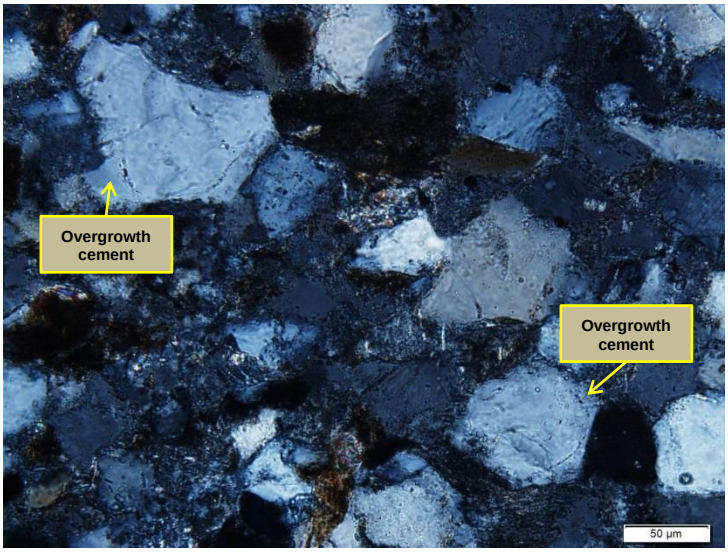


Fig. 4-184: Photomicrograph in XPL showing rare quartz overgrowth cements observed in a sandy portion of the sample.

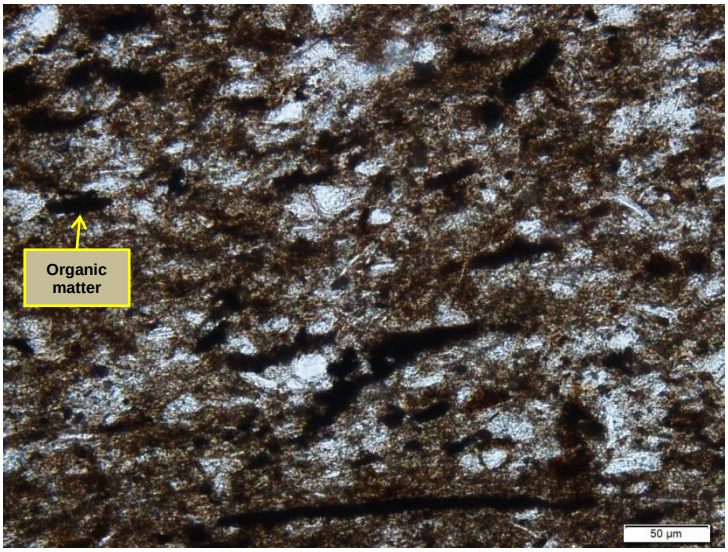


Fig. 4-185: Photomicrograph in PPL showing possible finely laminated clay-rich bedding or lenses (see location in Figure 4-178). Clay- to fine silt-sized particles of quartz are embedded within the clay-rich matrix along with some mica and chert. Note thin streaks or short “trails” of organic matter.

4.2.18 SAMPLE 13431

Sample ID	**13431**		
Sample type	**Core**	**UWI/Well**	**100/08-30-049-04W5/00**
Strat. Unit	**Cardium Formation**	**Depth**	**1244.86 m**

XRD/SRA results

Quartz (%)	Fsp (%)	Cb (%)	Clays (%)	Pyrite (%)
69.8	2.4	0	27.3	0.4

Composition (*in order of abundance*)

Grain size	%	Variety (%)	Variety (%)	Variety (%)	Variety (%)
sand	50	Quartz/chert (94)	Mica (2)	Feldspar (1)	
silt	10	Quartz/chert (96)	Mica (4)		
clay	30	Clay mins (100)			
Cement	7	Quartz (100)			
Bioclasts	0				
Organics	3	Amorphous (100)			
Opaques	<1	Pyrite (100)			
	100				

*Intensively altered to clay minerals

^ Including bitumen

Sedimentary structures

Primary	Sandy and clay-rich bedding and possible faint laminae.
Biogenic	Possible burrow structures.

Fractures	Common epoxy-filled fractures. Likely artificial.
Porosity	6-10% intergranular porosity in sandy beds.

Description

Clayey sandstone comprised of subrounded (common) to angular (rare) very fine silt- to fine sand-sized (average grain size is very fine sand) detrital quartz (45-60%), chert (10-14%), mica (1-8%), and feldspar (<4%). The sandstone consists of interbedded clay-rich and sandy horizons, with both convoluted bedding and sections of distinct layering present. 6-10% intergranular porosity is observed in sandy layers.

Thin Section Quality

Poor. Common artificial fractures and exposed thin section glass.

Rock Classification

Clayey sandstone.

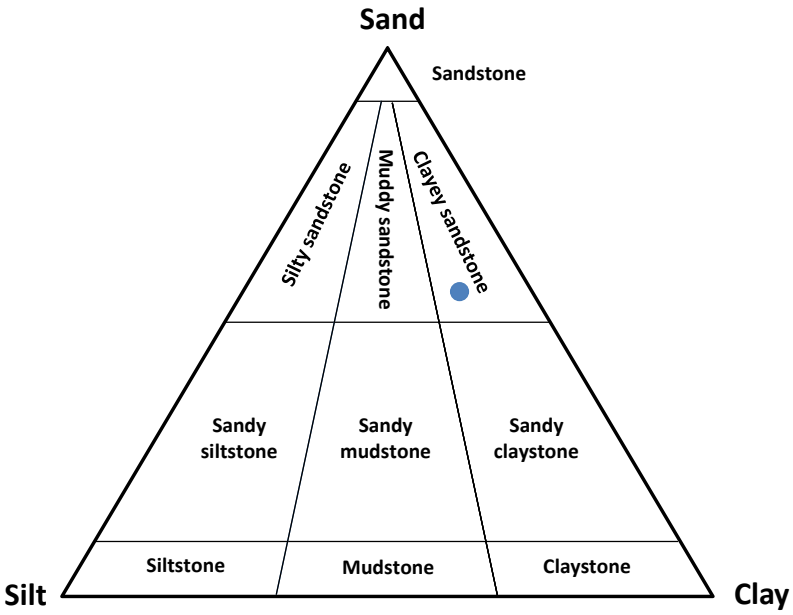


Fig. 4-186: Ternary plot showing the grain size composition of the sample based on the Wentworth scale (after Folk, 1954). Sample 13431 is classified as a clayey sandstone.



Fig. 4-187: Core photograph of sample 13431 from the Cardium Formation, well 100/08-30-049-04W5/00 (depth 1244.86 m). The thin section prepared from this sample was cut from the area marked with an X. The sample was received with no up direction. Scale is in mm.

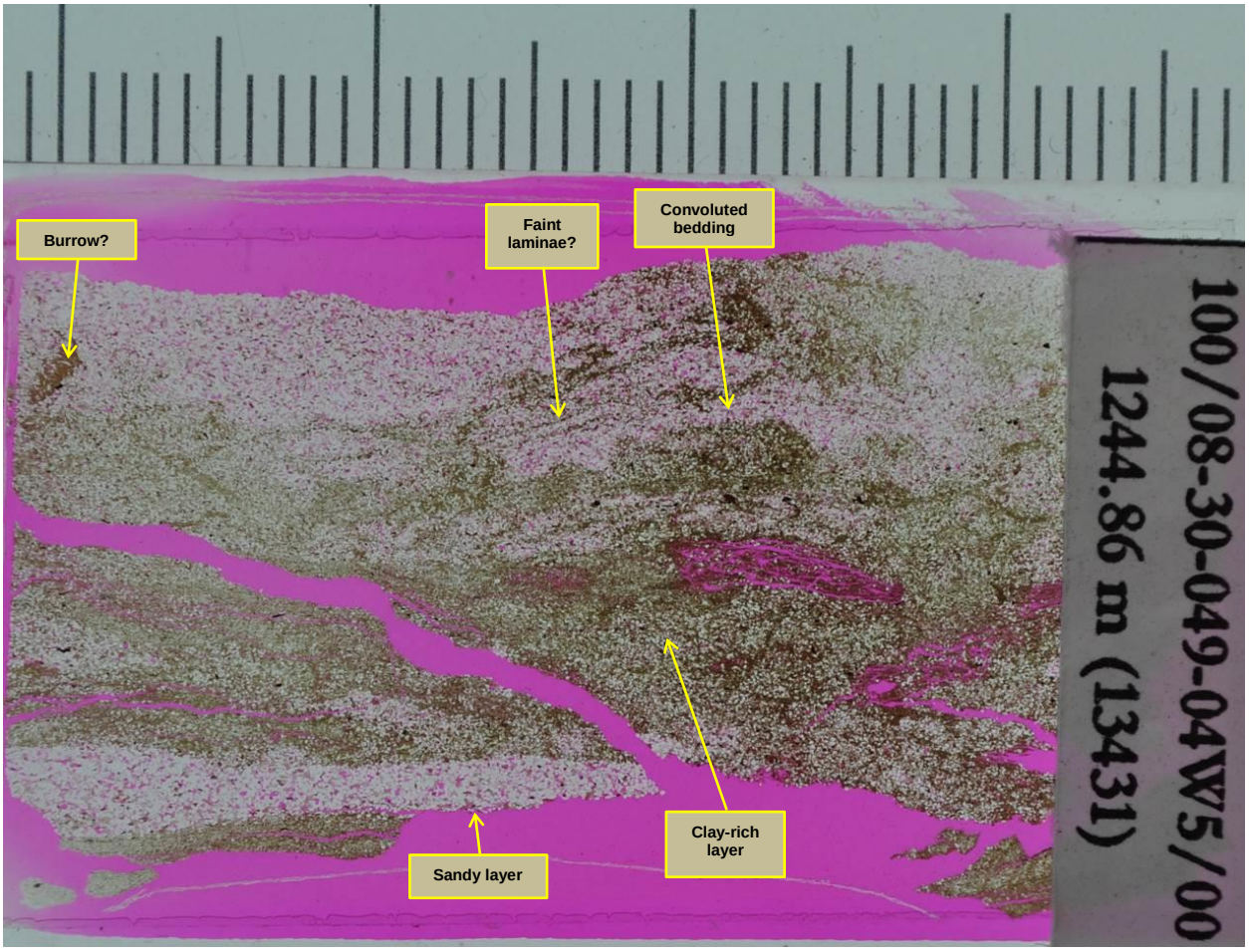


Fig. 4-188: Thin section photograph of sample 13431 from the Cardium Formation, well 100/08-30-049-04W5/00 (depth 1244.86 m). The sample is a clayey sandstone with interbedded sandy and clay-rich layers. Irregular, convoluted bedding structures are observed. Scale is in mm. Note: up-direction was not positively identified.

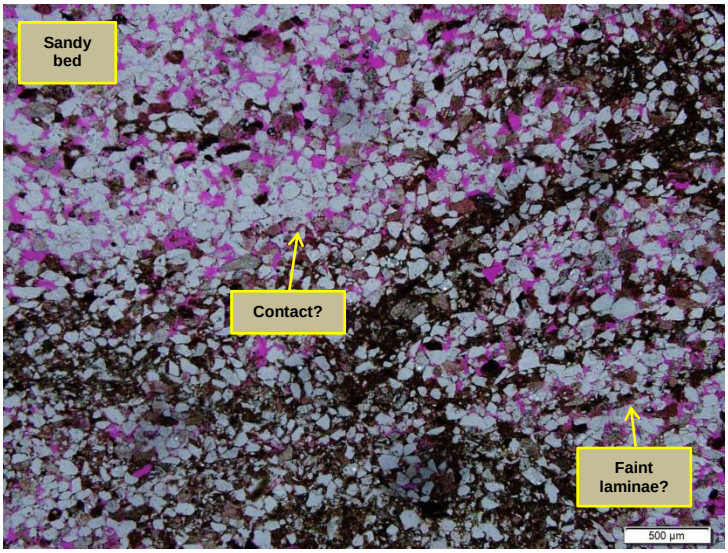


Fig. 4-189: Photomicrograph in PPL showing an overview image of the clayey sandstone. The sample is comprised of interbedded clay-rich and sandy layers, some of which show subtle convoluted bedding contacts or form patches. Porosity is highest in the sandy layers.

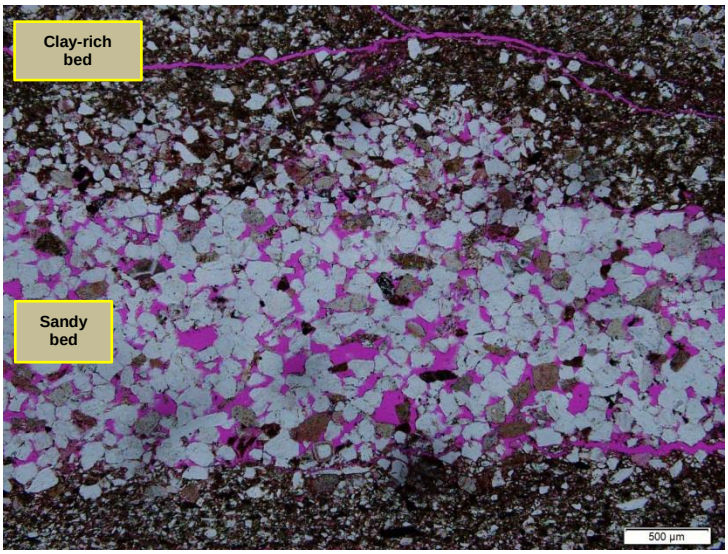


Fig. 4-190: Photomicrograph in PPL showing a sandy bed bound between clay-rich layers. Very little clay matrix occurs in the sandy layers, which have an estimated 6-10% intergranular porosity. Note artificial fractures filled with pink epoxy along the top half of the image.

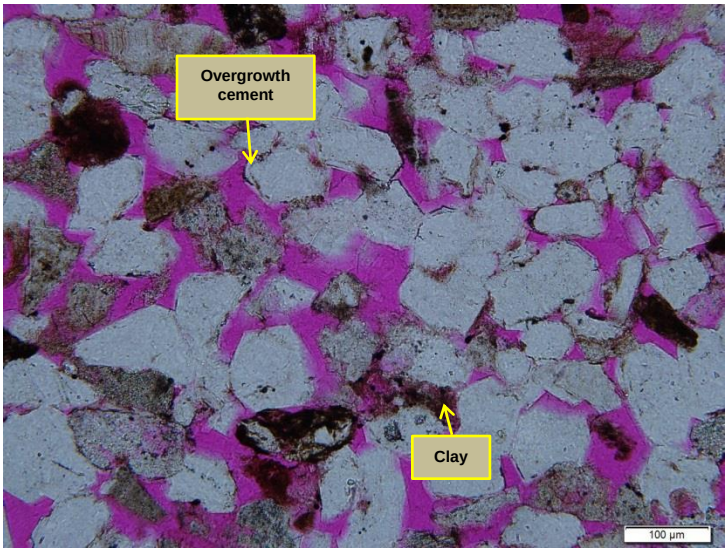


Fig. 4-191: Photomicrograph in PPL detailing intergranular porosity (filled with pink epoxy) observed in a sandy layer. Quartz overgrowth cements and rare interstitial clays are observed in these layers. Some oversized pores are likely the result of grain dissolution (or possible grain plucking during sample preparation).

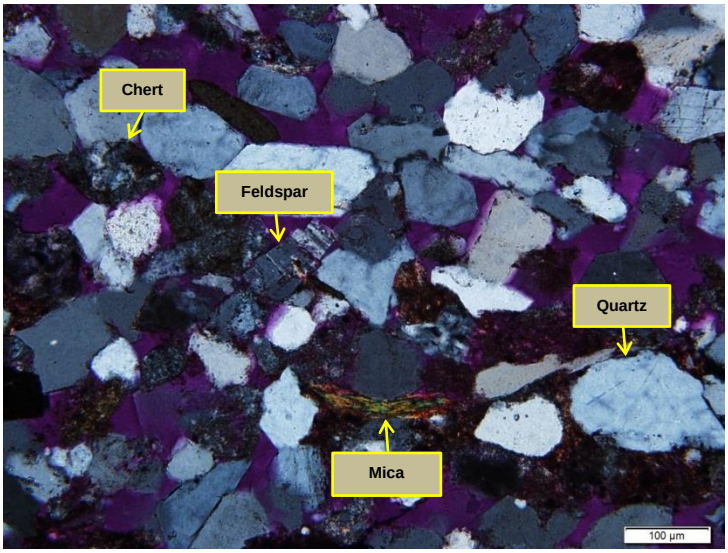


Fig. 4-192: Photomicrograph in XPL showing subrounded (common) to angular (rare) very fine silt- to fine sand-sized (average grain size is very fine sand) detrital quartz (45-60%), chert (10-14%), mica (1-8%), and feldspar (<4%) observed in the sandstone. Note polysynthetic twinning of feldspar, and a mica lathe with high birefringent colours, in XPL.

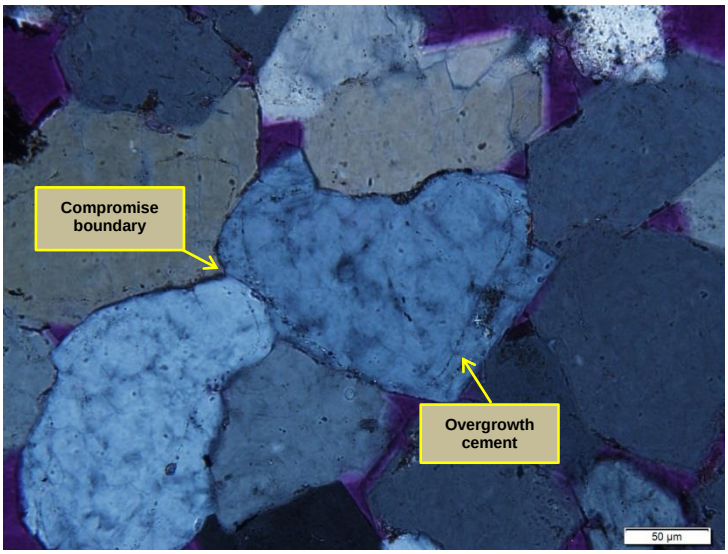


Fig. 4-193: Photomicrograph in XPL detailing quartz overgrowth cements observed in a sandy layer. These cements occasionally completely fill intergranular space. Note a dust rim around the original detrital grain.

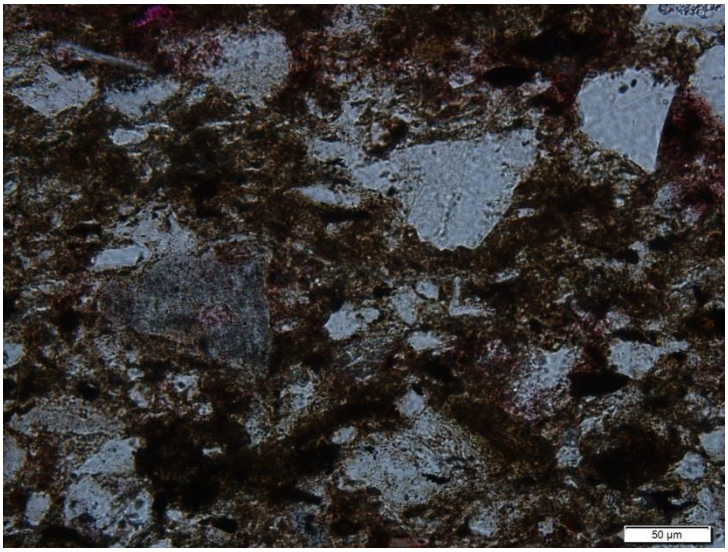


Fig. 4-194: Photomicrograph in PPL showing detail of a clay-rich layer. These layers contain many silt-sized grains embedded within the clay matrix, and have little to no intergranular porosity. Organic matter and finely disseminated pyrite are also observed.

4.2.19 SAMPLE 13432

Sample ID	**13432**		
Sample type	**Core**	**UWI/Well**	**100/08-30-049-04W5/00**
Strat. Unit	**Cardium Formation**	**Depth**	**1247.23 m**

XRD/SRA results

Quartz (%)	Fsp (%)	Cb (%)	Clays (%)	Pyrite (%)
54.5	3.6	1.4	40.1	0.3

Composition (*in order of abundance*)

Grain size	%	Variety (%)	Variety (%)	Variety (%)	Variety (%)
sand	27	Quartz/chert (94)	Mica (4)	Feldspar (<3)	
silt	18	Quartz/chert (90)	Mica (10)		
clay	50	Clay mins (100)			
Cement	<1	Quartz (100)			
Bioclasts	0				
Organics	4	Amorphous (100)			
Opaques	1	Pyrite (100)			
	100				

*Intensively altered to clay minerals

^ Including bitumen

Sedimentary structures

Primary	Convoluted clay-rich and sandy interbedding.
Biogenic	None apparent.

Fractures	Common epoxy-filled fractures and partings. Likely artificial.
Porosity	~5% intergranular porosity in a single sandy bed; otherwise non-porous.

Description

Sandy claystone comprised of subrounded (common) to angular (rare) very fine silt- to fine sand-sized quartz (20-40%), chert (2-8%), mica (1-5%), and feldspar (<2%). The rock consists of convoluted clay-rich and sandy interbeds, which lack distinct laminae and bedding contacts.

Thin Section Quality

Poor. Common exposed thin section glass and numerous fractures/partings.

Rock Classification

Sandy claystone.

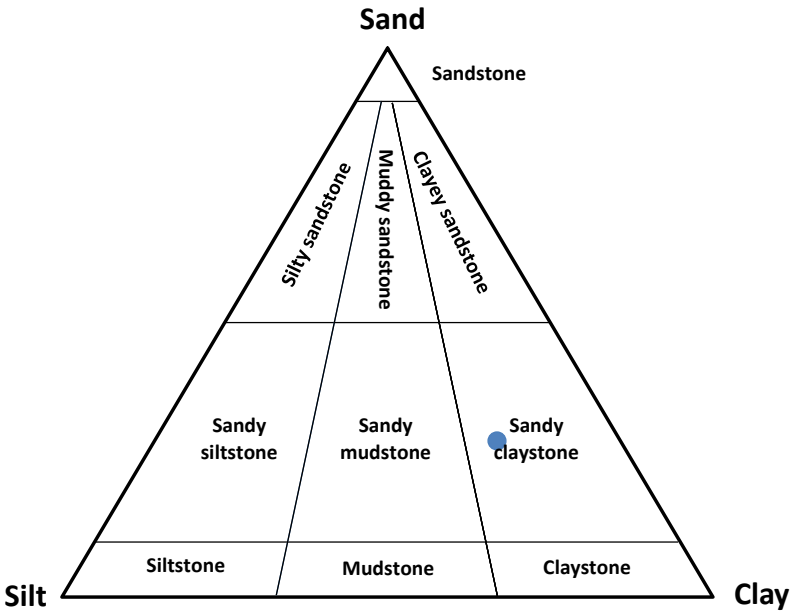


Fig. 4-195: Ternary plot showing the grain size composition of the sample based on the Wentworth scale (after Folk, 1954). Sample 13432 is classified as a sandy claystone.



Fig. 4-196: Core photograph of sample 13432 from the Cardium Formation, well 100/08-30-049-04W5/00 (depth 1247.23 m). The thin section prepared from this sample was cut from the area marked with an X. The sample was received with no up direction. Note the abundant missing sample material due to rock cutting with water. Scale is in mm.



Fig. 4-197: Thin section photograph of sample 13432 from the Cardium Formation, well 100/08-30-049-04W5/00 (depth 1247.23 m). The sample is a sandy claystone with convoluted clay-rich and sandy interbedding. A single sandy lens is observed. Partings are artifical and indicate the presence of swelling clay minerals. Scale is in mm.

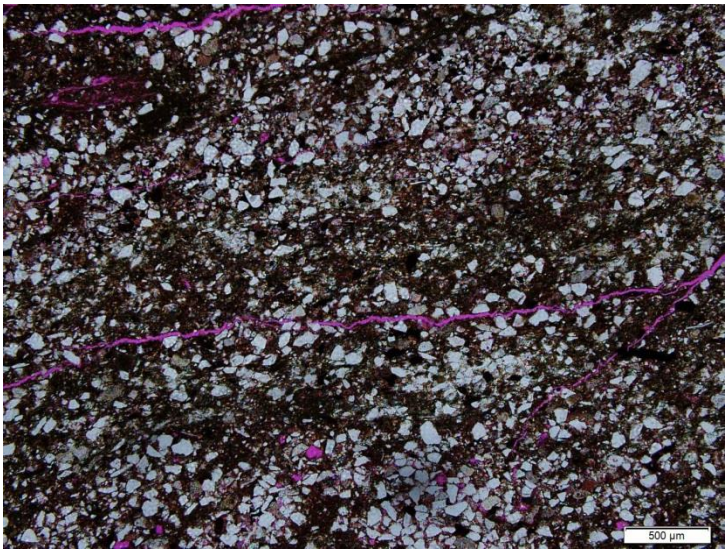


Fig. 4-198: Photomicrograph in PPL showing an overview of the sandy claystone. The sample is comprised of convolute, interbedded sandy and clay-rich horizons, which lack distinct laminae and bed contacts. Light-coloured minerals consist of quartz, chert, mica and feldspar, whereas the darker patches are composed mostly of clays, organic matter and pyrite. Note several artificial fractures (filled with pink epoxy).

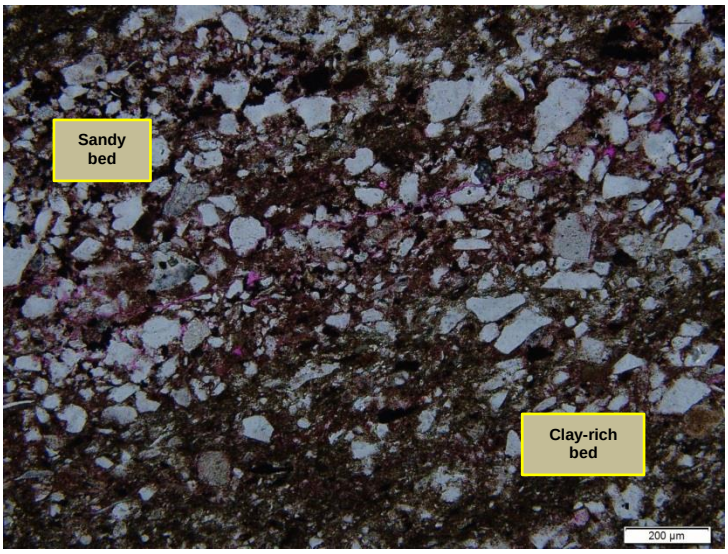


Fig. 4-199: Photomicrograph in PPL detailing mixed coarse- and fine-grained sediments. No distinct grading is observed. Grains are up to 200 µm in size. Note patchy porosity (pink epoxy).

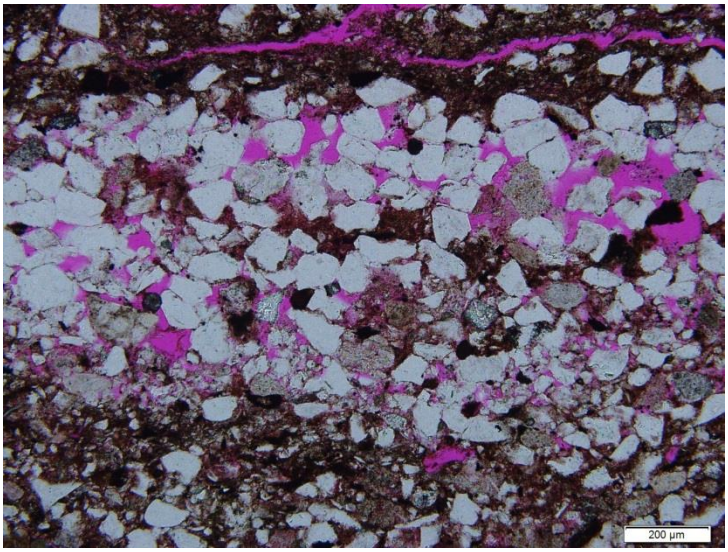


Fig. 4-200: Photomicrograph in PPL showing a single porous sandy lens (~830 µm thick in the image). This horizon has ~5% intergranular porosity (filled with pink epoxy), but some oversized pores are likely due sample preparation (grain plucking).

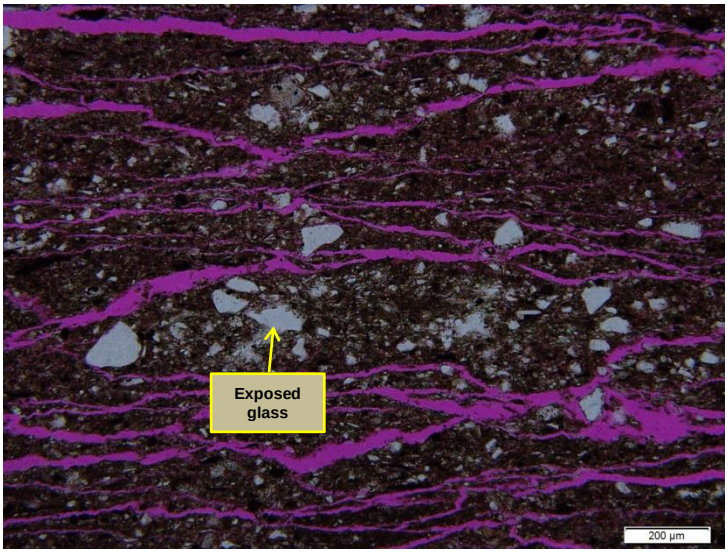


Fig. 4-201: Photomicrograph in PPL showing heavy artificial fracturing. Artificial fractures and exposed thin section glass suggest that water-sensitive clay minerals are present in the sample. Clay-size quartz is embedded within the matrix.

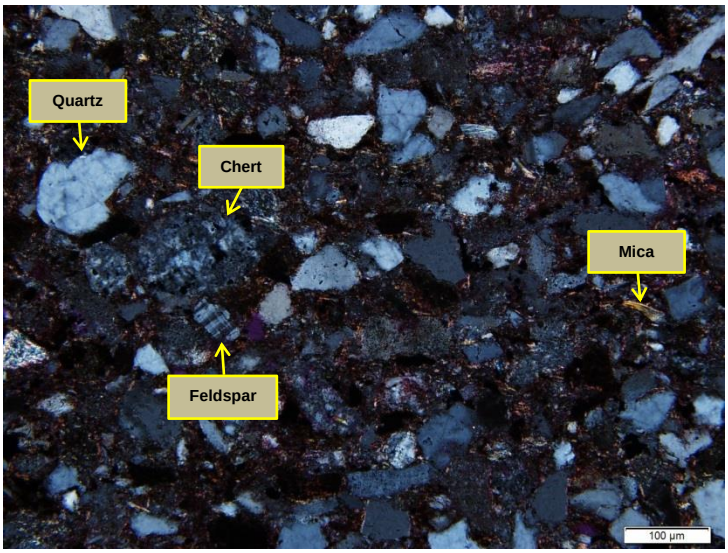


Fig. 4-202: Photomicrograph in XPL showing subrounded (common) to angular (rare) very fine silt- to fine sand-sized quartz (20-40%), chert (2-8%), mica (1-5%), and feldspar (<2%) observed in the claystone. Note “tartan” twinning associated with feldspar.

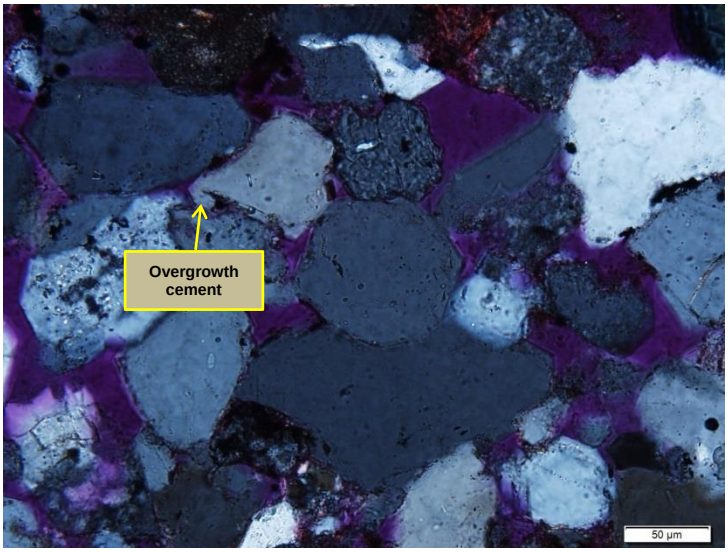


Fig. 4-203: Photomicrograph in XPL detailing minor quartz overgrowths observed in the single porous sandy lens seen in Figure 4-200. Some interstitial clay is observed lining/rimming open pores.

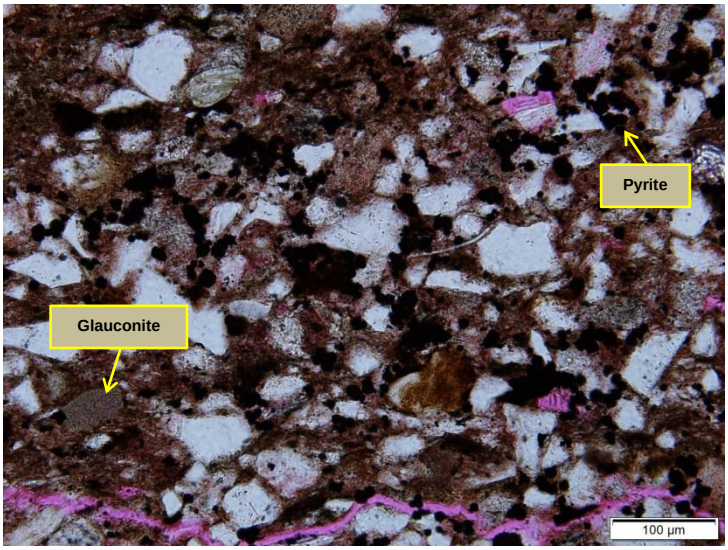


Fig. 4-204: Photomicrograph in PPL illustrating finely disseminated pyrite idiomorphs (opaque), which are occasionally clustered together. Patchy intergranular porosity is observed, with additional secondary microporosity associated with grain dissolution (see pink epoxy within a glauconite grain).

4.2.20 SAMPLE 13436

Sample ID	**13436**		
Sample type	**Core**	**UWI/Well**	**100/07-32-045-12W5/00**
Strat. Unit	**Cardium Formation**	**Depth**	**2177.13 m**

XRD/SRA results

Quartz (%)	Fsp (%)	Cb (%)	Clays (%)	Pyrite (%)
67.6	3.7	2.4	25.7	0.7

Composition (*in order of abundance*)

Grain size	%	Variety (%)	Variety (%)	Variety (%)	Variety (%)
sand	43	Quartz/chert (97)	Mica (2)	Feldspar (<2)	
silt	20	Quartz/chert (92)	Mica (8)		
clay	29	Clay mins (100)			
Cement	4	Quartz (100)			
Bioclasts	0				
Organics	4	Amorphous (100)			
Opaques	<1	Pyrite (100)			
	100				

*Intensively altered to clay minerals

^ Including bitumen

Sedimentary structures

Primary	Discontinuous (bioturbated?) clay-rich laminae.
Biogenic	Apparent bioturbation features, including possible *Planolites* burrows.

Fractures	Occasional thin (6-8 μm thickness) epoxy-filled fractures. Likely artificial.
Porosity	Minor (<4%) intergranular porosity in clay-poor patches. Largely non-porous.

Description

Bioturbated sandy mudstone comprised of subangular (common) to subrounded (rare) fine silt- to fine sand-sized (average grain size is very-fine sand) detrital quartz (45-50%), chert (5-10%), mica (1-5%), and feldspar (<4%). Several discontinuous (bioturbated?) clay-rich laminae occur in the mudstone, which largely appears unstratified. Minor (<4%) intergranular porosity is observed in rare clay-poor patches of the mudstone.

Thin Section Quality

Good. Some exposed thin section glass.

Rock Classification

Sandy mudstone.

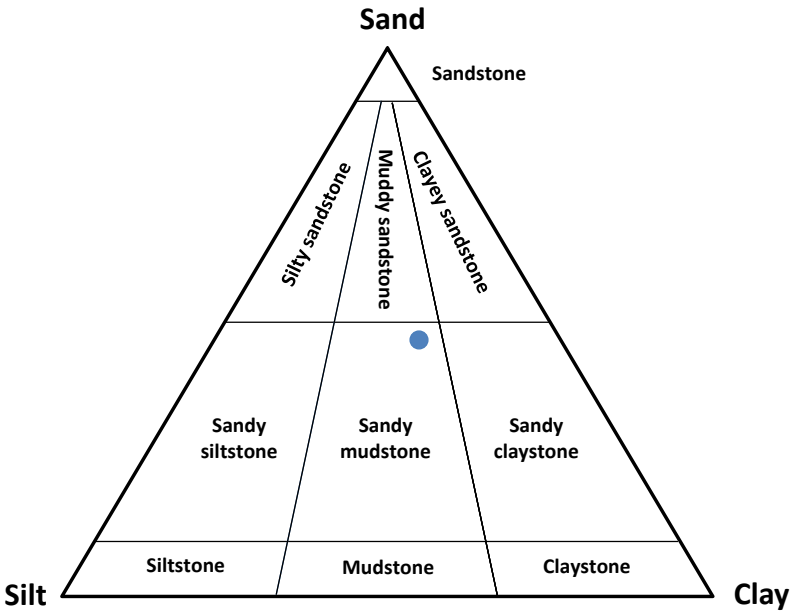


Fig. 4-205: Ternary plot showing the grain size composition of the sample based on the Wentworth scale (after Folk, 1954). Sample 13436 is classified as a sandy mudstone.

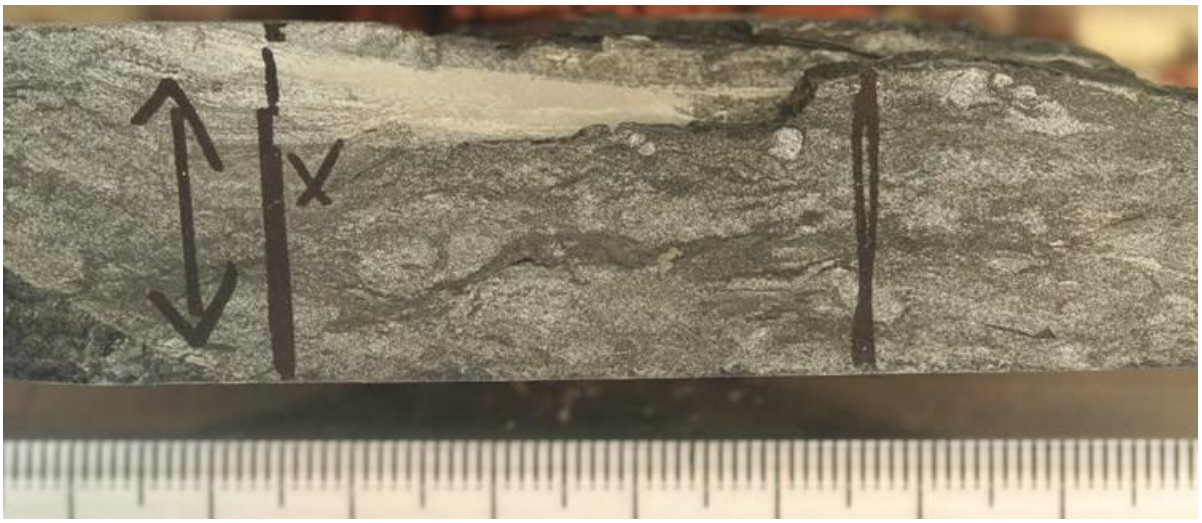


Fig. 4-206: Core photograph of sample 13436 from the Cardium Formation, well 100/07-32-045-12W5/00 (depth 2177.13 m). The thin section prepared from this sample was cut from the area marked with an X. The sample was received with no up direction. Scale is in mm.

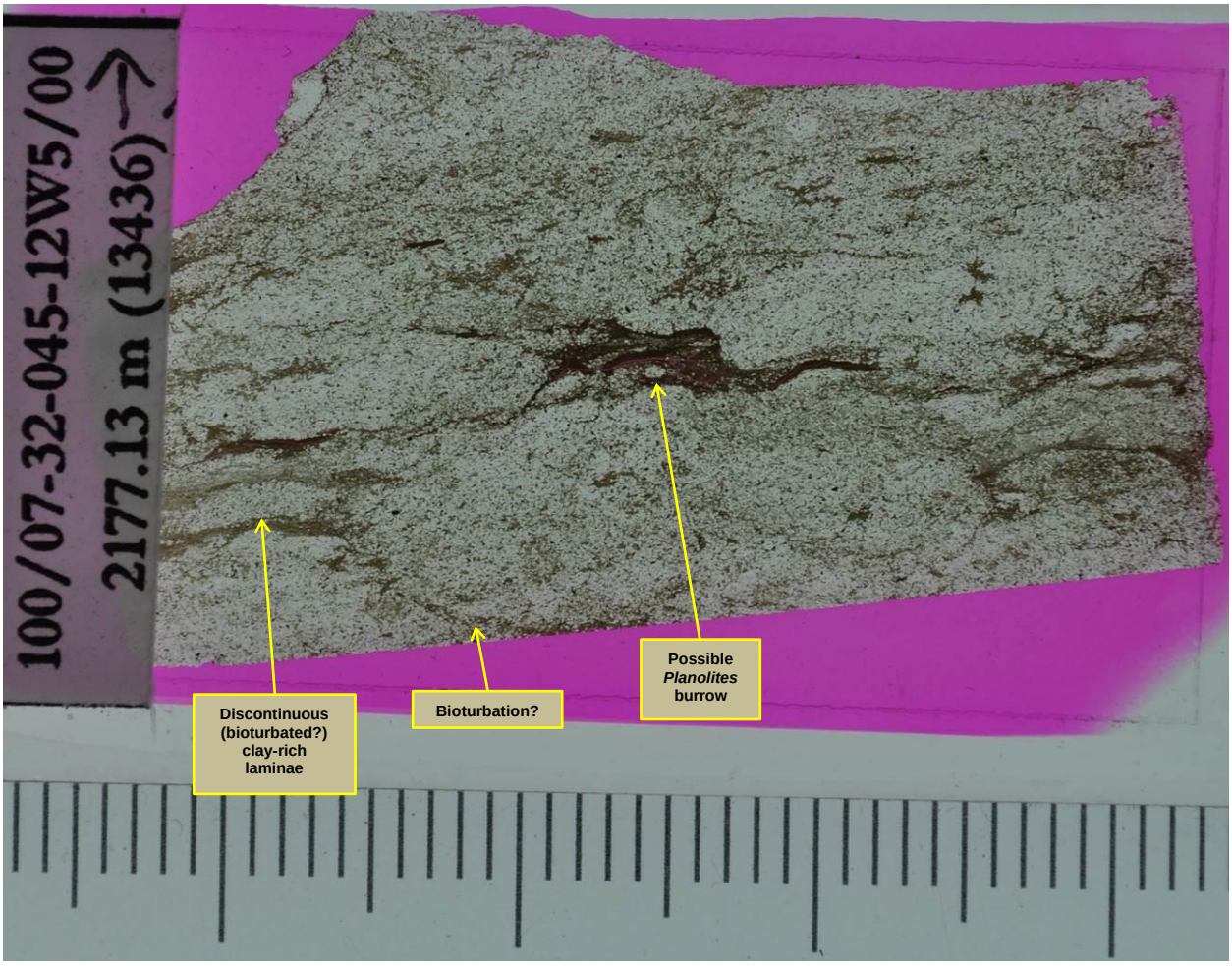


Fig. 4-207: Thin section photograph of sample 13436 from the Cardium Formation, well 100/07-32-045-12W5/00 (depth 2177.13 m). The sample is a bioturbated sandy mudstone. Although the sample largely appears unstratified, several discontinuous clay-rich laminae and lenses are present suggesting that some original bedding features were likely disturbed by bioturbation (as well as sediment compaction). Clay-rich patches and thin wisps are also observed. Scale is in mm.

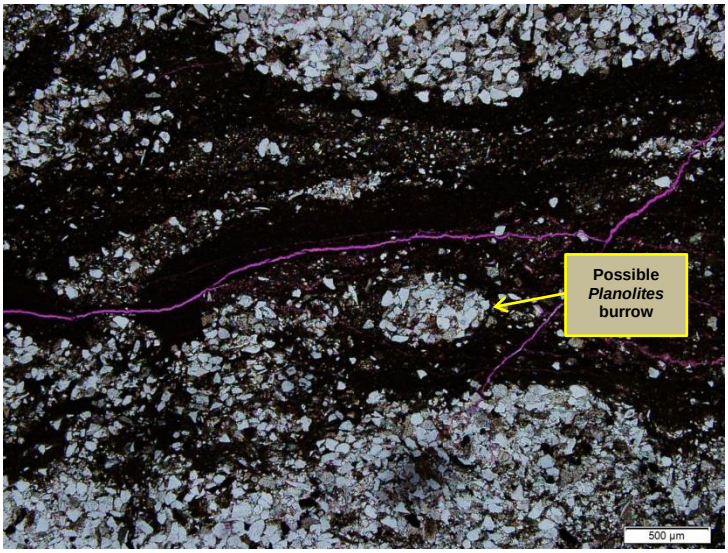


Fig. 4-208: Photomicrograph in PPL showing an overview of the sandy mudstone. Several discontinuous (bioturbation?) clay-rich laminae are observed. A possible *Planolites* burrow is present near the center of the image (see location within sample in Figure 4-207).

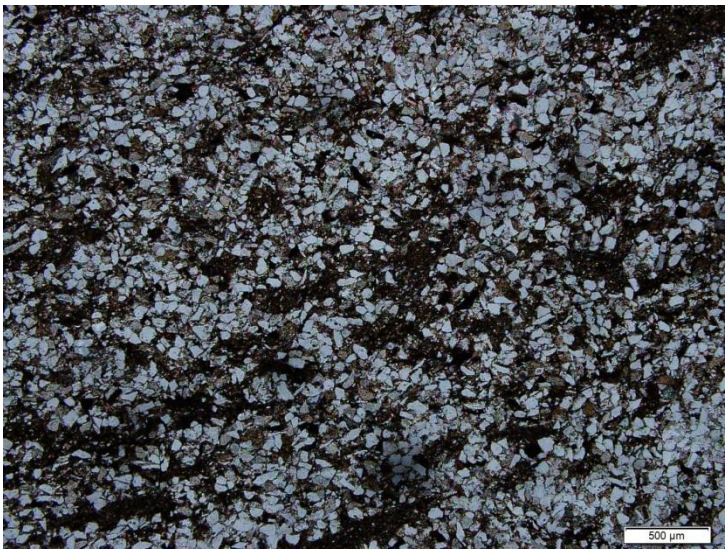


Fig. 4-209: Photomicrograph in PPL showing an overview of a typical mixed or bioturbated portion of the sample with numerous clay-rich patches (dark-colour). Light-coloured minerals consist of quartz, chert, mica and feldspar. The lack of primary sedimentary structures is likely the result of bioturbation.

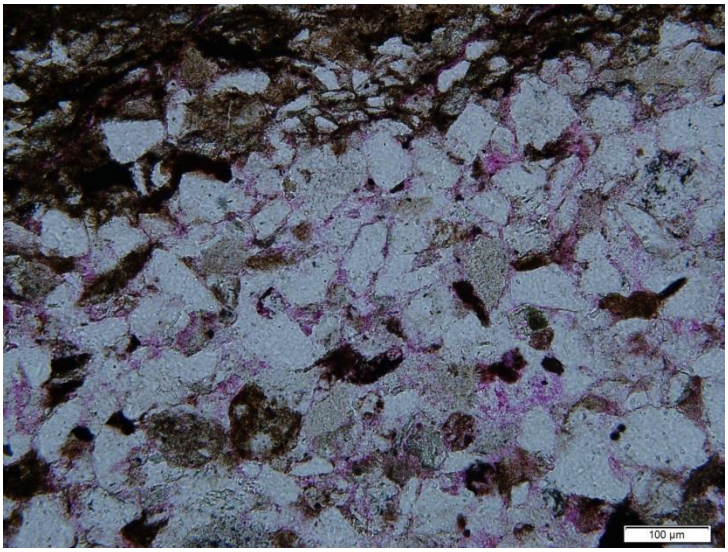


Fig. 4-210: Photomicrograph in PPL showing minor (<4%) intergranular porosity observed in a clay-poor patch of the sample. Clays are estimated at ~30% of the total sample composition, and are also associated with organic matter and pyrite.

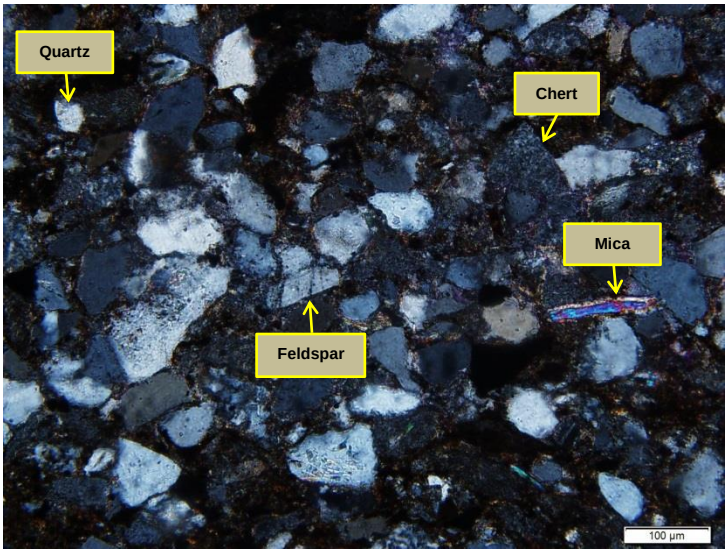


Fig. 4-211: Photomicrograph in XPL showing subangular (common) to subrounded (rare) fine silt- to fine sand-sized (average grain size is very-fine sand) detrital quartz (45-50%), chert (5-10%), mica (1-5%), and feldspar (<4%) present throughout the mudstone. Note a mica lathe (~120 µm in length) with high birefringent colours.

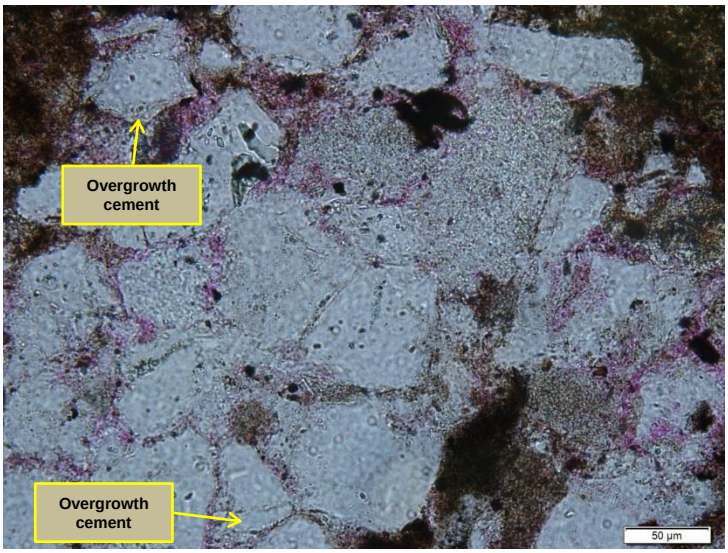


Fig. 4-212: Photomicrograph in PPL showing quartz overgrowths observed in a clay-poor patch of the sample. These cements do not occur in areas where abundant clay matrix is present. Note some minor intergranular porosity (pink epoxy), finely disseminated pyrite (opaque) and interstitial clays (brown).

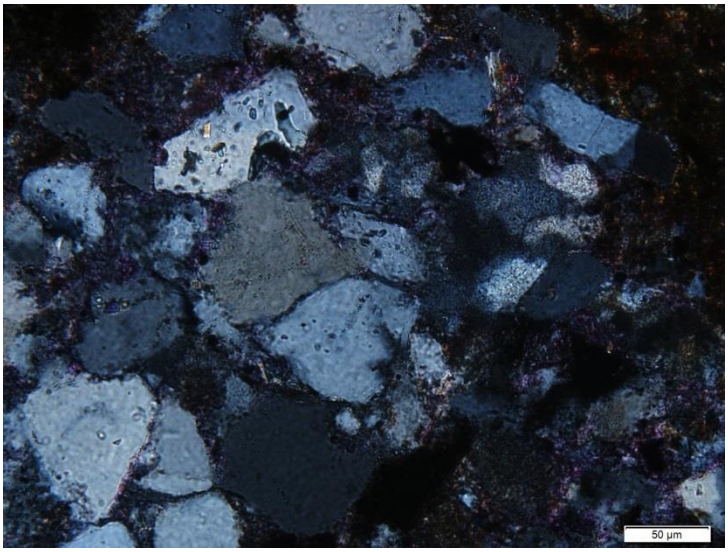


Fig. 4-213: Photomicrograph illustrating Figure 4-212 in XPL. Quartz overgrowths account for ~4% of the sample.

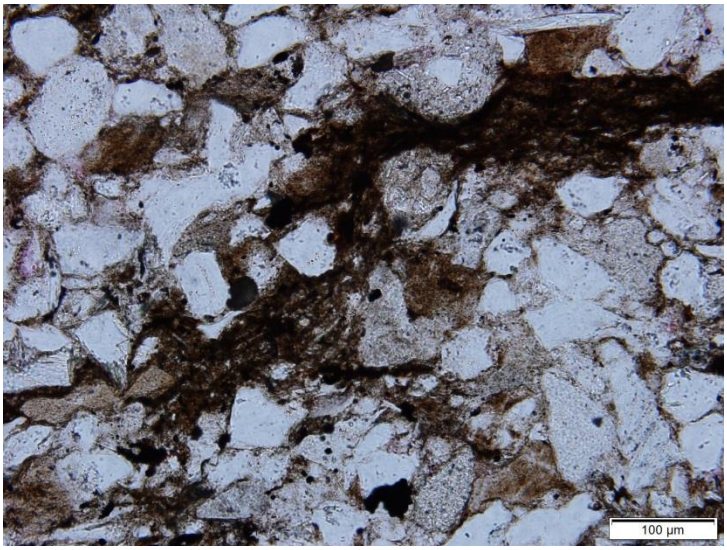


Fig. 4-214: Photomicrograph in PPL detailing a deformed and compacted opaque-rich (clays, organic matter, and pyrite) lens. Note larger grains embedded into the softer, clay-rich material.

4.2.21 SAMPLE 13437

Sample ID	**13437**		
Sample type	**Core**	**UWI/Well**	**100/07-32-045-12W5/00**
Strat. Unit	**Cardium Formation**	**Depth**	**2180.19 m**

XRD/SRA results

Quartz (%)	Fsp (%)	Cb (%)	Clays (%)	Pyrite (%)
67.1	3.1	0.8	28.6	0.6

Composition (*in order of abundance*)

Grain size	%	Variety (%)	Variety (%)	Variety (%)	Variety (%)
sand	25	Quartz/chert (94)	Mica (4)	Feldspar (2)	
silt	38	Quartz/chert (97)	Mica (3)		
clay	25	Clay mins (100)			
Cement	5	Chert (90)	Quartz (10)		
Bioclasts	0				
Organics	5	Amorphous (100)			
Opaques	2	Pyrite (100)			
	100				

*Intensively altered to clay minerals

^ Including bitumen

Sedimentary structures

Primary	None apparent (structureless mixture of clay-rich and sandy sediments).
Biogenic	Possible burrow structures. Appears heavily bioturbated.

Fractures	Occasional thin (7-34 μm thickness) epoxy-filled fractures. Likely artificial.
Porosity	Mostly non-porous. <3% intergranular porosity in some sandy patches.

Description

Bioturbated sandy mudstone comprised of subrounded (common) to angular (rare) very fine silt- to fine sand-sized (average grain size is coarse silt) detrital quartz (40-60%), chert (10-15%), mica (1-4%), and feldspar (<4%). Limited intergranular porosity (<3%) occurs in some sand-dominated patches of the rock (including possible burrow structures). Sand-dominated patches are cemented by chert (pore-filling) and quartz (overgrowth cements).

Thin Section Quality

Moderate. Exposed thin section glass is fairly abundant.

Rock Classification

Sandy mudstone.

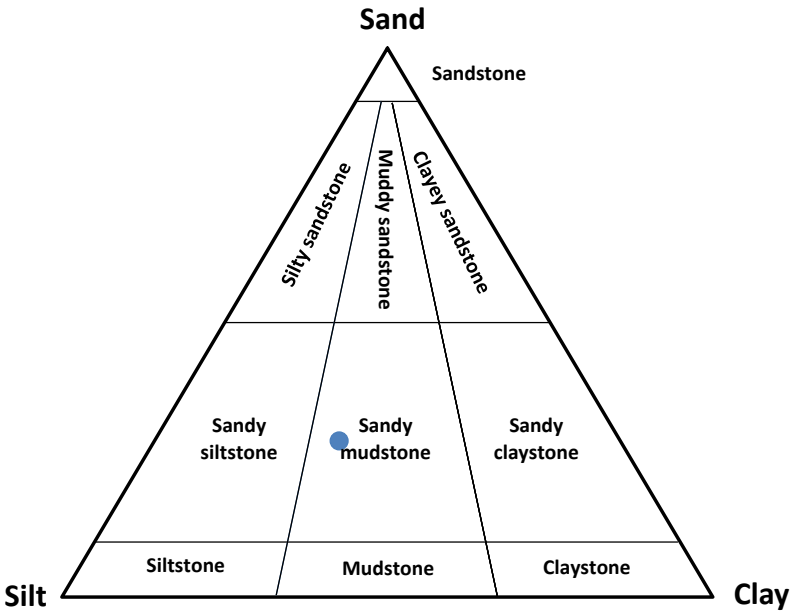


Fig. 4-215: Ternary plot showing the grain size composition of the sample based on the Wentworth scale (after Folk, 1954). Sample 13437 is classified as a sandy mudstone.

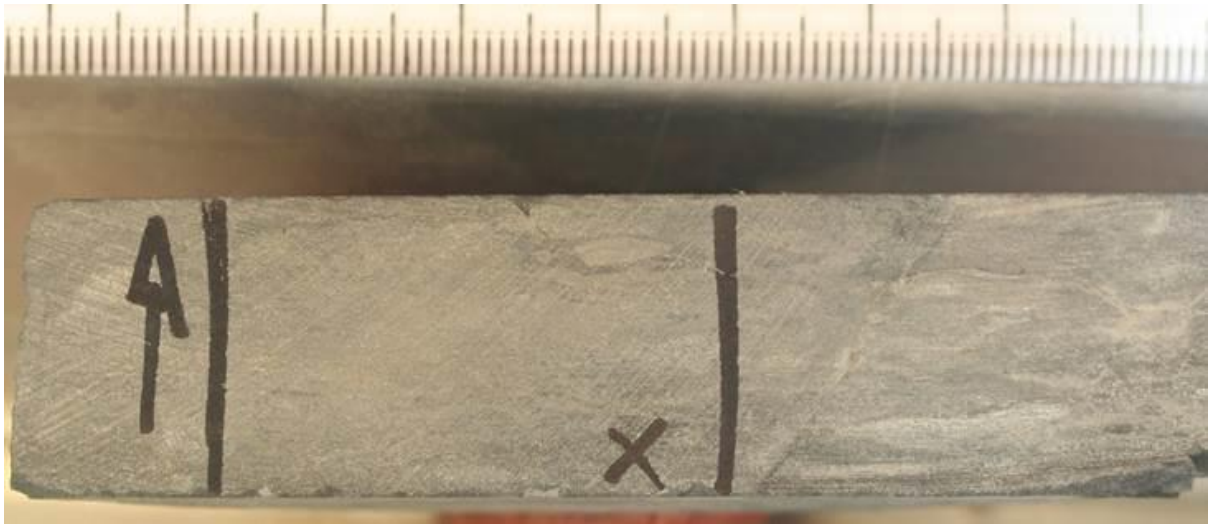


Fig. 4-216: Core photograph of sample 13437 from the Cardium Formation, well 100/07-32-045-12W5/00 (depth 2180.19 m). The thin section prepared for this sample was cut from the area marked with an X. The depositional up direction is indicated by the arrow (left). Scale is in mm.

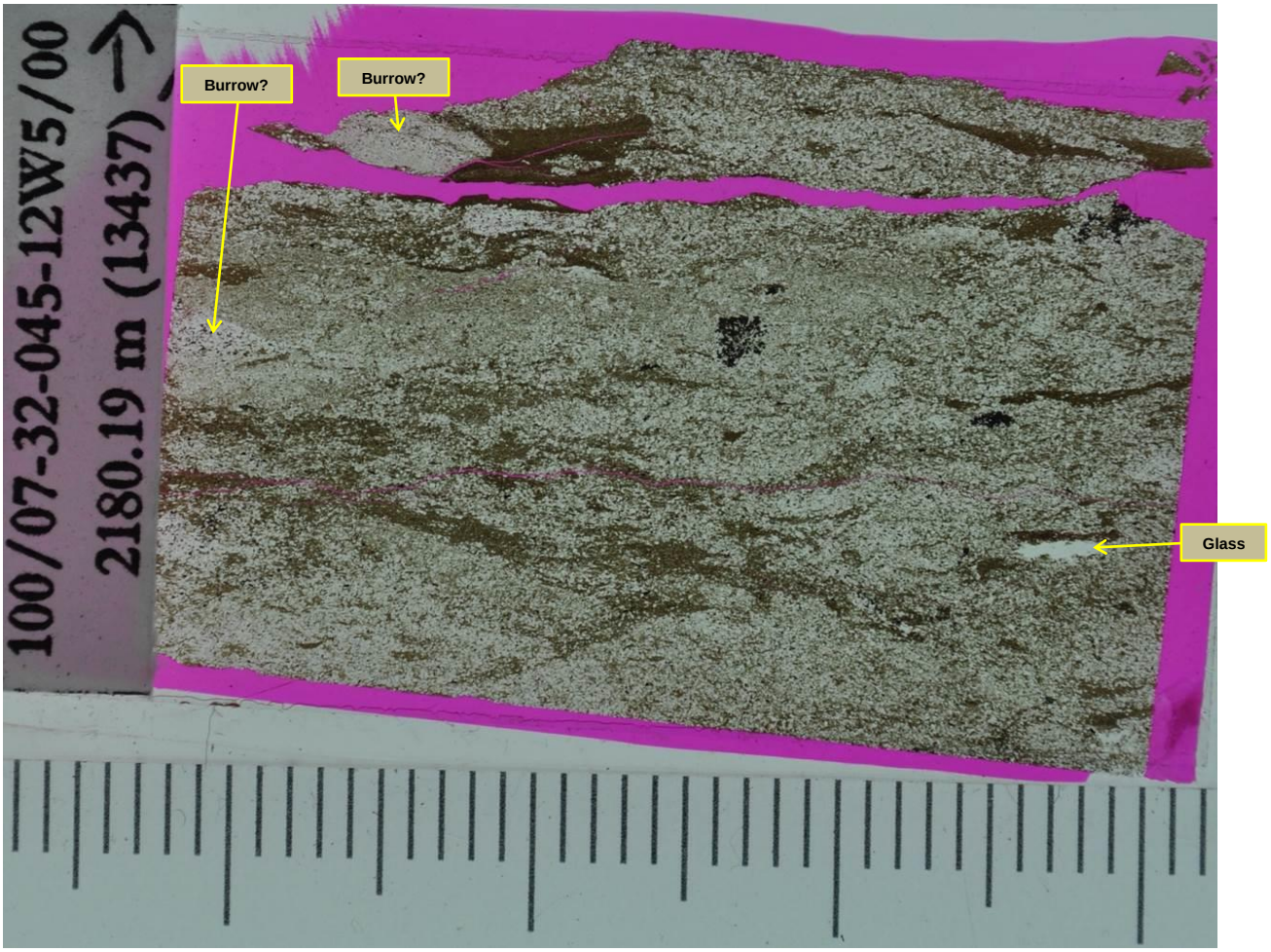


Fig. 4-217: Thin section photograph of sample 13437 from the Cardium Formation, well 100/07-32-045-12W5/00 (depth 2180.19 m). The sample is a bioturbated sandy mudstone, which lacks primary sedimentary structures, possibly indicating pervasive bioturbation following deposition of the original sediment. Dark-coloured patches consist of clay and organic-rich material. Light-coloured areas contain very fine silt- to fine sand-sized detrital quartz grains and abundant exposed thin section glass (white), which suggests that water-sensitive clays are present. Scale is in mm.

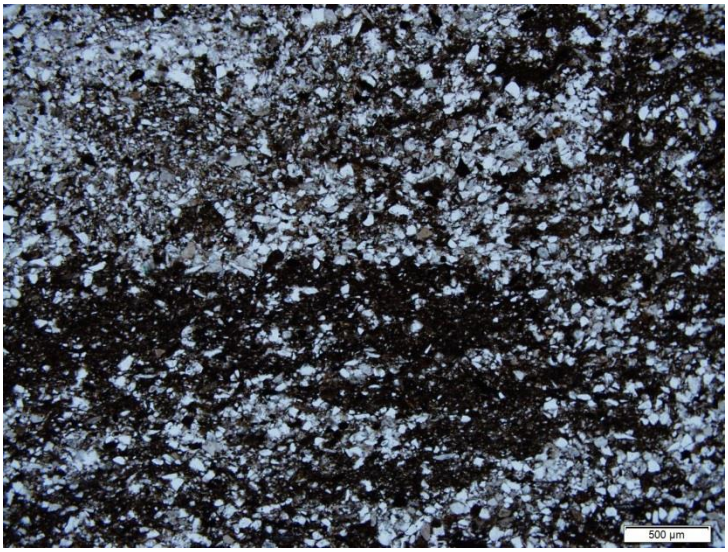


Fig. 4-218: Photomicrograph in PPL showing an overview of the sandy mudstone. The sample lacks primary depositional features, being composed of patches of clay-rich and sandy sediments that appear to be heavily bioturbated or mixed. Light-coloured minerals consist mostly of quartz, chert, feldspar and mica, whereas the dark patches are composed of opaque-material (clays, organic matter and pyrite).

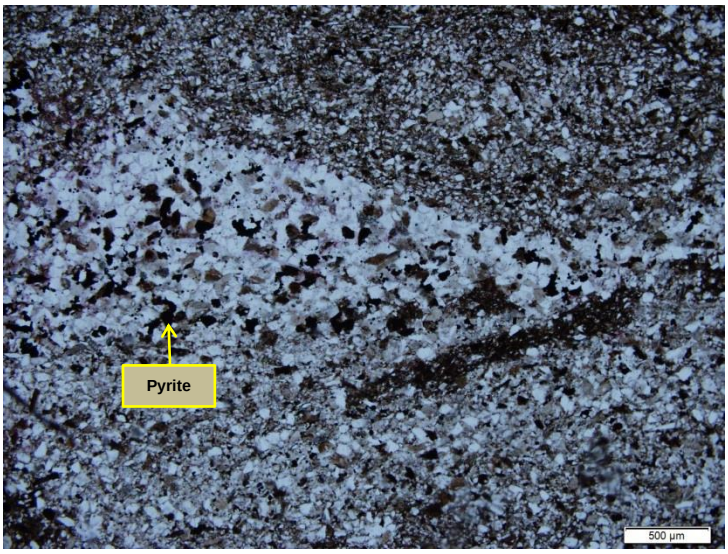


Fig. 4-219: Photomicrograph in PPL showing a well-sorted sandy lens. Note sharp contact between the sandy lens and the surrounding finer grained clay-rich sediment. Opaques (pyrite) are observed within the lens, which may be fecal in origin.

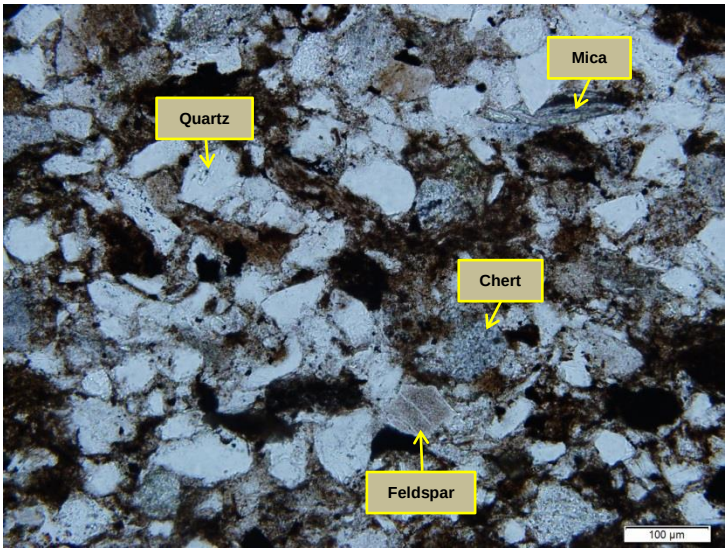


Fig. 4-220: Photomicrograph in PPL showing a typical example of subrounded (common) to angular (rare) very fine silt- to fine sand-sized (average grain size is coarse silt) detrital quartz (40-60%), chert (10-15%), mica (1-4%) and feldspar (<4%).

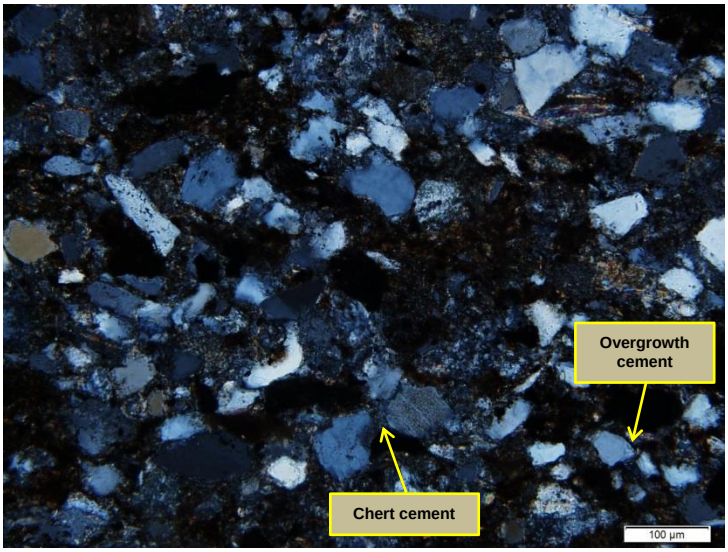


Fig. 4-221: Photomicrograph in XPL illustrating pore-filling microcrystalline quartz (chert) and quartz overgrowth cements observed in a sand-dominated patch of the sample (same field of view as Figure 4-220).

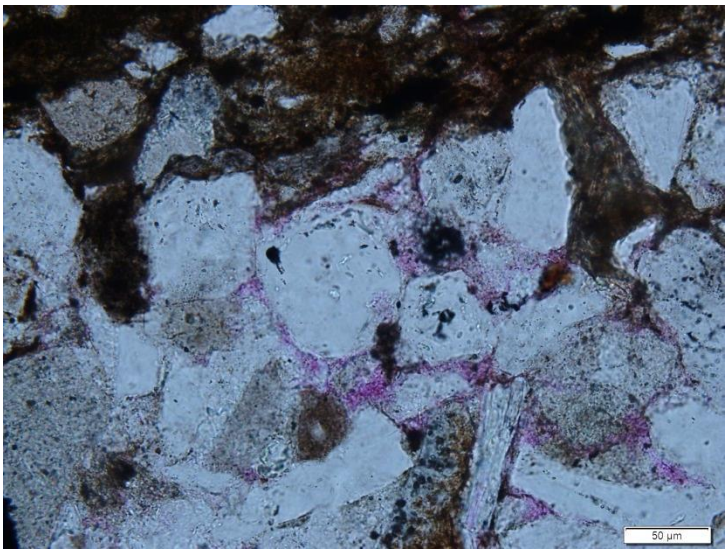


Fig. 4-222: Photomicrograph in PPL showing limited (<3%) intergranular porosity (pink) observed in a sand-dominated patch of the sample. Quartz and chert cementation appear to have significantly reduced intergranular porosity.

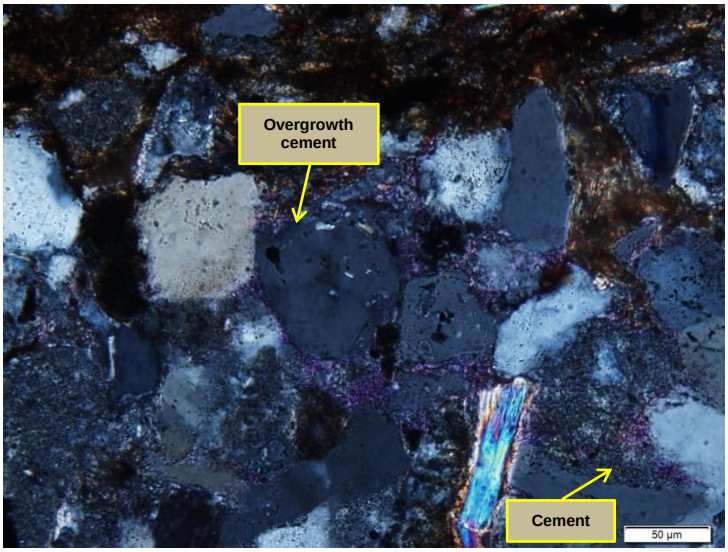


Fig. 4-223: Photomicrograph in XPL showing detail of chert and quartz cements (same field of view as Figure 4-222). Cement comprises ~5% of the total sample composition. Note a muscovite lathe, which has high birefringent colours.

4.2.22 SAMPLE 13438

Sample ID	**13438**		
Sample type	**Core**	**UWI/Well**	**100/07-32-045-12W5/00**
Strat. Unit	**Cardium Formation**	**Depth**	**2181.70 m**

XRD/SRA results

Quartz (%)	Fsp (%)	Cb (%)	Clays (%)	Pyrite (%)
61.4	5.8	1	31.5	0.3

Composition (*in order of abundance*)

Grain size	%	Variety (%)	Variety (%)	Variety (%)	Variety (%)
sand	32	Quartz/chert (97)	Mica (2)	Feldspar (1)	
silt	23	Quartz/chert (98)	Mica (2)		
clay	33	Clay mins (100)			
Cement	6	Chert (85)	Quartz (10)	Siderite (5)	
Bioclasts	0				
Organics	4	Amorphous (100)			
Opaques	2	Pyrite (100)			
	100				

*Intensively altered to clay minerals

^ Including bitumen

Sedimentary structures

Primary	None apparent.
Biogenic	Apparent pervasive bioturbation.

Fractures	Few thin (4-30 μm thickness) epoxy-filled fractures. Likely artificial.
Porosity	Non-porous.

Description

Heavily bioturbated sandy mudstone consisting of subrounded (common) to angular (rare) fine silt- to fine sand-sized (average grain size is very fine sand) detrital quartz (40-50%), chert (8-12%), mica (2 3%), and feldspar (1-3%). Rare (<1%) secondary dolomite crystals are observed in sandy parts of the rock, which are cemented by chert, quartz (overgrowth cements), and siderite. No intergranular porosity is observed in the rock.

Thin Section Quality

Good.

Rock Classification

Sandy mudstone.

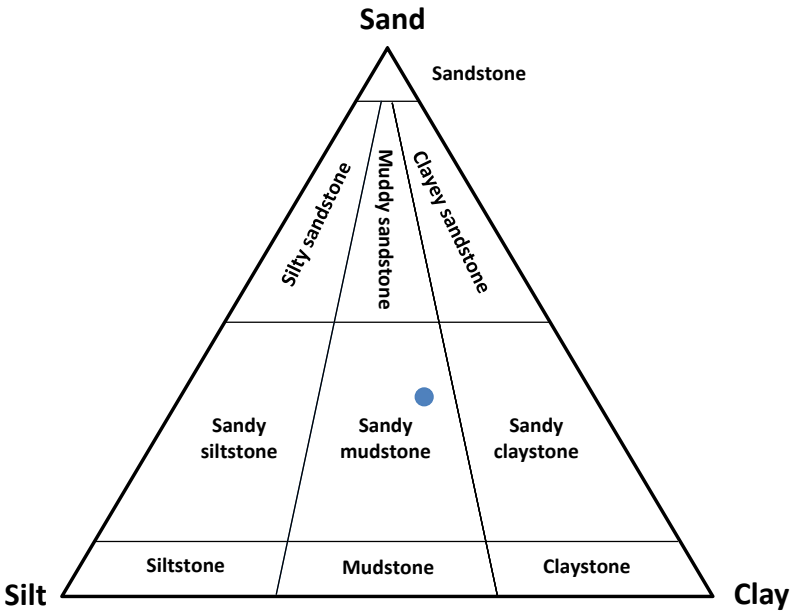


Fig. 4-224: Ternary plot showing the grain size composition of the sample based on the Wentworth scale (after Folk, 1954). Sample 13438 is classified as a sandy mudstone.

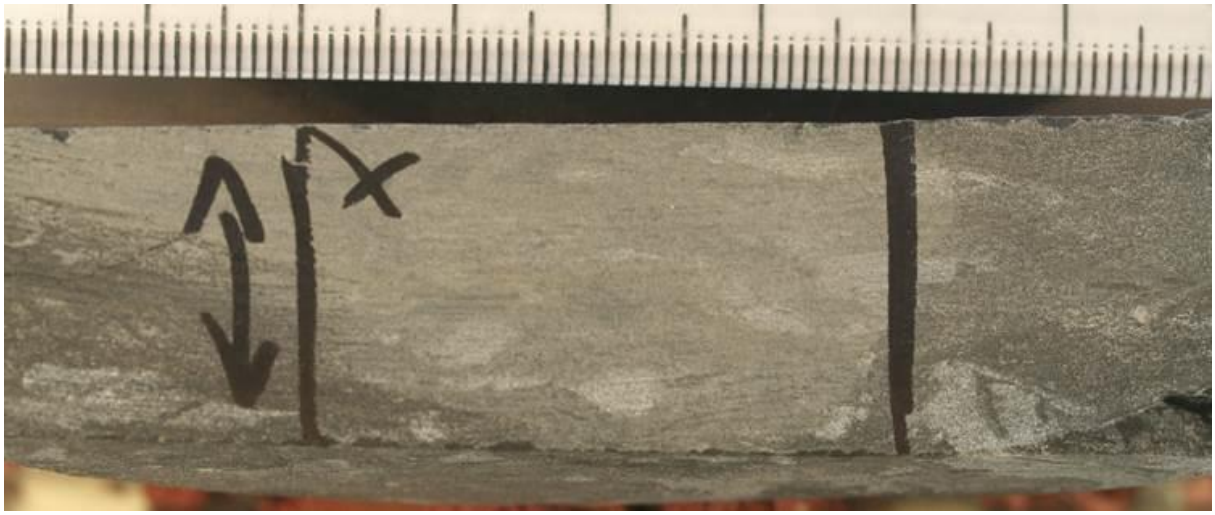


Fig. 4-225: Core photograph of sample 13438 from the Cardium Formation, well 100/07-32-045-12W5/00 (depth 2181.70 m). The thin section prepared from this sample was cut from the area marked with an X. The sample was received with no top orientation. Scale is in mm.

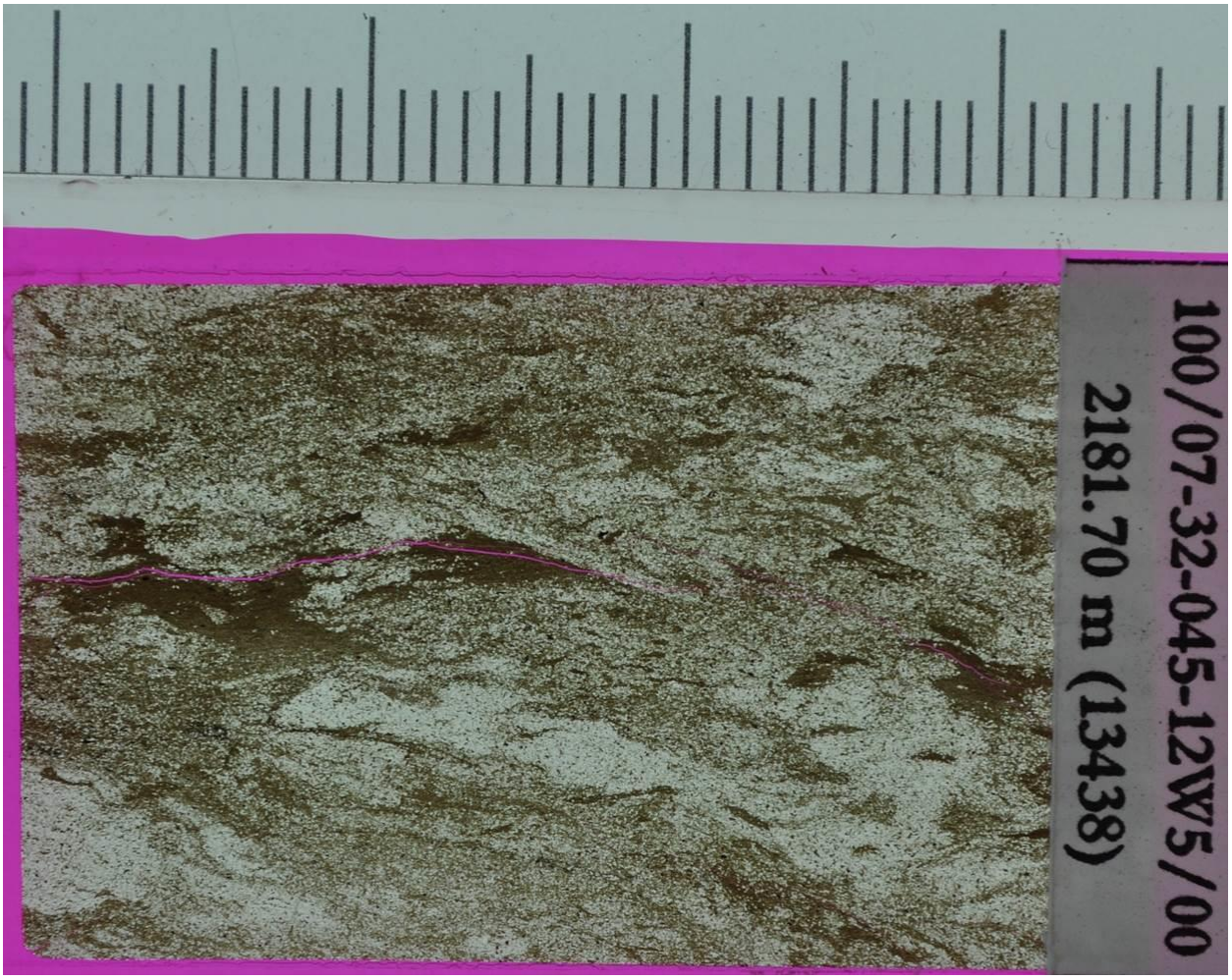


Fig. 4-226: Thin section photograph of sample 13438 from the Cardium Formation, well 100/07-32-045-12W5/00 (depth 2181.70 m). The sample is a heavily bioturbated sandy mudstone, which lacks primary depositional features. The sample consists of a mixture of amorphous clay- and sand-dominated patches, possibly indicating pervasive bioturbation. Scale is in mm.

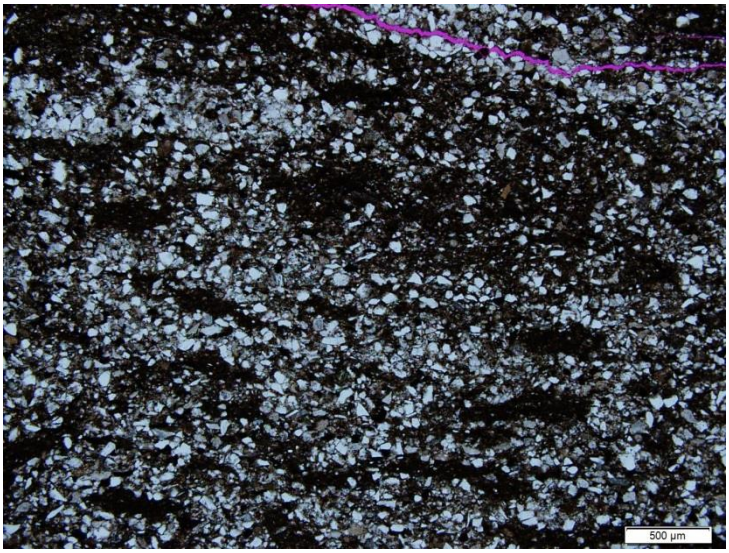


Fig. 4-227: Photomicrograph in PPL showing an overview of the sandy mudstone. The sample lacks primary depositional features, which indicates pervasive mixing (bioturbation?). Light-coloured minerals in the image consist of quartz, chert, mica and feldspar, whereas the darker patches consist predominantly of clays. Note an artificial fracture in the top right corner of the image (pink epoxy).

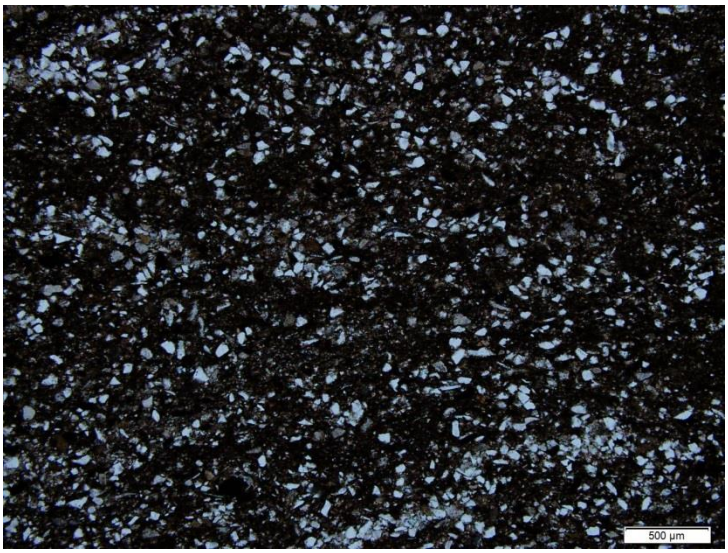


Fig. 4-228: Photomicrograph in PPL showing a clay-dominated patch observed in the sample. The sample consists of abundant amorphous patches of clay- (~30-35%) and sand-dominated (~32%) sediments.

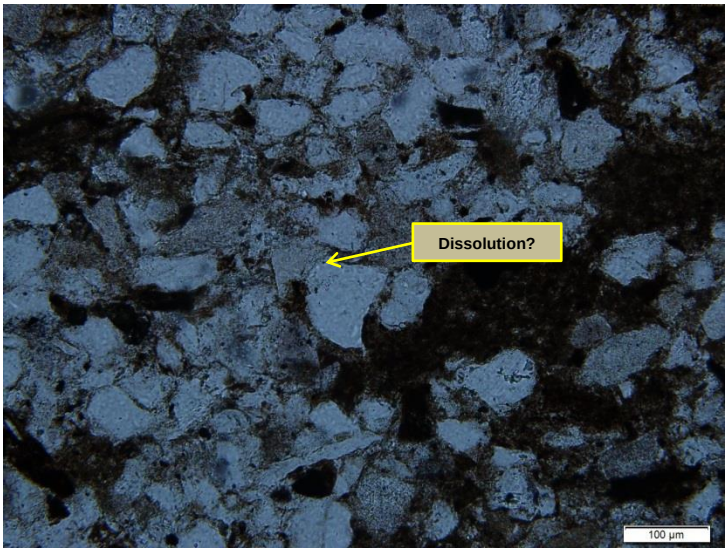


Fig. 4-229: Photomicrograph in PPL showing detail of a sand-dominated patch. Grains are tightly compacted, indicating that the original sediment experienced moderate to high compaction during burial. Irregularly-shaped grain boundaries may indicate partial mineral dissolution (pressure solution).

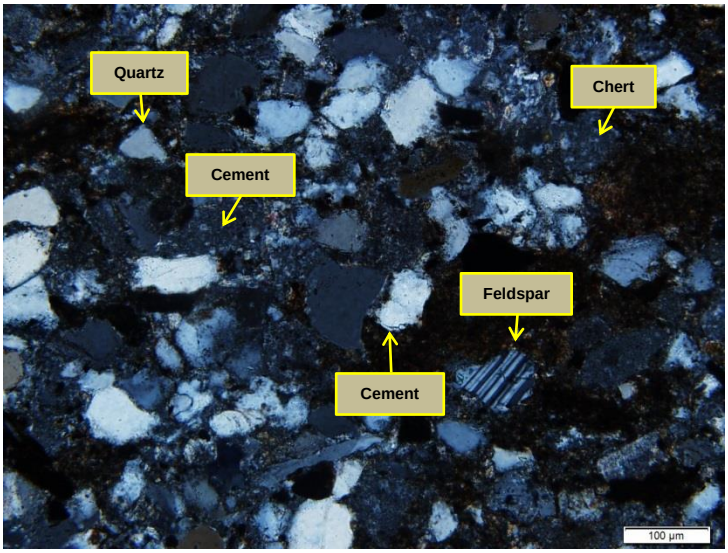


Fig. 4-230: Photomicrograph in XPL showing detail of subrounded (common) to angular (rare) fine silt- to fine sand-sized (average grain size is very fine sand) detrital quartz (40-50%), chert (8-12%), and feldspar (1-3%) observed in a sand-dominated patch (same field of view as shown in Figure 4-229). Quartz overgrowths and pore-filling chert cements are commonly observed in the sandy patches. Note polysynthetic twinning associated with feldspar (albite).

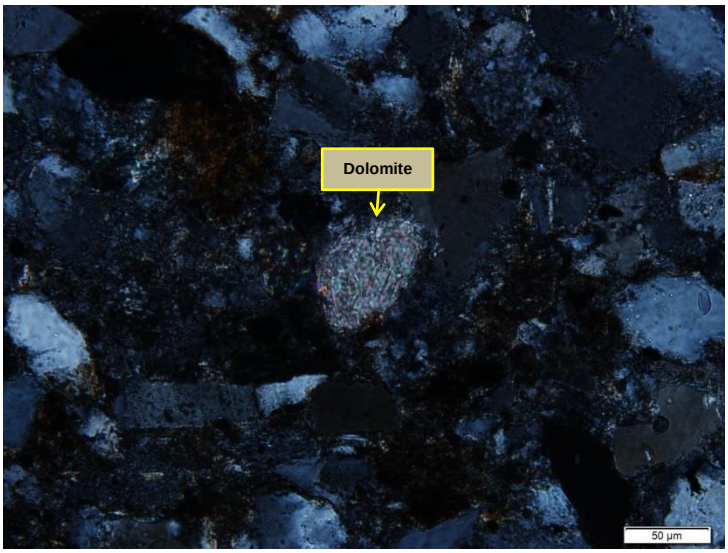


Fig. 4-231: Photomicrograph in XPL illustrating a rare, degraded secondary dolomite crystal. XRD analysis indicates that dolomite comprises <1% of the sample.

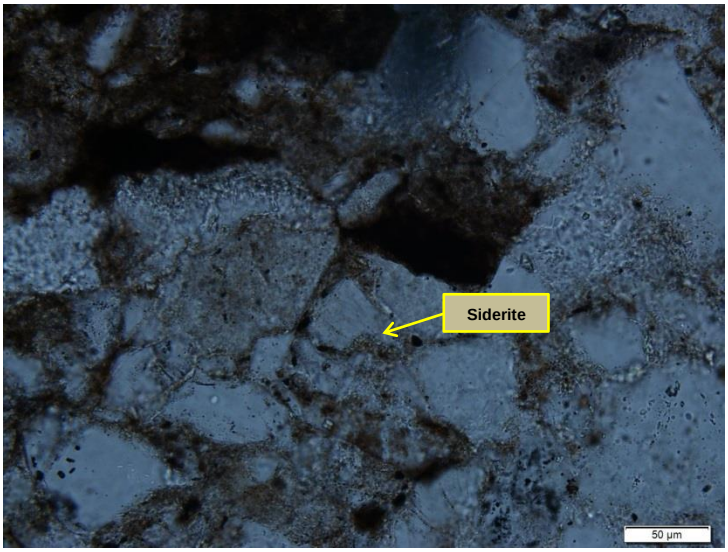


Fig. 4-232: Photomicrograph in PPL showing minor siderite cement. XRD analysis indicates that siderite comprises 0.4% of the rock. Note clay minerals forming rims or drapes.

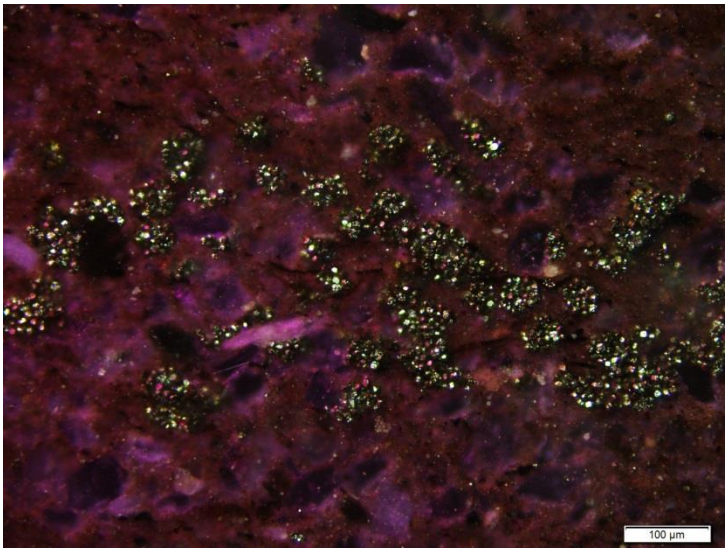


Fig. 4-233: Photomicrograph in reflected light showing framboidal pyrite (gold colour) observed in a clay-dominated patch of the sample. Pyrite comprises ~2% of the rock.

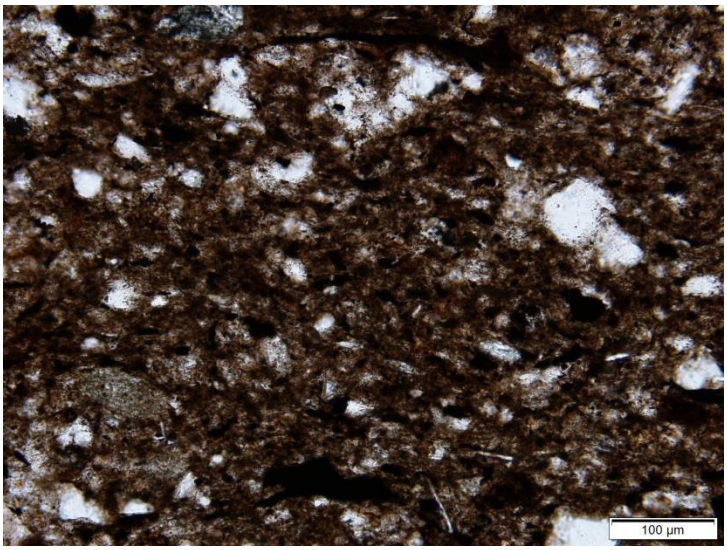


Fig. 4-234: Photomicrograph in PPL detailing a clay-rich patch observed in the sample. The patch contains finely disseminated (also occasional streaks and pockets) pyrite and organic matter, mica lathes and embedded clay- to very fine sand-sized quartz/chert grains.

4.2.23 SAMPLE 13441

Sample ID	**13441**		
Sample type	**Core**	**UWI/Well**	**100/16-03-052-13W5/0**
Strat. Unit	**Cardium Formation**	**Depth**	**0 1742.23 m**

XRD/SRA results

Quartz (%)	Fsp (%)	Cb (%)	Clays (%)	Pyrite (%)
69.3	4.2	0.3 (Siderite)	25.3	1

Composition (*in order of abundance*)

Grain size	%	Variety (%)	Variety (%)	Variety (%)	Variety (%)
sand	50	Quartz/chert (95)	Feldspar (4)	Mica (1)	
silt	20	Quartz/chert (96)	Mica (4)		
clay	20	Clay mins (100)			
Cement	2	Quartz (100)			
Bioclasts	0				
Organics	6	Amorphous (100)			
Opaques	2	Pyrite (100)			
	100				

*Intensively altered to clay minerals

^ Including bitumen

Sedimentary structures

Primary	Faint laminae and clay-rich interbeds.
Biogenic	Possible *Planolites* burrows. Clay-rich interbeds appear heavily bioturbated.

Fractures	Occasional thin (10-30 μm thickness) epoxy-filled fractures. Likely artificial.
Porosity	5-8% intergranular porosity is observed in the uppermost, sandy layer of the sample, and in apparent burrow structures.

Description

Bioturbated muddy sandstone consisting of subangular (common) to subrounded (rare) very fine silt- to fine sand-sized (average grain size is very fine sand) detrital quartz/chert (65-75%), feldspar (2-5%), and mica (<3%). Quartz overgrowth cements are observed in porous sandy layers and burrow structures, both of which have 5-8% intergranular porosity.

Thin Section Quality

Good. Minor exposed thin section glass.

Rock Classification

Muddy sandstone.

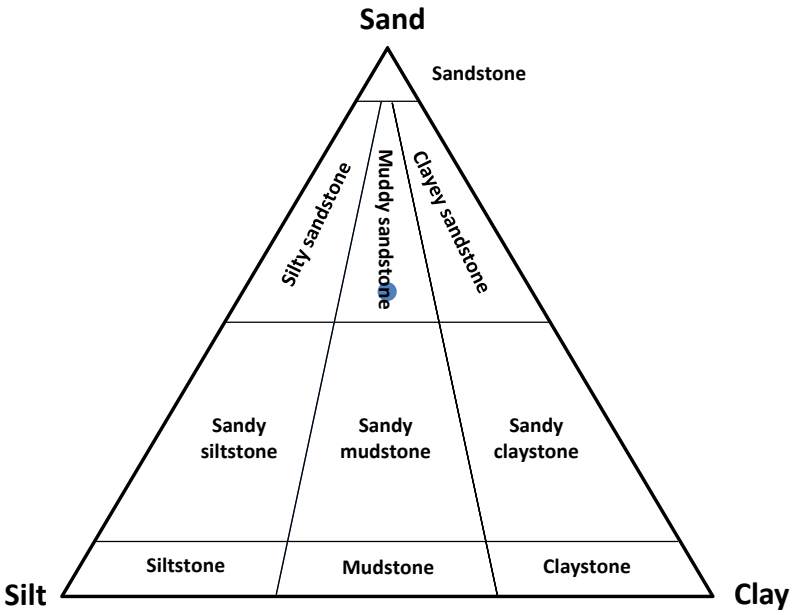


Fig. 4-235: Ternary plot showing relative abundance of different grain sizes within the clastic rock (after Folk 1954). Sample 13441 is classified as a muddy sandstone.

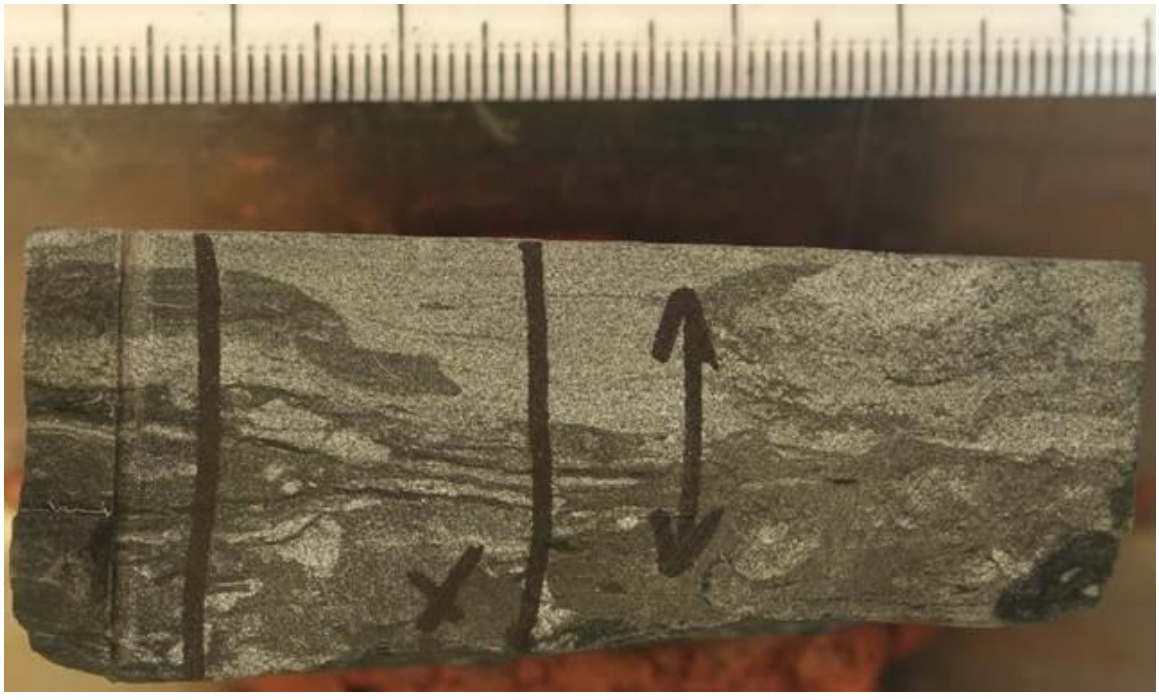


Fig. 4-236: Core photograph of sample 13441 from the Cardium Formation, well 100/16-03-052-13W5/00 (depth 1742.23 m). The thin section prepared for this sample was cut from the area marked with an X. The sample was received without a way-up orientation. Scale is in mm.

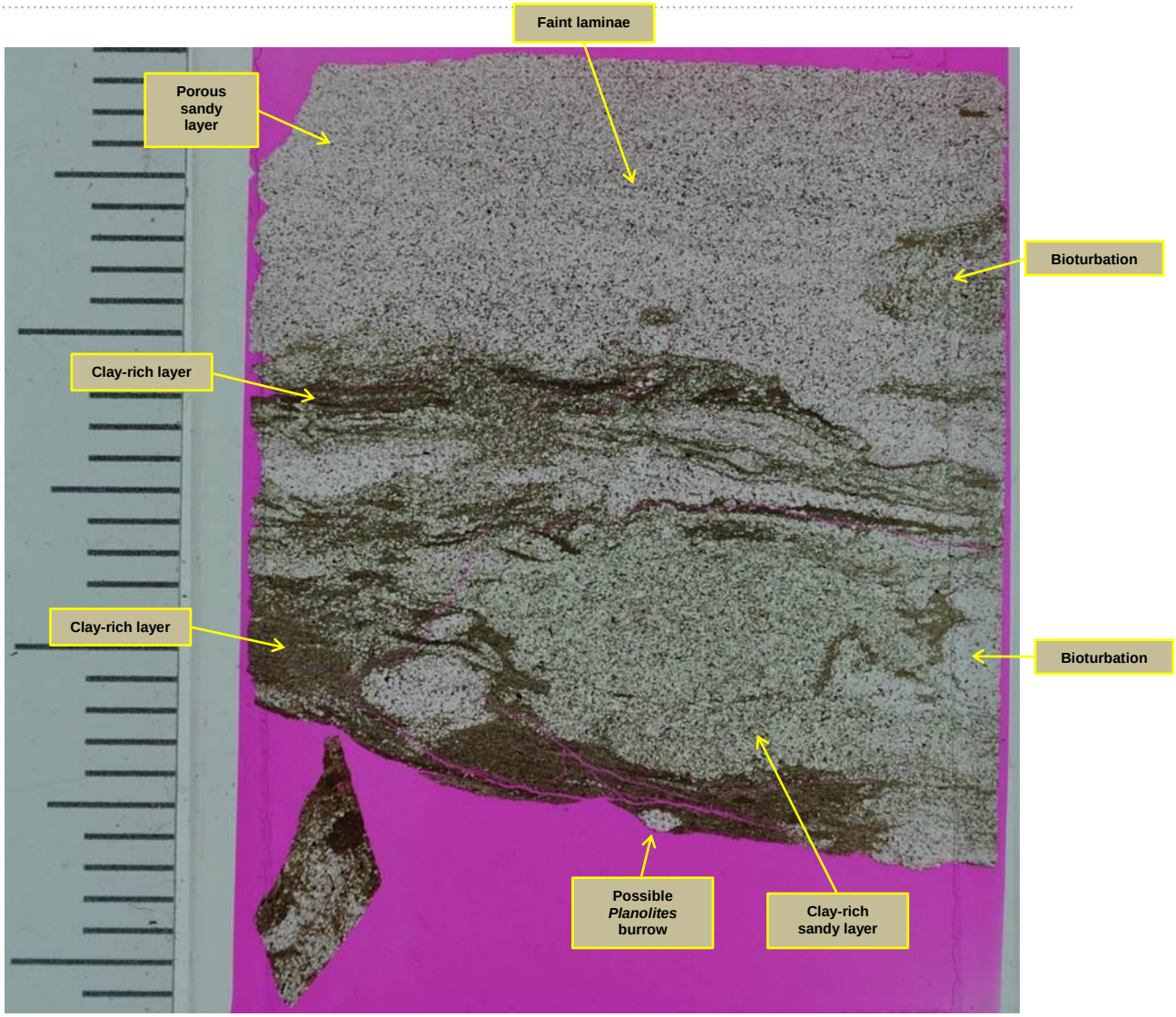


Fig. 4-237: Thin section photograph of sample 13441 from the Cardium Formation, well 100/16-03-052-13W5/00 (depth 1742.23 m). The sample is a heavily bioturbated muddy sandstone with clay-rich (dark brown) interbeds. Light-coloured areas contain abundant very fine silt- to fine sand-sized detrital quartz grains. Some subtle laminae are observed in the top, sandy layer. The depositional way up was not indicated on this sample, and may differ from the orientation shown in the above image. Scale is in mm.

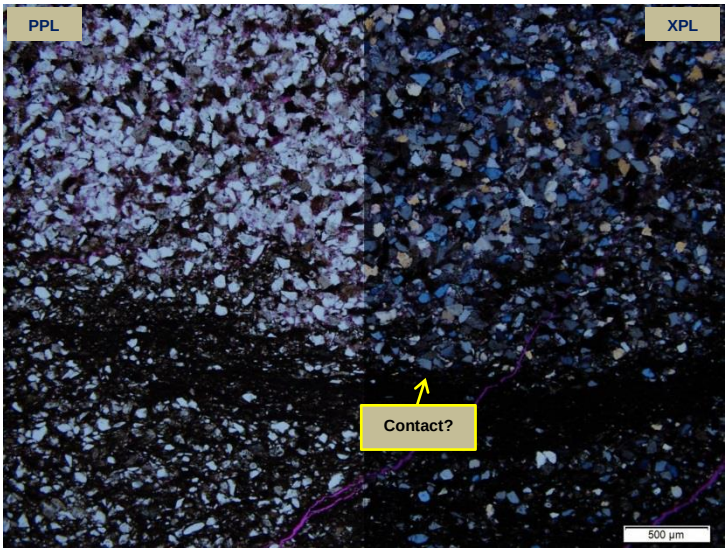


Fig. 4-238: Photomicrograph in PPL (left) and XPL (right) showing an overview of the sample, classified as a muddy sandstone. Light-coloured minerals consist of quartz, chert, feldspar and mica with the darker patches or layers consisting mostly of clays. The contacts between the sandy layers and interbedded clay-rich horizons are diffuse (due to mixing and bioturbation?).

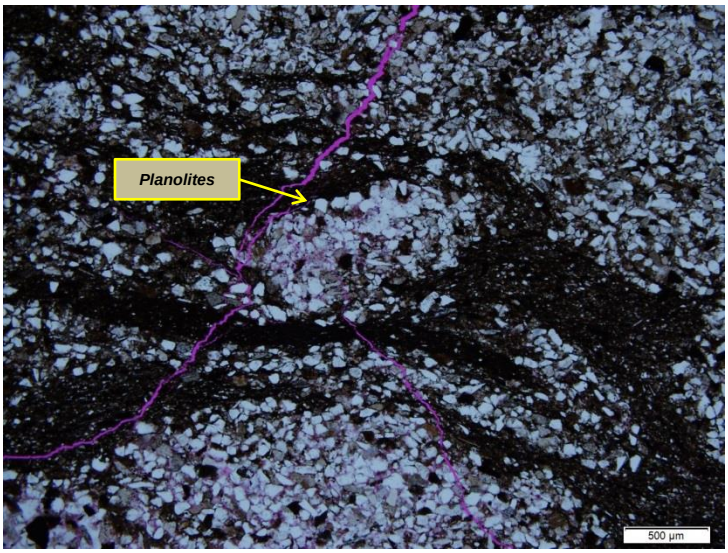


Fig. 4-239: Photomicrograph in PPL showing an overview from the bottom half of the thin section, illustrating bioturbated, clay-rich layers. The clay-rich layers present in this image enclose a possible *Planolites* burrow, as well as many indistinct bioturbation features. Note artificial fractures (pink epoxy).

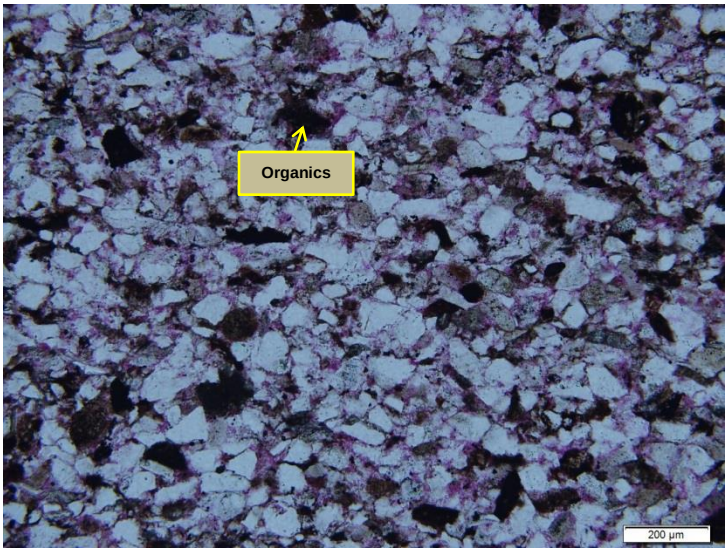


Fig. 4-240: Photomicrograph in PPL illustrating the porous sandy layer from the top half of the sample. Intergranular porosity, which is infilled with pink epoxy, is estimated at ~5-8% in this layer. Solid amorphous organic matter (opaque) comprises ~6% of the total sample composition.

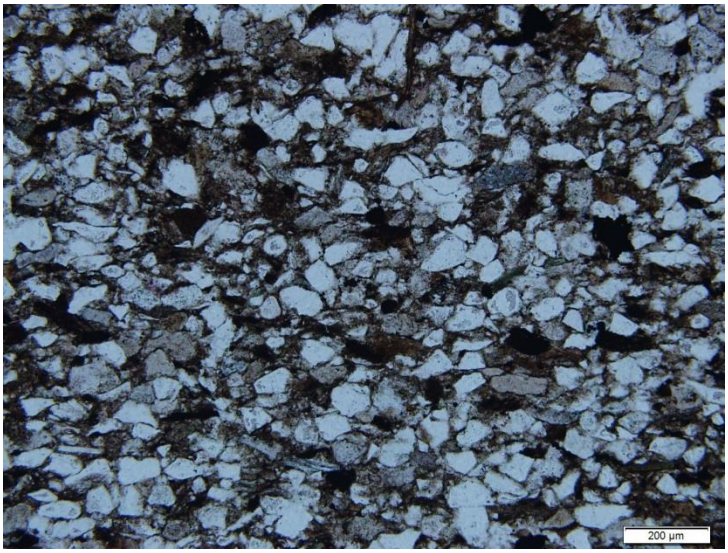


Fig. 4-241: Photomicrograph in PPL showing the clay-rich sandy layer observed near the base of the sandstone. The mineralogical composition of this layer is similar to the horizon shown in Figure 4-240, but elevated clay content has significantly reduced porosity.

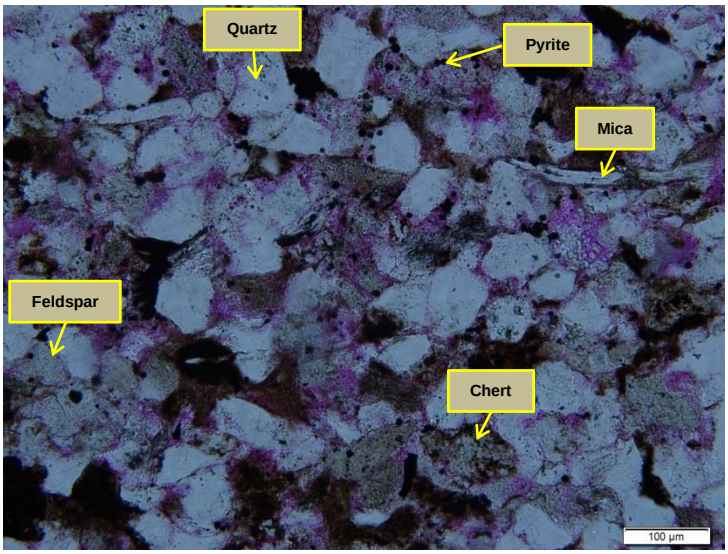


Fig. 4-242: Photomicrograph in PPL detailing the porous sandy layer shown in Figure 4-240. This layer contains subangular (common) to subrounded (rare) very fine silt- to fine sand-sized (average grain size is very fine sand) detrital quartz/chert (65-75%), feldspar (2-5%), and mica (<3%). Note finely disseminated pyrite idiomorphs (opaque).

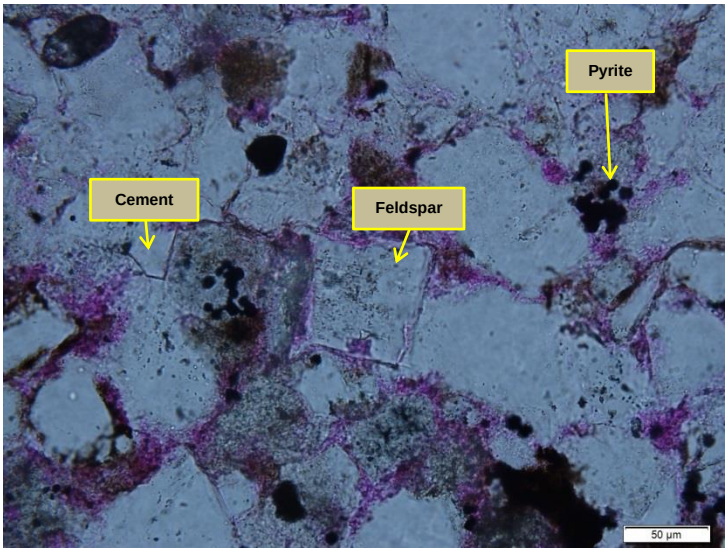


Fig. 4-243: Photomicrograph in PPL illustrating quartz overgrowth cements observed in the porous sandy layer. These cements have reduced pore size and connectivity. Some interstitial clays are also observed. Pyrite is present within pore spaces as well as embedded within some grains.

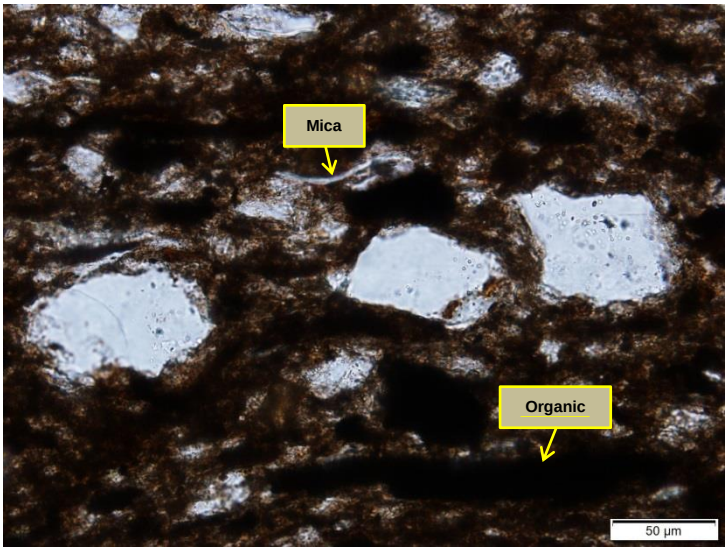


Fig. 4-244: Photomicrograph in PPL detailing the clay-rich layer, which contains numerous organic flakes, short streaks and pockets. Clay- to very fine sand-sized quartz and chert are embedded within the clay-rich matrix. Note a bent mica lathe near the center of the image.

4.2.24 SAMPLE 13442

Sample ID	**13442**		
Sample type	**Core**	**UWI/Well**	**100/16-03-052-13W5/0**
Strat. Unit	**Cardium Formation**	**Depth**	**0 1743.24 m**

XRD/SRA results

Quartz (%)	Fsp (%)	Cb (%)	Clays (%)	Pyrite (%)
69.6	2.2	0.3 (Siderite)	27.5	0.6

Composition (*in order of abundance*)

Grain size	%	Variety (%)	Variety (%)	Variety (%)	Variety (%)
sand	49	Quartz/chert (95)	Feldspar (4)	Mica (1)	
silt	20	Quartz/chert (98)	Mica (2)		
clay	25	Clay mins (100)			
Cement	<1	Quartz (100)			
Bioclasts	0				
Organics	5	Amorphous			
Opaques	1	Pyrite (100)			
	100				

*Intensively altered to clay minerals

^ Including bitumen

Sedimentary structures

Primary	Faint laminae and possible clay-rich interbedding visible.
Biogenic	Possible bioturbation features apparent. No distinctive burrow structures.

Fractures	Occasional thin (4-60 μm thickness) epoxy-filled fractures. Likely artificial.
Porosity	~5% intergranular porosity observed in the main sandy layer of the rock.

Description

Bioturbated muddy sandstone consisting of subangular (common) to subrounded (rare) very fine silt- to fine sand-sized (average grain size is very fine sand) detrital quartz/chert (65-80%), feldspar (4-8%), and mica (1-3%). Most of the rock shows ~5% intergranular porosity, with the exception of non-porous clay-rich features (possibly bioturbated interbeds) present near the base and top of the sample.

Thin Section Quality

Moderate. Exposed thin section glass is visible throughout the sample.

Rock Classification

Muddy sandstone.

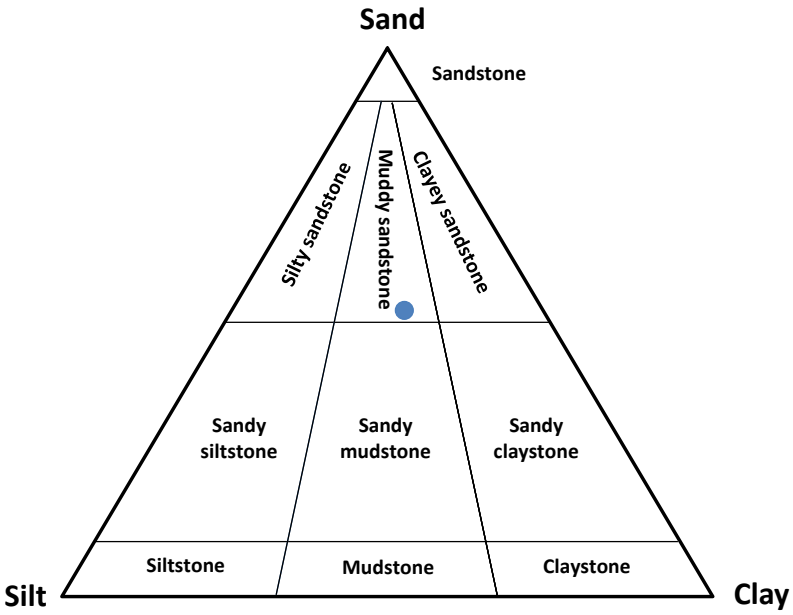


Fig. 4-245: Ternary plot showing the grain size composition of the sample based on the Wentworth scale (after Folk, 1954). Sample 13442 is classified as a muddy sandstone.

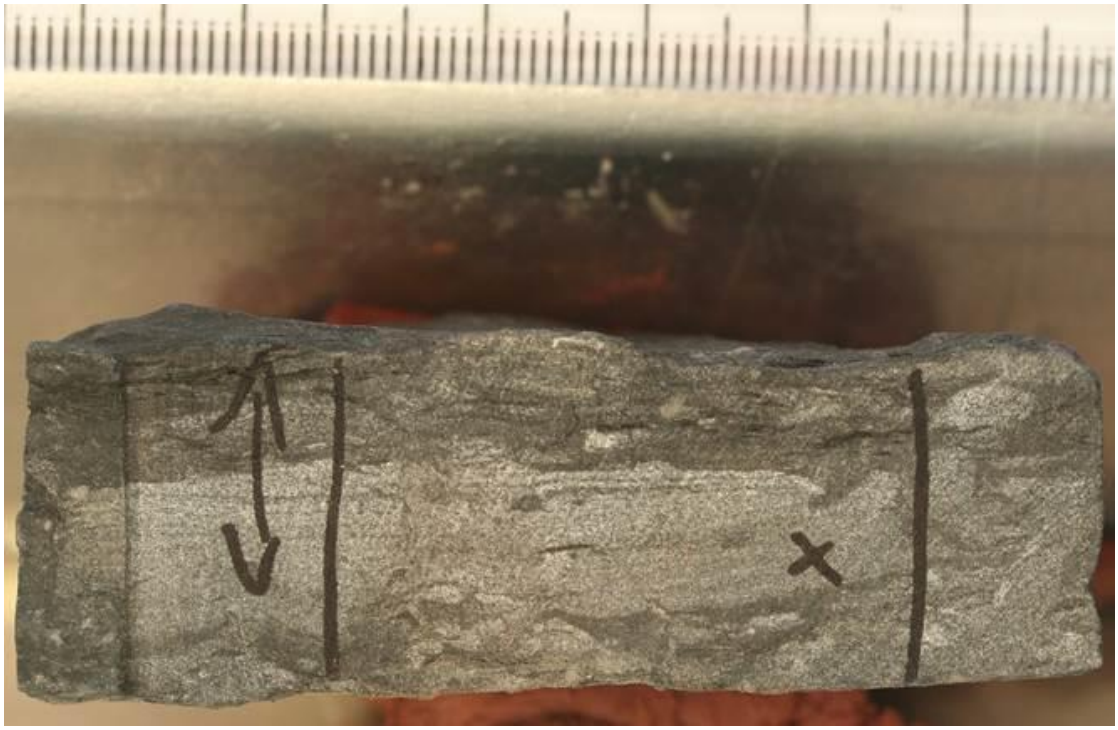


Fig. 4-246: Core photograph of sample 13442 from the Cardium Formation, well 100/16-03-052-13W5/00 (depth 1743.24 m). The thin section prepared from this sample was cut from the area marked with an X. Scale is in mm.

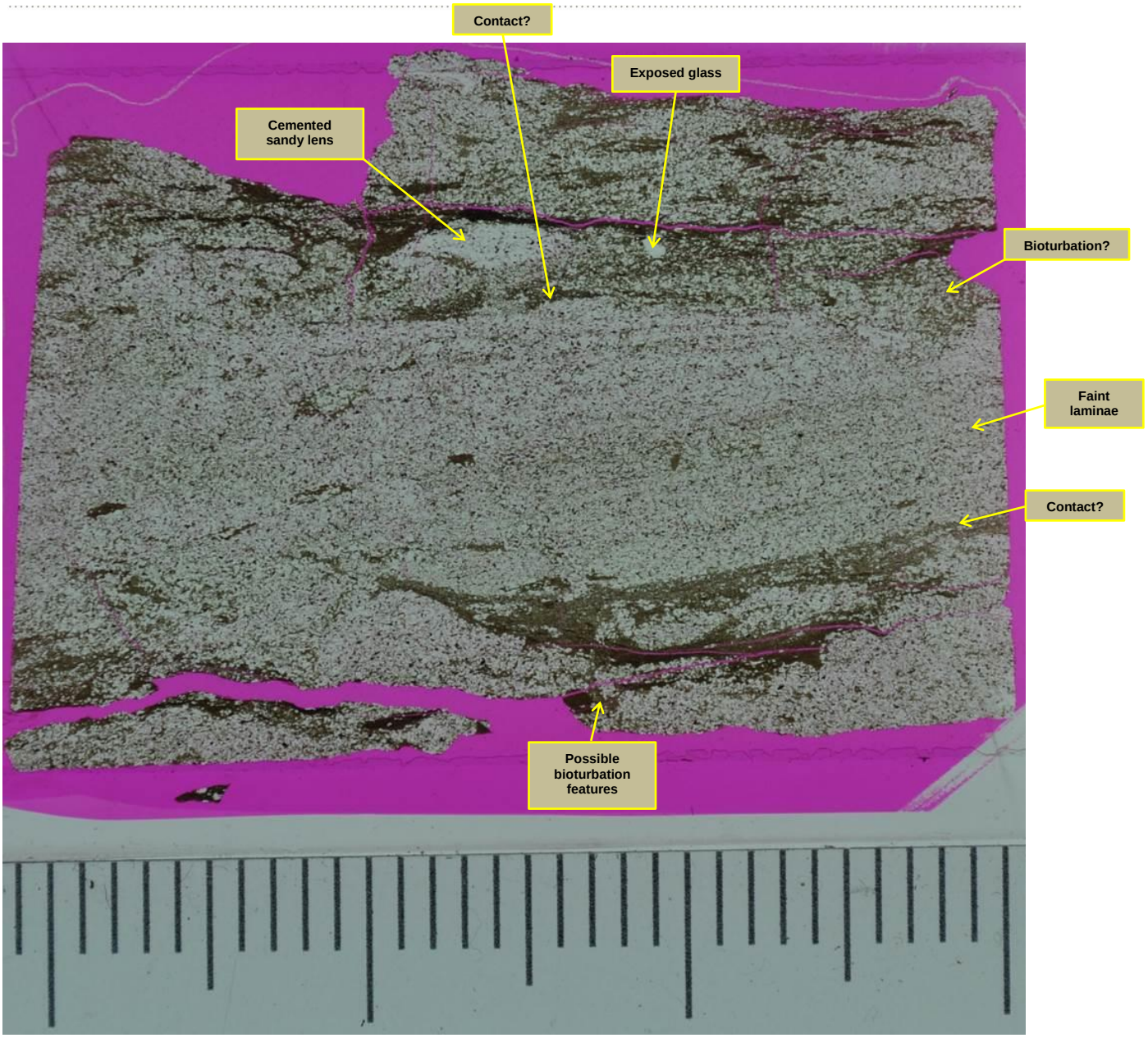


Fig. 4-247: Thin section photograph of sample 13442 from the Cardium Formation, well 100/16-03-052-13W5/00 (depth 1743.24 m). The sample is a bioturbated muddy sandstone, with faint laminae observed in the middle, sandy layer. Clay-rich streaks, lenses and patches are observed and are likely the result of bioturbation. Note that the depositional way up direction was not indicated on this sample, but was interpreted based on sedimentary structures. Scale is in mm.

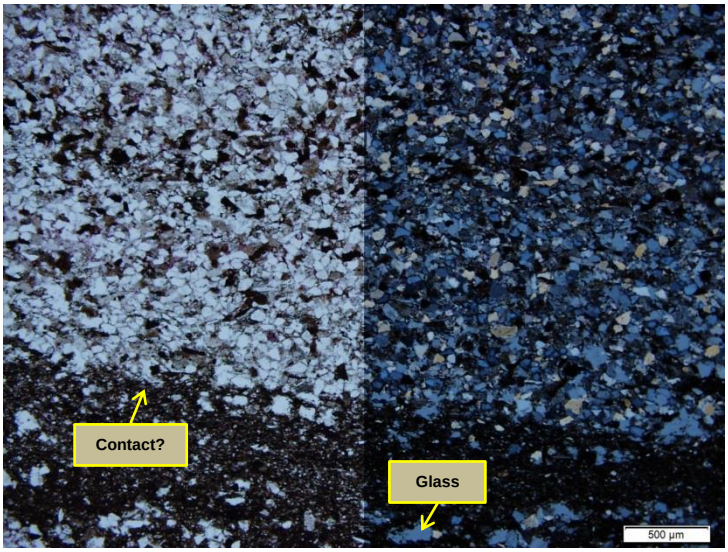


Fig. 4-248: Photomicrograph (left half in PPL, right half in XPL) showing an overview of the muddy sandstone. The sample consists of well-compacted quartz and chert grains (light-coloured) with interbedded clay-rich layers and patches (dark-coloured; see bottom of image).

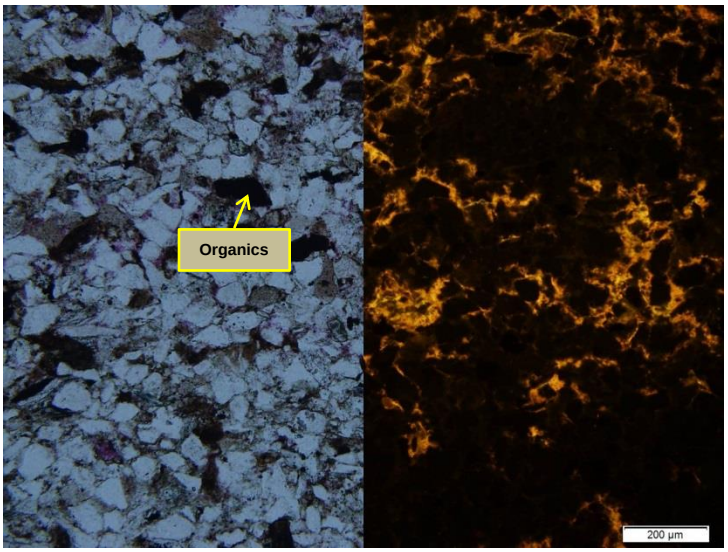


Fig. 4-249: Photomicrograph (left half in PPL, right half in UV light) showing ~5% intergranular porosity (estimated) observed in the main, sandy layer. Most of this layer shows little or no quartz overgrowth cementation. Amorphous organic matter is observed throughout and is estimated at ~5% of the total composition.

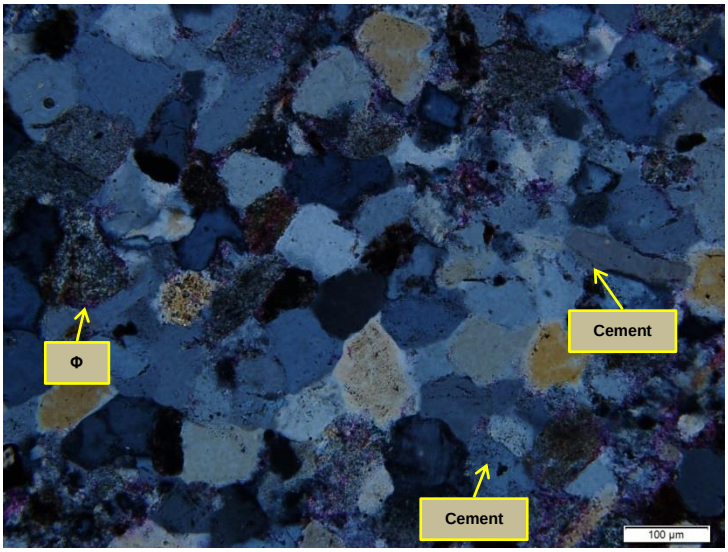


Fig. 4-250: Photomicrograph in XPL showing an isolated cemented sandy lens (see Figure 4-247 for location in the sample). Narrow pores are observed between some grains in this lens, which exhibits much lower porosity and pore connectivity than the main sandy layer.

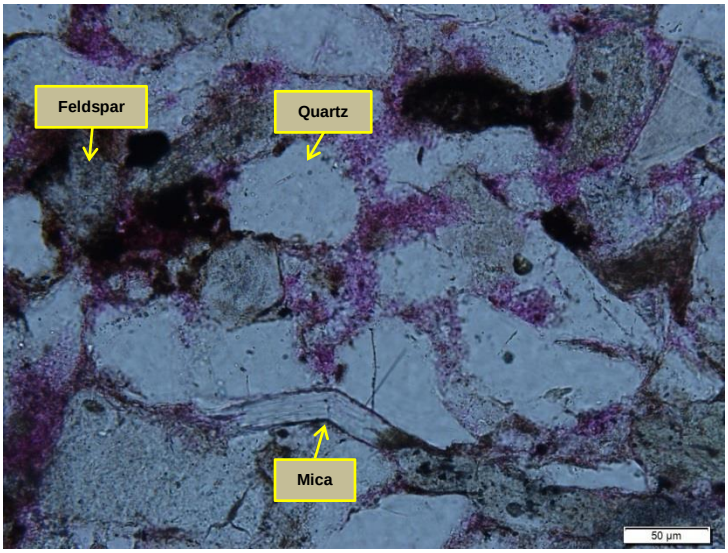


Fig. 4-251: Photomicrograph in PPL detailing subangular (common) to subrounded (rare) very fine silt- to fine sand-sized (average grain size is very fine sand) detrital quartz/chert (65-80%), feldspar (4-8%), and mica (1-3%) observed in the main sandy layer. Note a mica lathe bent due to grain compaction.

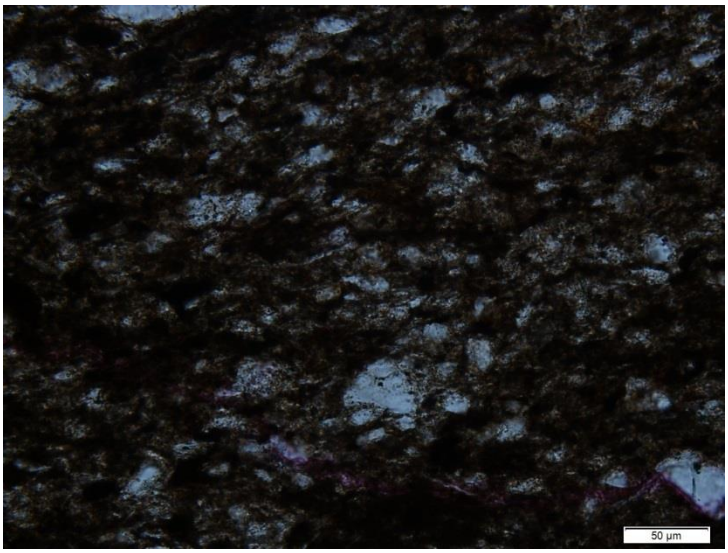


Fig. 4-252: Photomicrograph in PPL detailing clay- to silt-sized quartz observed in the clay-rich patches or layers. The clay-rich sediment contains fewer sand-sized detrital grains, suggesting possible sediment sorting by infaunal organisms or periods of lower depositional energy.

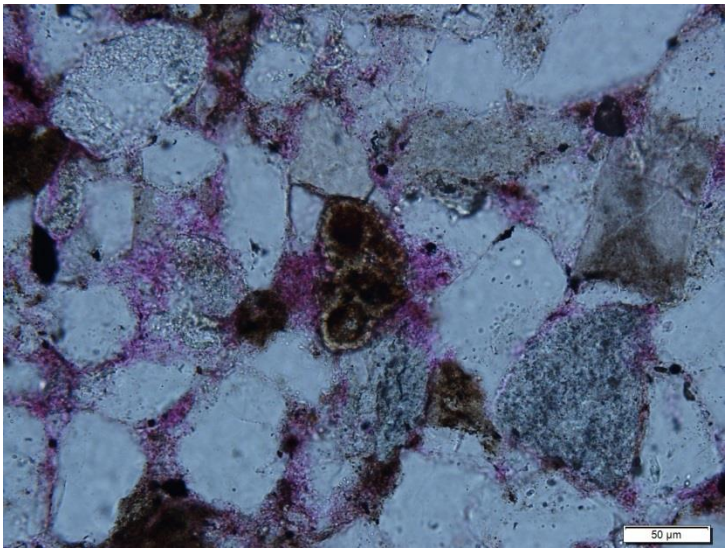


Fig. 4-253: Photomicrograph in PPL showing a rare foraminiferan test. This imperforate test is composed of microcrystalline calcite, and is filled with organic matter. Note intergranular porosity (pink epoxy) with some interstitial clays observed within the open pores between the surrounding fine sand-size grains.

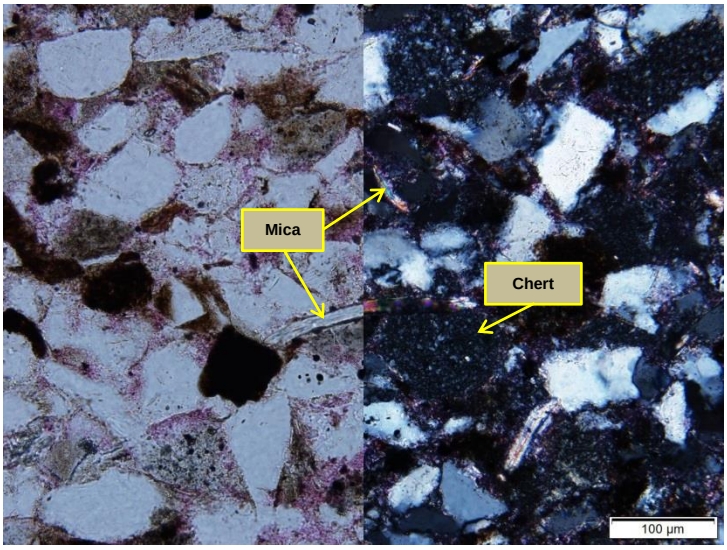


Fig. 4-254: Photomicrograph (left halt in PPL, right half in XPL) detailing medium silt- to very fine sand-sized quartz and chert grains. Chert grains show characteristic microcrystalline textures. Several mica lathes with variable orientations are observed.

4.2.25 SAMPLE 13443

Sample ID	**13443**		
Sample type	**Core**	**UWI/Well**	**100/05-17-049-08W5/00**
Strat. Unit	**Cardium Formation**	**Depth**	**1505.30 m**

XRD/SRA results

Quartz (%)	Fsp (%)	Cb (%)	Clays (%)	Pyrite (%)
63.9	4.5	0	30.6	1

Composition (*in order of abundance*)

Grain size	%	Variety (%)	Variety (%)	Variety (%)	Variety (%)
sand	38	Quartz/chert (92)	Feldspar (5)	Mica (3)	
silt	20	Quartz/chert (98)	Mica (2)		
clay	35	Clay mins (100)			
Cement	<1	Quartz (100)			
Bioclasts	0				
Organics	4	Amorphous (100)			
Opaques	3	Pyrite (100)			
	100				

*Intensively altered to clay minerals

^ Including bitumen

Sedimentary structures

Primary	None visible.
Biogenic	Apparent bioturbation.

Fractures	Occasional thin (5-30 μm thickness) epoxy-filled fractures, and one large (370 μm thickness) parting. Likely artificial.
Porosity	Non-porous. Limited artificial porosity occurs in association with epoxy-filled fractures.

Description

Sandy mudstone comprised of subrounded (common) to subangular (rare) very fine silt- to fine sand sized detrital quartz/chert (40-85%), feldspar (2-8%), and mica (1-6%). The rock is non-porous, although limited artificial porosity is sometimes observed due to epoxy "bleeding" through grain boundaries around fractures.

Thin Section Quality

Poor. Large patches of exposed thin section glass.

Rock Classification

Sandy mudstone.

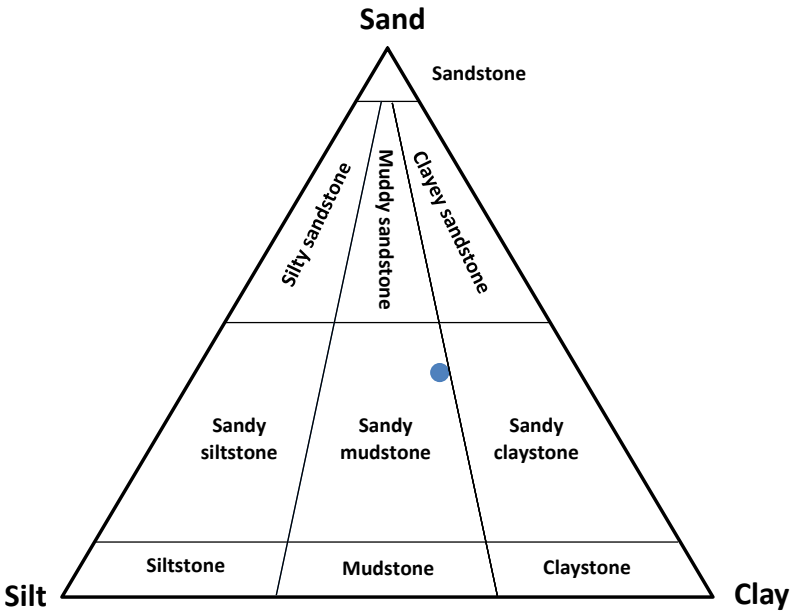


Fig. 4-255: Ternary plot showing the grain size composition of the sample based on the Wentworth scale (after Folk, 1954). Sample 13443 is classified as a sandy mudstone.



Fig. 4-256: Core photograph of sample 13443 from the Cardium Formation, well 100/05-17-049-08W5/00 (depth 1505.30 m). The thin section prepared for this sample was cut from the area marked with an X. Depositional up direction is indicated by the arrow (right). Scale is in mm.

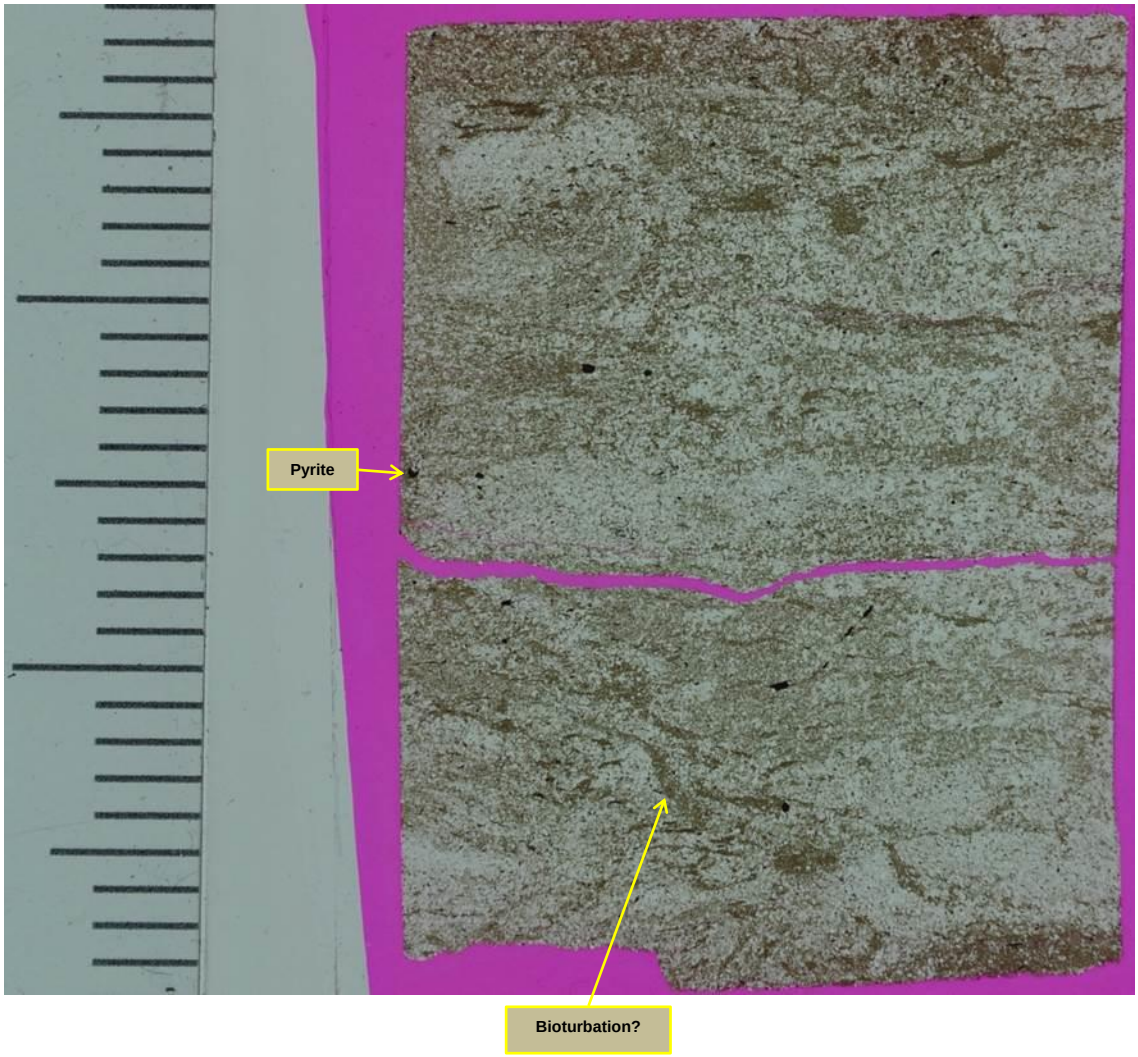


Fig. 4-257: Thin section photograph of sample 13443 from the Cardium Formation, well 100/05-17-049-08W5/00 (depth 1505.30 m). The sample is a sandy mudstone that lacks primary sedimentary structures (possibly indicating pervasive bioturbation?). Dark-coloured patches, lenses and wisps consisting of clay material are interspersed between light-coloured areas, which contain very fine silt- to fine sand-sized detrital quartz grains. Portions of the sample show abundant exposed thin section glass, which suggests the presence of water-sensitive clays (removed during sample cutting and polishing). Scale is in mm.

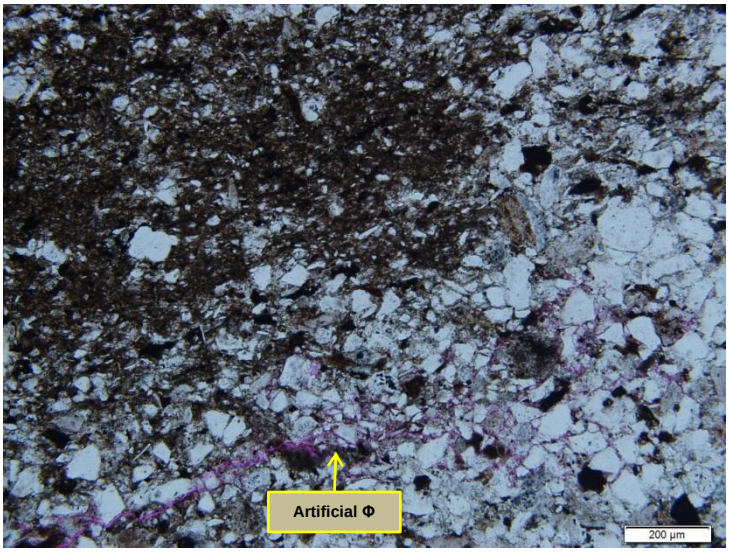


Fig. 4-258: Photomicrograph in PPL showing an overview of the sandy mudstone. The sample lacks primary sedimentary features, and consists of largely amorphous clay-rich and sandy patches, possibly indicating pervasive bioturbation. Although the sample is non-porous, artificial porosity is observed where epoxy has "bled" through grain boundaries in association with fractures. Lighter patches consist of quartz, chert, mica and feldspar with the darker patches consisting mostly of clays and opaque material.

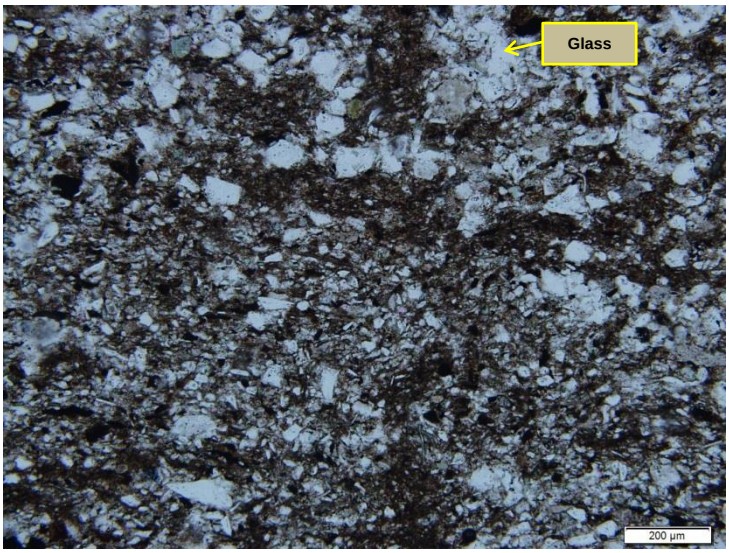


Fig. 4-259: Photomicrograph in PPL showing a patch with elevated clay material. Silt-sized grains predominantly occur within the clay-rich patches, possibly indicating sediment sorting by burrowing organisms. Exposed thin section glass is common within this sample, indicating removal of material (water sensitive clays?) during cutting and polishing.

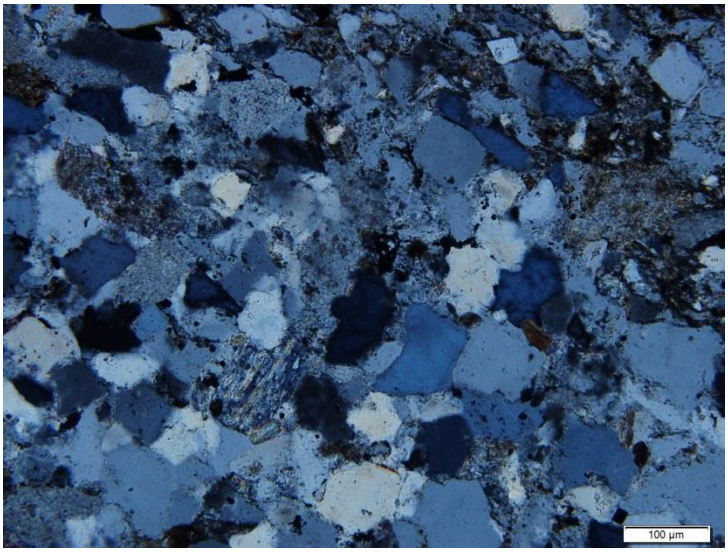


Fig. 4-260: Photomicrograph in XPL showing a sandy patch observed in the sample. An absence of dust rims in the constituent detrital quartz grains makes identification of cements difficult. Several "dirty" grains are likely feldspar.

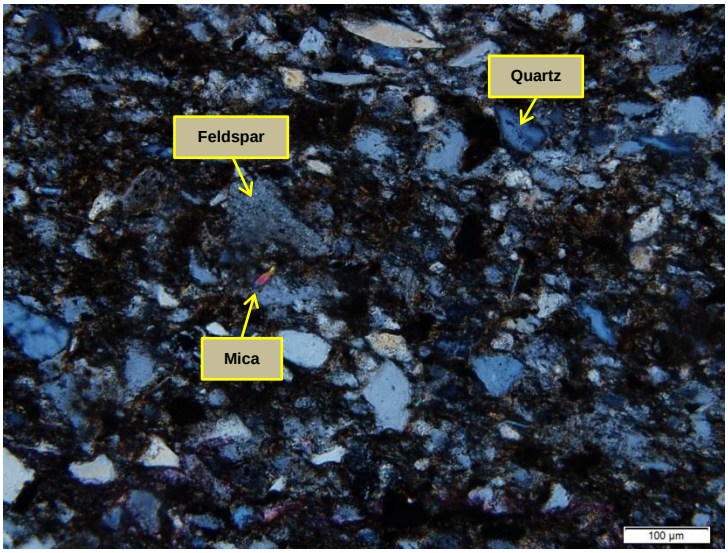


Fig. 4-261: Photomicrograph in XPL showing subangular to subrounded, very fine silt- to fine sand-sized detrital quartz/chert (40-85%), feldspar (2-8%), and mica (1-6%) set within a clay-rich matrix.

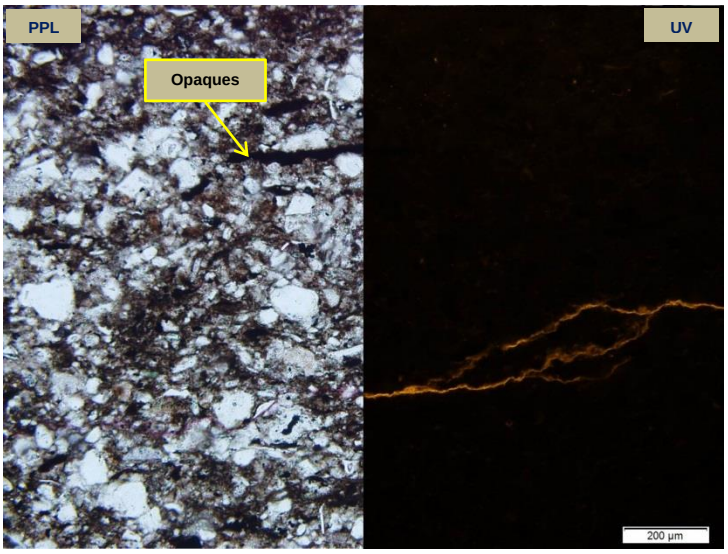


Fig. 4-262: Photomicrograph in PPL (left) and UV (right) showing thin micro-fractures present in the sample. These fractures may have been enhanced during sample preparation. Note short, opaque streaks or “trails”.

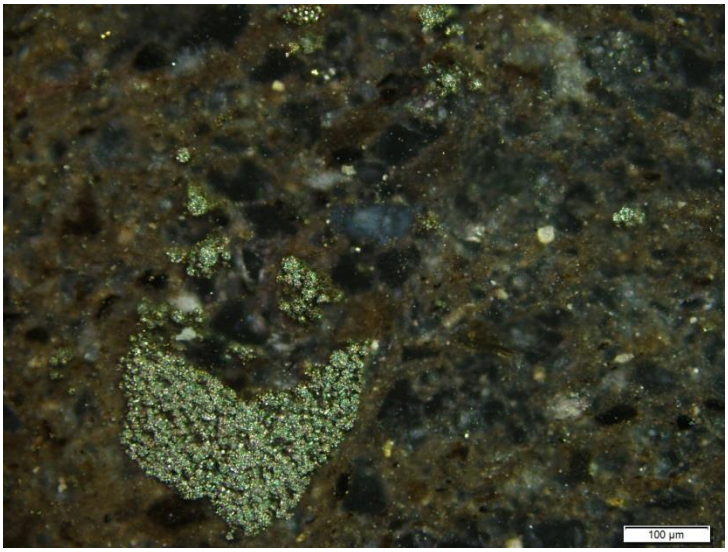


Fig. 4-263: Photomicrograph in reflected light showing disseminated framboidal and idiomorphic pyrite, which occasionally forms clusters. Pyrite accounts for ~3% of the sample.

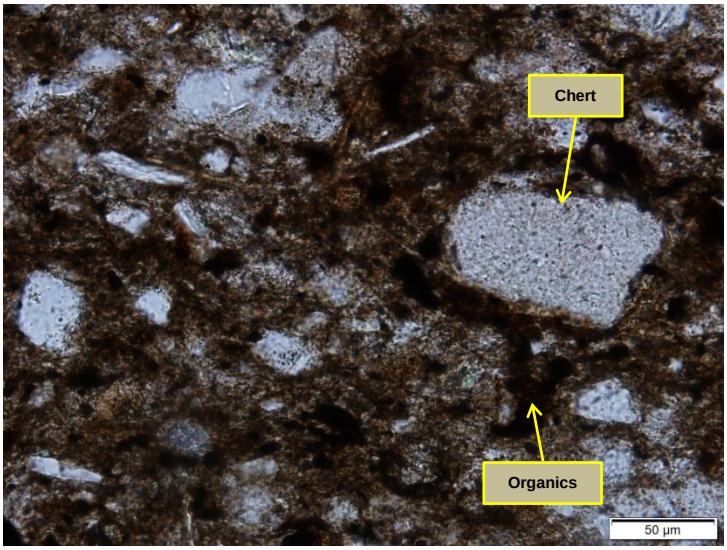


Fig. 4-264: Photomicrograph in PPL detailing a clay-rich portion of the sample, which contains clay- to sand-size quartz, chert and mica grains embedded within the clay matrix. Organic matter is associated with the clay material and is also observed rimming some grains.

4.2.26 SAMPLE 13446

Sample ID	**13446**		
Sample type	**Core**	**UWI/Well**	**100/05-17-049-08W5/00**
Strat. Unit	**Cardium Formation**	**Depth**	**1514.67 m**

XRD/SRA results

Quartz (%)	Fsp (%)	Cb (%)	Clays (%)	Pyrite (%)
73.4	3.6	0	22.3	0.6

Composition (*in order of abundance*)

Grain size	%	Variety (%)	Variety (%)	Variety (%)	Variety (%)
sand	60	Quartz/chert (95)	Feldspar (3)	Mica (2)	
silt	20	Quartz/chert (100)			
clay	14	Clay mins (100)			
Cement	0				
Bioclasts	0				
Organics	2	Amorphous (100)			
Opaques	4	Pyrite (100)			
	100				

*Intensively altered to clay minerals

^ Including bitumen

Sedimentary structures

Primary	Clay-rich patches and streaks may be depositional features.
Biogenic	Possible *Palaeophycus* and *Skolithos* burrows.

Fractures	Occasional thin (20-100 μm thickness) epoxy-filled fractures. Likely artificial.
Porosity	Variable and discontinuous. Some clay-rich patches are non-porous, whereas burrow structures and clay-poor areas show up to 10% intergranular porosity.

Description

Bioturbated muddy sandstone comprised of subrounded (common) to subangular (rare) fine silt- to fine sand-sized (average grain size is very fine sand) detrital quartz/chert (70-80%), feldspar (2-4%), and mica (< 3%). Porosity is variable and discontinuous in the sandstone, with burrow structures and clay-poor areas of the sample having up to 10% intergranular porosity, and sections of the rock with more interstitial clay being non-porous.

Thin Section Quality

Good. Occasional fractures and exposed glass.

Rock Classification

Muddy sandstone.

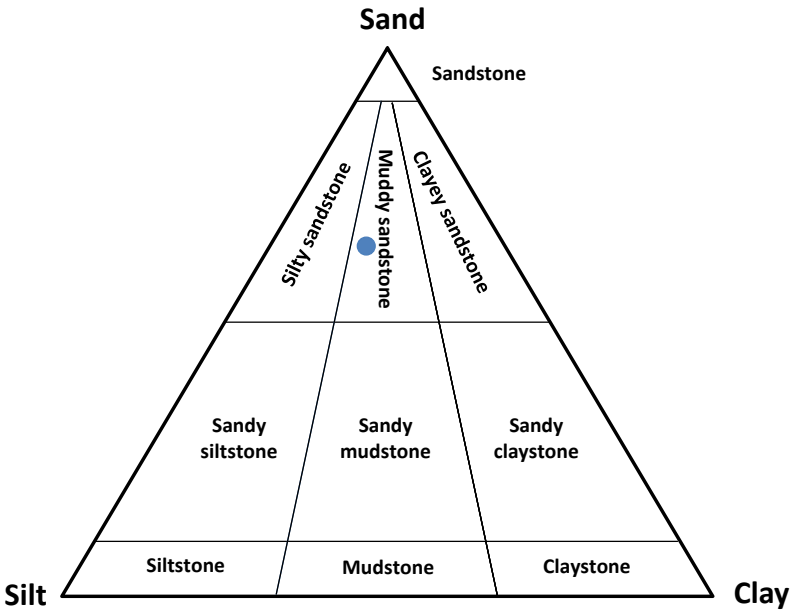


Fig. 4-265: Ternary plot showing the grain size composition of the sample based on the Wentworth scale (after Folk, 1954). Sample 13446 is classified as a muddy sandstone.



Fig. 4-266: Core photograph of sample 13446 from the Cardium Formation, well 100/05-17-049-08W5/00 (depth 1514.67 m). The thin section prepared from this sample was cut from the area marked with an X. Up-direction was not indicated. Scale is in mm.

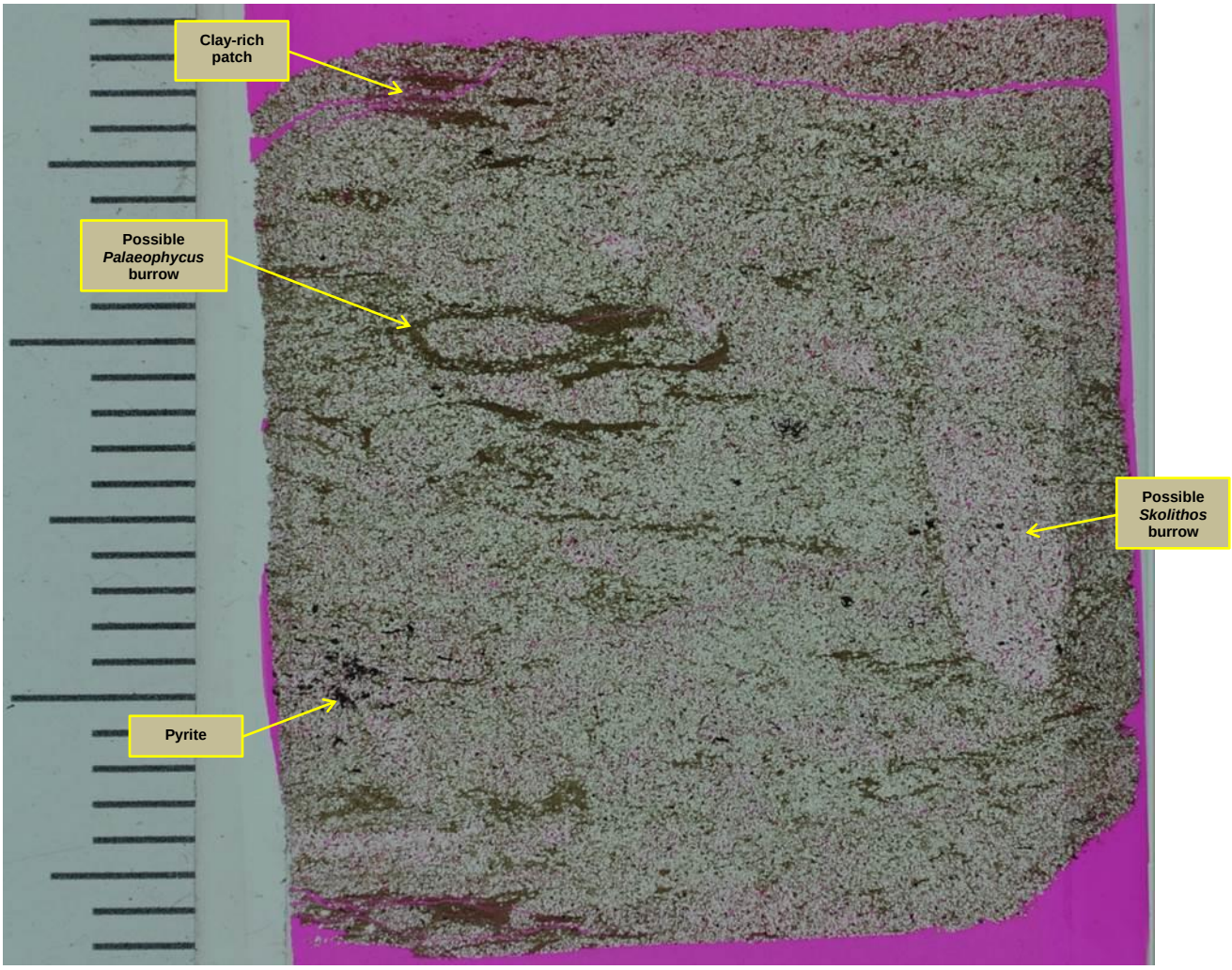


Fig. 4-267: Thin section photograph of sample 13446 from the Cardium Formation, well 100/05-17-049-08W5/00 (depth 1514.67 m). The sample is a bioturbated muddy sandstone with numerous clay-rich patches, wisps and streaks observed, which likely represent depositional and bioturbation features. At least two different bioturbation features are observed in the sample, including a possible* Palaeophycus *burrow (circular/ovate burrow lined with clay and infilled with sediments undifferentiated from the surrounding rock), and a* Skolithos *burrow (vertical burrow with structureless infill). The* Skolithos *burrow was used for orientation of the thin section. Scale is in mm.

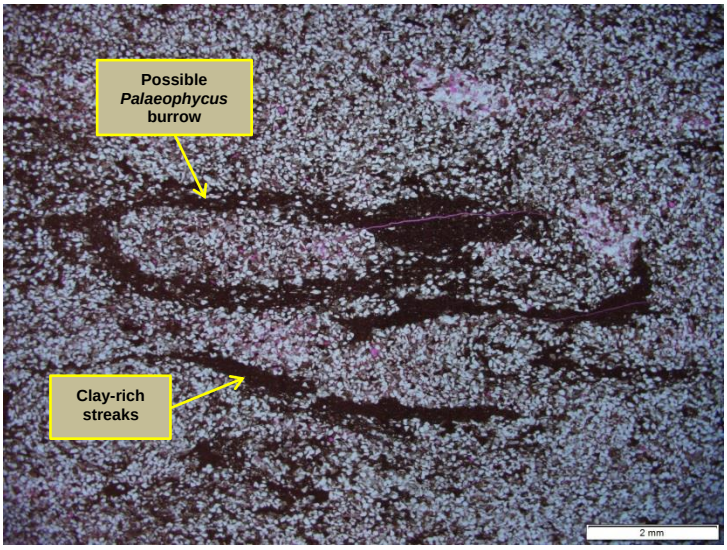


Fig. 4-268: Photomicrograph in PPL showing an overview of the heavily mixed (bioturbated) muddy sandstone. The sample lacks recognizable bedding planes or laminae. Light-coloured minerals consisit of quartz, chert, feldspar and mica with the darker patches and wisps composed mostly of clays and organics.

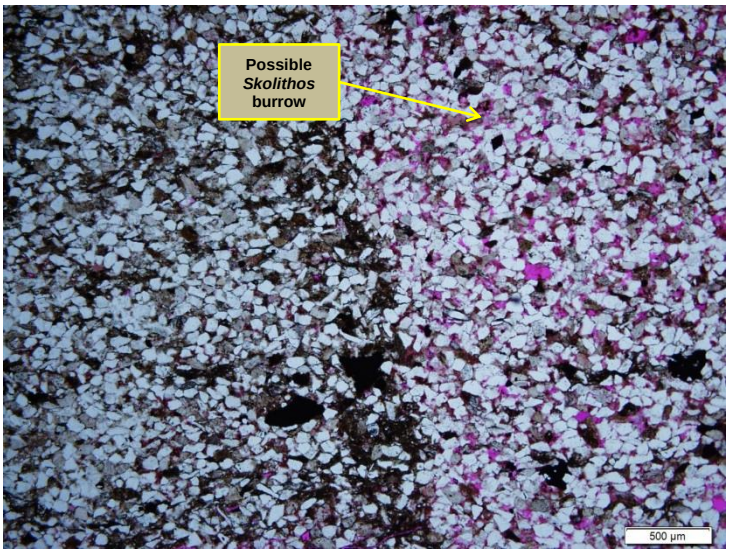


Fig. 4-269: Photomicrograph in PPL showing part of the possible *Skolithos* burrow (see Figure 4-267) in contact with the surrounding sediment. The burrow infill has much higher intergranular porosity (pink epoxy) than the adjacent sediment, in which clays/organics occupy the space between grains.

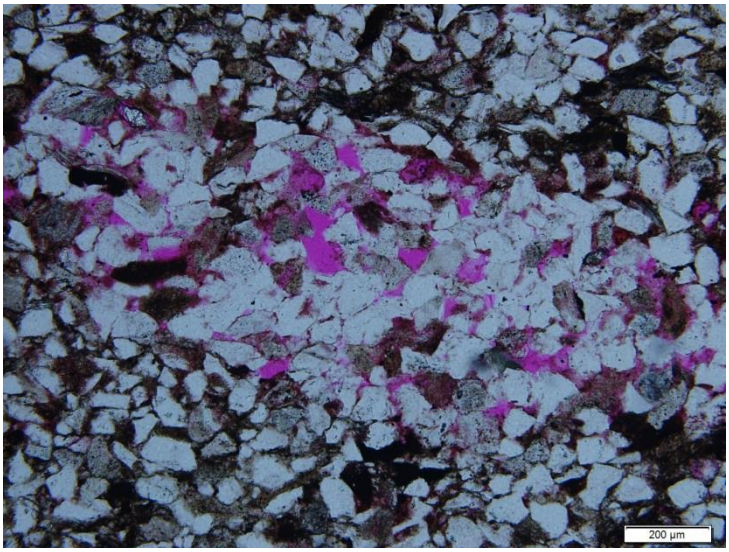


Fig. 4-270: Photomicrograph in PPL detailing patchy porosity (pink epoxy), likely associated with bioturbation. Intergranular porosity in the sample is estimated at ~8-10%.

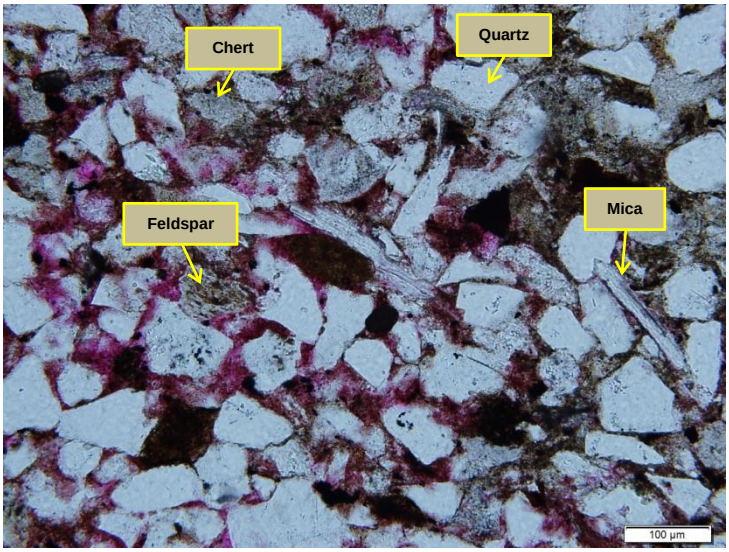


Fig. 4-271: Photomicrograph in PPL detailing subrounded (common) to subangular (rare) fine silt- to fine sand-sized (average grain size is very fine sand) detrital quartz/chert (70-80%), feldspar (2-4%), and mica (<3%). Mica lathes are up to ~120 µm in size.



Fig. 4-272: Photomicrograph in PPL showing a degraded mica lathe observed in a porous section of the sample. Low to moderate levels of sediment compaction during burial (indicated by common undeformed micas) may have helped to preserve porosity. Note clay material between the detrital grains.

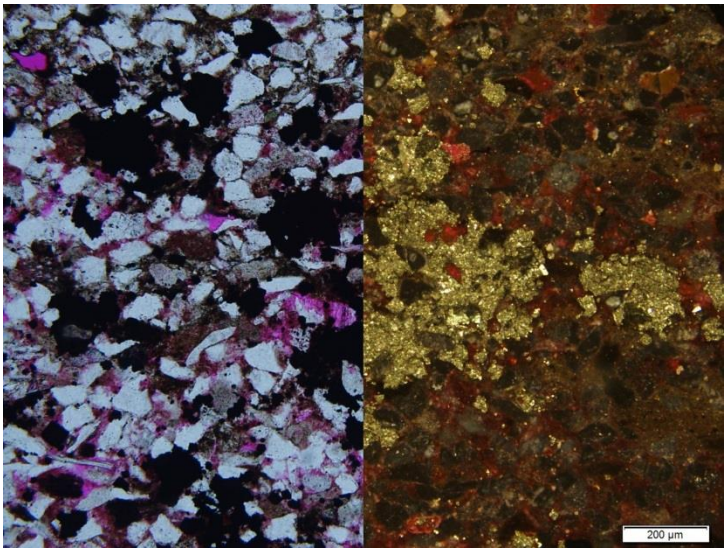


Fig. 4-273: Photomicrograph (left half in PPL, right half in reflected light) showing a rare patch of pore-filling and disseminated pyrite (opaque in PPL, gold in reflected light) observed in the sample. Pyrite accounts for ~4% of the total composition.

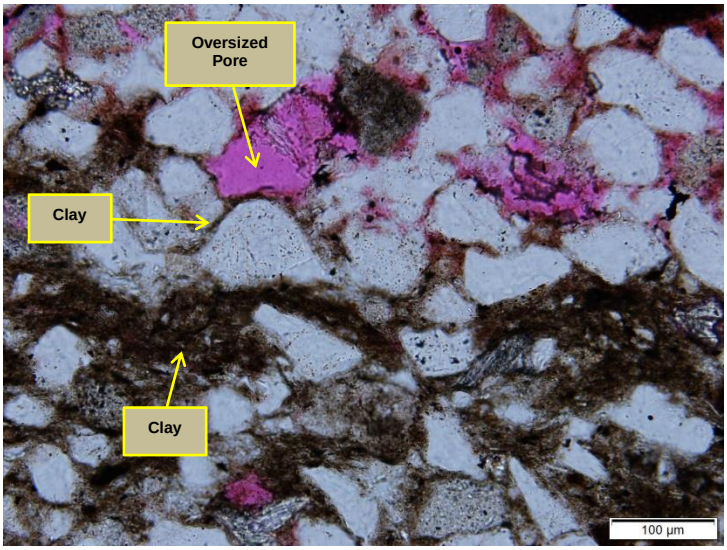


Fig. 4-274: Photomicrograph in PPL illustrating organic- and clay-rich streaks. The top half of the image shows an oversized pore that is likely the result of grain dissolution. Clays are also observed lining pore spaces.

4.2.27 SAMPLE 13448

Sample ID	**13448**		
Sample type	**Core**	**UWI/Well**	**100/05-17-049-08W5/00**
Strat. Unit	**Cardium Formation**	**Depth**	**1521.54 m**

XRD/SRA results

Quartz (%)	Fsp (%)	Cb (%)	Clays (%)	Pyrite (%)
72.9	3.6	0	23.2	0.1

Composition (*in order of abundance*)

Grain size	%	Variety (%)	Variety (%)	Variety (%)	Variety (%)
sand	65	Quartz/chert (95)	Feldspar (3)	Mica (2)	
silt	12	Quartz/chert (100)			
clay	20	Clay mins (100)			
Cement	0				
Bioclasts	0				
Organics	3	Amorphous (100)			
Opaques	<1	Pyrite (100)			
	100				

*Intensively altered to clay minerals

^ Including bitumen

Sedimentary structures

Primary	Clay-rich patches and streaks may be depositional features.
Biogenic	Possible *Helminthopsis* burrows.

Fractures	Occasional thin (5-40 μm thickness) epoxy-filled fractures. Likely artificial.
Porosity	Largely non-porous. Some discontinuous patches of the sample have minor intergranular porosity (<8%), some of which may be artificial.

Description

Bioturbated muddy sandstone comprised of subrounded fine silt- to fine sand-sized (average grain size is very fine sand) detrital quartz/chert (25-85%), feldspar (2-5%), and mica (2-4%). Clay-rich patches and streaks occur throughout the rock, and likely represent a combination of depositional and bioturbation features. Discontinuous patches with minor intergranular porosity (<8%) are present, and may be partly artificial.

Thin Section Quality

Good. Some epoxy-filled fractures and plucked grains.

Rock Classification

Muddy sandstone.

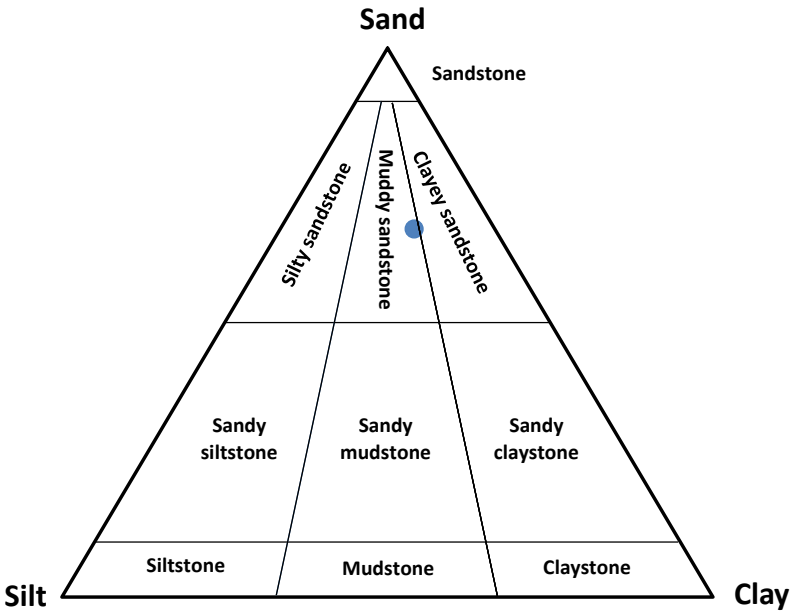


Fig. 4-275: Ternary plot showing the grain size composition of the sample based on the Wentworth scale (after Folk, 1954). Sample 13448 is classified as a muddy sandstone.



Fig. 4-276: Core photograph of sample 13448 from the Cardium Formation, well 100/05-17-049-08W5/00 (depth 1521.54 m). The thin section prepared from this sample was cut from the area marked with an X. Stratigraphic up-direction was not indicated. Scale is in mm.

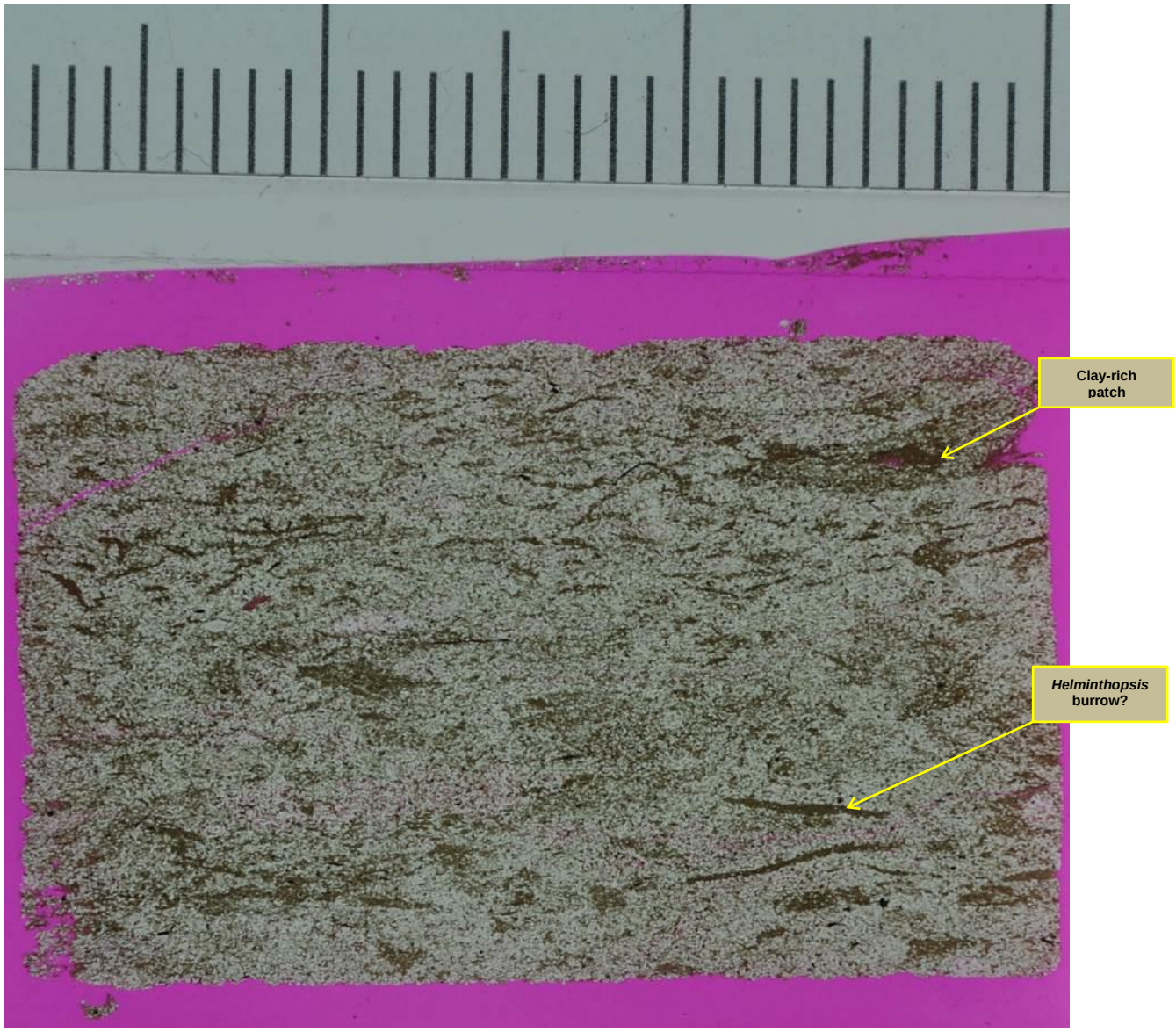


Fig. 4-277: Thin section photograph of sample 13448 from the Cardium Formation, well 100/05-17-049-08W5/00 (depth 1521.54 m). The sample is a bioturbated muddy sandstone with clay-rich patches, wisps and streaks throughout that may represent both depositional and bioturbation features. Possible* Helminthopsis *burrows (elongate clay streaks containing few detrital grains) are present in the sample. Scale is in mm.

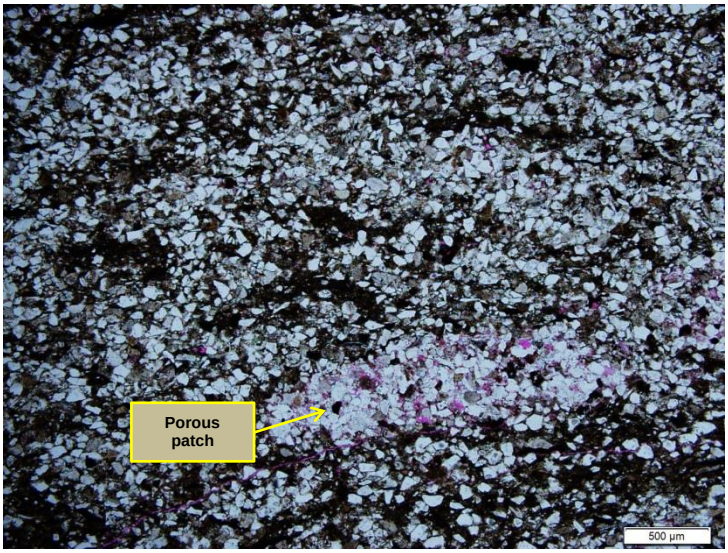


Fig. 4-278: Photomicrograph in PPL showing an overview of the muddy sandstone. The sample contains numerous clay-rich patches, wisps and streaks, most of which are non-porous. Some of the coarser-grained patches and lenses have <8% intergranular porosity. Light-coloured minerals include quartz, chert, mica and feldspar with the darker patches consisting mostly of clay material and some organics.

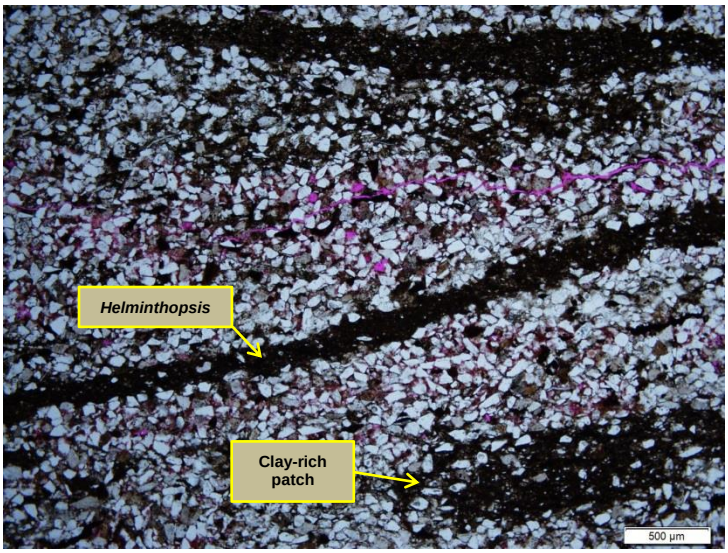


Fig. 4-279: Photomicrograph in PPL showing possible *Helminthopsis* burrows (elongate clay streaks containing few detrital grains). Other clay-rich patches and streaks observed in the sample contain more silt and sand-sized detrital grains, and may be depositional, rather than bioturbation features (lower right corner of image).

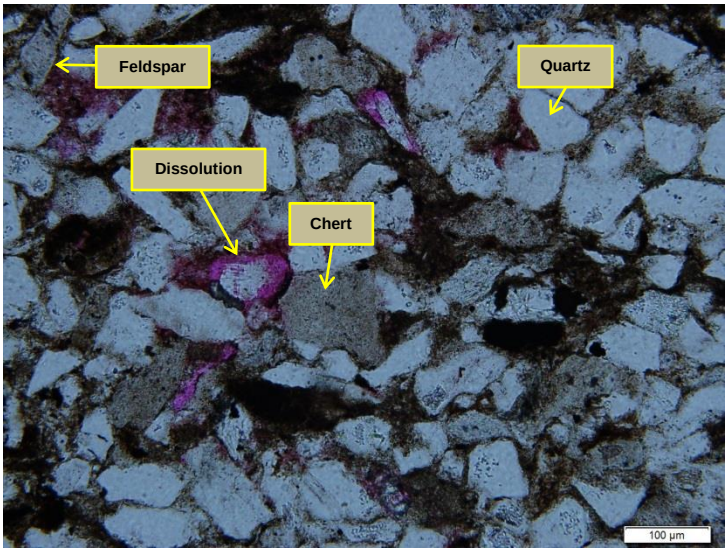


Fig. 4-280: Photomicrograph in PPL detailing subangular to subrounded, fine silt- to fine sand-sized (average grain size is very fine sand) detrital quartz/chert (25-85%) and feldspar (2-5%). Some feldspars exhibit a more dusty or “dirty” appearance compared to quartz and chert. Note several grains exhibiting partial dissolution.

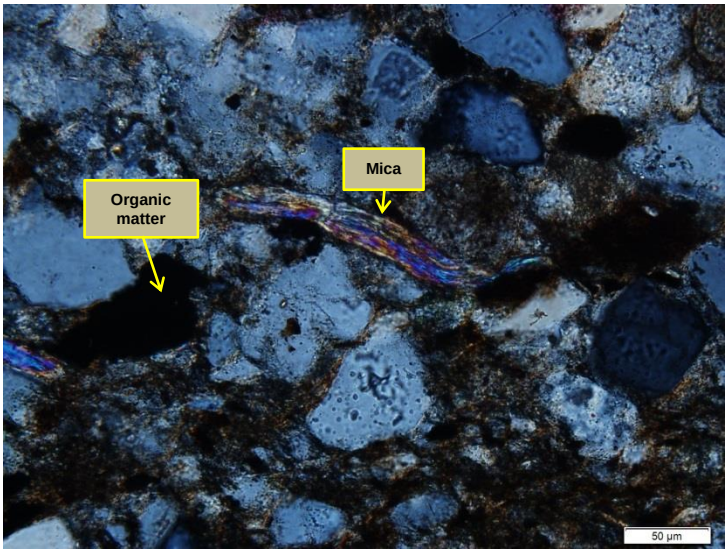


Fig. 4-281: Photomicrograph in XPL showing a partially deformed mica sheet (deformation likely due to sediment compaction during burial). Detrital mica grains comprise 2-4% of the sample. Solid organic matter fragments occur throughout the sample (estimated at ~2-5%).

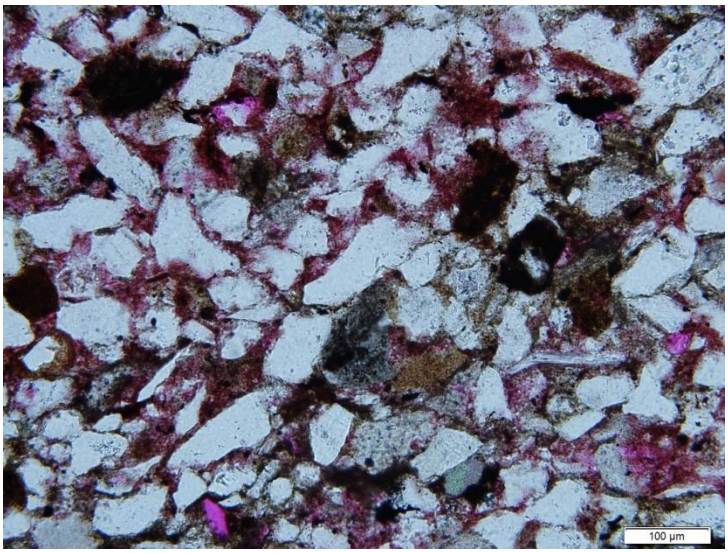


Fig. 4-282: Photomicrograph in PPL detailing patchy intergranular porosity (pink epoxy) estimated at ~8%. Few intergranular pores observed appear to be free of clay, indicating that some of the porosity apparent in thin section may be artificial.

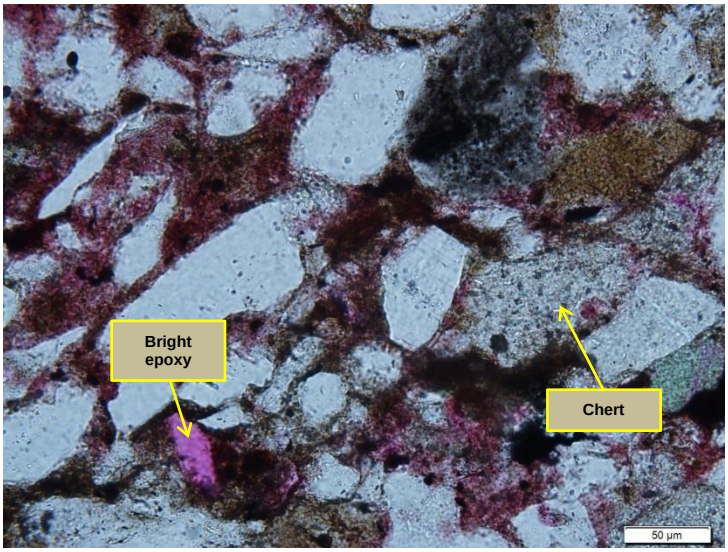


Fig. 4-283: Photomicrograph in PPL showing detail of intergranular porosity and clay material. A single pore observed in this image shows little/no interstitial clay (bright epoxy with apparent grain shape outline – possibly due to grain plucking during sample preparation?).

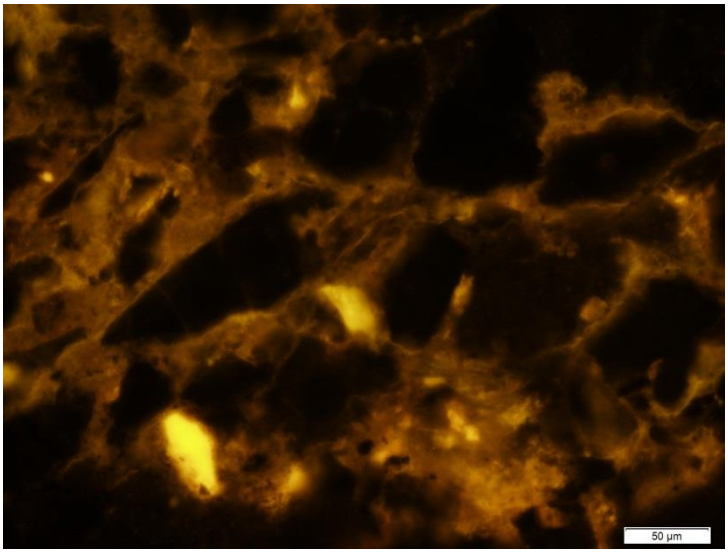


Fig. 4-284: Photomicrograph in UV light showing detail of intergranular porosity (same field of view as shown in Figure 4-283). Faint yellow patches observed under UV light may represent epoxy “bleeding” through clays (possible microporosity) rather than true intergranular porosity.

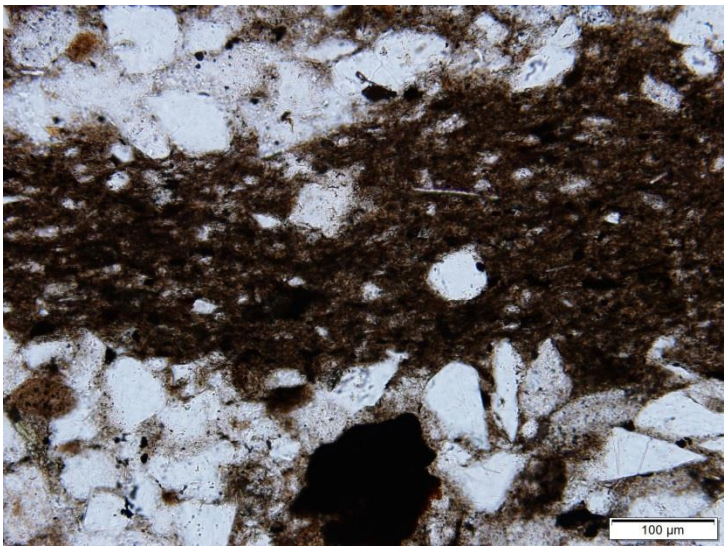


Fig. 4-285: Photomicrograph in PPL detailing a clay-rich streak observed in the sample. Small amounts of clay- to coarse silt-sized quartz and chert are found embedded within the clay matrix. Opaque material such as pyrite and organic matter are also present. Note an amorphous organic blob in the sandy portion along the bottom of the image, which also contains finely disseminated pyrite.

4.2.28 SAMPLE 15107

Sample ID	**15107**		
Sample type	**Core**	**UWI/Well**	**100/16-15-050-06W5/00**
Strat. Unit	**Cardium Formation**	**Depth**	**1170.27 m**

XRD/SRA results

Quartz (%)	Fsp (%)	Cb (%)	Clays (%)	Pyrite (%)
76.5	2.9	0	20.1	0.4

Composition (*in order of abundance*)

Grain size	%	Variety (%)	Variety (%)	Variety (%)	Variety (%)
sand	59	Quartz/chert (97)	Feldspar (2)	Mica (1)	
silt	8	Quartz/chert (98)	Mica (2)		
clay	25	Clay mins (100)			
Cement	5	Quartz (100)			
Bioclasts	0				
Organics	3	Amorphous (100)			
Opaques	<1	Pyrite (100)			
	100				

*Intensively altered to clay minerals

^ Including bitumen

Sedimentary structures

Primary	None apparent.
Biogenic	Possible burrow strutures.

Fractures	Rare thin (10-13 μm thickness) epoxy-filled fractures.
Porosity	5-10% porosity in possible burrow structures and clay-poor areas.

Description

Bioturbated clayey sandstone comprised of subrounded (common) to subangular (rare) very fine silt- to fine sand-sized (average grain size is very fine sand) detrital quartz (45-65%), chert (6-12%), feldspar (<2%), and mica (<2%). The sample appears unstratified, with no primary sedimentary structures visible. 5-10% intergranular porosity is observed in possible burrow structures and areas of clay-poor sediment.

Thin Section Quality

Moderate. Common exposed thin section glass. 1/2 stained for carbonates.

Rock Classification

Clayey sandstone.

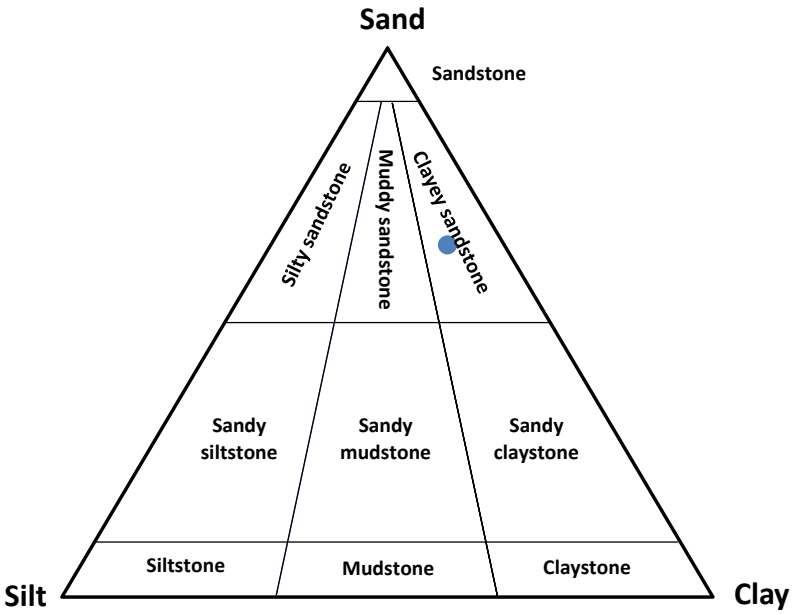


Fig. 4-286: Ternary plot showing the grain size composition of the sample based on the Wentworth scale (after Folk, 1954). Sample 15107 is classified as a clayey sandstone.



Fig. 4-287: Core photograph of sample 15107 from the Cardium Formation, well 100/16-15-050-06W5/00 (depth 1170.27 m). The thin section prepared from this sample was cut from the area marked with an X. The sample was received with no way-up direction. Scale is in mm.

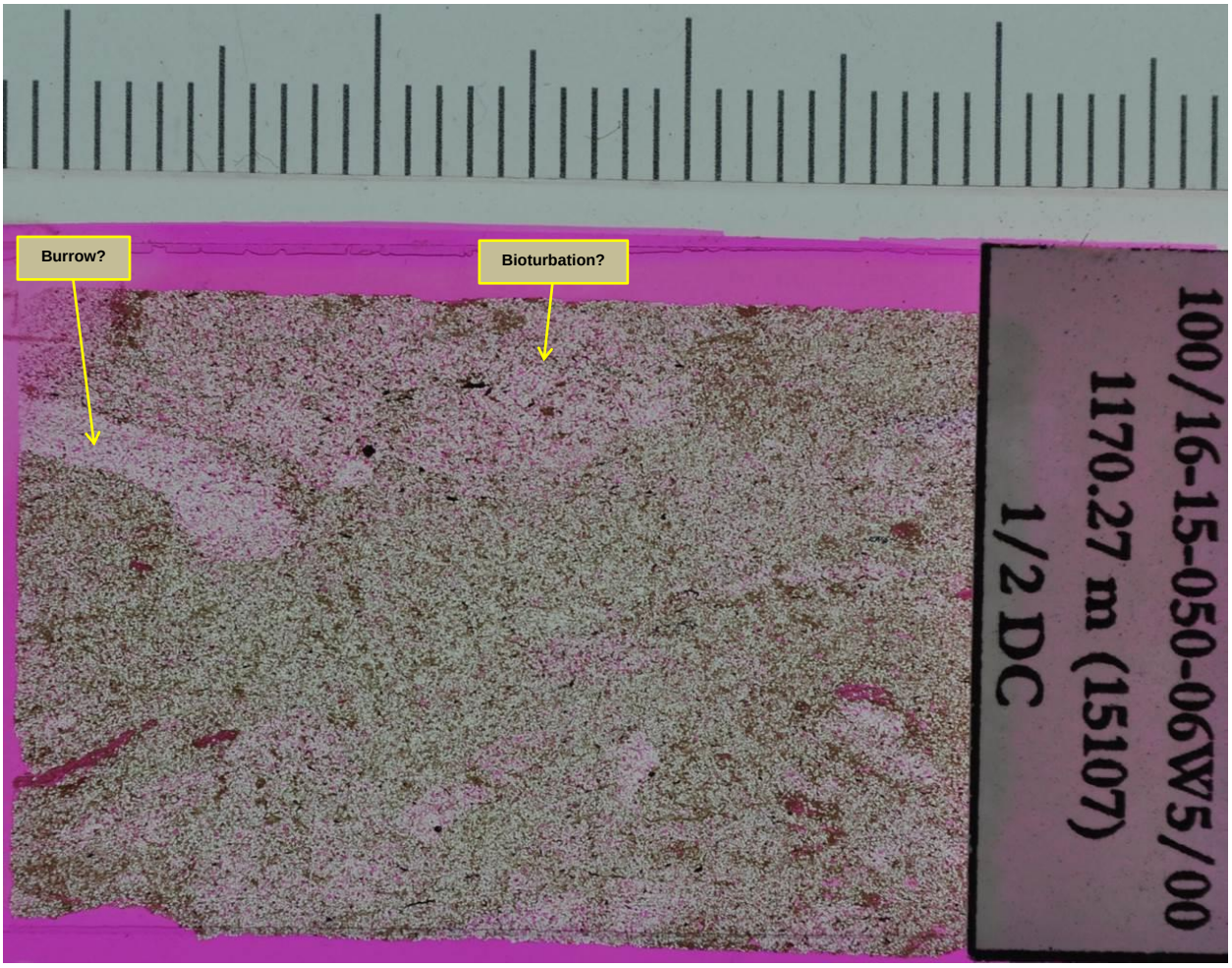


Fig. 4-288: Thin section photograph of sample 15107 from the Cardium Formation, well 100/16-15-050-06W5/00 (depth 1170.27 m). The sample is a bioturbated clayey sandstone that lacks primary sedimentary structures. Numerous clay-poor patches and structures (burrowing?) are observed that contain elevated intergranular porosity compared to most of the surrounding sediment. Scale is in mm. Note: way-up direction was not indicated and is difficult to positively identify due to pervasive mixing of the sediment.

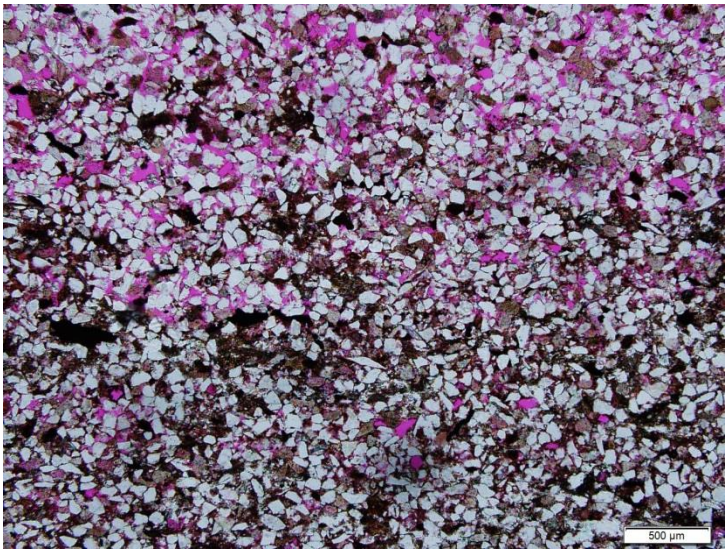


Fig. 4-289: Photomicrograph in PPL showing an overview of the clayey sandstone. The sample lacks primary sedimentary structures and consists of unstratified areas of clay-rich (bottom half of image) and clay-poor (porous; top half of image) sandy sediments. Light-coloured minerals consist mostly of quartz as well as chert, feldspar and mica. Darker material also includes chert, but is mostly made up of clay minerals.

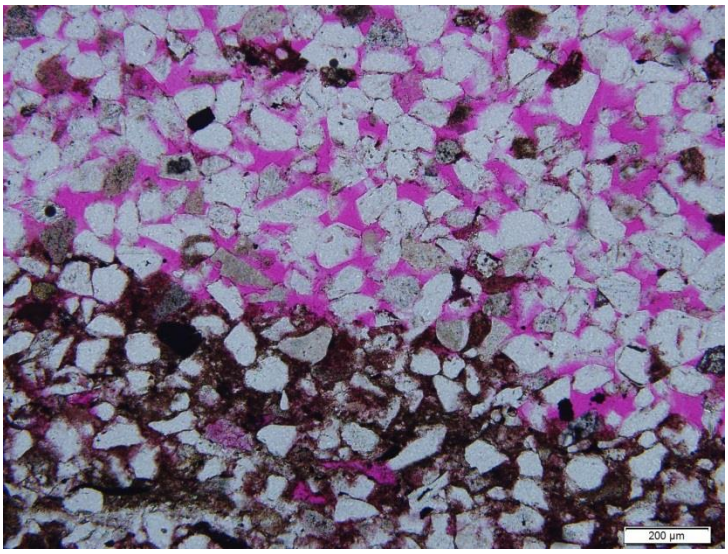


Fig. 4-290: Photomicrograph in PPL showing a contact between a possible burrow structure (see location in Figure 4-288) and a clay-rich area of the sample. The top half of the image shows elevated intergranular porosity (pink epoxy).

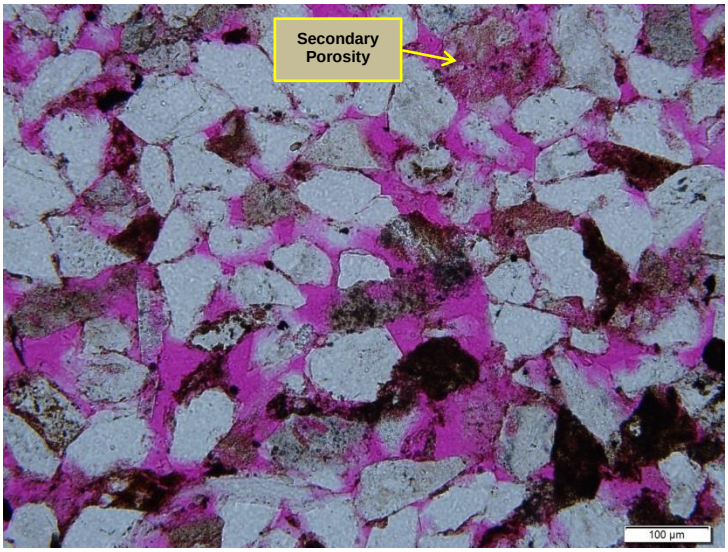


Fig. 4-291: Photomicrograph in PPL illustrating patchy intergranular porosity within a clay-poor lens. Porosity (pink) is estimated at ~5-10% but can exceed 15% in these patches. Small amounts of secondary porosity are observed associated with grain dissolution. Compaction likely occurred prior to dissolution with the majority of the pores relatively well preserved.

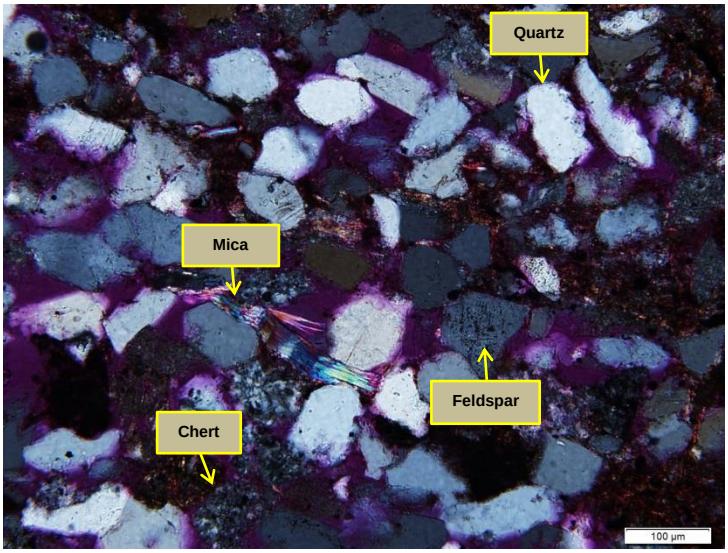


Fig. 4-292: Photomicrograph in XPL showing subangular to subrounded, very fine silt- to fine sand-sized (average grain size is very fine sand) detrital quartz (45-65%), chert (6-12%), feldspar (<2%), and mica (<2%). Some mica lathes are bent due to grain compaction. Chert grains are predominantly composed of microquartz.

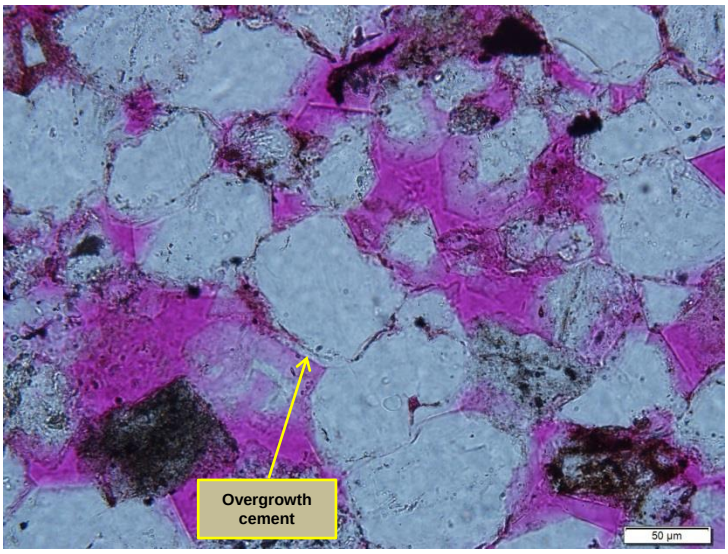


Fig. 4-293: Photomicrograph in PPL showing quartz overgrowths observed in the porous patches/lenses of the sandstone. Overgrowth cements are common in these clay-poor areas, but occur only as thin rims, never completely filling intergranular pore space.

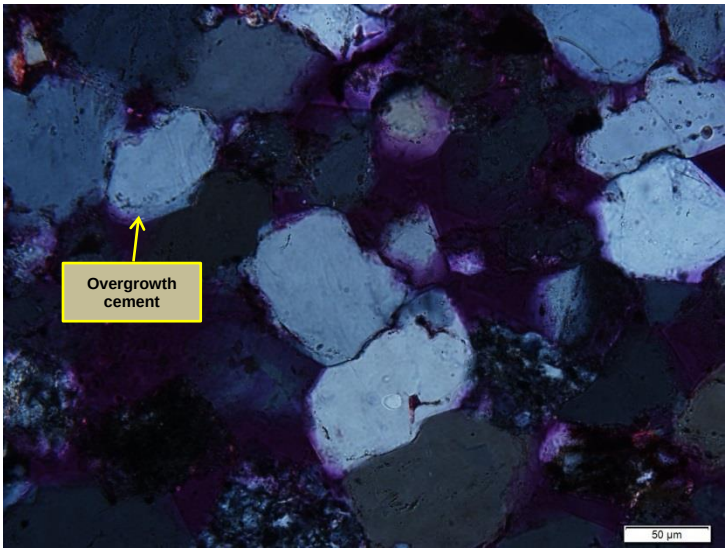


Fig. 4-294: Photomicrograph in XPL showing quartz overgrowth cements observed in a porous area of the sample (same field of view as Figure 4-293). A dust rim is typically observed separating overgrowths from detrital grains. Quartz overgrowths comprise ~5% of the sample.

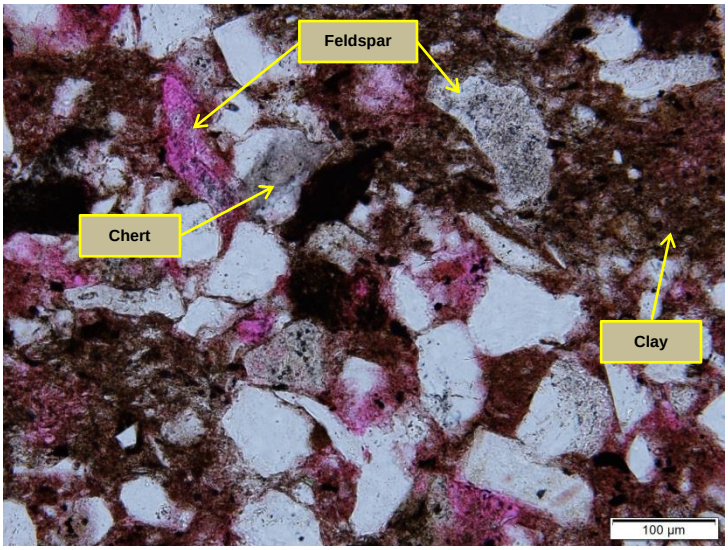


Fig. 4-295: Photomicrograph in PPL detailing a clay-rich portion of the sample. Porosity (intergranular and secondary) is still present within the clay-rich layers. Pyrite, organic material and fine silt- to very fine sand-sized quartz grains are observed embedded in the clay matrix (brown). Total clay content is estimated at ~25%. Some feldspars exhibit subtle overgrowths or are partially dissolved.

4.2.29 SAMPLE 15109

Sample ID	**15109**		
Sample type	**Core**	**UWI/Well**	**100/16-15-050-06W5/00**
Strat. Unit	**Cardium Formation**	**Depth**	**1177.05 m**

XRD/SRA results

Quartz (%)	Fsp (%)	Cb (%)	Clays (%)	Pyrite (%)
62.5	5.8	0	29.6	0.8

Composition (*in order of abundance*)

Grain size	%	Variety (%)	Variety (%)	Variety (%)	Variety (%)
sand	38	Quartz/chert (93)	Mica(5)	Feldspar(2)	
silt	26	Quartz/chert(94)	Mica(6)		
clay	30	Clay mins (100)			
Cement	1	Quartz (100)			
Bioclasts	0				
Organics	5	Amorphous (100)			
Opaques	<1	Pyrite (100)			
	100				

*Intensively altered to clay minerals

^ Including bitumen

Sedimentary structures

Primary	Possible convoluted bedding (likely reworked by bioturbation).
Biogenic	Many apparent bioturbation features, including possible *Planolites* burrows.

Fractures	Common epoxy-filled fractures and partings. Likely artificial.
Porosity	1-5% intergranular porosity in convoluted sandy bedding and some possible burrow structures. Mostly non-porous.

Description

Bioturbated sandy mudstone comprised of subrounded (common) to angular (rare) very fine silt- to fine sand-sized (average grain size is very fine sand) quartz (30-50%), chert (8-12%), mica (1-4%), and feldspar (<2%). The mudstone appears heavily reworked, with few discernible primary sedimentary structures. 1-5% intergranular porosity (possibly artificial) is observed in convoluted sandy bedding and some possible burrow structures present in the rock.

Thin Section Quality

Moderate. Common exposed thin section glass.

Rock Classification

Sandy mudstone.

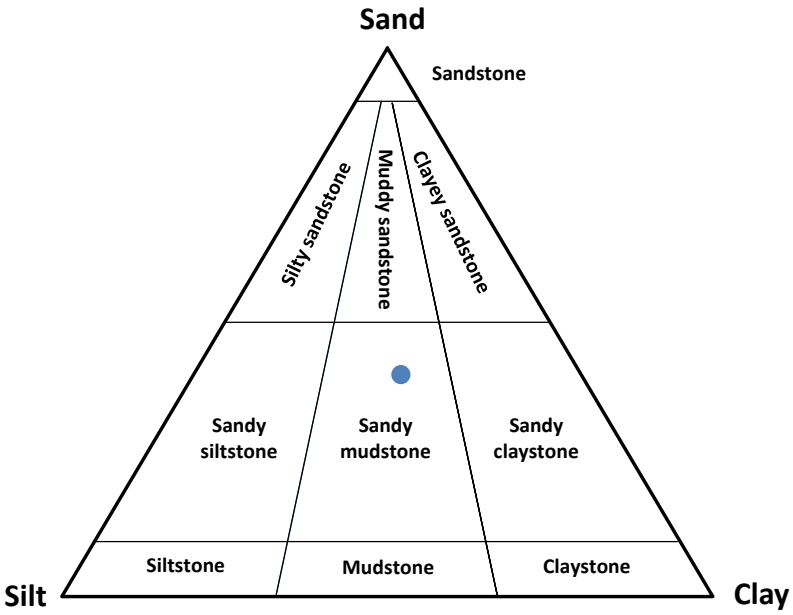


Fig. 4-296: Ternary plot showing the grain size composition of the sample based on the Wentworth scale (after Folk, 1954). Sample 15109 is classified as sandy mudstone.

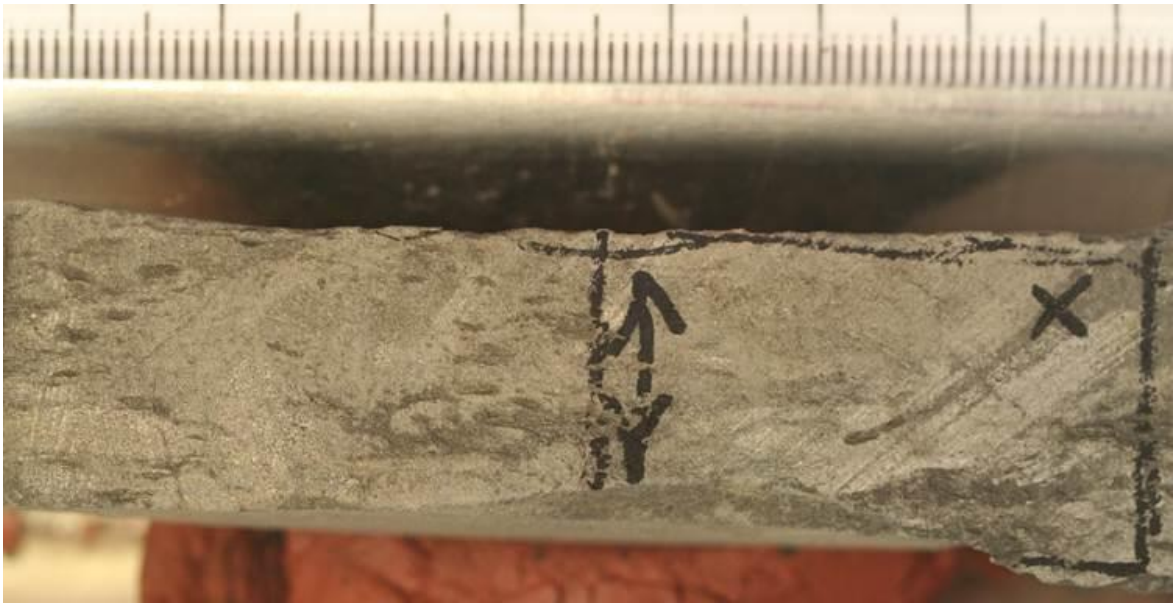


Fig. 4-297: Core photograph of sample 15109 from the Cardium Formation, well 100/16-15-050-06W5/00 (depth 1177.05 m). The thin section prepared from this sample was cut from the area marked with an X. The sample was received with no way-up direction. Scale is in mm.

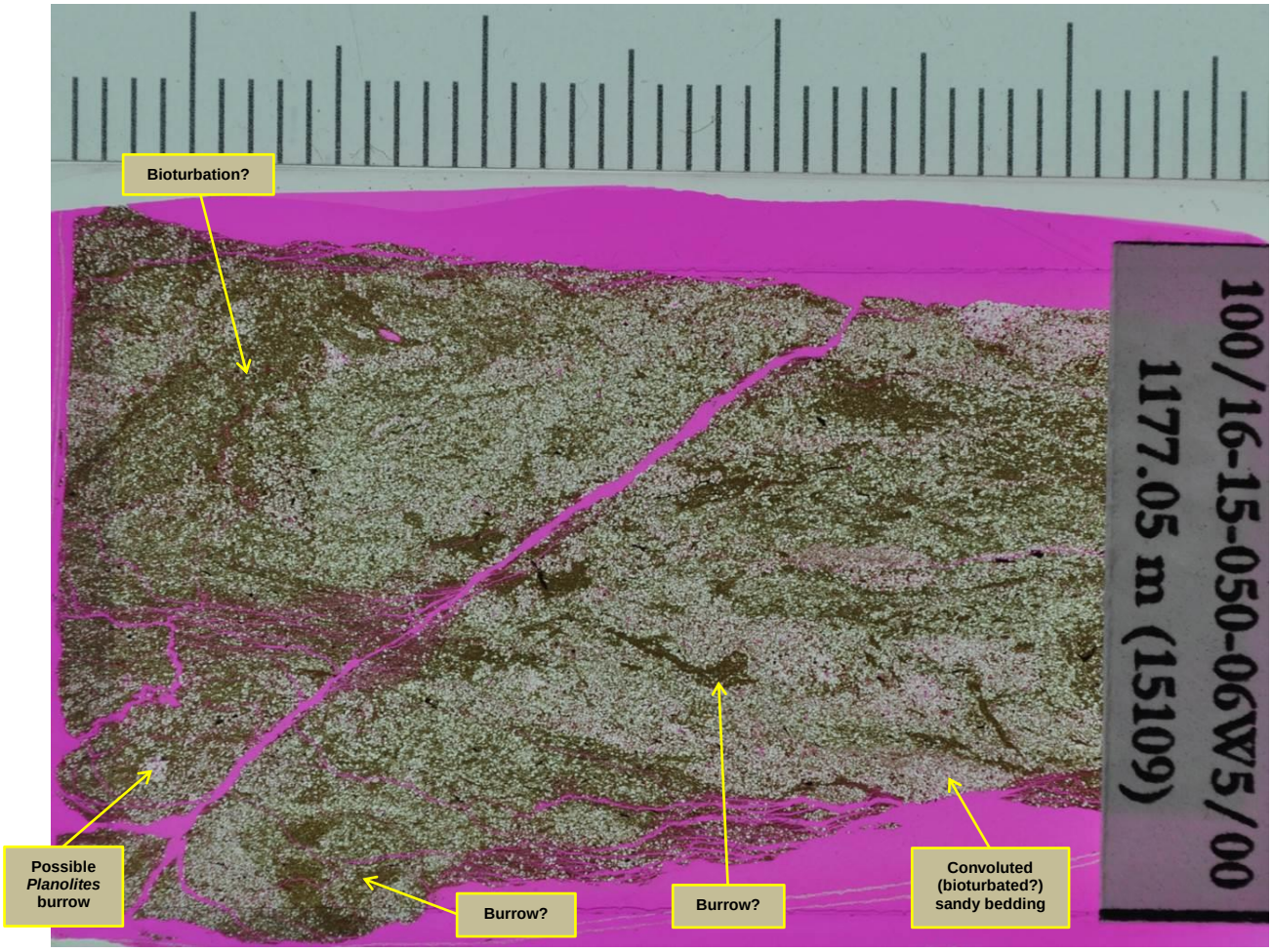


Fig. 4-298: Thin section photograph of sample 15109 from the Cardium Formation, well 100/16-15-050-06W5/00 (depth 1177.05 m). The sample is a bioturbated sandy mudstone with strongly mixed and convoluted sandy bedding observed near the base (as shown) of the sample. Bioturbation or sediment mixing have obliterated the original depositional fabric, which appears largely unstratified with numerous clay-rich patches, lenses and wisps. Note common artificial partings. Scale is in mm. Note: way-up direction was difficult to infer and may be different from the orientation shown.

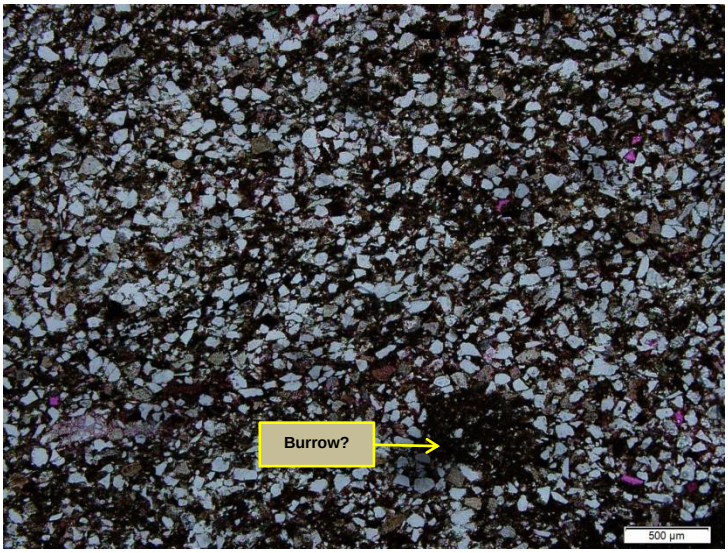


Fig. 4-299: Photomicrograph in PPL showing an overview of the sandy mudstone. The sample has few discernible primary sedimentary structures due to heavy mixing (pervasive bioturbation?). Light-coloured minerals consist of quartz, chert, feldspar and mica with the darker patches consisting mostly of clay. Clay-rich patches are likely the result of bioturbation. Note a subcircular, clay-rich structure, which is likely a burrowing feature.

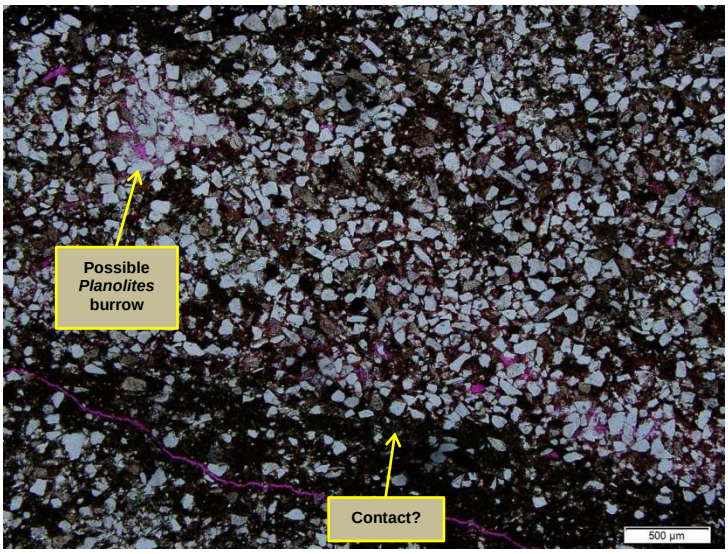


Fig. 4-300: Photomicrograph in PPL showing possible convoluted sandy bedding. Bioturbation features may have obscured much of the original bedding structure. Note a possible *Planolites* burrow (coarser-grained material with concentrated porosity).

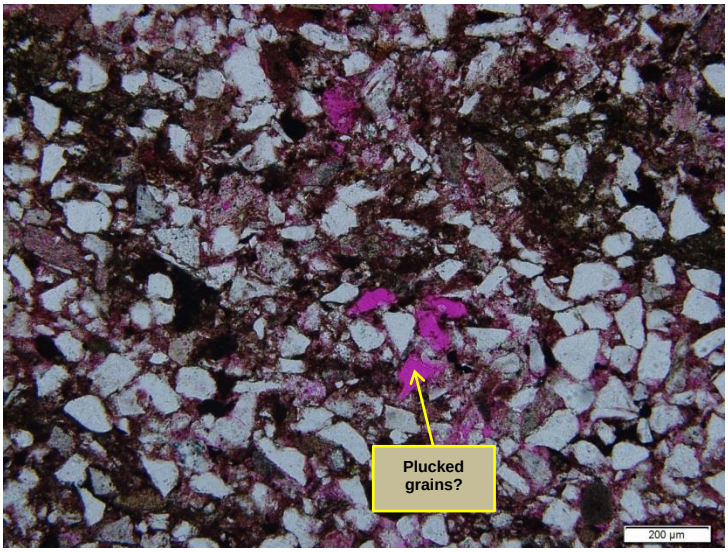


Fig. 4-301: Photomicrograph in PPL showing 1-5% estimated intergranular porosity observed in a section of possible convoluted sandy bedding (see Figure 4-298). Some of this porosity may be artificial, resulting from plucking of detrital grains (angular pores near center of image) and thin section epoxy “bleeding” around grain edges.

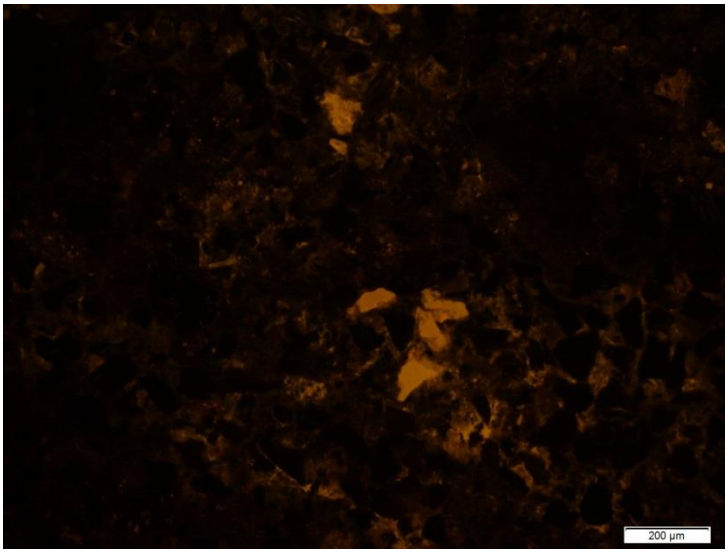


Fig. 4-302: Photomicrograph in UV light detailing intergranular porosity observed in Figure 4-301. Some pores are possibly artificial.

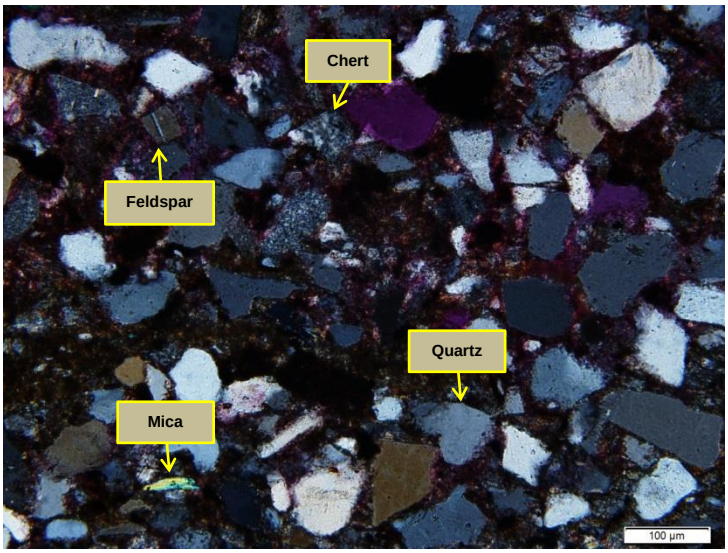


Fig. 4-303: Photomicrograph in XPL showing angular to subrounded, very fine silt- to fine sand-sized (average grain size is very fine sand) quartz (30-50%), chert (8-12%), mica (1-4%), and feldspar (<2%). Microcrystalline quartz represents chert grains.

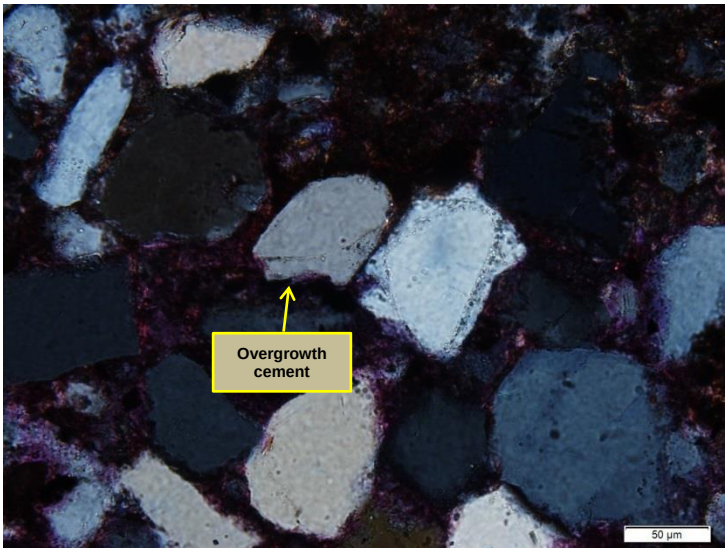


Fig. 4-304: Photomicrograph in XPL showing rare quartz overgrowth cementation. Quartz cement comprises ~1% of the total composition.

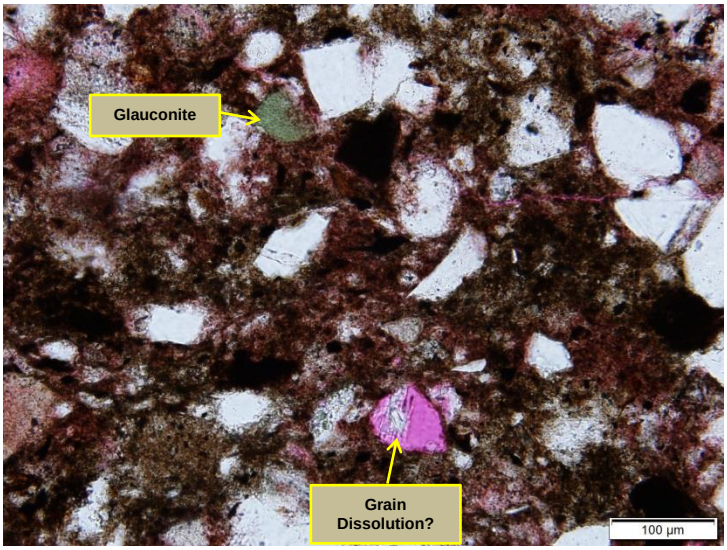


Fig. 4-305: Photomicrograph in PPL illustrating a clay-rich patch of the sample, which includes embedded clay- to very fine sand-sized quartz and chert grains. Finely dispersed pyrite and organic matter are also present. Some microporosity is observed as well as possible secondary porosity associated with grain dissolution (feldspar?). A rare glauconite grain (green), which is deformed due to compaction, is also observed.

5. Banff Formation Overview

This chapter presents a petrographic analysis of four core samples from three wells of the Banff Formation (see Table 5-A). Core samples were impregnated using rhodamine-B epoxy (pink) in order to identify porosity and fractures using UV fluorescence microscopy. Three of the samples were half stained for carbonates. The following summary focuses on observations of sample compositional variability (i.e., lithofacies groupings), and provides photomicrographs of the most common depositional and bioturbation structures, diagenetic features, clay and organic matter distributions, and the occurrence of porosity and fractures. Several lithofacies were identified (Table 5-B) and the mineralogical XRD data for each lithofacies was averaged in order to determine common compositional parameters (Table 5-C).

5.1 SUMMARY

5.1.1 CORE SAMPLES:

Well Location	Depth m (Sample ID)
102/04-32-003-17W4/00	1320.5 (13034)
100/01-03-002-20W4/00	1524.9 (13041), 1532.1 (13044)
102/08-07-075-05W5/00	1077.3 (13822)

Table 5-A: Well locations and core sample depths.

5.1.2 LITHOFACIES, GROUPINGS AND DESCRIPTIONS:

Well Location	Lithofacies	Depth m (Sample ID)
102/04-32-003-17W4/00	1	1320.5 (13034)
100/01-03-002-20W4/00	2	1524.9 (13041)
100/01-03-002-20W4/00	3	1532.1 (13044)
102/08-07-075-05W5/00	4	1077.3 (13822)

Table 5-B: Lithofacies distribution by Well.

Lithofacies	Classification	Quartz/Chert %	Feldspar %	Calcite %	Dolomite %	Ankerite %	Clay/Mica %	Pyrite %
1	Carbonate-rich siliceous siltstone	58.8	20.7	0	9.5	6.4	3.2	1.7
2	Silica-rich wackestone	23.2	9.7	46.2	9.2	7.3	3.4	0.8
3	Silty subarkose sandstone	61.5	15.8	0	7.0	9.2	5.9	0.5
4	Silica-rich carbonate mudstone	21.3	4.0	59.7	0	4.1	7.9	2.9

Table 5-C: Average lithofacies composition, based on XRD data.

5.1.2.1 LITHOFACIES 1: CARBONATE-RICH SILICEOUS SILTSTONE

Samples 13034 is a moderately to heavily bioturbated, carbonate-rich siliceous siltstone. The sample shows irregular laminae and lenses defined by elevated opaque material and dolomite cement. Thin opaque-rich laminae occur interbedded between thicker coarser-grained laminae that are comprised of quartz (predominant), feldspar (K-feldspar and albite), mica, and chert.

5.1.2.2 LITHOFACIES 2: SILICA-RICH WACKESTONE

Sample 13041 is classified as a silica-rich wackestone. The texture of the sample is characterized by abundant micrite supporting detrital quartz grains, common fragmented bivalve shells, and

minor phosphatic grains and bryozoan fragments. Several mm-scale burrows and areas of possible bioturbated sediment occur in the sample, which otherwise appears to lack primary sedimentary structures.

5.1.2.3 LITHOFACIES 3: SILTY SUBARKOSE SANDSTONE

Sample 13044 is classified as a silty subarkose sandstone. The sample is comprised of subrounded (common) to angular (rare) fine silt- to very fine sand-sized (average grain size is very fine sand) detrital quartz (50-65%) and feldspar (6-10%).

5.1.2.4 LITHOFACIES 4: SILICA-RICH CARBONATE MUDSTONE

Sample 13822 is classified as a silica-rich carbonate mudstone. The texture of the sample is characterized by alternating sparry calcite and organic-rich mixed siliceous/calcareous laminae.

5.1.3 SEDIMENTARY STRUCTURES & BIOTURBATION:

Primary sedimentary structures and bioturbation features are observed in samples 13034, 13041, and 13822. Sample 13034 shows irregular laminae and lenses of silt- to sand-sized grains, with thin interspersed opaque-rich laminations. Patches of bioturbated or mixed sediment and possible mm-scale burrows occur in sample 13044. Sample 13822 is characterized by alternating laminae with distinct sparry calcite and organic-rich mixed siliceous/carbonate compositions.

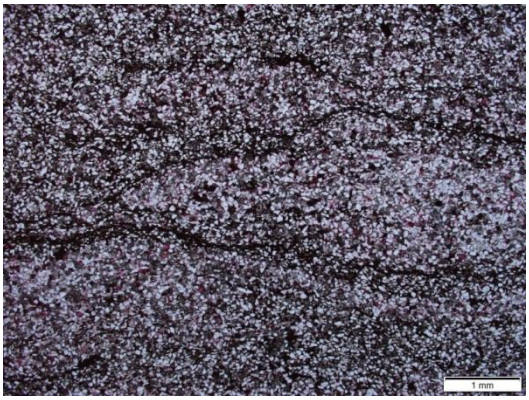


Fig. 5.1.3-1: Photomicrograph in PPL showing wavy, disturbed laminae and lenses and interspersed opaque-rich laminae in sample 13034.



Fig. 5.1.3-2: Photomicrograph in PPL showing a section of bioturbated sediment (right side of image) containing abundant glauconite (green) grains observed in sample 13041.

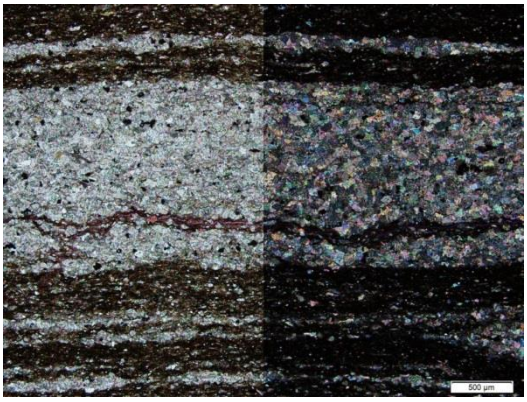


Fig. 5.1.3-3: Photomicrograph (left half in PPL, right half in XPL) showing alternating sparry calcite (light-coloured) and organic-rich mixed siliceous/calcareous (dark-coloured) laminae present in sample 13822.

5.1.4 DIAGENESIS:

Diagenetic features are observed in samples 13034 and 13044. Sample 13034 shows common quartz cementation (predominately as overgrowths) as well as subhedral to euhedral authigenic dolomite (some with overgrowths), patchy calcite cement, and rare feldspathic cement. Sample 13044 shows at least four diagenetic features, including: dolomite cementation, feldspar overgrowths, pore-filling feldspar cementation, and quartz overgrowths.

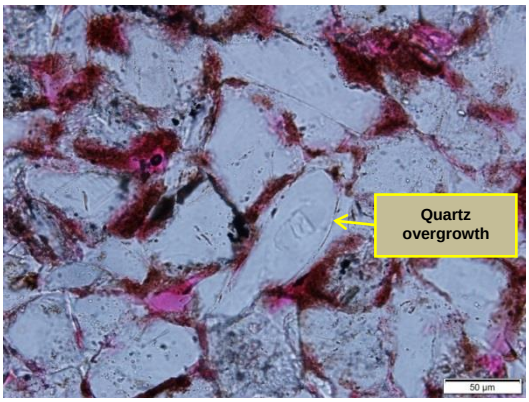


Fig. 5.1.4-1: Photomicrograph in PPL showing abundant quartz overgrowths in sample 13034, which have reduced both pore space and pore throat sizes.

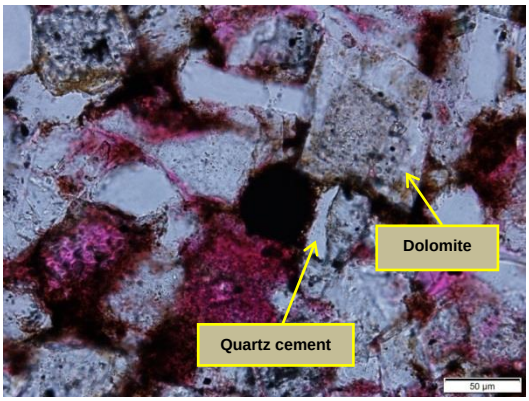


Fig. 5.1.4-2: Photomicrograph in PPL showing dolomite and quartz cements in sample 13034. The large dolomite rhomb exhibits a “dirty” inner surface, surrounded by a clean secondary overgrowth. Note possible dissolution pores. Calcite and minor feldspar cements are also observed in the sample.

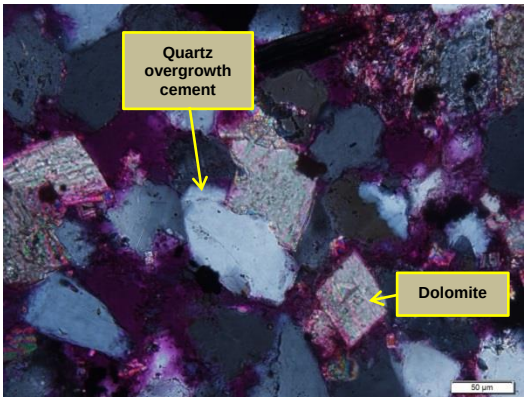


Fig. 5.1.4-3: Photomicrograph in XPL showing dolomite and quartz cements observed in sample 13044. Dolomite cement occurs as subhedral to euhedral pore-filling crystals or rhombs, whereas quartz cement occurs as anhedral to euhedral overgrowths.

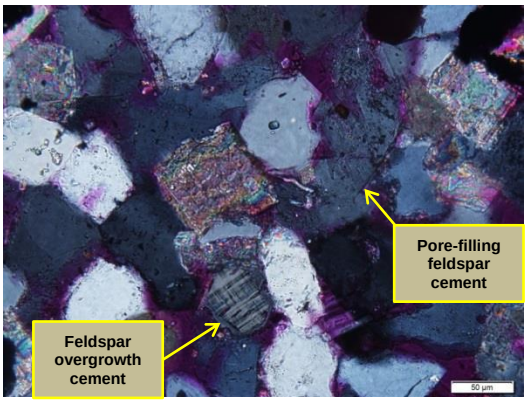


Fig. 5.1.4-4: Photomicrograph in XPL showing dolomite cements, feldspar overgrowths, pore-filling feldspar cements, and quartz overgrowths present in sample 13044.

5.1.5 ORGANIC MATTER & CLAYS:

With the exception of sample 13822, <5% clay is observed in the samples. Sample 13822 contains organic-rich mixed siliceous/carbonate compositional laminae with ~15-20% organic matter and ~8% clay. <2% organic matter occurs in samples 13034 and 13041 (organics are absent from sample 13044), typically as finely dispersed particles or elongate streaks associated with pyrite.

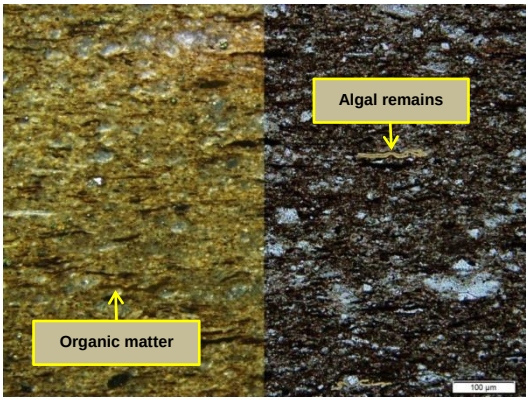


Fig. 5.1.5-1: Photomicrograph (left half in reflected light, right half in PPL) showing detail of an organic-rich mixed siliceous/calcareous lamination in sample 13822. The lamination contains elongate, bedding-parallel organic strands and algal remains.

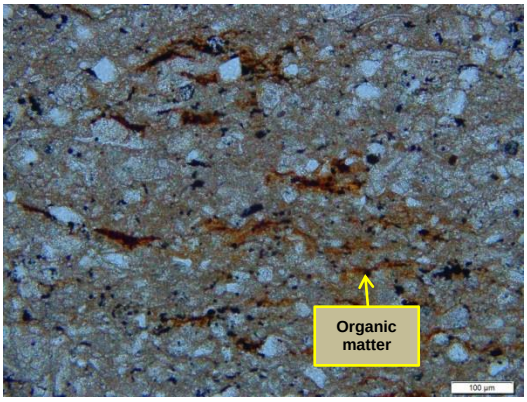


Fig. 5.1.5-2: Photomicrograph in HDR (high dynamic range) PPL showing rare organic strands, wisps, and blebs present in sample 13041.

5.1.6 POROSITY & FRACTURING:

Significant porosity (>5%) occurs only in sample 13044. Fractures are observed only in sample 13822, and are concentrated in organic-rich mixed siliceous/calcareous laminae.

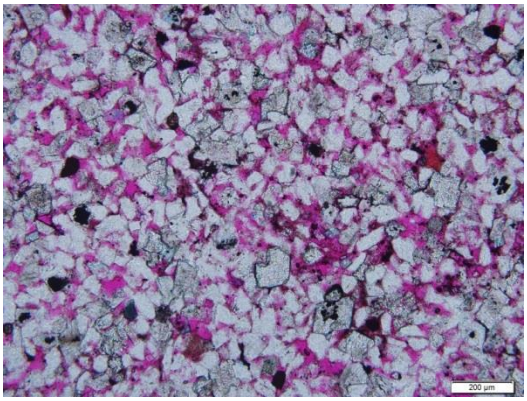


Fig. 5.1.6-1: Photomicrograph in PPL showing 10-15% intergranular porosity (pink epoxy) common throughout sample 13044. Despite extensive secondary cementation, the sample shows well connected pore throats.

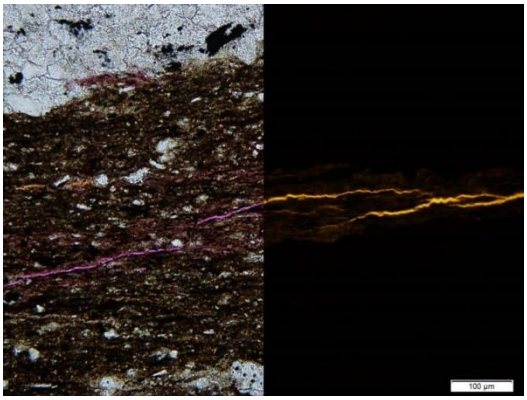


Fig. 5.1.6-2: Photomicrograph (left half in PPL, right half in UV light) showing common thin, artificial epoxy-filled fractures in sample 13822. Thin section epoxy (pink) is observed to “bleed” through the organic-rich material surrounding the fractures, creating apparent microporosity.

5.2 RESULTS

5.2.1 SAMPLE 13034

Sample ID 13034
Sample type Core
Strat. Unit Banff

102/04-32-033-17W4/00
Depth 1320.50 m

XRD/SRA results

Quartz (%)	Fsp (%)	Cb (%)	Clays (%)	Pyrite (%)	
58.7	20.7	15.8	3.2	1.7	

Composition (*in order of abundance*)

Grain size	%	Variety (%)	Variety (%)	Variety (%)	Variety (%)	Variety (%)
sand	15-17	Quartz (60)	K-feldspar (25)	Albite (15)	Muscovite (<1)	
silt	44-47	Quartz (70)	K-feldspar (20)	Albite (6)	Muscovite (2)	Chert (2)
clay	4	Clay minerals (100)				
Cement	28-33	Dolomite (55)	Quartz (30)	Calcite (10)	K-feldspar (3)	
Opaques	3	Pyrite (100)				
Organics	1	AOM^(100)				
Bioclasts	0					
	100					

*Heavily degraded
^ Including bitumen

Sedimentary structures

Primary	Thin, silt to sand-sized, irregular laminae and lenses defined by elevated amounts of opaque material and dolomite cement. Thin, compacted, opaque-rich laminations are interbedded between the coarser-grained laminae.
Biogenic	Moderately to heavily bioturbated with laminae and lenses due to burrowing activity. Opaque clusters and "trails" may be fecal derived.

Fractures	Fracturing is absent.
Porosity	Estimated to be ~3-5%. Most porosity is associated with open/partially cemented intergranular space (<5-10 µm) as well as thin, elongate pores along grain edges. Secondary porosity due to partial grain dissolution is also observed.
Organics	Estimated at ~1%. Organic material is associated with pyrite and clay material within intergranular spaces , opaque pockets, "trails" and finely dispersed between grains and cements.

Description

Classified as a moderate to heavily bioturbated, carbonate-rich siliceous siltstone with irregular laminae and lenses defined by elevated amounts of opaque material and dolomite cement. Several, fine-grained, thin opaque-rich laminae are observed interbedded between the coarser-grained laminae. Grains are fine-silt to very fine sand-size (predominantly coarse-silt), subangular to subround and moderate to well sorted. The rock framework composition consists of quartz (predominant), feldspar (K-feldspar and albite), muscovite and chert. Authigenic minerals consist predominantly of subhedral to euhedral dolomite crystals and rhombs some of which show overgrowths. Calcite cement is patchy. Secondary quartz cementation is common and occurs predominantly as overgrowths. Some feldspathic cement is also observed. Opaque material consists of clays along with idiomorphic pyrite and organic material occurring in intergranular spaces, along laminae and forming clusters and “trails”, which may be fecal derived. Porosity is estimated at 3-5% and is present within intergranular spaces and as secondary porosity associated with grain dissolution. Fracturing in the sample is absent. In general the sample is grain-supported, well sorted as well as texturally and compositionally mature.

Thin Section Quality

Good; 1/2 stained for carbonates

Rock Classification

Carbonate-rich siliceous siltstone (Folk, 1954)

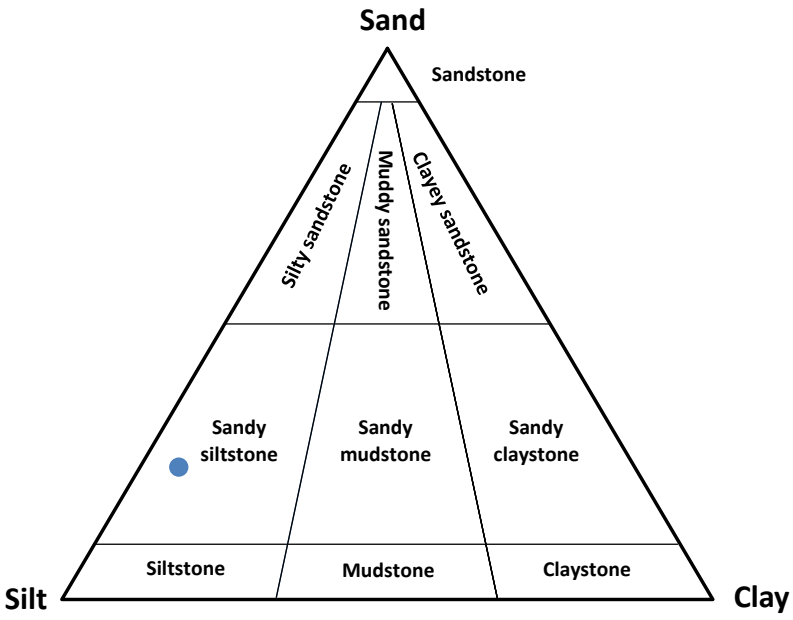


Fig. 5-1: Ternary plot showing the grain size composition of the sample based on the Wentworth scale (after Folk, 1954). Using this classification scheme, the sample can be described as a sandy siltstone.

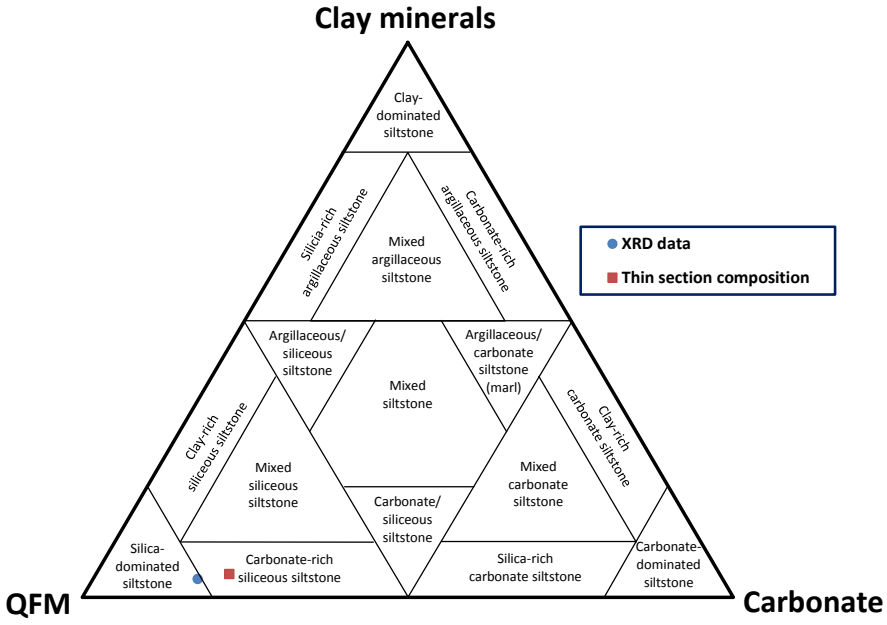


Fig. 5-2: Ternary plot of the mineralogical composition of the sample according to the XRD data (blue) and estimated thin-section composition (red) in terms of clay minerals, QFM (quartz, feldspar and mica) and carbonate content. The sample is classified as a carbonate-rich siliceous siltstone due to the abundance of quartz and feldspar with respect to carbonate content. Thin section analysis shows slightly greater amounts of carbonate compared to the XRD data (silica-dominated siltstone).

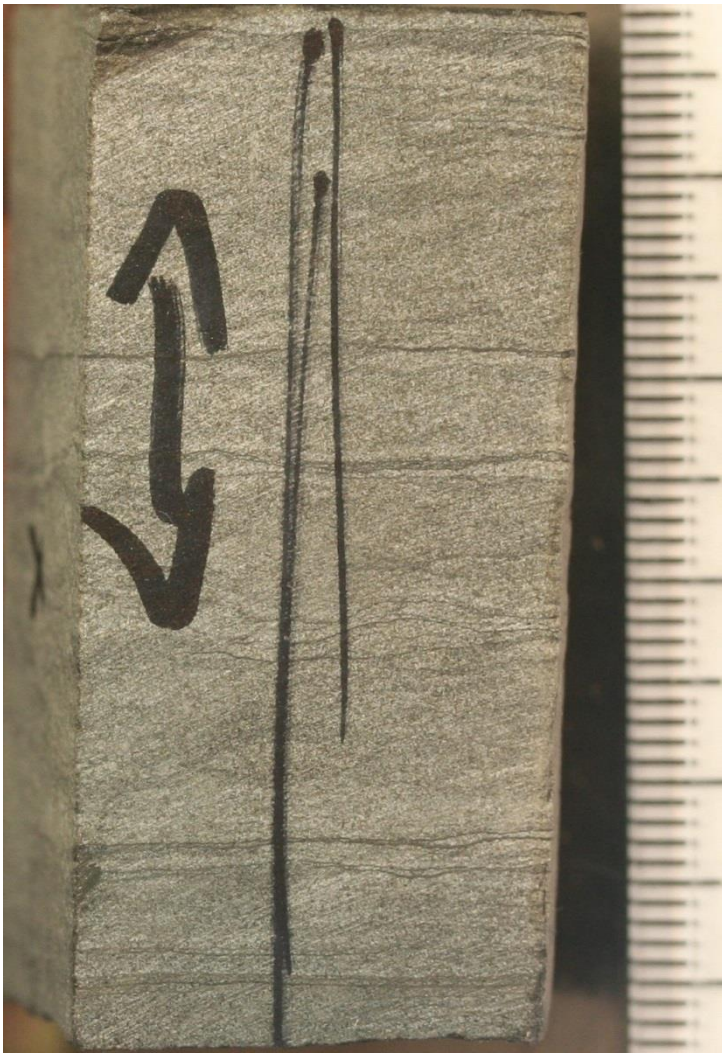


Fig. 5-3: Core photograph of sample 13034 from the Banff Formation, well 102/04-32-033-17W4/00 (depth 1320.50 m). The thin section prepared from this sample was cut from the area marked with an X. The sample was received with no way-up direction. Scale is in mm.



Fig. 5-4: Thin section photograph of sample 13034 from the Banff Formation, well 102/04-32-003-17W4 (1320.5 m). The sample is a moderately to heavily bioturbated, carbonate-rich siliceous siltstone, with wavy, disturbed laminae and lenses that possibly represent burrowing features. Several thin, wavy, occasionally discontinuous opaque-rich laminae are observed. Scale is in mm.

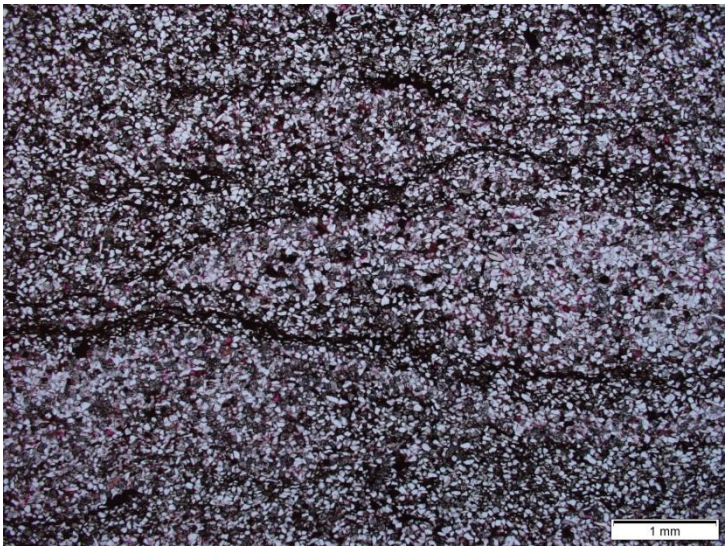


Fig. 5-5: Photomicrograph in PPL showing an overview of sample 13034 (1320.5 m). The sample is a moderately to heavily bioturbated, carbonate-rich siliceous siltstone with wavy, disturbed laminae and lenses, some of which are possibly burrowing features. The light coloured minerals in the image consist predominantly of quartz, dolomite, and feldspar. Grains are fine silt- to very fine sand-sized (predominantly coarse-silt) and subangular to subrounded.

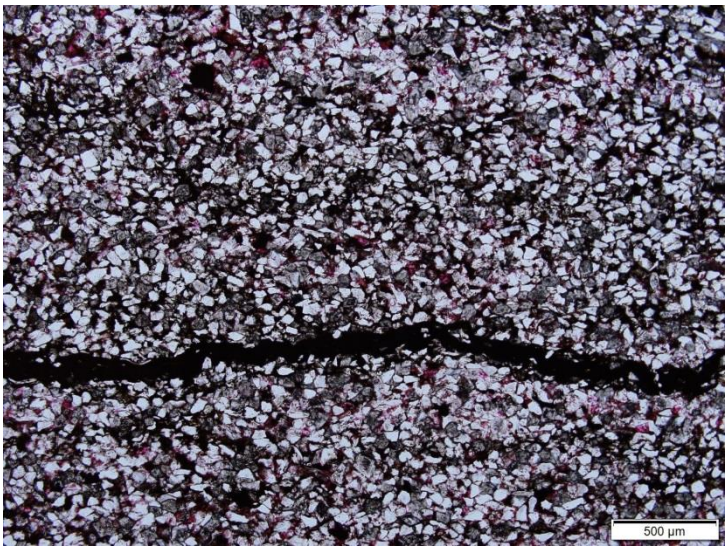


Fig. 5-6: Photomicrograph in PPL from the lower half of the slide illustrating a thin, slightly undulating opaque-rich lamination (~140 µm thick). The lamination likely represents an accumulation of organic and fine-grained material during a period of low energy.

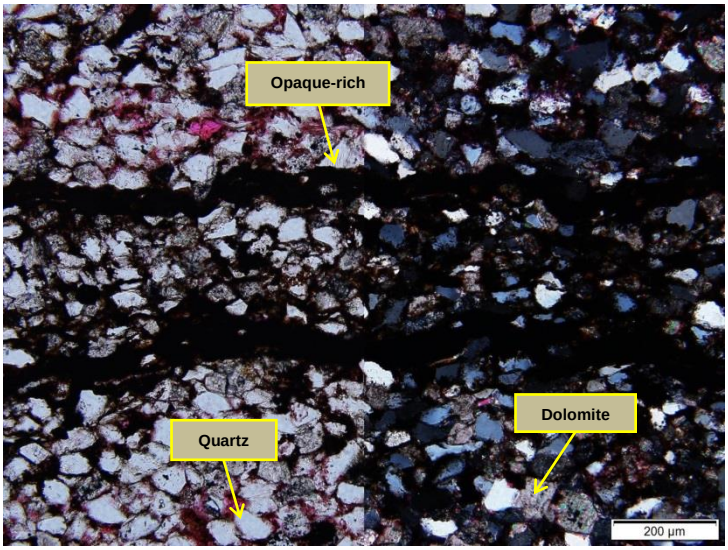


Fig. 5-7: Photomicrograph in PPL (left) and XPL (right) showing medium silt- (~15 µm) to very fine sand-sized (~75 µm) grains and cements with interbedded opaque-rich laminae (~50-75 µm thick). Quartz grains and cements (estimated at ~55%) are colourless and subangular to subrounded. Feldspars can be difficult to distinguish from quartz in thin section. Some feldspars may exhibit twinning (polysynthetic or tartan) as well as dusty or altered surfaces. Potassium feldspar is estimated at ~10-12% with albite estimated at 4%. Dolomite (grey in PPL, dull birefringence in XPL) is abundant and estimated at ~15-20%.

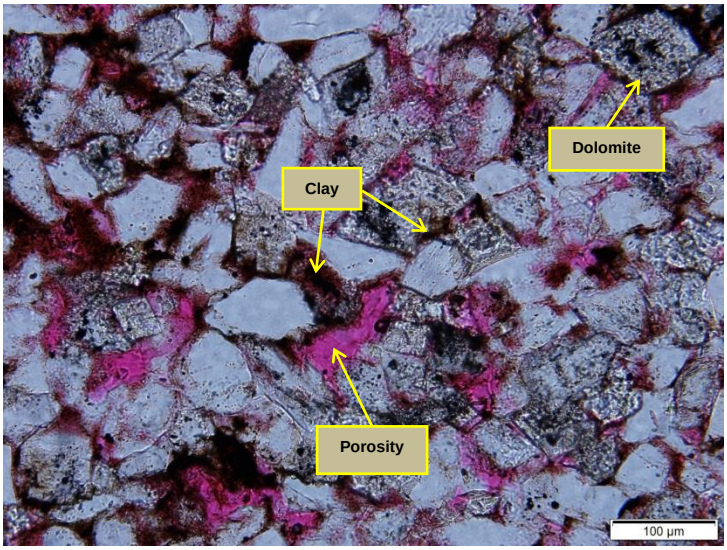


Fig. 5-8: Photomicrograph in PPL showing intergranular porosity highlighted by pink epoxy. Clays (dark-brown to black; estimated at ~4%) and organic material (black; estimated at ~1%) are observed rimming grains and lining pores. The primary controls on porosity and permeability include compaction, dolomite cementation, quartz cement and clay/organic material. Overall porosity in the sample is estimated at ~3-5%. Note 25-70 µm, subedral to euhedral, dolomite rhombs, which exhibit "dirty" surfaces and corroded edges. Dolomite is estimated at ~15-20%.

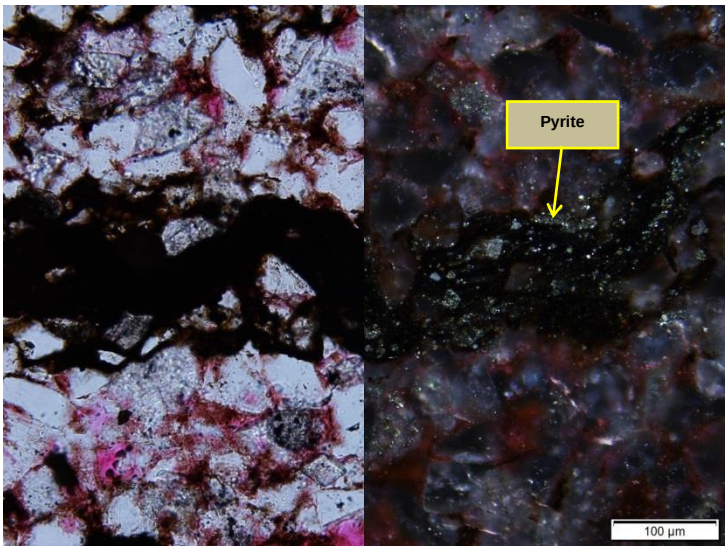


Fig. 5-9: Photomicrograph in PPL (left) and reflected light (right) detailing an opaque-rich lamination (clays, pyrite and organics), which is deformed due to compaction. Within the reflected light image, pyrite idiomorphs (gold colour; estimated at ~3%) are dispersed within the lamination. Note intergranular porosity above and below the lamination (pink epoxy).

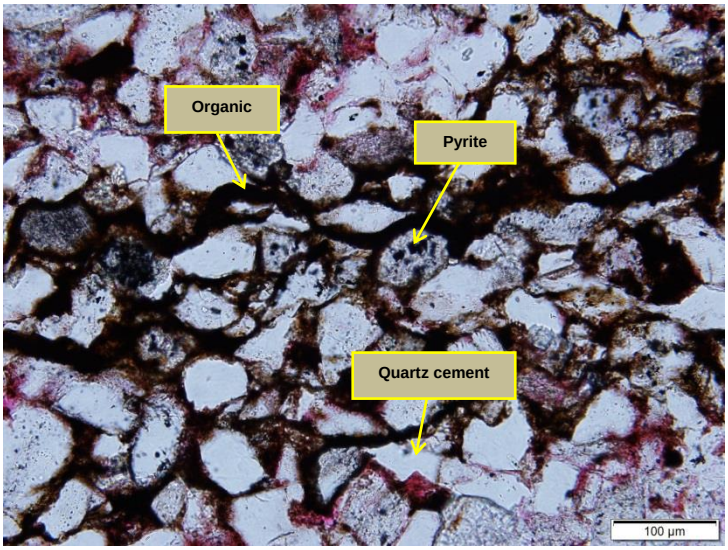


Fig. 5-10: Photomicrograph in PPL showing opaque material, both finely dispersed and interfingering between grains and cements. Opaque material may accumulate along trails or form clusters, which are possibly fecal derived. Some pyrite may occur as inclusions. Note a quartz particle with pyrite inclusions.

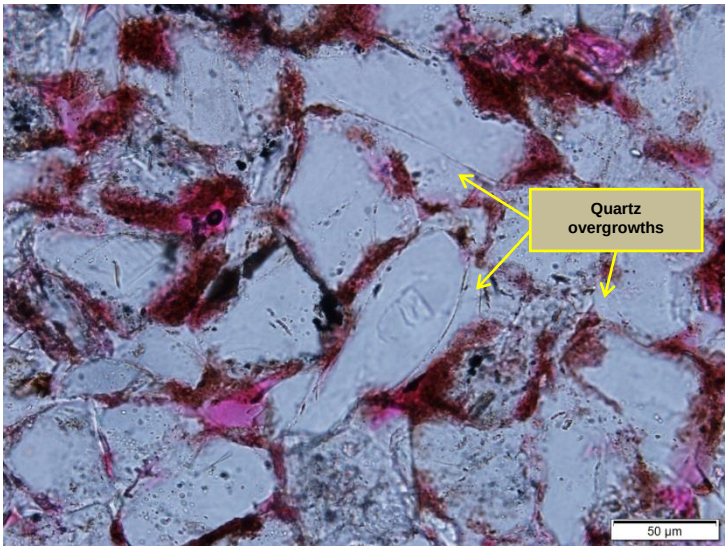


Fig. 5-11: Photomicrograph in PPL showing abundant quartz overgrowths that have reduced pore space and pore throat sizes. Dust rims separate quartz overgrowths from the original detrital grains.

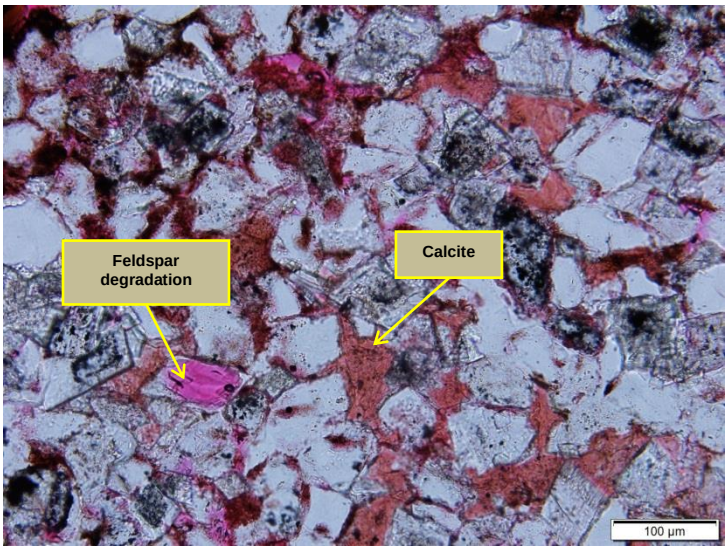


Fig. 5-12: Photomicrograph in PPL illustrating secondary calcite cement (red/pink stained). Calcite cement is patchy and is estimated at ~2% of the total composition. Calcite appears to be a relatively late diagenetic phase. Some degraded feldspar grains are observed, some of which contain diagenetic cements.

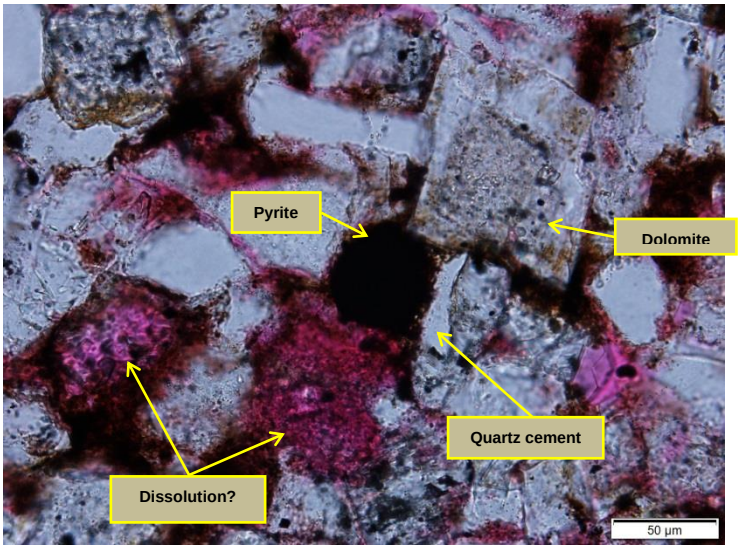


Fig. 5-13: Photomicrograph in PPL detailing a dolomite rhomb (~100 µm in size), which exhibits a “dirty” surface and clean overgrowth phase. Some clay material (brown) is observed coating and rimming dolomite in the image. Note a cluster of pyrite (fecal derived?) in the centre of the image.

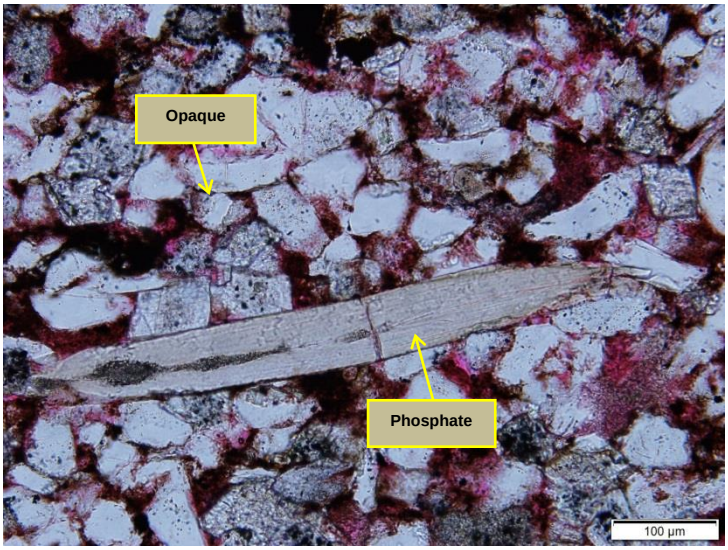


Fig. 5-14: Photomicrograph in PPL illustrating a rare phosphatic fragment (~590 µm in length), which may be remnant bone material.

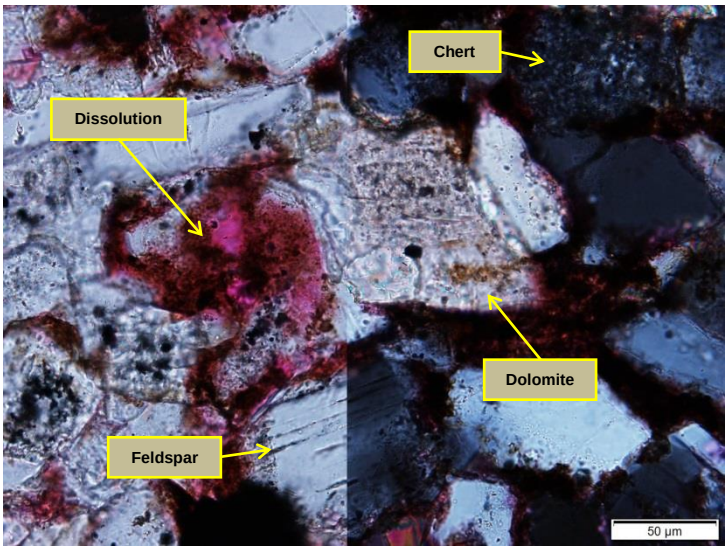


Fig. 5-15: Photomicrograph in PPL (left) and XPL (right) showing a feldspar grain (bottom centre) exhibiting slight twinning as well as a feldspathic overgrowth. The centre of the image shows a dolomite rhomb (dull birefringence in XPL) with a poorly formed overgrowth that is adjacent to a grain (feldspar?) that has been almost completely dissolved. Pyrite occurs within some of the secondary dolomite. Grain disolution generates secondary porosity. A rare microcrystalline chert grain is also present (top right).

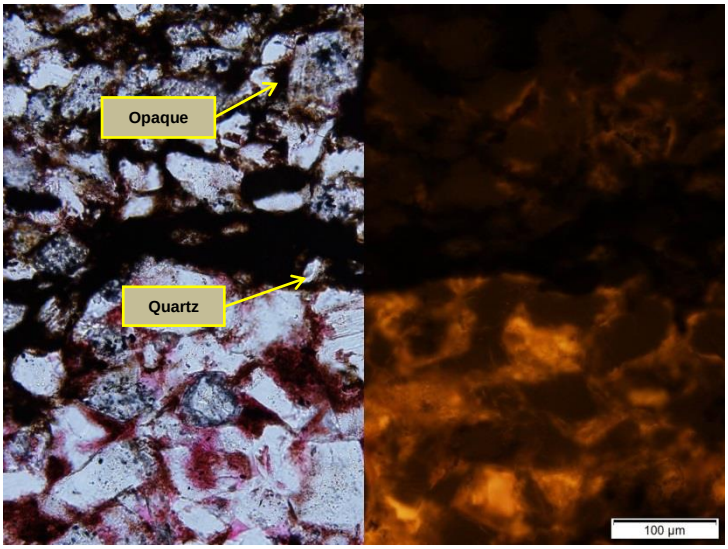


Fig. 5-16: Photomicrograph in PPL (left) and UV-light (right) detailing a reduction in porosity (pink epoxy) observed within the more dolomitic, opaque-rich laminae shown in the top half of the image. Note quartz grains entrained within the thin, opaque-rich lamination.

5.2.2 SAMPLE 13041

Sample ID	**13041**		
Sample Type	**Core**	**UWI/Well**	**100/01-03-002-20W4/00**
Strat. Unit	**Banff**	**Depth**	**1524.90 m**

XRD results

Quartz (%)	Feldspar (%)	Calcite (%)	Dolomite/ankerite (%)	Clays (%)
23.2	9.7	46.2	16.5	3.4

Pyrite (%)
0.8

Composition (*in order of abundance*)

	%	Variety (%)	Variety (%)	Variety (%)	Variety (%)
Cement (spar)	25	Dolomite (98)	Calcite (2)		
Cement (micrite)	40	Micrite (100)			
Clay	0				
Other grains	30	Quartz (96)	Glauconite (3)	Feldspar (1)	
Opaques	5	Pyrite (100)			
Organics	<1	Amorphous (100)			
	100				

Allochems	40	Bivalve shells (95)	Phosphatic material (2)	Bryozoan debris (2)	Brachiopod spines (<1)
Matrix	60	Micrite (100)			
Porosity	0				
	100				

Sedimentary structures

Primary	None apparent.
Biogenic	Several mm-scale burrow structures and areas of apparently bioturbated sediment occur in the rock.

Fractures	None apparent.
Porosity	None apparent.
Opaques	Pyrite is abundant throughout the sample, and occurs as common finely dispersed crystals, µm-(common) to mm-scale (rare) "streaks", and rare 300-500 µm ovate particles.
Organics	Rare (<1%) organic matter strands.
Diagenetic	Euhedral to subhedral dolomite (common) and calcite (rare) crystals occur throughout the rock.

Bioclasts *(in order of abundance)*

Type	*Size (µm)*	*Preservation*	*Recrystallisation*
Bivalve shells	Up to 850 µm	Fragmental	Complete recrystallization
Phosphatic material	Up to 250 µm	Fragmental	N/A
Bryozoan debris	Up to 350 µm	Fragmental	Complete recrystallization
Brachiopod spines	58 µm	Cross-section	Partially recrystallized

Description

Sample 13041 is a silica-rich wackestone. The texture of the sample is mainly characterized by abundant micrite, supporting common quartz grains, and fragmentary bivalve shells. Several mm-scale burrow structures and areas of possible bioturbated sediment occur in the rock, which otherwise appears to lack original sedimentary structures. Formation of euhedral dolomite appears to be the main diagenetic process that occurred in the rock.

Rock Classification

Silica-rich wackestone (Dunham, 1962).

Thin Section Quality

Good. 1/2 stained for carbonates.

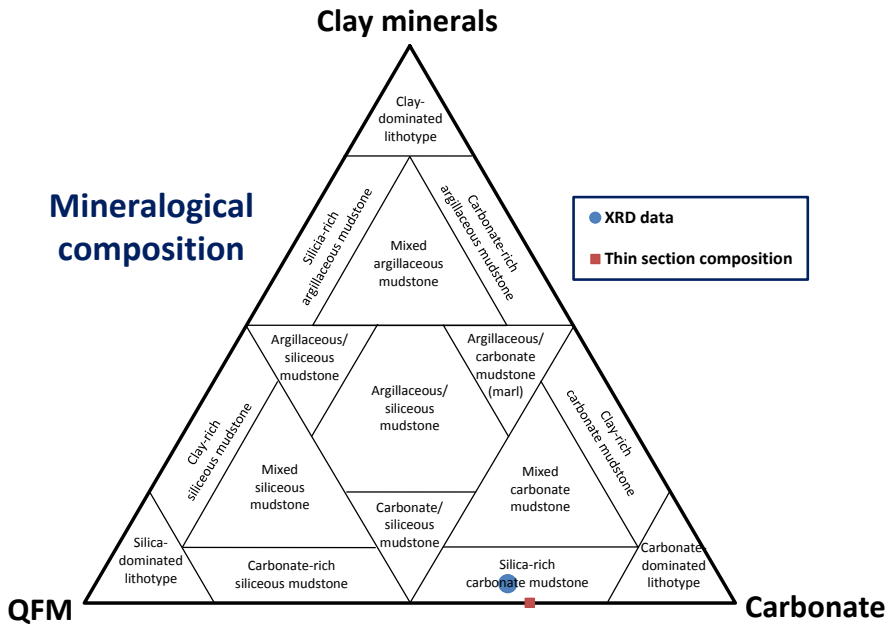


Fig. 5-17: Ternary plot of the mineralogical composition of the carbonate rock according to XRD data (blue) and estimated thin section composition (red). According to this scheme, sample 13041 is classified as a silica-rich carbonate mudstone. Using a classification scheme based on depositional texture, sample 13041 is classified as a silica-rich wackestone (Dunham, 1962).

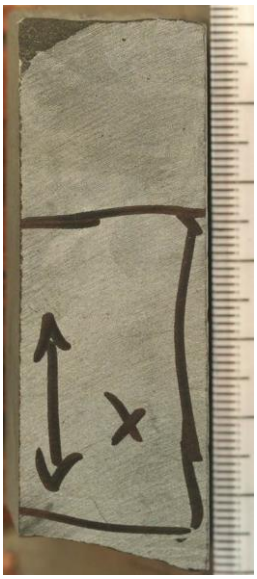


Fig. 5-18: Core photograph of sample 13041 from the Banff Formation, well 100/01-03-002-20W4/00 (depth 1524.90 m). The thin section prepared from this sample was cut from the area marked with an X. The sample was received with no way-up direction. Scale is in mm.

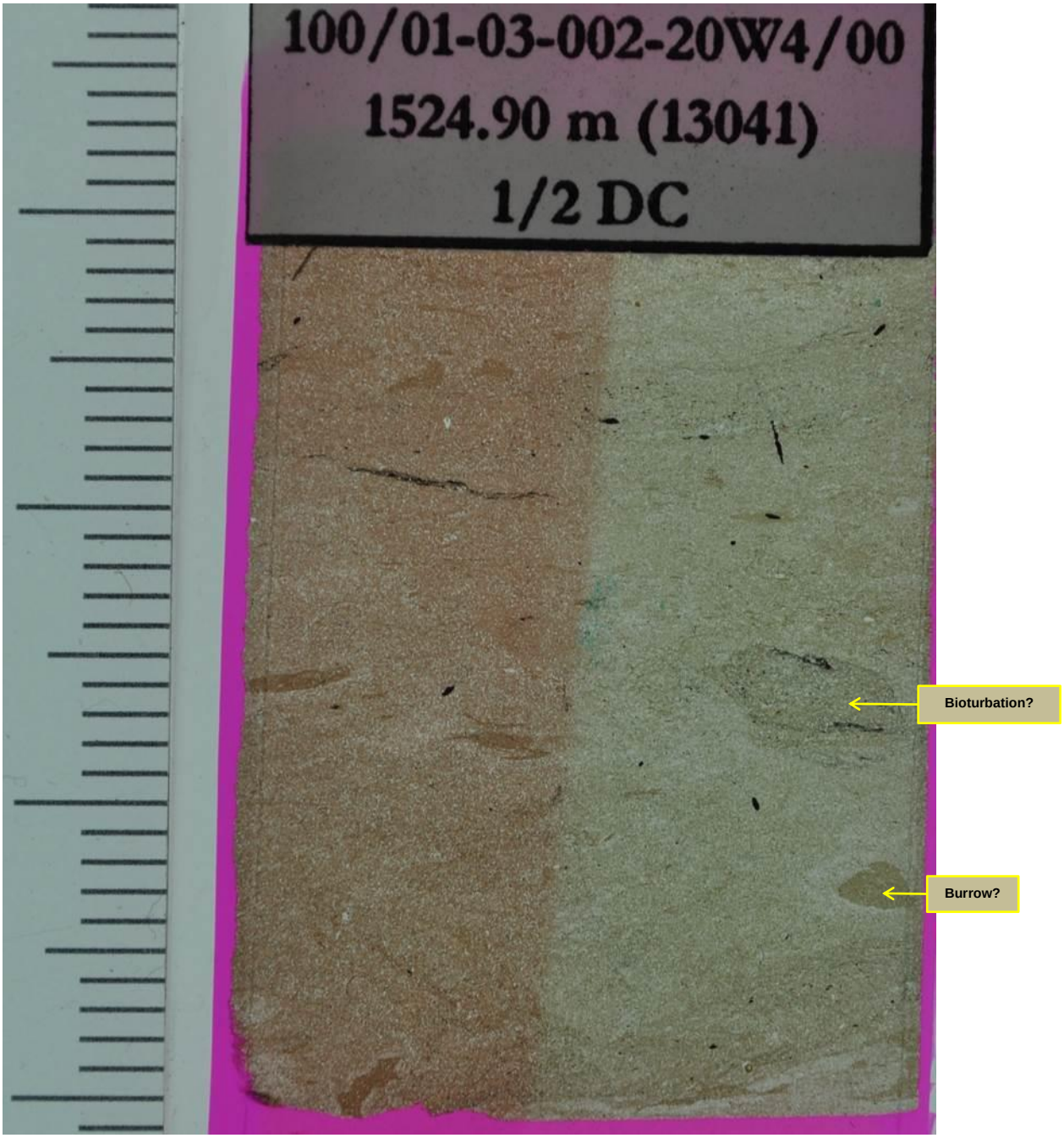


Fig. 5-19: Thin section photograph of sample 13041 from the Banff Formation, well 100/01-03-002-20W4/00 (depth 1524.90 m). The sample is a silica-rich wackestone. The sample mostly lacks distinct sedimentary structures with the exception of several mm-scale burrow structures and areas of possible bioturbated sediment. Scale is in mm.

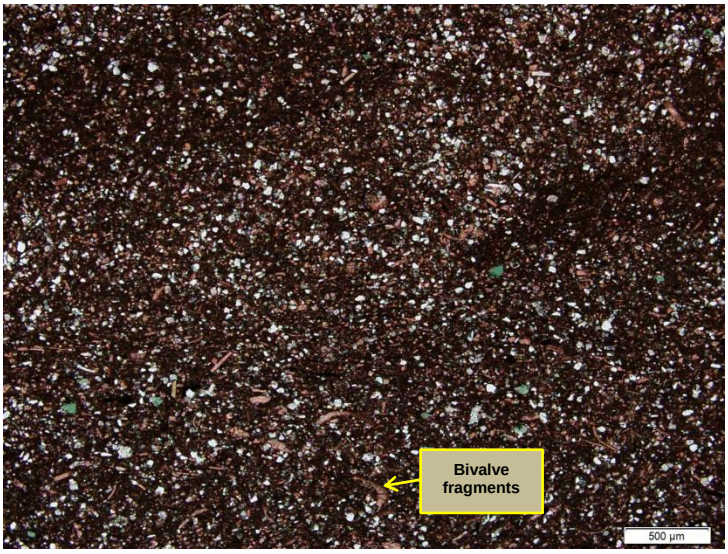


Fig. 5-20: Photomicrograph in PPL showing an overview of the sample, classified as a silica-rich wackestone. This image shows the half of the sample that is stained for carbonates, in which particles composed of calcite appear red. Quartz (~28%), dolomite (~24%), and feldspar (<1%) comprise the light-colored grains present in the stained portion of the sample.

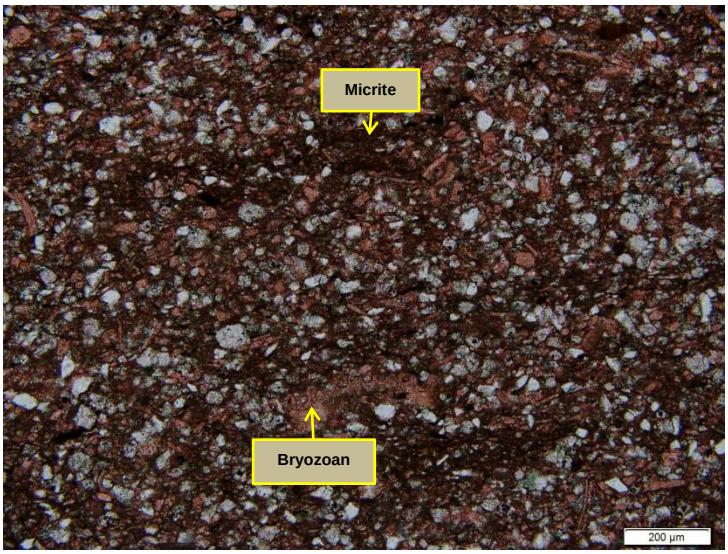


Fig. 5-21: Photomicrograph in PPL illustrating the texture of the sample. Micrite is predominant and comprises ~40% of the total composition. The sample lacks articulated fossil material, likely indicating an allochthonous origin.

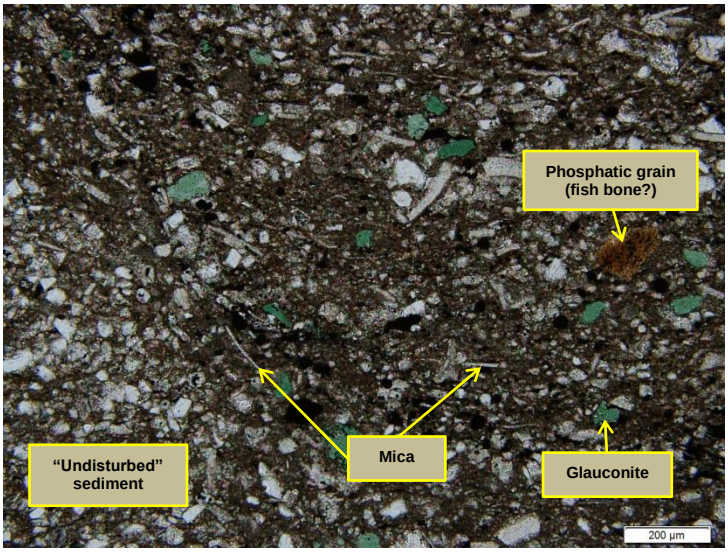


Fig. 5-22: Photomicrograph in PPL showing a section of bioturbated sediment (right side of image) observed in the wackestone. Glauconite grains are abundant within this area of the sample. Glauconite is present as green coloured, silt- to very fine sand-sized grains, which are occasionally deformed due to compaction. A rare phosphatic grain or fragment (fish bone?) is observed. Note variable orientation of the mica lathes.

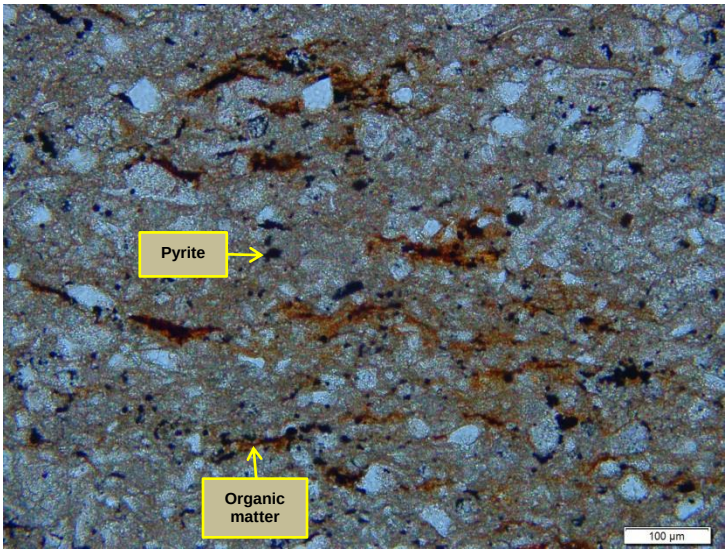


Fig. 5-23: Photomicrograph in HDR (high dynamic range) PPL showing common finely dispersed pyrite (opaque; estimated at ~5%) and rare organic matter strands, wisps and blebs (dark-brown/reddish colour; estimated at <1%) observed in the wackestone.

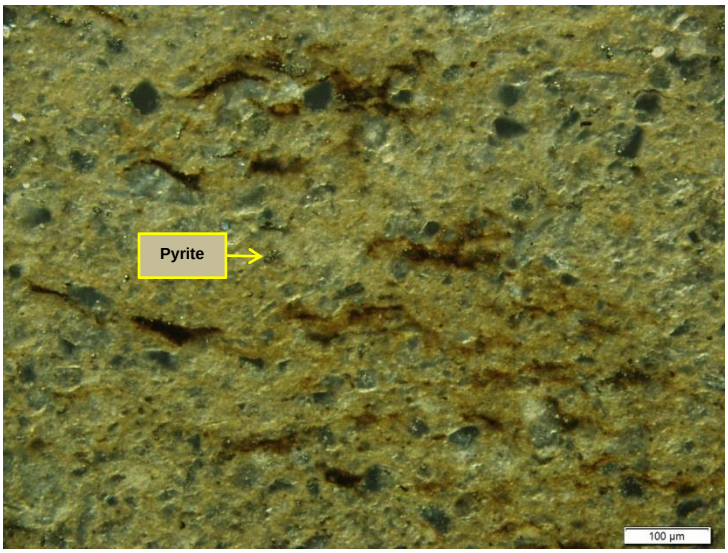


Fig. 5-24: Photomicrograph of Figure 5-23 in reflected light highlighting finely dispersed pyrite (gold colour) and rare organic matter in the wackestone.

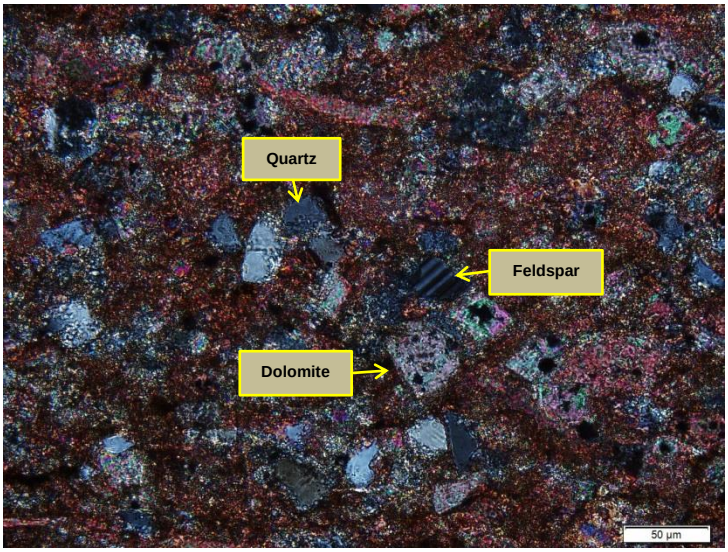


Fig. 5-25: Photomicrograph in XPL showing quartz (~28%), dolomite (~24%), and feldspar (<1%) observed in the sample. X-ray diffraction analysis indicates that feldspars comprise 10% of the total composition. Since few twinned or altered feldspar grains are visible in the sample, petrographic analysis likely underestimates the true amount of feldspar present. Note some dolomite rhombs up to ~50 µm in size.

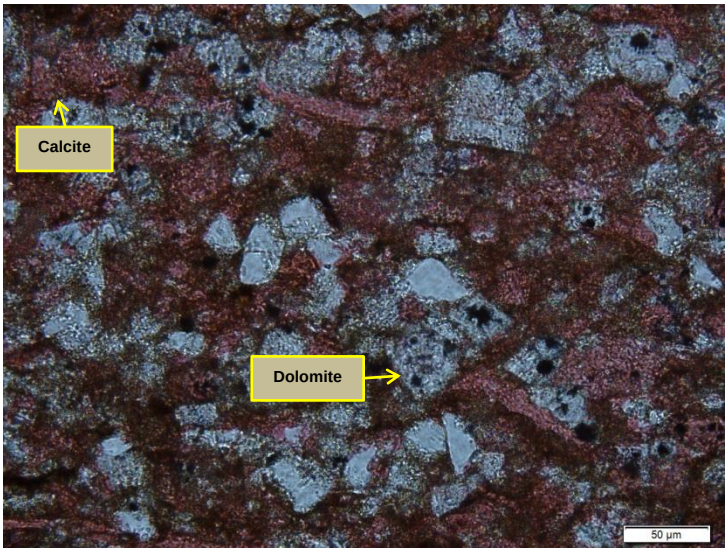


Fig. 5-26: Photomicrograph of Figure 5-25 in PPL showing rare subhedral to euhedral dolomite crystals observed in the wackestone. Pyrite inclusions within the secondary dolomite illustrates that initial dolomite with euhedral habit dissolved and microcrystalline dolomite precipitated within the open pore space.

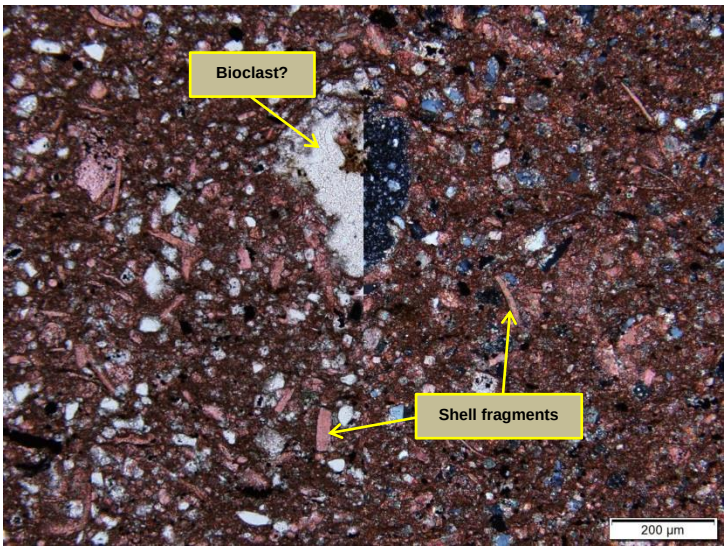


Fig. 5-27: Photomicrograph in PPL (left) and XPL (right) showing a possible bioclast or shell fragment (~325 µm in size), which has been replaced with chert. Note abundant calcareous shell debris in the micritic matrix.

5.2.3 SAMPLE 13044

Sample ID	**13044**		
Sample type	**Core**	**UWI/Well**	**100/01-03-002-20W4/00**
Strat. Unit	**Banff Formation**	**Depth**	**1532.10 m**

XRD/SRA results

Quartz (%)	Fsp (%)	Cb (%)	Clays (%)	Pyrite (%)
61.5	15.8	16.2	5.9	0.5

Composition (*in order of abundance*)

Grain size	%	Variety (%)	Variety (%)	Variety (%)	Variety (%)
sand	50	Quartz (90)	Feldspar (10)		
silt	30	Quartz (100)			
clay	<2	Clay mins (100)			
Cement	18	Dolomite (90)	Feldspar (8)	Quartz (2)	
Bioclasts	0				
Organics	0				
Opaques	2	Pyrite (100)			
	100				

*Intensively altered to clay minerals

^ Including bitumen

Sedimentary structures

Primary	None apparent.
Biogenic	None apparent.

Fractures	None apparent.
Porosity	10-15% intergranular porosity.

Description

Silty subarkose comprised of subrounded (common) to angular (rare) fine silt- to very fine sand-sized (average grain size is very fine sand) detrital quartz (50-65%) and feldspar (6-10%). The sandstone is cemented by dolomite, feldspar (overgrowth and intergranular cements), and quartz (overgrowth cement). 10-15% intergranular porosity is observed throughout the sample.

Thin Section Quality

Good. 1/2 stained for carbonates.

Rock Classification

Silty sandstone.

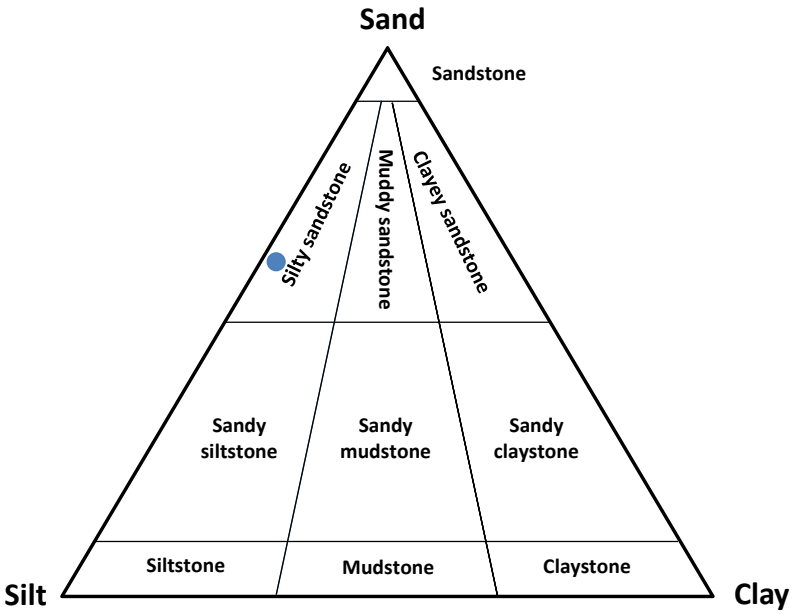


Fig. 5-28: Ternary plot showing the grain size composition of the sample based on the Wentworth scale (after Folk, 1954). Sample 13044 is classified as a silty sandstone.

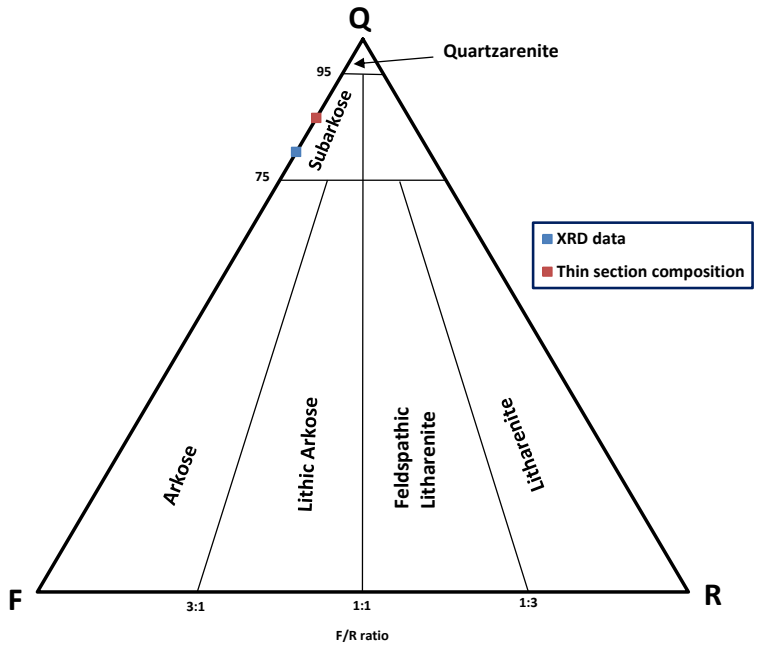


Fig. 5-29: Ternary plot showing the relative abundance of different detrital grains within the sandstone. Sample 13044 is classified as a subarkose due to the abundance of quartz and feldspar.

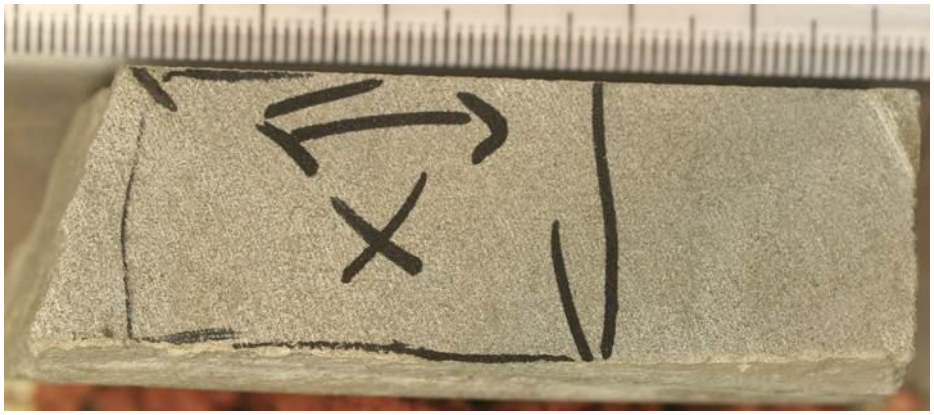


Fig. 5-30: Core photograph of sample 13044 from the Banff Formation, well 100/01-03-002-20W4/00 (depth 1532.10 m). The thin section prepared from this sample was cut from the area marked with an X. The sample was received with no way-up direction.

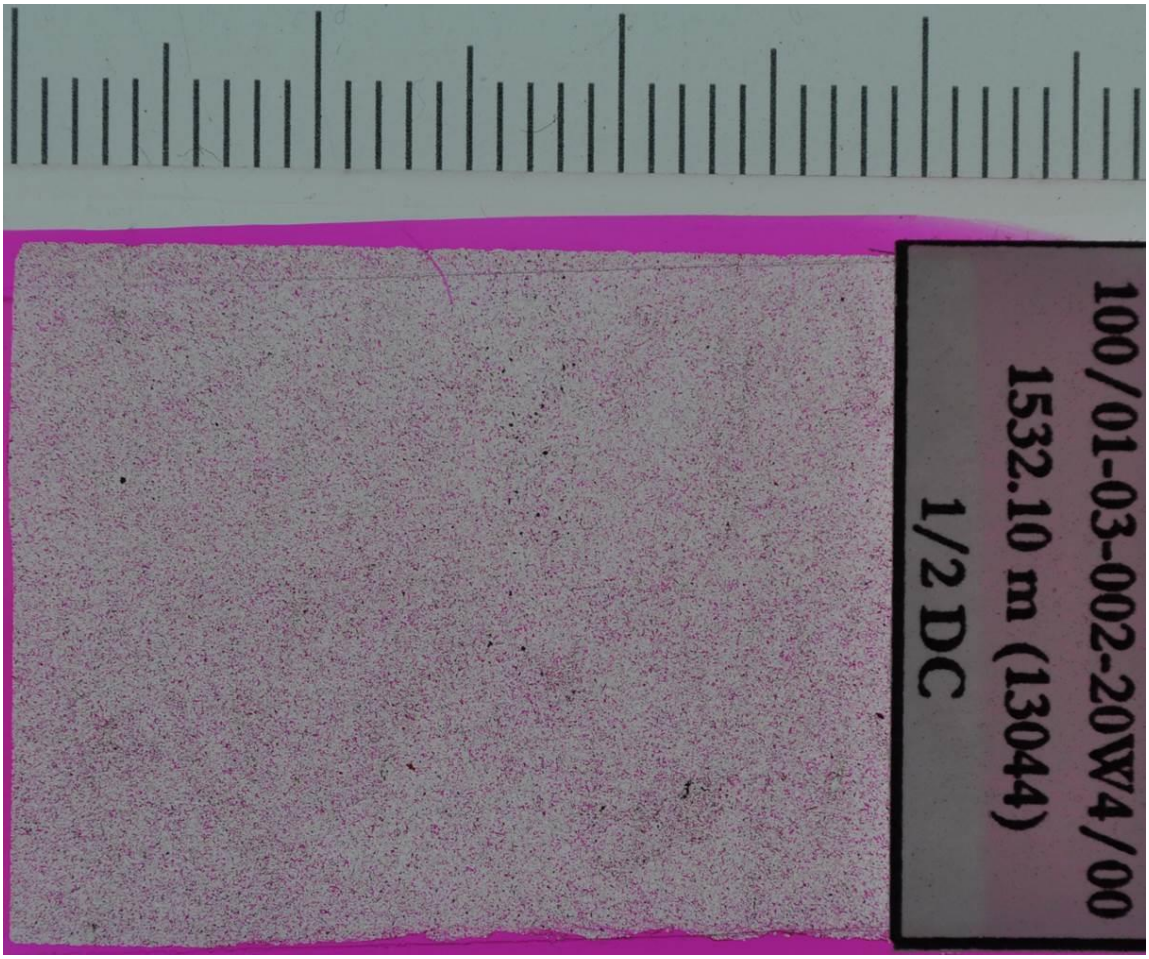


Fig. 5-31: Thin section photograph of sample 13044 from the Banff Formation, well 100/01-03-002-20W4/00 (depth 1532.10 m). The sample is a silty sandstone. The sandstone is unstratified and lacks identifiable primary sedimentary structures.

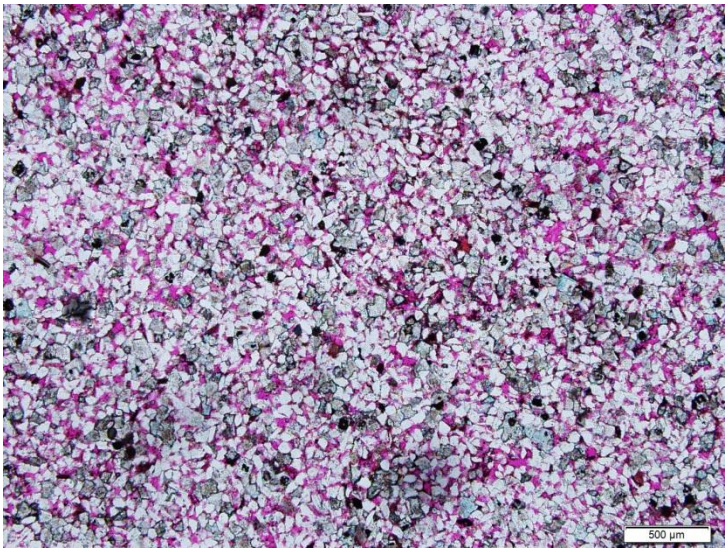


Fig. 5-32: Photomicrograph in PPL showing an overview of the silty subarkose sandstone, which appears to lack primary sedimentary structures. Light-coloured minerals consist of quartz and feldspar, with the grey minerals consisting of dolomite.

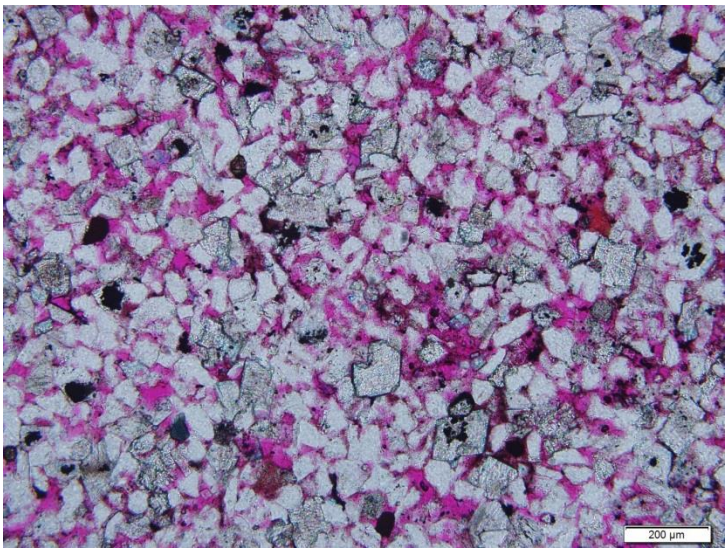


Fig. 5-33: Photomicrograph in PPL showing 10-15% intergranular porosity (pink epoxy) observed throughout the sample. Despite extensive secondary cementation, the sample shows well connected pore throats.

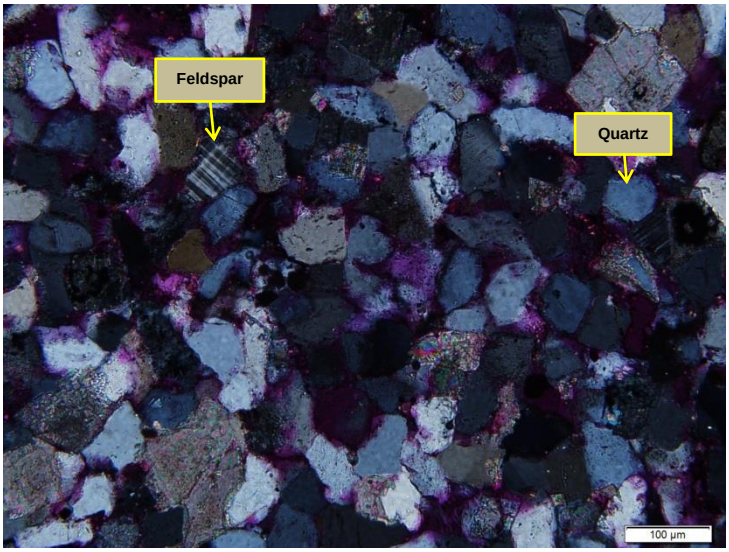


Fig. 5-34: Photomicrograph in XPL showing angular (rare) to subrounded, fine silt- to very fine sand-sized (average grain size is very fine sand) detrital quartz (50-65%) and feldspar (6-10%). Note “tartan-twinning” associated with some feldspars.

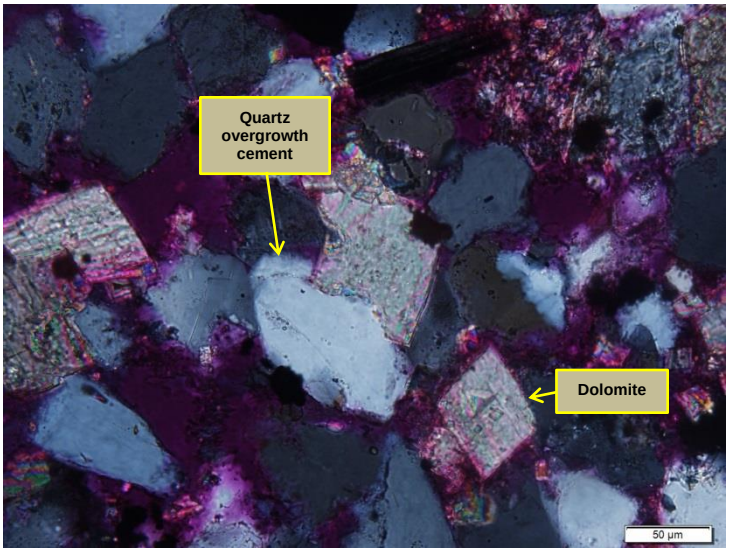


Fig. 5-35: Photomicrograph in XPL showing dolomite and quartz cements observed in the sample. Dolomite cement (~90% of all cements) occurs as euhedral to subhedral (rare) pore-filling crystals or rhombs, whereas quartz cement (~2%) occurs as anhedral to euhedral overgrowths. Dolomite has a dull birefringent colour. The remainder of the cement present in the sample is composed of secondary feldspar.

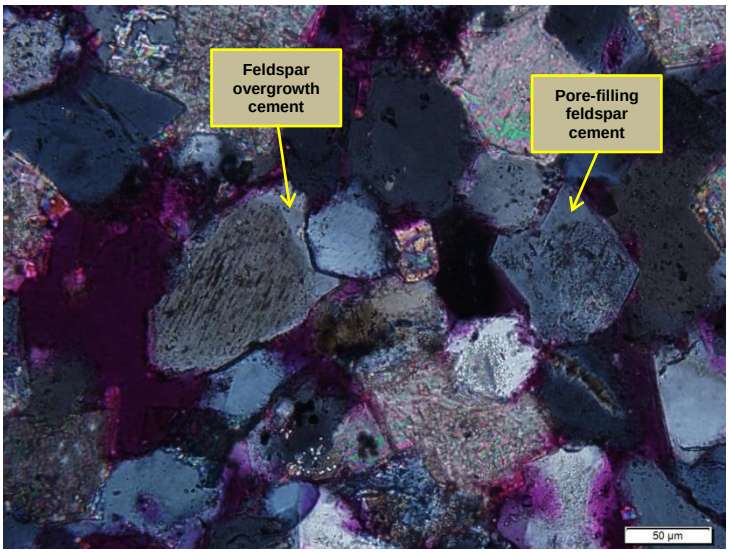


Fig. 5-36: Photomicrograph in XPL showing feldspar cements, which occur as both pore-filling and overgrowth cements. Feldspar is the second most abundant (~8%) type of cement observed in the sample.

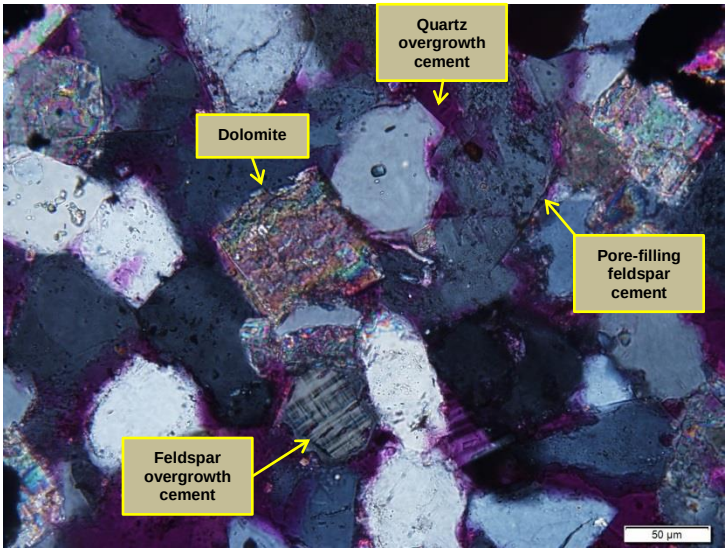


Fig. 5-37: Photomicrograph in XPL showing an overview of diagenetic features observed in the sample, with at least four identified, including: dolomite cementation, feldspar overgrowths, pore-filling feldspar cementation, and quartz overgrowths.

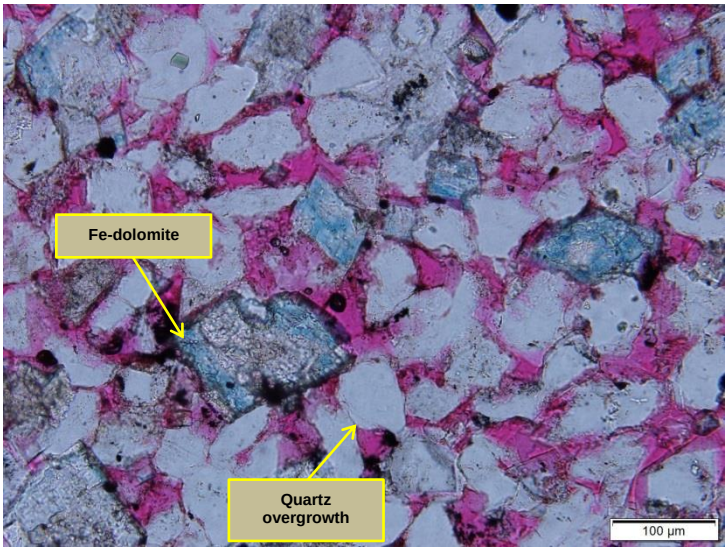


Fig. 5-38: Photomicrograph in PPL showing several dolomite rhombs exhibiting partial blue staining, indicating the presence of iron. In many cases Fe-dolomite occurs as rims around earlier crystals. Note occasional quartz overgrowths.

5.2.4 SAMPLE 13822

Sample ID	**13822**		
Sample Type	**Core**	**UWI/Well**	**102/08-07-075-05W5/00**
Strat. Unit	**Banff**	**Depth**	**1077.30 m**

XRD results

Quartz (%)	Feldspar (%)	Calcite (%)	Dolomite/ankerite (%)	Clays (%)
21.3	4	59.7	4.1	7.9

Pyrite (%)
2.9

Composition (*in order of abundance*)

	%	Variety (%)	Variety (%)	Variety (%)	Variety (%)
Cement (spar)	60	Calcite (100)			
Cement (micrite)	0				
Clay	8	Clay mins* (100)			
Detrital grains	16	Quartz (99)	Feldspar (<1)		
Opaques	6	Pyrite (100)			
Organics	10	Amorphous (100)			
	100				

** Based on XRD data*

Allochems	2	Sponge spicules (100)			
Matrix	98	Clay* (100)			
Porosity	<1	Sponge spicules (100)			
	100				

** Based on XRD data*

Sedimentary structures

Primary	Alternating sparry calcite and organic-rich mixed siliceous/calcareous compositional laminae.
Biogenic	One possible burrow structure (replaced by sparry calcite).

Fractures	Several large partings, and common thin epoxy-filled fractures. Likely artificial.
Porosity	Rare intragranular porosity in sponge spicules with uncemented central canals (3-5 µm pores). Apparent microporosity is observed in association with fractures.
Opaques	Finely dispersed (most common in organic-rich laminae) and framboidal (most common in sparry calcite laminae) pyrite accounts for ~6% of the rock.
Organics	Common stringers of bedding-parallel organic matter in mixed siliceous/calcareous laminae. Possible plant detritus occurs in both sparry calcite and mixed siliceous/calcareous laminae.
Diagenetic	Calcite spar accounts for ~65% of the sample, and forms distinct compositional laminae in the rock.

Bioclasts *(in order of abundance)*

Type	*Size (µm)*	*Preservation*	*Recrystallisation*
Sponge spicules	30 x 195 µm	Good	N/A

Description

Silica-rich carbonate mudstone comprised of alternating sparry calcite and organic-rich mixed siliceous/calcareous compositional laminae. Sparry calcite layers account for ~60% of the rock, and contain ~5-10% detrital quartz. Mixed siliceous/calcareous laminae contain ~15-20% organic matter, and ~20% quartz.

Rock Classification

Silica-rich carbonate mudstone.

Thin Section Quality

Good.

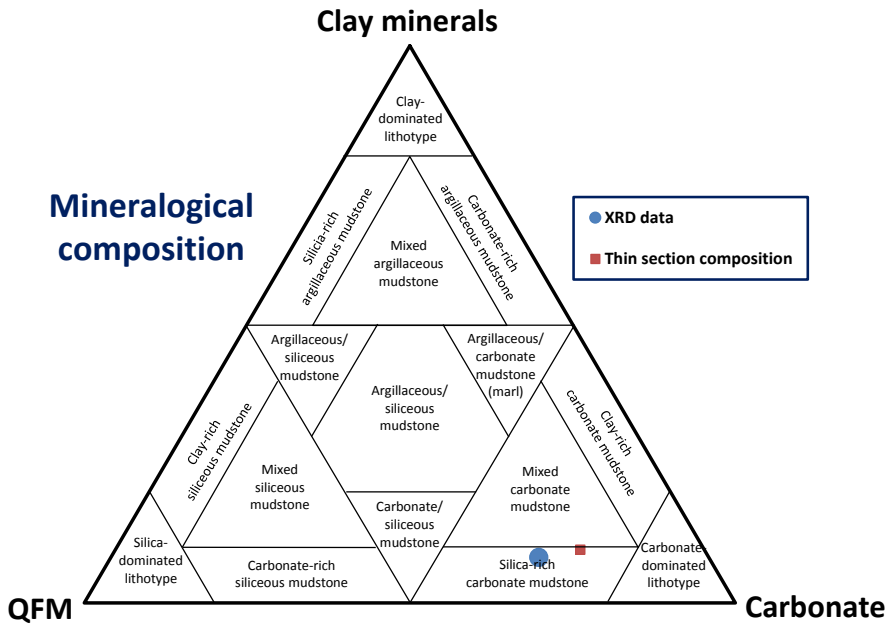


Fig. 5-39: Ternary plot of the mineralogical composition of the carbonate rock according to XRD data (blue) and estimated thin section composition (red). Sample 13822 is classified as a silica-rich carbonate mudstone.



Fig. 5-40: Core photograph of sample 13822 from the Banff Formation, well 102/08-07-075-05W5/00 (depth 1016.32 m). The thin section prepared from this sample was cut from the face shown in this image. The sample was received with no way-up direction. Scale is in mm.

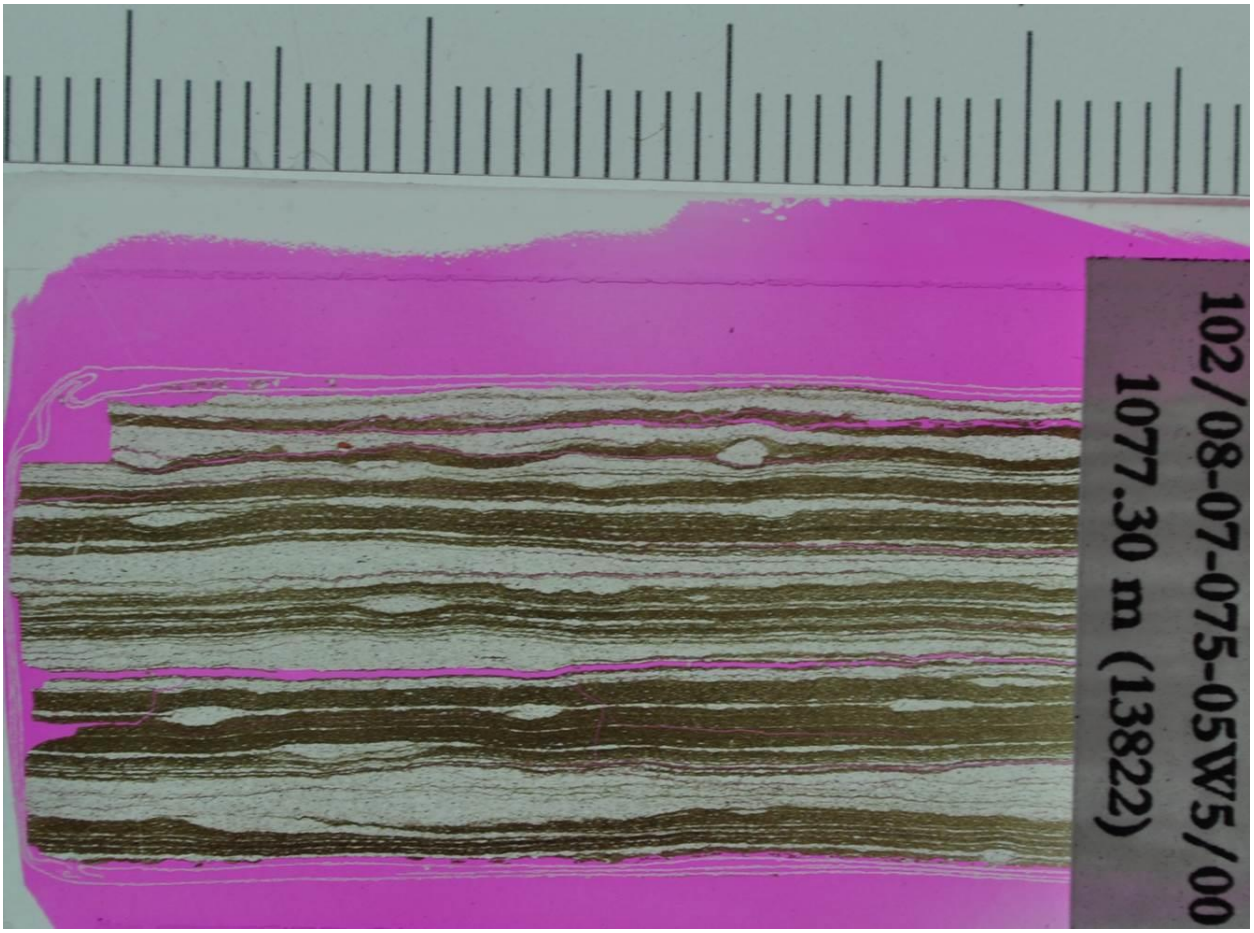


Fig. 5-41: Thin section photograph of sample 13822 from the Banff Formation, well 102/08-07-075-05/00 (depth 1077.30 m). The sample is a silica-rich carbonate mudstone, characterized by alternating sparry calcite and organic-rich mixed siliceous/calcareous laminae. Scale is in mm.

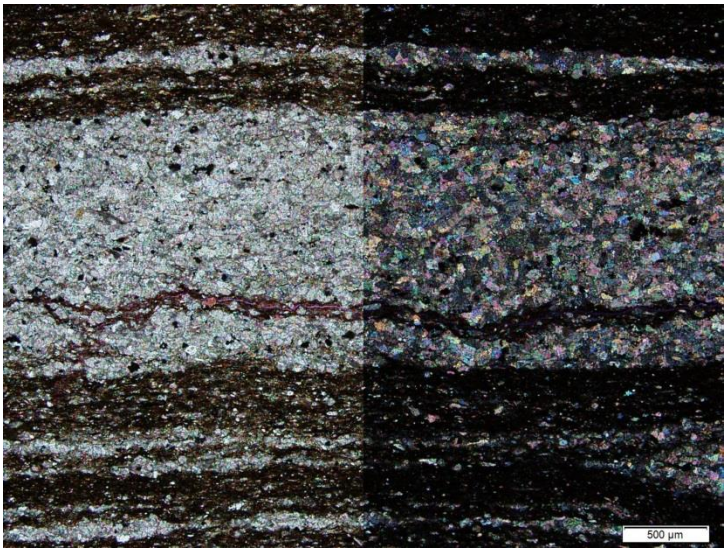


Fig. 5-42: Photomicrograph (left half in PPL, right half in XPL) showing an overview of alternating sparry calcite (light-coloured) and organic-rich mixed siliceous/calcareous (dark-coloured) laminae that characterize the sample, which is classified as a silica-rich carbonate mudstone.

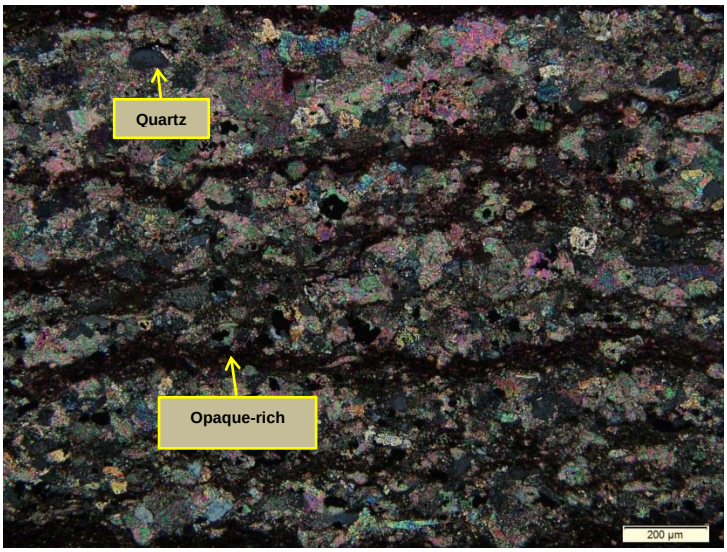


Fig. 5-43: Photomicrograph in XPL detailing a sparry calcite lamination, which contains interbedded opaque-rich streaks. These laminae account for ~60% of the sample. Silt-size detrital quartz grains comprise ~5-10% of these laminae.

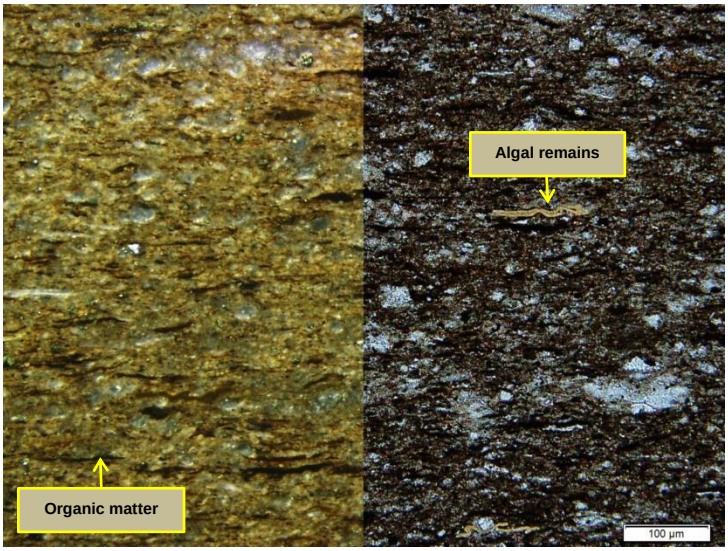


Fig. 5-44: Photomicrograph (left half in reflected light, right half in PPL) showing an organic-rich mixed siliceous/calcarous lamination, which contains elongate, bedding-parallel organic strands and algal remains. Small amounts of phosphate also occurs around some of the strands.

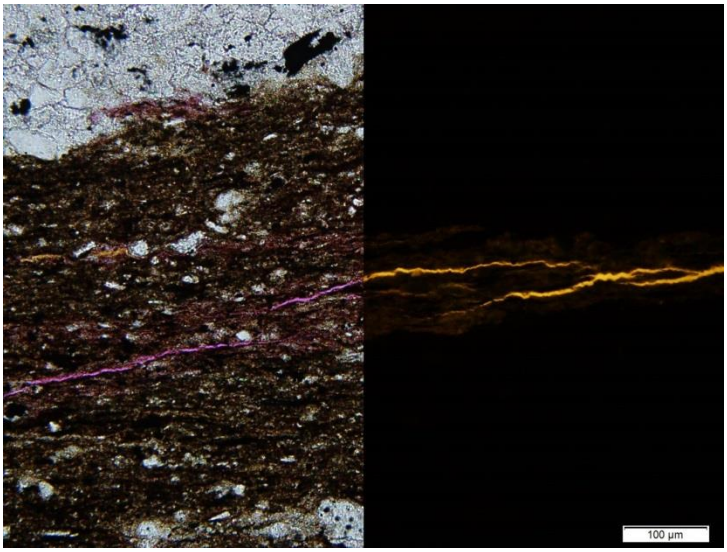


Fig. 5-45: Photomicrograph (left half in PPL, right half in UV light) showing a typical example of thin, possibly artificial, epoxy-filled fractures commonly observed in the sample. Thin section epoxy is observed to “bleed” through material surrounding these fractures, creating apparent microporosity.

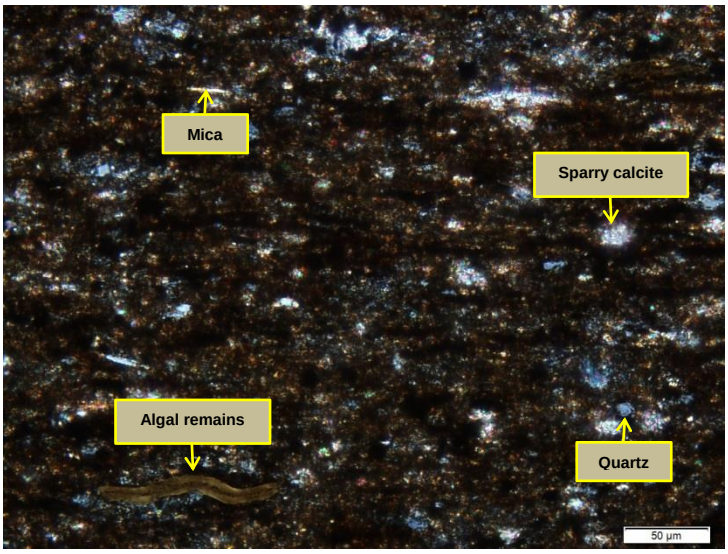


Fig. 5-46: Photomicrograph in XPL (slightly overexposed) detailing an organic-rich mixed siliceous/calcareous lamination. Clay- to fine silt-sized quartz particles are abundant in these laminae, accounting for ~20% of the composition. Some short mica lathes are observed and are oriented parallel to bedding.

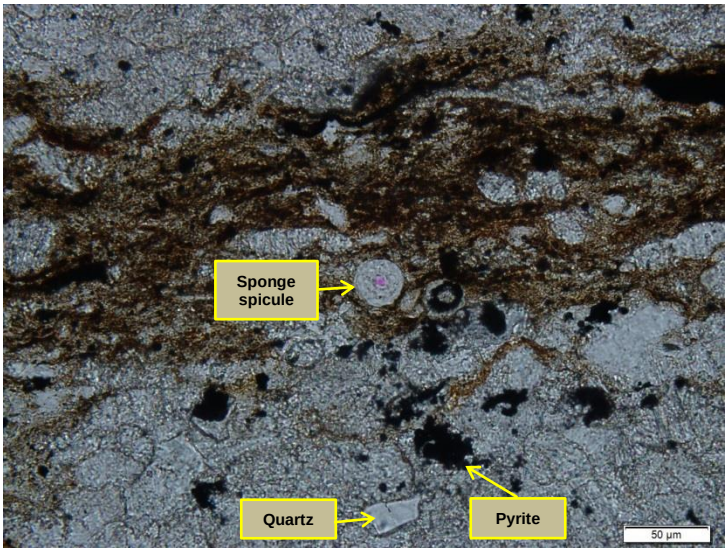


Fig. 5-47: Photomicrograph in PPL illustrating a siliceous sponge spicule with a rare uncemented central canal (pink epoxy) set at the edge of a clay-rich lamination bound between calcareous laminae. The porous canal measures ~5 µm in diameter. Note pyrite (opaque) occuring as dispersed framboids and occasionally forming clusters.

6. Exshaw Formation Overview

This chapter presents a petrographic analysis of seven core samples from six wells of the Exshaw Formation (see Table 6-A). Core samples were cut into small blocks, and impregnated using rhodamine-B epoxy (pink) in order to identify porosity and fractures using UV fluorescence. Half of each slide was stained for carbonates. The following summary focuses on observations of rock compositional variability (i.e., lithofacies groupings), and provides photomicrographs of the most common depositional and bioturbation structures, diagenetic features, clay and organic matter distributions, and the occurrence of porosity and fractures. Several lithofacies were identified (Table 6-B) and the mineralogical XRD data for each lithofacies was averaged in order to determine common compositional parameters (Table 6-C).

6.1 SUMMARY

6.1.1 CORE SAMPLES:

Well Location	Depth m (Sample ID)
100/14-07-001-21W4/00	1945.2 (13032)
102/04-32-003-17W4/00	1327.0 (13035)
100/01-03-002-20W4/00	1536.8 (13048), 1541.7 (13184)
100/16-06-010-22W4/00	1870.3 (13190)
102/14-10-007-19W4/00	1441.2 (13193)
102/10-07-077-04W5/00	705.5 (13818)

Table 6-A: Well locations and core sample depths.

6.1.2 LITHOFACIES, GROUPINGS AND DESCRIPTIONS:

Well Location	Lithofacies	Depth m (Sample ID)
100/14-07-001-21W4/00	1	1945.2 (13032)
102/04-32-003-17W4/00	1	1327.0 (13035)
100/01-03-002-20W4/00	1	1536.8 (13048), 1541.7 (13184)
100/16-06-010-22W4/00	1	1870.3 (13190)
102/14-10-007-19W4/00	1	1441.2 (13193)
102/10-07-077-04W5/00	2	705.5 (13818)

Table 6-B: Lithofacies distribution by Well.

Lithofacies	Classification	Quartz/Chert %	Feldspar %	Calcite %	Dolomite %	Ankerite %	Clay/Mica %	Pyrite %
1	Siliceous dolostone	32.5	18.8	2.3	12.8	11.5	19.9	2.2
2	Muddy sandstone	14.0	35.8	14.0	0	3.5	4.8	24.6

Table 6-C: Average lithofacies composition, based on XRD data.

6.1.2.1 LITHOFACIES 1: FINELY CRYSTALLINE SILICEOUS/ SILICA-RICH DOLOSTONE

Samples 13032, 13035, 13048, 13184, 13190, and 13193 are classified as finely crystalline siliceous/silica-rich dolostones. Dolomite spar (and rarely lesser calcite spar) comprises ~30-50% of these samples, and forms a characteristic diagenetic fabric due to its common occurrence as euhedral to subhedral crystals. All of these samples contain >29% detrital grains, including abundant quartz, and lesser micas and feldspars. Clay material comprises 8-25% of the total composition of these samples.

6.1.2.2 LITHOFACIES 2: MUDDY SANDSTONE

Sample 13818 is classified as a muddy arkose sandstone. Coarse silt- to coarse sand-sized (average medium sand) detrital feldspar (30-50%) and quartz (10-15%) comprise the framework of this sample. Calcite, feldspar, and dolomite cements are observed and account for ~25% of the total composition. Clay material is a relatively minor (~8%) component of the sample.

6.1.3 SEDIMENTARY STRUCTURES & BIOTURBATION:

Few original sedimentary structures are visible in the samples. Elongate, clay-rich burrow structures are the only distinct sedimentary structures observed in all of the samples of Lithofacies 1. Sample 13818 (Lithofacies 2) contains minor clay minerals (see Figure 6.1.5-2) that occur concentrated in thin laminae visible in the core sample.

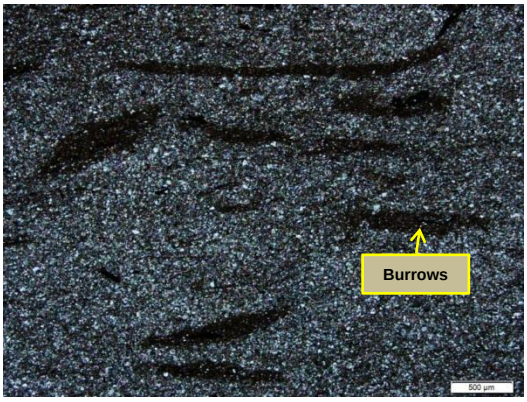


Fig. 6.1.3-1: Photomicrograph in PPL showing elongate, clay-rich burrow structures present in a finely crystalline siliceous dolostone. These burrows are common in samples of Lithofacies 1.

6.1.4 DIAGENESIS:

All of the samples belonging to Lithofacies 1 show a characteristic dolomitized fabric, in which the original depositional texture has been overprinted (i.e., nonmimic fabric) by subhedral (planar-s) to euhedral (planar-e) dolomite crystals. Sample 13818 shows a more complex diagenetic history, with at least four distinct processes observed.

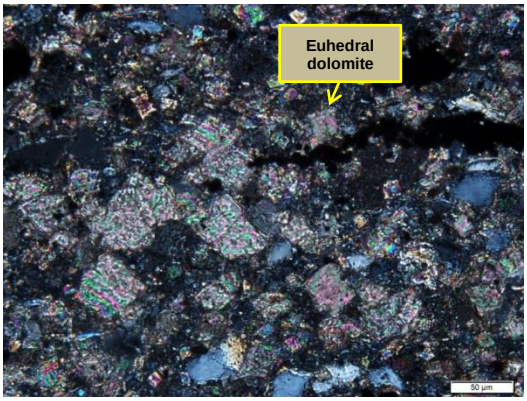


Fig. 6.1.4-1: Photomicrograph in XPL showing subhedral to euhedral dolomite cementation characteristic of finely crystalline siliceous dolostone samples.

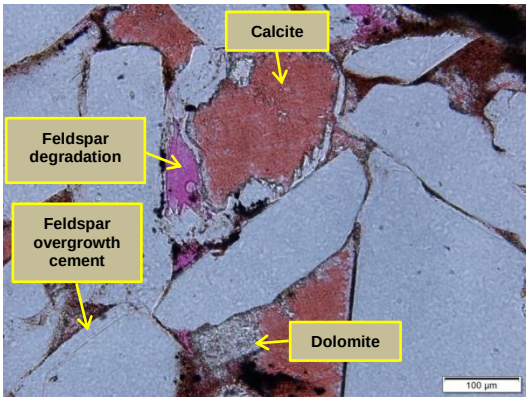


Fig. 6.1.4-2: Photomicrograph in PPL detailing diagenetic features observed in sample 13818. At least four diagenetic features are observed, including: partial feldspar degradation, feldspar overgrowth, dolomite and calcite cementation.

6.1.5 ORGANIC MATTER & CLAYS:

In Lithofacies 1, clay material occurs both within burrow structures (Figure 6.1.3-1) and as finely dispersed interstitial material surrounding larger siliceous and carbonate particles. Total clay content is difficult to estimate in these samples due to its finely dispersed texture, and overprinting by extensive secondary dolomitization. Minor clay material occurs in sample 13818, and corresponds to fine laminae visible in the core sample.

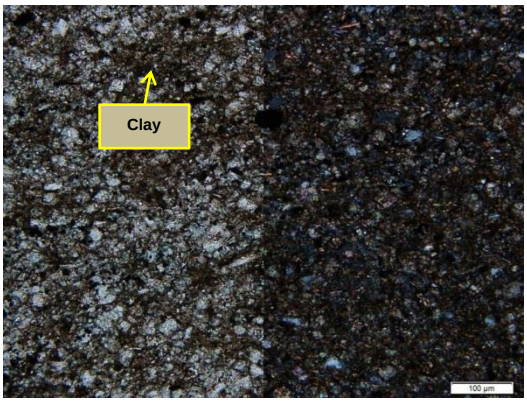


Fig. 6.1.5-1: Photomicrograph (left half in PPL, right half in XPL) illustrating finely dispersed interstitial clay typical of Lithofacies 1.

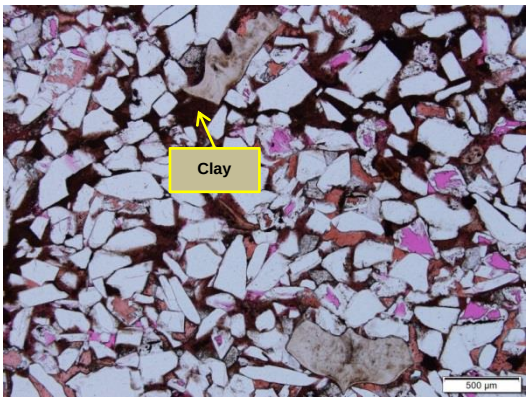


Fig. 6.1.5-2: Photomicrograph in PPL showing an area of elevated clay matrix observed in sample 13838. This area of the thin section corresponds to a faintly laminated interval.

6.1.6 POROSITY & FRACTURING:

With the exception of rare dissolution pores (possible moldic porosity) and possible thin micropores occurring along the boundaries of some carbonate crystals, no significant porosity is observed in Lithofacies 1. Common intragranular pores (due to feldspar degradation) and less prevalent intergranular pores (in areas poor in interstitial clay and carbonate cements) occur in sample 13818. Fractures are rare in both lithofacies, possibly due to heavy secondary cementation.

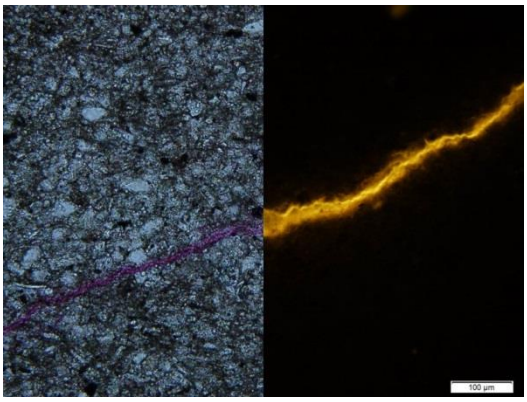


Fig. 6.1.6-1: Photomicrograph (left half in PPL, right half in UV light) showing a rare artificial fracture (filled with pink epoxy) present in a finely crystalline siliceous dolostone.

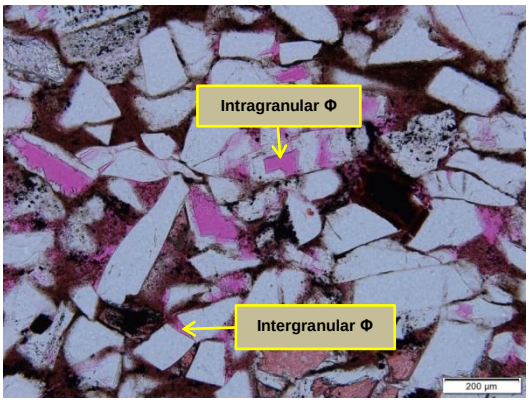


Fig. 6.1.6-2: Photomicrograph in PPL illustrating intra- and intergranular porosity in sample 13818. Intragranular porosity (6-8%) occurs in partially degraded feldspar grains. Minor (<3%) intergranular porosity occurs throughout the sample.

6.2 RESULTS

6.2.1 SAMPLE 13032

Sample ID	**13032**		
Sample Type	**Core**	**UWI/Well**	**100/14-07-001-21W4/00**
Strat. Unit	**Exshaw**	**Depth**	**1945.20 m**

XRD results

Quartz (%)	Feldspar (%)	Calcite (%)	Dolomite/ankerite (%)	Clays (%)
35.7	16.1	0	22.5	23.3

Pyrite (%)
2

Composition (*in order of abundance)*

	%	Variety (%)	Variety (%)	Variety (%)	Variety (%)
Cement (spar)	30	Dolomite (100)			
Cement (micrite)	0				
Clay	25	Clay minerals (100)			
Other grains	37	Quartz (98)	Mica (1)	Feldspar (1)	
Opaques	8	Pyrite (100)			
Organics	<1	Amorphous (100)			
	100				

Sedimentary structures

Primary	None apparent.
Biogenic	Common elongate clay streaks may represent burrow structures.

Fractures	Occasional thin, epoxy-filled fractures.
Porosity	None apparent.
Opaques	Pyrite is common throughout the rock, both as finely dispersed crystals (common) and large, irregular masses (rare).
Organics	Rare (<1%) amorphous organic particles.
Diagenetic	Heavily dolomitized, with nonmimic planar-e to planar-s fabric.

Description

Sample 13032 is a finely crystalline siliceous dolostone. Elongate clay streaks, possibly representing burrow structures, are the only original sedimentary features apparent in the sample. The rock is characterized by a nonmimic planar-e to planar-s dolomite fabric with no intergranular porosity. Pyrite is abundant throughout the rock, occurring as both finely dispersed crystals and large, irregular masses.

Rock Classification

Finely crystalline siliceous dolostone.

Thin Section Quality

Good. 1/2 stained for carbonates.

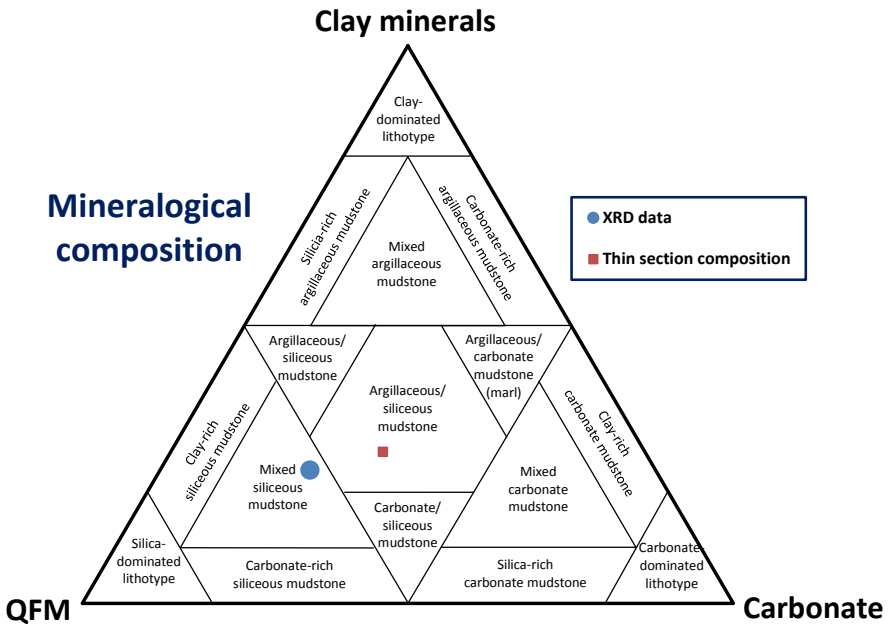


Fig. 6-1: Ternary plot of the mineralogical composition of the carbonate rock according to XRD data (blue) and estimated thin section composition (red). According to this scheme, sample 13035 is classified as an argillaceous/siliceous mudstone. Using a grain- and crystal-size classification scheme for crystalline carbonate rocks, sample 13032 is classified as a finely crystalline siliceous dolostone (Folk, 1962).

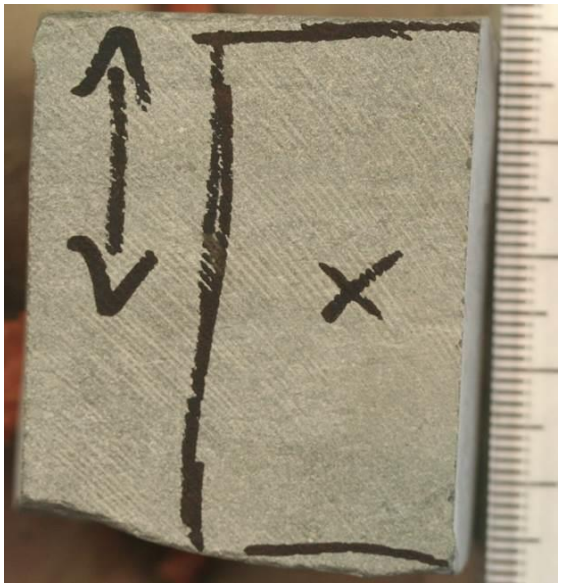


Fig. 6-2: Core photograph of sample 13032 from the Exshaw Formation, well 100/14-07-001-21W4/00 (depth 1945.20 m). The thin section prepared from this sample was cut from the area marked with an X. The sample was received with no way-up direction. Scale is in mm.

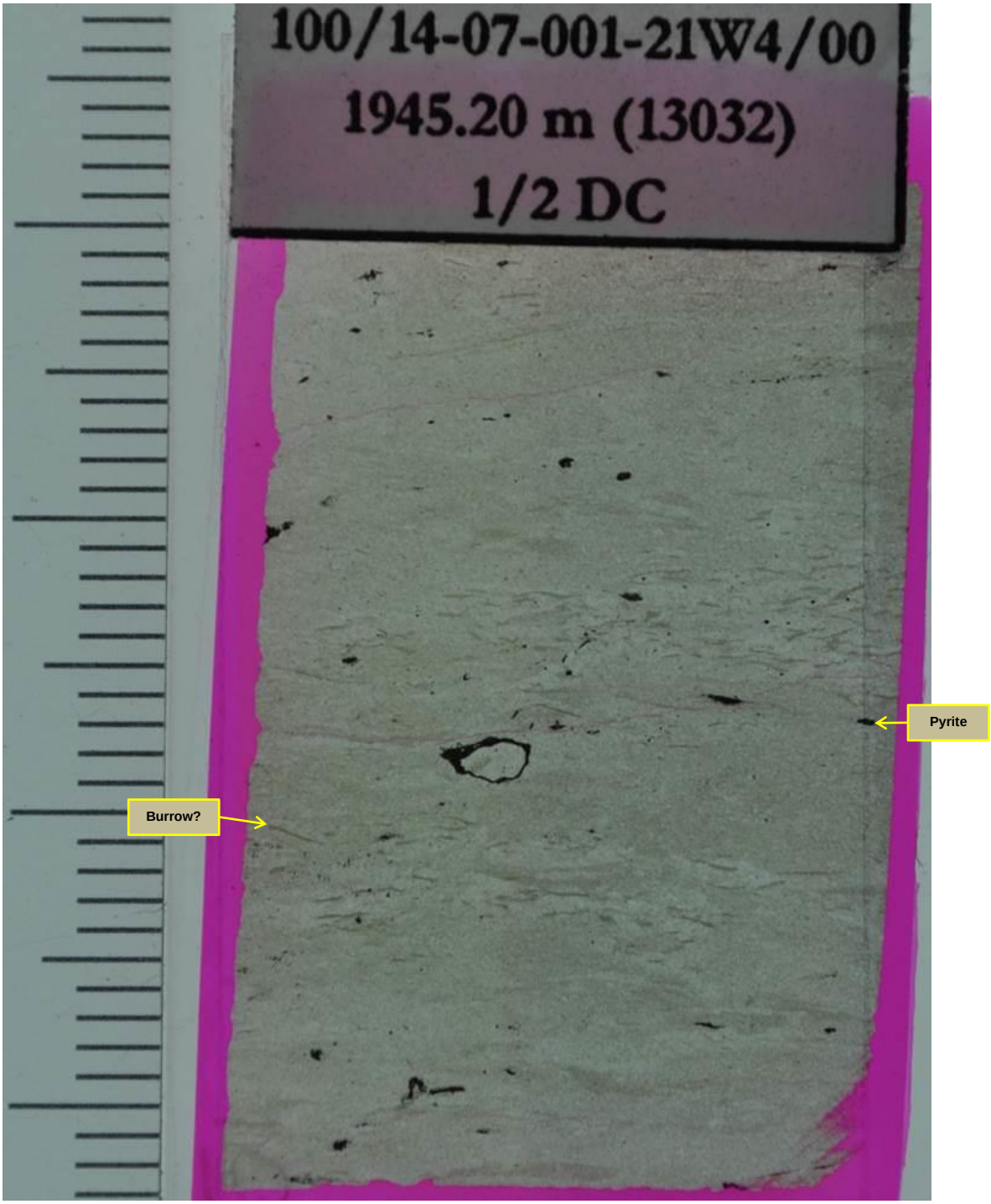


Fig. 6-3: Thin section photograph of sample 13032 from the Exshaw Formation, well 100/14-07-001-21W4/00 (depth 1945.20 m). The sample is a finely crystalline siliceous dolostone. Common elongate clay streaks, possibly representing burrow structures, are the only original sedimentary structures apparent in the sample. Scale is in mm.

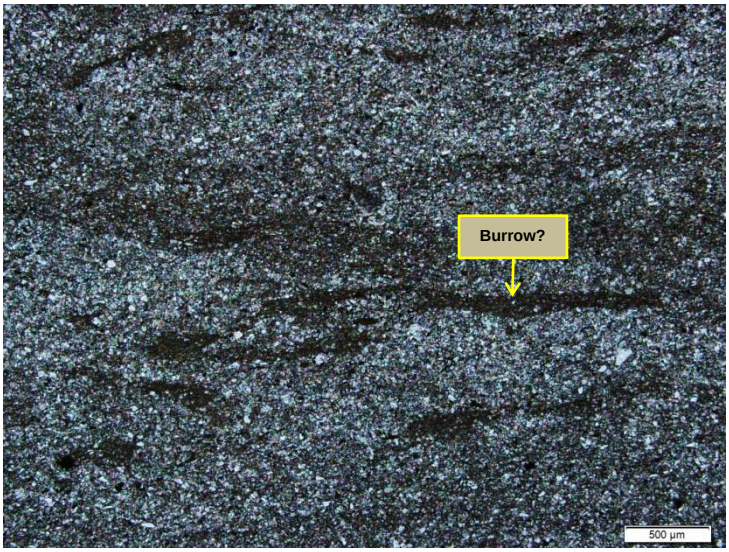


Fig. 6-4: Photomicrograph in PPL showing an overview of the sample, classified as a finely crystalline siliceous dolostone. Elongate clay streaks and patches (dark-coloured), possibly representing burrow structures, are the only original sedimentary features apparent in the sample. Light-coloured minerals consist predominantly of quartz and dolomite.

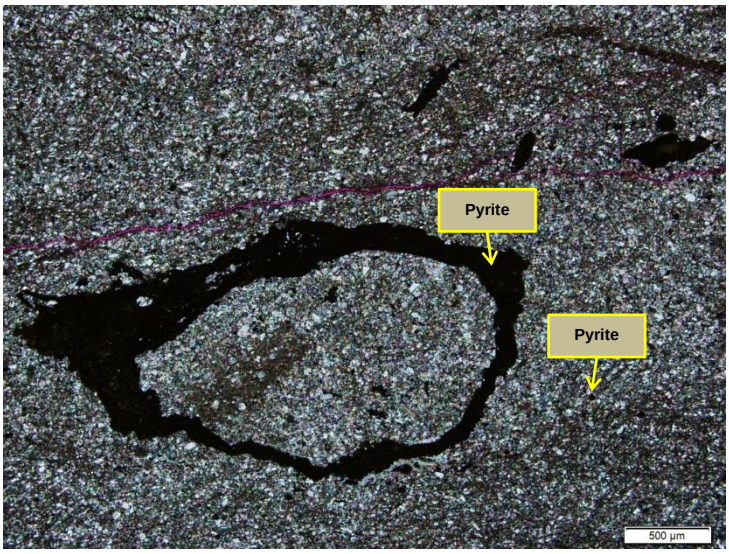


Fig. 6-5: Photomicrograph in PPL showing finely dispersed pyrite (opaque) within a possible dissolved shell. Pyrite accounts for ~8% of the total composition.

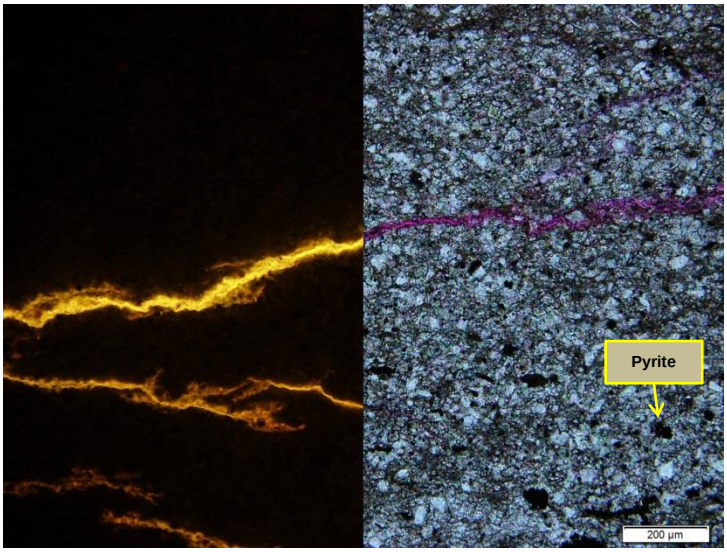


Fig. 6-6: Photomicrograph (left half in UV light, right half in PPL) showing a series of thin, epoxy-filled (pink) fractures observed in the sample. These fractures may have been enhanced or created during thin section preparation. Note common finely dispersed pyrite crystals.

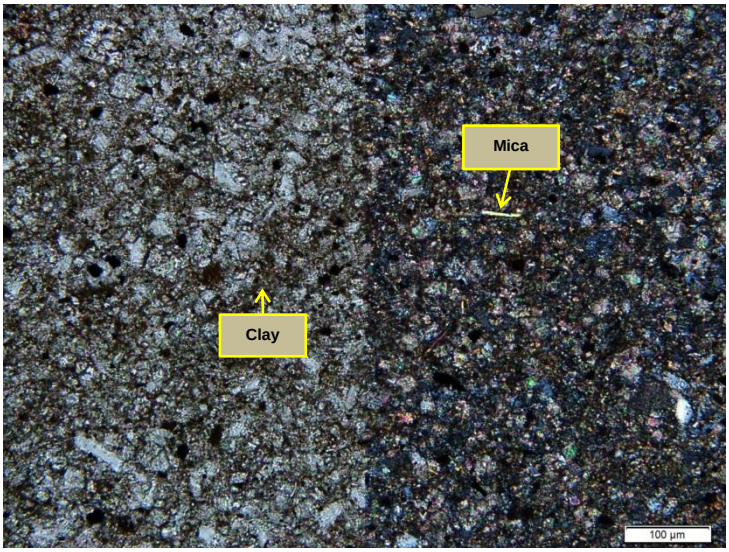


Fig. 6-7: Photomicrograph (left half in PPL, right half in XPL) showing common interstitial clays (dark-brown to black) observed in the dolostone. X-ray diffraction analysis indicates that clays comprise 23% of the sample. Estimation of clay abundance is difficult due to a combination of extensive fine-grained dolomitization and fine distribution of clays around larger siliceous and carbonate particles; therefore, the compositional abundance of clay minerals in the sample is given based on the XRD data, rather than petrographic estimation. Note several mica lathes with high birefringent colours.

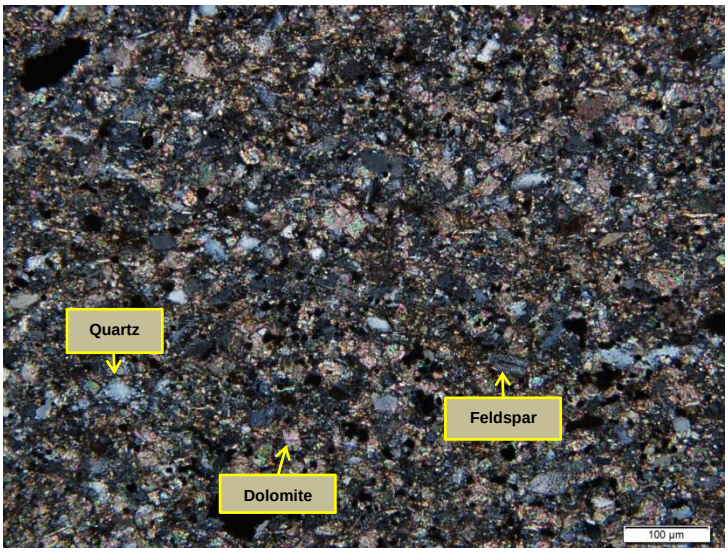


Fig. 6-8: Photomicrograph in XPL illustrating quartz (~36%), dolomite (~30%), mica (1-2%), and feldspar (1%). X-ray diffraction analysis indicates that feldspars comprise 16% of the sample, however, because very few twinned or altered grains were observed in thin section, some grains identified petrographically as quartz are likely feldspars. Dolomite crystals present in this sample measure between 16 and 62 µm in size.

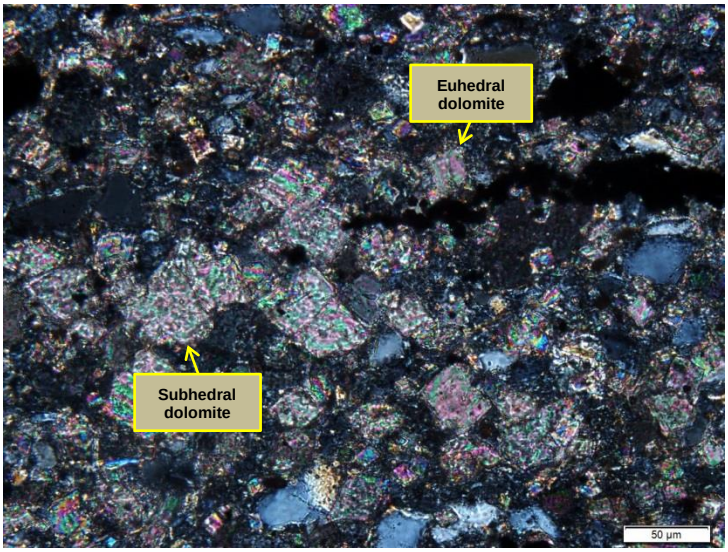


Fig. 6-9: Photomicrograph in XPL showing nonmimic fabric, in which dolomitization has destroyed all evidence of original depositional texture. Planar-e and planar-s fabrics (examples of both are observed in this sample) refer to dolostones with cements predominately made up of euhedral and subhedral crystals, respectively. Note a short “trail” of clustered pyrite idiomorphs, which possibly represents former fecal remains.

6.2.2 SAMPLE 13035

Sample ID	**13035**		
Sample Type	**Core**	**UWI/Well**	**102/04-32-033-17W4/00**
Strat. Unit	**Exshaw**	**Depth**	**1327.00 m**

XRD results

Quartz (%)	Feldspar (%)	Calcite (%)	Dolomite/ankerite (%)	Clays (%)
30.9	16.7	0	31.8	18.8

Pyrite (%)
1.8

Composition (*in order of abundance*)

	%	Variety (%)	Variety (%)	Variety (%)	Variety (%)
Cement (spar)	45	Dolomite (100)			
Cement (micrite)	0				
Clay	20	Clay minerals (100)			
Other grains	29	Quartz (98)	Mica (1)	Feldspar (1)	
Opaques	6	Pyrite (100)			
Organics	<1	Amorphous (100)			
	100				

Sedimentary structures

Primary	None apparent.
Biogenic	Common elongate clay streaks may be burrow features.

Fractures	None apparent.
Porosity	None apparent.
Opaques	Finely dispersed pyrite is common throughout the sample. Pyrite also occurs as large, irregular masses, and elongate particles, some of which may represent replaced organic matter.
Organics	Rare (<1%) amorphous organic particles.
Diagenetic	Heavily dolomitized, with nonmimic planar-e to planar-s fabric.

Description

Sample 13035 is a finely crystalline siliceous dolostone. Common elongate clay streaks, possibly representing burrow features, are the only original sedimentary structues visible in the rock. Dolomite is the most abundant component of the rock, which is characterized by a nonmimic planar-e to planar-s fabric with no intergranular porosity. Pyrite is common throughout the sample, and occurs as finely dispersed crystals, large, irregular masses, and as elongate particles.

Rock Classification

Finely crystalline siliceous dolostone.

Thin Section Quality

Good. 1/2 stained for carbonates.

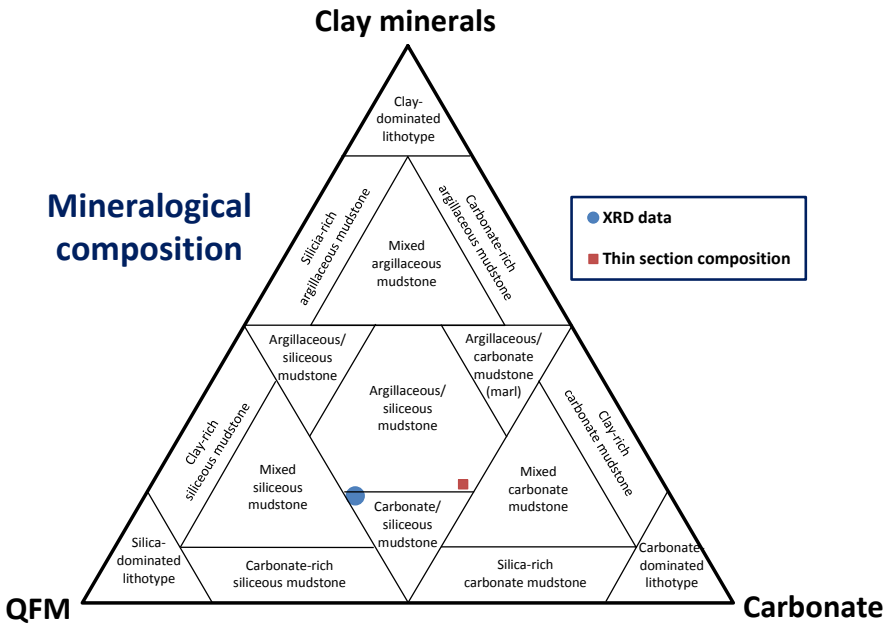


Fig. 6-10: Ternary plot of the mineralogical composition of the carbonate rock according to XRD data (blue) and estimated thin section composition (red). According to this scheme, sample 13035 is classified as an argillaceous/siliceous mudstone. Using a grain- and crystal-size classification scheme for crystalline carbonate rocks, sample 13035 is classified as a finely crystalline siliceous dolostone (Folk, 1962).

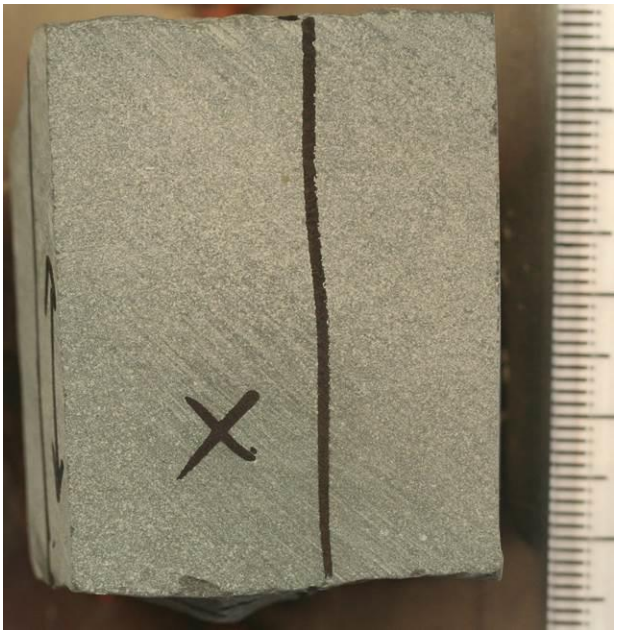


Fig. 6-11: Core photograph of sample 13035 from the Exshaw Formation, well 102/04-32-033-17W4/00 (depth 1327.00 m). The thin section prepared from this sample was cut from the area marked with an X. The sample was received with no way-up direction. Scale is in mm.



Fig. 6-12: Thin section photograph of sample 13035 from the Exshaw Formation, well 102/04-32-033-17W4/00 (depth 1327.00 m). The sample is a finely crystalline siliceous dolostone. Elongate clay streaks and patches, possibly representing burrow features, are the only original sedimentary structures apparent in the sample. Scale is in mm.

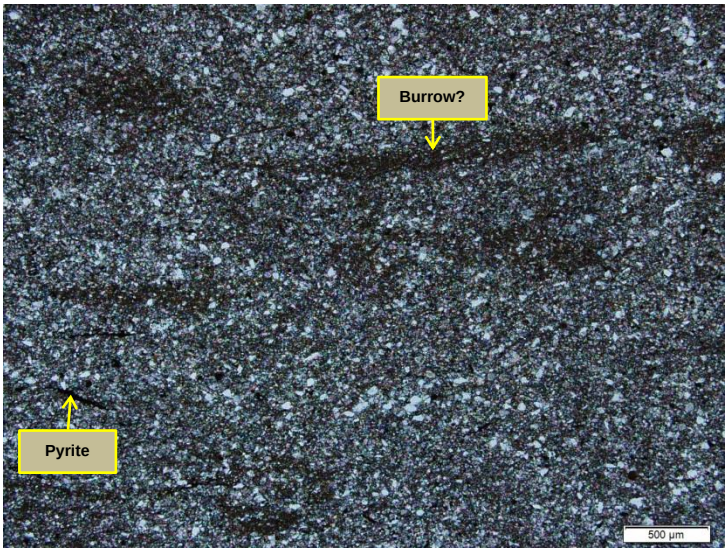


Fig. 6-13: Photomicrograph in PPL showing an overview of the sample, classified as a finely crystalline siliceous dolostone. Elongate clay streaks and patches (dark-coloured), possibly representing burrow structures, are common in the sample, and are the only original sedimentary features visible. Light-coloured minerals consist predominantly of dolomite and quartz.



Fig. 6-14: Photomicrograph in PPL showing pyrite (estimated at ~6% of total composition; opaque) observed in the sample. Pyrite occurs most commonly as finely dispersed crystals, but also forms larger, irregular masses and elongate particles (replaced organic matter?).

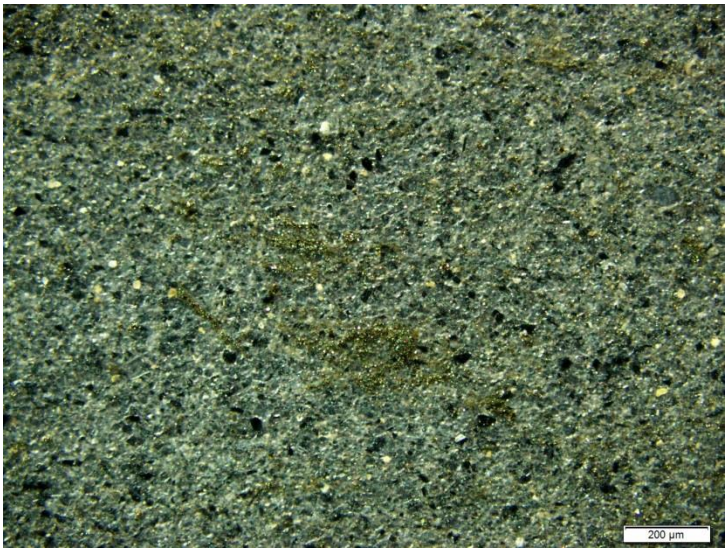


Fig. 6-15: Photomicrograph of Figure 6-14 in reflected light detailing the distribution of pyrite (gold colour) in the sample.

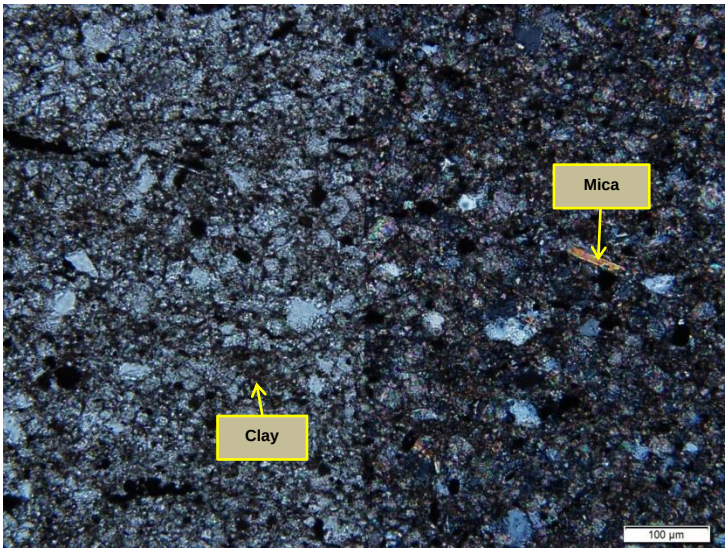


Fig. 6-16: Photomicrograph (left half in PPL, right half in XPL) showing finely dispersed clays and rare mica flakes. X-ray diffraction analysis indicates that clays comprise 19% of the sample. Estimation of clay abundance is difficult due to a combination of extensive dolomitization and fine distribution of clays around larger siliceous and carbonate particles; therefore, the compositional abundance of clay minerals in the sample is given based on the XRD data, rather than petrographic estimation. The rare mica lathes have high birefringent colours.

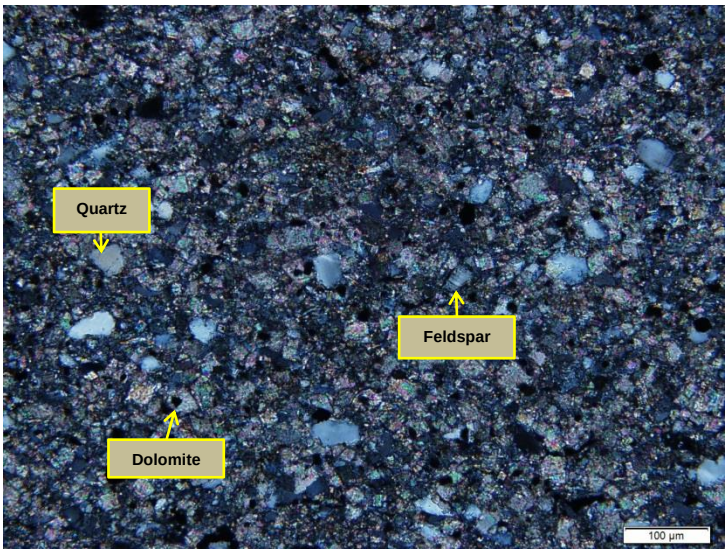


Fig. 6-17: Photomicrograph in XPL showing dolomite (~45%), quartz (~28%), mica (1-4%), and feldspar (<1%) observed in the dolostone. XRD analysis indicates that feldspars account for 17% of the total composition; however, because very few twinned or altered grains were observed in thin section, some grains identified petrographically as quartz are likely feldspars. Dolomite crystals present in this sample measure between 16 and 62 µm in size.

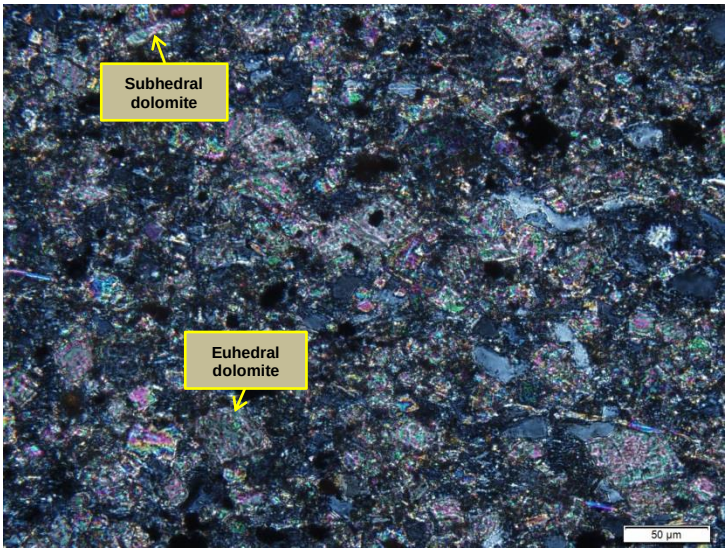


Fig. 6-18: Photomicrograph in XPL showing nonmimic fabric observed in the sample. Nonmimic fabrics occur in rocks where dolomitization has destroyed all evidence of original depositional texture. Euhedral and subhedral dolomite crystals are abundant in this sample (dull birefringent colours).

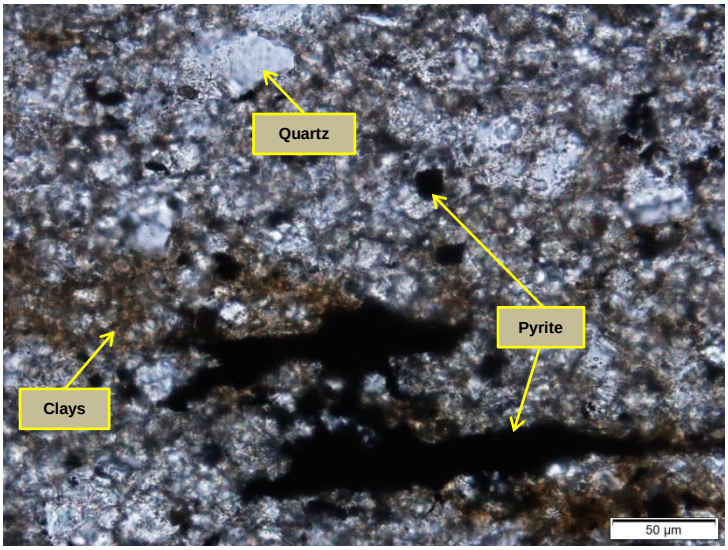


Fig. 6-19: Photomicrograph in PPL detailing interstitial clays (brown) and pyrite (opaque) forming short “trails” (likely fecal derived) in the sample. Note fine to medium silt-size quartz particles.

6.2.3 SAMPLE 13048

Sample ID	**13048**		
Sample Type	**Core**	**UWI/Well**	**100/01-03-002-20W4/00**
Strat. Unit	**Exshaw**	**Depth**	**1536.80 m**

XRD results

Quartz (%)	Feldspar (%)	Calcite (%)	Dolomite/ankerite (%)	Clays (%)
29.7	21.6	0	24.1	23

Pyrite (%)
1.6

Composition (*in order of abundance)*

	%	Variety (%)	Variety (%)	Variety (%)	Variety (%)
Cement (spar)	30	Dolomite (100)			
Cement (micrite)	0				
Clay	23	Clay minerals* (100)			
Detrital grains	39	Quartz (97)	Mica (2)	Feldspar (1)	
Opaques	8	Pyrite (100)			
Organics	<1	Amorphous (100)			
	100				

**Percent abundance based on XRD data*

Sedimentary structures

Primary	None apparent.
Biogenic	Common elongate burrow structures.

Fractures	Rare thin epoxy-filled fractures.
Porosity	None apparent.
Opaques	Pyrite occurs in abundance throughout the rock, including common finely dispersed and framboidal forms, as well as large, irregularly distributed masses.
Organics	Rare (<1%) amorphous organic particles.
Diagenetic	Heavily dolomitized, with a nonmimic planar-e to planar-s fabric.

Description

Sample 13048 is a finely crystalline siliceous dolostone. Elongate clay-rich burrow structures are the only original sedimentary structures apparent in the rock, which is heavily dolomitized and characterized by a nonmimic planar-e to planar-s diagenetic fabric. Pyrite is abundant in the sample, occuring as both common finely dispersed and framboidal forms, as well as large, irregularly distributed masses.

Rock Classification

Finely crystalline siliceous dolostone.

Thin Section Quality

Good. 1/2 stained for carbonates.

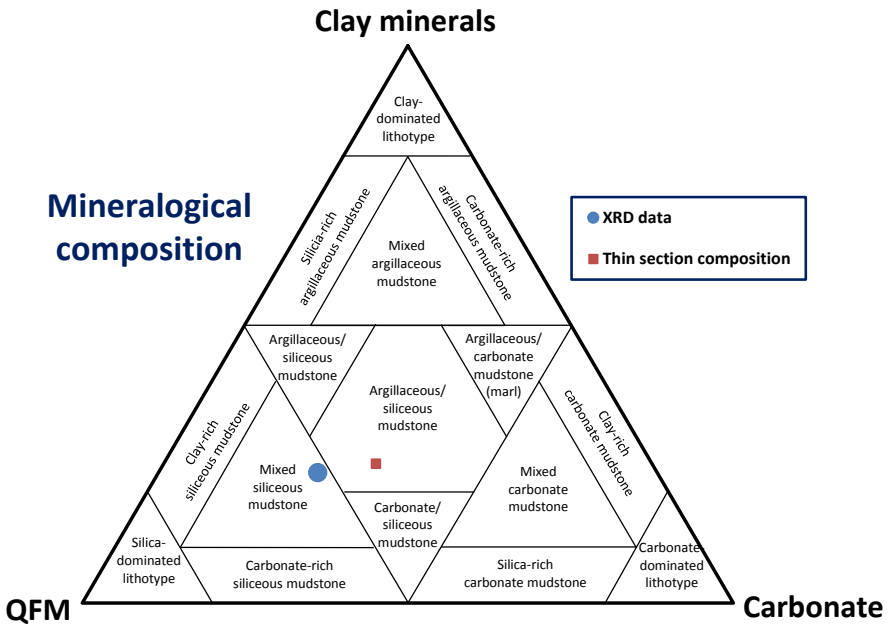


Fig. 6-20: Ternary plot of the mineralogical composition of the carbonate rock according to XRD data (blue) and estimated thin section composition (red). According to this scheme, sample 13048 is classified as an argillaceous/siliceous mudstone. Using a grain- and crystal-size classification scheme for crystalline carbonate rocks, sample 13048 is classified as a finely crystalline siliceous dolostone (Folk, 1962).



Fig. 6-21: Core photograph of sample 13048 from the Exshaw Formation, well 100/01-03-002-20W4/00 (depth 1536.80 m). The thin section prepared from this sample was cut from the face shown in this image. The sample was received with no way-up direction. Scale is in mm.

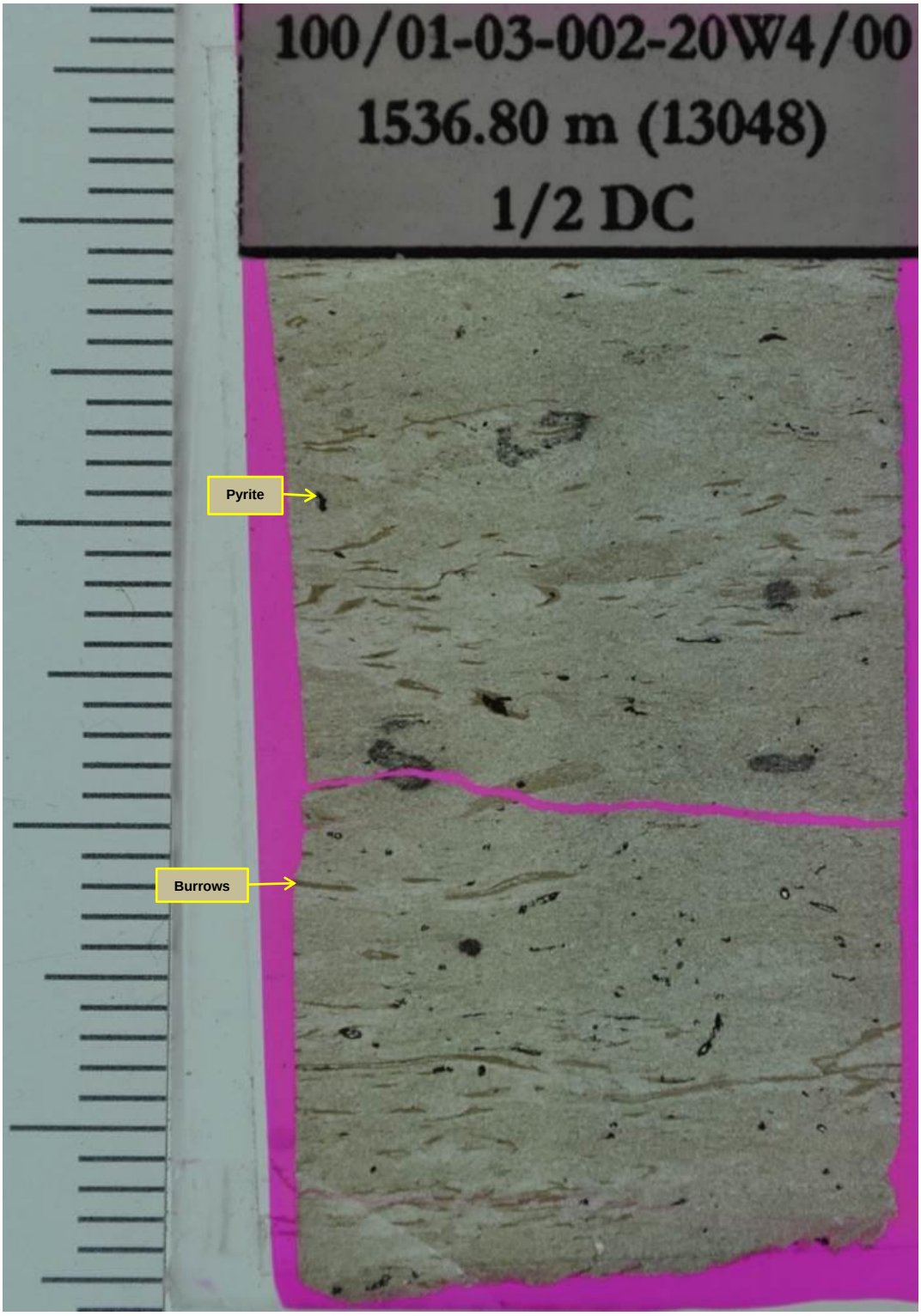


Fig. 6-22: Thin section photograph of sample 13048 from the Exshaw Formation, well 100/01-03-002-20W4/00 (depth 1536.80 m). The sample is a finely crystalline siliceous dolostone. Elongate clay-rich burrow structures and irregular pyrite masses are common throughout the sample. Scale is in mm.

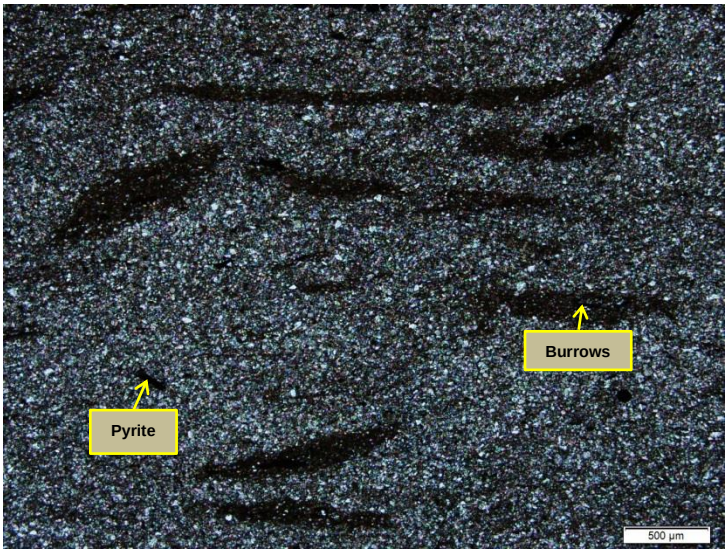


Fig. 6-23: Photomicrograph in PPL showing an overview of the sample, classified as a finely crystalline siliceous dolostone. Elongate clay-rich burrow structures are common (dark-coloured), and are the only original sedimentary structures apparent. Light-coloured minerals consist predominantly of dolomite and quartz.

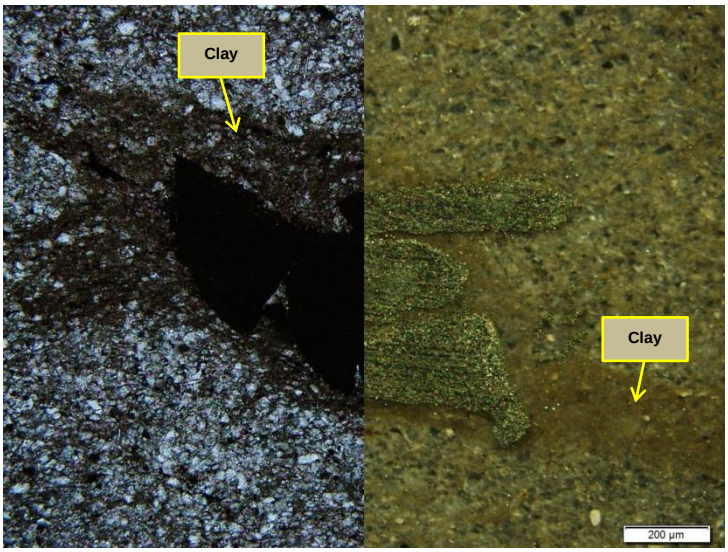


Fig. 6-24: Photomicrograph (left half in PPL, right half in reflected light) showing a patch of concentrated pyrite (opaque in PPL, gold colour in reflected light). This patch occurs within a clay-rich (brown) burrow structure, and may be associated with fecal remains.

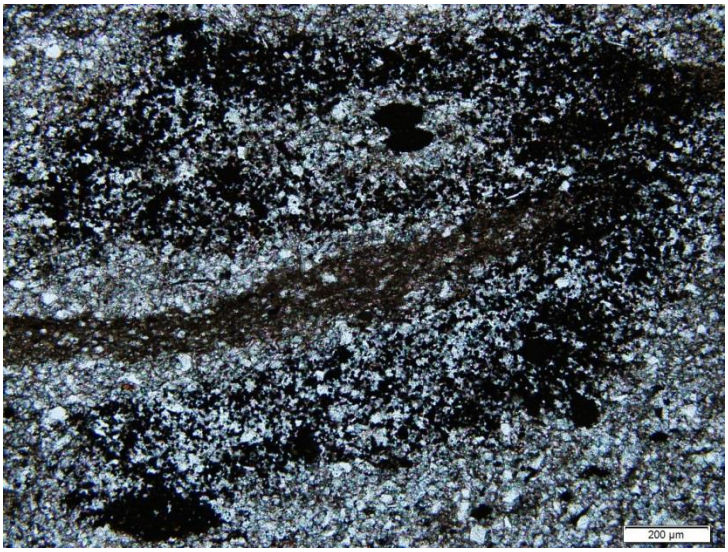


Fig. 6-25: Photomicrograph in PPL showing one of several irregular masses of pyrite crystals and framboids. These irregular masses occur in addition to finely dispersed and framboidal pyrite idiomorphs that are present throughout the sample. Pyrite is estimated at ~8% of the total composition.

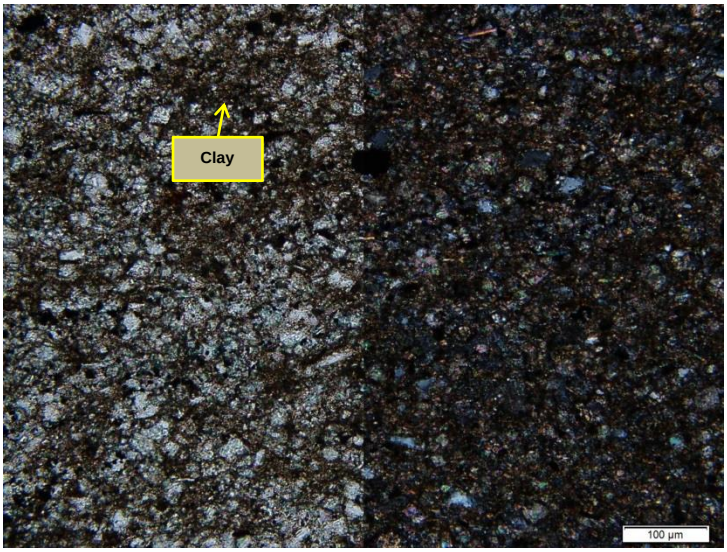


Fig. 6-26: Photomicrograph (left half in PPL, right half in XPL) illustrating common finely dispersed clay (dark-brown). X-ray diffraction analysis indicates that clays comprise 23% of the sample. Estimation of clay abundance in this rock is difficult due to a combination of extensive dolomitization and fine distribution of interstitial clays around larger siliceous and carbonate particles; therefore, the compositional abundance of clay minerals in the sample is given based on the XRD data, rather than petrographic estimation.

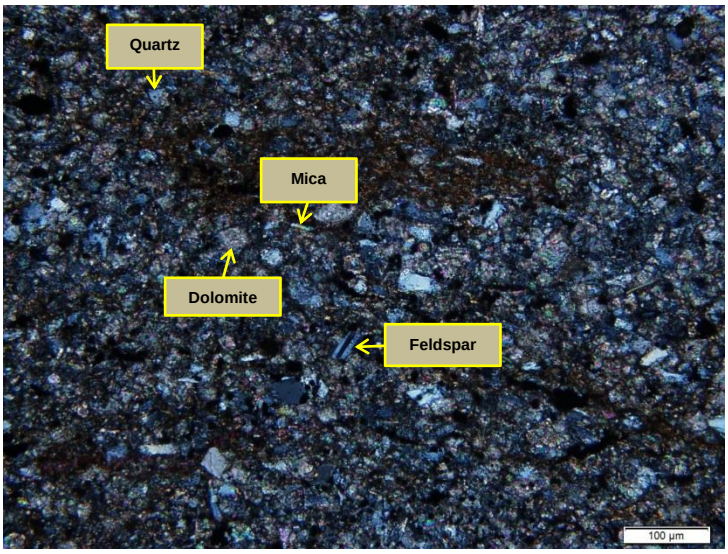


Fig. 6-27: Photomicrograph in XPL showing quartz (~38%), dolomite (~30%), mica (1-2%), and feldspar (<1%) observed in the sample. X-ray diffraction analysis indicates that feldspars comprise 22% of the sample; however, because very few twinned or altered grains were observed in thin section, some grains identified petrographically as quartz are likely feldspars. Dolomite crystals present in this sample measure between 16 and 62 µm in size.

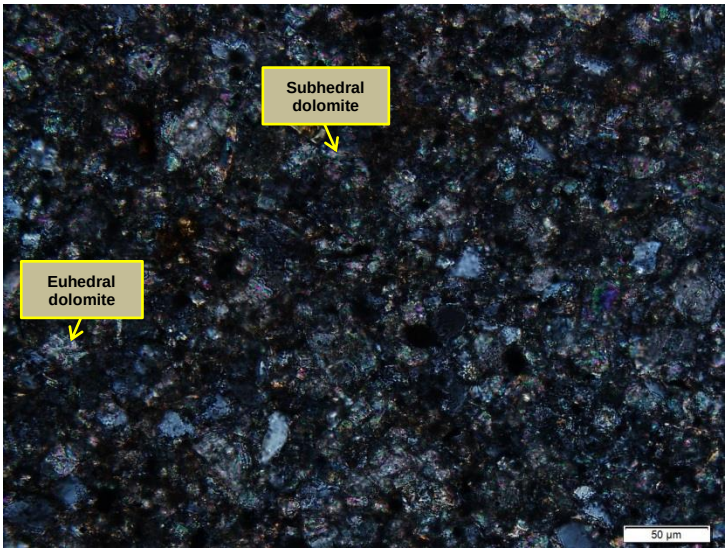


Fig. 6-28: Photomicrograph in XPL showing nonmimic diagenetic fabric, in which dolomitization has destroyed all evidence of original depositional texture. Planar-e and planar-s fabrics (examples of both are observed in this sample) refer to dolostones with cements predominately made up of euhedral and subhedral crystals, respectively.

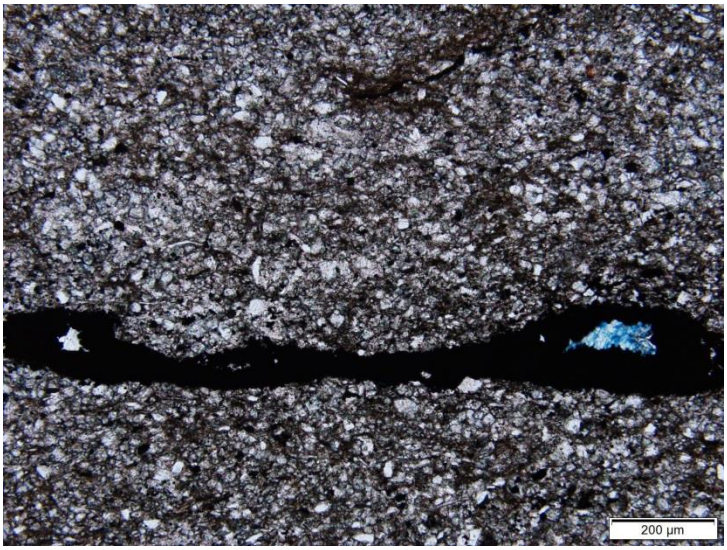


Fig. 6-29: Photomicrograph in PPL detailing an accumulation of opaque material, which may represent a dissolved shell fragment (~1.4 mm in length). Pyrite and some organics are present, as well as small secondary grains of quartz (left) and ferroan dolomite (right; blue stain).

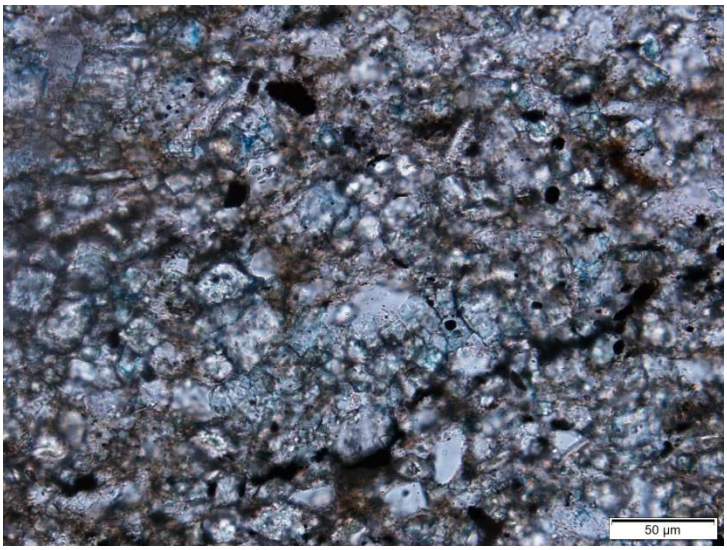


Fig. 6-30: Photomicrograph in PPL illustrating a faint blue stain associated with ferroan dolomite. Half of the sample was stained for calcite and ferroan carbonates. Note thin, short “trails” of pyrite, which are possibly fecal in origin.

6.2.4 SAMPLE 13184

Sample ID	**13184**		
Sample Type	**Core**	**UWI/Well**	**100/01-03-002-20W4/00**
Strat. Unit	**Exshaw**	**Depth**	**1541.65 m**

XRD results

Quartz (%)	Feldspar (%)	Calcite (%)	Dolomite/ankerite (%)	Clays (%)
28.6	21.5	8.5	17.2	21

Pyrite (%)
3.1

Composition (*in order of abundance)*

	%	Variety (%)	Variety (%)	Variety (%)	Variety (%)
Cement (spar)	30	Dolomite (82)	Calcite (18)		
Cement (micrite)	0				
Clay	21	Clay minerals* (100)			
Detrital grains	43	Quartz (97)	Mica (2)	Feldspar (1)	
Opaques	6	Pyrite (100)			
Organics	<1	Amorphous (100)			
	100				

**Percent abundance based on XRD data*

Allochems	100	Brachiopod shells (60)	Echinoderm debris (40)		
Matrix	0				
Porosity	0				
	100				

Sedimentary structures

Primary	None apparent.
Biogenic	Common clay streaks may be bioturbation features.

Fractures	Rare thin epoxy-filled fractures.
Porosity	None apparent.
Opaques	Abundant pyrite, including framboidal, finely-dispersed, and replacement forms. Numerous elongate pyrite particles are observed in the rock, which may represent pyritized brachiopod shells and/or organic matter.
Organics	Rare amorphous organic matter, including possible plant material.
Diagenetic	Heavy dolomitization, including ferroan dolomite, with a nonmimic planar-e to planar-s fabric.

Bioclasts *(in order of abundance)*

Type	*Size (µm)*	*Preservation*	*Recrystallisation*
Brachiopod shells	Up to 6000 µm	Fair	Often partially pyritized
Echinoderm debris	300-940 µm	Fair	Often partially pyritized

Description

Sample 13184 is a finely crystalline siliceous dolostone. Common clay streaks, which may represent burrows, are the only original sedimentary features apparent in the rock. Fragmental brachiopod shells and echinoderm plates are common in the sample, and are often partially pyritized. Pyrite is abundant (~6%) in the rock, with framboidal, finely dispersed, and replacement forms occurring throughout the sample. Heavy dolomitization is apparent in the rock, which shows a nonmimic planar-e to planar-s fabric with no porosity.

Rock Classification

Finely crystalline siliceous dolostone.

Thin Section Quality

Good. 1/2 stained for carbonates.

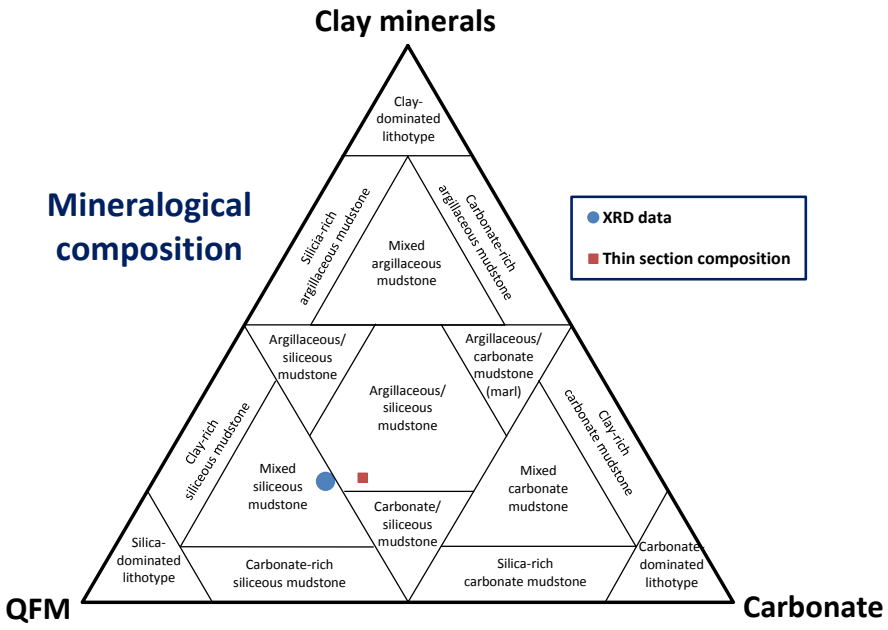


Fig. 6-31: Ternary plot of the mineralogical composition of the carbonate rock according to XRD data (blue) and estimated thin section composition (red). According to this scheme, sample 13184 is classified as an argillaceous/siliceous mudstone. Using a grain- and crystal-size classification scheme for crystalline carbonate rocks, sample 13184 is classified as a finely crystalline siliceous dolostone (Folk, 1962).

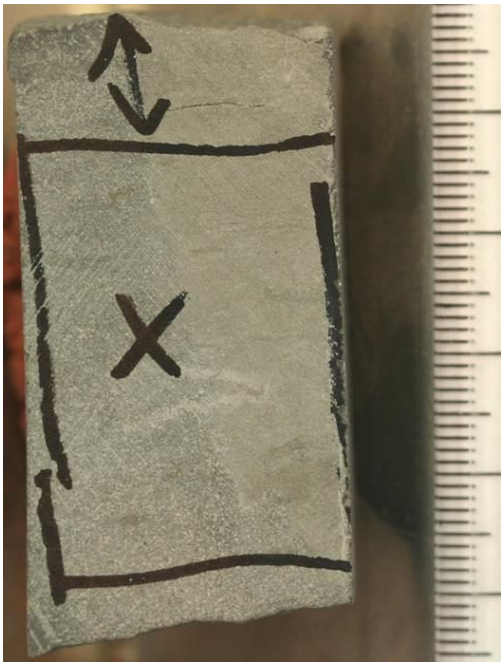


Fig. 6-32: Core photograph of sample 13184 from the Exshaw Formation, well 100/01-03-002-20W4/00 (depth 1541.65 m). The thin section prepared from this sample was cut from the area marked with an X. The sample was received with no way-up direction. Scale is in mm.

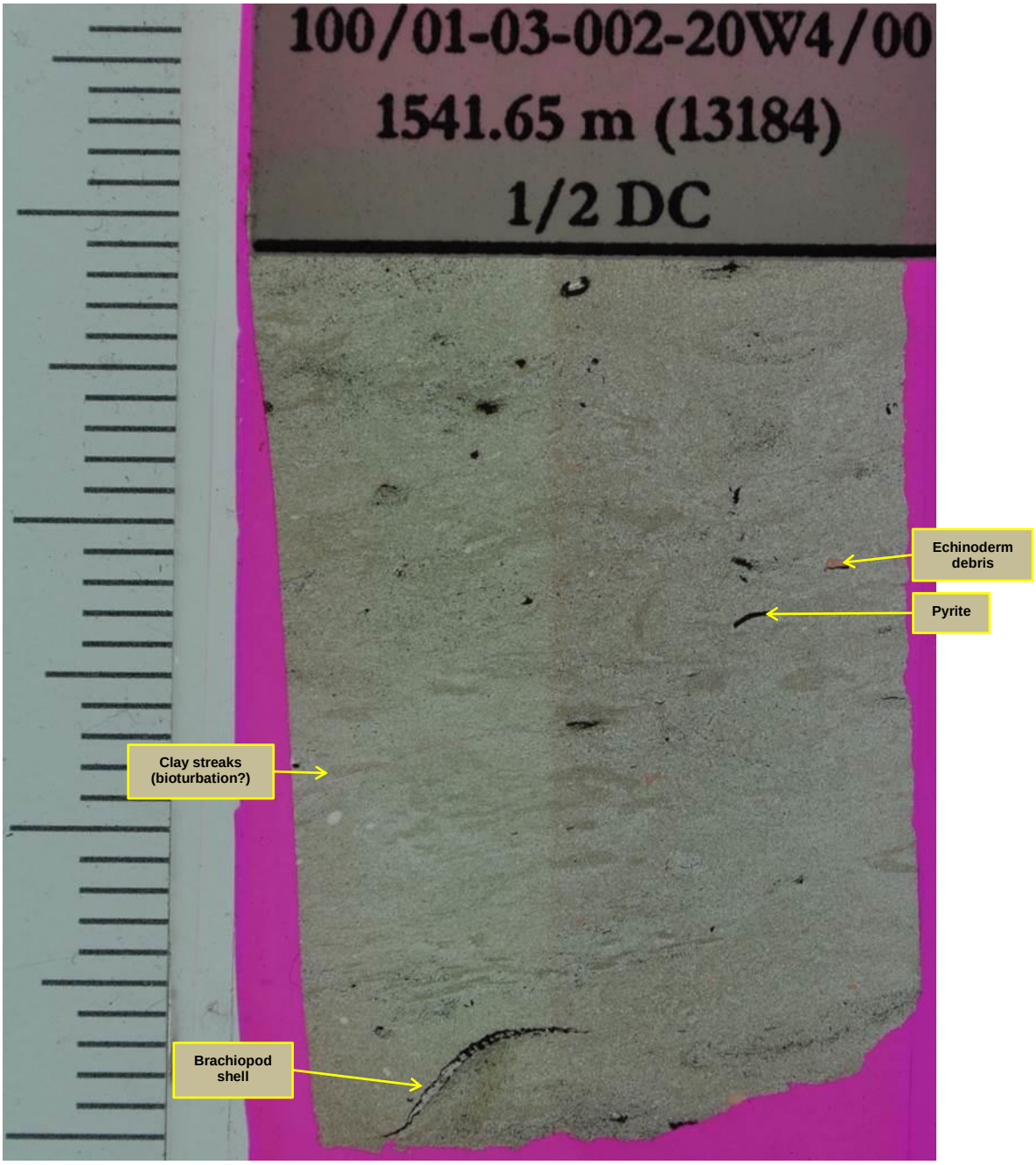


Fig. 6-33: Thin section photograph of sample 13184 from the Exshaw Formation, well 100/01-03-002-20W4/00 (depth 1541.65 m). The sample is a finely crystalline siliceous dolostone. Fragmental brachiopod shells and echinoderm plates are common throughout, and often show partial pyritization. Clay streaks and patches, possibly representing bioturbation features, are the only original sedimentary features apparent in the sample. Scale is in mm.

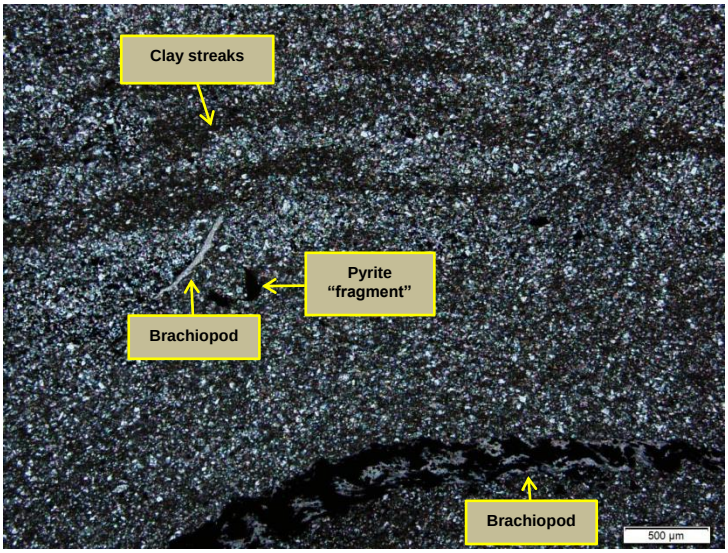


Fig. 6-34: Photomicrograph in PPL showing an overview of the finely crystalline siliceous dolostone. Clay streaks and patches (darker-coloured), possibly representing bioturbation features, are the only original sedimentary structures apparent. Light-coloured minerals consist predominantly of dolomite and quartz. Brachiopod shell fragments are common in the rock, and are often partially replaced by pyrite (the shell fragment shown at the bottom of the image contains >50% pyrite).

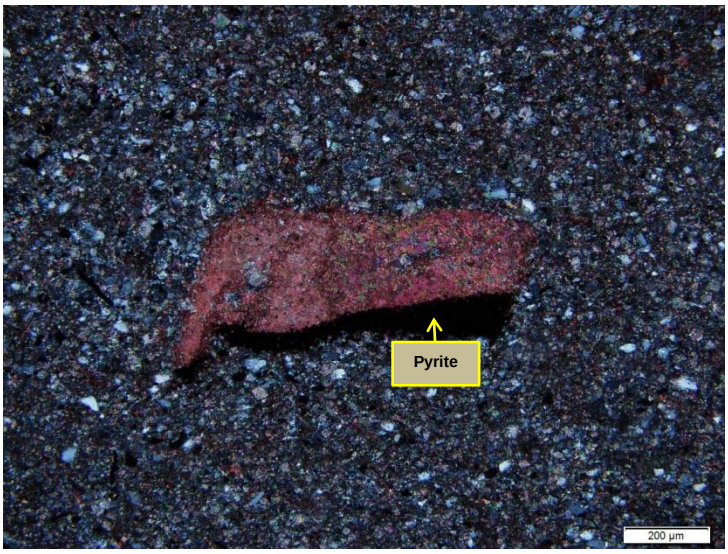


Fig. 6-35: Photomicrograph in XPL detailing a partially pyritized echinoderm fragment (~800 µm in size). The fragment is stained red, indicating that it is composed of calcite. Most of the grain shows unit extinction, with the exception of possible secondary calcite that appears to have crystallized within the original pores of the fossil. The lowermost part is dissolved and infilled with pyrite (opaque).

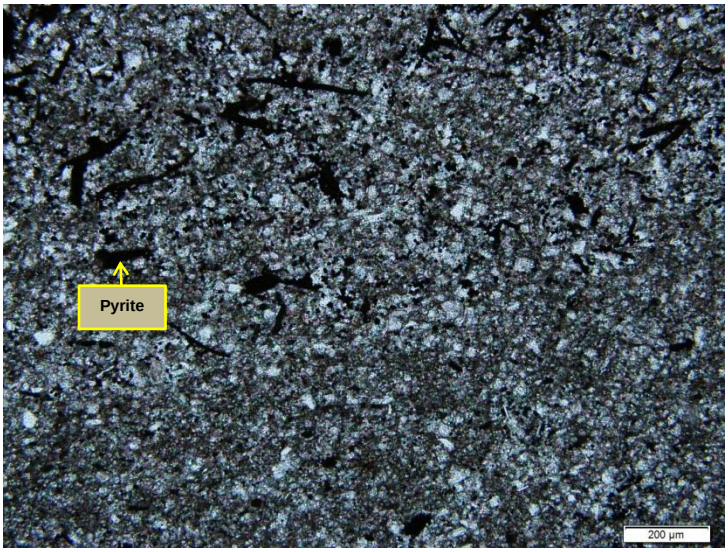


Fig. 6-36: Photomicrograph in PPL illustrating several elongate (up to ~300 µm in size) pyrite particles. These are common and may represent pyritized brachiopod shell fragments (dissolved shells infilled with opaques, including pyrite and/or organic matter). Pyrite is estimated at ~6% of the total composition.

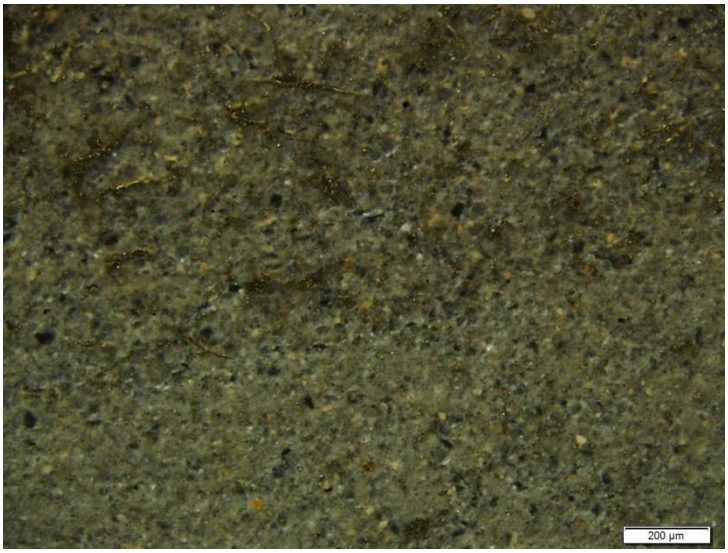


Fig. 6-37: Photomicrograph of Figure 6-36 in reflected light illustrating the distribution of pyrite in the sample (gold colour).

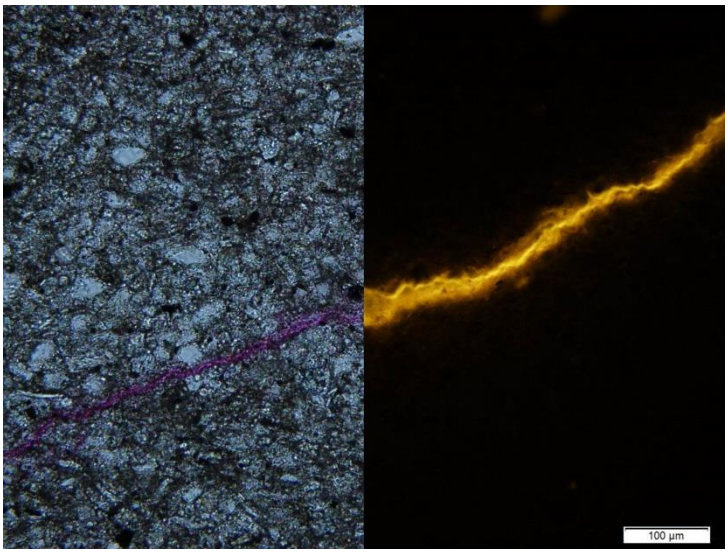


Fig. 6-38: Photomicrograph (left half in PPL, right half in UV light) showing a rare epoxy-filled (pink) fracture. None of the fractures are observed cutting across the entire sample, or bifurcating into a series of connected fractures.

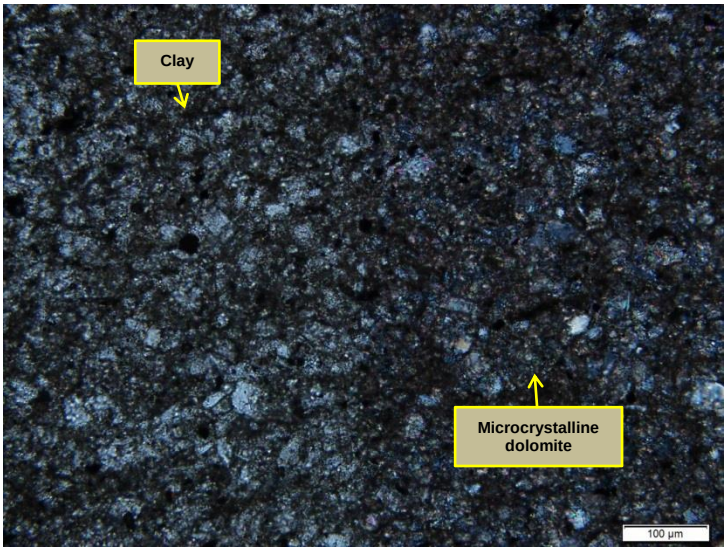


Fig. 6-39: Photomicrograph (left half in PPL, right half in XPL) showing the heavily cemented fabric of the dolostone. X-ray diffraction analysis indicates that clays comprise ~20% of the sample. Petrographic estimation of clay abundance is difficult due to a combination of extensive dolomitization and fine distribution of interstitial clays around larger siliceous and carbonate particles. Microcrystalline dolomite is commonly observed in the sample, possibly indicating several stages of dolomitization.

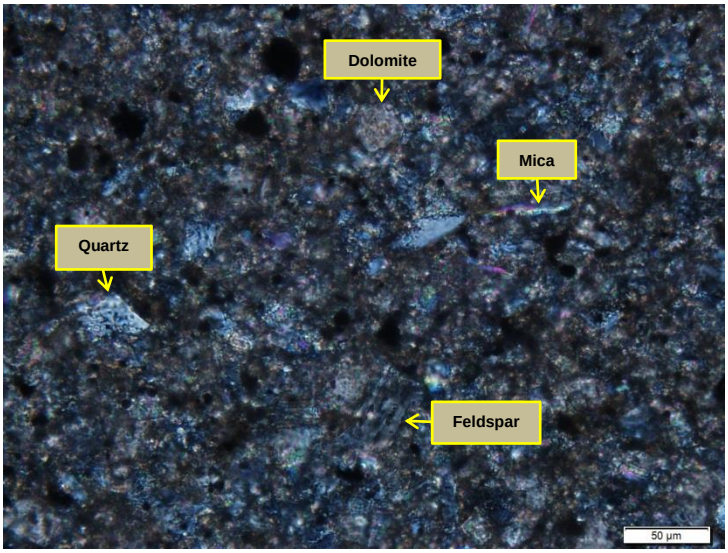


Fig. 6-40: Photomicrograph in XPL showing quartz (~40%), dolomite (~30%), mica (1-4%), and feldspar (>1%). X-ray diffraction analysis indicates that feldspars comprise 22% of this sample, but very few twinned or altered grains were observed in thin section. Hence, some grains identified petrographically as quartz are likely feldspars. Dolomite crystals present in this sample measure between 16 and 62 µm in size.

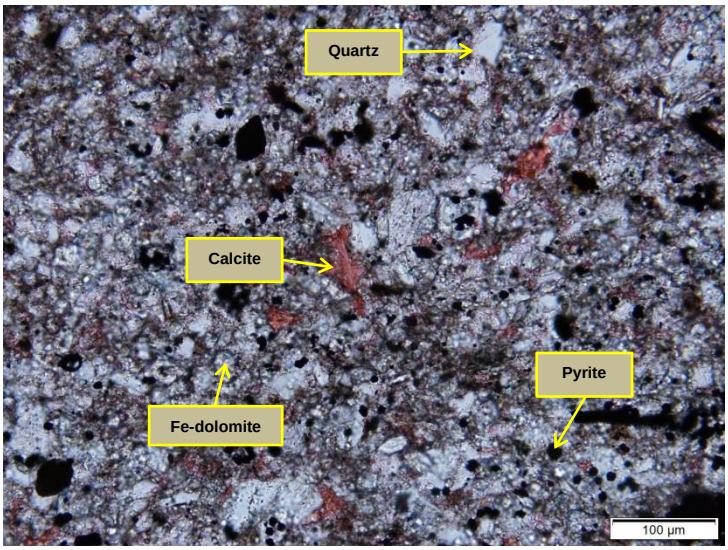


Fig. 6-41: Photomicrograph in PPL detailing minor (~5%) pore-filling calcite cements (red stain). A slight blue-stain is also observed and is associated with Fe-dolomite. Note numerous finely dispersed pyrite framboids and micro-nodules (opaque).

6.2.5 SAMPLE 13190

Sample ID	**13190**		
Sample Type	**Core**	**UWI/Well**	**100/16-06-010-22W4/00**
Strat. Unit	**Exshaw**	**Depth**	**1870.27 m**

XRD results

Quartz (%)	Feldspar (%)	Calcite (%)	Dolomite/ankerite (%)	Clays (%)
34.7	20.3	0	21.9	20.4

Pyrite (%)
2.7

Composition (*in order of abundance)*

	%	Variety (%)	Variety (%)	Variety (%)	Variety (%)
Cement (spar)	35	Dolomite (100)			
Cement (micrite)	0				
Clay	20	Clay minerals* (100)			
Detrital grains	37	Quartz (97)	Mica (2)	Feldspar (1)	
Opaques	8	Pyrite (100)			
Organics	<1	Amorphous (100)			
	100				

**Percent abundance based on XRD data*

Sedimentary structures

Primary	None apparent.
Biogenic	Common clay streaks may be bioturbation features.

Fractures	None apparent.
Porosity	Non-porous (heavily cemented).
Opaques	Finely dispersed and framboidal pyrite are common throughout the sample. Several (<10) larger pyrite "streaks" are also observed in the rock.
Organics	Rare amorphous organic particles, possibly representing plant material.
Diagenetic	Heavily dolomitized, with nonmimic planar-e to planar-s fabric.

Description

Sample 13190 is a finely crystalline siliceous dolostone. This non-porous rock is heavily dolomitized, showing a nonmimic planar-e to planar-s diagenetic fabric. Clay streaks are commonly observed in the rock, and may represent bioturbation features.

Rock Classification

Finely crystalline siliceous dolostone.

Thin Section Quality

Good. 1/2 stained for carbonates.

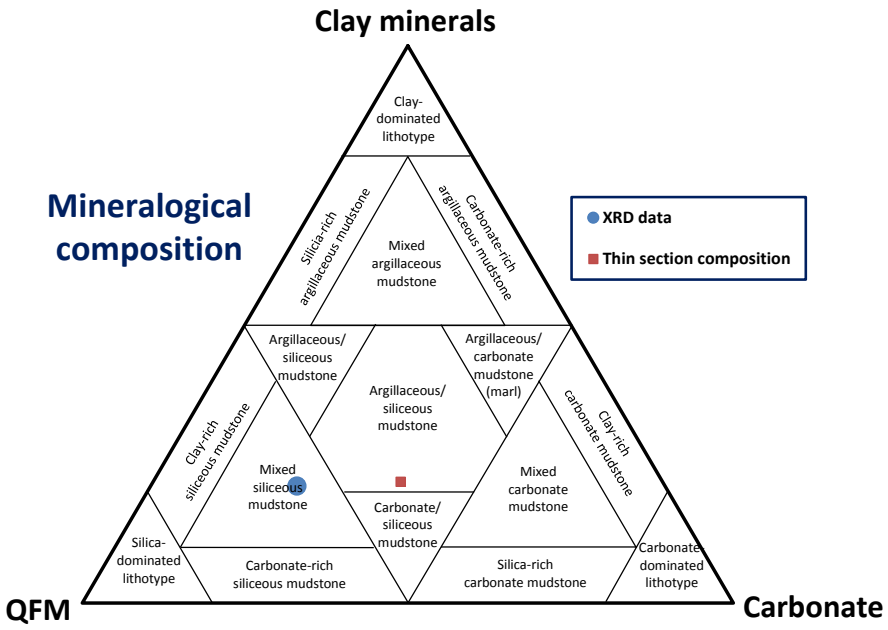


Fig. 6-42: Ternary plot of the mineralogical composition of the carbonate rock according to XRD data (blue) and estimated thin section composition (red). According to this scheme, sample 13190 is classified as an argillaceous/siliceous mudstone. Using a grain- and crystal-size classification scheme for crystalline carbonate rocks, sample 13190 is classified as a finely crystalline dolostone (Folk, 1962).

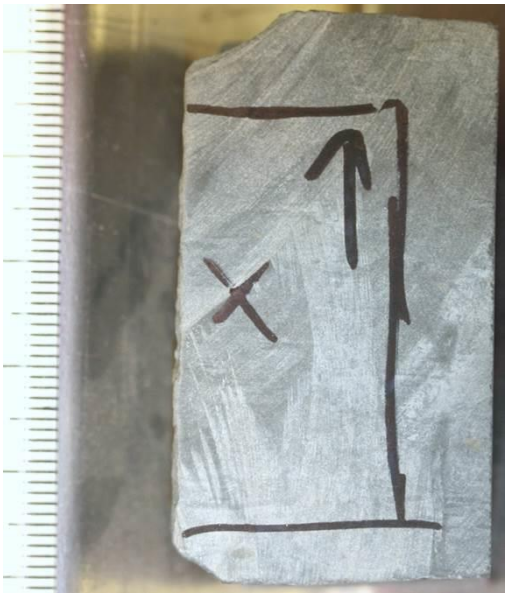


Fig. 6-43: Core photograph of sample 13190 from the Exshaw Formation, well 100/16-06-010-22W4/00 (depth 1870.27 m). The thin section prepared from this sample was cut from the area marked with an X. The arrow indicates stratigraphic up direction. Scale is in mm.

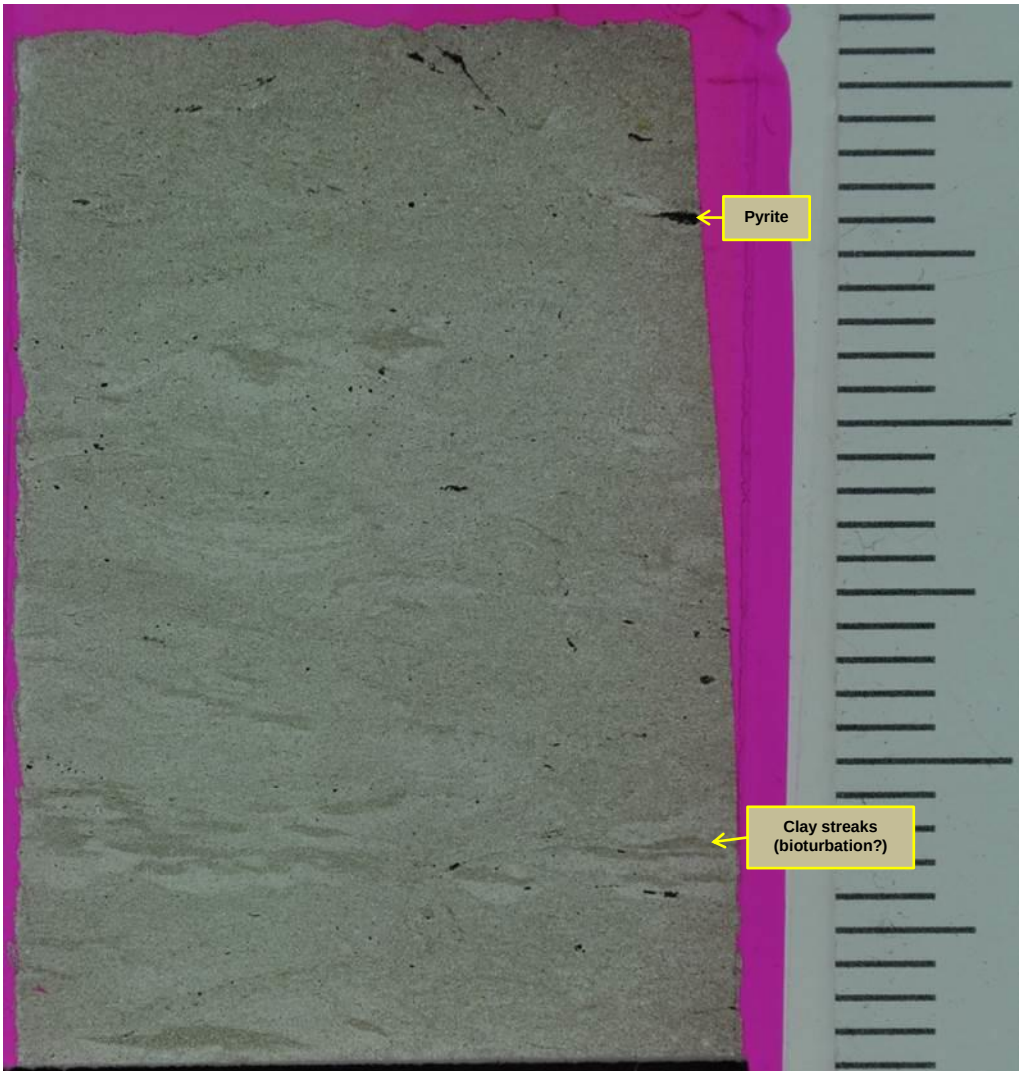


Fig. 6-44: Thin section photograph of sample 13190 from the Exshaw Formation, well 100/16-06-010-22W4/00 (depth 1870.27 m). The sample is a finely crystalline siliceous dolostone. Most of the original depositional fabric has been destroyed due to extensive dolomitization. Scale is in mm.

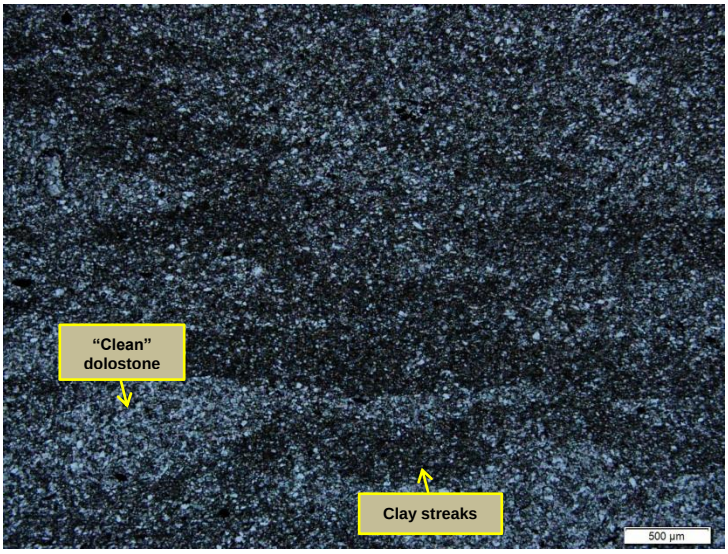


Fig. 6-45: Photomicrograph in PPL showing an overview of the sample, classified as a finely crystalline siliceous dolostone. Dark, elongate clay streaks are common and may represent bioturbation features. Much of the sample has a buff gray appearance (see Figure 6-44) associated with patches of lighter-colored "clean" dolostone (dolomite and quartz) around the clay streaks.

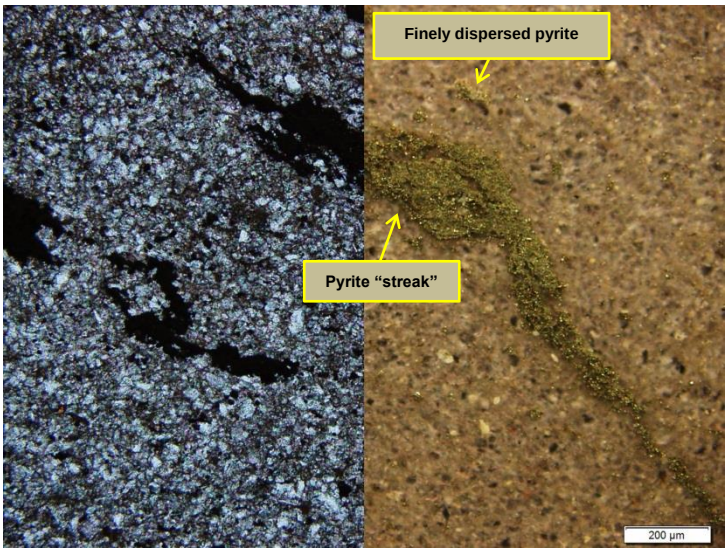


Fig. 6-46: Photomicrograph (left half in PPL, right half in reflected light) showing finely dispersed pyrite (opaque) and large pyrite "streaks" observed in the dolostone. Pyrite comprises ~8% of the sample.

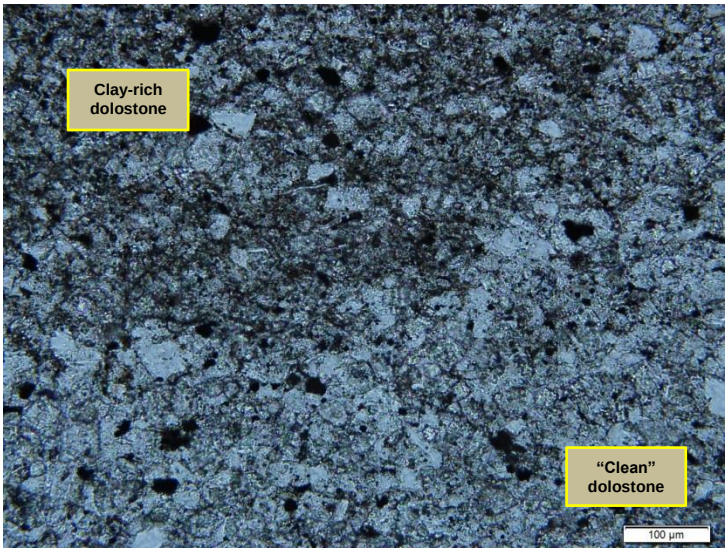


Fig. 6-47: Photomicrograph in PPL showing contrast between clay-rich and "clean" areas of the dolostone. X-ray diffraction analysis indicates that clays comprise 20% of the sample. Estimation of clay abundance in this sample is difficult due to a combination of extensive dolomitization and fine distribution of interstitial clays around larger siliceous and carbonate particles; therefore, the compositional abundance of clay minerals in the sample is given based on the XRD data, rather than petrographic estimation.

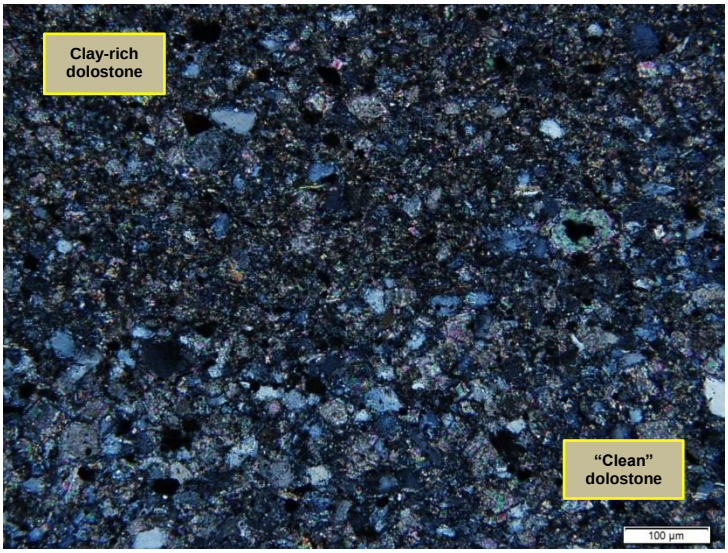


Fig. 6-48: Photomicrograph of Figure 6-47 in XPL highlighting the contrast between clay-rich and "clean" areas of the dolostone. Boundaries of siliceous and carbonate particles are less clear in clay-rich areas.

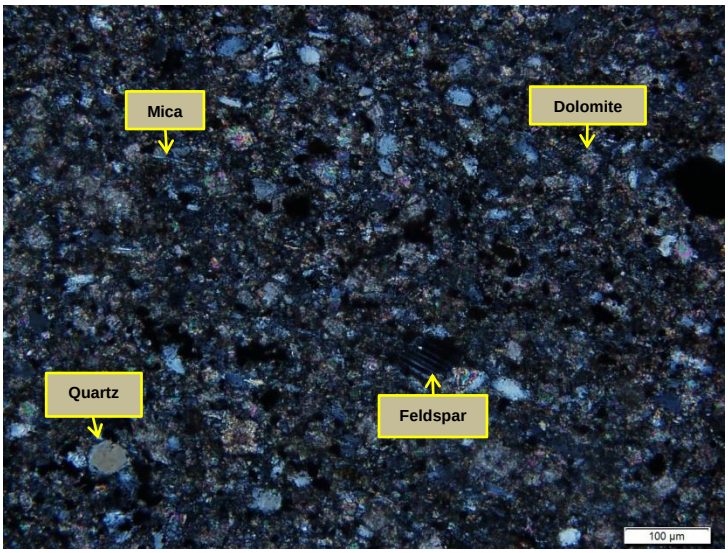


Fig. 6-49: Photomicrograph in XPL showing quartz (~35%), dolomite (~35%), mica (1-4%), and feldspar (1-2%). X-ray diffraction analysis indicates that feldspars comprise 20% of the sample; however, because very few twinned or altered grains were observed in thin section, some grains identified petrographically as quartz are likely feldspars. Dolomite crystals present in this sample measure between 16 and 62 µm in size.

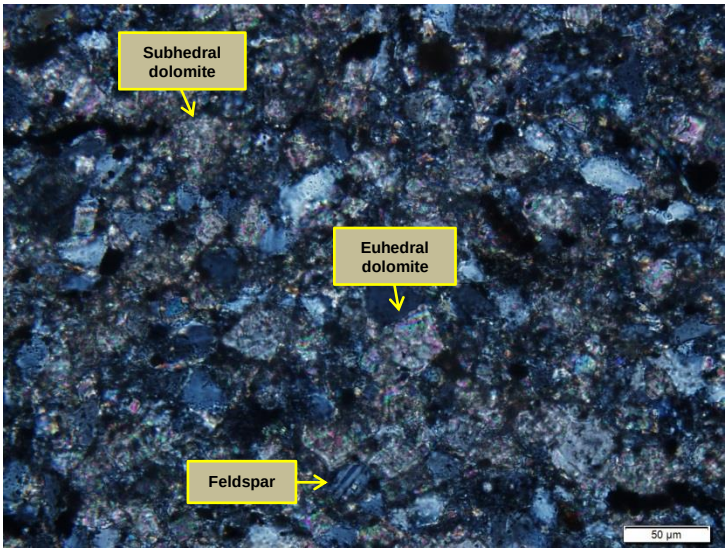


Fig. 6-50: Photomicrograph in XPL showing nonmimic diagenetic fabric, in which dolomitization has destroyed all evidence of original depositional texture, and euhedral to subhedral dolomite crystals occur in abundance.

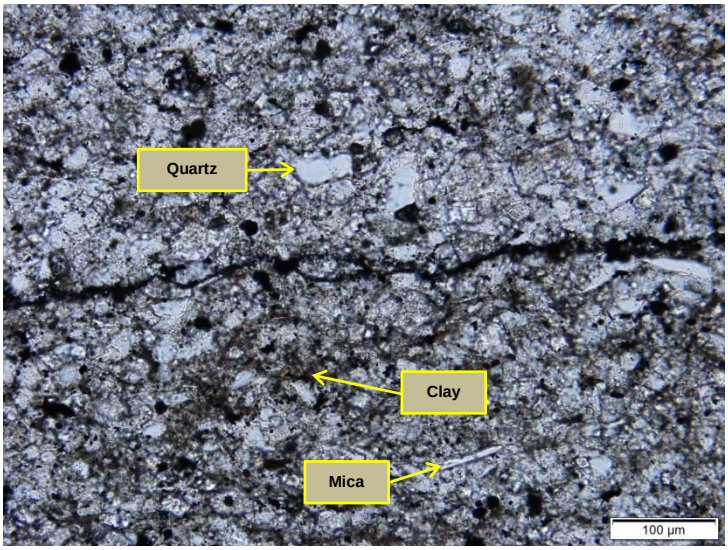


Fig. 6-51: Photomicrograph in PPL detailing a thin streak of pyrite (opaque) that has possibly replaced or infilled a former fracture. Some organic matter and clay material are likely associated with the feature as well. Note common fine to coarse silt-size quartz, scattered mica lathes and finely dispersed clays.

6.2.6 SAMPLE 13193

Sample ID	**13193**		
Sample Type	**Core**	**UWI/Well**	**102/14-10-007-19W4/00**
Strat. Unit	**Exshaw**	**Depth**	**1441.20 m**

XRD results

Quartz (%)	Feldspar (%)	Calcite (%)	Dolomite/ankerite (%)	Clays (%)
35.2	16.3	5.1	28.3	12.9

Pyrite (%)
2.1

Composition (*in order of abundance)*

	%	Variety (%)	Variety (%)	Variety (%)	Variety (%)
Cement (spar)	50	Dolomite (85)	Calcite (15)		
Cement (micrite)	0				
Clay	8	Clay minerals (100)			
Detrital grains	34	Quartz (96)	Mica (4)		
Opaques	8	Pyrite (100)			
Organics	<1	Amorphous (100)			
	100				

Allochems	100	Echinoderm debris (98)	Brachiopod shells (2)		
Matrix	0				
Porosity	<1	Shell dissolution vug			
	100				

Sedimentary structures

Primary	No bedding/stratification apparent.
Biogenic	Common clay streaks may be bioturbation features.

Fractures	None apparent.
Porosity	A single elongate vug, possibly resulting from dissolution of a bivalve shell, accounts for all of the porosity in this heavily cemented rock.
Opaques	Finely dispersed and framboidal pyrite are common throughout the sample. Pyrite is also observed to partially replace some echinoderm debris.
Organics	Rare amorphous organic matter (<1%).
Diagenetic	Heavily dolomitized, with nonmimic planar-e to planar-s fabric.

Bioclasts *(in order of abundance)*

Type	*Size (µm)*	*Preservation*	*Recrystallisation*
Echinoderm debris	200-4000 µm	Fair	Partial pyrite replacement
Brachiopod shells	1200 µm	Fair	N/A

Description

Sample 13193 is a finely crystalline silica-rich dolostone containing common echinoderm debris and rare brachiopod shell fragments. Clay streaks are commonly observed in the dolostone, and possibly represent bioturbation features. The rock is heavily dolomitized, and shows a nonmimic planar-e to planar-s fabric. Finely dispersed and framboidal pyrite are common in the sample, with pyrite also partially replacing some echinoderm fossils. The rock is almost entirely non-porous, with the exception of a single elongate vug that possibly resulted from dissolution of a bivalve shell.

Rock Classification

Finely crystalline silica-rich dolostone.

Thin Section Quality

Good. 1/2 stained for carbonates.

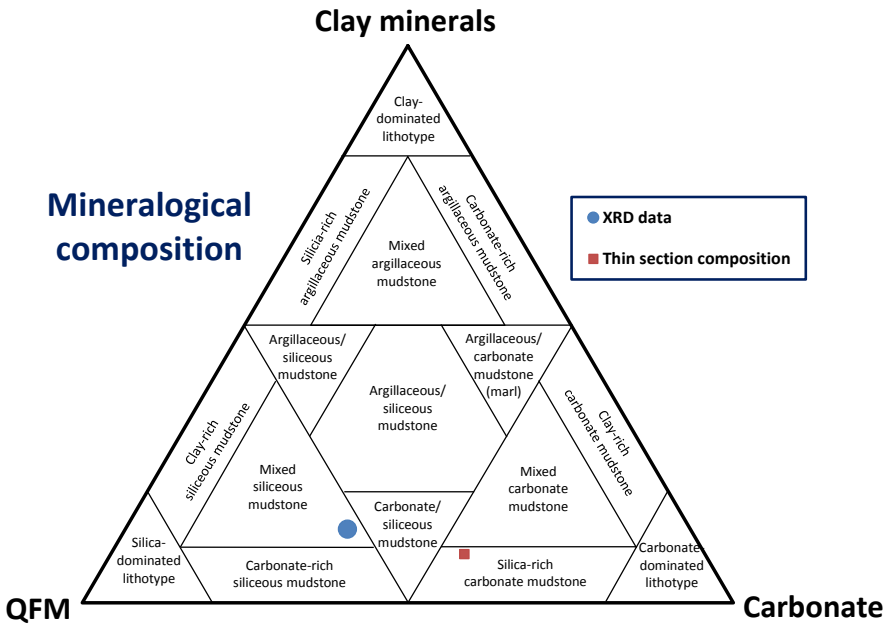


Fig. 6-52: Ternary plot of the mineralogical composition of the carbonate rock according to XRD data (blue) and estimated thin section composition (red). According to this scheme, sample 13193 is classified as a silica-rich carbonate mudstone. Using a grain- and crystal-size classification scheme for crystalline carbonate rocks, sample 13193 is classified as a finely crystalline dolostone (Folk, 1962).

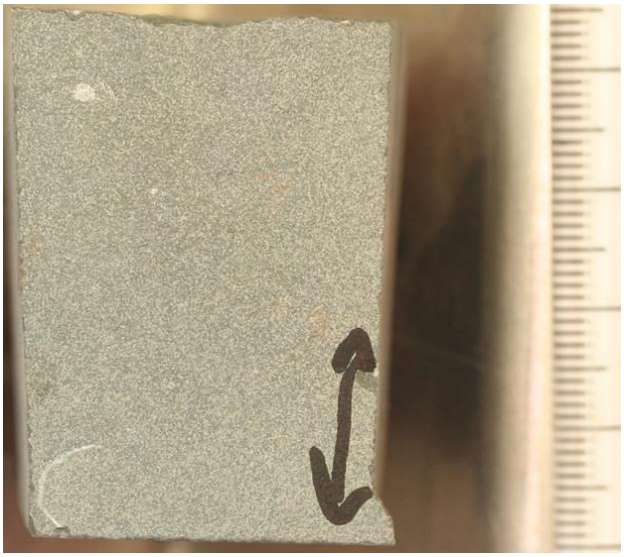


Fig. 6-53: Fig. 2: Core photograph of sample 13193 from the Exshaw Formation, well 102/14-10-007-19W4/00 (depth 1441.20 m). The thin section prepared from this sample was cut from the face shown in this image. The sample was received with no way-up direction. Scale is in mm.

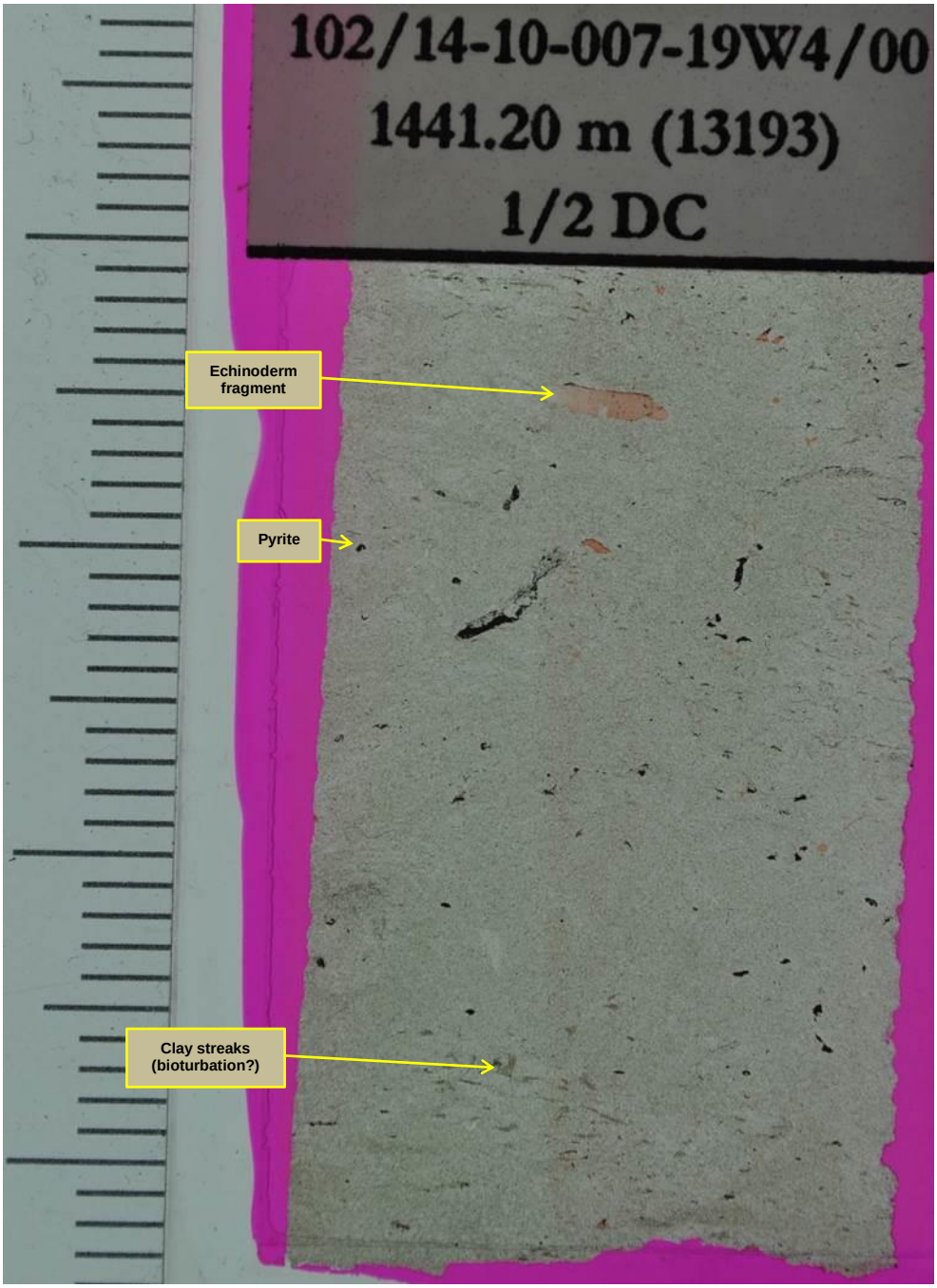


Fig. 6-54: Thin section photograph of sample 13193 from the Exshaw Formation, well 102/14-10-007-19W4/00 (depth 1441.20 m). The sample is a finely crystalline silica-rich dolostone. Clay streaks and patches are common and possibly represent bioturbation features. Common echinoderm fragments (likely crinoid columnals) and rare brachiopod shell fragments comprise the allochems present in the sample. Scale is in mm.

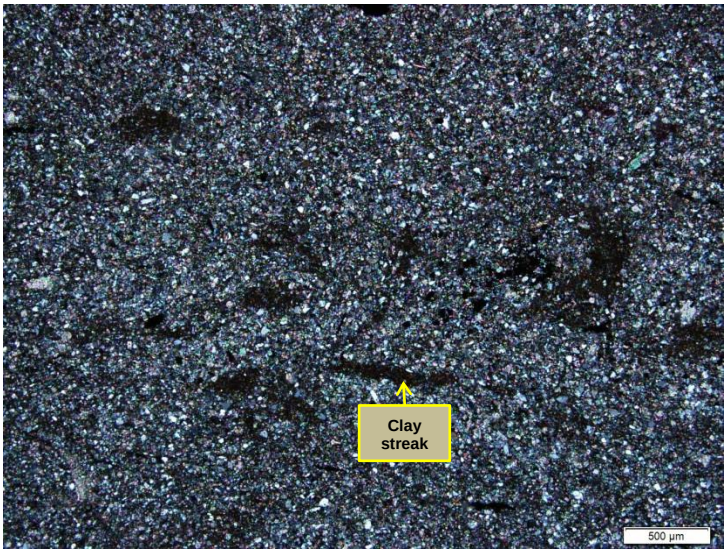


Fig. 6-55: Photomicrograph in XPL showing an overview of the sample, classified as a finely crystalline siliceous dolostone. The sample consists of extensive dolomite cementation and lacks distinct bedding or stratification features. Clay streaks and patches are common throughout the sample, and may represent bioturbation features.

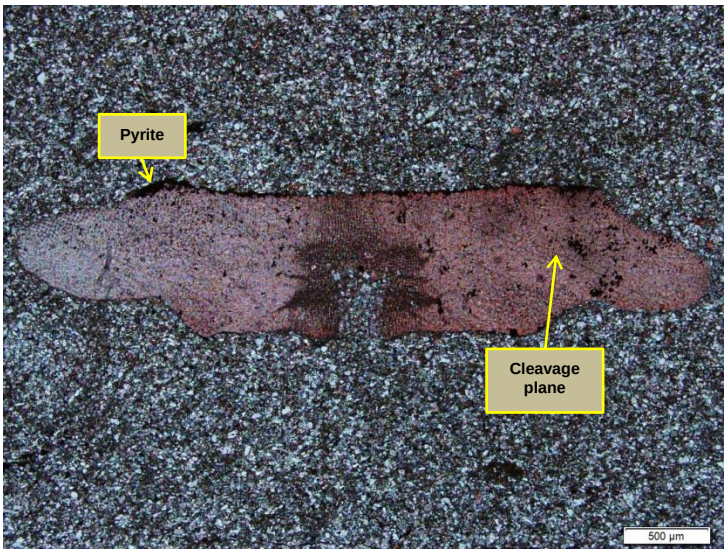


Fig. 6-56: Photomicrograph in PPL showing a well-preserved echinoderm fragment (~4.2 mm in length). The red stain indicates that it is composed of calcite. The visible cleavage planes indicate that it is made up of a single calcite crystal, a feature diagnostic of echinoderms. Note partial replacement of the fossil by pyrite (opaque).

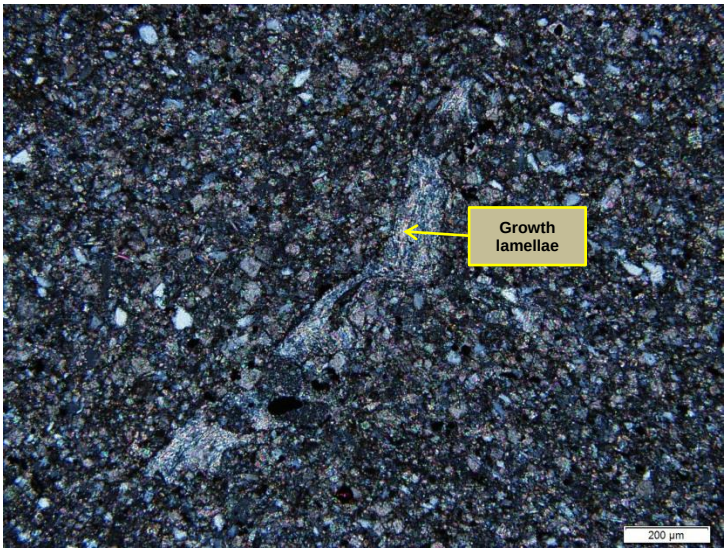


Fig. 6-57: Photomicrograph in XPL illustrating a brachiopod shell fragment (composed of calcite, unstained half of the slide). Growth lamellae are still visible on this shell, indicating that the fossil has not been extensively recrystallized.

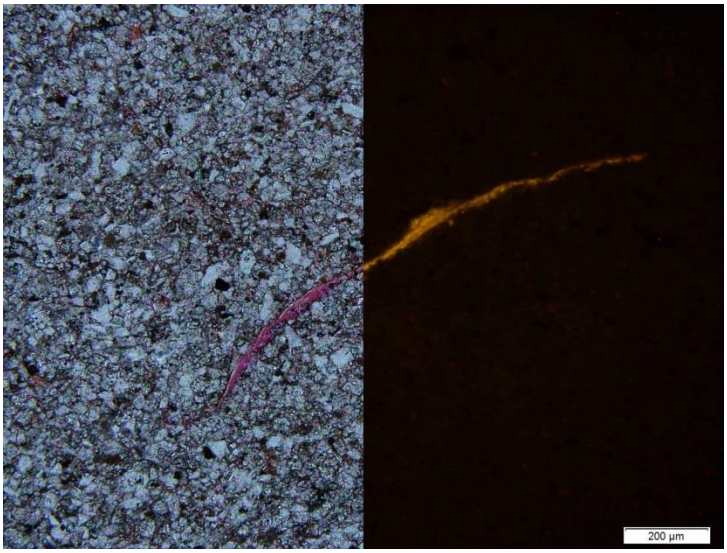


Fig. 6-58: Photomicrograph (left half in PPL, right half in UV light) showing an elongate pore (moldic bivalve shell?). Possible thin micropores are observed along grain and crystal boundaries, but are difficult to positively identify (see Figure 6-61).

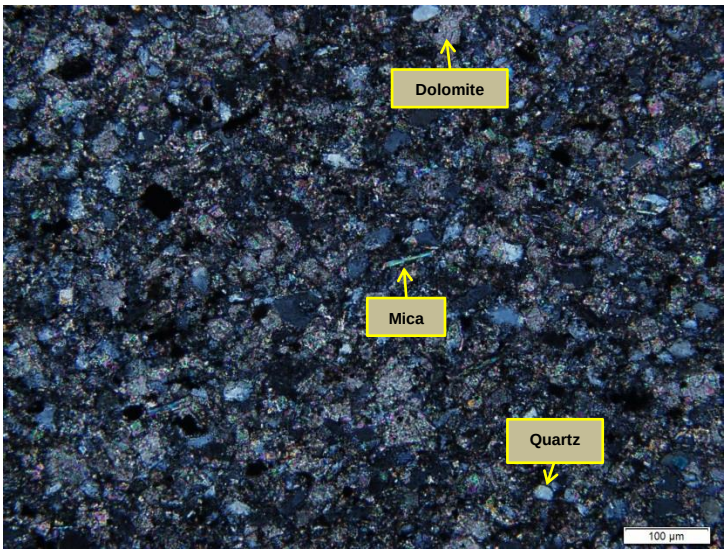


Fig. 6-59: Photomicrograph in XPL showing the mineralogy of sample 13193. The sample is composed primarily of dolomite (~43%), quartz (~33%), and mica (1-2%). Minor (~8%) calcite also occurs in the rock, typically as echinoderm debris or remnants of other shell fragments (see Figure 6-56). X-ray diffraction analysis indicates that feldspars comprise 16%; however, because no twinned or altered grains were observed in thin section, some grains identified petrographically as quartz are likely feldspars. Dolomite crystals present in this sample are between ~16 and 62 µm in size. Note higher birefringent colours associated with mica lathes compared to the more dull colours associated with dolomite.

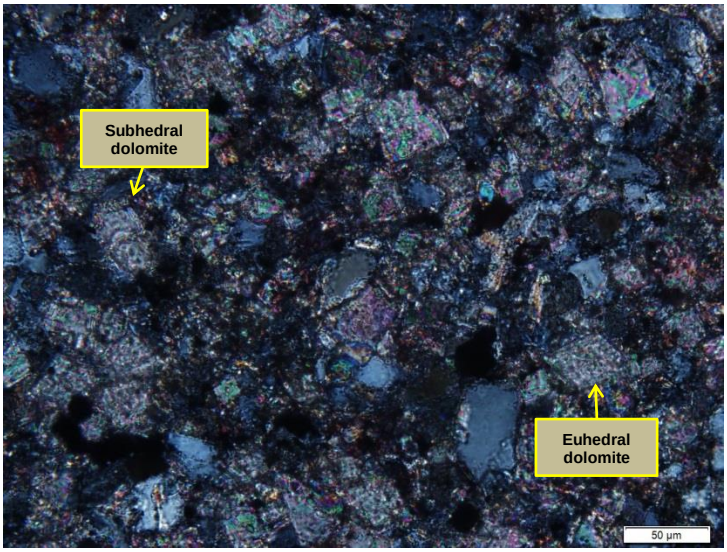


Fig. 6-60: Photomicrograph in XPL showing nonmimic diagenetic fabric due to multiple phases of dolomitization. The original depositional texture is replaced by abundant euhedral and subhedral dolomite crystals.

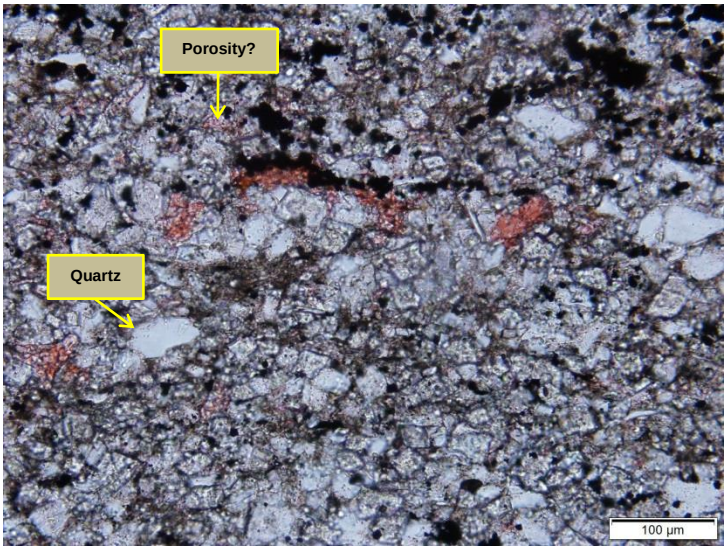


Fig. 6-61: Photomicrograph in PPL illustrating calcite (red stain), some of which may represent recrystallized shell fragments. The top half of the image shows concentrated finely dispersed pyrite (opaque), which forms clusters or pockets (former fecal remains?). Possible microporosity is observed along grain and crystal boundaries (pink epoxy), but is sometimes difficult to distinguish from calcite. Note silt- (common) to very fine sand-sized (rare) quartz grains.

6.2.7 SAMPLE 13818

Sample ID	**13818**		
Sample type	**Core**	**UWI/Well**	**102/10-07-077-04W5/00**
Strat. Unit	**Exshaw Formation**	**Depth**	**705.50 m**

XRD/SRA results

Quartz (%)	Fsp (%)	Cb (%)	Clays (%)	Pyrite (%)
14	35.8	17.5	4.8	24.6

Composition (*in order of abundance*)

Grain size	%	Variety (%)	Variety (%)	Variety (%)	Variety (%)
sand	45	Feldspar (95)	Quartz (5)		
silt	5	Feldspar (98)	Quartz (2)		
clay	8	Clay mins (100)			
Cement	25	Calcite (70)	Feldspar (25)	Dolomite (5)	
Bioclasts	5	?Phosphatic (100)			
Organics	2	Amorphous (100)			
Opaques	10	Pyrite (100)			
	100				

*Intensively altered to clay minerals

^ Including bitumen

Sedimentary structures

Primary	Apparent clay-rich laminae (rare).
Biogenic	None apparent.

Fractures	None apparent.
Porosity	6-8% intragranular porosity (feldspar degradation), <3% intergranular porosity.

Description

Muddy arkose comprised of angular (common) to subrounded (rare) coarse silt- to coarse sand-sized (average grain size is medium sand) detrital feldspar (30-50%) and quartz (10-15%). Many of the feldspar grains present in the sandstone show evidence of degradation, including open intergranular pores (6-8% porosity observed throughout the rock) and feldspar grains containing secondary calcite and dolomite cements. The majority of the feldspar grains present in the rock show complete (common) or partial (rare) overgrowth cementation. Much of the intergranular space in the sandstone is filled with poikilotopic calcite cement, dolomite cement, or clay matrix; however, minor (<3%) intergranular porosity is observed throughout the rock.

Thin Section Quality

Good. 1/2 stained for carbonates.

Rock Classification

Muddy sandstone.

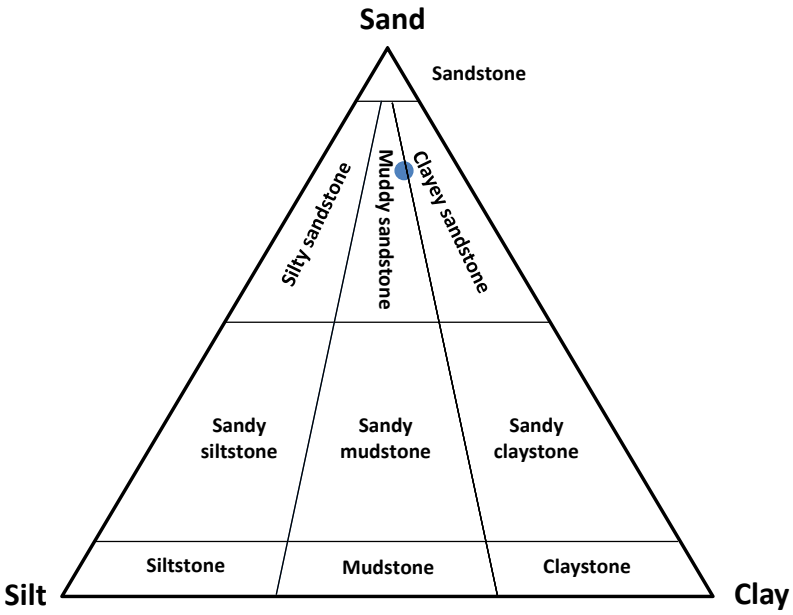


Fig. 6-62: Ternary plot showing the grain size composition of the sample based on the Wentworth scale (after Folk, 1954). Sample 13818 is classified as a muddy sandstone.

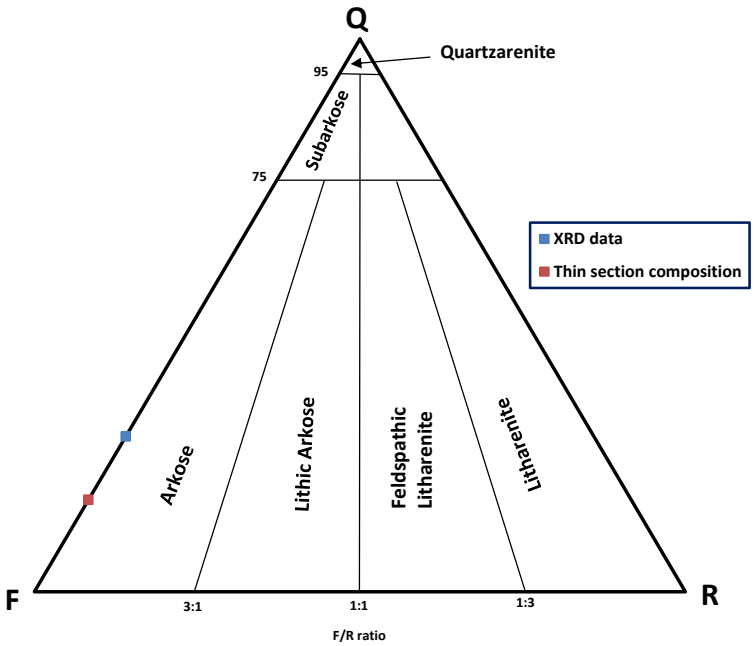


Fig. 6-63: Ternary plot showing the relative abundance of different detrital grains within the sandstone. Sample 13818 is classified as an arkose due to the abundance of feldspar in the sample.



Fig. 3: Core photograph of sample 13818 from the Exshaw Formation, well 102/10-07-077-04W5/00 (depth 705.50 m). The thin section prepared from this sample was cut from the area marked with an X. The sample was received with no way-up direction. Scale is in mm.

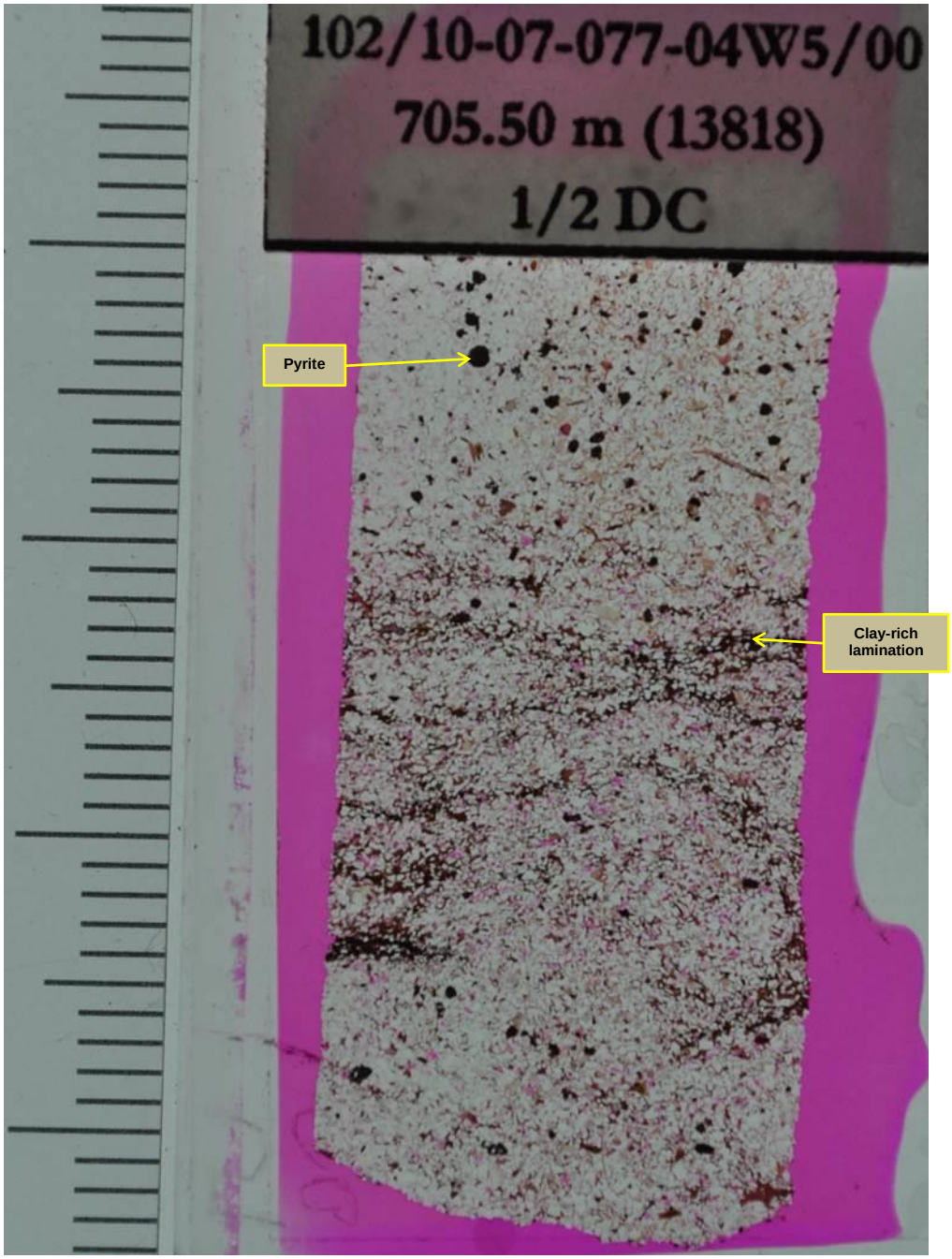


Fig. 6-64: Thin section photograph of sample 13818 from the Exshaw Formation, well 102/10-07-077-04W5/00 (depth 705.50 m). The sample is a muddy arkose with minor clay-rich laminae. Stratigraphic up-direction was not indicated and may differ from that shown here. Scale is in mm.

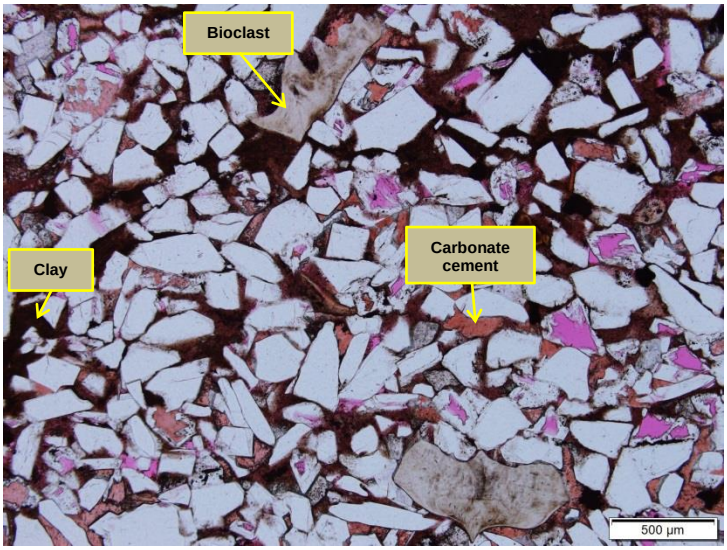


Fig. 6-65: Photomicrograph in PPL showing an overview of the muddy arkose sandstone. Most of the sample has calcite (stained red) and dolomite cements between the detrital grains. Faint laminae (see Figure 6-64) are visible in the thin section as areas of elevated clay matrix. Phosphatic bioclasts with thinly laminated microstructures (fish bone fragments?) comprise ~5% of the sandstone.

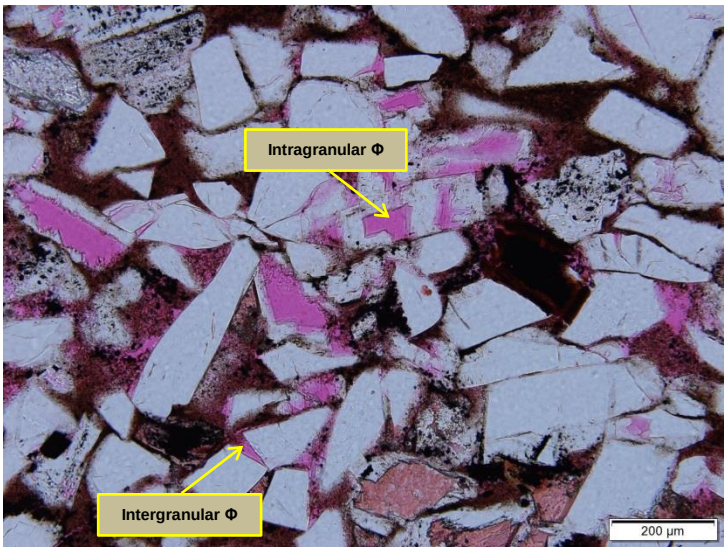


Fig. 6-66: Photomicrograph in PPL illustrating intra- and intergranular porosity. Intragranular porosity (6-8%) occurs in partially degraded feldspar grains. Minor (<3%) intergranular porosity occurs throughout the sample. Some microporosity (~1-2%) is also associated with clay material.

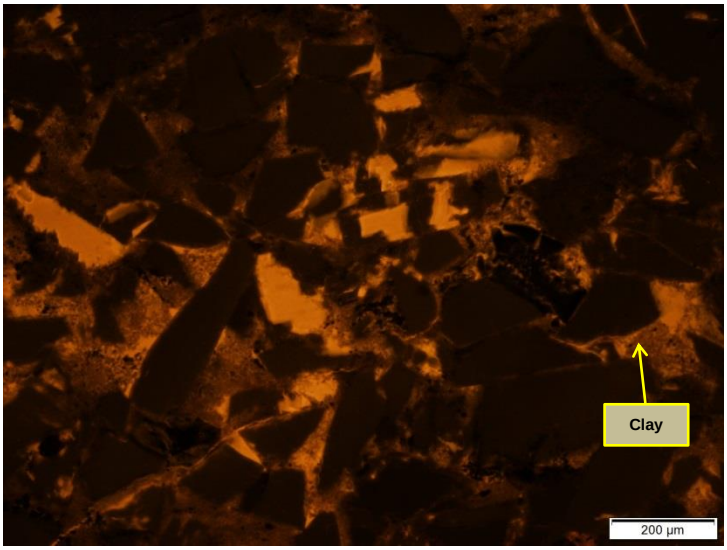


Fig. 6-67: Photomicrograph of Figure 6-66 in UV light illustrating intra- and intergranular porosity. Intragranular porosity shows the brightest yellow colour in UV light, whereas areas of intergranular porosity and clay (microporosity) show faint yellow and speckled yellow colours, respectively.

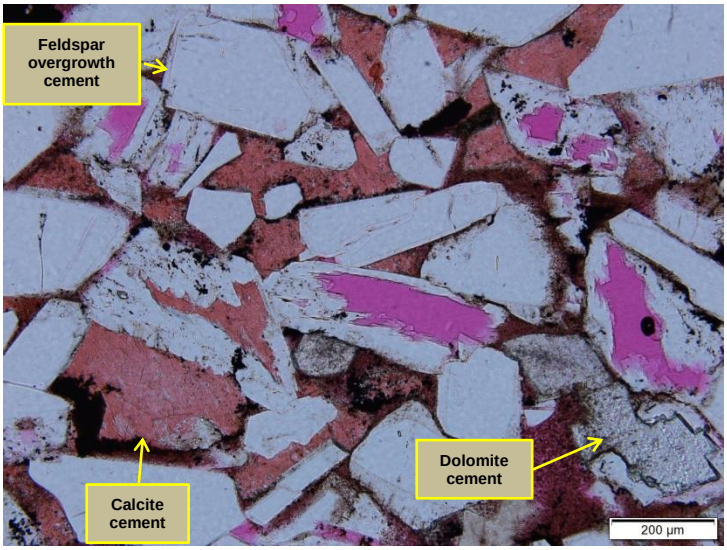


Fig. 6-68: Photomicrograph in PPL detailing carbonate and feldspar cements observed in the sample. Calcite (red stained crystals) and dolomite (grey-white rhombic crystals) cement intergranular space, and fill some partially degraded feldspar grains. The majority of the feldspar grains present in the arkose show complete or partial (rare) overgrowths.

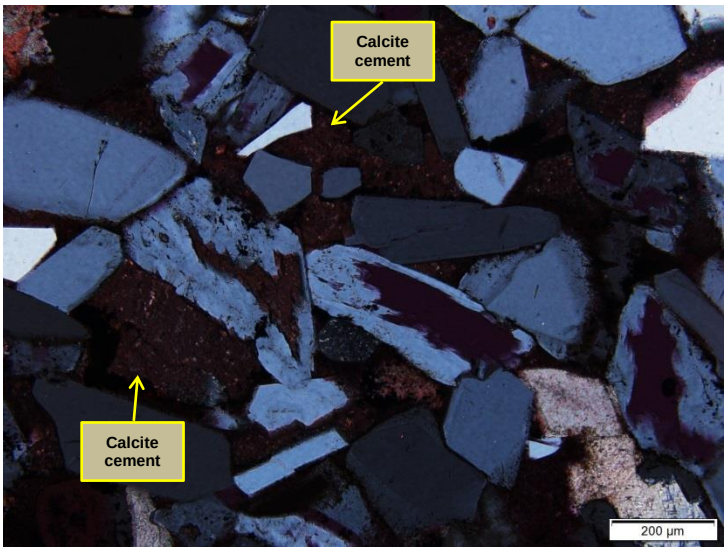


Fig. 6-69: Photomicrograph of Figure 6-68 in XPL (stage rotated ~10 degrees) illustrating poikilotopic calcite cement present throughout the sample. Poikilotopic refers to cement that exhibits a uniform extinction.

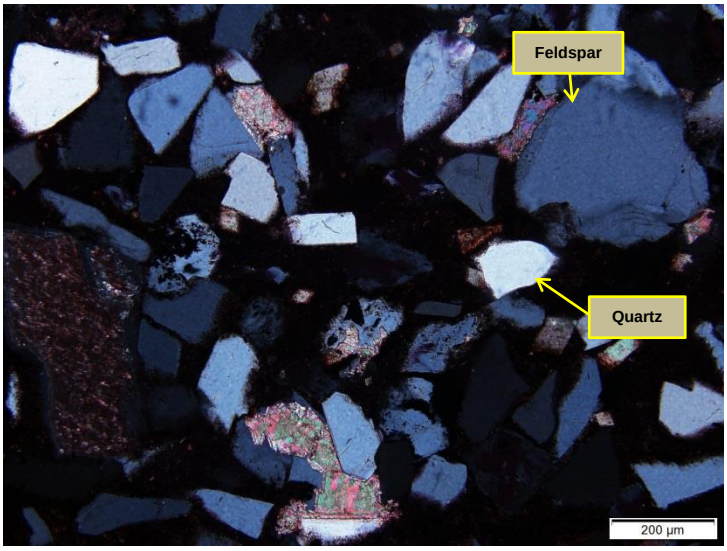


Fig. 6-70: Photomicrograph in XPL showing angular to subrounded (rare) coarse silt- to coarse sand-sized (average grain size is medium sand) detrital feldspar (30-50%) and quartz (10-15%) present throughout the sample. Quartz is distinguished from feldspar by its slightly higher birefringence and lack of authigenic feldspar overgrowths.

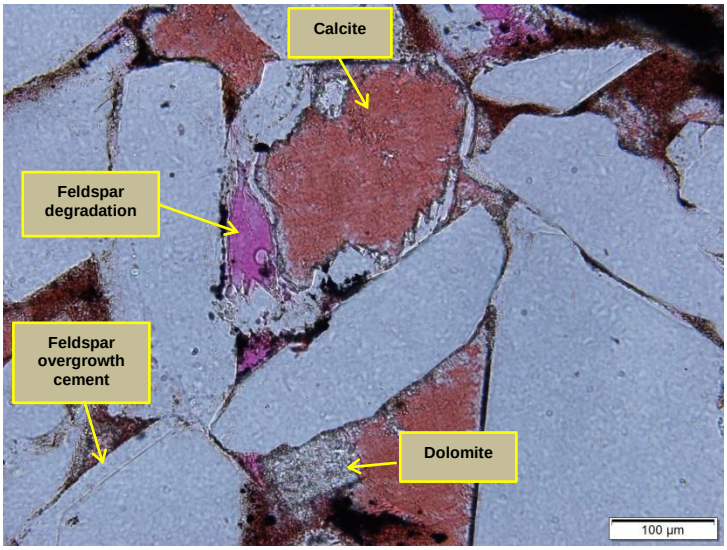


Fig. 6-71: Photomicrograph in PPL detailing diagenetic features observed in the sample. At least four diagenetic features are observed, including: partial feldspar degradation, feldspar overgrowths, dolomite cementation, and calcite cementation.

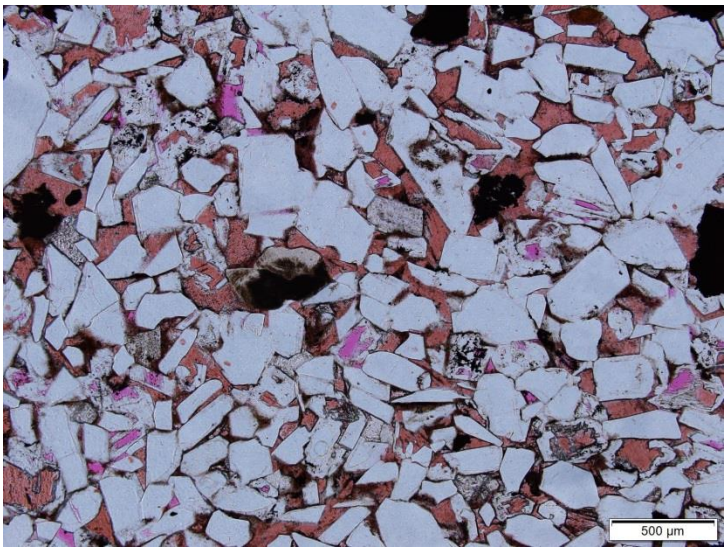


Fig. 6-72: Photomicrograph in PPL illustrating an overview of the top half of the thin section, which shows pervasive calcite cementation (red stain).

7. Duvernary Formation Overview

Petrographic thin sections were prepared from five core samples from two wells (see Table 7-A) of the Duvernay Formation. Samples were examined using transmitted light microscopy. Thin sections were impregnated with rhodamine-B epoxy (pink), allowing porosity and fracture characterization using UV fluorescence microscopy. Four of the samples were also dual-stained to aid in carbonate identification. Sample 15010 was not carbonate-stained due to clay sensitivity issues. The following summary focuses on observations of sediment composition, cementation, diagenesis, clays/organics, porosity and fracture characteristics. The samples constitute three lithofacies (Table 7-A). The mineralogical summary of these lithofacies is given in Table 7- B.

7.1 SUMMARY

7.1.1 CORE SAMPLES:

Well Location	Lithofacies	Depth (Sample ID)
100/12-06-035-20W4/00	1	1886.4 m (11127)
100/13-14-035-25W4/00	2	7796.5 ft. (15027)
100/13-14-035-25W4/00	2	7745.7 ft. (15013)
100/13-14-035-25W4/00	3	7738.5 ft. (15010)
100/13-14-035-25W4/00	2	7713.2 ft. (15005)

Table 7-A: Lithofacies distribution by Well.

7.1.2 LITHOFACIES, GROUPINGS AND DESCRIPTIONS:

Lithofacies	Classification	Quartz %	Feldspar %	Dolomite %	Calcite %	Pyrite %	Organics %	Clay /Mica %
1	Bio-pel extramicrite	~2	0	~25	~70	<1	~2	0
2	Biomicrite/biosparite	~1-5	~1-3	~1-7	~80-95	<1	<1	~1-5
3	Organic-rich biomicrite	~10	~8	~6	~50	~4	~5	~20

Table 7-B: Mineralogical summary of lithofacies.

7.1.2.1 LITHOFACIES 1: BIO-PEL EXTRAMICRITE

Lithofacies 1 (sample 11127) consists of a bio-pel extramicrite that contains abundant peloidal material, rounded extraclasts and a diverse bioclast assemblage. Sedimentary structures are poorly defined although some organic-and/or clay-rich layers are present within extraclasts. The sample is moderately to heavily bioturbated as indicated by large amounts of peloidal material. The sample predominantly consists of micrite with some diagenetic calcite and dolomite spar. These more coarsely-crystalline patches may represent cemented coral/reef debris (extraclasts). Other bioclast fragments include brachiopods, crinoids, ostracods, green algae, and some possible tentaculitids, which are generally replaced by microcrystalline calcite. Bioclasts are usually moderately well preserved. Organic matter (~2%) is largely present as compressed algal material, which fills interparticle space and wraps around cements. Some fluid organic matter (including hydrocarbons?) is also observed within extraclasts. Opaque material (pyrite) is rare. Visual porosity is low (~2%) with some interparticle porosity observed within sparry extraclasts. One vertical fracture runs from the center to the top of the sample and is completely healed by microcrystalline calcite.

7.1.2.2 LITHOFACIES 2: BIOMICRITE/BIOSPARITE

Lithofacies 2 consists of sparse biomicrites and biosparites with varying fossil content. Sedimentary structures such as laminae are generally not visible, although a few faintly defined bedding planes (sample 15027) are present. Some samples are very lightly bioturbated and contain varying concentrations of peloidal material and lighter-coloured sparry lenses (burrowing structures?). All samples are composed predominantly of sparry calcite cements (samples 15013 & 15005) and/or lime mud (sample 15027), with smaller amounts of dolomite, quartz, feldspar and clays present (see Table B for summary). Bioclast fragments are moderately abundant and consist of recrystallized brachiopods, tentaculitids, crinoids and ostracods. Organic content is generally low (<1%) and is interpreted to be mainly algal in origin. Visual porosity is <1% due to high amounts of diagenetic cementation. Sub-horizontal and vertical fractures are rare and likely artificial.

7.1.2.3 LITHOFACIES 3: ORGANIC-RICH BIOMICRITE

Lithofacies 3 consists of an argillaceous biomicrite, which is very organic- and opaque-rich compared to the samples of Lithofacies 1 & 2. Bedding planes and laminae are poorly defined. Abundant lighter-coloured lenticular features are relatively organic-poor compared to the surrounding matrix and may represent burrowing structures. Peloidal material is absent. The sample predominantly consists of lime mud and clay minerals (including muscovite mica lathes) with some carbonate spar, quartz and feldspar grains. However, mineralogical composition is difficult to determine in thin section as most grains and cements are heavily obscured by organic matter and opaque material. Carbonate-replaced bioclasts are also difficult to identify due to poor preservation. Organic matter is abundant (~5%) and is uniformly distributed throughout the sample. Pyrite is also commonly observed and consists of disseminated as well as small idiomorphic crystals. Visual porosity is low or absent. Discontinuous, bedding-parallel microfractures are also rare, and were likely produced during sample preparation.

7.1.3 SEDIMENTARY STRUCTURES & BIOTURBATION:

Sedimentary structures (such as bedding planes and laminae) are generally absent in all the samples due to destructive diagenetic cementation and recrystallization. However, sample 15027 contains some very faintly defined bedding planes that may indicate low energy sediment transport. Bedding-parallel organic- and/or clay-rich layers are also present within sparry extraclasts in sample 11127. Bioturbation within the samples is generally light to moderate and consists of peloidal material, which may represent fecal pellets. Elevated amounts of peloids in sample 11127 indicates that bioturbation and sediment mixing was higher. Lighter-coloured lenticular patches (samples 15005 and 15010) are likely burrowing structures which could also explain the lack of structure within the samples.

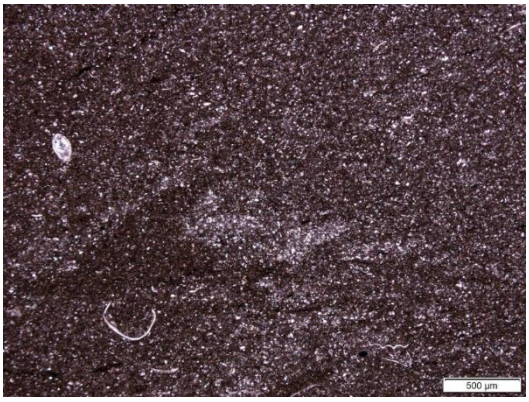


Fig. 7.1.3-1: Overview photomicrograph in PPL showing a biomicrite with some fossil fragments. Sedimentary structures such as bedding planes and laminae are absent. Lighter-coloured lenses are likely bioturbation structures. Also note numerous opaque-rich peloids which may represent fecal pellets (sample 15005, 7713.2 ft.).

7.1.4 DIAGENESIS:

All of the samples have been diagenetically altered, replaced and/or recrystallized with microcrystalline calcite, calcite spar, dolomite (rare), quartz, and anhydrite (rare; see sample 15013). Sparry carbonate patches within sample 11127 are likely loosely consolidated coral/reef debris dolomitized during early diagenesis. Bioclast fragments have also been replaced with carbonate minerals, and often feature edge or end dissolution. Very few quartz pseudomorphs (after dolomite crystals, sample 15013) and angular diagenetic quartz cements (sample 15010) are observed. The quartz in these samples sometimes features carbonate and (rarely) anhydrite overgrowths.

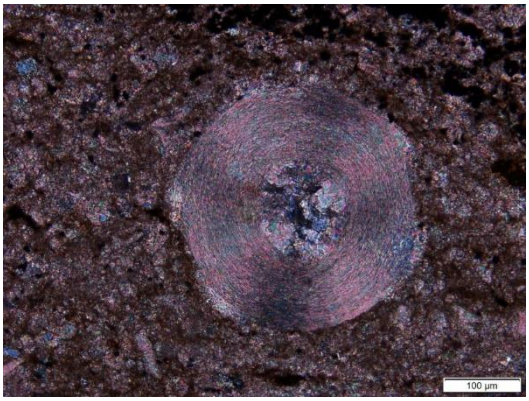


Fig. 7.1.4-1: Photomicrograph in XPL showing a bioclast fragment (brachiopod spine) surrounded by a matrix consisting of micrite cement and diagenetic carbonate spar (sample 15013, 7745.7 ft.)

7.1.5 ORGANIC MATTER & CLAYS:

Organic, clay and opaque content is generally fairly low. Organic matter is enriched within the micrite material that fills interparticle space and makes up the matrix of most samples. Organics are usually observed as ‘wispy’ or ‘netty’ brown material that forms strings, and is likely algal in origin. These strings are sometimes partially pyritized. Other organic material includes plant fragments, which are abundant in samples 11127 and 15005.

Pyrite is generally present as cubic and idiomorphic crystals and is observed as inclusions within (and lining the edges of) replaced bioclast fragments. Finely disseminated pyrite crystals are also present within micritic matrix.

Fine-grained clay minerals (e.g. illite) cannot be easily resolved using standard petrographic analysis due to their close association with organic matter. However, clay minerals are rarely observed and where present often fill the space between sparry carbonate cements.

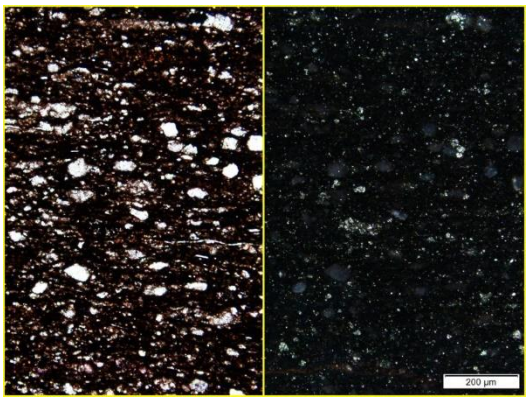


Fig. 7.1.5-1: Photomicrograph in overexposed PPL (left) and reflected light (right) showing a representative overview of Lithofacies 3. Abundant organic matter and clay minerals obscure grains and cements. Reflected light shows that disseminated pyrite crystals are also finely dispersed throughout (sample 15010, 7738.5 ft.)

7.1.6 BIOCLASTS:

Bioclasts mainly consist of bivalve and/or brachiopod shell fragments, spines and valves, which are often replaced by microcrystalline calcite cement and contain cubic pyrite inclusions. Articulated brachiopod shells are often filled by organic- and/or opaque-poor micrite, which contains smaller bioclast fragments. Lenticular and circular tentaculitid fragments are also commonly observed throughout the samples and are often replaced with both microcrystalline and sparry calcite cements. Ostracod fragments are less commonly observed and usually consist of a thin outer carapace replaced with microcrystalline calcite. Some bioclast fragments are rimmed by pyrite and organic matter. Crinoid fragments are rarely observed.

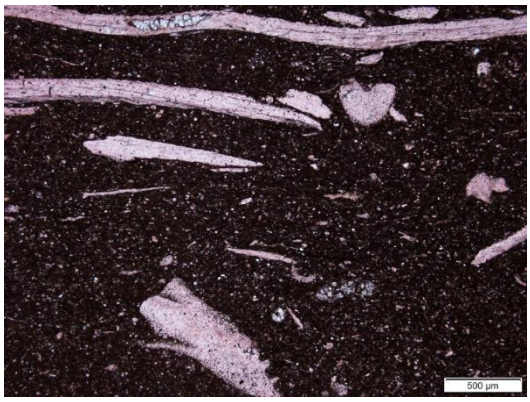


Fig. 7.1.6-1: Photomicrograph in PPL showing abundant bioclasts, including: brachiopod shells, crinoid fragments and tentaculitid fragments. The bioclasts are often replaced with microcrystalline calcite and (more rarely) dolomite spar. Also note small cubic pyrite inclusions within the crinoid fragment to the bottom of the image (sample 15027, 7796.5 ft.)

7.1.7 POROSITY & FRACTURING:

Porosity is low or absent in the samples, with diagenetic cements and micrite occupying most intergranular space. Compaction may also be a control on porosity and permeability, as evidenced by the presence of compressed algal strings within some samples. Porosity is typically associated with the edges of fossil fragments, and also commonly observed within sparry extraclasts (sample 11127). Discontinuous sub-parallel and vertical microfractures present in the samples were likely produced during sample preparation or unloading.

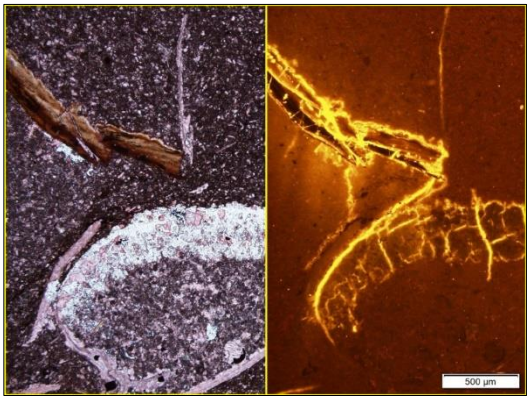


Fig. 7.1.7-1: Photomicrograph in PPL (left) and UV light (right) showing porosity associated with bioclast fragments and associated sparry carbonate infills. Porosity within the surrounding matrix is very low or absent, which is characteristic of these samples (sample 15013, 7745.7 ft.).

7.2 RESULTS

7.2.1 SAMPLE 11127

Sample ID	**11127**		
Sample Type	**Core**	**UWI/Well**	**100/12-06-035-20W4/00**
Strat. Unit	**Duvernay**	**Depth**	**1886.4 m**

XRD results

Quartz (%)	Feldspar (%)	Calcite (%)	Dolomite/ankerite (%)	Clays (%)
1.9	0	73.8	24.4	0

Pyrite (%)
0

Composition (*in order of abundance)*

%	Variety (%)	Variety (%)	Variety (%)	Variety (%)
Cement (micrite) 57	Calcite (100)	Clay minerals (trace)		
Cement (spar) 40	Dolomite (75)	Calcite (25)		
Organics 2	Amorphous* (90)	Plant (10)		
Opaques 1	Pyrite (100)			
100				

** Including hydrocarbons (bitumen?)*

Allochems 65	Extraclasts (40)	Bioclasts (30)	Peloids (30)	
Matrix 33	Micrite (60)	Spar (40)		
Porosity 2				
100				

Sedimentary structures

Primary	Some bedding-parallel laminations within extraclasts (alternating sparry (~1 mm wide) and opaque- and/or clay-rich (300-350 µm) layers)
Biogenic	Abundant peloids range in size (generally 40-60 µm, up to 160 µm) and are concentrated within the micrite matrix. This indicates sediment mixing and/or bioturbation.

Fractures	One vertical microfracture (10 µm wide, completely healed by microcrystalline calcite cement) runs from the center to the top of the sample and cross-cuts extraclasts. This indicates that the fracture was created after the incorporation of extraclasts into the sediment. Bedding-parallel microfractures are obscured by opaque material and likely represent opening fractures which were produced during sample preparation/unloading.
Porosity	Very minor porosity (<1%) associated with peloidal micrite. Interparticle porosity (between cements) commonly observed within sparry extraclasts.
Opaques	Some intraclasts/coral fragments feature abundant cubic pyrite crystals (<10 µm) and clusters (up to 200 µm) which fill the space between sparry carbonate cements and overprint some dolomite rhombs. Pyrite is rare elsewhere.
Organics	Organic matter (possibly representing compressed algal material/mats) fills interparticle space and wraps around cements. Some plant spores and fragments are also observed. A few extraclasts feature fluid organic matter (hydrocarbons, including bitumen?) and brown-stained carbonate spar indicating oil migration.
Diagenetic	Bioclast fragments completely replaced/recrystallized with microcrystalline calcite cements and (more rarely) calcite/dolomite spar. Sparry carbonate patches represent coral/reef debris that was loosely cemented and dolomitized during early diagenesis. Peloids likely formed via 'micritization' of primary carbonate grains.

Bioclasts *(in order of abundance)*

Type	*Size (µm)*	*Preservation*	*Recrystallisation*
Coral fragments	Up to ~5500	Moderate to good	Cal; micrite; dol
Brachiopods	Up to ~2000	Poor to good	Cal
Crinoids	Up to ~1700	Poor to good	Cal
Green algae	Up to ~1000	Moderate to good	Cal; micrite
Ostracods	Up to ~300	Poor	Cal
Tentaculitids	Up to ~200	Moderate	Cal; micrite; dol
Stromatoporid	~1500	Moderate	Cal; micrite; dol
Unidentified	Up to ~2500	Poor to moderate	Cal; micrite; dol

Description

Sample 11127 is a bio-pel extramicrite featuring a sparse biomicrite matrix with abundant peloids and extraclasts. The majority of the sample consists of a fine-grained micrite matrix containing some carbonate spar, abundant well-sorted peloids and a diverse bioclast assemblage (including brachiopods, crinoids, ostracods, green algae, some possible tentaculitids and a stromatoporid). Bioclast fragments exhibit a variety of preservation states (generally moderately well preserved) and are replaced by microcrystalline calcite and (more rarely) sparry carbonate cements. The extraclasts (sometimes >1 cm in length) are generally fairly rounded and composed of sparry carbonate cements (dolomite with some calcite) which interlock to form a rigid framework and contain some bioclastic debris (including crinoids and brachiopod shell fragments). Restricted interparticle space is filled by opaque- and/or organic-rich micrite. The extraclasts likely represent coral/reef debris that was loosely cemented and dolomitized during early diagenesis, broken apart and transported (during a storm?) and incorporated into a back-reef sediment. Pyrite is generally very finely dispersed throughout the sample but is concentrated within some extraclasts where it fills interparticle space and overprints rhombic dolomite cements. Organic matter is also concentrated within extraclasts, wraps around sparry carbonate cements and may represent compressed algal mats. In addition, some fluid hydrocarbons (including bitumen) and plant fragments are observed. One vertical microfracture cross-cuts extraclasts and is completely healed by microcrystalline calcite cement. Porosity is low within the sparse biomicrite matrix but is high within extraclasts where loosely cemented carbonate spar leads to abundant open interparticle space.

Rock Classification

Bio-pel extramicrite (Folk, 1962); mixed-fossil pelletal extraclastic wackestone/packstone (Dunham, 1962)

Thin Section Quality

Good; 1/2 stained for carbonates.

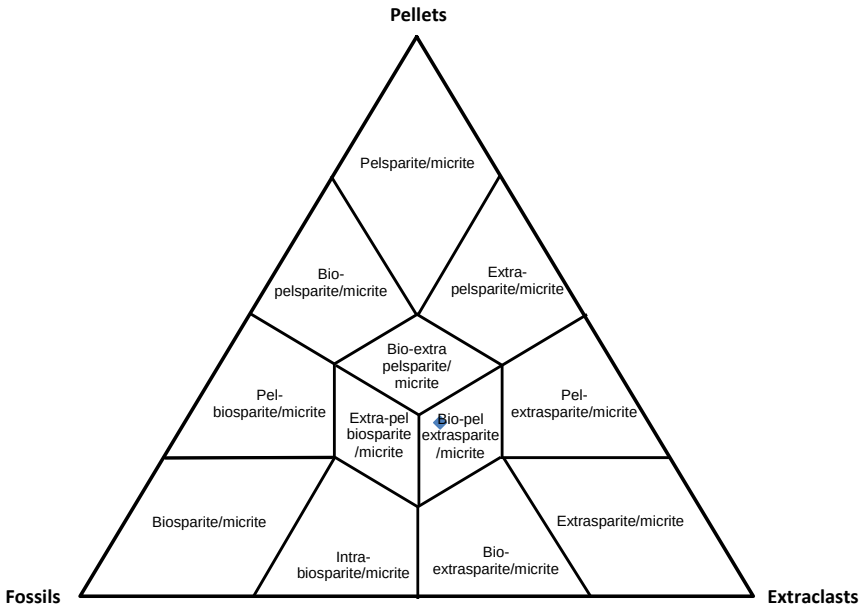


Fig. 7-1: Ternary plot showing the relative abundance of different allochem types within the carbonate rock (based on Folk's classification scheme, 1962). Sample 11127 is classified as bio-pel extramicrite as the rock has a predominantly micrite matrix with many extraclasts (sparry coral/reef debris), abundant peloidal material and 10-50% bioclasts.

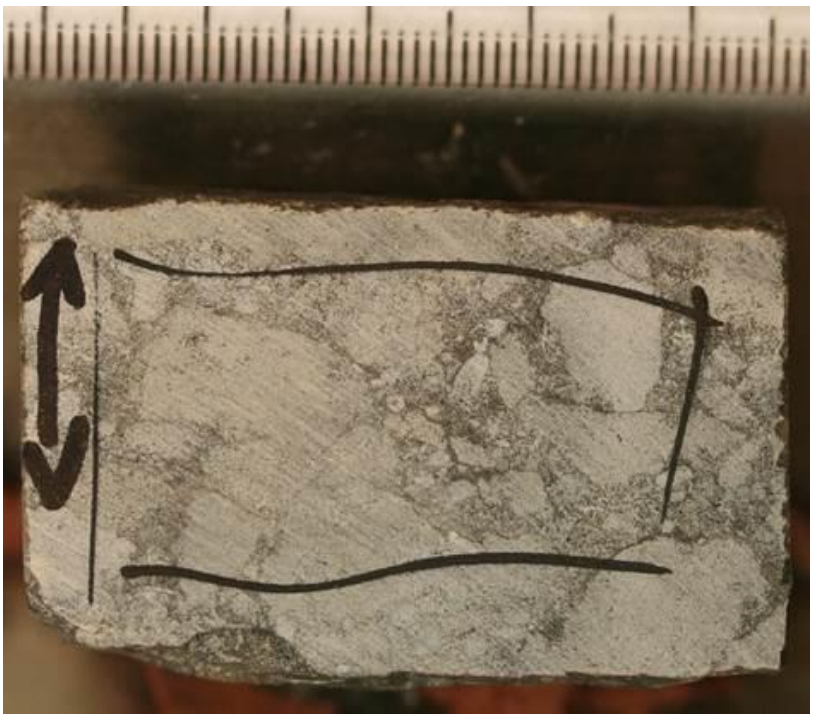


Fig. 7-2: Core photograph of sample 11127 from the Duvernay Formation, well 100/12-06-035-20W4/00 (depth 1886.40 m). The thin section prepared from this sample was cut from the area outlined in black marker. The sample was received with no up direction. Scale is in mm.

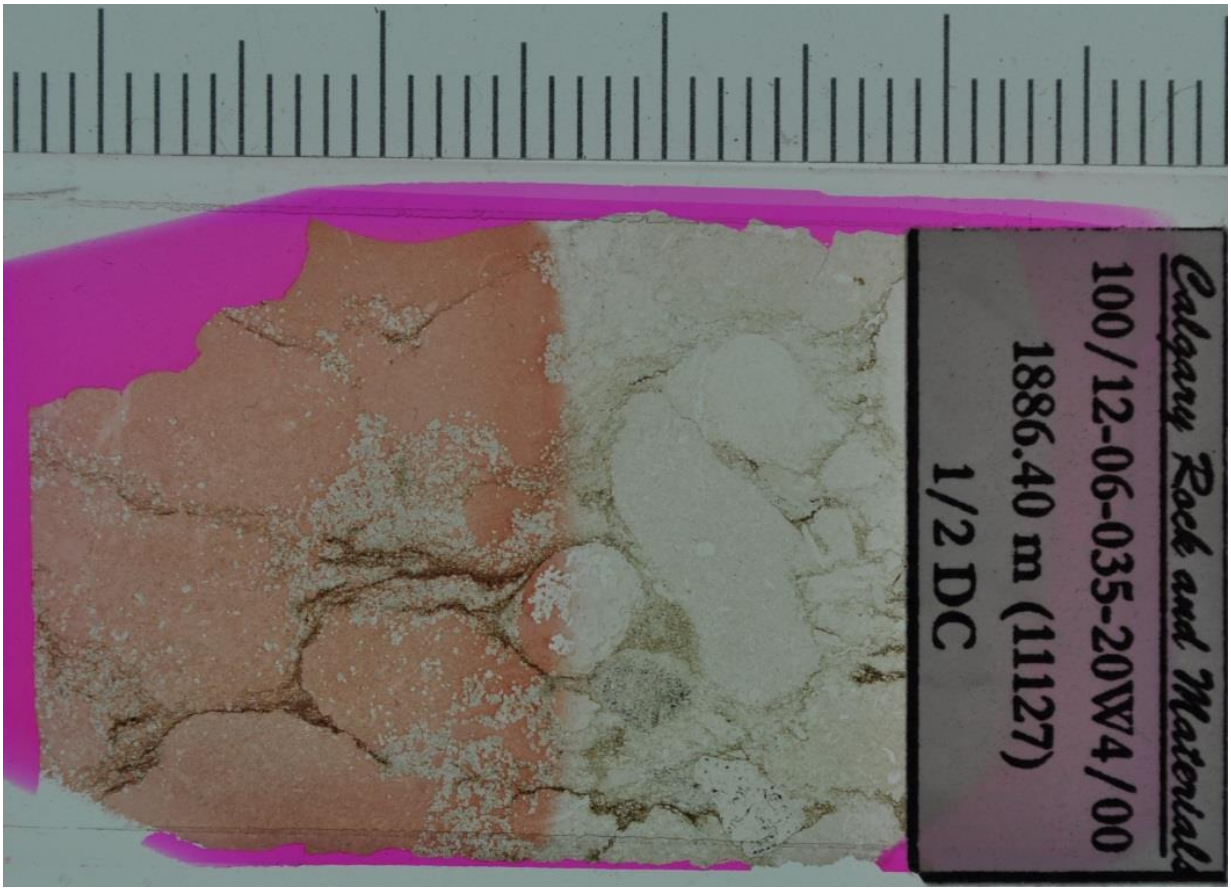


Fig. 7-3: Thin section photograph of sample 11127 from the Duvernay Formation, well 100/12-06-035-20W4/00 (depth 1886.40 m). The image reveals a carbonate rock containing several sparry clasts (representing extraclasts and/or coral fragments) which are separated by micritic material and organic matter. Some of the clasts appear to feature opaque (minor pyrite) inclusions (e.g. bottom-right). Intensive pink staining within the carbonate-stained half of the thin section (left of image) shows the dominance of calcite in the sample. Scale is in mm.

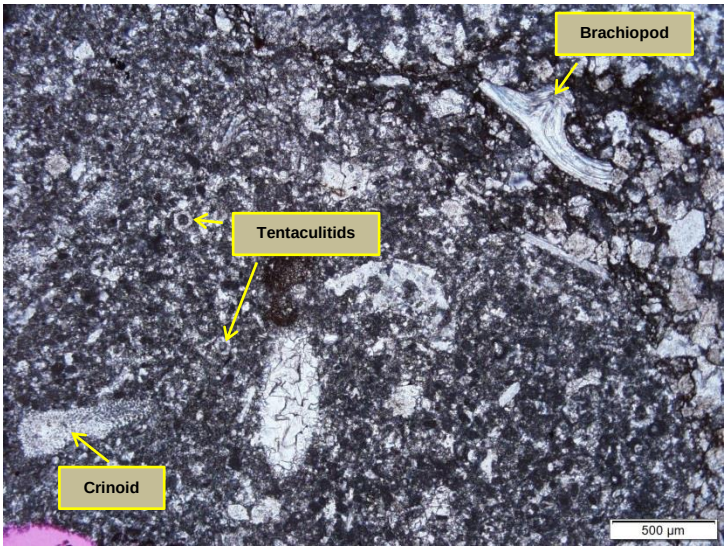


Fig. 7-4: Photomicrograph in PPL showing an overview of sample 11127 (well 12-6, depth 1886.4 m) within the unstained part of the thin section. The image illustrates a carbonate rock containing abundant bioclast fragments replaced by both microcrystalline and sparry carbonate cements. Bioclasts include crinoids (~700 µm), brachiopod shells (750 µm, some showing internal structures), and circular to lenticular fragments (including possible tentaculitids, 100-800 µm). The matrix is composed of a mixture of micritic material, carbonate spar and abundant peloids (~65 µm). Opaque, organic and/or clay material also fills interparticle space (i.e. top-right of the image).

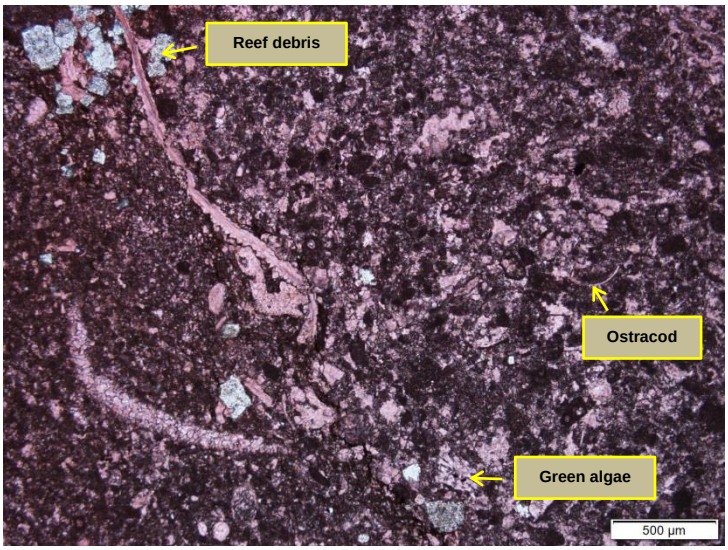


Fig. 7-5: Photomicrograph in PPL showing abundant calcite (stained) with minor amounts of dolomite. Several shell fragments are visible including an ostracod carapace (250 µm) and a green algal fragment (250 µm). The angular coarse blocky dolomite cements (up to 250 µm, top-left) represent diagenetically altered coral/reef debris.

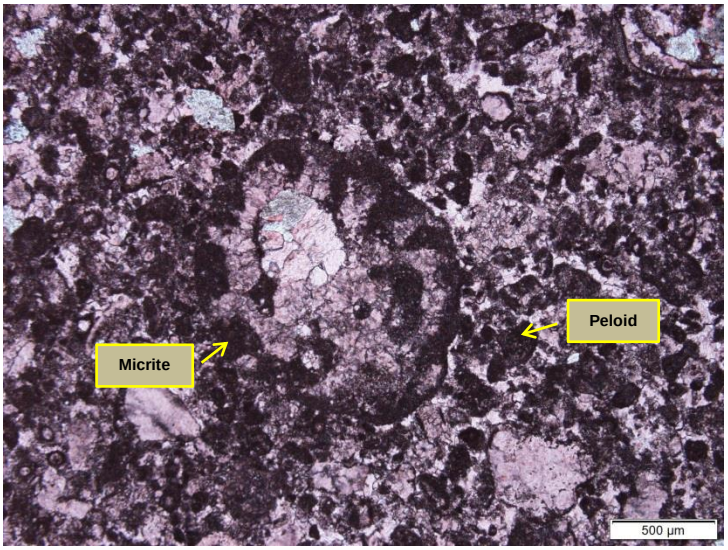


Fig. 7-6: Photomicrograph in PPL showing a sub-circular bioclast (possible stromatoporid (*Amphipora*?, 1.5 mm) which has been replaced by microcrystalline calcite cement, and is rimmed by micrite material. Some internal structure is also outlined/filled by micrite or sparry calcite and dolomite cements (e.g. the 450 µm circular feature to the top-left of the fragment). Peloidal remains are abundant within the matrix.

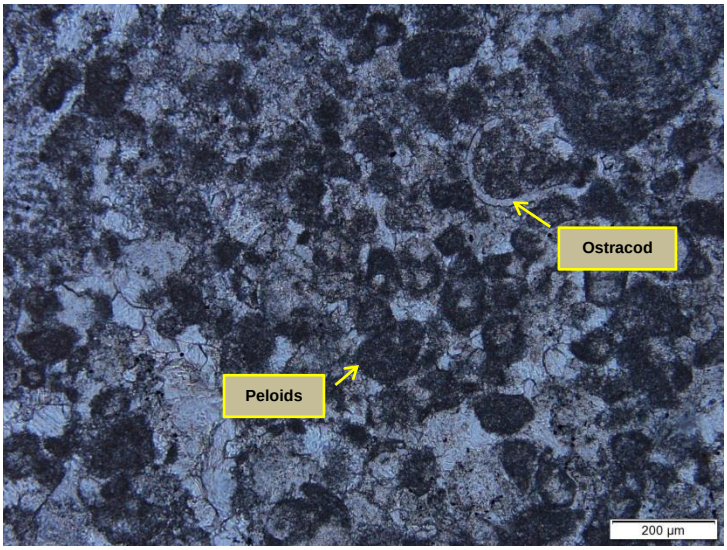


Fig. 7-7: Photomicrograph in PPL showing magnification of abundant peloids which range in size (generally 40-60 µm, up to 160 µm) and are characteristic of the sample. Also note the small (250 µm) ostracod carapace to the right of the image.

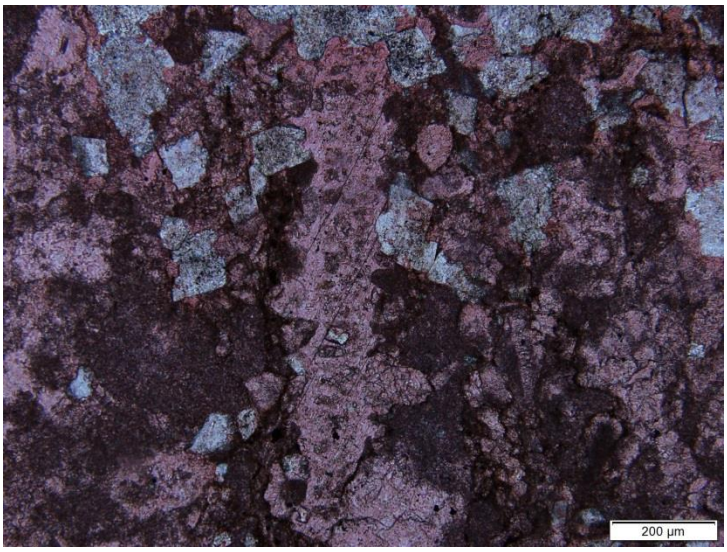


Fig. 7-8: Photomicrograph in PPL showing bioclast fragments (up to ~850 µm) that have been fully recrystallized or replaced by microcrystalline calcite, sparry calcite and/or sparry dolomite.

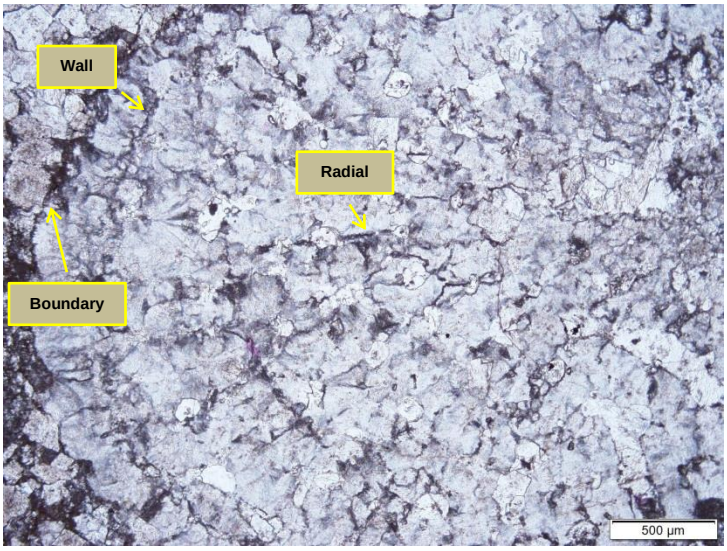


Fig. 7-9: Photomicrograph in PPL showing a recrystallized coral fragment showing some internal structure, a poorly defined outer wall and radial layering.

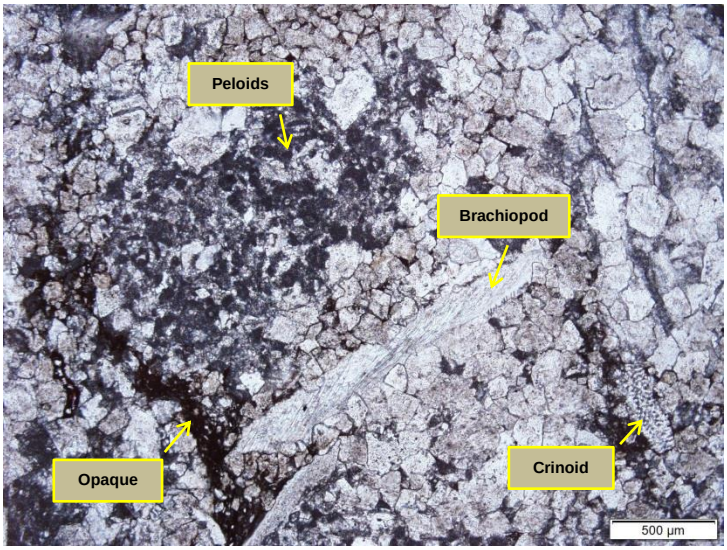


Fig. 7-10: Photomicrograph in PPL (unstained part of the thin section) showing sparry carbonate (up to ~350 µm) with both bioclast and peloidal remains concentrated in a small patch. Bioclast fragments include brachiopod shells (up to 2 mm) and crinoids (up to 550 µm). Organic and/or opaque material (left of image) is concentrated in stylolitic lineations.

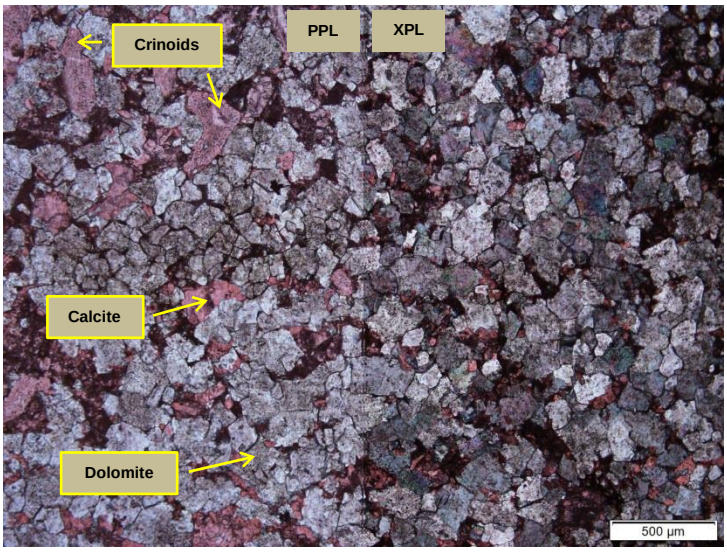


Fig. 7-11: Photomicrograph in PPL (left) and XPL (right) showing part of an extraclast that is predominantly composed of sparry dolomite (up to 300 µm), with some calcite spar. Several bioclast fragments (e.g. crinoid fragments, 400 µm, top-left of image) are embedded in the interlocking spar, which also contains some opaque- and/or organic-rich micrite. Peloids are absent. Sparry carbonate patches of this type may represent coral/reef debris that was loosely cemented and dolomitized during early diagenesis. The clasts were subsequently transported, broken apart and incorporated into the micrite and peloid-rich matrix of a sediment typical of back-reef material (e.g. Figures 7-4 through 7-7).

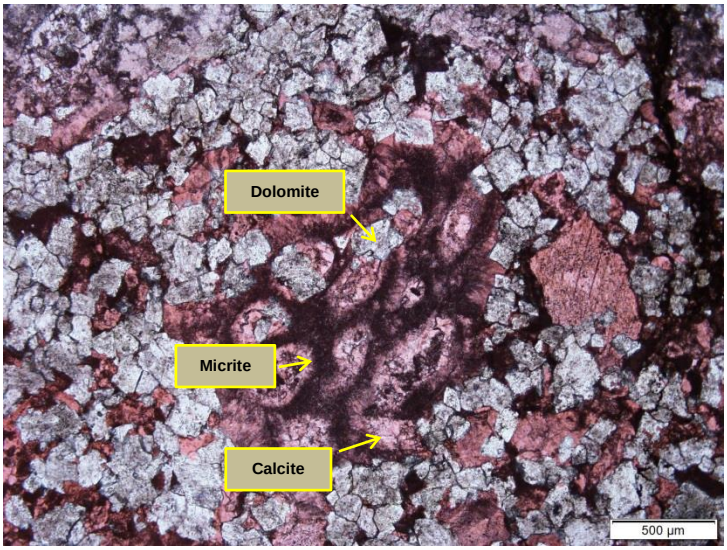


Fig. 7-12: Photomicrograph in PPL showing lobate bioclast fragments composed of micritic calcite and some opaque material.



Fig. 7-13: Photomicrograph in PPL showing magnification of a possible plant spore (~110 µm) and an organic fragment (~400 µm).

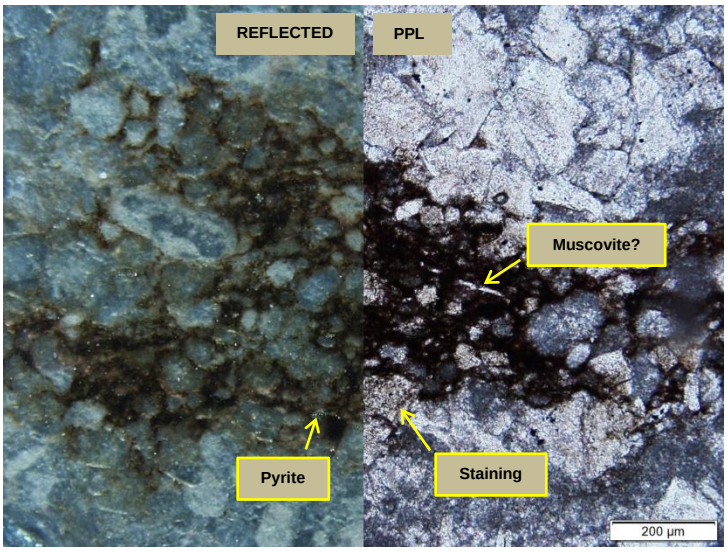


Fig. 7-14: Photomicrograph in reflected light (left) and PPL (right) showing a patch of opaque material filling interparticle space within an extraclast. The opaque material appears to predominantly consist of clay minerals (including detrital muscovite lathes, 95 µm) and organic matter (bitumen?). Reflected light shows that the opaque material also incorporates a few small (up to ~20 µm) cubic pyrite crystals. Some of the sparry carbonate cements adjacent to the opaque feature are brown-stained, indicating oil migration.

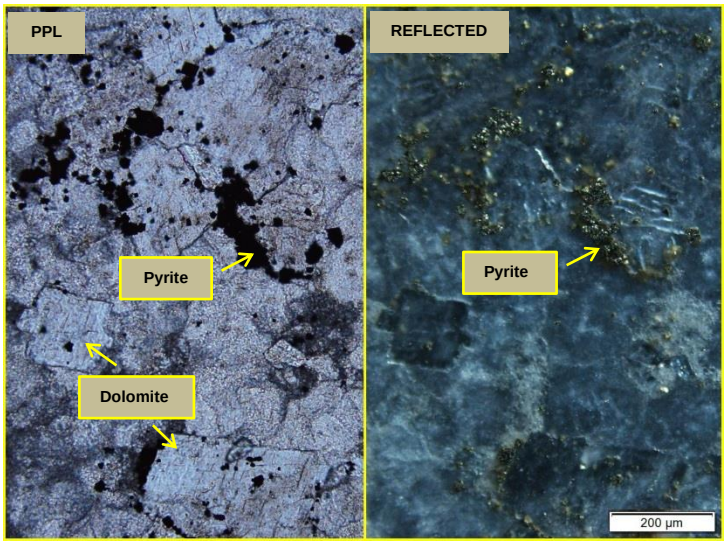


Fig. 7-15: Split-image photomicrograph in PPL (left) and reflected light (right) showing a section of an extraclast with abundant cubic pyrite crystals (<10 µm) and clusters (up to 200 µm). Pyrite generally fills space between sparry carbonate cements and overprints some dolomite rhombs.

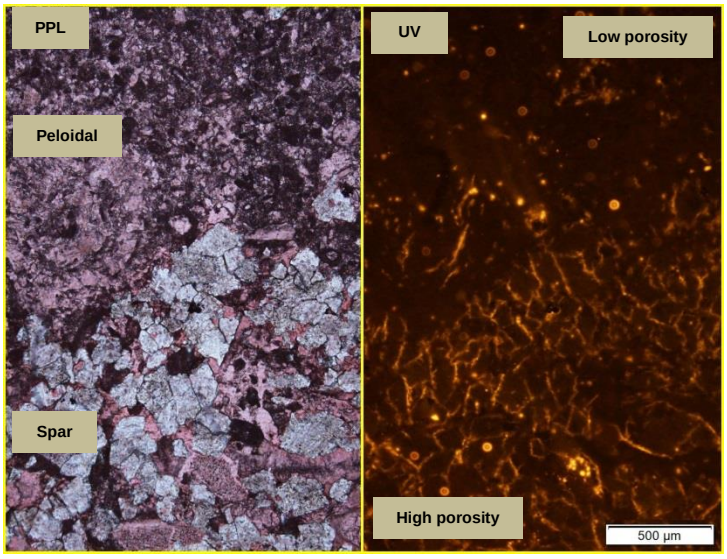


Fig. 7-16: Split-image photomicrograph in PPL (left) and UV light (right) showing differences in porosity between sparry carbonate intraclasts (bottom) and background peloidal micrite (top). Low fluorescence under UV light shows that very minor porosity is associated with the micritic layers. However, interparticle porosity (between carbonate cements) is commonly observed within the sparry extraclasts.

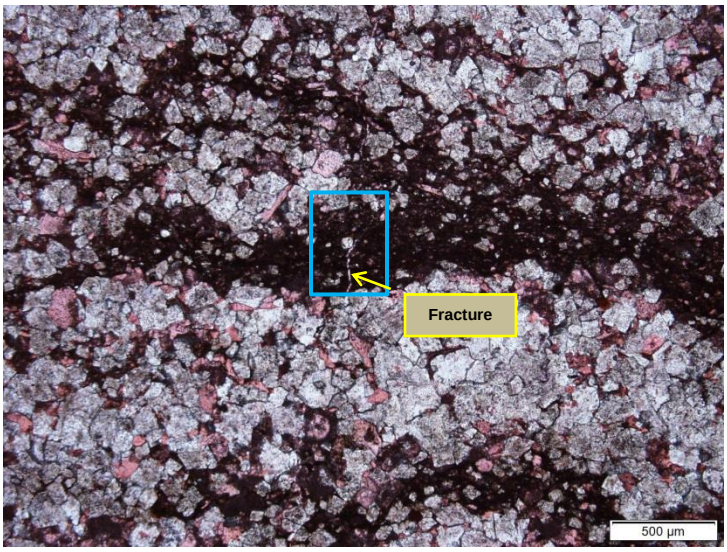


Fig. 7-17: Photomicrograph in PPL showing bedding-parallel sparry calcite and dolomite-rich laminae (~1 mm) within an extraclast. The laminae are interrupted by opaque and/or clay-rich layers (300-350 µm; algal remains?). A discontinuous, vertical microfracture runs from the center of the image to the top of the sample (see Figure 7-18 for further detail).

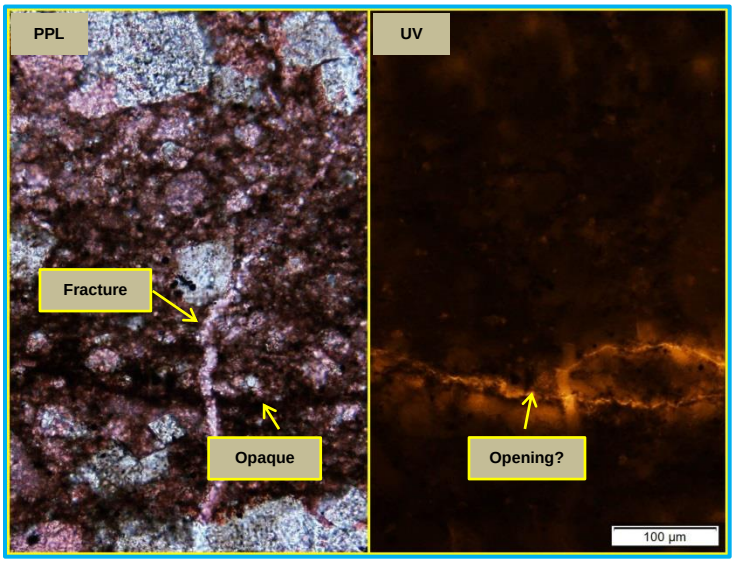


Fig. 7-18: Split-image photomicrograph in PPL (left) and UV light (right) showing magnification of the microfracture (10 µm) imaged in Figure 7-17. The vertical to sub-vertical fracture is completely healed by microcrystalline calcite cements (not visible under UV light) and wraps around more competent cements. The bedding-parallel microfracture towards the center of the image is obscured by opaque material and is visible only under UV light.

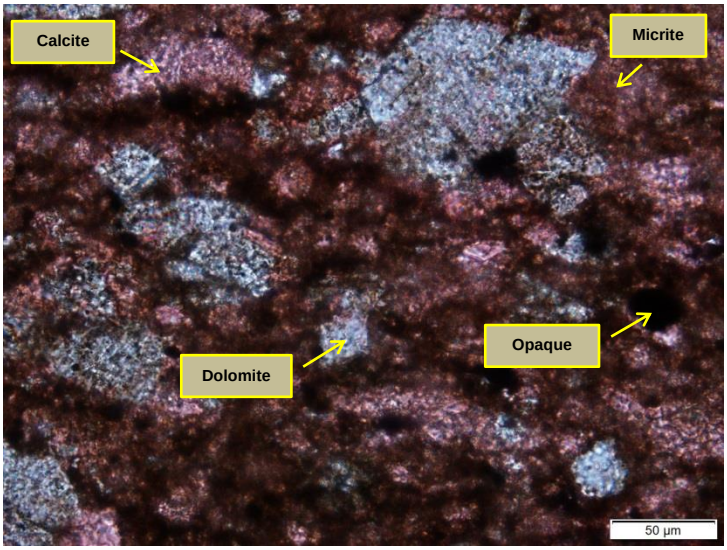


Fig. 7-19: Photomicrograph in PPL showing magnification of the clay-/micrite-rich layer imaged in Figures 7-17 & 7-18. The area is mainly composed of micrite (lime mud), with the remainder consisting of sparry dolomite (up to 110 µm, generally 30-35 µm) and rare calcite spar. Opaque material is estimated to comprise ~5% of the layer with organic matter representing ~80% of this value.

7.2.2 SAMPLE 15005

Sample ID	**15005**		
Sample Type	**Core**	**UWI/Well**	**100/13-14-035-25W4/00**
Strat. Unit	**Duvernay**	**Depth**	**7713.2 ft.**

XRD results

Quartz (%)	Feldspar (%)	Calcite (%)	Dolomite/ankerite (%)	Clays (%)
3.1	1.7	89.2	0.8	5.2

Pyrite (%)
0.1

Composition (*in order of abundance)*

	%	Variety (%)	Variety (%)	Variety (%)	Variety (%)
Cement (spar)	47	Calcite (95)	Dolomite (5)	Quartz (trace)	
Cement (micrite)	50	Calcite (95)	Clay minerals (5)		
Opaques	2	Pyrite (100)			
Organics	1	Amorphous^(50)	Plant (50)		
	100				

^ including fluid hydrocarbons

Allochems	20	Bioclasts (100)			
Matrix	80	Micrite (50)	Spar (50)		
Porosity	0				
	100				

Sedimentary structures

Primary	None observed.
Biogenic	Lighter patches or lenses (up to ~750 µm) of calcite and dolomite spar may represent burrowing structures.

Fractures	Bedding sub-parallel fractures (up to ~15 µm wide) are visible in both PPL (infiltration of epoxy) and under UV light (high fluorescence) indicating that they were likely produced during sample preparation and/or unloading. Finer vertical micro-fractures (<5 µm wide) may be natural and are filled/obscured by opaque material and/or micrite.
Porosity	Some fracture porosity. Interparticle porosity minor to absent.
Opaques	Bedding-parallel pyrite clusters are abundant. Cubic to idiomorphic pyrite crystals (up to 20 µm) also line the exterior and interior edges of bioclast fragments and are sometimes observed as inclusions. Smaller disseminated pyrite grains are dispersed throughout the matrix.
Organics	Organic (algal?) strings and pockets (up to 75 µm in length) are enriched within the micrite matrix and sometimes cross-cut bedding direction. Yellow/orange-stained plant fragments and spores (50-150 µm) are finely dispersed throughout the sample. One sinuous stylolite (~45 µm wide) within the concretion at the top of the sample incorporates sparry carbonate cements and contains fluid hydrocarbons.
Diagenetic	Bioclast fragments completely replaced/recrystallized with microcrystalline calcite cements and (minor) dolomite. Small amounts of dolomite spar observed within matrix.

Bioclasts *(in order of abundance)*

Type	*Size (µm)*	*Preservation*	*Recrystallisation*
Tentaculitids	Up to ~1000	Moderate to good	Calcite; micrite; dolomite
Ostracods	Up to ~400	Poor to moderate	Calcite; micrite
Bivalve shells	Up to ~650	Poor to moderate	Calcite
Crinoids	Up to ~150	Moderate	Calcite
Unidentified	Up to ~650	Poor	Calcite; dolomite; micrite; quartz

Description

Sample 15005 is a poorly-washed bio-sparite containing abundant tentaculitid and ostracod fragments with some other bioclastic debris. Bioclast fragments are generally replaced or infilled by pure microcrystalline calcite cements, micrite and (more rarely) dolomite with preservation ranging from poor (unidentifiable) to good (particularly tentaculitid fragments). The matrix contains a mixture of sparry calcite and (minor) dolomite cements with interparticle space filled by micrite material which is often enriched in disseminated pyrite crystals and organic matter. Pyrite also forms bedding-parallel clusters and is observed as inclusions within some bioclast fragments. Organic debris includes abundant yellow/orange-stained plant fragments (including spores), algal strings and a stylolite containing fluid hydrocarbons (within a concretion). Porosity within the sample is very low due to limited interparticle space.

Rock Classification

Poorly-washed bio-sparite (Folk, 1962); mixed-fossil lime wackestone (Dunham, 1962)

Thin Section Quality

Good; stained for carbonates.

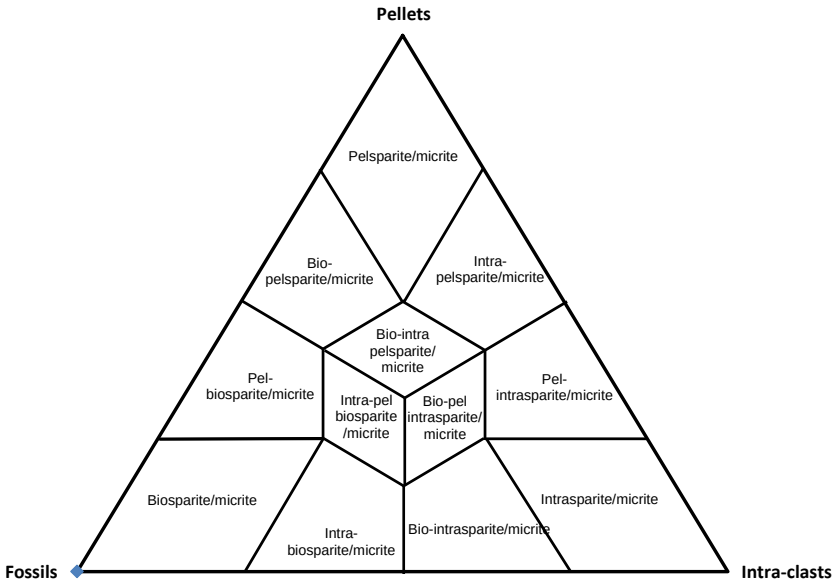


Fig. 7-20: Ternary plot showing the relative abundance of different allochem types within the carbonate rock (based on Folk's classification scheme, 1962). Sample 15005 is classified as (poorly-washed) biosparite as the rock has a mixed microcrystalline calcite (micrite) and sparry calcite/dolomite matrix with 10-50% bioclasts and no peloids or intraclasts.

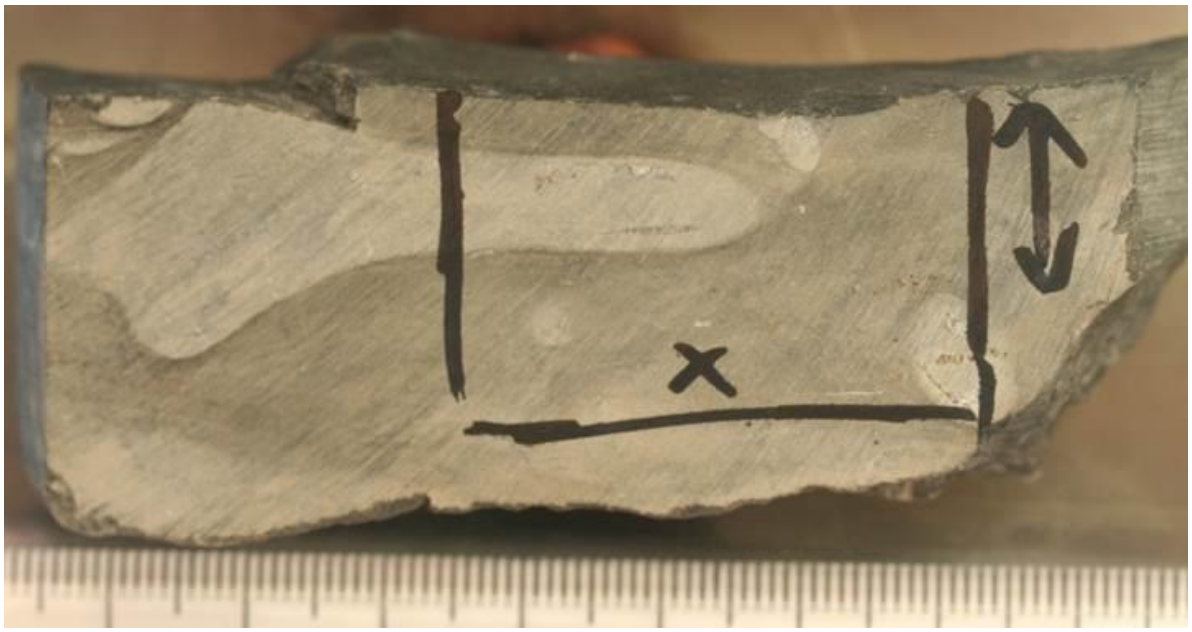


Fig. 7-21: Core photograph of sample 15005 from the Duvernay Formation, well 100/13-14-035-25W4/00 (depth 7713.2 m). The sample contains several small calcite concretions and microfossils are visible. The thin section was not prepared from the suggested area but rather from the bottom and part of the concretion was not preserved. The sample was received with no up direction. Scale is in mm.



Fig. 7-22: Thin section photograph of sample 15005 from the Duvernay Formation, well 100/13-14-035-25W4/00 (depth 7713.2 m). The image shows a fine-grained carbonate rock containing finely dispersed bioclast fragments and opaque strings. A light-coloured patch to the top-right of the thin section represents part of an early diagenetic calcite concretion. Intensive pink staining within the carbonate-stained half of the thin section (left of image) shows the dominance of calcite in the sample. Scale is in mm.

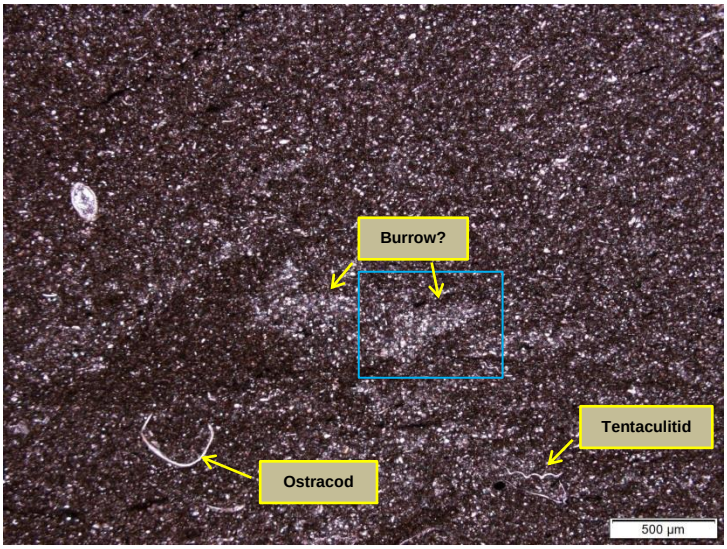


Fig. 7-23: Photomicrograph in PPL showing an overview of sample 15005 (depth 7713.2 ft.). The image shows a micritic calcite matrix containing abundant sparry carbonate cements and bioclast fragments (including tentaculid, ostracod and bivalve fragments). Opaque material (including pyrite and organic matter) is finely dispersed throughout. Lighter-coloured lenses (up to 750 µm, see Figure 7-24) are abundant throughout the sample, and may represent burrowing structures. The darker area to the left of the image contains less sparry carbonate.

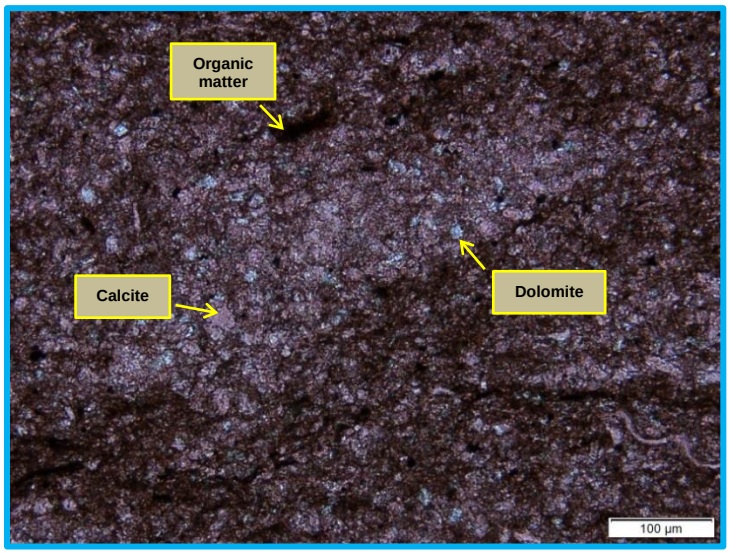


Fig. 7-24: Photomicrograph in PPL showing magnification of the area shown in Figure 4. These lighter patches or lenses (burrowing structures?) of sparry calcite (up to 35 µm) and white/blue-stained dolomite/ankerite cements (up to 15 µm) contain very sparse opaques, organic matter and clay minerals. The surrounding matrix is composed of clay-rich micritic material containing fewer sparry carbonate cements and abundant organic strands (bituminous; up to 75 µm in length).

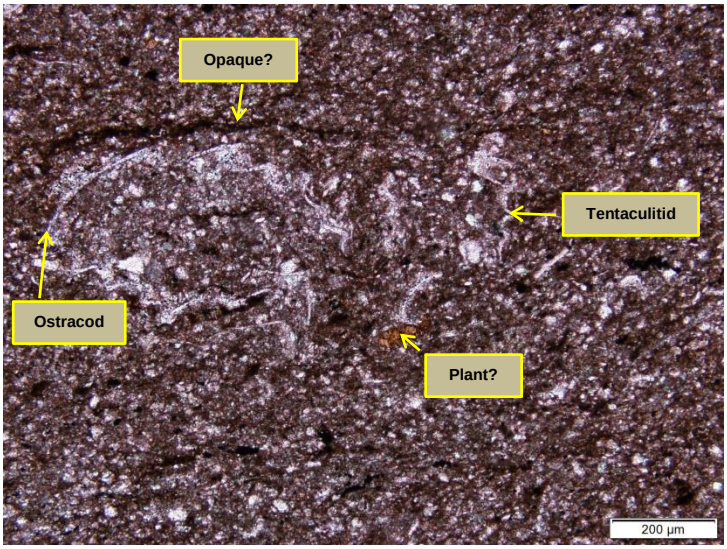


Fig. 7-25: Photomicrograph in PPL showing abundant poorly preserved bioclast debris including ostracod carapaces (up to 300 µm), bivalve shell fragments, tentaculitid fragments and an organic (plant?) fragment (~90 µm). Also note the bedding-parallel opaque string near the top of the image, which is predominantly composed of pyrite.

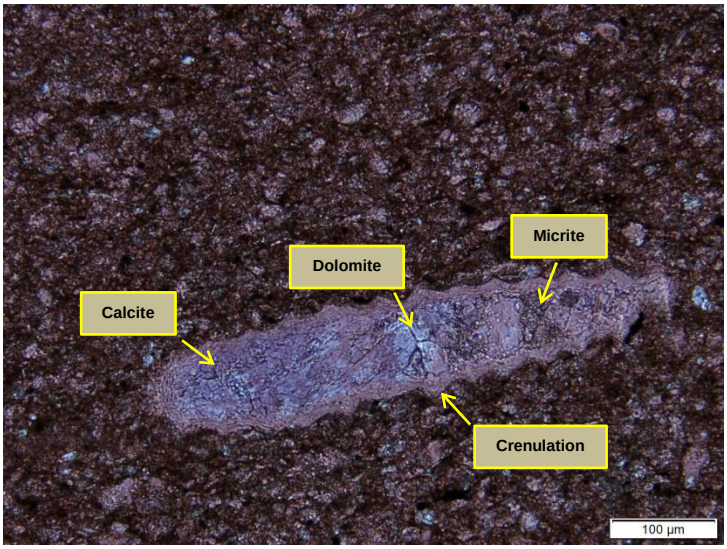


Fig. 7-26: Photomicrograph in PPL showing a recrystallized tentaculitid fragment (~520 µm). The outer wall of the fragment is composed of calcite and features some layering/growth lines. The center of the bioclast is filled with sparry calcite (up to 60 µm) and dolomite (up to 50 µm) cements, and micrite. Bioclasts of this type are commonly observed throughout the sample, and often feature partially dissolved edges and ends.

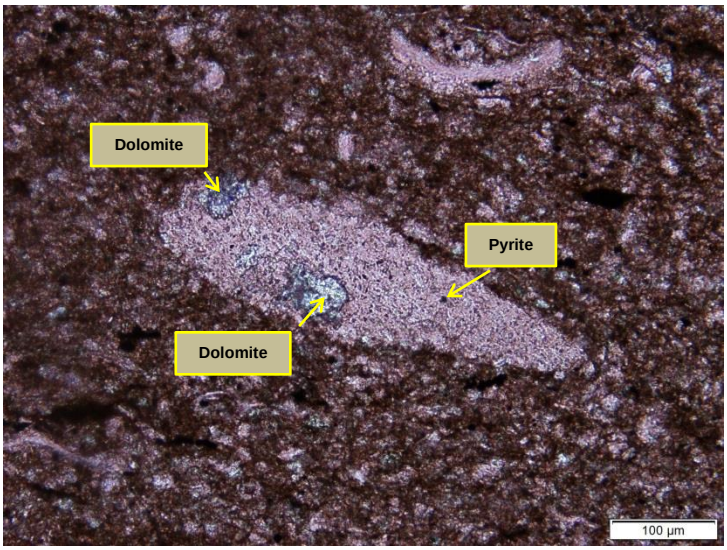


Fig. 7-27: Photomicrograph in PPL showing a lenticular bioclast fragment (tentaculitid; ~440 µm long), which has been completely replaced by microcrystalline calcite and some microcrystalline dolomite/ankerite cements. The dolomite cements form small patches (up to 40 µm) within the interior of the bioclast. Also note very small (<5 µm) idiomorphic pyrite inclusions within the fragment.

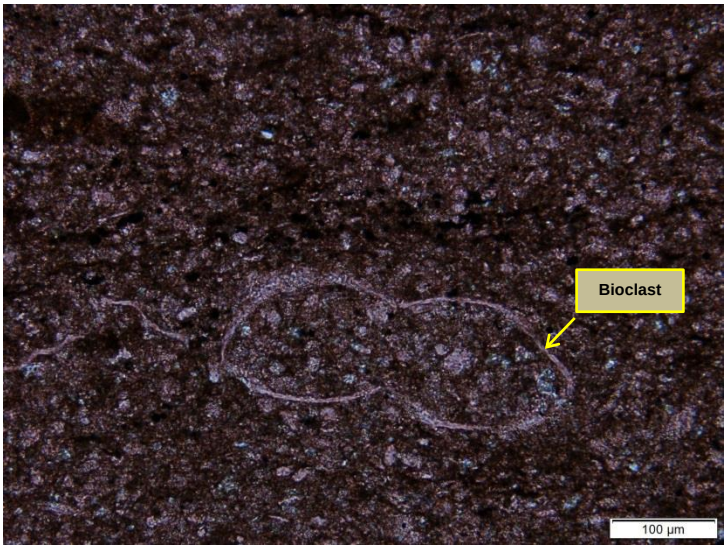


Fig. 7-28: Photomicrograph in PPL showing a ~340 µm tentaculitid fragment with a thin (~5 µm) outer wall composed of microcrystalline calcite.

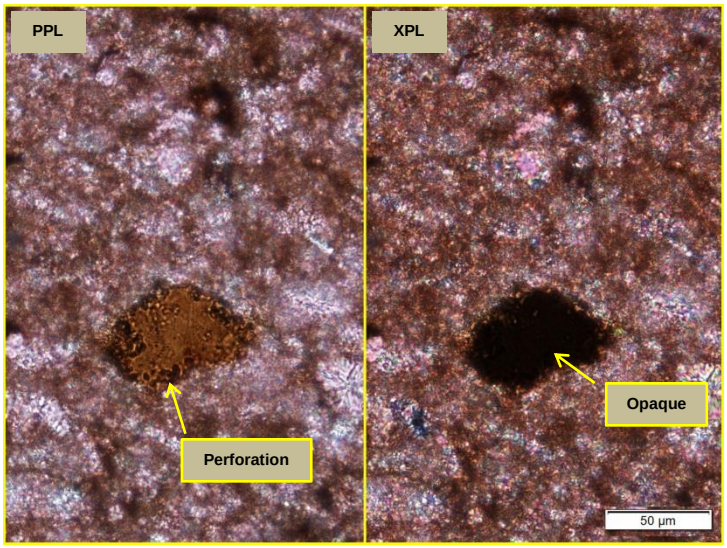


Fig. 7-29: Split-image photomicrograph in PPL (left) and XPL (right) showing magnification of a 70 µm plant fragment featuring some internal perforations. The fragment is opaque in XPL. Organic debris (including plant fragments) is abundant throughout the sample.

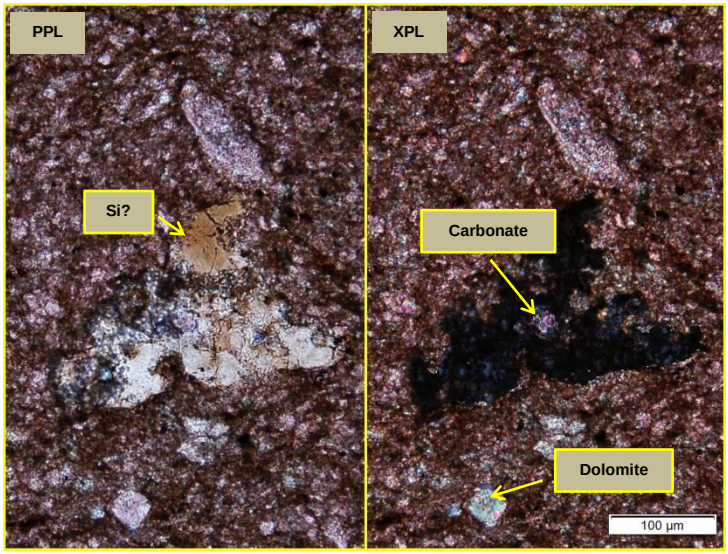


Fig. 7-30: Split-image photomicrograph in PPL (left) and XPL (right) showing a patch (~250 µm) of cream, white and brown-coloured cements (~35 µm) which show low order birefringence colours and incorporate small (<30 µm) sparry carbonate crystals. The cements possibly represent siliceous (i.e. quartz or chert) infilling of a bioclast fragment. Also note a rare dolomite rhomb (~40 µm) to the bottom of the image.

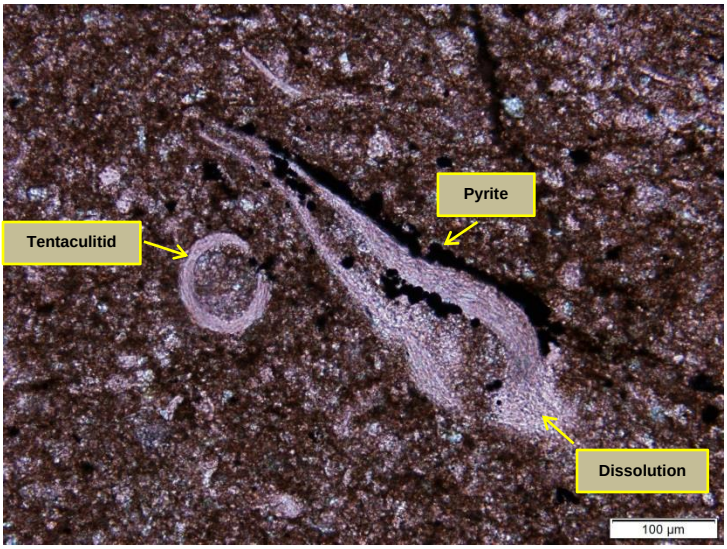


Fig. 7-31: Photomicrograph in PPL showing two tentaculitid fragments. The circular bioclast (~100 µm in diameter) to the left of the image is filled with lime mud (micrite) and features a calcite outer wall. The larger bioclast fragment (~465 µm in length) is partially dissolved and features internal layering and/or growth lines. Cubic and idiomorphic pyrite crystals (up to 20 µm) and some organic matter line both the interior and exterior edges of the fragment.

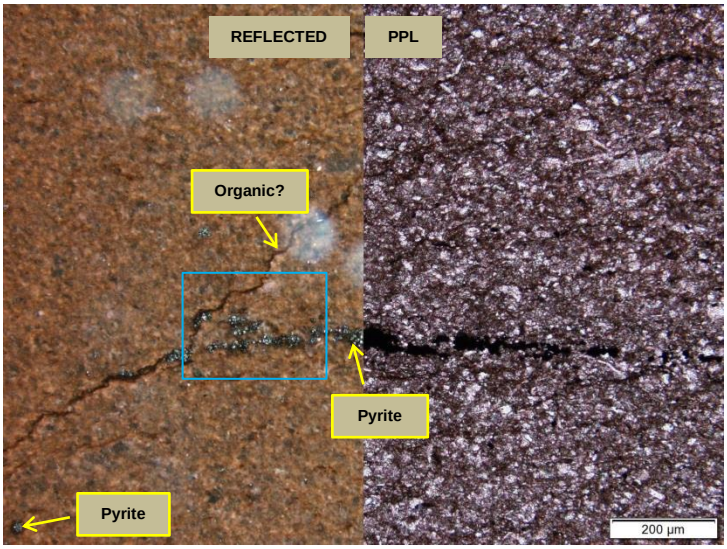


Fig. 7-32: Photomicrograph in reflected light (left) and PPL (right) showing bedding-parallel pyrite clusters (~55 µm wide) and an opaque (organic?) string that cross-cuts bedding. Smaller disseminated pyrite grains are dispersed throughout the matrix.

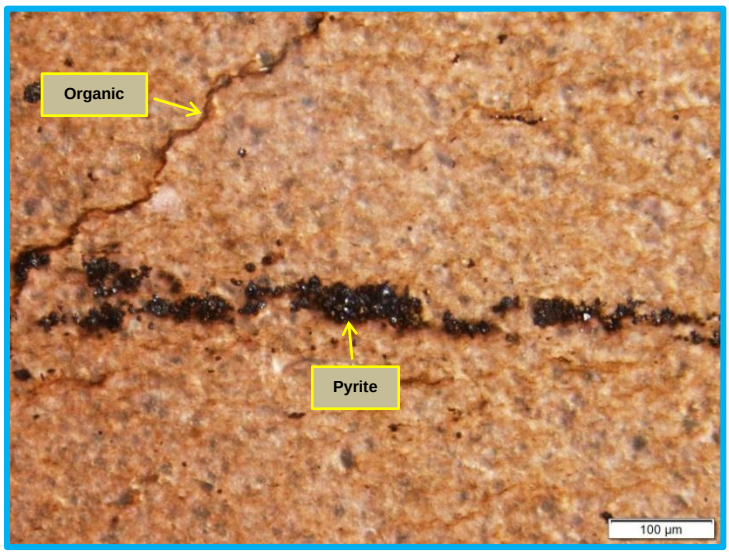


Fig. 7-33: Photomicrograph in reflected light showing magnification of the area shown in Figure 7-32. The pyrite clusters consist of cubic and idiomorphic crystals (<5 µm) together with very sparse organic matter. The opaque string to the top left of the image (~2 µm wide) is composed of brown organic matter (algal?) which may represent infilling of a fracture with organics/clays.

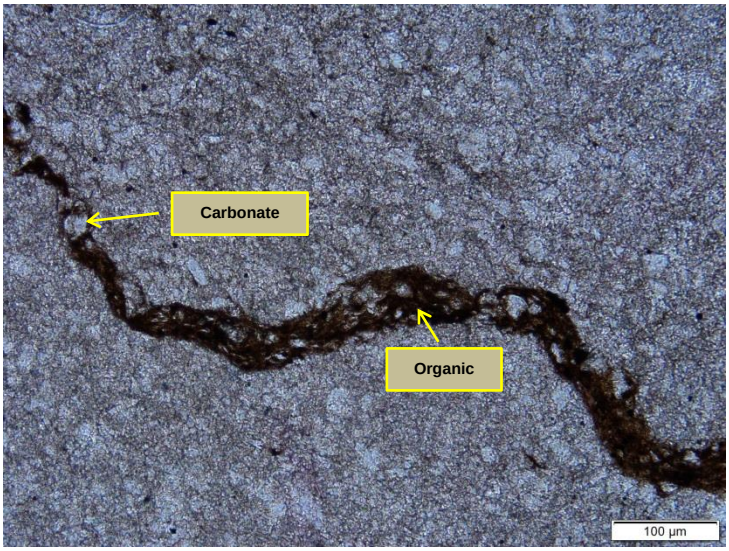


Fig. 7-34: Photomicrograph in PPL showing magnification of a concretion within the unstained part of the thin section (top of the sample) which features an organic layer (stylolite? ~45 µm wide). The surrounding matrix contains more abundant sparry cements and less micrite than the rest of the sample.

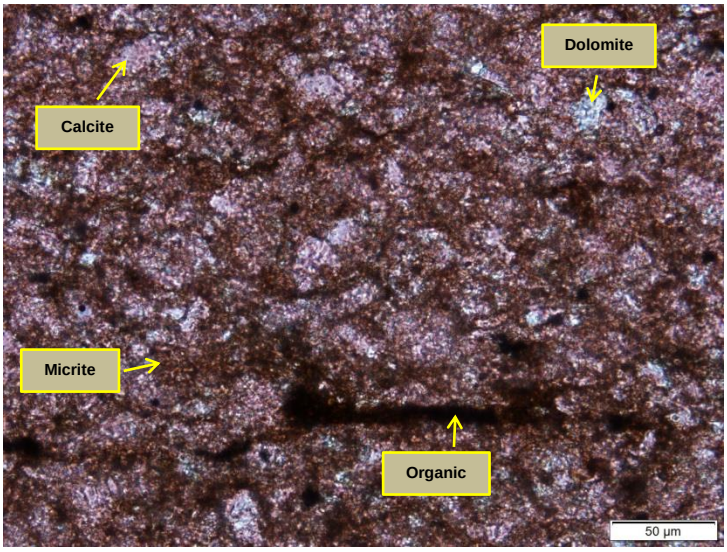


Fig. 7-35: Photomicrograph in slightly overexposed PPL showing details of the matrix. ~50% of the image consists of micrite (microcrystalline carbonates and clay minerals) with abundant sparry calcite cements (up to ~30 µm) and rare dolomite spar (up to 20 µm). Organic matter and disseminated pyrite crystals are enriched within the micritic material, which fills interparticle space. Organic strings (up to ~100 µm in this image) are likely to be algal in origin.

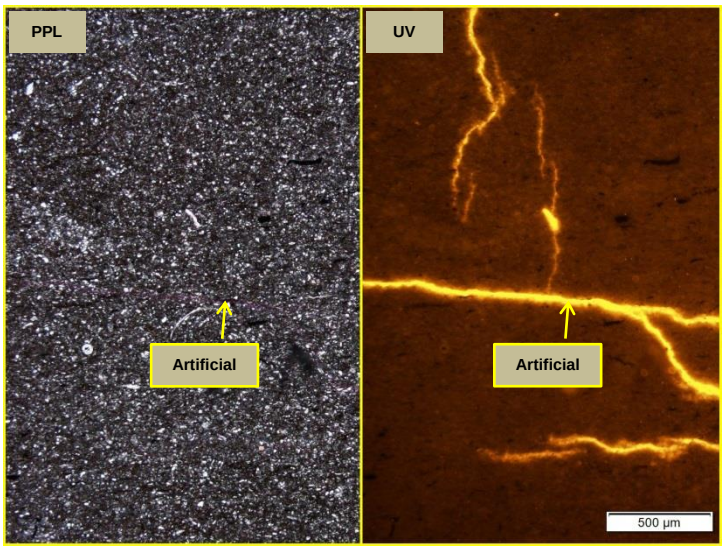


Fig. 7-36: Split-image photomicrograph in PPL (left) and UV light (right) showing an overview of porosity and fracturing within the sample. The bedding sub-parallel fracture to the center of the image (~15 µm wide) is visible in PPL due to the infiltration of epoxy indicating that it was likely produced during sample preparation or unloading. The finer vertical fractures observed to the top of the image are examined in further detail in Figure 7-37. Porosity within the sample is low to absent (<1%).

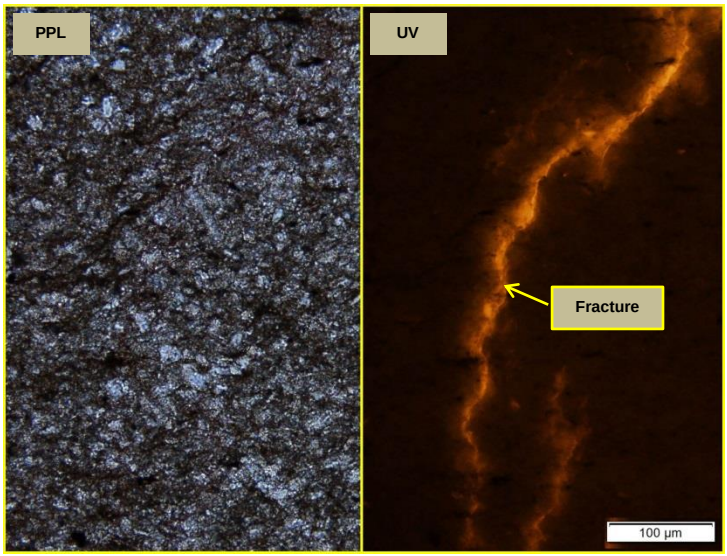


Fig. 7-37: Split-image photomicrograph in PPL (left) and UV light (right) showing magnification of some vertical micro-fractures (<5 µm wide) imaged in Figure 7-36. The fractures are not visible in PPL suggesting that they are obscured or filled by opaque material and/or micrite.

7.2.3 SAMPLE 15010

Sample ID	**15010**		
Sample Type	**Core**	**UWI/Well**	**100/13-14-035-25W4/00**
Strat. Unit	**Duvernay**	**Depth**	**7738.5 ft.**

XRD results

Quartz (%)	Feldspar (%)	Calcite (%)	Dolomite/ankerite (%)	Clays (%)
9.3	8	52.6	6.3	19.9

Pyrite (%)
4

Composition (*in order of abundance)*

	%	Variety (%)	Variety (%)	Variety (%)	Variety (%)
Cement (micrite)	31	Calcite (100)			
Cement (spar)	25	Calcite (65)	Dolomite (20)	Quartz (15)	Anhydrite (trace)
Clay	20	Clay minerals (100)			
Detrital grains	15	Feldspar* (55)	Quartz* (35)	Muscovite (10)	
Organics	5	Amorphous^(100)			
Opaques	4	Pyrite (100)			
	100				

^ including fluid hydrocarbons

** not observed in thin section*

Allochems	12	Bioclasts (100)			
Matrix	88	Micrite (35)	Clay (25)	Detrital grains (15)	Spar (15)
		Opaques/organics (10)			
Porosity	0				
	100				

Sedimentary structures

Primary	None observed.
Biogenic	Abundant bedding-parallel lenticular features (up to 1 mm in length) are relatively organic-poor compared to the surrounding matrix and may represent burrowing structures.

Fractures	Many bedding-parallel to bedding sub-parallel fractures (up to 100 µm wide) are filled with epoxy and were likely created during sample preparation and/or unloading. Finer micro-fractures (<3 µm wide) that are not visible in PPL are likely opening fractures which are often discontinuous and feature tear patterning.
Porosity	Some fracture porosity. Interparticle porosity absent.
Opaques	Opaque material is abundant and obscures grains and cements. The matrix contains some large pyrite clusters (possibly representing replaced/recrystallized bioclasts), discrete idiomorphic to cubic pyrite crystals and very small disseminated pyrite grains. Carbonate cements often feature very small (<5 µm) pyrite inclusions.
Organics	Very abundant organic matter obscures grains and cements and is uniformly dispersed throughout the sample. Possible burrowing structures are relatively organic-poor.
Diagenetic	Small unidentified bioclasts and possible tentaculitid/bivalve shell fragments are replaced or recrystallized with carbonate cements. Very rare diagenetic dolomite rhombs observed.

Bioclasts *(in order of abundance)*

Type	*Size (µm)*	*Preservation*	*Recrystallisation*
Unidentified	Up to ~160	Poor	Carbonates
Tentaculitids/bivalves	Up to ~500	Poor to moderate	Carbonates

Description

Sample 15010 is a sparse biomicrite/wackestone characterized by abundant opaque material (including organic matter and pyrite) and clay minerals. Unidentified bioclasts are generally poorly preserved and are replaced by carbonate cements (unable to differentiate between calcite and dolomite due to absence of dual carbonate stain). Some bedding-parallel tentaculitid and/or bivalve shell fragments are also observed. Matrix minerals are difficult to identify as pyrite and organic matter obscures grains and cements. However, the matrix is likely to be composed predominantly of lime mud (micrite/microcrystalline calcite) and clay minerals, with some sparry carbonate cements, quartz and feldspar grains (not observed in thin section, refer to XRD data) and abundant detrital muscovite lathes. Pyrite is observed as clusters (replaced bioclasts?), discrete idiomorphic to cubic crystals and small disseminated grains which are dispersed throughout the matrix. Organic matter is abundant and uniformly dispersed throughout. Porosity is absent due to limited interparticle space.

Rock Classification

Organic-rich argillaceous sparse biomicrite (Folk, 1962); organic-rich argillaceous wackestone (Dunham, 1962)

Thin Section Quality

Moderate: removal and plucking of material during sample preparation has led to patches of glass/balsam which are visible in thin section. The sample is unstained due to this sensitivity making differentiation of calcite from dolomite difficult (mineral composition estimates based heavily on XRD data).

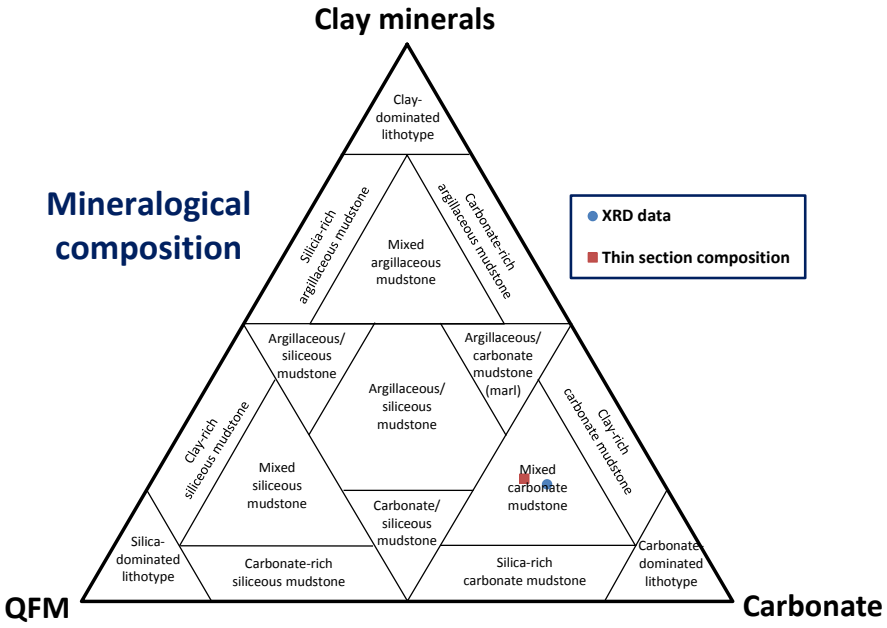


Fig. 7-38: Ternary plot of the mineralogical composition of the sample according to the XRD data (blue) and estimated thin section composition (red) in terms of clay minerals, QFM (quartz, feldspar and mica) and carbonate content. The sample is classified as a mixed carbonate mudstone (i.e. an argillaceous sparse biomicrite/wackestone) due to its high percentage of carbonate cements and relatively high clay mineral content.

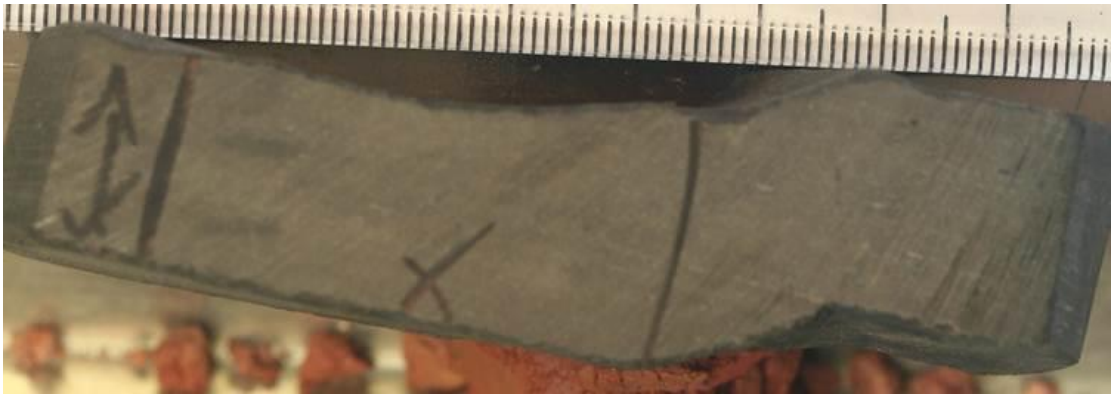


Fig. 7-39: Core photograph of sample 15010 from the Duvernay Formation, well 100/13-14-035-25W4/00 (depth 7738.5 ft.). The thin section prepared from this sample was cut from the area marked with an X. The sample was received with no up direction. Scale is in mm.



Fig. 7-40: Thin section photograph (with flash on) of sample 15010 from the Duvernay Formation, well 100/13-14-035-25W4/00 (depth 7738.5 ft.). The image shows a dark (opaque and/or organic-rich) fine-grained carbonate mudrock (shale) with abundant clay minerals. Bedding-parallel to bedding sub-parallel fractures are filled with epoxy and were likely created during sample preparation. White patches represent balsam and/or thin section glass indicating material removal (also due to sample preparation). The thin section has not been dual-carbonate stained due to water-sensitivity of the sample. Scale in in mm.

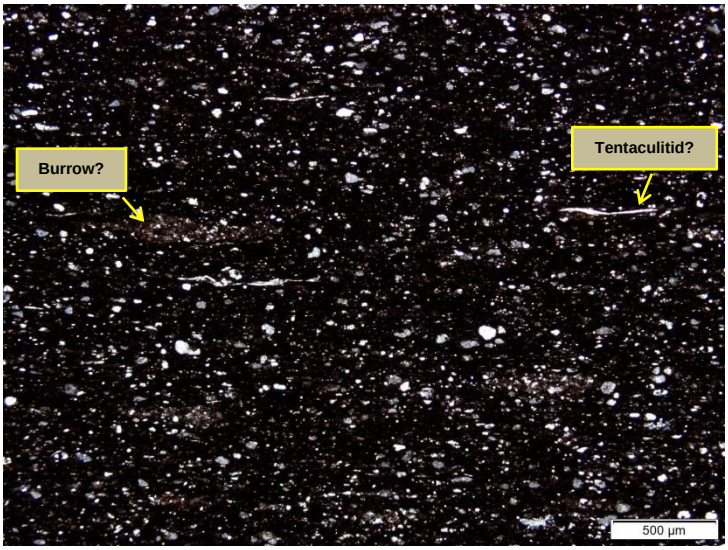


Fig. 7-41: Photomicrograph in PPL showing an overview of sample 15010 (well 13-4, depth 7738.5 ft.). The image shows an organic and/or opaque-rich carbonate mudstone (shale) containing abundant silt- to very fine sand-sized grains (up to 150 µm, see Figure 10) and some tentaculitid or bivalve shell fragments (up to ~700 µm), which are aligned parallel to bedding (see Figure 9). Some bedding-parallel features (~900 µm in length) may represent burrowing structures, which are abundant throughout the sample (see Figure 7-42 for more details).

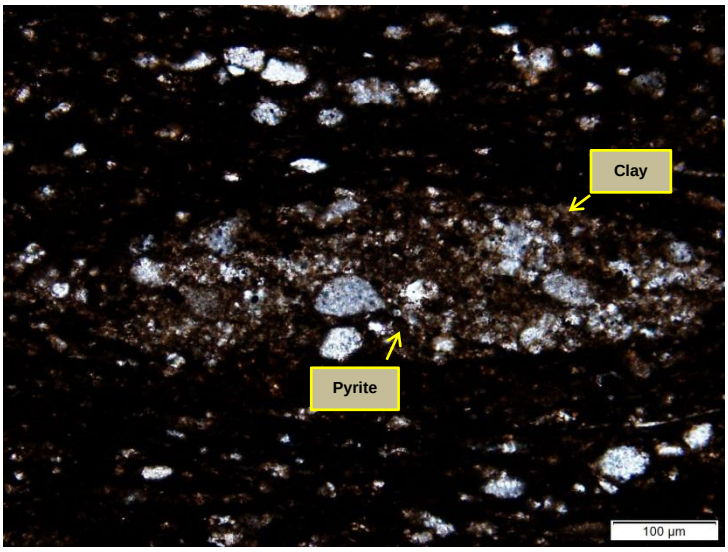


Fig. 7-42: Photomicrograph in PPL showing magnification of a bedding-parallel lenticular feature (~700 µm in length), which contains less opaque and/or organic material compared to the surrounding matrix (possible burrowing structure?). The feature is composed of clay minerals, silt- to very fine sand-sized grains and cements (up to 65 µm, examined in further detail in Figure 7-43), and small idiomorphic pyrite crystals (generally <10 µm).

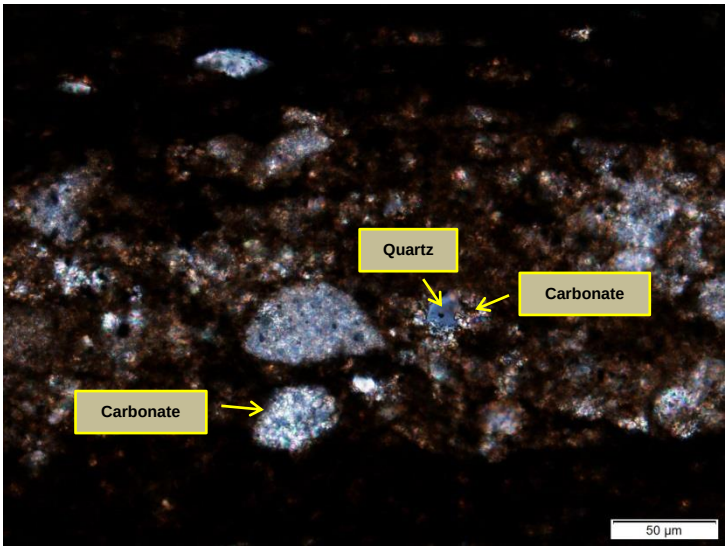


Fig. 7-43: Photomicrograph in XPL showing magnification of silt- to sand-sized particles within the burrowing structure (Figure 7-42). Most of the particles consist of sub-rounded carbonates (generally ~45 µm) featuring high order birefringence colours. The larger carbonate particles contain very small pyrite inclusions (<5 µm). Rare angular quartz cements (20 µm) are also observed.

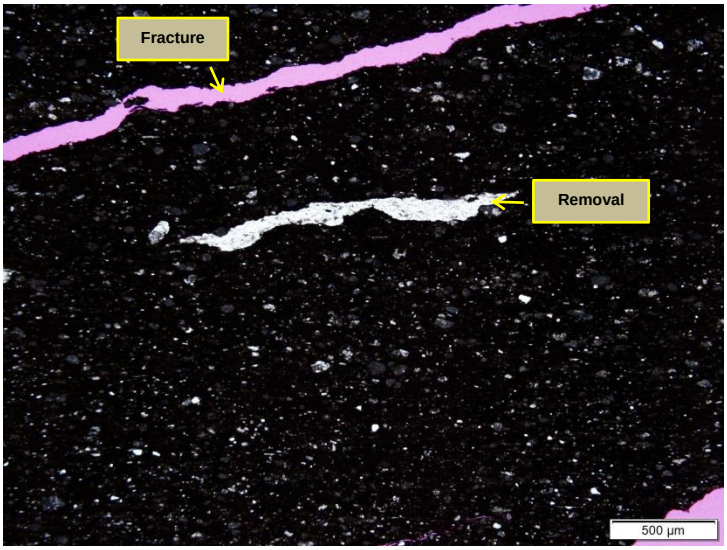


Fig. 7-44: Photomicrograph in PPL showing a 1.7 mm long white patch that may represent a removed bioclast fragment (examined further in Figure 7-46). These patches are commonly observed in the sample. The bedding sub-parallel fracture to the top of the image (~95 µm wide) is filled with epoxy and was likely produced during sample preparation.

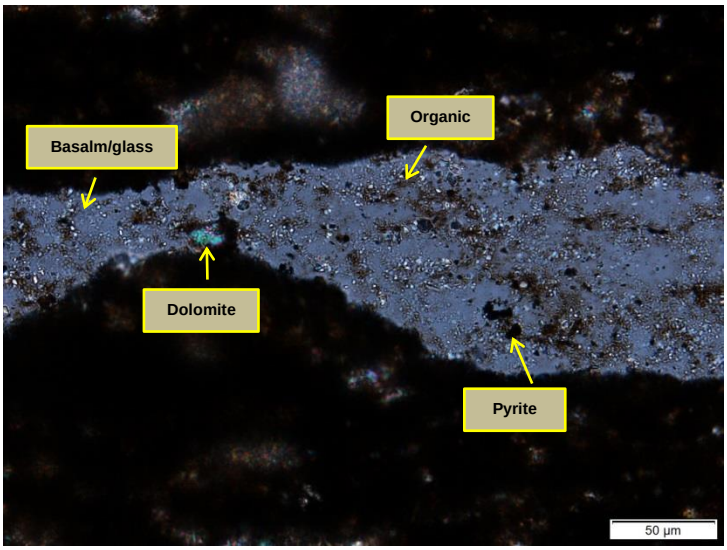


Fig. 7-45: Photomicrograph in XPL showing magnification of the removed material (former bioclast fragment?) imaged in Figure 7-44. The feature exhibits 'flat' first order birefringence colours (glass or balsam infill) and incorporates sparse, 'wispy' organic matter remnants (brown-coloured) and small (<7 µm) pyrite crystals and clusters. Some rhombic dolomite cements (20 µm) are also observed. The feature likely represents removal of material during sample preparation.

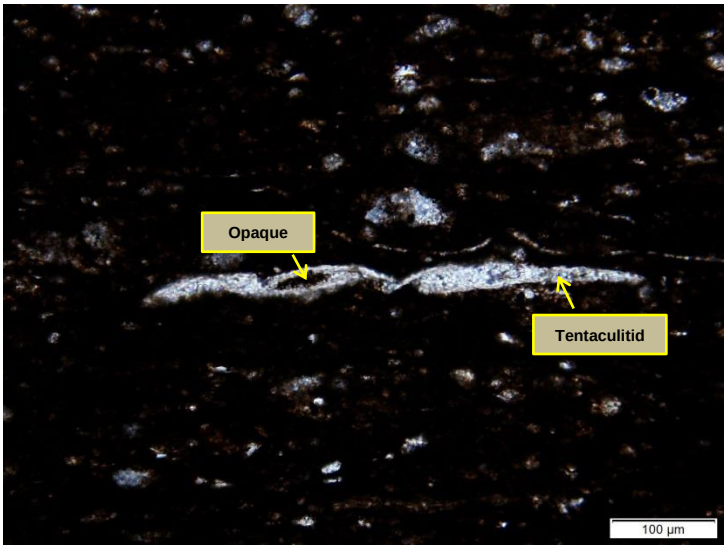


Fig. 7-46: Photomicrograph in PPL showing magnification of a rare ~500 µm bioclast fragment (possible tentaculitid), which is poorly preserved and oriented parallel to bedding (see Figure 7-41). The fragment has been replaced by microcrystalline carbonates, features a thin outer wall (~5 µm) and contains an ~55 µm long opaque/organic inclusion.

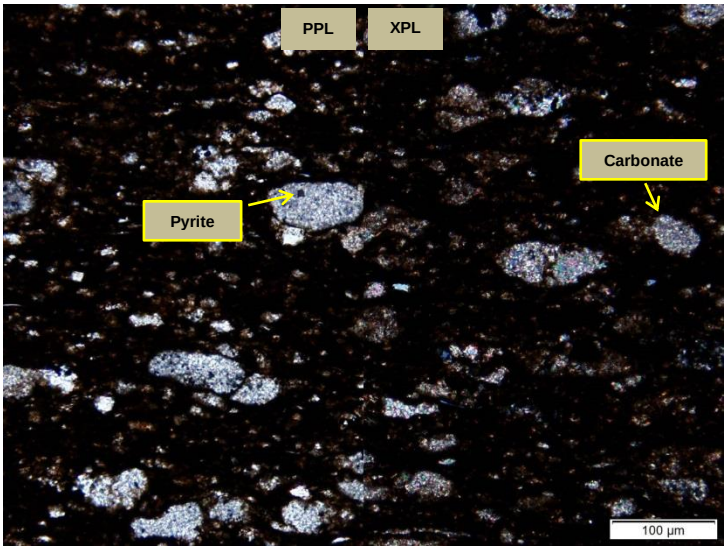


Fig. 7-47: Photomicrograph in PPL (left) and XPL (right) showing magnification of some sub-rounded carbonate particles (up to ~105 µm) containing very small pyrite crystals (<<5 µm). The particles likely represent recrystallized bioclasts, and are commonly observed throughout the sample. Dull birefringence colours indicate that the cements are microcrystalline (dolomite?).

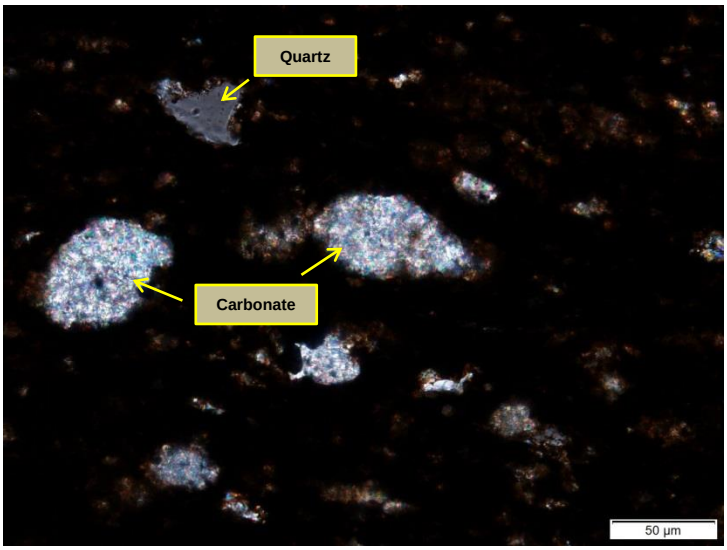


Fig. 7-48: Photomicrograph in XPL showing magnification of the matrix and some of the silt-size carbonate and quartz particles These particles are all secondary cements and may represent replacement of microfossils. The matrix is opaque rich and contains high amounts of clays.

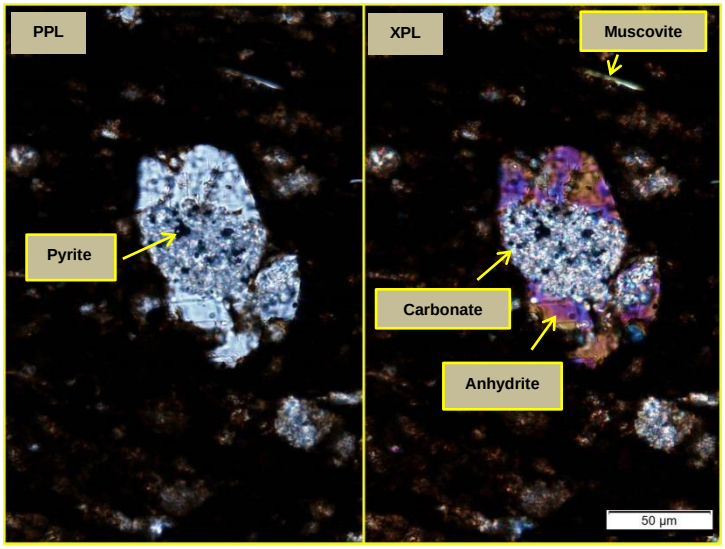


Fig. 7-49: Split-image photomicrographs in PPL (left) and XPL (right) showing magnification of a carbonate cement (105 µm) containing small pyrite inclusions (<7 µm, typical of carbonate cements within the sample) and anhydrite overgrowths (especially around cement edges), which feature high relief (PPL), some cleavage and high order birefringence colours (XPL). Also note the detrital muscovite lathe (30 µm) to the top of the image, which shows a preferred orientation sub-parallel to bedding.

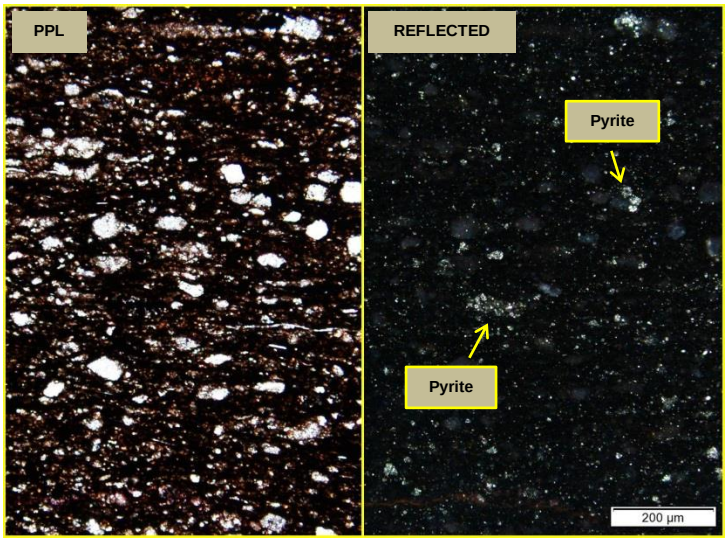


Fig. 7-50: Split-image photomicrograph in overexposed PPL (left) and reflected light (right) showing the abundance of recrystallized microfossils, pyrite and organic matter within the sample. Opaques (including both pyrite and organic matter) obscure grains and are uniformly dispersed throughout (i.e. are not concentrated in pockets or layers). The matrix contains some large pyrite clusters (up to 120 µm) which may represent replaced bioclasts, and abundant discrete idiomorphic to cubic pyrite crystals (up to ~22 µm). The remainder of the matrix consists of very small disseminated pyrite.

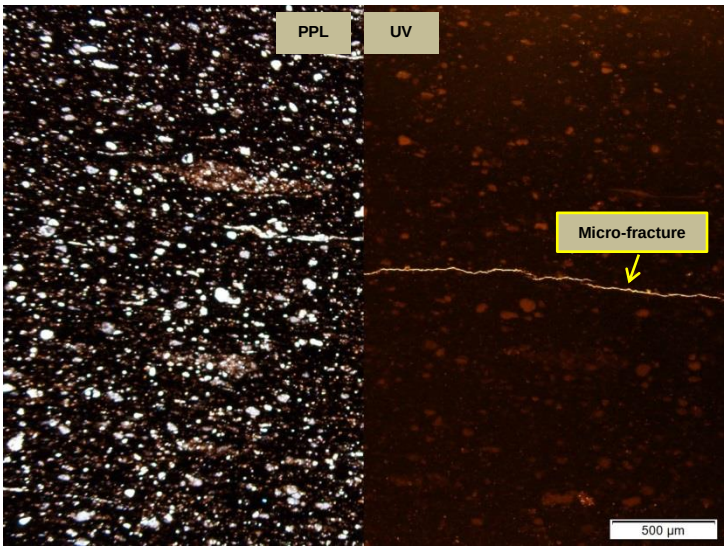


Fig. 7-51: Photomicrograph in PPL (left) and UV light (right) showing a fine bedding-parallel micro-fracture, which is discontinuous and features tear patterns (examined in further detail in Figure 7-52). Porosity is absent.

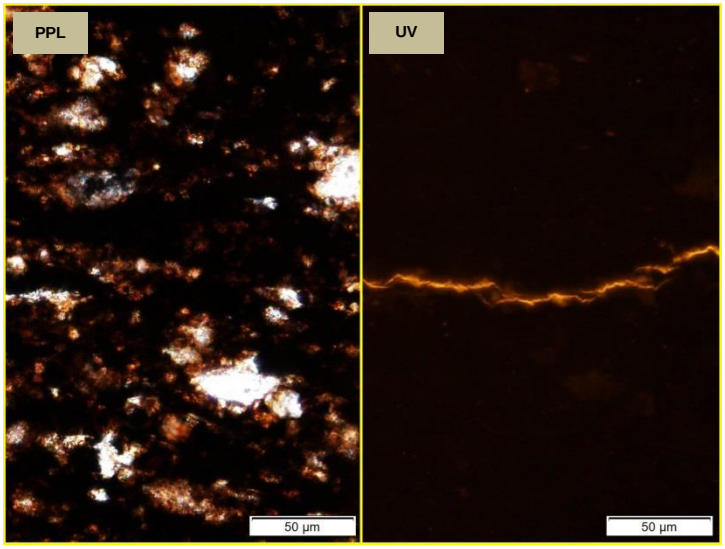


Fig. 7-52: Split-image photomicrograph in overexposed PPL (left) and UV light (right) showing magnification of a bedding-parallel micro-fracture (<3 µm wide). The fracture is not visible in PPL, suggesting that it is an opening fracture (produced during sample preparation or unloading).

7.2.4 SAMPLE 15013

Sample ID	**15013**
Sample Type	**Core**
Strat. Unit	**Duvernay**
UWI/Well	**100/13-14-035-25W4/00**
Depth	**7745.7 ft.**

XRD results

Quartz (%)	Feldspar (%)	Calcite (%)	Dolomite/ankerite (%)	Clays (%)
0.9	1	95.9	1.5	0.8

Pyrite (%)
0

Composition (*in order of abundance*)

	%	Variety (%)	Variety (%)	Variety (%)	Variety (%)
Cement (spar)	50	Calcite (85)	Dolomite (10)	Anhydrite (5)	Quartz (trace)
Cement (micrite)	47	Calcite (95)	Clay minerals (5)		
Opaques	2	Pyrite (100)			
Organics	1	Amorphous (100)			
	100				
Allochems	20	Bioclasts (75)	Peloids? (25)		
Matrix	80	Spar (55)	Micrite (45)		
Porosity	<1				
	100				

Sedimentary structures

Primary	None observed.
Biogenic	Some circular micrite patches may represent peloidal material, indicating minor amounts of bioturbation within the sample. One (vertical?) feature (~5 mm in length) is filled with sparry cements and possibly represents an escape trace/bore hole.

Fractures	Some fractures/open pore space observed around the edges of large bioclast fragments.
Porosity	Interparticle porosity is observed within infilled bioclast fragments (between sparry carbonate cements). Some fracture porosity (see above). Interparticle porosity within matrix minor to absent.
Opaques	Large cubic pyrite crystals are observed as overprints or inclusions within bioclast fragments. Very rare discrete pyrite grains are also present in the matrix (increased concentrations where bioclast fragments are abundant) and around the edges of bioclasts. Very fine (disseminated) pyrite crystals (sample 5010) are rare to absent.
Organics	Wispy' organic (algal?) strings and pockets (up to ~60 µm in length) are enriched within the micrite matrix and fill interparticle space.
Diagenetic	Bioclast fragments completely replaced/recrystallized with microcrystalline calcite cements, calcite/dolomite spar and rare anhydrite. Small amounts of dolomite spar and trace quartz cement observed within matrix. Some quartz replacement of dolomite cements.

Bioclasts *(in order of abundance)*

Type	*Size (µm)*	*Preservation*	*Recrystallisation*
Brachiopods/(bivalves?)	Up to ~8000	Moderate to good	Calcite; micrite; dolomite; anhydrite; none
Tentaculitids	Up to ~ 800	Moderate	Calcite; dolomite; micrite
Crinoids?	Up to ~550	Moderate	Calcite
Bryozoa?	Up to ~300	Moderate	Calcite

Description

Sample 15013 is a poorly-washed biosparite containing abundant brachiopod fragments (including shells, spines and valves), a few tentaculitid fragments and some other bioclastic debris (including possible crinoids and bryozoans). Bioclast fragments are generally replaced or infilled by pure microcrystalline calcite cements, calcite and dolomite spar, micrite and rare anhydrite and often contain large cubic pyrite inclusions and/or overprints. Some bioclast fragments feature their original composition indicating that preservation is generally moderate to good. The matrix (similar to sample 15005) contains a mixture of sparry calcite, minor dolomite spar and trace amounts of quartz cement with interparticle space filled by micrite material and 'wispy' organic matter (including strings and pockets). Disseminated pyrite crystals are rarely observed within the matrix and are generally associated with bioclasts. Darker, circular patches of micrite may indicate that some minor bioturbation has occured. Porosity within the sample is very low due to limited interparticle space (matrix). However, some open pore space is observed around the edges of bioclasts and between sparry carbonate cements (within bioclast fragments).

Rock Classification

Poorly-washed bio-sparite (Folk, 1962); brachiopod lime wackestone (Dunham, 1962).

Thin Section Quality

Good; stained for carbonates.

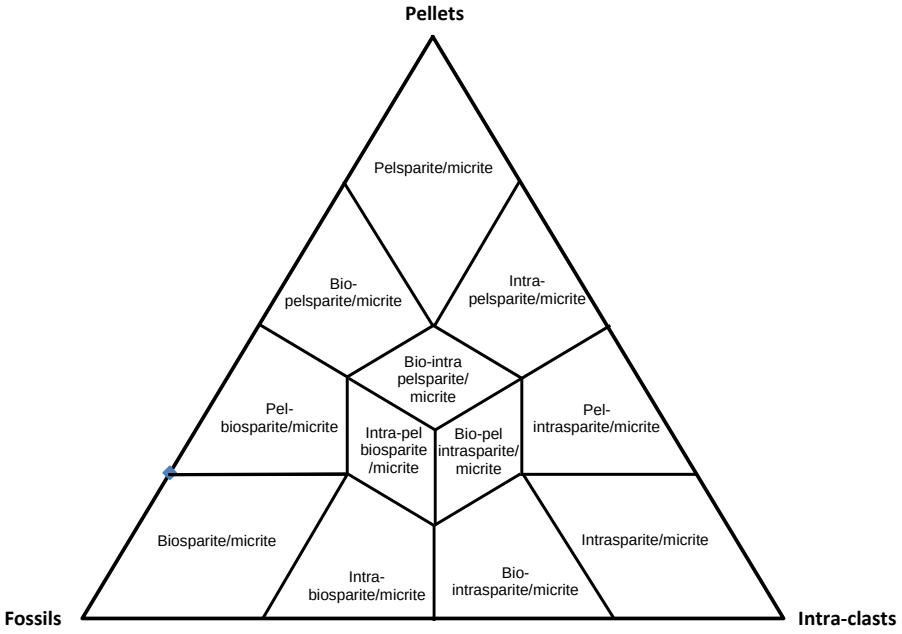


Fig. 7-53: Ternary plot showing the relative abundance of different allochem types within the carbonate rock (based on Folk's classification scheme, 1962). Sample 15013 is classified as biosparite as the rock has a mixed microcrystalline calcite (micrite) and sparry calcite/dolomite matrix with 10-50% bioclasts, some possible peloidal material and no intraclasts.



Fig. 7-54: Core photograph of sample 15013 from the Duvernay Formation, well 100/13-14-035-25W4/00 (depth 7745.7 ft.). The thin section prepared from this sample was cut from the area marked with an X. The sample was received with no up direction. Scale is in mm.



Fig. 7-55: Thin section photograph of sample 15013 from the Duvernay Formation, well 100/13-14-035-25W4/00 (depth 7745.7 ft.). The image reveals a fine-grained carbonate rock containing abundant bioclasts (especially towards the top of the sample), which predominantly consist of brachiopod and/or bivalve shell fragments. Some darker patches and lenses may represent burrow structures, indicating sediment disturbance or bioturbation. Intensive pink staining within the carbonate-stained half of the thin section (left of image) shows the dominance of calcite in the sample. Scale is in mm.

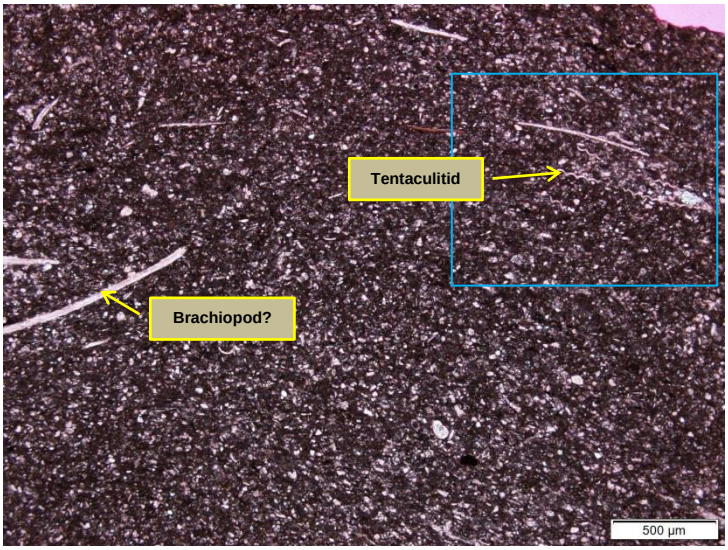


Fig. 7-56: Photomicrograph in PPL showing an overview of sample 15013 (well 13-4, depth 7745.7 ft.). The image reveals a calcite-rich carbonate rock containing both sparry cements (predominantly calcite with some dolomite) and micritic material (some of which may represent peloids). Bioclast fragments are generally sparsely dispersed throughout the sample and predominantly consist of bivalve and/or brachiopod shell fragments (up to 700 µm in this image) and tentaculitids (up to 850 µm in this image; see Figures 7-57 & 7-58 for further detail). Some darker patches may represent concentrated organic matter and/or opaque material.

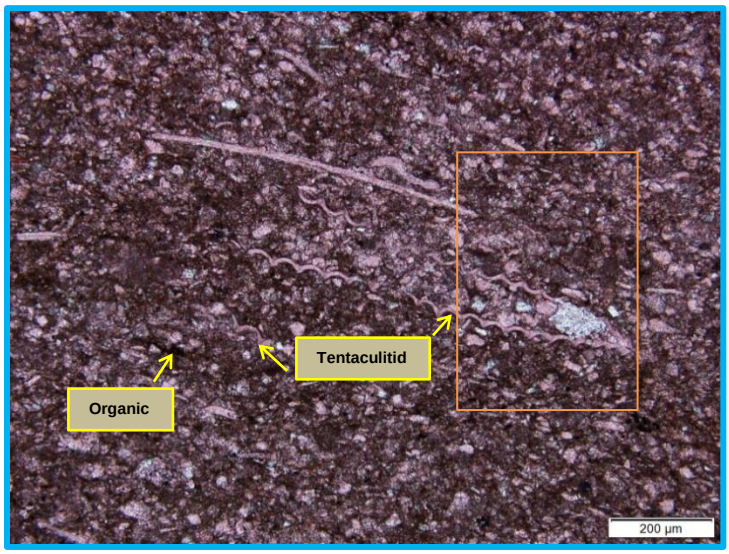


Fig. 7-57: Photomicrograph in PPL showing magnification of the ~800 µm tentaculitid fragment imaged in Figure 7-56. The fragment is composed of microcrystalline calcite and infilled by both sparry and micritic carbonates (microcrystalline material). Smaller, broken tentaculitid fragments (100-150 µm) are finely dispersed throughout the image. Also note organic matter (generally wispy; algal?) which is concentrated in the matrix.

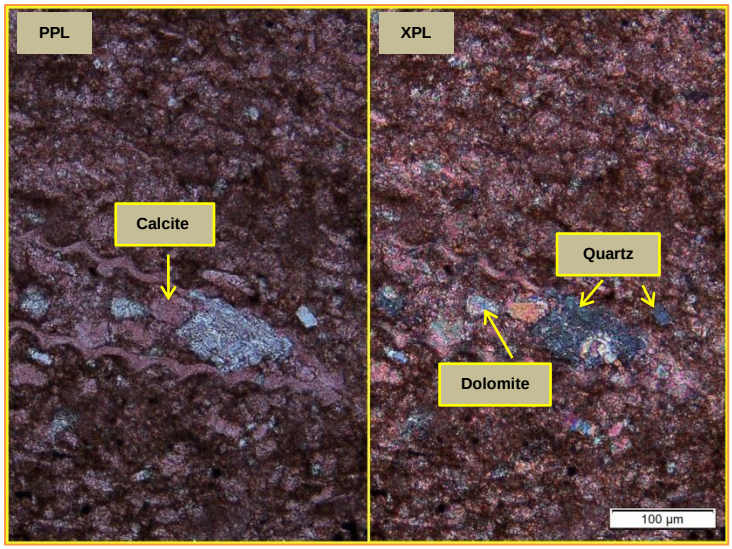


Fig. 7-58: Split-image photomicrograph in PPL (left) and XPL (right) showing further magnification of the cements infilling a tentaculitid fragment (see Figure 7-57). Most of the sparry cements are composed of pink-stained calcite (25-40 µm) with very rare sparry dolomite (generally up to 35 µm) and some quartz. The rare angular quartz (20 µm) within the matrix to the right represents a pseudomorph after dolomite.

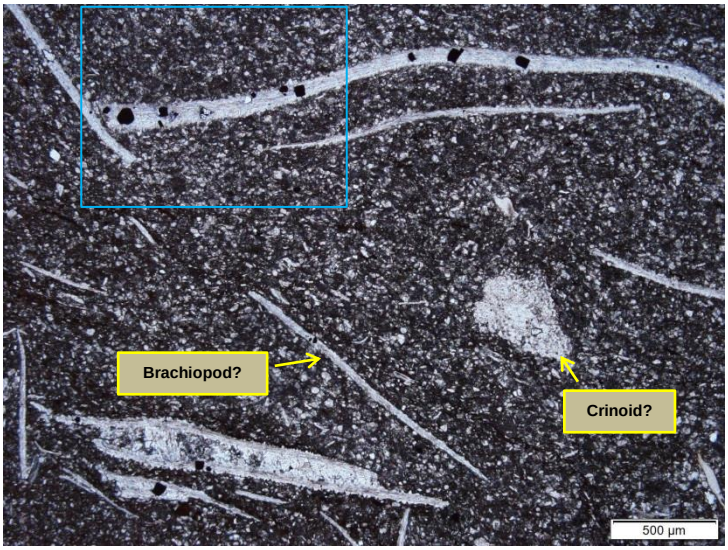


Fig. 7-59: Photomicrograph in PPL (unstained part of thin section) showing abundant bivalve and/or brachiopod shell fragments (up to ~5.5 mm) many of which contain large (up to 80 µm) cubic pyrite crystals (see Figure 7-60). Also note the possible crinoid fragment (550 µm) to the center-right of the image.

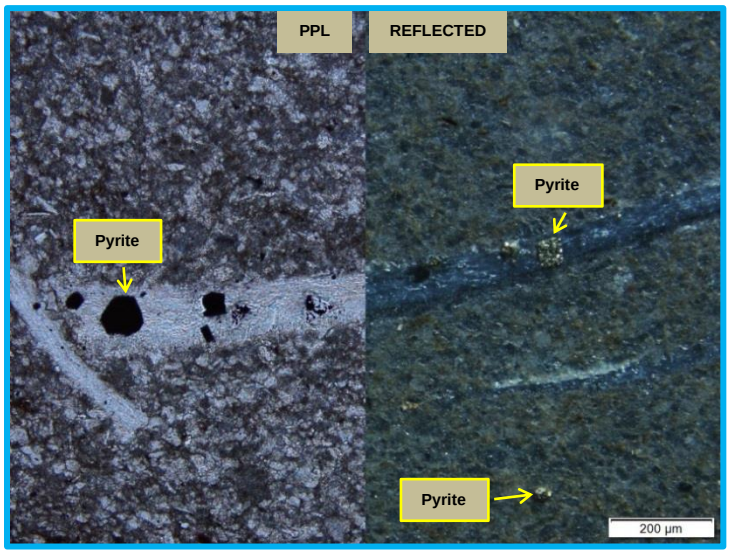


Fig. 7-60: Photomicrograph in PPL (left) and reflected light (right) showing magnification of the pyrite crystals within a brachiopod shell fragment (see Figure 7-59). Some rare discrete pyrite grains (up to 40 µm) are also observed in the surrounding matrix. Finely dispersed disseminated pyrite crystals (such as those observed in sample 15010) are absent.

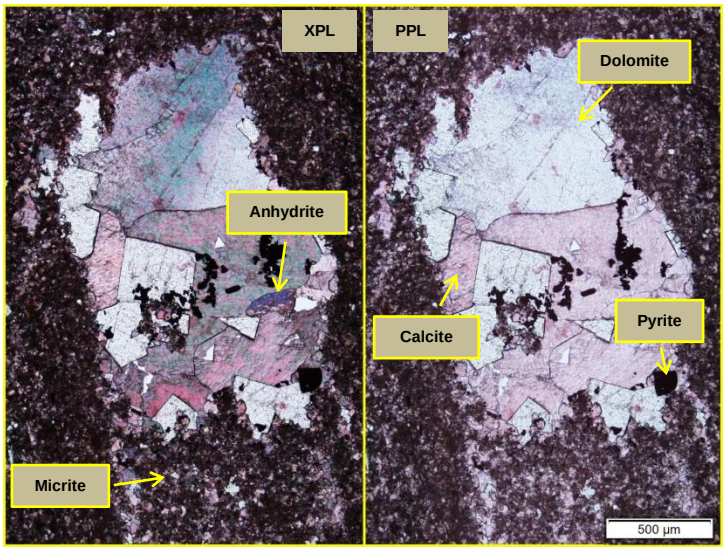


Fig. 7-61: Split-image photomicrograph in XPL (left) and PPL (right) showing a completely replaced bioclast (shell fragment, ~5 mm in length). The top part is filled by sparry dolomite (up to 950 µm), calcite (up to 650 µm) and rare anhydrite cements (250 µm), and contains pyrite inclusions (150 µm) and clusters. The bottom part is more faintly outlined/defined, contains less sparry carbonate cements, and is dominated by micrite material.

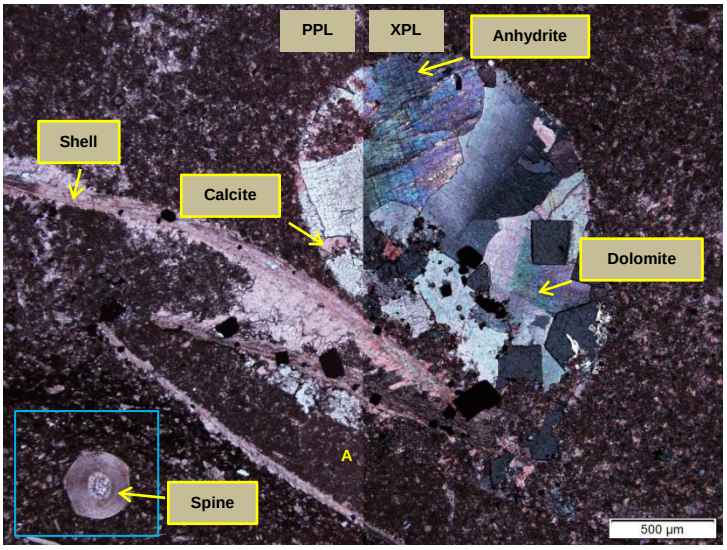


Fig. 7-62: Photomicrograph in PPL (left) and XPL (right) showing abundant bioclastic debris including a V-shaped shell (tentacilitid), a circular brachiopod spine (bottom-left, examined further in Figure 7-63) and a possible lobate valve. The V-shaped shell wall is composed of microcrystalline calcite and has been partially filled by micrite and sparry calcite cements. The large (~2 mm) lobate (valve?) fragment is completely replaced by massive sparry dolomite (up to 950 µm), rare pink-stained sparry calcite (up to 200 µm) and anhydrite cements (~1 mm) which feature high order birefringence colours and strongly defined cleavage planes.

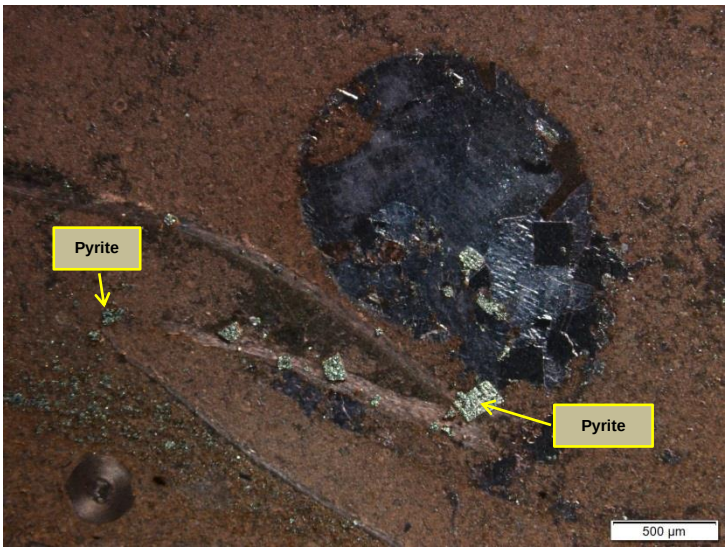


Fig. 7-63: Photomicrograph in reflected light showing abundant cubic pyrite inclusions (up to 125 µm) and overprints within the bioclast fragments imaged in Figure 7-62. Some finer pyrite grains are also observed rimming the lower edge of the shell fragment to the bottom-left of the image. In general, pyrite is associated with bioclasts and is rarely observed within the matrix.

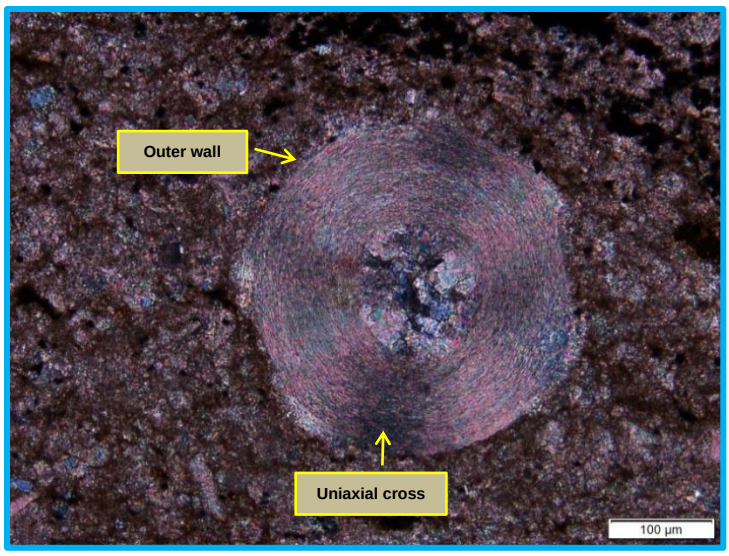


Fig. 7-64: Photomicrograph in XPL of the brachiopod spine (~335 µm) shown in Figure 7-62. The hollow center of the spine (135 µm diameter) is filled by sparry calcite cements (~20 µm), whereas the outer wall is composed of finely layered microcrystalline calcite. Also note the pseudo-uniaxial cross observed under XPL which aids in the classification of this fossil as a brachiopod spine.

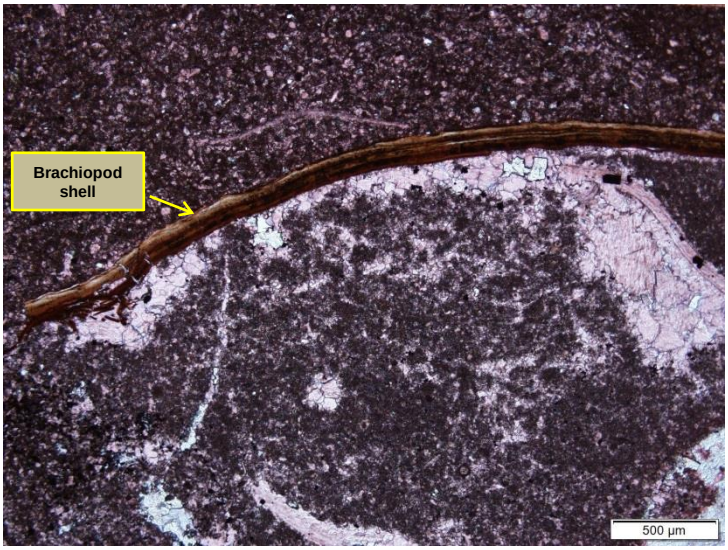


Fig. 7-65: Photomicrograph in PPL showing a section of a large (~8 mm) shell fragment (opaque in XPL). The fragment (phosphatic brachiopod?) is rimmed by sparry calcite. The matrix of the sample is mostly micritic with few sparry calcite and dolomite cements observed.

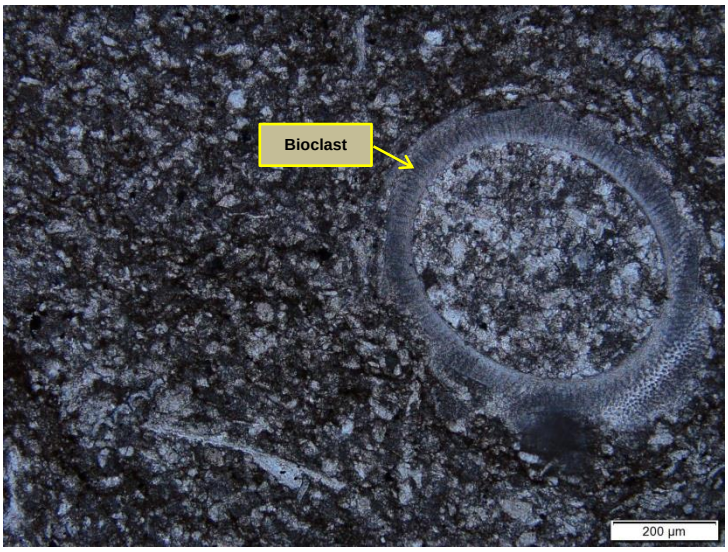


Fig. 7-66: Photomicrograph in PPL showing a ~600 µm circular bioclast fragment within the unstained part of the thin section. The fragment features some internal structure including an outer wall (70 µm wide) and a hollow center filled by sparry carbonate cements and some micrite.

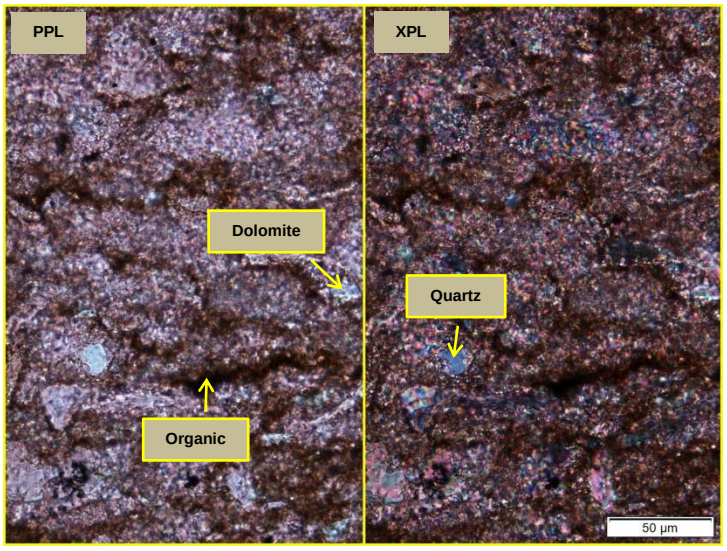


Fig. 7-67: Split-image photomicrograph in overexposed PPL (left) and overexposed XPL (right) showing details of the matrix. ~40-50% of the matrix consists of micrite (microcrystalline carbonates and clay minerals), with abundant sparry calcite cements (up to ~45 µm), rare dolomite spar (15 µm) and trace concentrations of quartz cement (20 µm). 'Wispy' brown (organic, clays?) strings (up to ~60 µm in length) and very rare disseminated pyrite crystals are also observed within the micritic material.

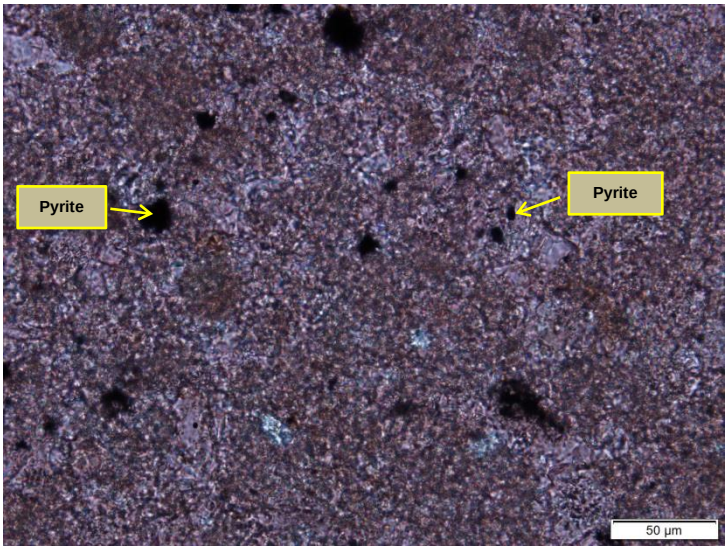


Fig. 7-68: Photomicrograph in slightly overexposed PPL showing magnification of the fine-grained material shown in Figure 7-62 (labeled A). Discrete pyrite crystals (up to 15 µm) and clusters are finely dispersed throughout.

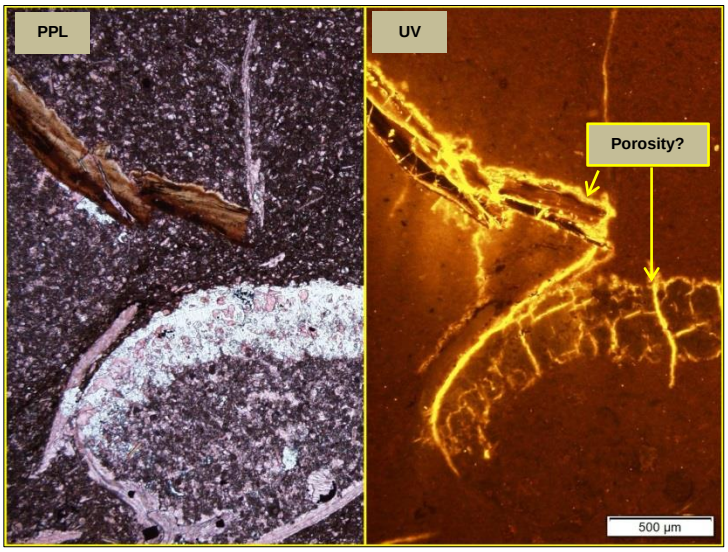


Fig. 7-69: Split-image photomicrograph in PPL (left) and UV light (right) showing an overview of porosity and fracturing within the sample. Open pore space/fractures are generally associated with the rims of bioclast fragments (e.g. the organic-replaced brachiopod shell fragment towards the left of the image). Some interparticle porosity is also observed between sparry carbonate cements in the infilled bioclast towards the bottom of the image. Porosity within the matrix is low to absent, causing overall porosity to be ~1%.

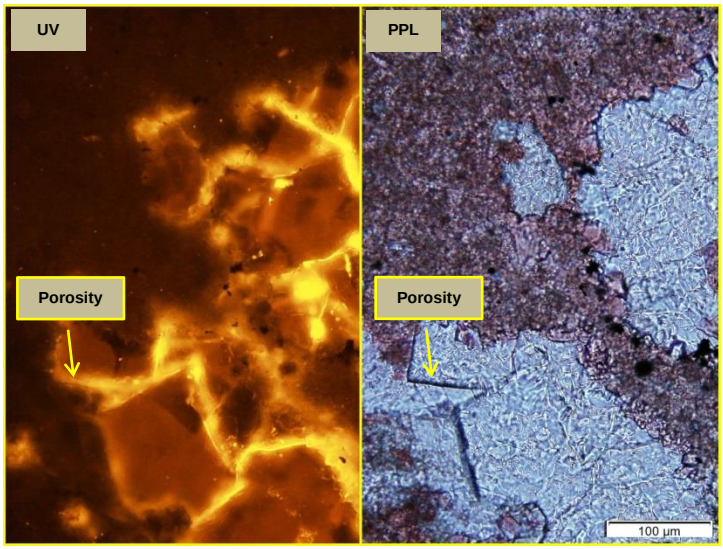


Fig. 7-70: Split-image photomicrograph in UV light (left) and PPL (right) showing magnification of interparticle porosity between sparry carbonates present within a cemented pocket/patch (replaced bioclast fragment?). Porosity is absent from the surrounding matrix.

7.2.5 SAMPLE 15027

Sample ID 15027
Sample Type Core
Strat. Unit Duvernay

UWI/Well 100/13-14-035-25W4/00
Depth 7796.5 ft.

XRD results

Quartz (%)	Feldspar (%)	Calcite (%)	Dolomite/ankerite (%)	Clays (%)
3.7	2.1	83.7	6.3	3.7

Pyrite (%)
0.7

Composition (*in order of abundance*)

	%	Variety (%)	Variety (%)	Variety (%)	Variety (%)
Cement (spar)	35	Calcite (60)	Dolomite (40)		
Cement (micrite)	61	Calcite (90)	Clay minerals (10)		
Opaques	3	Pyrite (100)			
Organics	1	Amorphous (100)			
	100				

Allochems	15	Bioclasts (100)	Peloids (trace)		
Matrix	85	Micrite (75)	Spar (25)		
Porosity	<1				
	100				

Sedimentary structures

Primary	Poorly defined bedding planes indicate sediment transport.
Biogenic	Some bioclast fragments filled with micrite enriched in peloidal material.

Fractures	Some fractures/open pore space associated with the internal structure of brachiopod fragments which may have been created naturally and enhanced/widened during sample preparation. Finer microfractures (<1 µm wide) likely represent opening fractures produced during sample preparation or unloading.
Porosity	Some fracture porosity (see above). Interparticle porosity within matrix absent.
Opaques	Small cubic pyrite crystals commonly observed as inclusions within bioclasts and rim/line some fragments. A few (brachiopod?) shell fragments are completely replaced by pyrite. Cubic pyrite crystals are also finely dispersed throughout the microcrystalline matrix.
Organics	Netty' organic matter that rims a brachiopod shell fragment has been partially pyritized and may represent a compressed algal mat. Some fluid organic matter (also possibly algal in origin) is also observed within the matrix.
Diagenetic	Bioclast fragments completely replaced/recrystallized with microcrystalline calcite cements, calcite/dolomite spar and pyrite. An irregularly shaped, light-coloured patch to the right of the thin section may represent a concretion, which contains fewer clay minerals, opaque material and organic matter than the rest of the sample. Diagenetic dolomite cements are more abundant than in previous samples.

Bioclasts *(in order of abundance)*

Type	*Size (µm)*	*Preservation*	*Recrystallisation*
Brachiopods	Up to ~7000	Moderate to good	Calcite; dolomite; pyrite
Crinoids	Up to ~1200	Moderate to good	Calcite
Tentaculitids	Up to ~1500	Moderate to good	Dolomite; calcite; micrite
Ostracods	Up to ~500	Moderate to good	Dolomite; calcite; micrite; pyrite

Description

Sample 15027 is a sparse biomicrite containing abundant bedding-parallel brachiopod fragments (predominantly shells with some valves), crinoid fragments, tentaculitids and ostracods. As in previous samples, bioclasts are well preserved and generally replaced with pure microcrystalline calcite cements. Many of the ostracod and tentaculitid fragments have also been infilled by dolomite/calcite spar and micrite material. The matrix is predominantly composed of micrite which contains a higher clay, pyrite and organic content than observed in previous samples (15005 &15013). Sparry calcite and dolomite cements are also incorporated within the matrix. One irregularly shaped, light-coloured area to the right of the thin section possibly represents a concretion (formed during early diagenesis). This concretion contains more micrite and less organic, opaque and sparry material than the rest of the sample. Bioclasts (especially tentaculitids) are also better preserved in this area. Cubic pyrite crystals are dispersed throughout the matrix and are commonly observed as inclusions within brachiopod shell fragments and crinoid fragments. Pyrite also sometimes completely replaces brachiopod shells and organic matter (algal mats?) and rims/lines bioclasts. As in sample 15013. porosity is very low due to limited interparticle space (matrix). However, some open pore space is related to fracturing within brachiopod fragments and artificial microfractures.

Rock Classification

Sparse biomicrite (Folk, 1962); brachiopod lime wackestone (Dunham, 1962)

Thin Section Quality

Good; 1/2 stained for carbonates.

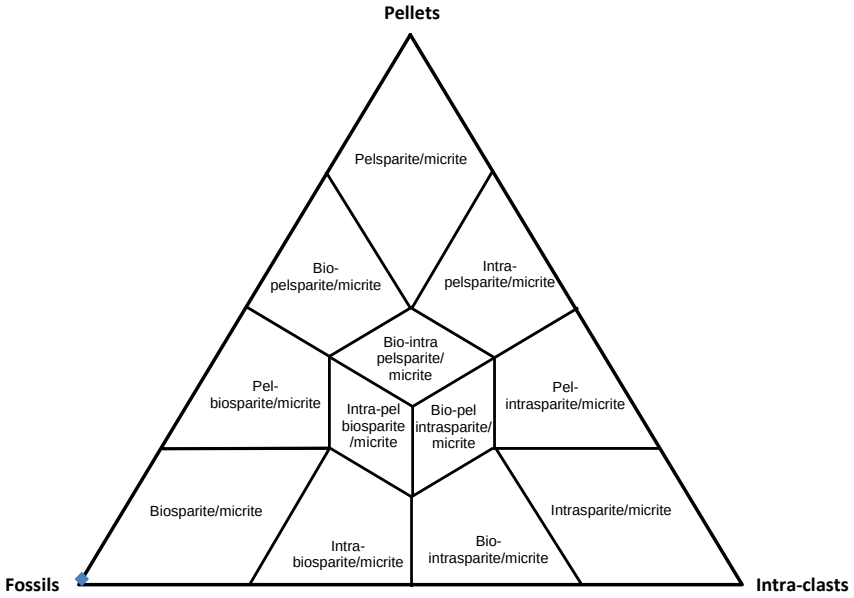


Fig. 7-71: Ternary plot showing the relative abundance of different allochem types within the carbonate rock (based on Folk's classification scheme, 1962). Sample 15027 is classified as (sparse) biomicrite as the rock has a predominantly micrite matrix with 10-50% bioclasts, some (possible) peloids and no intraclasts.

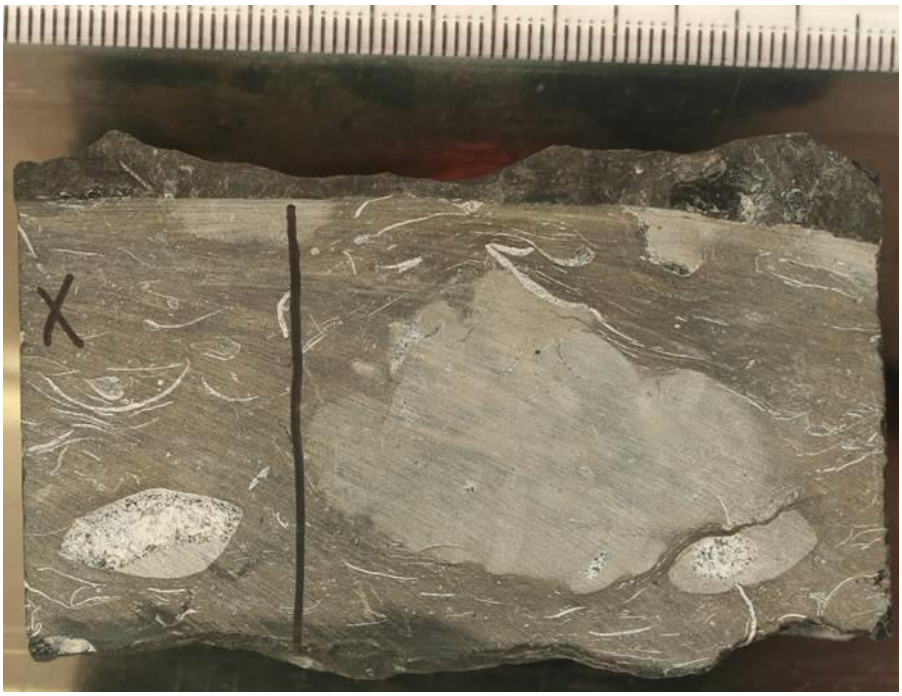


Fig. 7-72: Core photograph of sample 15027 from the Duvernay Formation, well 100/13-14-035-25W4/00 (depth 7796.5 ft.). Common recrystallized bioclasts and abundant shell fragments are observed together with several concretionary patches. The sample was received with no up direction. Scale is in mm.



Fig. 7-73: Thin section photograph of sample 15027 from the Duvernay Formation, well 100/13-14-035-25W4/00 (depth 7796.5 ft.). The image shows a fine-grained carbonate rock containing abundant bedding-parallel shell fragments and other bioclasts. An irregularly shaped, lighter-coloured patch to the right of the image also contains also some well-preserved bioclasts, and represents a concretion that formed during early diagenesis. Intensive pink staining within the carbonate-stained half of the thin section (left of image) shows the abundance of calcite in the sample. Scale is in mm.

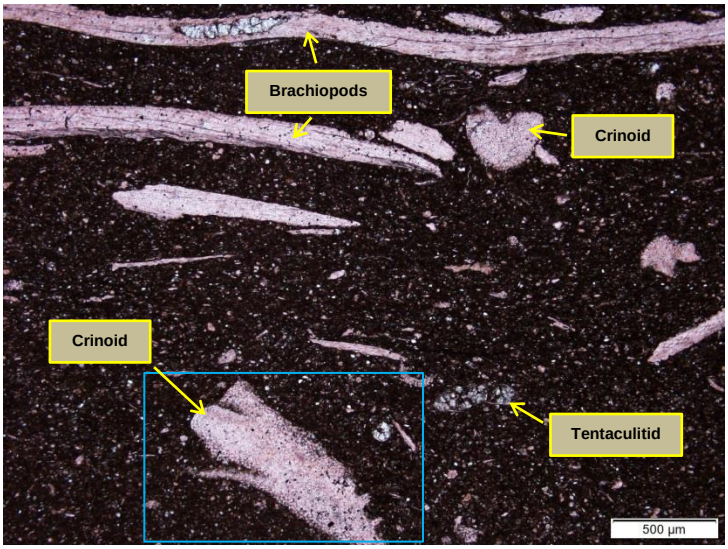


Fig. 7-74: Photomicrograph in PPL showing an overview of sample 15027 (well 13-4, depth 7796.5 ft.). The image shows a carbonate rock with abundant brachiopod shells and shell fragments (120 µm to over 5 mm in this image), which are generally oriented bedding-parallel to bedding sub-parallel. Other bioclasts include crinoid fragments (up to 1.1 mm) and tentaculitids (450 µm). Bedding planes are poorly defined.

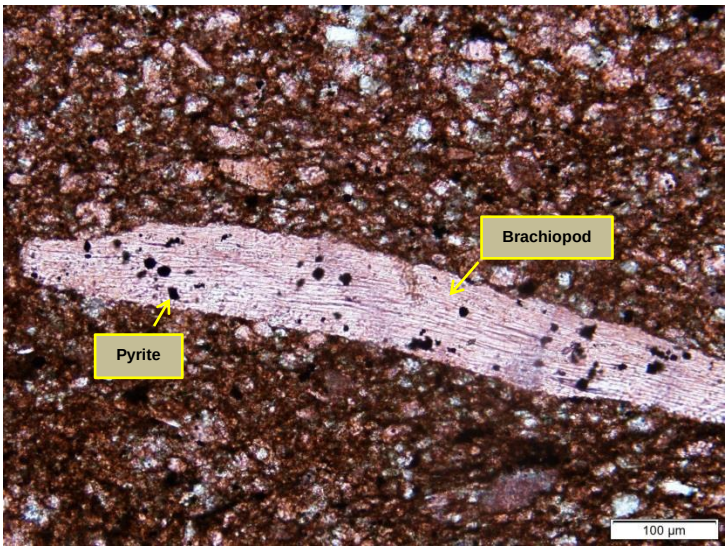


Fig. 7-75: Photomicrograph in overexposed PPL showing magnification of a brachiopod shell fragment. The fragment features growth lines and abundant cubic pyrite inclusions (up to 15 µm in this image) which are common in the brachiopod shells in this sample.

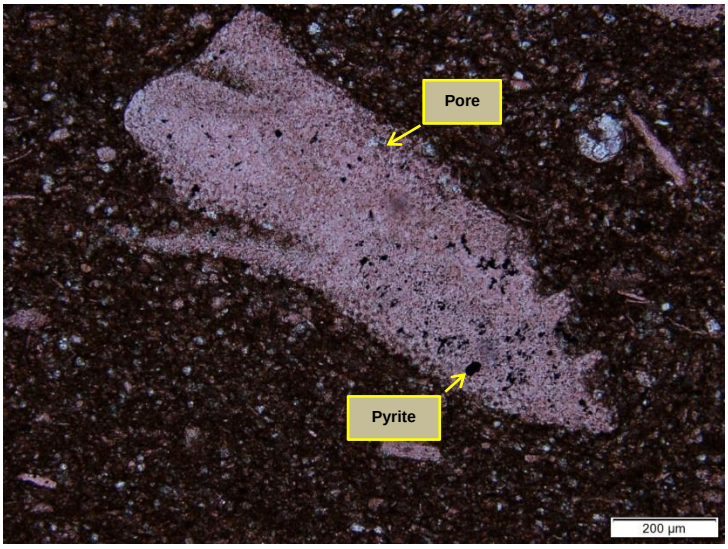


Fig. 7-76: Photomicrograph in PPL showing magnification of the crinoid fragment (~1.1 mm) imaged in Figure 7-74. Some internal features (such as micropores) are preserved.

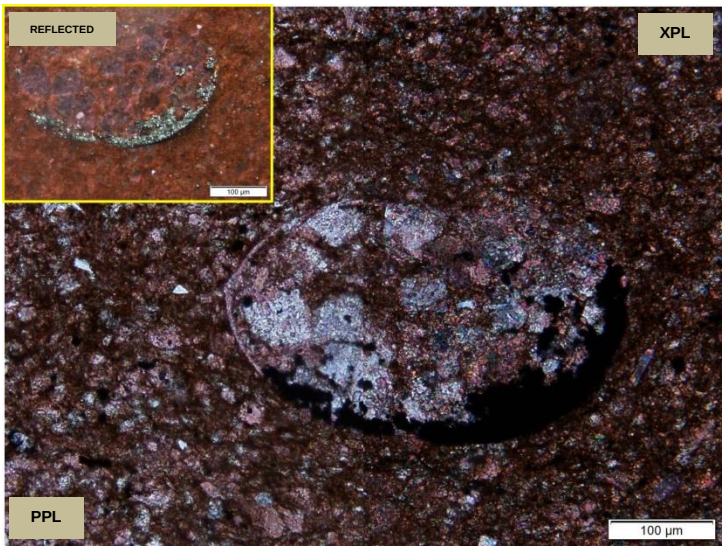


Fig. 7-77: Photomicrograph in PPL (left), XPL (right) and reflected light (inset) showing an ostracod (400 µm) with a microcrystalline calcite carapace. The interior of the bioclast has been filled with clay-rich micrite and sparry carbonates (dolomite and some calcite, up to ~70 µm), which is characteristic of ostracod preservation throughout the sample. The right-hand side of the bioclast is rimmed and filled by cubic pyrite crystals (see inset image).

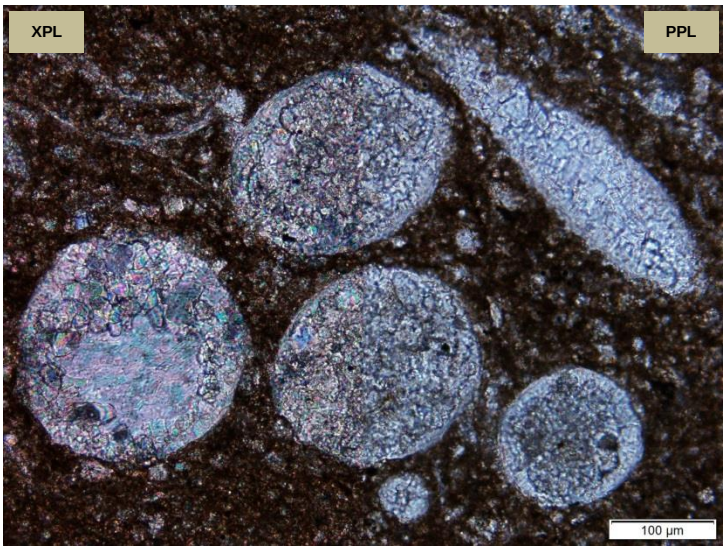


Fig. 7-78: Photomicrograph in XPL (left) and PPL (right) showing abundant circular to ovoid tentaculitid fragments (45-230 µm). The lenticular (flattened?) fragment towards the right of the image likely represents the crenulate exterior of a tentaculitid shell wall (335 µm). All of the fragments have been replaced by (or recrystallized by) sparry carbonate cements (up to 135 µm; generally ~30-35 µm). Calcite and dolomite cements cannot be differentiated due to absence of staining within this part of the thin section.

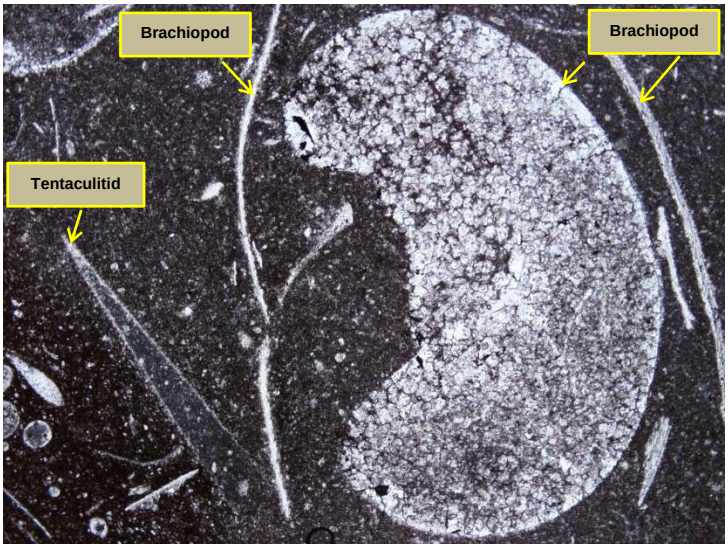


Fig. 7-79: Photomicrograph in PPL showing a large (2.6 mm) bean-shaped bioclast fragment (brachiopod?) within the concretion (unstained). The fragment features an outer wall (~65 µm wide) and a sparry interior. The image also shows a well preserved tentaculitid fragment (~1.2 mm) and abundant brachiopod shell fragments. The matrix is less organic/opaque-rich than the matrix observed throughout the rest of the sample (see left of image).

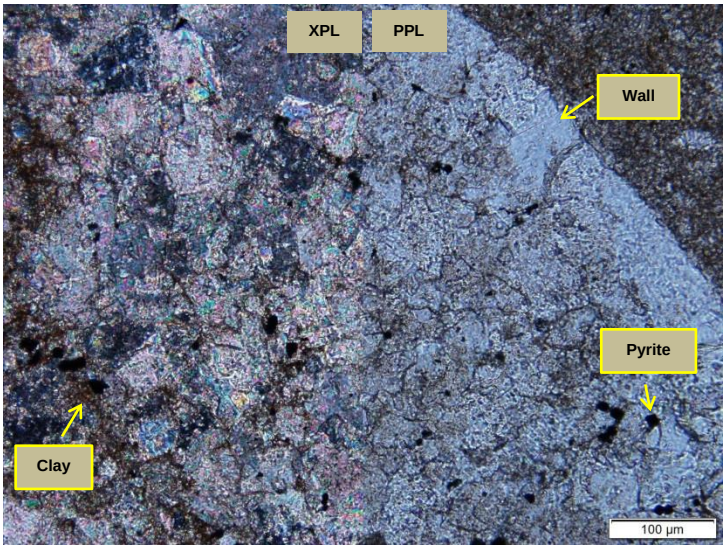


Fig. 7-80: Photomicrograph in XPL (left) and PPL (right) showing magnification of the brachiopod interior, which is predominantly composed of sparry carbonate cements, pyrite crystals (~10 µm) and small amounts of clay and organic-rich material. Calcite and dolomite cements cannot be differentiated due to lack of staining within this part of the thin section.

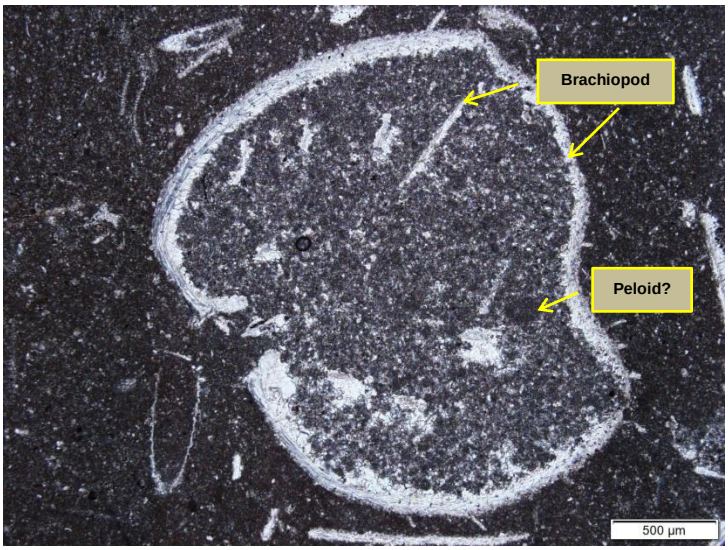


Fig. 7-81: Photomicrograph in PPL showing a brachiopod valve (~2.5 mm) that is surrounded by abundant tentaculitid fragments present within the concretion. The interior is filled by organic-and/or opaque-poor micrite, bioclasts (predominantly shell fragments; up to 600 µm) and abundant peloidal material (up to 200 µm, generally ~50 µm).

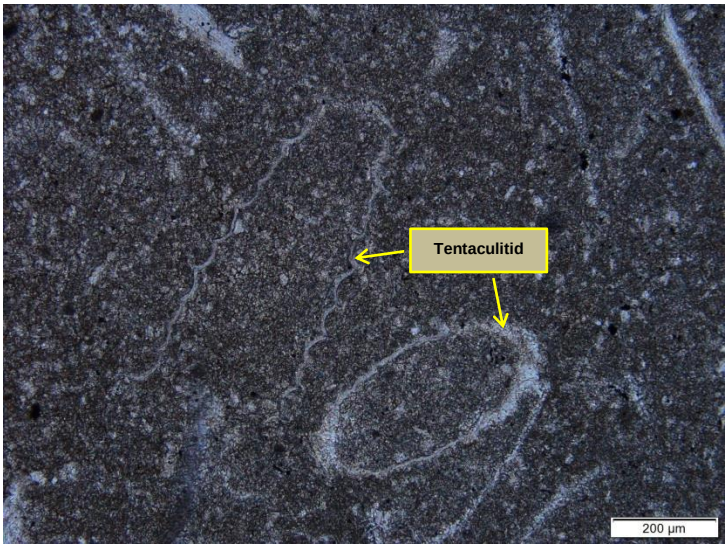


Fig. 7-82: Photomicrograph in PPL showing magnification of some well-preserved tentaculitid fragments (up to 650 µm) within the concretion (early diagenetic). Space between the crenulate shell walls of the tentaculitid towards the left of the image is wide (~230 µm) indicating that the bioclast has not been compressed.

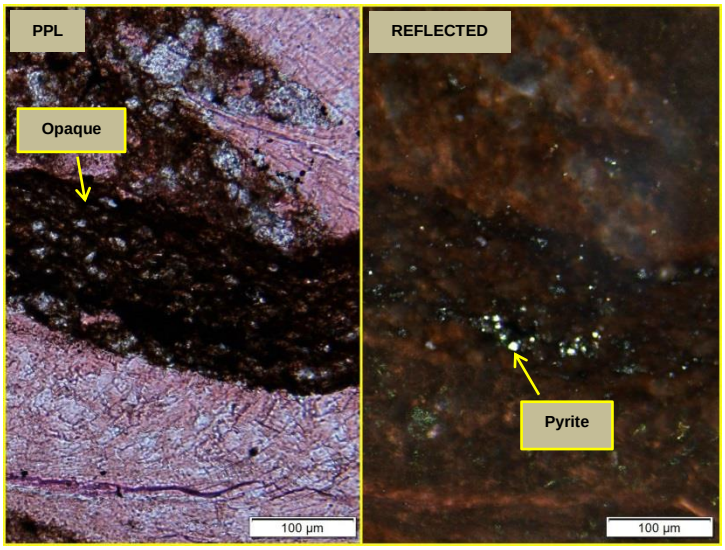


Fig. 7-83: Split-image photomicrograph in PPL (left) and reflected light (right) showing opaque material (predominantly organic matter with some pyrite) rimming a large brachiopod shell. The 'netty' texture and laterally continuous nature of the opaque material indicates that it may represent a partially pyritized algal mat that has been compressed and therefore bends around bioclasts.

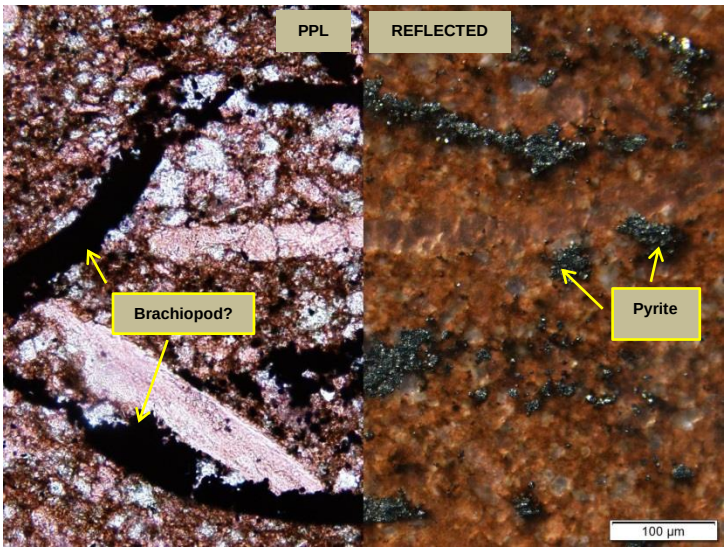


Fig. 7-84: Photomicrograph in PPL (left) and reflected light (right) showing an area of the slide with high pyrite content. Some pyrite clusters (up to ~350 µm in this image) have very defined shapes and may represent completely pyritized brachiopod shell fragments (see left of image). Pyrite clusters and patches of this type are commonly throughout the sample.

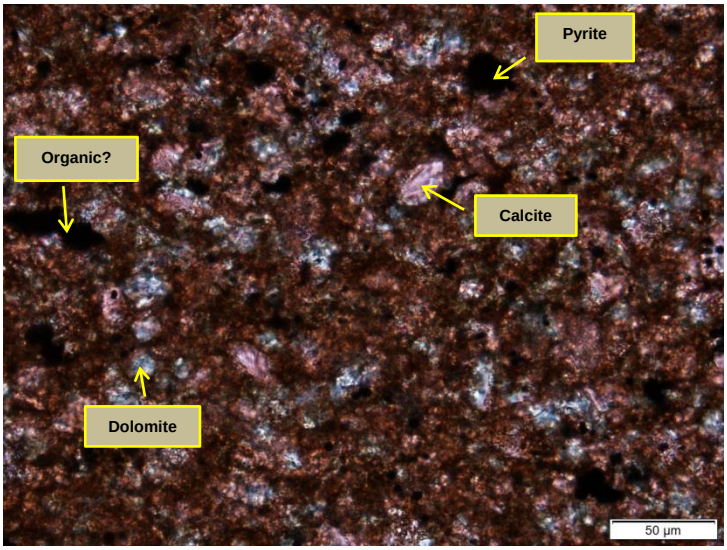


Fig. 7-85: Photomicrograph in slightly overexposed PPL showing details of the matrix. ~65% of the matrix consists of micrite and contains a higher concentration of clay minerals compared to previous samples (15005 & 15013). The remainder of the image consists of sparry calcite (up to 30 µm) and dolomite (up to 25 µm) cements. ~4% of the matrix is composed of opaque material with ~75% of this value represented by discrete pyrite crystals (5 µm) and clusters (up to ~40 µm). The remainder of the opaque material consists of organic matter.

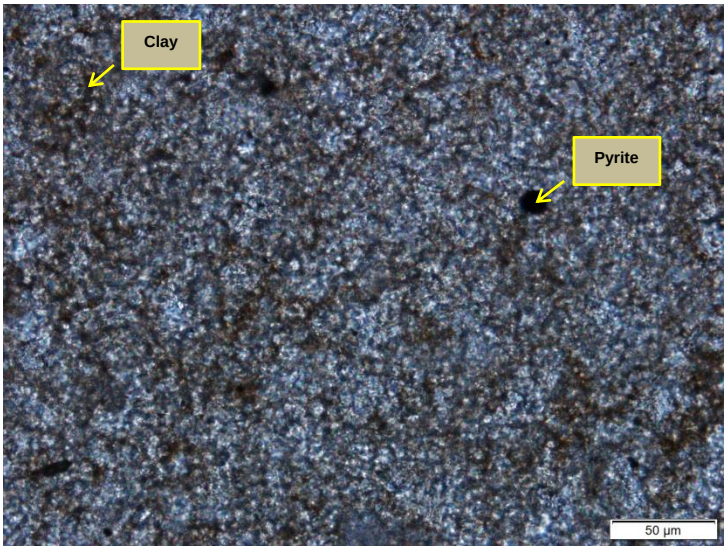


Fig. 7-86: Photomicrograph in overexposed PPL showing magnification of the matrix within the concretion. The majority of the concretion is composed of microcrystalline carbonates (cannot differentiate between calcite and dolomite due to lack of carbonate staining) with clay minerals filling very limited interparticle space. Organic matter and pyrite (15 µm) are much reduced compared to the rest of the sample (see Figure 7-85).

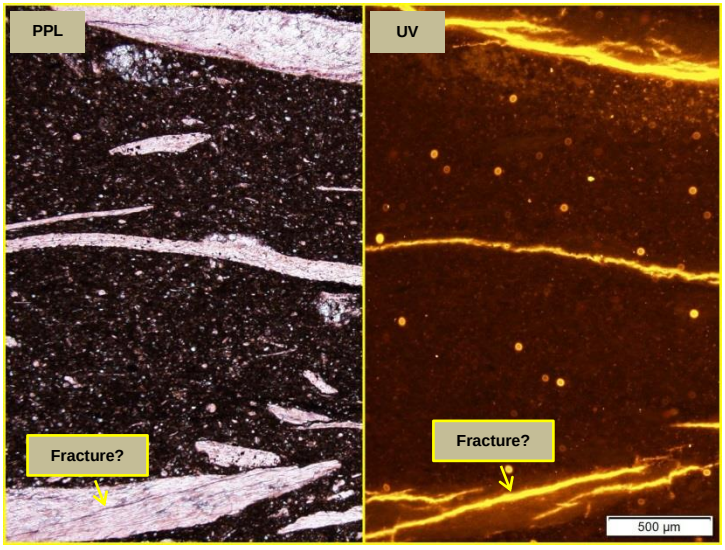


Fig. 7-87: Split-image photomicrograph in PPL (left) and UV light (right) showing an overview of porosity and fracturing within the sample. Most fracturing is associated with the internal structure of brachiopod fragments, which may have been created naturally and enhanced/widened during sample preparation (see Figure 7-88 for further detail).

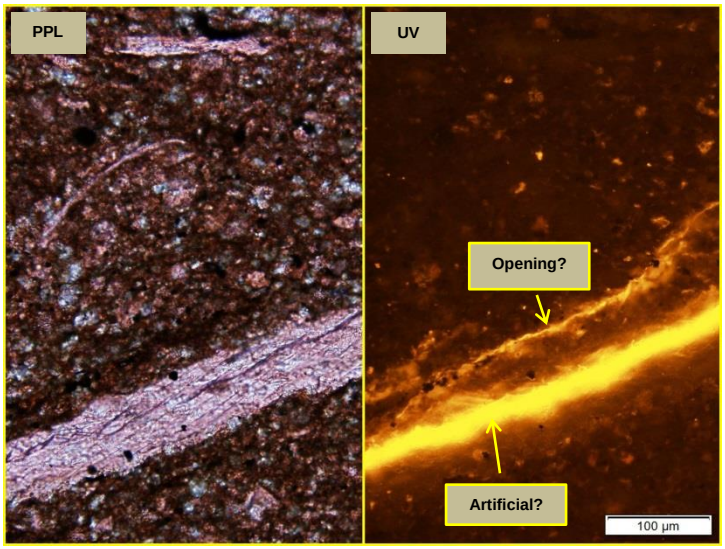


Fig. 7-88: Split-image photomicrograph in PPL (left) and UV light (right) showing magnification of some fractures. The ~5 µm fracture towards the bottom of the image is related to the internal structure of the brachiopod shell and is likely artificial (produced during sample preparation). The finer microfracture (~1 µm wide) is not visible in PPL and may represent an opening fracture (also produced during sample preparation or unloading), which is obscured by clay minerals and/or opaque material. Porosity is absent within the surrounding matrix, with patches of high fluorescence representing dolomite cements that have been partially removed or thinned.

8. Slave Point Formation Overview

Petrographic thin sections were prepared from six core samples from three wells (see Table 8-A) of the Slave Point Formation. Samples were impregnated using rhodamine-B epoxy (pink) for porosity and fracture characterization using UV fluorescence microscopy. In addition, all of the samples were dual-stained for carbonate identification. The following summary focuses on observations of sediment composition, cementation, diagenesis, clays/organics, porosity and fracture characteristics. The samples constitute five lithofacies (Table 8-B). The mineralogical summary of these lithofacies is given in Table 8-C.

8.1 SUMMARY

8.1.1 CORE SAMPLES:

Well Location	Depth (Sample ID)
100/12-08-088-08W5/00	4275.70 ft. (13451); 4257.45 ft. (13452); 4233.45 ft. (13455)
100/02-21-084-14W5/00	1706.20 m (13461); 1700.00 m (13462)
100/15-11-091-13W5/00	1629.80 m (13479)

Table 8-A: Well locations and core sample depths.

8.1.2 LITHOFACIES, GROUPINGS AND DESCRIPTIONS:

Well Location	Lithofacies	Depth (Sample ID)
100/12-08-088-08W5/00	1	4275.70 ft. (13451)
100/12-08-088-08W5/00	2	4257.45 ft. (13452)
100/12-08-088-08W5/00	3	4233.45 ft. (13455)
100/02-21-084-14W5/00	4	1706.20 m (13461); 1700.00 m (13462)
100/15-11-091-13W5/00	5	1629.80 m (13479)

Table 8-B: Lithofacies distribution by Well.

Lithofacies	Folk Classification	Dunham Classification	Quartz %	Feldspar %	Dolomite %	Calcite %
1	Bio-pelsparite	Mixed fossil peloidal grainstone	0.5	trace	0.5	99
2	Sparse biomicrite	Coral wackestone	trace	0	1	95
3	Crystalline limestone	Floatstone (Embry & Klovan, 1971)	1	0	2	97
4	Dolomitic biosparite	Coral/stromatoporoid dolostone	trace	trace	97	0
5	Sparse pel-biomicrite	Mixed fossil peloidal wackestone/packstone	trace	trace	trace	95

Table 8-C: Mineralogical summary of lithofacies.

8.1.2.1 LITHOFACIES 1: BIO-PELSPARITE

Lithofacies 1 consists of a bio-pelsparite (sample 13451) with abundant poorly preserved calcispheres, ostracods and some possible gastropod fragments. Although sedimentary structures are absent, the sample contains widespread peloidal material, which indicates moderate to heavy bioturbation. Mineralogically, the sample consists of sparry calcite with trace amounts of dolomite and quartz. Organic matter (<1%) and opaque material is rarely observed. Although fractures are absent, visual porosity is fairly high (~10%) due to the partial dissolution of bioclast fragments and abundant open interparticle space.

8.1.2.2 LITHOFACIES 2: SPARSE BIOMICRITE

Lithofacies 2 consists of a sparse biomicrite (sample 13452) which contains elevated concentrations of organic matter and lime mud compared to Lithofacies 1. Both sedimentary and biogenic structures (including peloidal material) are absent. The sample predominantly consists of microcrystalline calcite with some sparry carbonate and very rare anhydrite cement. Bioclasts are abundant (~40% of thin section) and include well-preserved coral/stromatoporoid fragments, poorly-preserved echinoderm/crinoid fragments and ostracod carapaces. Organic matter (~3%) is enriched within stylolites. Pyrite is more rarely observed and is generally present as disseminated crystals within the matrix and organic-rich stylolites. Visual porosity (~5%) is lower than in Lithofacies 1 and is associated with the dissolution and/or removal of organic matter and micrite. Some intercrystalline and moldic porosity is also observed within bioclast fragments.

8.1.2.3 LITHOFACIES 3: CRYSTALLINE LIMESTONE

Lithofacies 3 consists of a crystalline limestone (sample 13455) composed of framework material (stromatoporoid). Sedimentary structures are absent, but poorly-defined micrite patches (fecal remains?) are observed. Some boring tubes/remnants of boring organisms are also present, indicating minor bioturbation. The sample is composed almost entirely of calcite spar with some micrite patches that outline the original internal structure of the framework organism. The texture and composition of the sample is fairly consistent throughout. Bioclast fragments and organic traces are absent. Visual porosity (~7%) is higher than in Lithofacies 2, but lower than in Lithofacies 1. This porosity is generally associated with the dissolution of calcite spar, which leaves behind angular pore space. Fractures are rare and likely to be artificial or ‘enhanced’.

8.1.2.4 LITHOFACIES 4: DOLOMITIC BIOSPARTIE

Lithofacies 4 consists of dolomitic biosparites (samples 13461 & 13462), which have been extensively diagenetically recrystallized and contain abundant sub-circular coral/stromatoporoid fragments. Both sedimentary and biogenic structures are absent. The samples within this lithofacies predominantly consist of diagenetic dolomite with trace amounts of calcite and quartz. Other bioclasts are very rare and often unidentifiable. Organic matter (1-2%) is enriched within strings and stylolites and is sometimes observed as more solid chunks and blobs (especially in sample 13461). Visual porosity is high (10-13%) due to extensive dissolution that has led to the creation of vugs and voids. Opaque material sometimes fills dissolution voids and intercrystalline pores. Microfractures are common and may have assisted in stylolite development.

8.1.2.5 LITHOFACIES 5: SPARSE PEL-BIOMICRITE

Lithofacies 5 consists of a sparse pel-biomicrite (sample 13479) which is characterized by increased concentrations of organic matter and opaque material. Ovular to circular peloids are abundant throughout, indicating moderate amounts of bioturbation. Mineralogically, the sample is composed of micritic material and ‘dirty’ calcite spar with trace concentrations of dolomite. Stromatoporoid/coral fragments are present but other bioclasts (calcispheres, ostracod fragments and tentaculitids) are more common. Organic matter (~2%) is enriched within abundant stylolites. Cubic pyrite clusters are also more abundant than in all previous lithofacies. Visual porosity (~5%) is lower than in Lithofacies 4 due to filled dissolution voids. Both artificial and natural fractures are rare and generally associated with stylolites.

8.1.3 SEDIMENTARY STRUCTURES & BIOTURBATION:

Sedimentary structures (such as bedding planes and laminae) are absent from all Slave Point samples due to destructive diagenetic recrystallization, which has obliterated primary depositional features.

Biogenic mixing is variable, with most samples experiencing light to moderate bioturbation (e.g. Lithofacies 2, 3 and 4). However, ovular to rounded peloids that may represent fecal remains (Figure 8.1.3-1; left) are abundant in both Sample 13451 (Lithofacies 1) and Sample 13479 (Lithofacies 5). In addition, bean-shaped and lenticular structures within Sample 13455 (Lithofacies 3) may represent boring tubes or remnants of boring organisms (Figure 8.1.3-1; right).

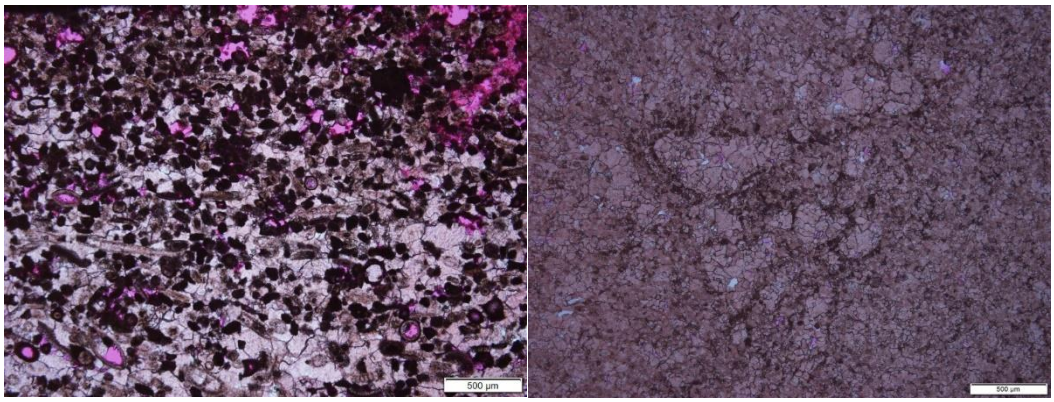


Fig. 8.1.3-1: Overview photomicrographs in PPL showing *(left)* abundant rounded peloids, which indicates moderate to heavy bioturbation within the sample (sample 13452, 4275.7 ft.), and *(right)* boring tubes and/or remnants of boring organisms which are faintly outlined by micrite material (sample 13455, 4233.45 ft.).

8.1.4 DIAGENESIS:

Lithofacies 3 (sample 13455) and Lithofacies 4 (samples 13461 & 13462) have been completely diagenetically recrystallized with calcite and medium-coarsely crystalline dolomite spar respectively (Figure 8.1.4-1). Although Samples 13451, 13452 and 13479 have not experienced as much diagenetic alteration, bioclast fragments within these samples are often completely replaced and/or recrystallized by microcrystalline calcite cement, micrite (13451) and spar (13452; 13462). Variation in birefringence colours, crystal sizes and extinction angles within the same bioclast fragments suggests that more than one phase of diagenetic recrystallization has occurred. The presence of stylolites within most samples indicates that pressure dissolution also occurred during early diagenesis.

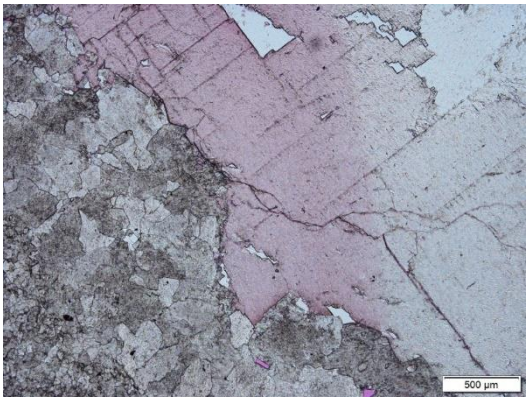


Fig. 8.1.4-1: Overview photomicrograph in PPL showing a carbonate rock that has been almost completely diagenetically recrystallized by medium to coarsely crystalline dolomite cement (white). Secondary calcite spar (pink) obliterates the fabric of a stromatoporoid fragment towards the right of the image (sample 13461, 1706.2 m).

8.1.5 ORGANIC MATTER & CLAYS:

Organic content is variable throughout the Slave Point Formation. Stylolites (samples 13452, 13461, 13462 & 13479) contain concentrated organics and cubic pyrite crystals (Figure 8.1.5-1). These features taper in thickness, wrap around larger sparry cements and are sometimes interconnected (e.g. sample 13479). Bedding-parallel organic strings and laminae in some samples may represent compressed algal material. Only trace amounts of organic matter are observed in Samples 13451 and 13455. Clay minerals are absent from the samples.

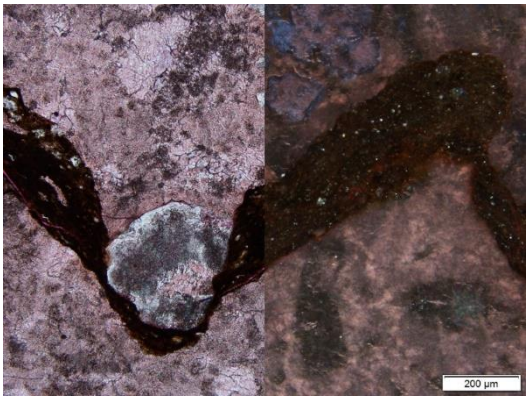


Fig. 8.1.5-1: Overview photomicrograph in PPL (left) and reflected light (right) showing an organic-rich stylolite that is characteristic of the Slave Point samples. The stylolite tapers in thickness, wraps around larger sparry carbonate cements and contains some small pyrite crystals (sample 13452, 4257.5 ft.)

8.1.6 BIOCLASTS:

Bioclasts mainly consist of stromatoporoid/coral fragments (especially in samples 13452, 13455, 13461 & 13462) that have been completed replaced by sparry carbonate cements (Figure 8.1.6-1, left). These fragments show a range of preservation states from poor (completely diagenetically obliterated) to good (radial internal structure visible; e.g. sample 13452). Sample 13455 is a stromatoporoid framework which has been completely replaced by sparry calcite cement. Original pore structures within the stromatoporoids/corals are usually filled by ‘dirty’ dolomite and/or calcite spar. This material has been removed in samples 13461 & 13462, leaving angular dissolution voids/vugs.

Samples 13451, 13452 and 13479 contain a more diverse bioclast assemblage (Figure 8.1.6-1, right) that includes poorly preserved ostracod carapaces, calcispheres, crinoids/echinoderms (sample 13452), and tentaculitids (sample 13479). These bioclast fragments are generally replaced by calcite spar and/or micrite (usually present as an infill). Calcispheres often consist of multiple concentric layers and feature dissolved centers that contribute to intraparticle porosity. Echinoderm/crinoid fragments are moderately well-preserved.

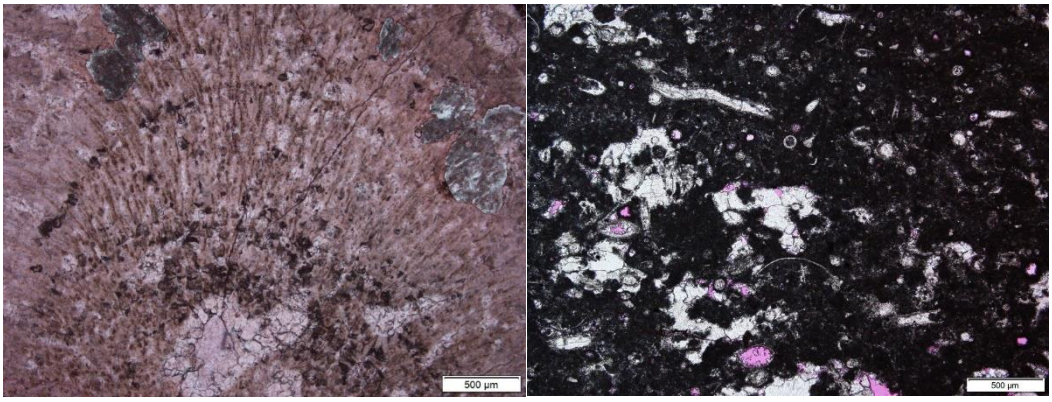


Fig. 8.1.6-1: Overview photomicrographs in PPL showing *(left)* a calcite-replaced stromatoporoid fragment with radial internal structure (sample 13452, 4257.5 ft.) and *(right)* a more diverse bioclast assemblage which includes calcispheres, ostracod carapaces and tentaculitid fragments (sample 13479, 1629.8 m).

8.1.7 POROSITY & FRACTURING:

Intraparticle porosity is generally fairly high within the Slave Point samples (Figure 8.1.7-1, left) due to the partial dissolution of bioclasts (especially ostracods and calcispheres; e.g. sample 13451). Interparticle porosity is also high in this sample, as open pores are only sporadically filled by dolomite spar or quartz cement. In addition, angular vugs and dissolution voids (samples 13461 & 13462, see Figure 8.1.7-1) are common. Porosity is lower within samples 13452 and 13455 as sparry cements are interlocking (13455). Porosity is also lower within sample 13479 as most voids are filled by calcite or dolomite spar. Most fractures within the Slave Point Formation were likely created or enhanced during sample preparation. However, some of the fractures associated with stylolites may be natural openings that encouraged stylolite development.

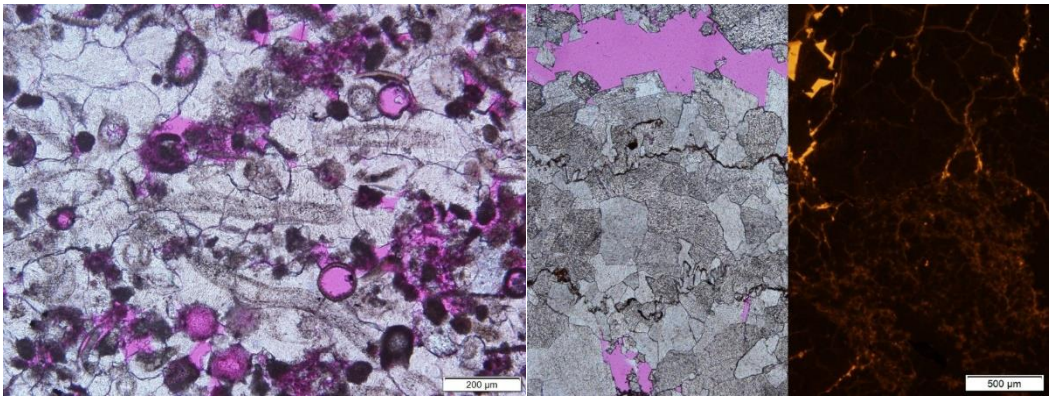


Fig. 8.1.7-1: *(Left)* Overview photomicrograph in PPL showing abundant porosity (pink epoxy) associated with calcispheres and ostracod fragments (sample 13451, 4275.7 ft.). *(Right)* Overview photomicrograph in PPL and UV light showing an open angular dissolution void/vug (top-left). UV light reveals that some intercrystalline porosity is also present between dolomite crystals (sample 13461, 1706.2 m).

8.2 RESULTS

8.2.1 SAMPLE 13451

Sample ID	**13451**		
Sample Type	**Core**	**UWI/Well**	**100/12-08-088-08W5/00**
Strat. Unit	**Slave Point Formation**	**Depth**	**4275.7 ft.**

XRD results

Quartz (%)	Feldspar (%)	Calcite (%)	Dolomite/ankerite (%)	Clays (%)
0.6	0.2	98.7	0.5	0

Pyrite (%)
0

Composition (*in order of abundance*)

	%	Variety (%)	Variety (%)	Variety (%)	Variety (%)
Cement (spar)	70	Calcite (100)	Dolomite (trace)	Quartz (trace)	
Cement (micrite)	30	Calcite* (100)			
Organics	trace	Amorphous (100)			
Opaques	trace	Pyrite (100)			
	100				

**predominantly incorporated in peloids*

Matrix	55	Spar (100)	Micrite (trace)		
Allochems	35	Peloids (55)	Bioclasts (45)	Intraclasts (trace)	
Porosity	10	Interparticle (75)	Intraparticle (25)		
	100				

Sedimentary structures

Primary	None observed.
Biogenic	Rounded peloids (up to 120 µm, generally 70-90 µm) are heavily dispersed throughout indicating sediment mixing and/or bioturbation. Slightly reduced concentrations are observed where bioclasts are abundant.

Fractures	None observed.
Porosity	Sample loosely consolidated leading to abudant open interparticle pore space. Intraparticle porosity (within bioclasts) is also commonly observed.
Opaques	Rare disseminated pyrite crystals are finely dispersed throughout the sample.
Organics	Some dark brown/black organic matter is sporadically observed.
Diagenetic	Bioclast fragments completely replaced/recrystallized with microcrystalline calcite cements and micrite. Rare dolomite and trace quartz cements fill some interparticle space and very rarely replace calcispheres.

Bioclasts *(in order of abundance)*

Type	*Size (µm)*	*Preservation*	*Recrystallisation*
Calcispheres	Up to ~300	Poor	Micrite; calcite; dolomite
Girvanella?	Up to ~550	Poor	Micrite
Ostracods	Up to ~550	Poor	Calcite; micrite
Gastropods?	Up to ~400	Poor	Micrite

Description

Sample 13451 is a bio-pelsparite containing abundant poorly preserved calcispheres, ostracod fragments and algal material (possibly *Girvanella*) with some other bioclastic debris (including gastropods). Bioclast fragments and algal remnants are generally replaced by pure microcrystalline calcite cements or faintly outlined by micrite. Peloidal material is heavily dispersed throughout but is slightly reduced where bioclast fragments are abundant. The matrix is composed (almost completely) of sparry calcite cement with very rare dolomite and quartz cements filling interparticle space. Disseminated pyrite crystals and organic matter are sporadically observed. Porosity within the sample is fairly high due to abundant open interparticle space. Many of the bioclasts (especially calcispheres) are partially dissolved contributing to further (intraparticle) porosity.

Rock Classification

Bio-pelsparite (Folk, 1962); mixed-fossil peloidal grainstone (Dunham, 1962)

Thin Section Quality

Good; 1/2 stained for carbonates.

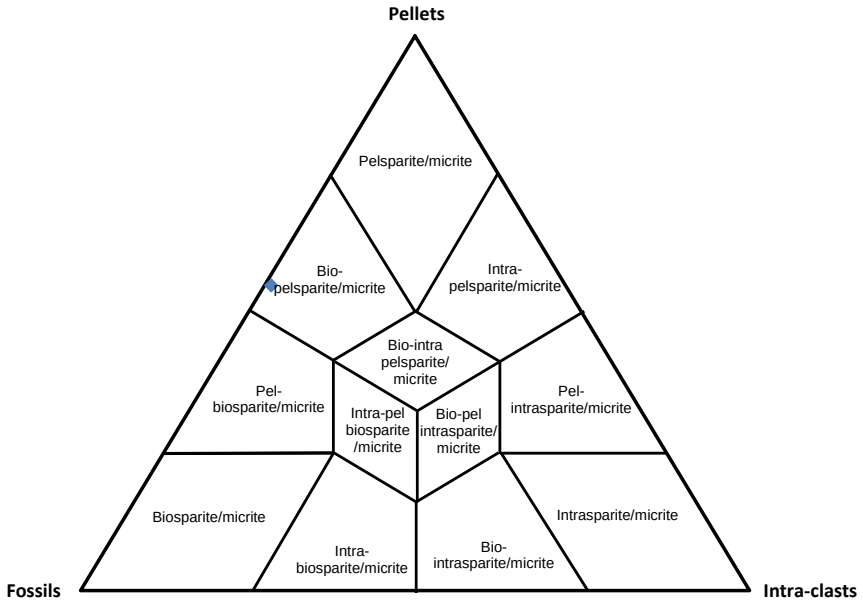


Fig. 8-1: Ternary plot showing the relative abundance of different allochem types within the carbonate rock (based on Folk's classification scheme, 1962). Sample 13451 is classified as bio-pelsparite as the sample has a sparry calcite matrix with abundant peloids, 10-50% bioclasts, and a few (possible) intraclasts.



Fig. 8-2: Core photograph of sample 13451 from the Slave Point Formation, well 100/12-08-088-08W5/00 (depth 4275.70 ft.). The thin section prepared from this sample was cut from the area marked with an X. The sample was received with no up direction. Scale is in mm.

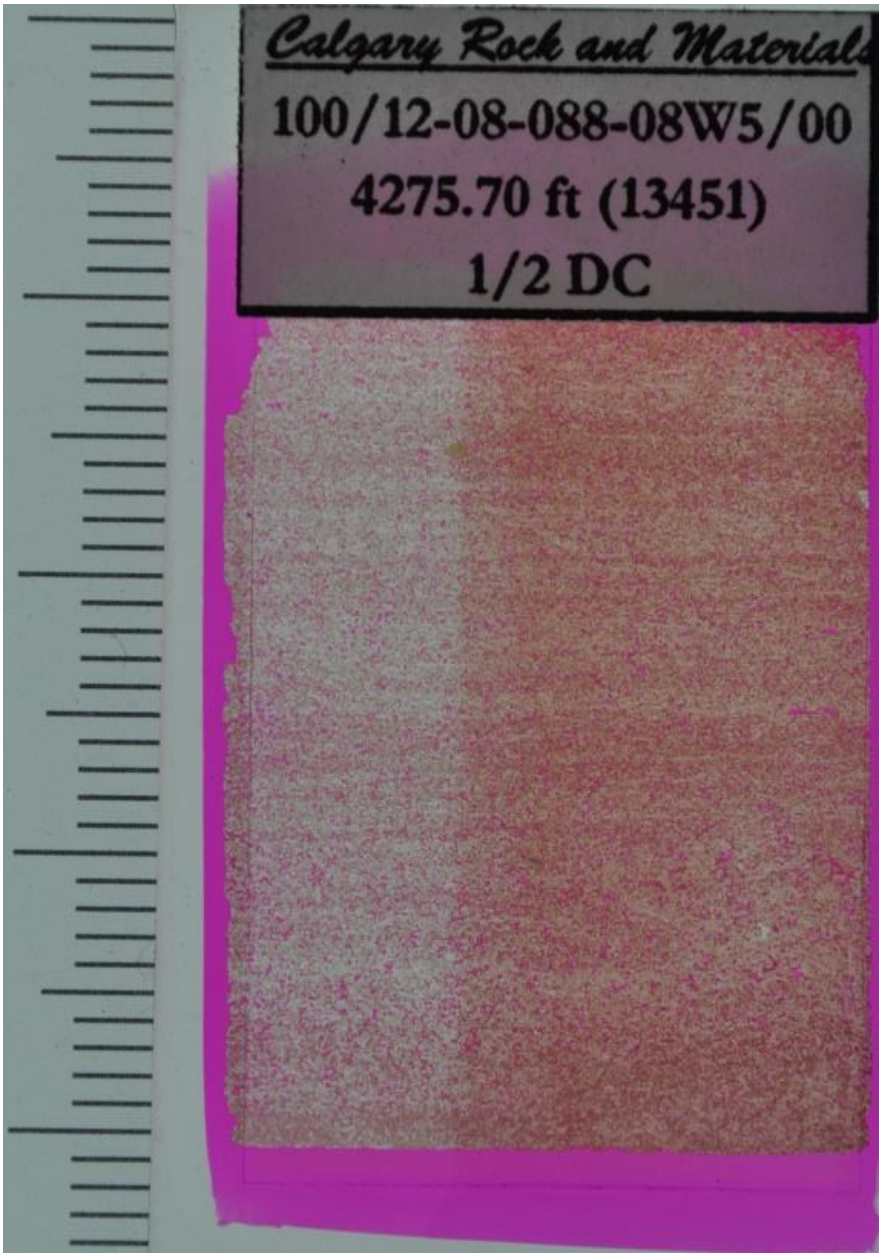


Fig. 8-3: Thin section photograph of sample 13451 from the Slave Point Formation, well 100/12-08-088-08W5/00 (depth 4275.70 ft.). The image shows a porous carbonate rock with several faintly-defined horizontal bedding-planes/laminations. Intensive pink staining within the carbonate-stained half of the thin section (right of image) shows the abundance of calcite in the sample.

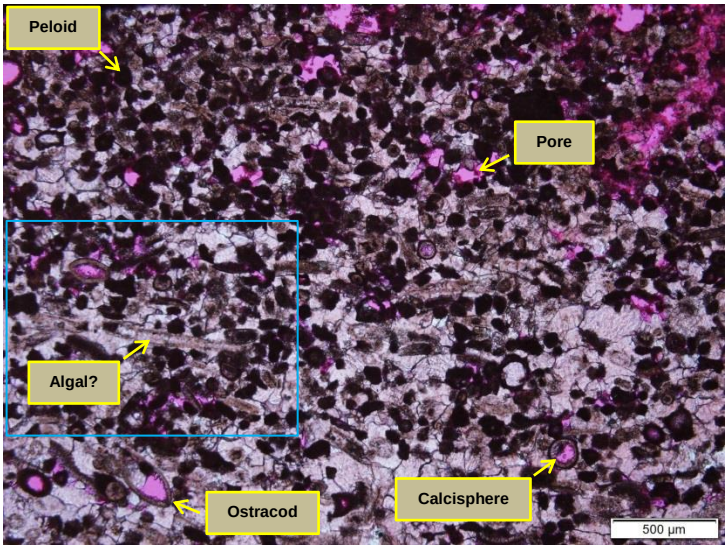


Fig. 8-4: Photomicrograph in PPL showing an overview of sample 13451 (well 12-8, depth 4275.7 ft.). The sample consists predominantly of sparry calcite with abundant open pore space (up to ~100 µm) which has been filled with epoxy. Most of the micrite material is incorporated in subspherical to spherical peloids (up to 120 µm, generally 70-90 µm) which are common throughout. Bioclast fragments are abundant and consist of poorly preserved ostracods (up to 350 µm in this image), calcispheres (up to 150 µm in this image) and algal material (see Figure 8-5 for further detail).

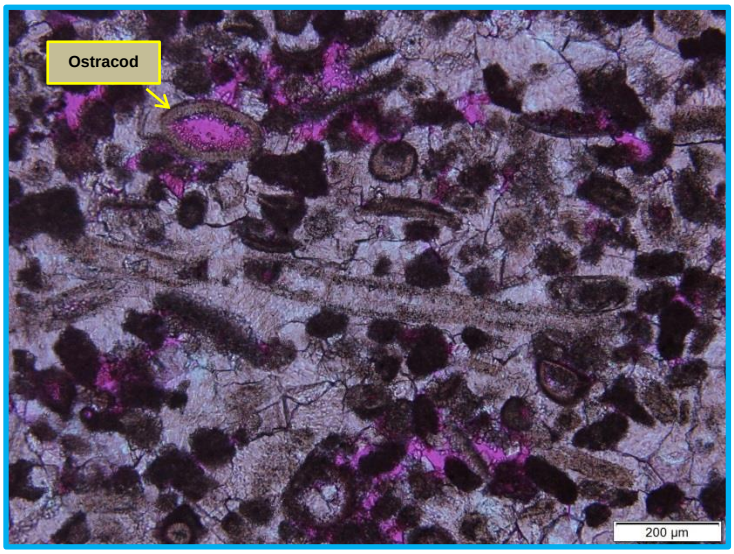


Fig. 8-5: Photomicrograph in PPL showing magnification of the abundant bioclast fragments (some up to ~750 µm) imaged in Figure 8-4. Some bioclasts have intact shell structures whereas others are fully recrystallized. The fragment in the centre may represent an individual *Girvanella* filament (abundant throughout the sample). Also note the ostracod (200 µm) with a dissolved center towards the top-left of the image.

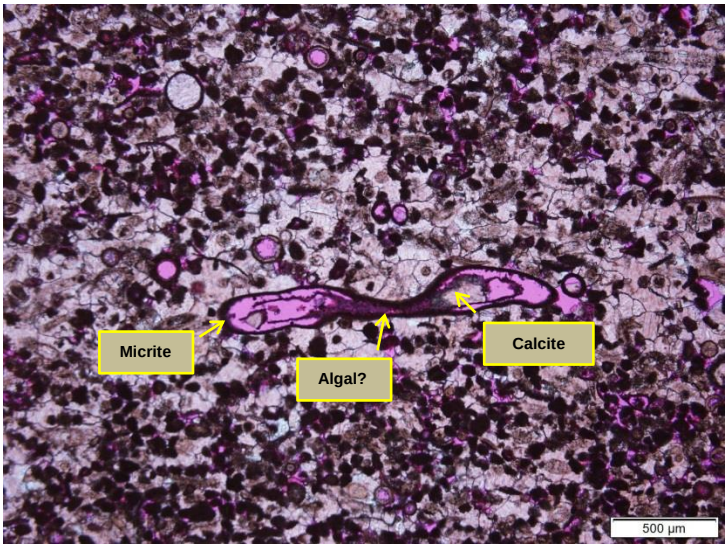


Fig. 8-6: Photomicrograph in PPL showing algal debris (~1.6 mm), which is outlined by micrite and contains a partial sparry calcite (~270 µm) and micrite infill (largely dissolved). Sparry calcite and peloids are common throughout.

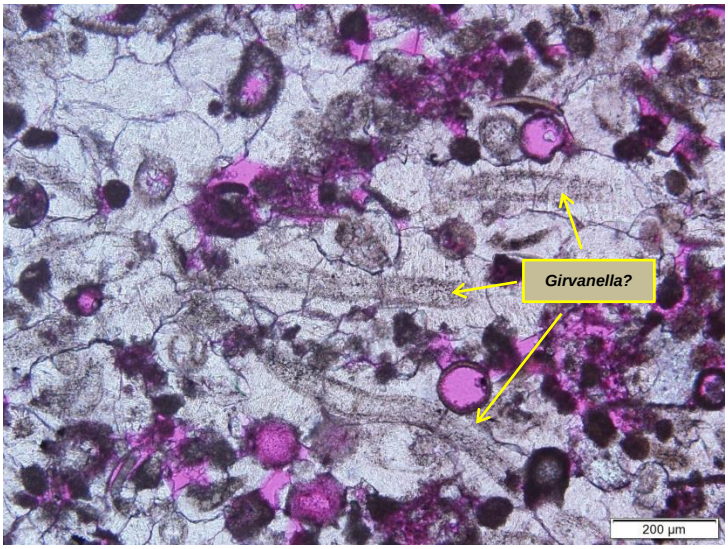


Fig. 8-7: Photomicrograph in PPL showing abundant bioclastic remains (similar to those in Figure 8-5), which are characteristic of the sample. These fragments (500-575 µm in length) are only faintly defined, indicating that they have been partially removed. The bioclasts are likely to represent individual algal *(Girvanella?)* filaments or filament sheets, and are only observed in the sparry carbonate patches.

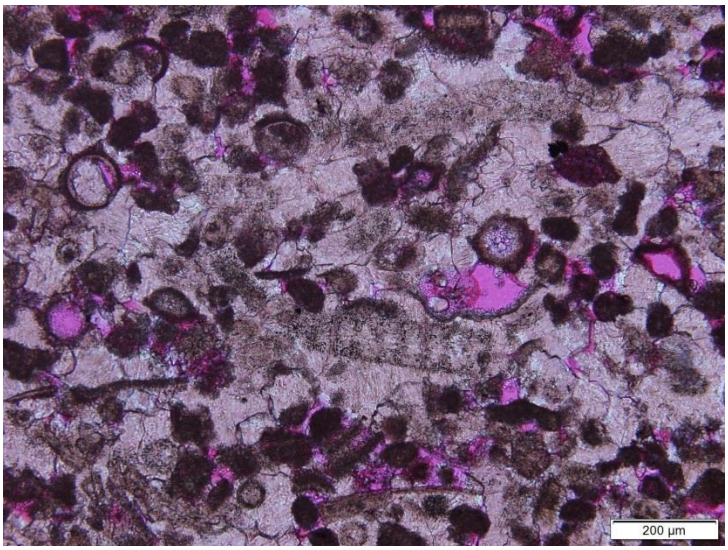


Fig. 8-8: Photomicrograph in PPL showing more algal remains (including circular structures), peloids, and shell fragments embedded within the blocky sparitic calcite matrix. Several large open pores occur throughout the sample.

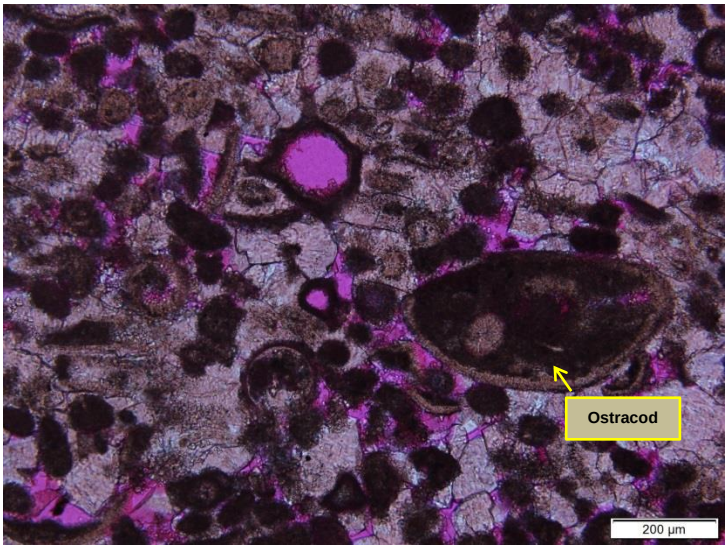


Fig. 8-9: Photomicrograph in PPL showing magnification of an ostracod (~525 µm) with a 'pure' microcrystalline calcite carapace. The interior of the ostracod is filled with lime mud (micrite), and retains some internal structure.

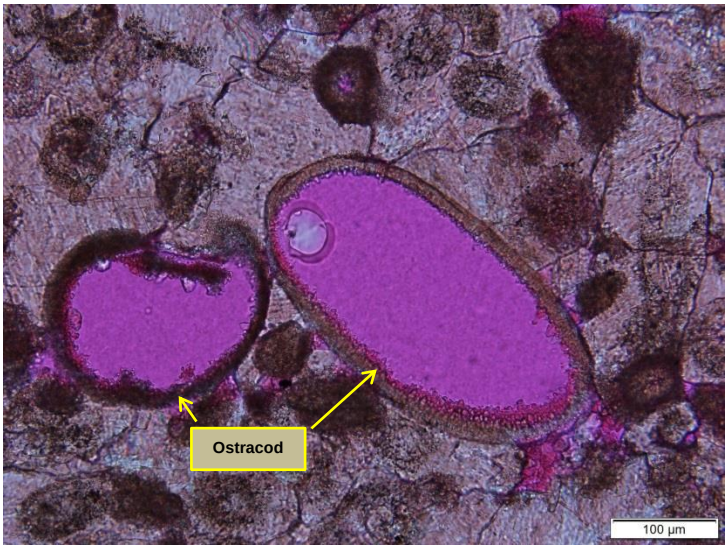


Fig. 8-10: Photomicrograph in PPL showing two ostracods (up to 370 µm) with microcrystalline calcite carapaces and empty interiors (intraparticle porosity).

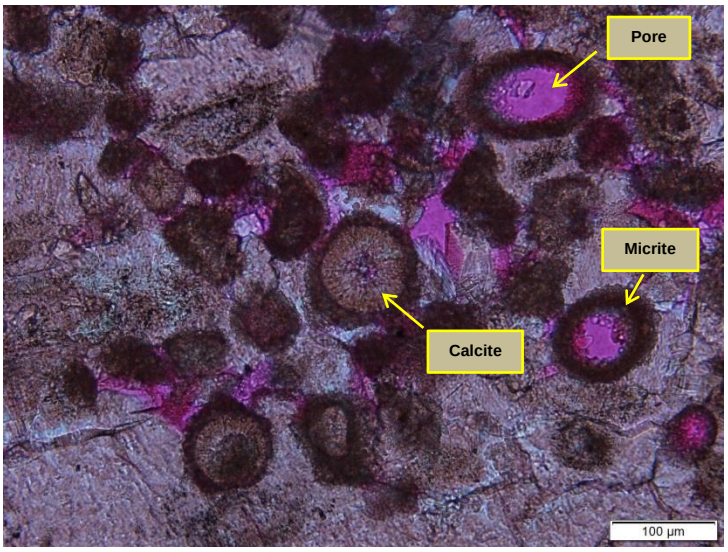


Fig. 8-11: Photomicrograph in PPL showing magnification of some small spherical bioclasts (algal remains?), which are abundant throughout the sample. These calcispheres (up to 140 µm in this image) feature a micrite outer layer and a microspar calcite interior, which is often partially or fully absent (dissolved, removed during sample preparation).

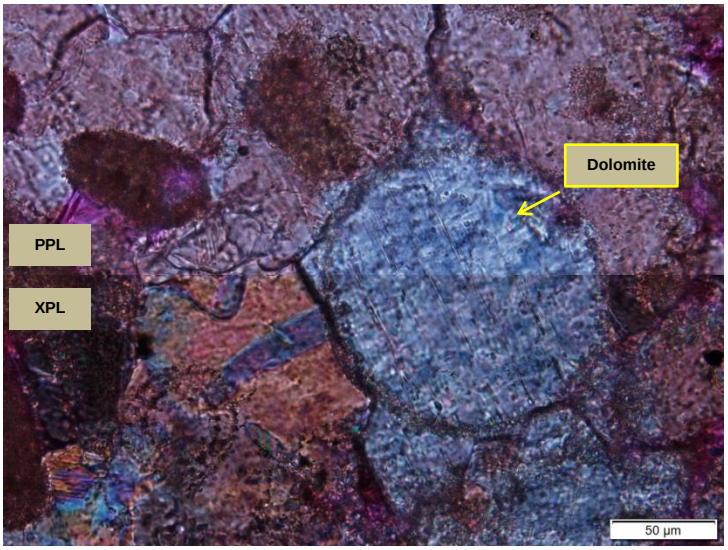


Fig. 8-12: Photomicrograph in PPL (top) and XPL (bottom) showing magnification of a calcisphere (~130 µm) that has been replaced by sparry dolomite cement (rarely observed).

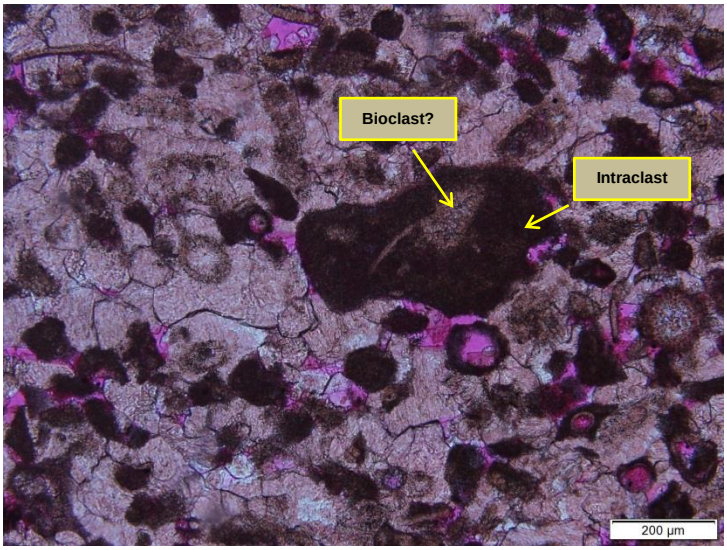


Fig. 8-13: Photomicrograph in PPL showing magnification of a rare lime mud (micrite) intraclast (~480 µm), which contains some pure microcrystalline calcite cement (up to 150 µm, possible recrystallized bioclast fragments).

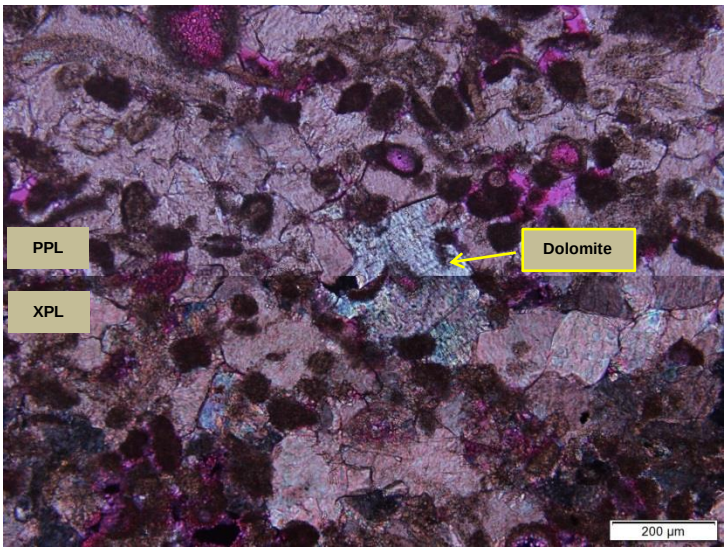


Fig. 8-14: Photomicrograph in PPL (top) and XPL (bottom) showing some sparry dolomite cements (200-250 µm), which fill interparticle space and are sporadically observed throughout the sample.

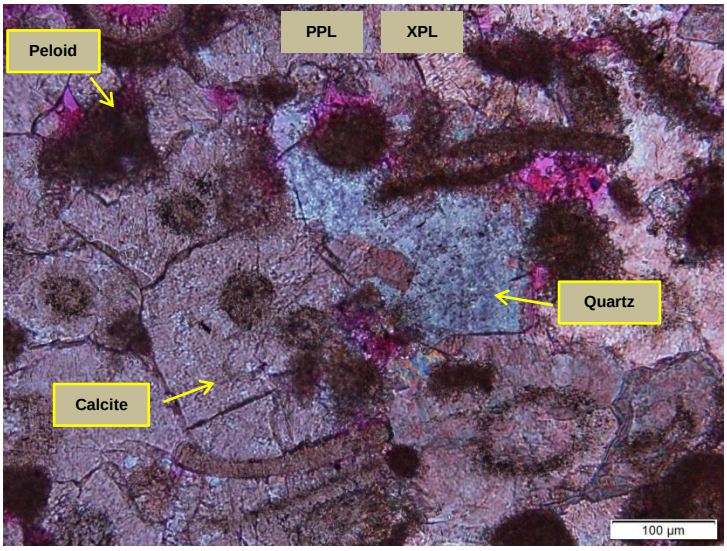


Fig. 8-15: Photomicrograph in PPL (left) and XPL (right) showing very rare quartz cement (~270 µm) filling former interparticle space. The remainder of the matrix is composed of massive sparry calcite cements, with some open pore space and peloidal material.

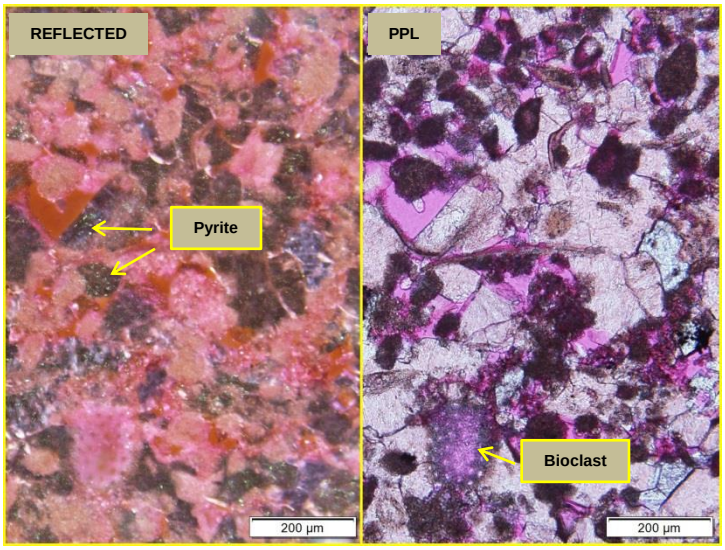


Fig. 8-16: Split-image photomicrograph in reflected light (left) and PPL (right) showing rare disseminated pyrite crystals, which are finely dispersed throughout the sample. Also note the partially dissolved bioclast (175 µm) with numerous circular white dimples to the bottom of the image.

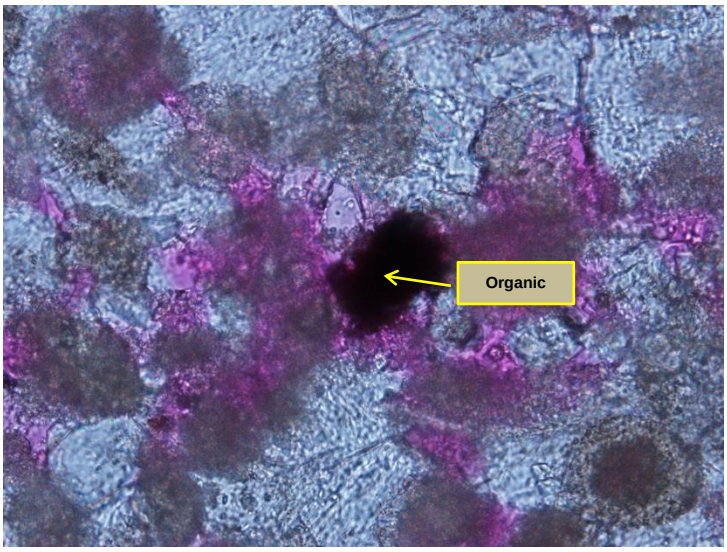


Fig. 8-17: Photomicrograph in PPL showing organic matter (~65 µm), which is sporadically observed throughout the sample.

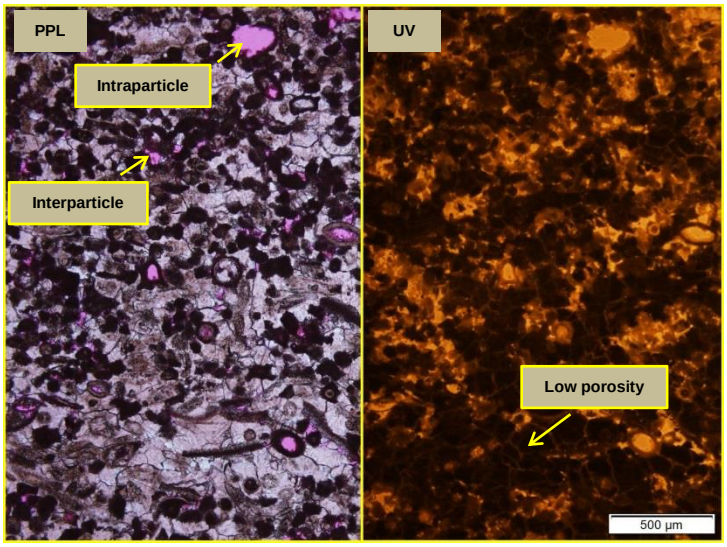


Fig. 8-18: Split-image photomicrograph in PPL (left) and UV light (right) showing an overview of porosity in the sample. The sample is generally loosely consolidated, leading to abundant open interparticle pore space. Some porosity is also associated with the dissolved interiors of calcispheres and ostracods (intraparticle porosity, up to 250 µm in this image). Reduced interparticle porosity is observed where the concentration of sparry calcite cements is high. No fractures are observed.

8.2.2 SAMPLE 13452

Sample ID	**13452**		
Sample Type	**Core**	**UWI/Well**	**100/12-08-088-08W5/00**
Strat. Unit	**Slave Point Formation**	**Depth**	**4257.5 ft.**

XRD results

Quartz (%)	Feldspar (%)	Calcite (%)	Dolomite/ankerite (%)	Clays (%)
4.1	0	94.9	1	0

Pyrite (%)
0

Composition (*in order of abundance)*

	%	Variety (%)	Variety (%)	Variety (%)	Variety (%)
Cement (micrite)	53	Calcite (100)	Dolomite (trace)	Quartz (trace)	
Cement (spar)	43	Calcite (95)	Dolomite (5)	Quartz (trace)	Anhydrite (trace)
Organics	3	Amorphous*(90)	Hydrocarbons (10)		
Opaques	1	Pyrite (100)			
	100				

**including algal material*

Matrix	55	Micrite (95)	Spar (5)		
Allochems	40	Bioclasts (100)	Peloids (trace)		
Porosity	5	Interparticle (95)	Moldic (5)		
	100				

Sedimentary structures

Primary	None observed.
Biogenic	None observed.

Fractures	Microfractures (<20 µm wide) both follow and cross-cut bedding direction and are likely predominantly artificial (filled with epoxy, created during sample preparation or recovery). Some bedding-parallel fractures may be filled with fluid organic material. A few discontinuous vertical microfractures (<15 µm wide) are healed with 'pure' microcrystalline calcite cement. Fractures often associated with stylolites and coral fragments.
Porosity	Porosity high within microcrystalline matrix (bottom part of thin section) due to dissolution of micrite and/or removal of organic material. Some intercrystalline porosity present between sparry cements within replaced/recrystallized bioclast fragments. Very rare moldic porosity observed.
Opaques	Rare disseminated pyrite crystals (up to ~15 µm) are finely dispersed throughout the sample. Cubic pyrite also sometimes forms clusters (up to ~65 µm) and is incorporated within organic-rich stylolites.
Organics	Organic matter (including both algal material and fluid hydrocarbons?) is enriched within the middle-bottom part of the sample where it fills stylolites & intergranular space and separates stromatoporoid fragments. Most organic strings are oriented parallel to bedding and may represent compressed algal remains/mats. The matrix within the top part of the sample is relatively organic-poor although some finely dispersed dark-brown organic matter (up to 75 µm) is observed.
Diagenetic	Bioclast fragments completely replaced/recrystallized with 'pure' microcrystalline calcite cements (possibly 2 phases), micrite and (rarely) dolomite. Trace amounts of bladed anhydrite observed. Micrite and/or organic matter appears to have been partially removed from bottom part of thin section. Presence of stylolites indicates that pressure dissolution has occurred.

Bioclasts *(in order of abundance)*

Type	*Size (µm)*	*Preservation*	*Recrystallisation*
Stromatoporoids	Up to ~10,000	Good	Calcite; dolomite; micrite; anhydrite
Echinoderms/crinoids	Up to ~1500	Poor to good	Calcite; micrite
Ostracods	Up to ~800	Moderate	Calcite; micrite

Description

Sample 13452 is a sparse biomicrite containing abundant well preserved stromatoporoid fragments (which retain some internal structure), poorly preserved echinoderm/crinoid fragments, ostracods (including carapaces) and some other unidentified bioclastic debris. Bioclast fragments are generally replaced by pure microcrystalline and/or sparry calcite cements with internal structure often outlined by micrite material. Bioclastic material is more abundant in the middle-bottom part of the thin section. The matrix is composed (almost completely) of microcrystalline calcite with some sparry calcite and dolomite cements. Organics are enriched within the matrix towards the bottom of the sample. Organic material is contained within stylolites (which incorporate small sparry dolomite cements and cubic pyrite crystals), forms bedding-parallel bands/laminae (compressed algal mats?) and separates stromatoporoid fragments. Disseminated pyrite crystals and clusters are sporadically observed within the matrix. Porosity within the sample is fairly high due to the removal of micrite and/or organic material (especially towards the bottom of the thin section). Some intercrystalline porosity is also associated with the completely replaced bioclast fragments. Fracturing (mostly artificial) is commonly observed.

Rock Classification

Sparse biomicrite (Folk, 1962); coral wackestone (Dunham, 1962).

Thin Section Quality

Good; 1/2 stained for carbonates.

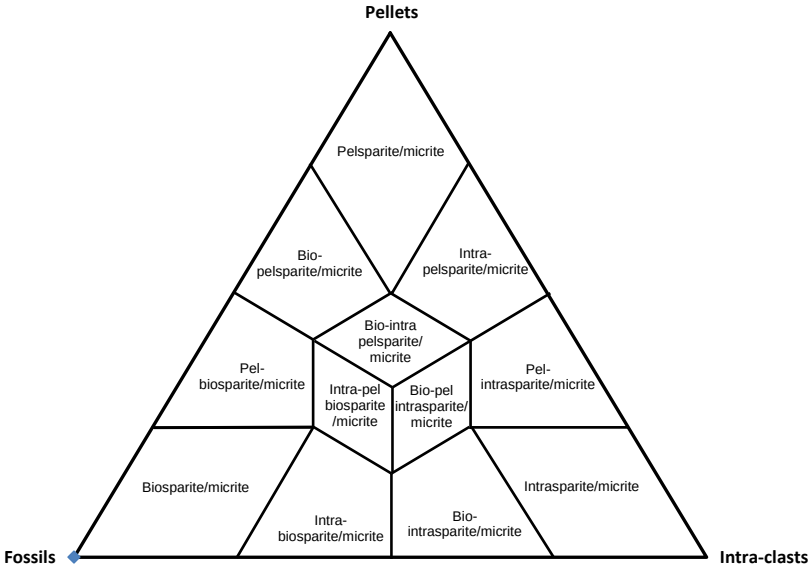


Fig. 8-19: Ternary plot showing the relative abundance of different allochem types within the carbonate rock (based on Folk's classification scheme, 1962). Sample 13452 is classified as (sparse) biomicrite as the rock has a microcrystalline calcite matrix with 10-50% bioclasts, trace amounts of peloids and no intraclasts.



Fig. 8-20: Core photograph of sample 13452 from the Slave Point Formation, well 100/12-08-088-08W5/00 (depth 4257.50 ft.). The thin section prepared from this sample was cut from the area marked with an X. The sample was received with no up direction. Scale is in mm.

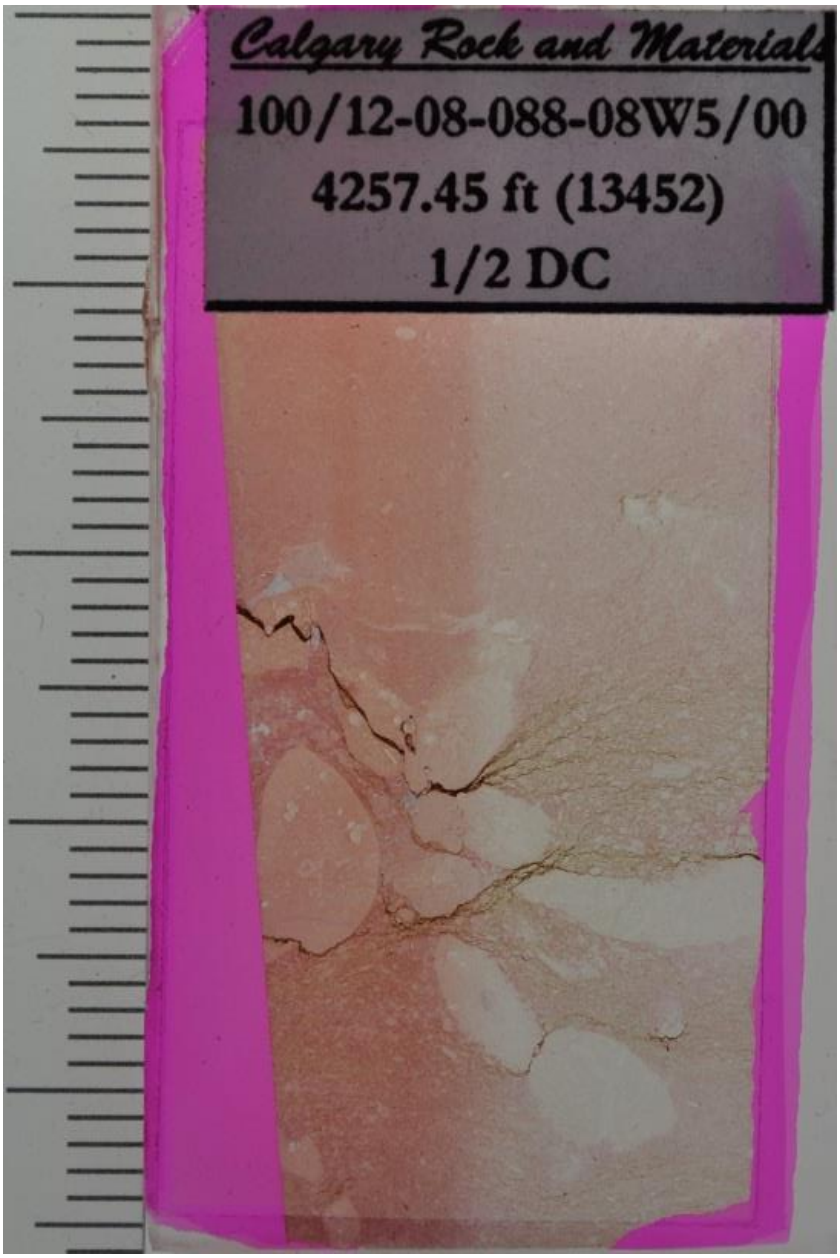


Fig. 8-21: Thin section photograph of sample 13452 from the Slave Point Formation, well 100/12-08-088-08W5/00 (depth 4257.50 ft.). The image shows a carbonate rock containing numerous rounded bioclast (stromatoporoid?) fragments (up to ~1 cm), which are concentrated in the middle and bottom parts of the thin section. The fragments are separated and cross-cut by organic matter (including bitumen?), which is often dendritic (center) or contained within stylolites (left of image). Porosity does not appear to be as high as in the previous sample (13451). Intensive pink staining within the carbonate-stained half of the thin section (left of image) shows the abundance of calcite in the sample. Scale is in mm.

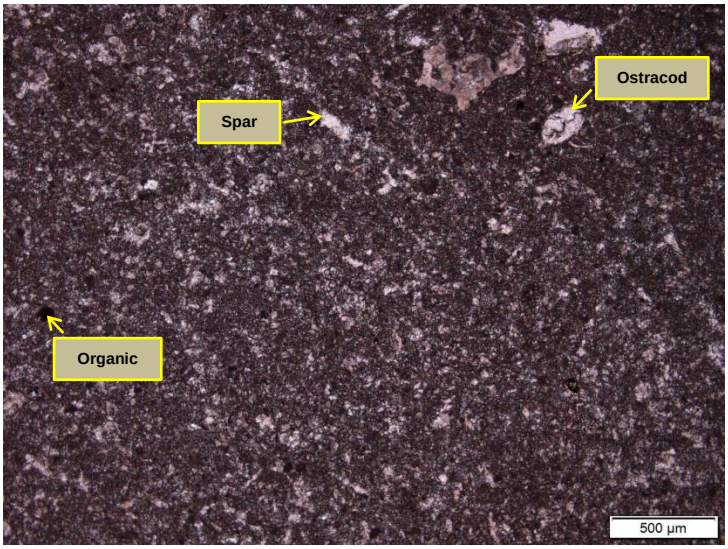


Fig. 8-22: Photomicrograph in PPL showing an overview of the top of sample 13452 (depth 4257.5 ft.). The sample consists predominantly of a microcrystalline calcite matrix containing finely dispersed dark brown/black organic material (up to 75 µm). Some of the sparry calcite patches (up to ~540 µm in this image) likely represent replaced/recrystallized bioclast fragments (including a 250 µm ostracod), which are abundant throughout the sample

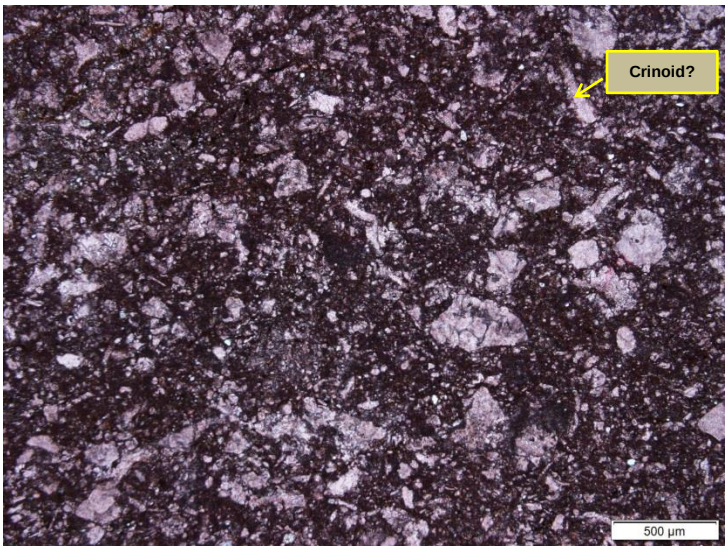


Fig. 8-23: Photomicrograph in PPL showing an overview of the bottom of the thin section. This part of the sample contains higher concentrations of sparry calcite cement (up to ~500 µm) which represent replaced/recrystallized bioclast fragments (predominantly echinoderms/crinoids?). The microcrystalline matrix is heavily enriched in organic matter (dark brown, algal?).

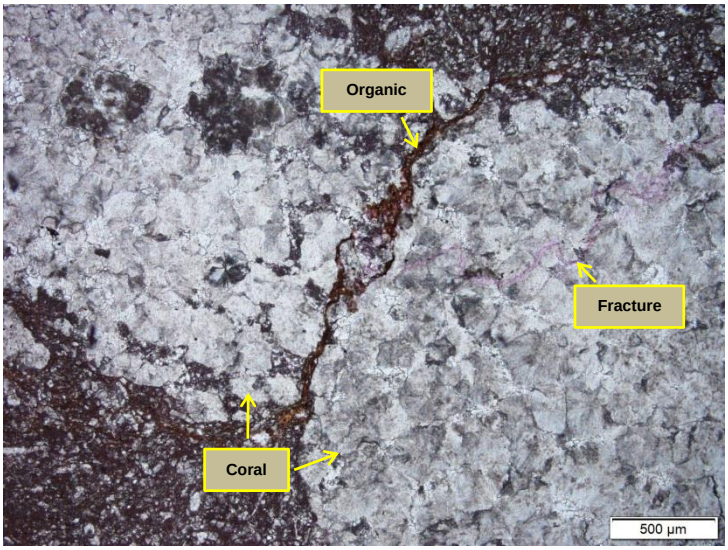


Fig. 8-24: Photomicrograph in PPL showing two adjacent coral fragments (unstained part of the thin section), which are separated by a thin layer of concentrated dark brown organic matter (stylolite?). These extraclasts occur in the middle and lower part of the sample. The fragments are likely to have been completely replaced by sparry cements, and contain isolated patches of micrite (peloidal?) that may be related to the original internal structure of the coral. Faint pink-staining through one stromatoporoid fragment (right-hand side of image) represents a fracture, which was likely created during sample preparation or recovery.

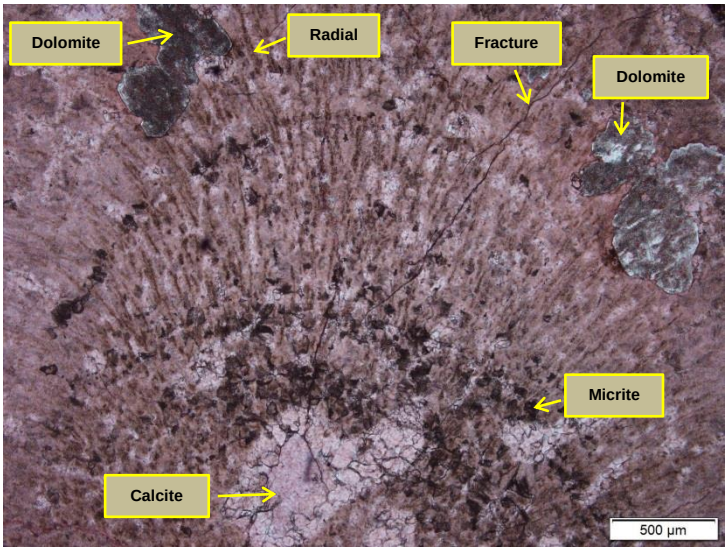


Fig. 8-25: Photomicrograph in PPL showing a section of a large stromatoporoid fragment with visible radial internal structure (outlined by micrite). Lighter-coloured sparry calcite to the bottom of image represents an infilled pore (relating to the original internal structure of the stromatoporoid), indicating two phases of cementation. Some former pores have also been filled with 'dirty' dolomite cement and micrite. Fine internal fracturing (<5 µm wide) is present within the fragment.

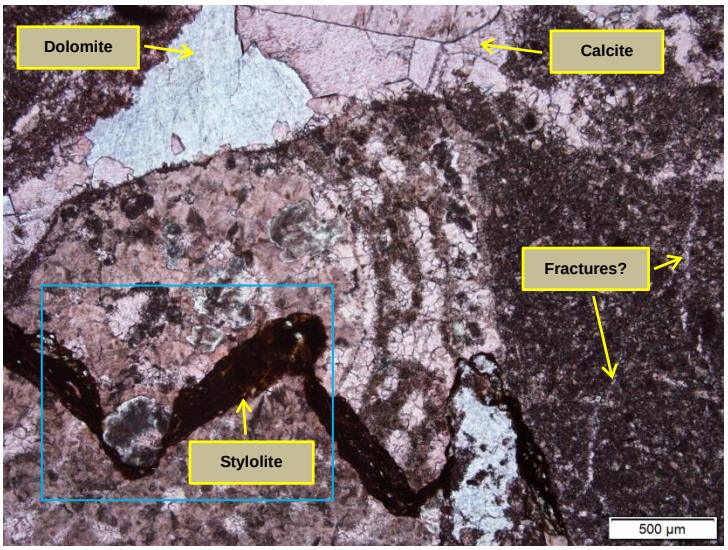


Fig. 8-26: Photomicrograph in PPL showing a stromatoporoid fragment with clearly defined internal structure (outlined/highlighted by micritic material) and moldic pores filled by dolomite cement. The fragment is cross-cut by a stylolite composed of fluid organic matter (including hydrocarbons?), which incorporates small dolomite particles (up to ~60 µm). The stylolite tapers in thickness (~50-250 µm) and wraps around larger sparry fragments. The structure of the top-left of the stromatoporoid fragment has been completely obliterated by dolomite and calcite spar (up to ~1 mm). Also note small (<15 µm wide) calcite-healed vertical microfractures towards the right of the image.

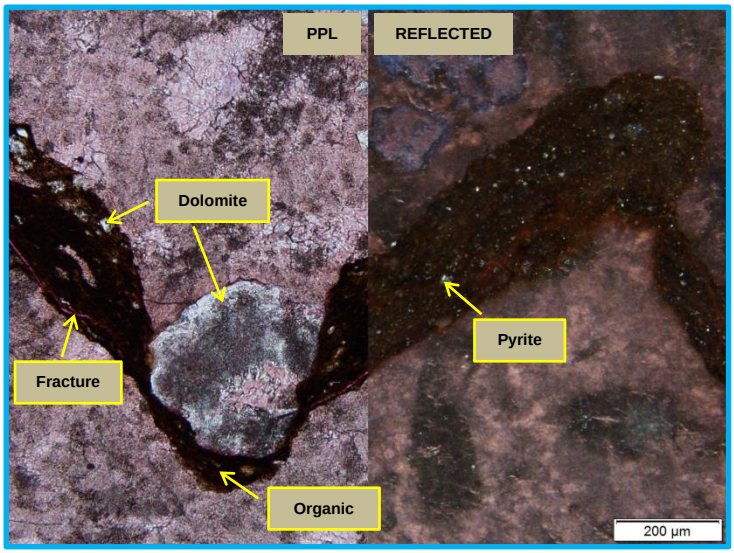


Fig. 8-27: Photomicrograph in PPL (left) and reflected light (right) showing magnification of the stylolite in Figure 8-26. The stylolite is composed predominantly of dark brown-black fluid organic matter (including hydrocarbons?), which incorporates small carbonate particles (up to ~35 µm) and cubic pyrite crystals (up to ~20 µm). The stylolite thins as it wraps around the sparry dolomite crystal (~350 µm) to the left of the image, and is associated with fracturing (e.g. far left).

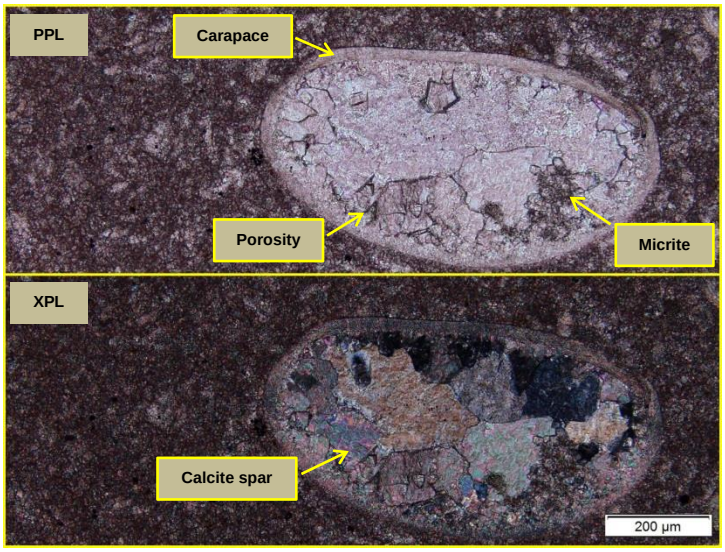


Fig. 8-28: Split-image photomicrograph in PPL (top) and XPL (bottom) showing an ostracod (~800 µm) with a clearly defined carapace (~25 µm thick). The interior of the ostracod has been filled by sparry calcite (with minor intercrystalline porosity) and minor amounts of micrite. Ostracods are abundant throughout the sample.

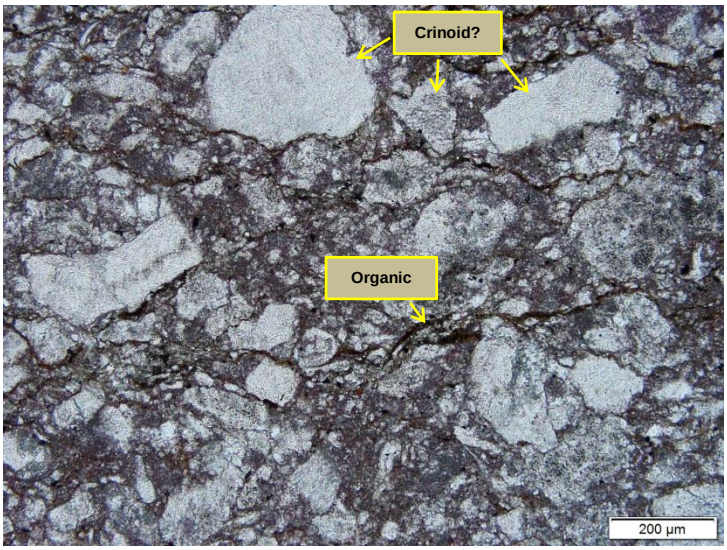


Fig. 8-29: Photomicrograph in PPL (unstained part of the thin section) showing abundant echinoderm/crinoid debris (up to 350 µm in this image) embedded in a microcrystalline carbonate matrix. Bedding-parallel organic strings/laminae are abundant and may represent compressed algal material.

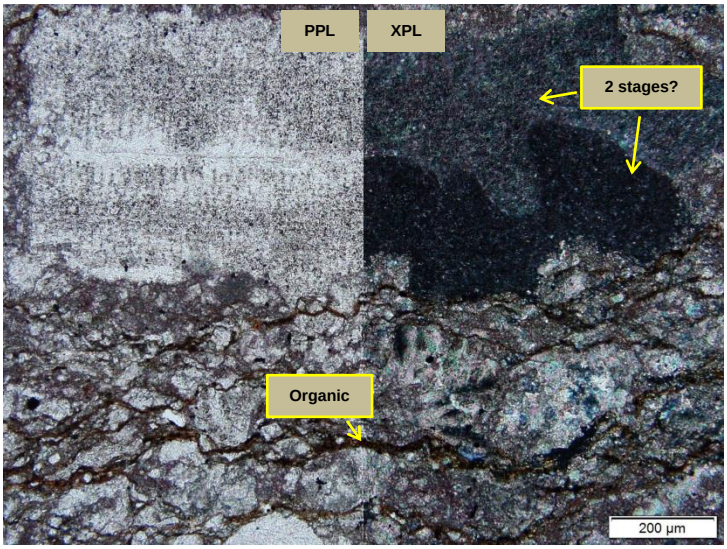


Fig. 8-30: Photomicrograph in PPL (left) and XPL (right) showing a large echinoderm (crinoid) fragment (~1.4 mm in length), which features a characteristic 'honeycomb' microtexture (small pores filled with micrite). Birefringence colours and the extinction angle at the top of the fragment are different from those at the bottom, indicating a diagenetic overprint.

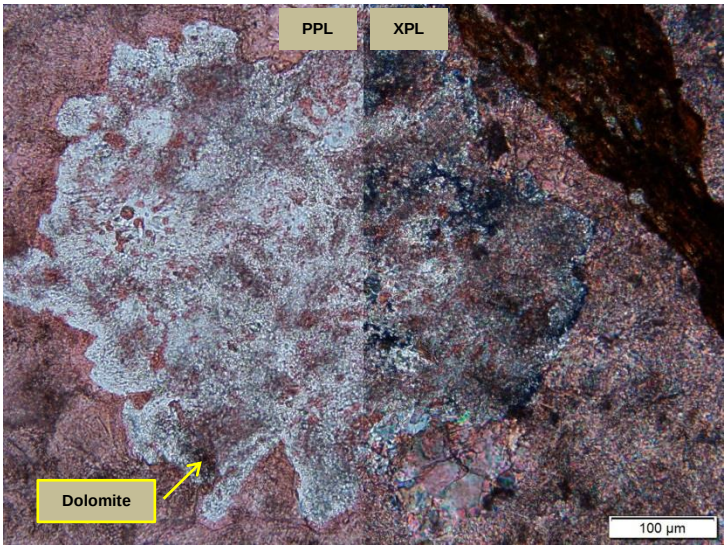


Fig. 8-31: Photomicrograph in PPL (left) and XPL (right) showing magnification of microcrystalline dolomite cement (and minor microcrystalline calcite) filling a moldic pore (~550 µm) within the large stromatoporoid fragment (see Figure 8-25). Also note the wide organic band (~110 µm wide) towards the right of the image, which incorporates small (up to 20 µm) dolomite particles (stylolite, similar to that observed in Figure 8-26?).

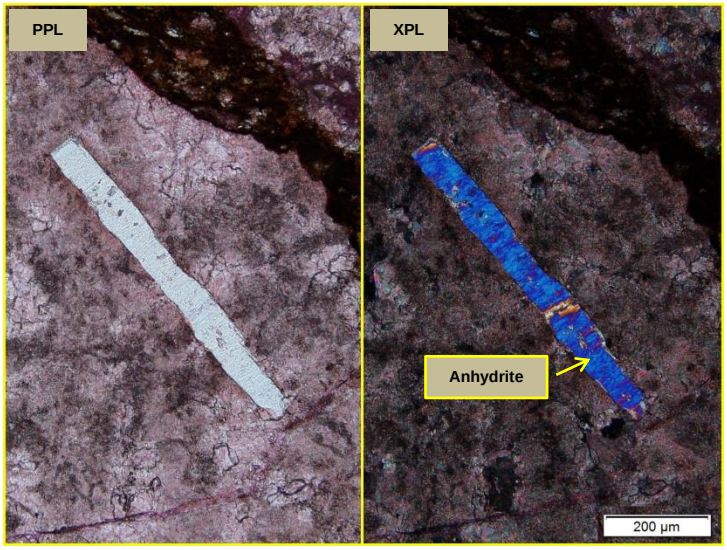


Fig. 8-32: Photomicrograph in PPL (left) and XPL (right) showing a rare bladed anhydrite particle (~680 µm in length) incorporated within a stromatoporoid fragment. The anhydrite particle is distinctive due to its high order birefringence colours (XPL).

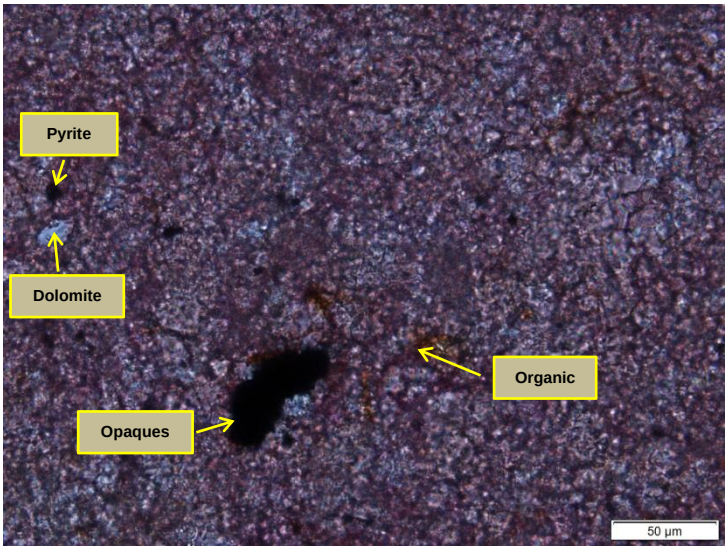


Fig. 8-33: Photomicrograph in PPL showing magnification of the matrix, which is predominantly composed of calcite (pink-stained) with lesser dolomite cement (up to 20 µm). Intercrystalline pore space is typically filled by wispy, brown organic matter. Opaque pockets and clusters (up to 65 µm in this image) are likely composed of both pyrite and organic matter, and are sporadically observed throughout the sample.

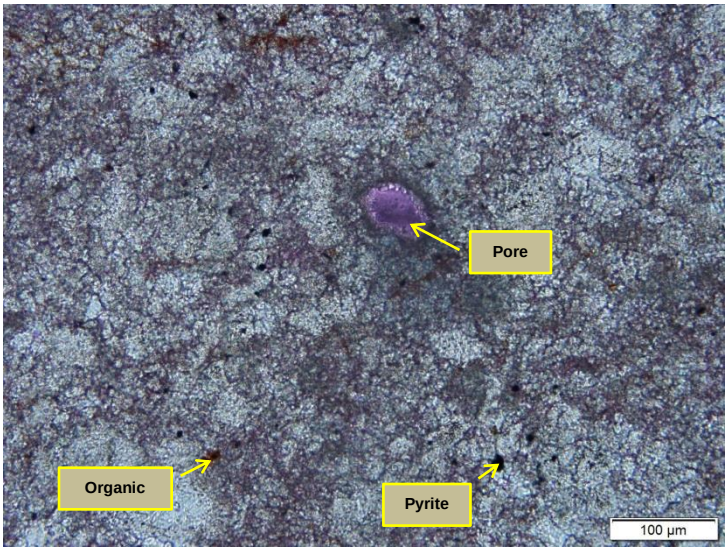


Fig. 8-34: Photomicrograph in PPL showing magnification of a rare rounded (moldic?) pore (~75 µm), which is open (filled with pink epoxy) and lined by microcrystalline carbonate cement. Also note finely dispersed pyrite crystals (up to ~15 µm) and organic matter within the surrounding matrix.

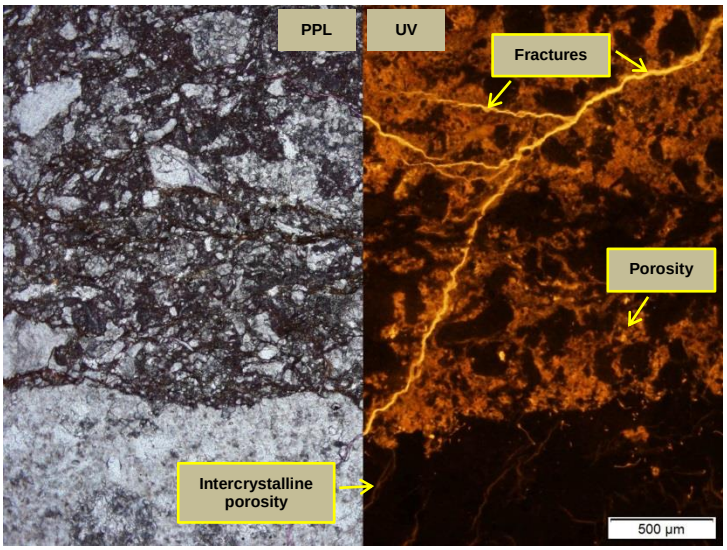


Fig. 8-35: Photomicrograph in PPL (left) and UV light (right) showing an overview of porosity and fracturing within the bottom part of the sample. Microfractures (<20 µm wide) both follow and cross-cut bedding, and are mainly artificial (filled by epoxy). Some high fluorescence under UV light is associated with bedding-parallel organic bands/strings which may represent healed natural fractures. Porosity within the sample is generally associated with the microcrystalline matrix (see Figure 8-36). Some intercrystalline porosity is also observed within replaced/recrystallized bioclast fragments (e.g. bottom of image).

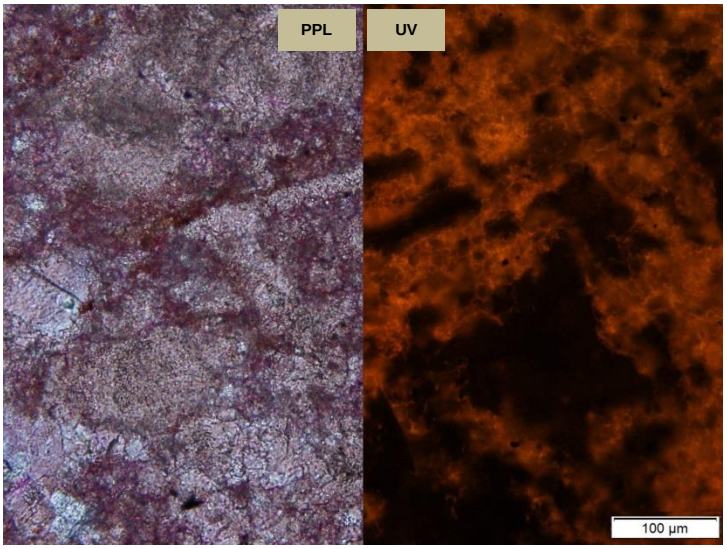


Fig. 8-36: Photomicrograph in PPL (left) and UV light (right) showing magnification of porosity within the microcrystalline matrix. Porosity is often high (>10%) between calcareous bioclast fragments, perhaps due to dissolution of microcrystalline cements and/or removal of organic material. Porosity is lower within the top part of the sample.

8.2.3 SAMPLE 13455

Sample ID	**13455**		
Sample Type	**Core**	**UWI/Well**	**100/12-08-088-08W5/00**
Strat. Unit	**Slave Point Formation**	**Depth**	**4233.45 ft.**

XRD results

Quartz (%)	Feldspar (%)	Calcite (%)	Dolomite/ankerite (%)	Clays (%)
1	0	96.9	2.1	0

Pyrite (%)
0

Composition (*in order of abundance)*

	%	Variety (%)	Variety (%)	Variety (%)	Variety (%)
Cement (spar)	80	Calcite (100)	Quartz (trace)		
Cement (micrite)	20	Calcite* (100)			
Organics	trace	Amorphous (100)			
Opaques	trace	Pyrite (100)			
	100				

Matrix	93	Spar (80)	Micrite (20)		
Porosity	7	Interparticle (75)	Intraparticle (25)		
Allochems	0				
	100				

Sedimentary structures

Primary	None observed.
Biogenic	Abundant small (generally 30-40 µm), poorly-defined micrite patches may represent fecal remains (NOT true pellets or peloids). These patches are concentrated around the edges of bean-shaped and lenticular structures (up to ~1 mm) which are possibly boring tubes or remanants of boring organisms.

Fractures	Branching microfractures (<10 µm wide) that cross-cut bedding direction are only observed towards the edges of the thin section and were likely created during sample preparation or recovery (filled with epoxy).
Porosity	Porosity at the top of sample is high (~10%) due to the dissolution of calcite spar (especially within boring tubes and/or remnants of boring organisms) which leaves angular open pores (generally ~75 µm, up to ~400 µm). The bottom part of the sample features very low porosity (<1%) as most intercrystalline pore space is filled by 'pure' microcrystalline calcite cement.
Opaques	None observed.
Organics	None observed.
Diagenetic	The whole sample has been diagentically recrystallized to calcite spar with some micrite lenses and layers (relics of the original framework?)

Description

Sample 13455 is a finely to medium crystalline limestone or floatstone which has been almost completely recrystallized to calcite spar and may represent a stromatoporid (due to absence of sedimentary or burrowing structures). The framework contains numerous bean-shaped and lenticular features (also recrystallized to calcite spar) which are likely to be boring tubes or remnants of boring organisms. These structures are faintly outlined by small patches of micritic material which may represent fecal remains (not true pellets or peloids). Micritic patches are also finely dispersed throughout the rest of the framework/matrix. Rare micrite lenses and layers may represent relicts of the original structure of the stromatoporid (prior to diagenetic recrystallization). Porosity is variable throughout the sample, with increased (angular) open pore space observed to the top of the sample where more dissolution appears to have occured (primarily related to the interior of boring tubes and/or boring organism remnants). Porosity is very low to the bottom of the thin section where most intercrystalline space is filled by microcrystalline calcite cement. Microfractures that cross-cut bedding direction are generally located to the edge of the sample and are likely artificial (created during sample preparation or recovery).

Rock Classification

Finely to medium crystalline limestone (Folk, 1962); crystalline limestone (Dunham, 1962); floatstone (Embry & Klovan, 1971)

Thin Section Quality

Good; 1/2 stained for carbonates.



Fig. 8-37: Core photograph of sample 13455 from the Slave Point Formation, well 100/12-08-088-08W5/00 (depth 4233.45 ft.). The thin section prepared from this sample was cut from the area marked with an X. The sample was received with no up direction. Scale is in mm.

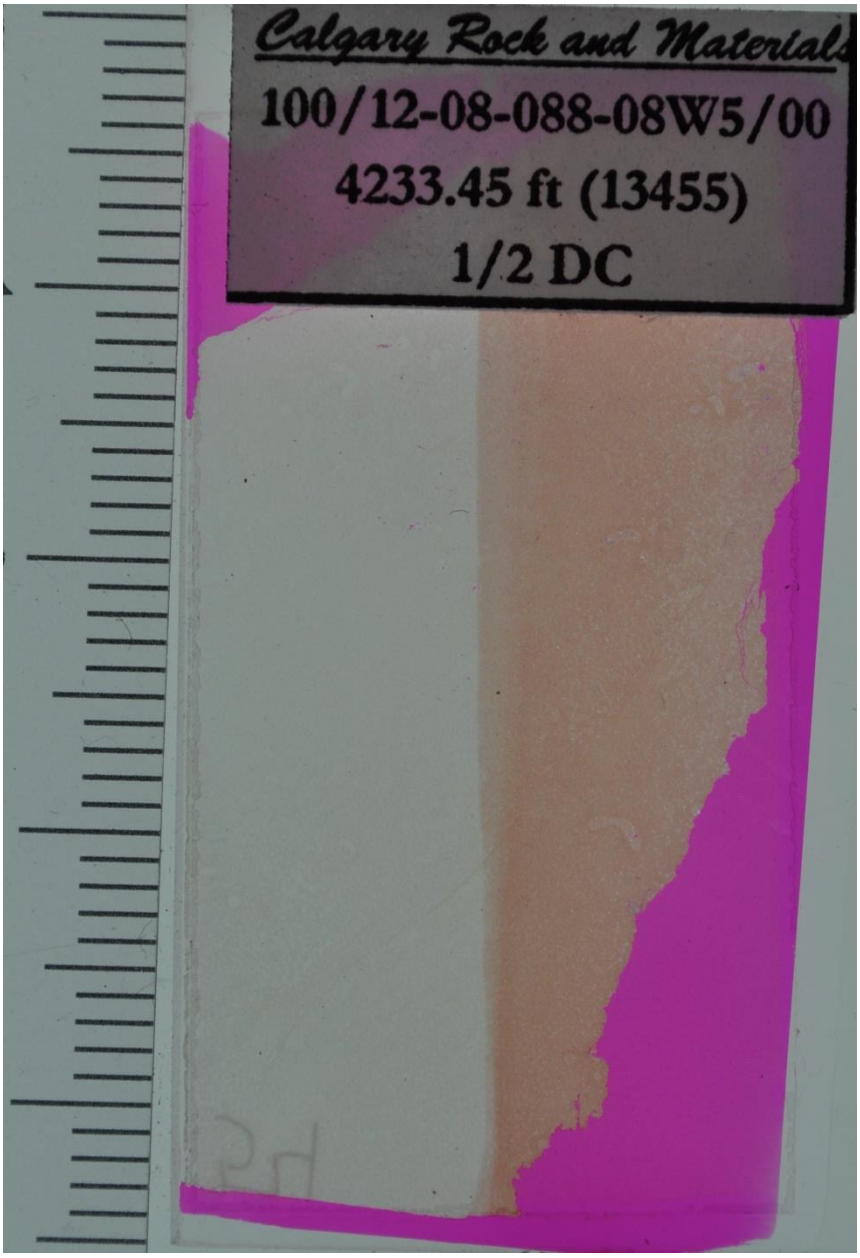


Fig. 8-38: Thin section photograph of sample 13455 from the Slave Point Formation, well 100/12-08-088-08W5/00 (depth 4233.45 ft.). The image reveals a carbonate rock with no visible sedimentary or biogenic features. Some lighter coloured bean-shaped patches are possible boring tubes or remnants of boring organisms. A few very faint lines/bands run from the bottom-left corner to the top-right of the thin section and may represent the original structure of a framework organism (prior to recrystallization). Scale is in mm.

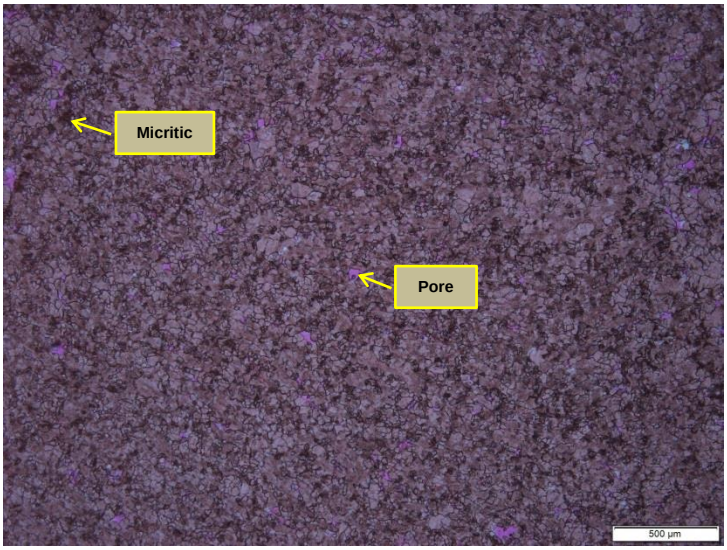


Fig. 8-39: Photomicrograph in PPL showing an overview of the top of sample 13455 (depth 4233.45 ft.). The sample has been extensively recrystallized, and predominantly consists of calcite spar with some open pore space (up to ~100 µm in this image) and abundant small micritic patches (slightly darker in colour than the surrounding matrix, generally ~30-40 µm). The texture and composition is fairly consistent throughout the sample. The sample contains few sedimentary or biogenic structures.

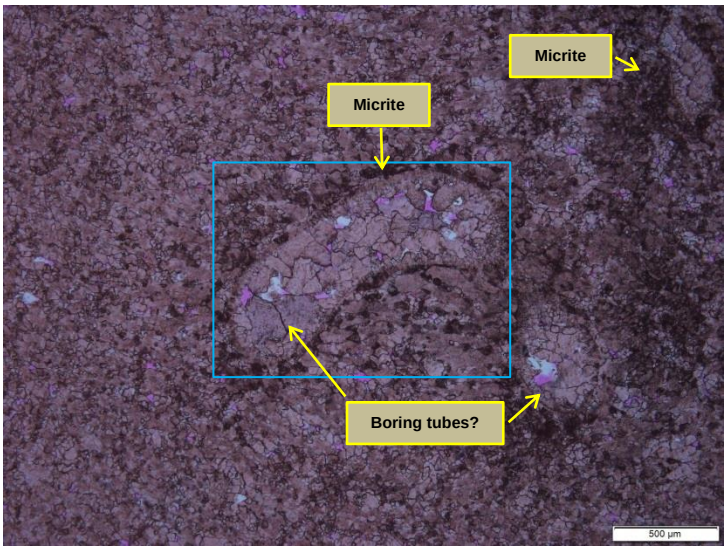


Fig. 8-40: Photomicrograph in PPL showing a ~1.5 mm bean-shaped feature and a ~650 µm lenticular feature. These features may represent boring tubes, or remnants of boring organisms that have been completely replaced by sparry calcite cement. Micrite patches are more concentrated towards the right of the image.

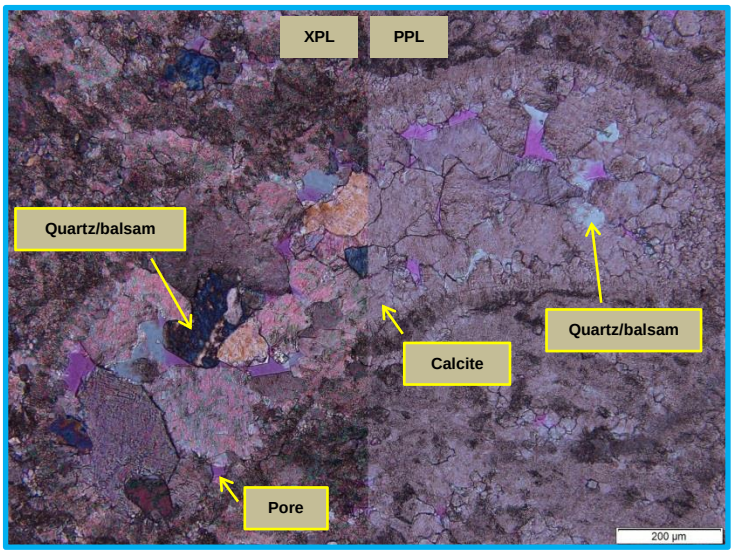


Fig. 8-41: Photomicrograph in XPL (left) and PPL (right) showing magnification of the bean-shaped feature in Figure 8-40. Calcite spar (up to 275 µm), small amounts of quartz (grey/white first order birefringence colours) and epoxy (relict of sample preparation) are observed in the feature.

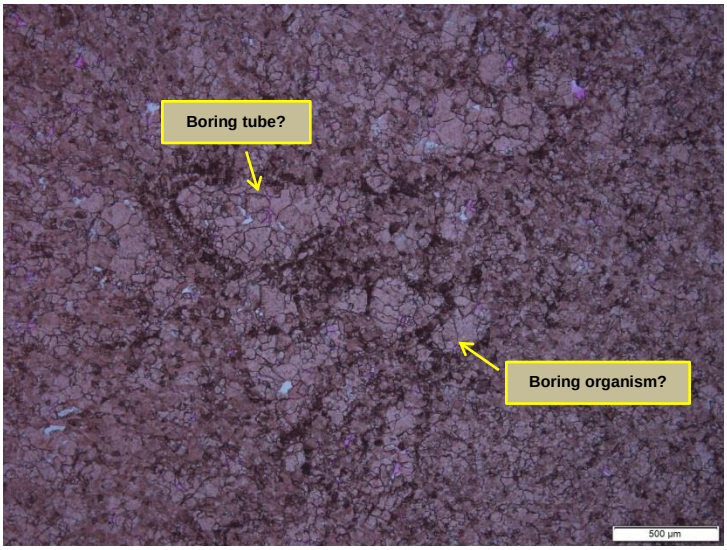


Fig. 8-42: Photomicrograph in PPL showing boring tubes (~1.9 mm in length, similar to those observed in Figure 8-40) and remains (~820 µm), which are incorporated within abundant sparry calcite and minor micritic matrix.

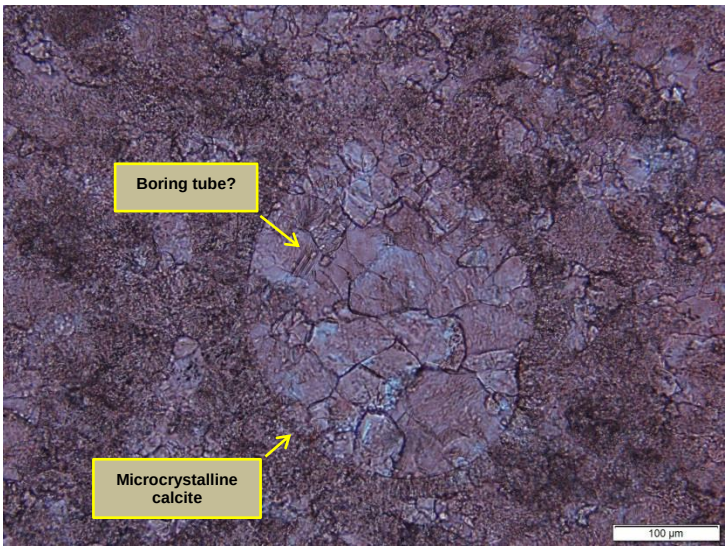


Fig. 8-43: Photomicrograph in PPL showing a recrystallized (~350 µm) boring structure which has been completely replaced by calcite spar (up to ~100 µm), and is embedded in a matrix of microcrystalline calcite.

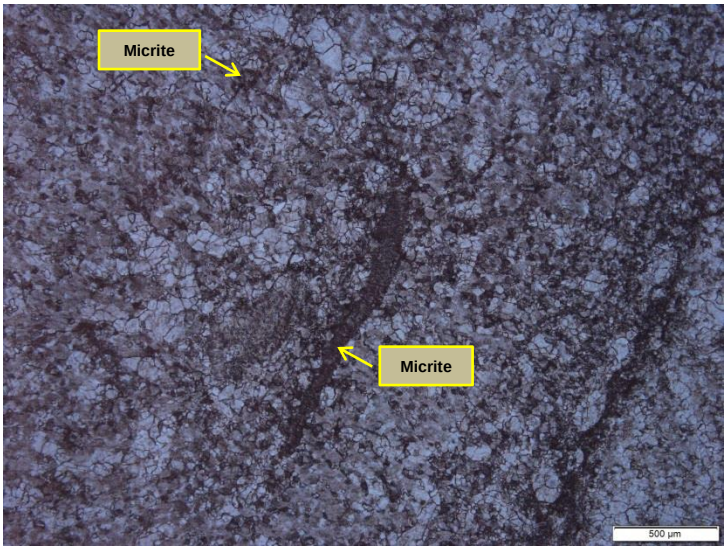


Fig. 8-44: Photomicrograph in PPL (unstained part of thin section) showing some discontinuous micritic bands (~1.4 mm in length), which cross-cut bedding (part of a framework structure?). Several small (~30-40 µm) micrite patches (fecal remains?) are also observed in the surrounding matrix.

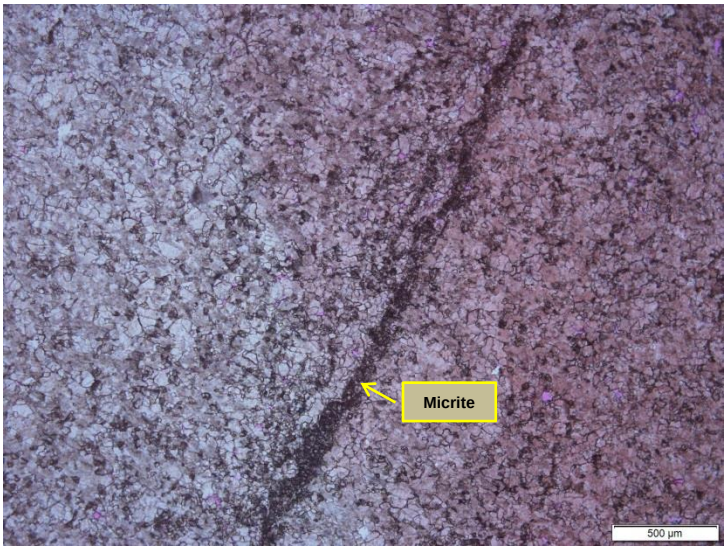


Fig. 8-45: Photomicrograph in PPL showing a section of a discontinuous micritic layer/band (~100 µm in width) which cross-cuts bedding and runs from the middle to the bottom of the thin section (also seen towards the right-hand side of Figure 8-44).

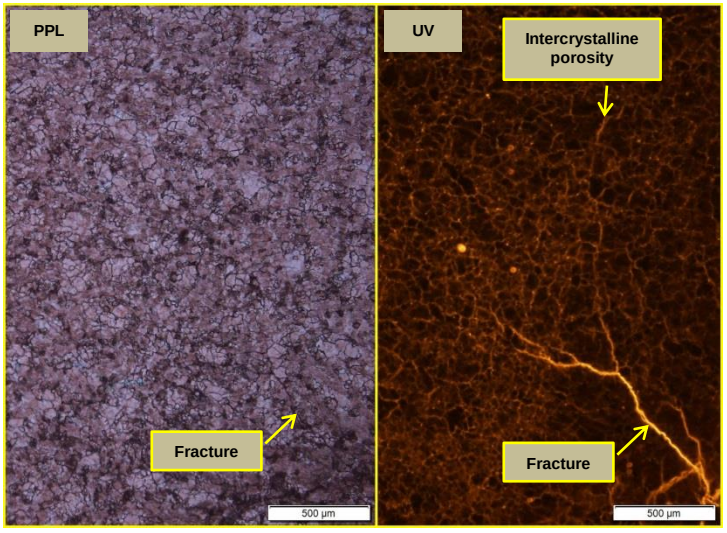


Fig. 8-46: Split-image photomicrograph in PPL (left) and UV light (right) showing an overview of porosity and fracturing within the bottom part of the sample. Porosity within this area of the thin section is very low (<1%) and is associated with the space between sparry calcite cements (i.e. intercrystalline porosity).

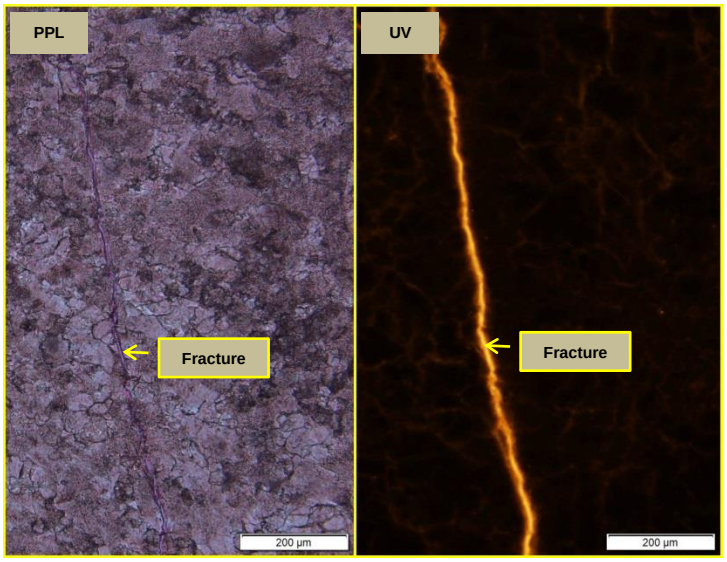


Fig. 8-47: Split-image photomicrograph in PPL (left) and UV light (right) showing magnification of a microfracture (<10 µm wide) located towards the bottom-right of the thin section (see Figure 8-46). The epoxy-filled fracture cross-cuts bedding and cement boundaries, indicating that it is likely artificial (created during sample preparation or recovery).

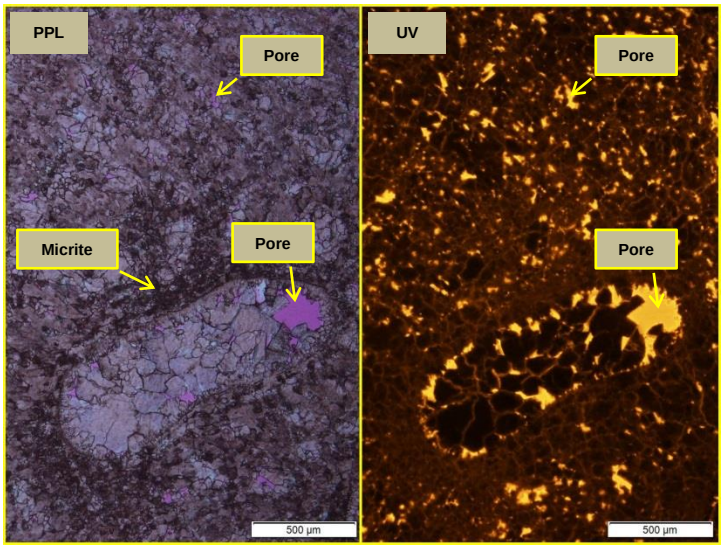


Fig. 8-48: Split-image photomicrograph in PPL (left) and UV light (right) showing porosity within the top part of the sample. Porosity is much higher (~10%) in this part of the thin section and is mainly related to the dissolution of calcite spar, which leaves angular open pores (up to 400 µm in this image). Also note the abundance of micritic material, which is concentrated around the edge of the boring tube.

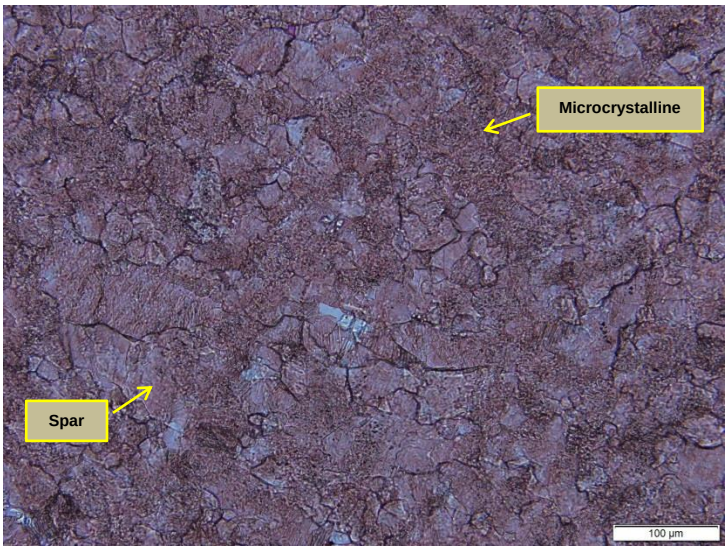


Fig. 8-49: Photomicrograph in PPL showing magnification of the matrix at the bottom of the thin section. As observed in Figure 8-46, this part of the sample features very low porosity (<1%) as most intercrystalline pore space is filled by microcrystalline calcite cement.

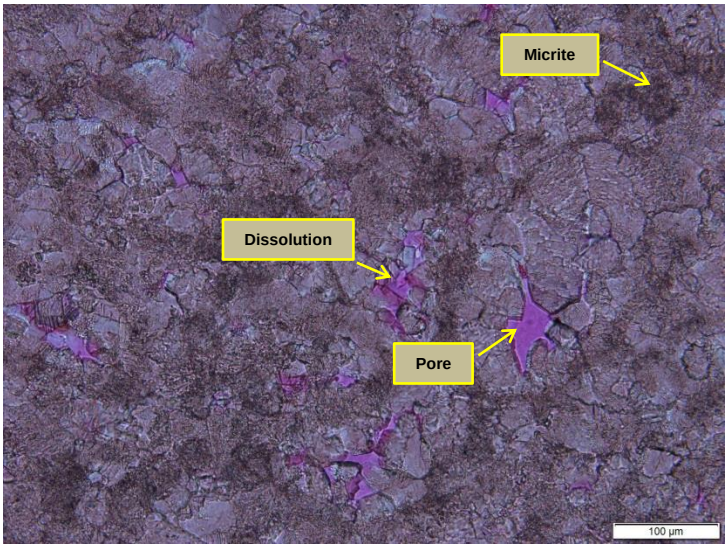


Fig. 8-50: Photomicrograph in PPL showing magnification of the matrix at the top of the sample. Angular open pore space (up to 75 µm in this image) is more abundant than at the bottom of the thin section. Poorly defined micrite patches (fecal remains?) are abundant, whereas organic matter and pyrite are virtually absent. Also note the decreased concentration of microcrystalline calcite (compared to Figure 8-49).

8.2.4 SAMPLE 13461

Sample ID	**13461**		
Sample Type	**Core**	**UWI/Well**	**100/02-21-084-14W5/00**
Strat. Unit	**Slave Point Formation**	**Depth**	**1706.2 m**

XRD results

Quartz (%)	Feldspar (%)	Calcite (%)	Dolomite/ankerite (%)	Clays (%)
1	0.1	1.4	97.5	0

Pyrite (%)
0

Composition (*in order of abundance)*

	%	Variety (%)	Variety (%)	Variety (%)	Variety (%)
Cement (spar)	97	Dolomite (100)	Calcite (trace)	Quartz (trace)	
Cement (micrite)	trace	Dolomite (100)			
Organics	2	Amorphous* (100)			
Opaques	1	Pyrite (100)			
	100				

** including bitumen?*

Allochems	70	Bioclasts (100)			
Matrix	17	Spar (100)	Micrite (trace)		
Porosity	13	Intraparticle (75)	Intercrystalline (25)		
	100				

Sedimentary structures

Primary	None observed.
Biogenic	None observed.

Fractures	Coral/stromatoporoid fragments are often separated from the surrounding matrix by (artificial?) epoxy-filled fractures (~40 µm wide), which are lined with organic matter. Some organic bands/strings cross-cut bioclasts and cements/cement boundaries suggesting that they may represent healed natural fractures.
Porosity	Porosity is high due to presence of large vugs/dissolution voids (often >550 µm in length) within many coral/stromatoporoid fragments. Some minor intercrystalline porosity is observed between sparry dolomite cements (often partially filled with organic matter). Dolomite spar is sometimes partially dissolved (especially around crystal edges), removed or plucked.
Opaques	Some styolites and organic strings incorporate large pyrite grains and clusters (up to ~145 µm) and a few disseminated pyrite crystals. Very rare small bioclast fragments (up to ~250 µm) are replaced by pyrite.
Organics	Abundant organic strings and organic-filled stylolites. Organic material (including large pockets, up to 225 µm) also fills intercrystalline space and is sometimes observed as more solid chunks and blobs (up to ~80 µm).
Diagenetic	The whole sample has been diagentically recrystallized to dolomite spar. Extensive dissolution (including pressure dissolution) has occurred as indicated by abundant vugs/dissolution voids and stylolites.

Bioclasts *(in order of abundance)*

Type	*Size (µm)*	*Preservation*	*Recrystallisation*
Stromatoporoid/coral frags	Up to ~5000	Poor to moderate	Dolomite
Unidentified (rare)	Up to ~250	Poor	Pyrite & Organics

Sample 13461 is a medium to coarsely crystalline coral/stromatoporoid dolostone/framestone which has been almost completely recrystallized to dolomite spar. The sample contains many psuedo-circular stromatoporoid/coral fragments (mm-scale) which are composed of medium-coarsely crystalline dolomite spar and often contain large, angular dissolution voids or vugs. Organic-rich stylolites are abundant throughout the thin section and are associated with reduced dolomite crystal size. Strings of organic matter also fill minor intercrystalline pore space and often separate bioclast fragments from the surrounding matrix/framework. Minor amounts of pyrite are observed as disseminated crystals and (rarely) as large grains which are generally entrained within stylolites or organic strings/bands. Most fractures within the sample are epoxy-filled and therefore likely to be artificial (created during sample preparation or recovery). However, some organic strings cross-cut bioclasts, cements and cement boundaries and may represent healed natural fractures. Porosity within the sample is generally high due to the partial dissolution of stromatoporoid/coral fragments to leave large voids/vugs. Some porosity is also associated with open intercrystalline space which is often only partially filled by organic material.

Rock Classification

Medium to coarsely crystalline dolomitic biosparite (Folk, 1962); medium to coarsely crystalline coral/stromatoporoid dolostone (Dunham, 1962); dolomitic framestone (Embry & Klovan, 1971).

Thin Section Quality

Good; 1/2 stained for carbonates.

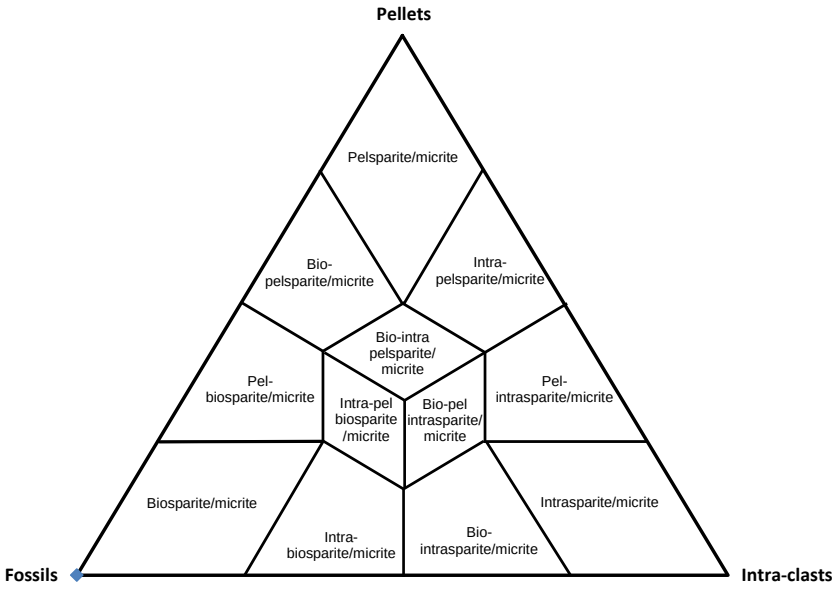


Fig. 8-51: Ternary plot showing the relative abundance of different allochem types within the carbonate rock (based on Folk's classification scheme, 1962). Sample 13461 is classified as a (dolomitic) biosparite as the rock has a sparry dolomite matrix with abundant coral/stromatoporoid fragments (~70% of the sample) and no peloids or intraclasts.



Fig. 8-52: Core photograph of sample 13461 from the Slave Point Formation, well 100/02-21-084-14W5/00 (depth 1706.2 m). The thin section prepared from this sample was cut from the area outlined in black. The sample was cut transverse (i.e. bedding parallel). Scale is in mm.

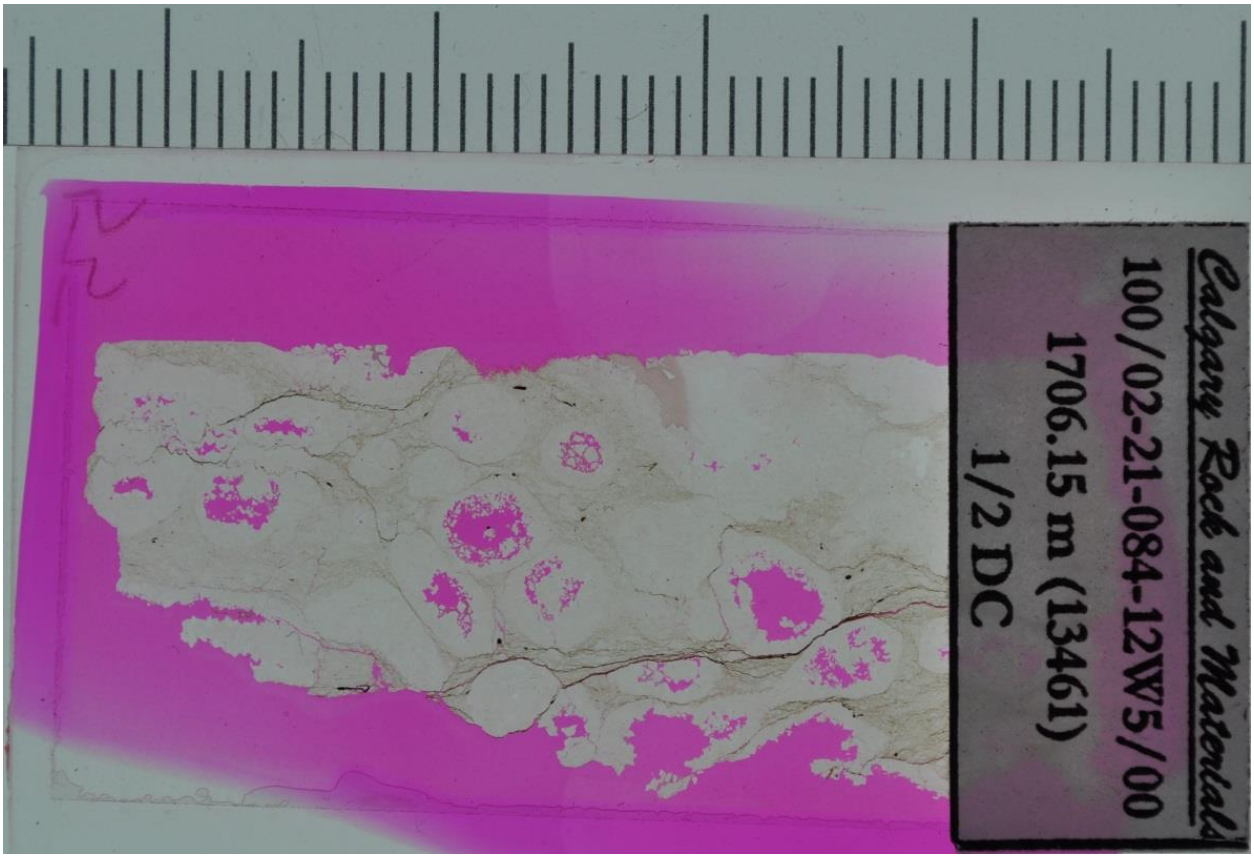


Fig. 8-53: Thin section photograph of sample 13461 from the Slave Point Formation, well 100/02-21-084-14W5/00 (depth 1706.2 m). The image shows a light-coloured carbonate rock that has been completely recrystallized (dolomite spar). The sample contains abundant sub-circular features (mm-scale) from framework builders (coral and/or stromatoporoid) with growth-framework porosity. Sinuous organic-rich strings or laminae (stylolites) of concentrated opaques are observed. An isolated patch of pink-stained calcite spar to the top-center of the thin section is also present. Scale is in mm.

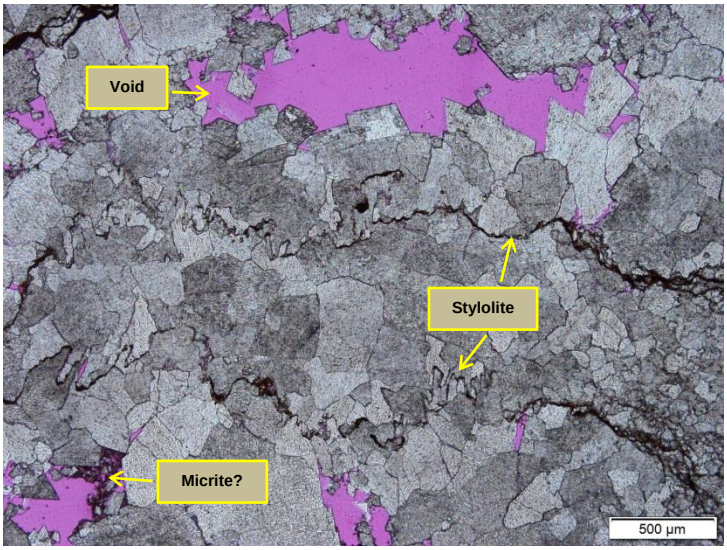


Fig. 8-54: Photomicrograph in PPL showing an overview of the lower part of sample 13461 (well 02-21, depth 1706.2 m) shown in Figure 8-53. Abundant medium to coarsely crystalline dolomite spar (up to ~550 µm in this image) with irregularly shaped dissolution voids or vugs (e.g. top of image, up to ~2.2 mm in length) are observed. Several fine organic-rich stylolites (<10 µm wide) are also present and associated with reduced dolomite crystal size (e.g. right of image).

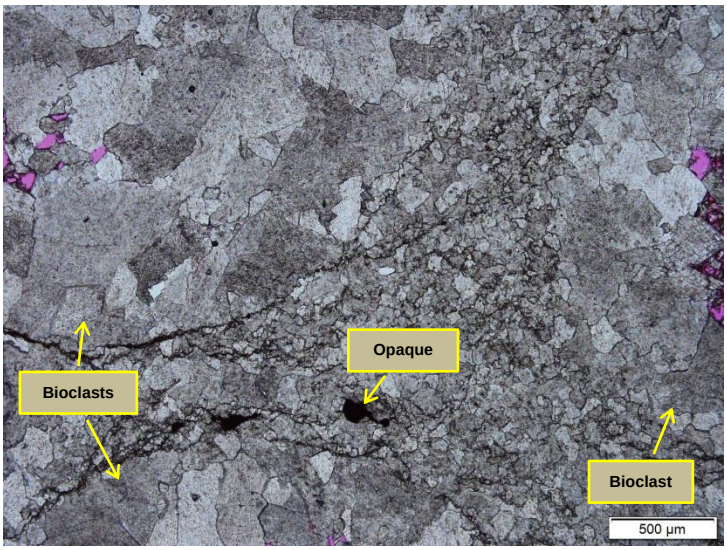


Fig. 8-55: Photomicrograph in PPL showing an overview taken towards the center of the thin section. This area of the sample contains fewer dissolution voids and/or vuggy pores than the previous figure (Figure 8-54). Micrite and organics fill minor intercrystalline space and outline three circular, recrystallized columns of the framework builders (coral, stromatoporoid?). The framework contains larger spar sizes than the surrounding matrix (~50-100 µm). Also note several blobs (70-150 µm) of opaque material (organic matter and pyrite) that are common throughout the sample.

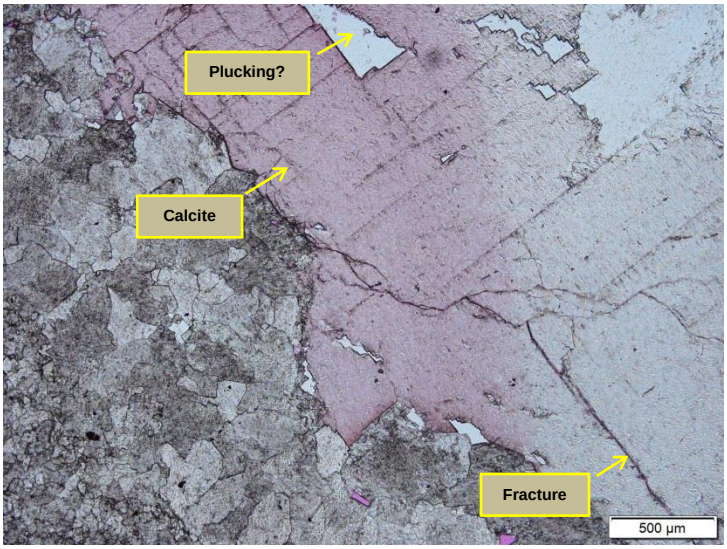


Fig. 8-56: Photomicrograph in PPL showing rare tabular calcite spar (very faintly stained towards right of image), which features strongly defined cleavage planes. Looking at the macro image (Figure 8-53), the calcite spar has likely obliterated the recrystallized internal structure of a coral or stromatoporoid fragment.

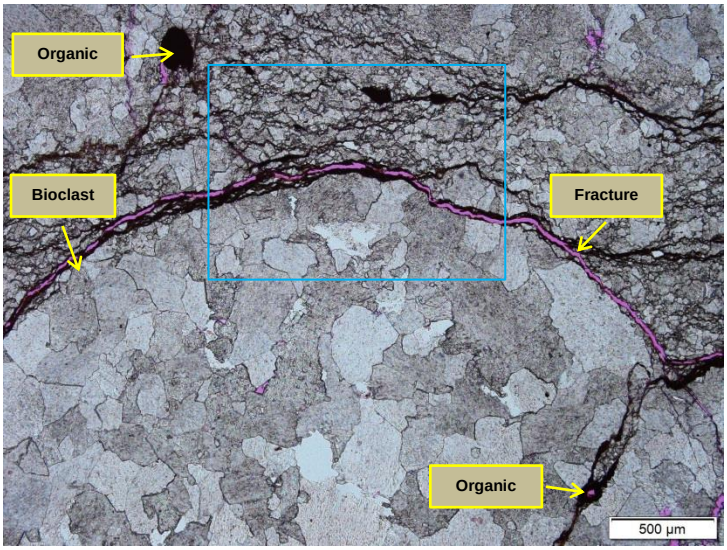


Fig. 8-57: Photomicrograph in PPL showing a coral/stromatoporoid with coarse blocky dolomite spar and minor open porosity. The surrounding matrix is finely-crystalline and has several lines with concentrated opaques, along which a fracture is observed (see Figure 8-58 for further detail). Some organic-filled fractures cross-cut dolomite cements, crystal boundaries and the framework builder (towards the bottom of the image). Organic material is also commonly observed within pockets (up to 225 µm), which fill intercrystalline space (e.g. top of image).

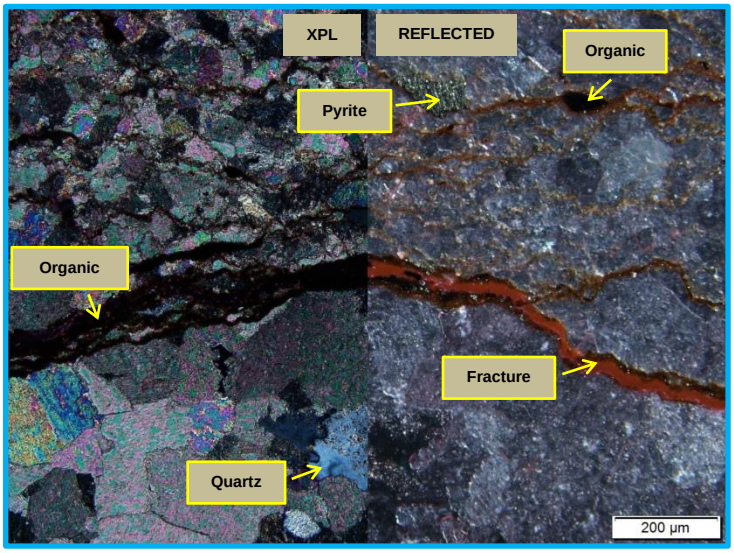


Fig. 8-58: Photomicrograph in XPL (left) and reflected light (right) showing magnification of the organic-lined fracture (see Figure 8-57). The dolomite crystals often feature high order birefringence colours (e.g. left of the image). Some of the organic matter filling intercrystalline space (and stylolites) incorporates large pyrite crystals and clusters (up to ~145 µm), and more solid organic chunks (up to ~80 µm). The organic material lining the fracture also contains a few disseminated pyrite crystals. Also note rare authigenic quartz cement towards the bottom and center of the image.

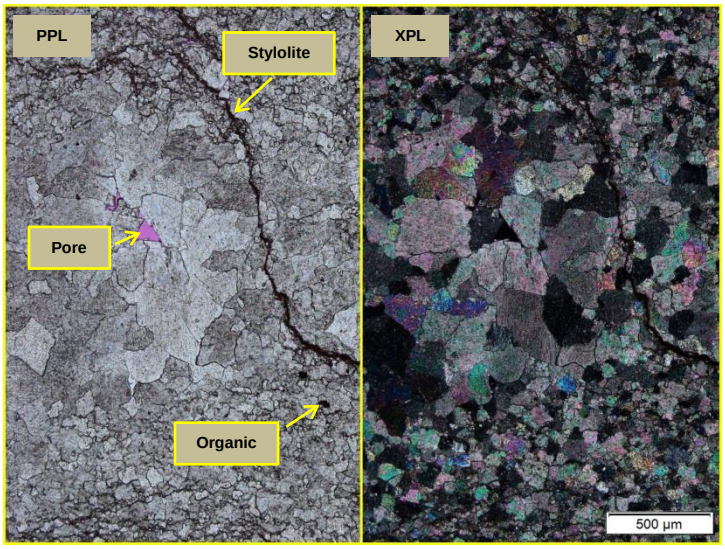


Fig. 8-59: Split-image photomicrograph in PPL (left) and XPL (right) showing a section of a stylolite (~40 µm wide) that separates coarsely crystalline and finely crystalline dolomite cements. A few open pores (120 µm; pink epoxy) and small opaque pockets (~50 µm) are also present.

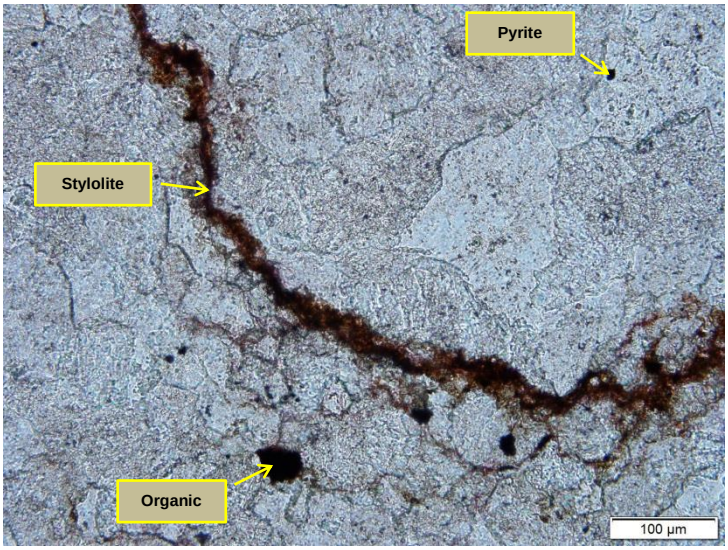


Fig. 8-60: Photomicrograph in PPL showing magnification of the stylolite in the previous figure (Figure 8-59). The stylolite contains dark brown organic matter and possibly incorporates some pyrite. The large opaque blob to the bottom of the image (~42 µm) remains black under reflected light (solid organics). Some disseminated pyrite crystals (generally <10 µm) are finely dispersed throughout the surrounding matrix/framework.

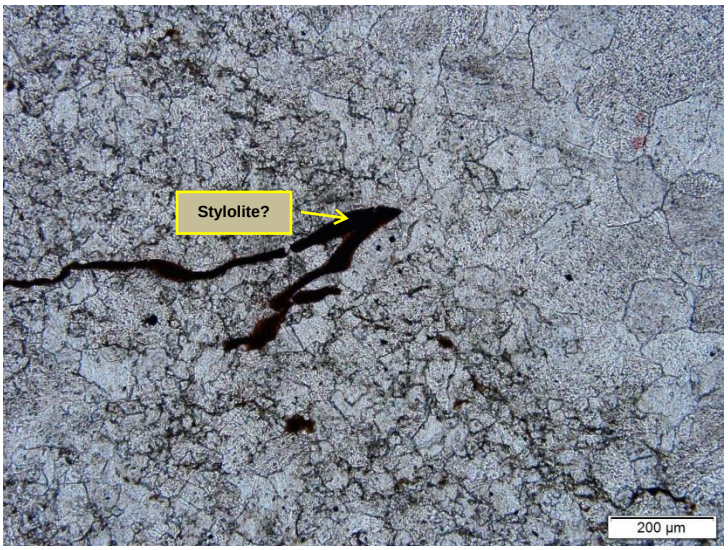


Fig. 8-61: Photomicrograph in PPL showing a thick stylolite (~45 µm wide), which is bedding-parallel towards the left of the image but changes orientation to cut across bedding (center of image). The stylolite appears to mainly consist of organic matter and is associated with the opaque pocket (~45 µm) to its right.

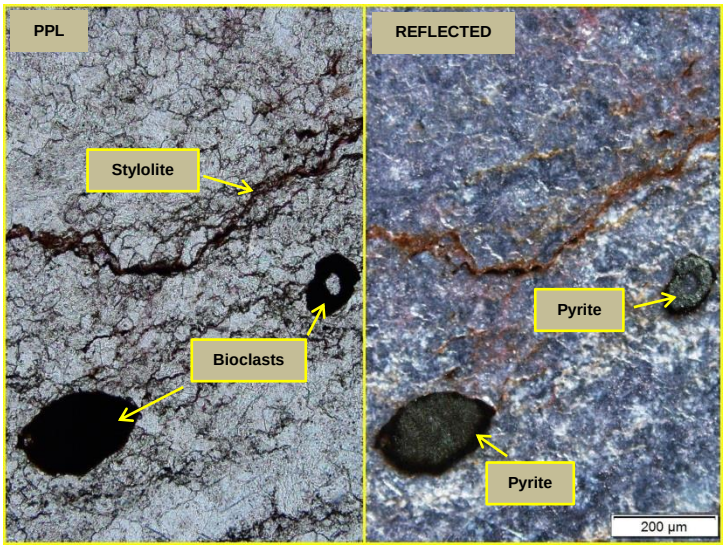


Fig. 8-62: Split-image photomicrograph in PPL (left) and reflected light (right) showing magnification of some possible bioclast fragments-(~250 µm, left and 125 µm, right) that have been almost completely replaced by microcrystalline pyrite (and some organic matter). The stylolite (~10 µm wide) above the fragments predominantly consists of organic matter with very rare disseminated pyrite.

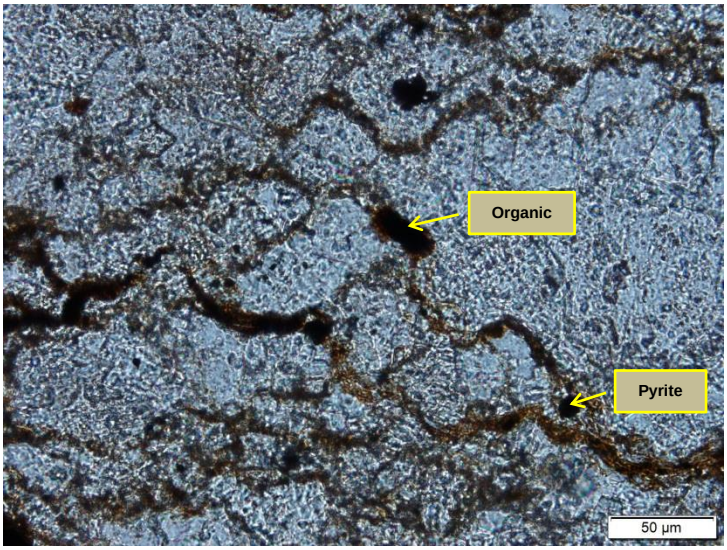


Fig. 8-63: Photomicrograph in PPL showing magnification of the matrix/framework. Dark brown organic matter fills intercrystalline space and sometimes incorporates organic blobs (up to 35 µm in this image) and pyrite clusters (including framboids, up to 10 µm). Some opaque material is not associated with intercrystalline pore space and instead overprints/obscures sparry dolomite cements (e.g. top of image).

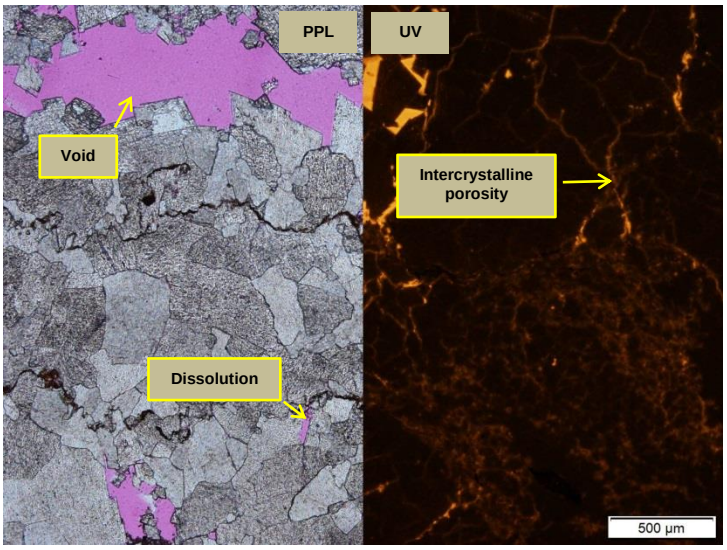


Fig. 8-64: Photomicrograph in PPL (left) and UV light (right) showing an overview of porosity within the sample. Large dissolution framework pores and voids/vugs (e.g. top-left of image) are generally associated with coarsely crystalline dolomite patches (i.e. stromatoporoid/coral fragments). Other porosity is related to the space between sparry dolomite cements (i.e. intercrystalline porosity), which is often only partially filled by micrite and/or organic material. Some dolomite cements are also partially dissolved (especially around crystal edges), removed or plucked.

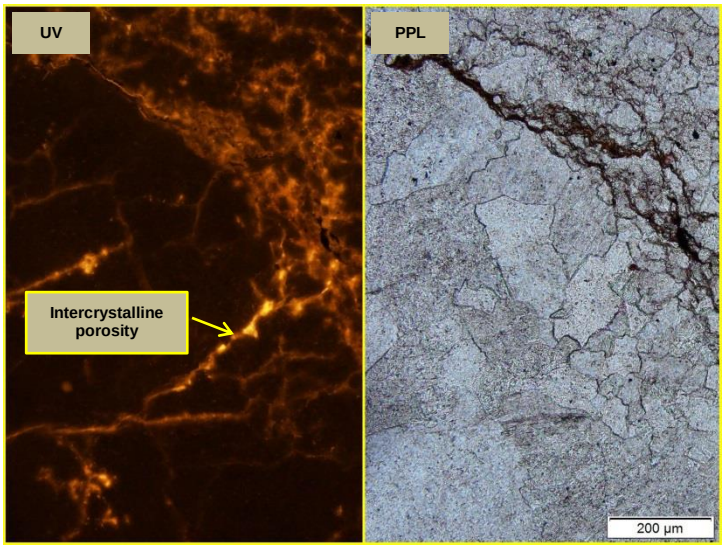


Fig. 8-65: Split-image photomicrograph in UV light (left) and PPL (right) showing magnification of intercrystalline porosity between sparry dolomite cements (e.g. left of image). Some minor porosity is also associated with the organics towards the top-right of the image, indicating that they only partially fill intercrystalline space.

8.2.5 SAMPLE 13462

Sample ID	**13462**		
Sample Type	**Core**	**UWI/Well**	**100/02-21-084-14W5/00**
Strat. Unit	**Slave Point Formation**	**Depth**	**1700.0 m**

XRD results

Quartz (%)	Feldspar (%)	Calcite (%)	Dolomite/ankerite (%)	Clays (%)
0.8	0.4	0	97.5	1.2

Pyrite (%)
0

Composition (*in order of abundance)*

	%	Variety (%)	Variety (%)	Variety (%)	Variety (%)
Cement (spar)	97	Dolomite (99)	Calcite (1)		
Cement (micrite)	trace	Dolomite (100)			
Organics	1.5	Amorphous* (100)			
Opaques	1.5	Pyrite (100)			
	100				

** including bitumen?*

Allochems	75	Bioclasts (100)			
Matrix	15	Spar (100)	Micrite (trace)		
Porosity	10	Intraparticle (75)	Intercrystalline (25)		
	100				

Sedimentary structures

Primary	None observed.
Biogenic	None observed.

Fractures	Fractures (up to ~25 µm in width) are often associated with stylolites and may have aided in stylolite development. These fractures were likely reopened or artificially enhanced during sample preparation/handling. Some artificial open fractures are rimmed by brown material (organics, clays) and pyrite.
Porosity	Most of the sample is very well cemented and lacks visible pore space. The top-left part of the thin section features increased porosity (up to 10%) in the form of angular pores and dissolution voids (up to ~600 µm) which may be related to the internal structure of large bioclast (stromatoporoid) fragments. Minor porosity is associated with intercrystalline space, fractures and stylolites.
Opaques	Larger pyrite clusters/pockets (up to ~130 µm) sometimes partially fill angular dissolution voids. Smaller idiomorphic and framboidal pyrite crystals (typically 5-10 µm) are very finely dispersed throughout and are often concentrated within stylolites and intercrystalline pores.
Organics	Organic-rich stylolites (generally <5 µm in width, up to 40 µm) are abundant throughout the sample and may separate stromatoporoid fragments from the surrounding framework.
Diagenetic	The whole sample has been diagentically recrystallized to dolomite spar. Extensive dissolution (including pressure dissolution) has occurred as indicated by abundant vugs/dissolution voids and stylolites. Microcrystalline dolomite and calcite spar sometimes fills the space between sparry dolomite crystals. Variations in dolomite birefringence colours and crystal size may indicate more than one phase of recrystallization. Some zoning observed within dolomite rhombs.

Bioclasts *(in order of abundance)*

Type	*Size (µm)*	*Preservation*	*Recrystallisation*
Stromatoporoid/coral frags	Up to ~6000	Poor to moderate	Dolomite

Sample 13462 is a (medium to coarsely crystalline?) coral/stromatoporoid framestone which has been almost completely recrystallized to dolomite spar. The thin section is compositionally and texturally similar to the previous sample (13461) which is from the same well and formation. However, mm-scale stromatoporoid fragments are not as well defined as in sample 13461 and feature lower intraparticle porosity. Fine stylolites (up to 40 µm in width) often separate these bioclast fragments and generally contain a mixture of dark brown organic matter and small disseminated pyrite crystals. Larger cubic and idiomorphic pyrite crystals are more abundant than in sample 13461 and are observed filling large angular dissolution voids/vugs and as isolated pockets/clusters. Smaller pyrite crystals are finely dispersed throughout the framework and are often associated with intercrystalline space. In general, the sample features lower porosity than sample 13461, partly due to the presence of microcrystalline dolomite (and very rare calcite spar) which fills some intercrystalline space and leads to a more well-cemented framework. This microcrystalline dolomite coupled with dulled or varied birefringence colours in dolomite spar suggests multiple phases of dolomitization and/or recrystallization. Fractures within the sample are generally associated with stylolites, indicating that fractures may have encouraged stylolite development. These fractures are only partially filled and may contribute to porosity within the sample.

Rock Classification

Medium to coarsely crystalline dolomitic biosparite (Folk, 1962); medium to coarsely crystalline coral/stromatoporoid dolostone (Dunham, 1962); dolomitic framestone (Embry & Klovan, 1971).

Thin Section Quality

Good; 1/2 stained for carbonates.

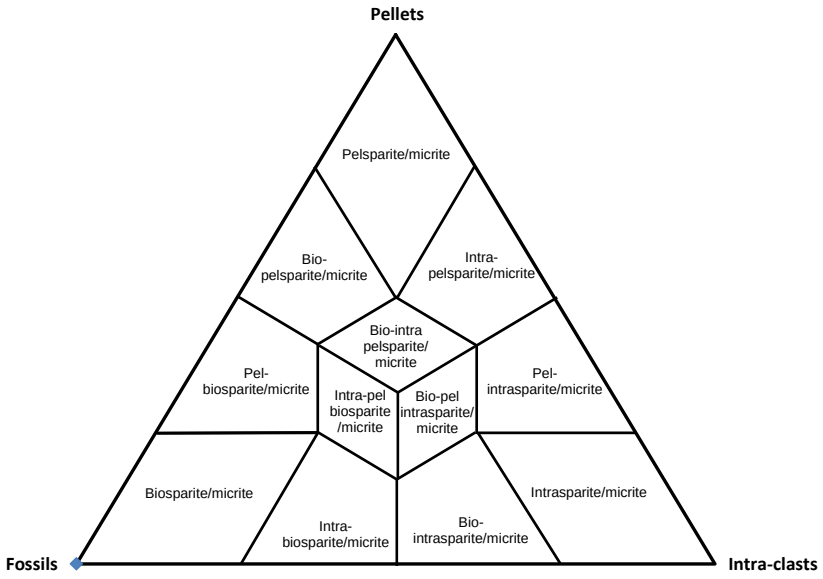


Fig. 8-66: Ternary plot showing the relative abundance of different allochem types within the carbonate rock (based on Folk's classification scheme, 1962). Sample 13462 is classified as a (dolomitic) biosparite as the rock has a sparry dolomite matrix with abundant coral/stromatoporoid fragments (~75% of the sample) and no peloids or intraclasts.

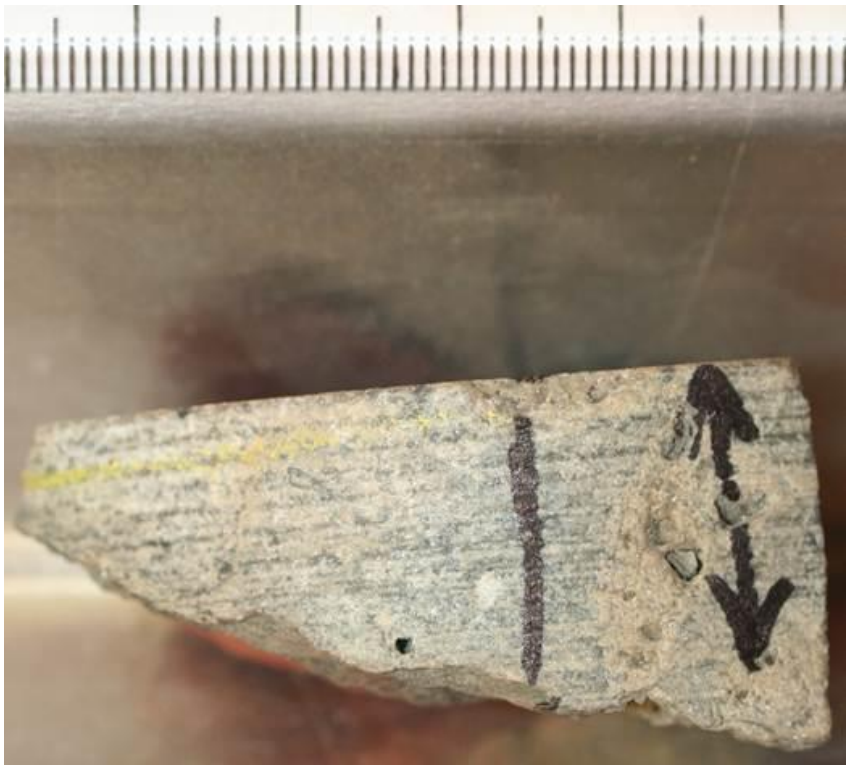


Fig. 8-67: Core photograph of sample 13462 from the Slave Point Formation, well 100/02-21-084-14W5/00 (depth 1700.0 m). The thin section prepared from this sample was cut from the area outlined in black marker. The sample was received with no up orientation. Scale is in mm.

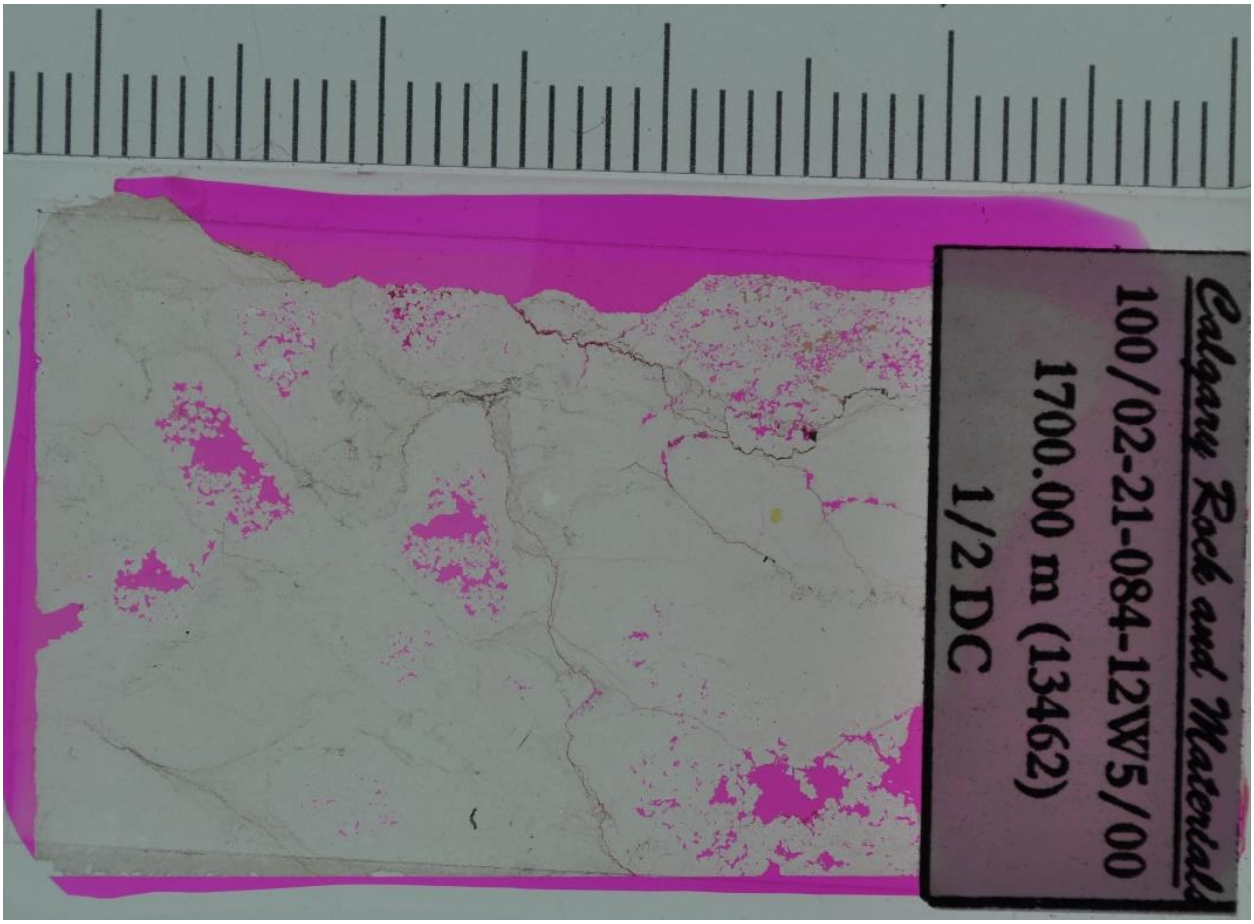


Fig. 8-68: Thin section photograph of sample 13462 from the Slave Point Formation, well 100/02-21-084-14W5/00 (depth 1700.0 m). The image shows a light-coloured carbonate rock that has been completely recrystallized to dolomite spar. The sample contains abundant faintly defined sub-circular features (mm-scale), some of which may be recrystallized coral and/or stromatoporoid fragments. The clasts are commonly separated or enveloped by sinuous organic and/or opaque-rich strings, some of which are stylolites. Open pore space is common (pink epoxy) and occurs within the clasts as well as between the fragments. Overall the sample appears to be very similar in texture and composition to sample 13462. Scale is in mm.

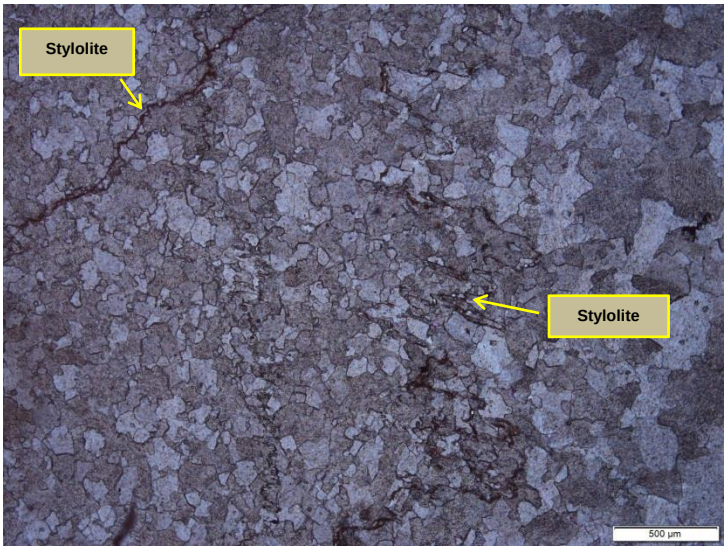


Fig. 8-69: Photomicrograph in PPL showing an overview of sample 13462 (well 02-21, 1700.0 m). Interlocking fine to coarse sparry dolomite crystals (~50 to 450 µm) dominate the sample. As in the previous sample (13461), fine stylolites (<5 µm wide in this image) are abundant and filled with dark brown opaque material. This area of the sample is well-cemented and lacks visible open pore space.

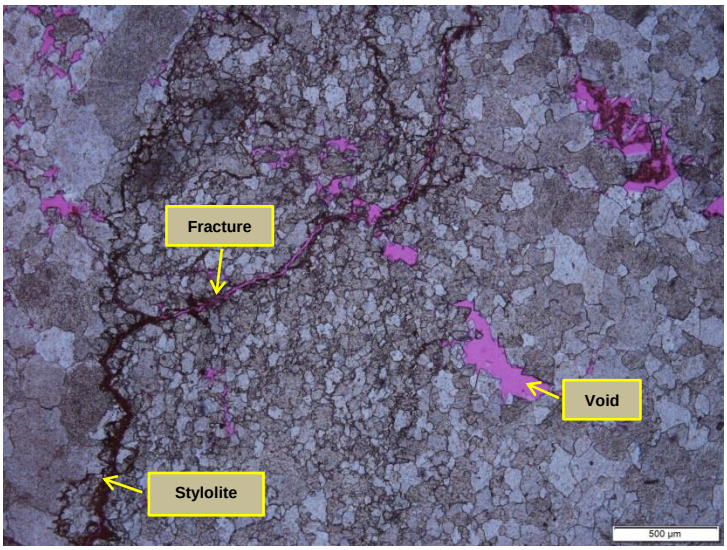


Fig. 8-70: Photomicrograph in PPL showing several opaque stylolites (up to ~40 µm in width) that are often associated with areas in which dolomite crystal sizes are smaller than within the clasts (~70 µm average compared to ~250 µm). Some of the stylolites are also associated with epoxy-filled fractures (~15 µm in width), which may have been re-opened or artificially enhanced during sample preparation. As in sample 13461, abundant angular dissolution voids or 'vugs' (up to 700 µm) are present.

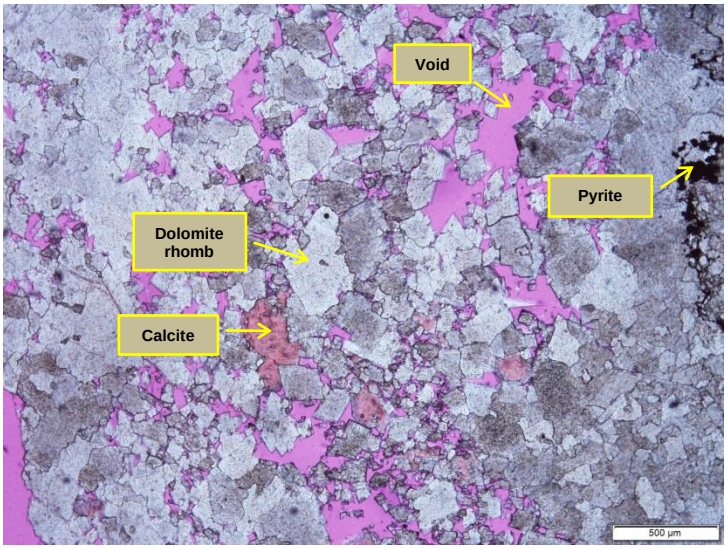


Fig. 8-71: Photomicrograph in PPL showing an area of the sample (top-left part of the thin section) with elevated porosity (estimated to be up to 10% of the image). Most of the angular pores (up to ~600 µm) likely formed through dissolution. Rhombic to sub-rhombic dolomite crystals (up to 540 µm) and idiomorphic and framboidal pyrite crystals (up to 30 µm) and clusters (up to 210 µm, e.g. right of image) are present and more abundant than in the previous sample.

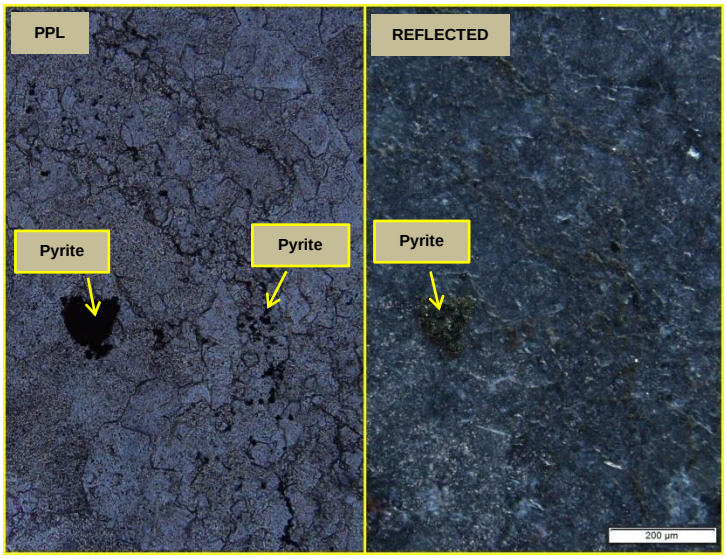


Fig. 8-72: Split-image photomicrograph in PPL (left) and reflected light (right) showing a large (~130 µm) pyrite cluster/pocket (left of image). Smaller, disseminated pyrite crystals (typically 5-10 µm) are observed throughout the surrounding dolomite framework and are often (although not always) associated with stylolites and/or the space between sparry dolomite crystals (i.e. intercrystalline space).

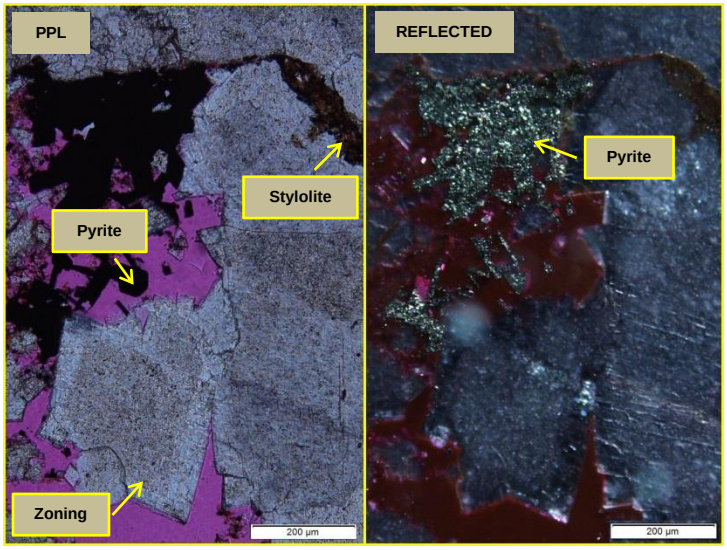


Fig. 8-73: Split-image photomicrograph in PPL (left) and reflected light (right) showing cubic and idiomorphic pyrite crystals within coarse blocky dolomite grains. The pyrite occurs within a stylolite (up to 70 µm in width), that contains both organic matter and smaller disseminated pyrite crystals. Most dolomite shows zoning and strongly defined cleavage planes.

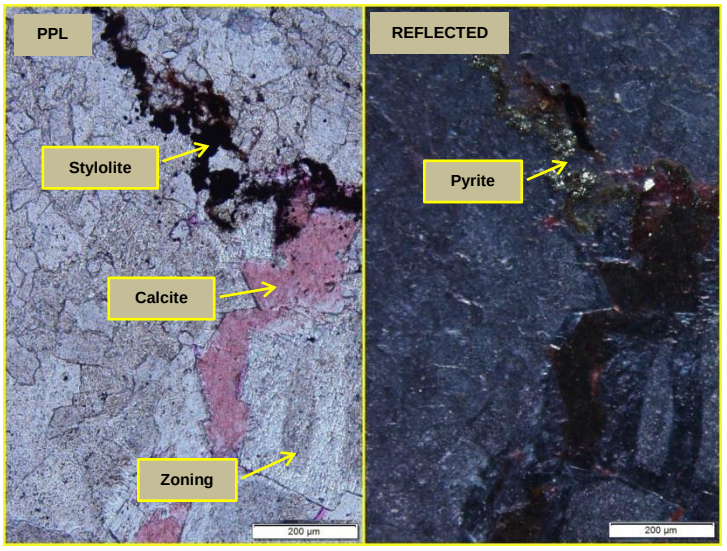


Fig. 8-74: Split-image photomicrograph in PPL (left) and reflected light (right) showing magnification of rare sparry calcite cement (pink stained, 250-275 µm) occurring between dolomite spar. The stylolite (up to ~65 µm in width) towards the top-left of both images partially obscures the top of the calcite spar and is predominantly composed of idiomorphic pyrite crystals (up to 30 µm), as well as some organic material. Also note zoning within the dolomite cement towards the right of the image.

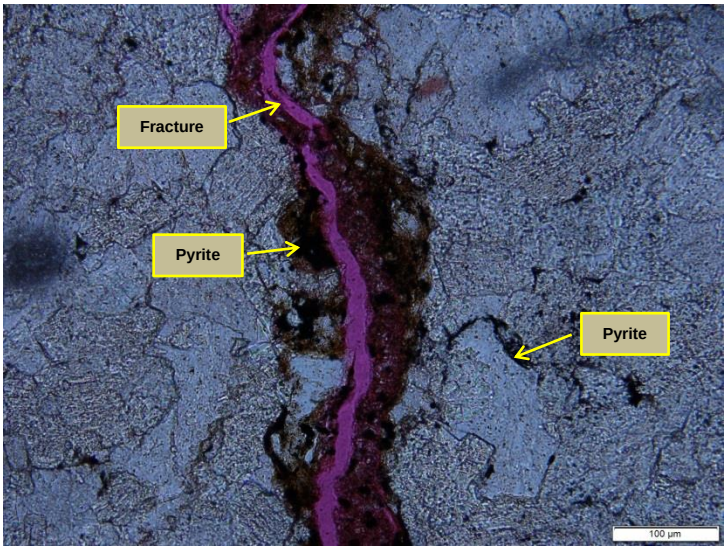


Fig. 8-75: Photomicrograph in PPL showing magnification of a fracture (~25 µm in width), which is rimmed by dark brown material (organics, clays) and some pyrite (typically ~10 µm). The fracture contains pink epoxy and likely opened during sample preparation or unloading. Pyrite and/or organic matter also line coarse blocky dolomite crystals adjacent to the fracture (stylolitic zone?).

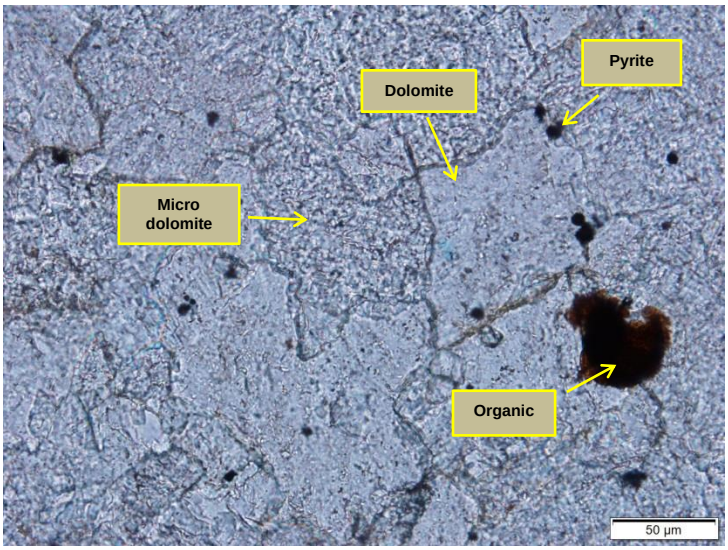


Fig. 8-76: Photomicrograph in PPL showing detail of the recrystallized clasts. The image shows that rhombic to massive dolomite spar (average ~140 µm) is often separated by microcrystalline dolomite, which has a less distinct form or habit (two different phases of recrystallization?). Very small pyrite crystals (generally <5 µm) and organic 'blobs' (~50 µm) are finely dispersed throughout.

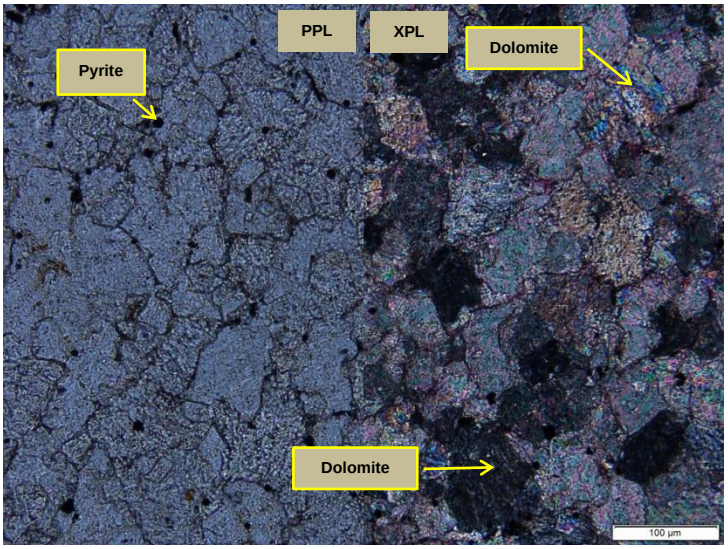


Fig. 8-77: Photomicrograph in PPL (left) and XPL (right) showing detail of the interlocking dolomite crystals that are the dominant component of this sample. Very small idiomorphic pyrite crystals (<10 µm) are finely dispersed throughout and are concentrated within intercrystalline space.

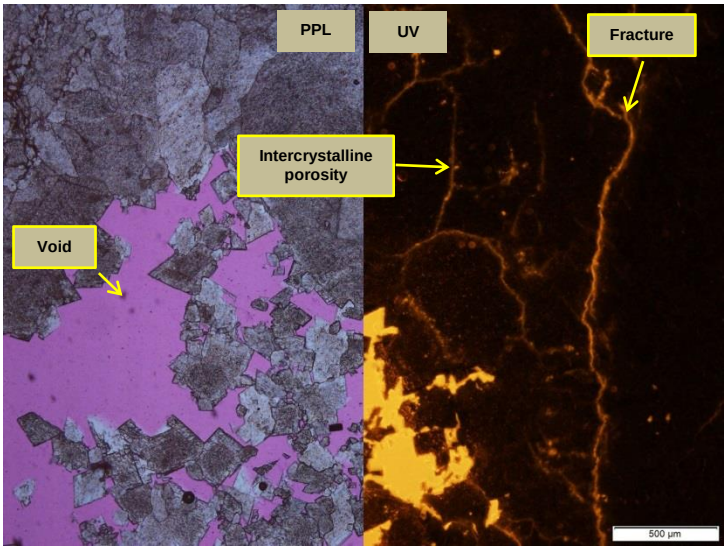


Fig. 8-78: Photomicrograph in PPL (left) and UV light (right) showing porosity within the sample. Most porosity is associated with angular voids or 'vugs' that likely formed through dissolution, and may be related to the internal structure of bioclast fragments (framework porosity). Further porosity is related to the space between sparry dolomite cements (i.e. intercrystalline porosity) and fractures (up to ~15 µm in width).

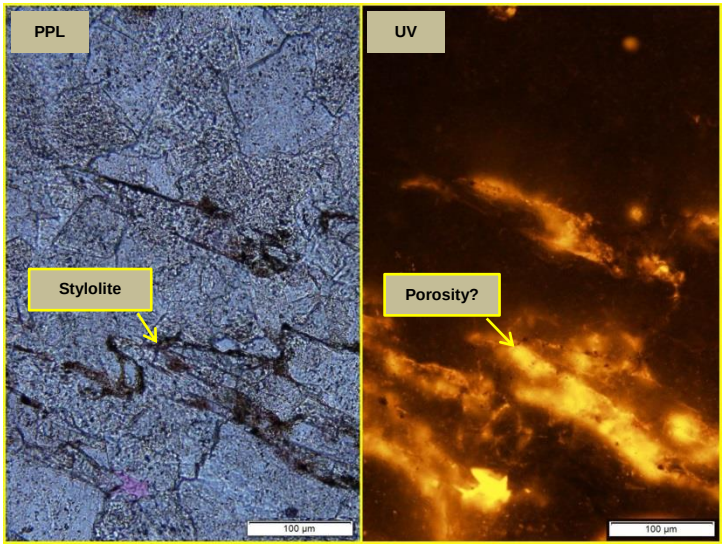


Fig. 8-79: Split-image photomicrograph in PPL (left) and UV light (right) showing porosity associated with fine stylolites (<5 µm in width). This porosity indicates that the stylolites are only partially filled by pyrite and/or organic matter. A small porous (pink epoxy) patch (~40 µm) towards the bottom-left of the image likely represents partial removal, plucking or thinning of some dolomite spar.

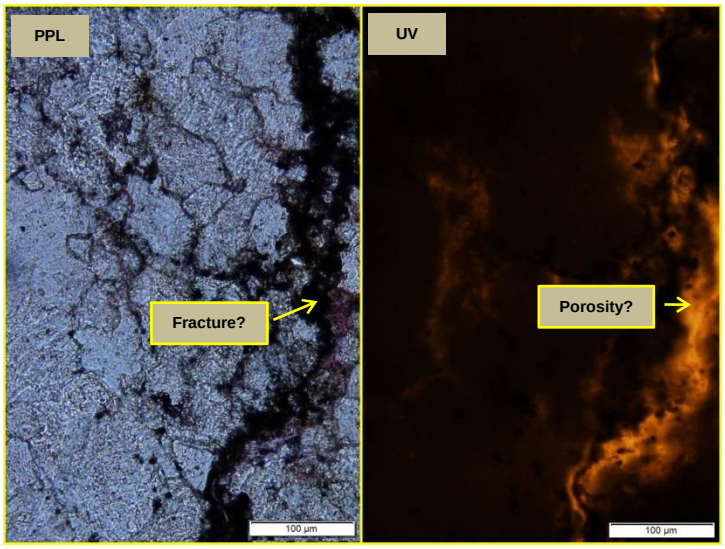


Fig. 8-80: Split-image photomicrograph in PPL (left) and UV light (right) showing partial filling of fractures and stylolites by pyrite and/or organic matter.

8.2.6 SAMPLE 13479

Sample ID	**13479**		
Sample Type	**Core**	**UWI/Well**	**100/15-11-091-13W5/00**
Strat. Unit	**Slave Point Formation**	**Depth**	**1629.8 m**

XRD results

Quartz (%)	Feldspar (%)	Calcite (%)	Dolomite/ankerite (%)	Clays (%)
0.6	0.4	97.6	0.5	0.9

Pyrite (%)
0

Composition (*in order of abundance*)

	%	Variety (%)	Variety (%)	Variety (%)	Variety (%)
Cement (micrite)	65	Calcite (100)			
Cement (spar)	30.5	Calcite (98)	Dolomite (2)		
Opaques	2.5	Pyrite (100)			
Organics	2	Amorphous* (100)			
	100				

** including bitumen?*

Matrix	65	Micrite (65)	Spar (35)		
Allochems	30	Bioclasts (65)	Peloids (35)	Intraclast? (trace)	
Porosity	5	Intraparticle (100)	Intercrystalline (trace)		
	100				

Sedimentary structures

Primary	None observed.
Biogenic	None observed.

Fractures	Some stylolites are likely associated with fractures that are joined to dissolution voids and partially filled/replaced by carbonate cement. Artificial fractures are rarely observed.
Porosity	Intraparticle porosity is widespread throughout the sample and is generally associated with bioclast fragments (particularly calcispheres, ostracods and stromatoporoids). In addition, the matrix is partially removed in some areas of the thin section contributing to further porosity. Very minor intercrystalline porosity is observed within sparry calcite patches.
Opaques	Cubic pyrite clusters (up to 420 µm) are often associated with sparry carbonate patches and incorporated within stylolites. Smaller (generally <10 µm) disseminated pyrite crystals and clusters are finely dispersed throughout the micritic matrix.
Organics	Amorphous organic-rich material is often concentrated in stylolites (up to 350 µm wide) which also incorporate carbonate crystals. Some of the stylolites feature fine organic 'offshoots' which connect one stylolite to another. Parallel organic-rich 'mats' also fill intercrystalline space.
Diagenetic	All bioclast fragments have been replaced by calcite spar. Large angular dissolution voids (often mm-scale) are filled by calcite and (more rarely) dolomite spar. Some of the sparry carbonate patches are folded. Abundance of stylolites indicates pressure dissolution.

Bioclasts *(in order of abundance)*

Type	*Size (µm)*	*Preservation*	*Recrystallisation*
Calcispheres	Generally ~125 (up to 300)	Poor to good	Calcite spar
Ostracods	Up to ~900	Poor to good	Calcite spar
Tentaculitids	Generally ~500 (up to 850)	Moderate	Calcite spar
Stromatoporoid frags	3200+	Poor to moderate	Calcite spar & micrite

Sample 13479 is a sparse pel-biomicrite containing a diverse assemblage of calcite replaced/recrystallized bioclast fragments (including calcispheres, ostracods, tentaculitids and stromatoporoids). Stromatoporoid fragments are not as common as in previous Slave Point samples (e.g. 13461 and 13462) and are often composed of 'dirty' calcite spar with internal pore space filled by micrite. The surrounding matrix is also composed predominantly of micrite, including abundant peloidal material. Large angular dissolution voids are filled by very coarsely crystalline calcite and (more rarely) dolomite crystals with very strongly defined cleavage planes. The dissolution voids are sometimes associated with partially filled vertical features, which may represent replaced stylolites or fractures. Large cubic pyrite crystals and clusters are also concentrated around sparry calcite patches. Abundant bedding-parallel stylolites vary in thickness and usually contain both organic matter and disseminated pyrite. Many of these stylolites are connected via organic-rich offshoots. Porosity within the sample is variable and is generally related to intraparticle porosity within bioclast fragments. However, some porosity can also be attributed to partial dissolution of the matrix and very minor open pore space between sparry calcite cements (i.e. intercrystalline porosity).

Rock Classification

Sparse pel-biomicrite (Folk, 1962); mixed fossil peloidal wackestone/packstone (Dunham, 1962).

Thin Section Quality

Good; 1/2 stained for carbonates.

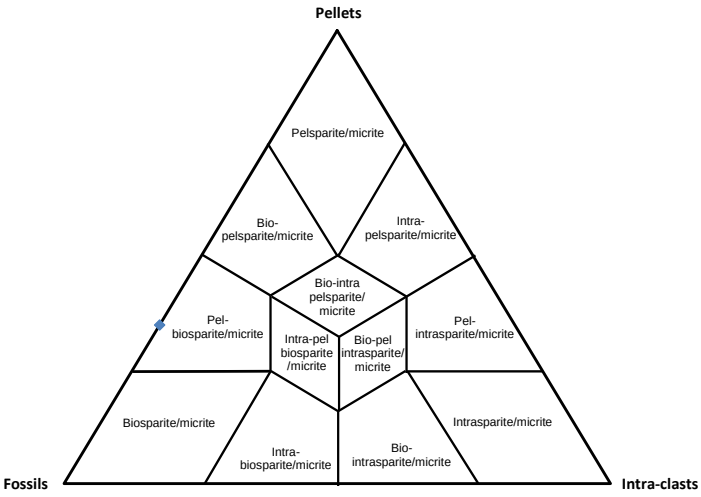


Fig. 8-81: Ternary plot showing the relative abundance of different allochem types within the carbonate rock (based on Folk's classification scheme, 1962). Sample 13479 is classified as (sparse) pel-biomicrite as the rock has a micrite matrix with a mixed bioclast assemblage (including calcispheres, ostracods, tentaculitids and stromatoporoids; ~20% of the sample), some peloids and trace amounts of intraclasts.



Fig. 8-82: Core photograph of sample 13479 from the Slave Point Formation, well 100/15-11-091-13W5/00 (depth 1629.8 m). The thin section prepared from this sample was cut from the area outlined in black marker. The sample was received with no up direction. Scale is in mm.



Fig. 8-83: Thin section photograph of sample 13479 from the Slave Point Formation, well 100/15-11-091-13W5/00 (depth 1629.8 m). The image shows a carbonate rock that is predominantly composed of micritic calcite (intensive pink staining in carbonate stained portion, right) and some dolomite (white). The lighter-coloured patches represent secondary calcite infilling of dissolution voids. Abundant organic-rich stylolites of varying thickness and cubic pyrite crystals/clusters (e.g. top-right of the image) are observed. The main stylolite zone shows a small (1.5 cm) vertical offset (left of image). Pink epoxy highlights a few open pores within some sections of the sample (e.g. top left and bottom-right of the thin section). Scale is in mm.

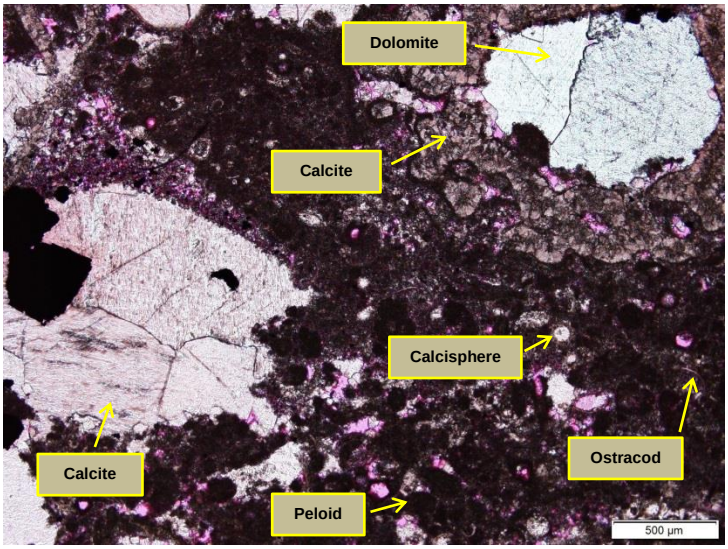


Fig. 8-84: Photomicrograph in PPL showing an overview of the top-right part of sample 13479. This area of the thin section consists of a micrite matrix containing abundant ovate-circular peloids (up to 250 µm, average ~130 µm), ostracod carapace remnants (up to ~200 µm) and calcispheres (~125 µm). Large blocky calcite crystals (up to ~1 mm, left) and dolomite spar (up to 1.2 mm, top-right) occasionally fill angular dissolution voids. Opaques (including some idiomorphic pyrite, left) occur throughout.

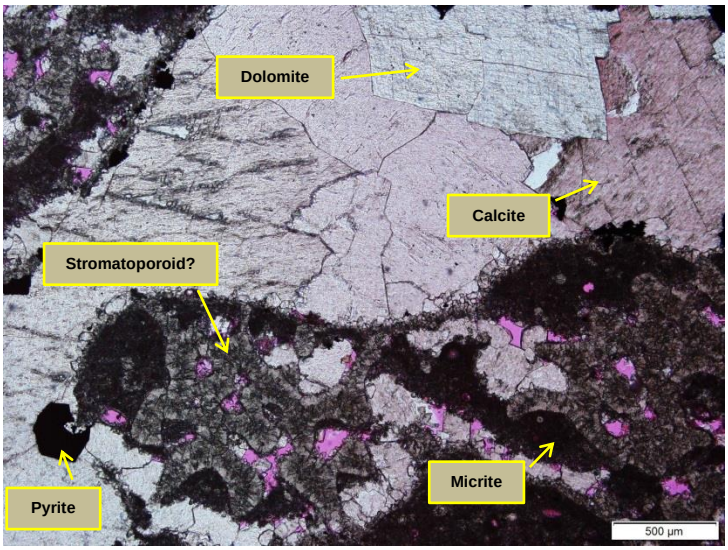


Fig. 8-85: Photomicrograph in PPL showing a large sparry carbonate patch that is composed of calcite and rhombic dolomite crystals (up to ~1.3 mm) with strongly defined cleavage planes. The sparry carbonates are adjacent to a lobate feature (~3.1 mm) that is composed of micrite and 'dirty' calcite spar. This feature contains several small pores (up to 200 µm) that may represent former framework space (stromatoporoid?). Also note abundant opaque material, including several cubic pyrite clusters (up to ~250 µm).

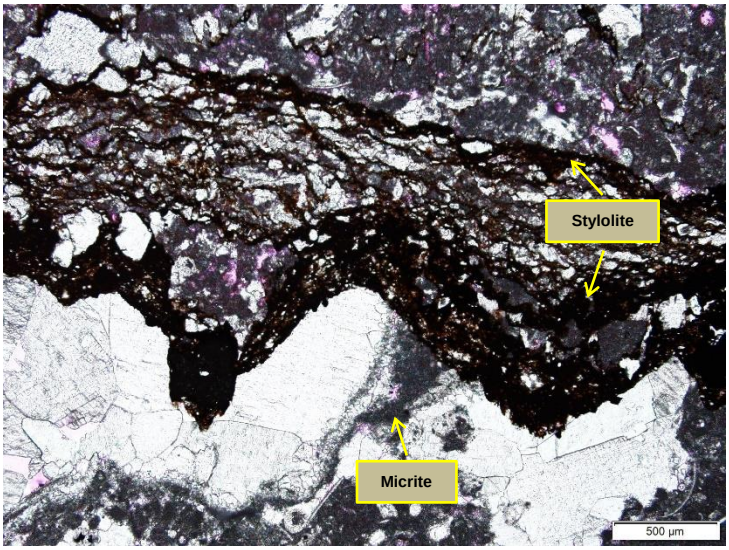


Fig. 8-86: Photomicrograph in overexposed PPL showing an overview of the middle part of the sample, where stylolites are present (unstained half of the thin section). The stylolite contains pyrite and other opaques (including organics) as well as some carbonate crystals (up to 250 µm). The area below the stylolite contains diagenetic sparry carbonate and some micrite. The top part of the image shows the typical micritic composition of the sample.

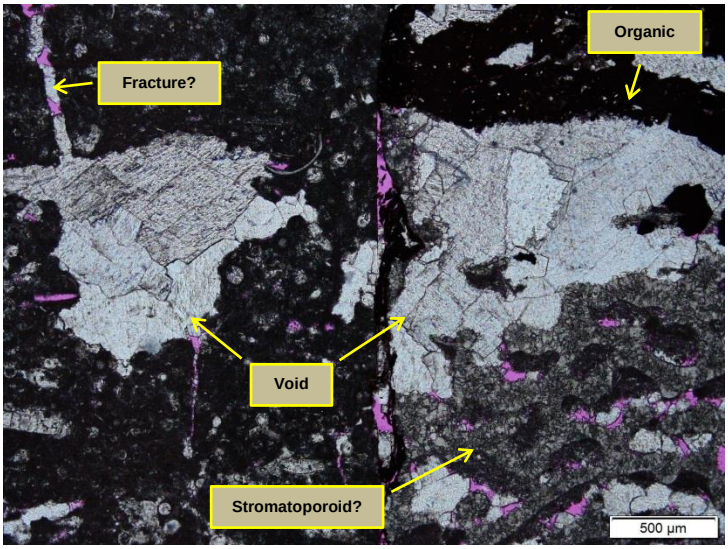


Fig. 8-87: Photomicrograph in PPL showing the top part of the thin section (see Figure 8-83), where the sample is offset by a stylolite. The carbonate-filled stylolite (~60 µm wide) cuts across former open pore space (~1.3 mm, left of image) that is filled by coarse blocky carbonate cements. The micritic framework is observed in the lower-right, whereas the left side of the stylolite contains abundant micritic bioclasts. Short vertical offsets filled with spar are also present.

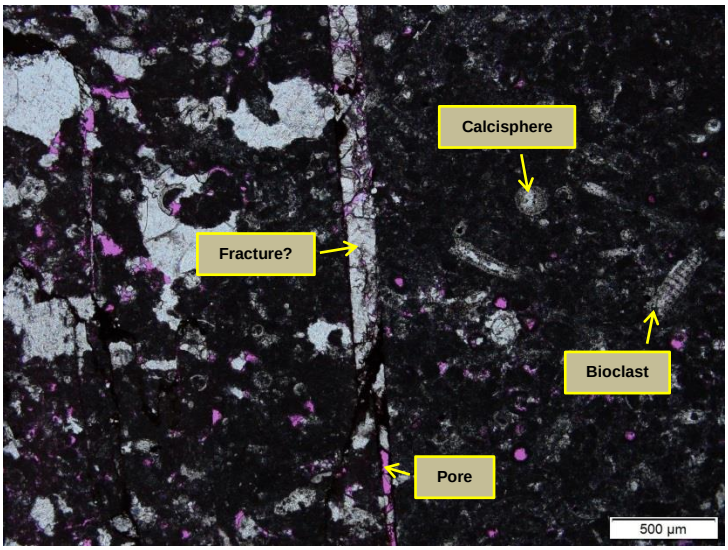


Fig. 8-88: Photomicrograph in PPL showing continuation of the carbonate-filled offset (stylolite), which tapers in thickness from the top to the bottom of the image (~165 µm to 50 µm wide). Abundant calcispheres (up to 220 µm) and other bioclast fragments (up to 380 µm) are observed in the microcrystalline matrix. Opaques are also common.

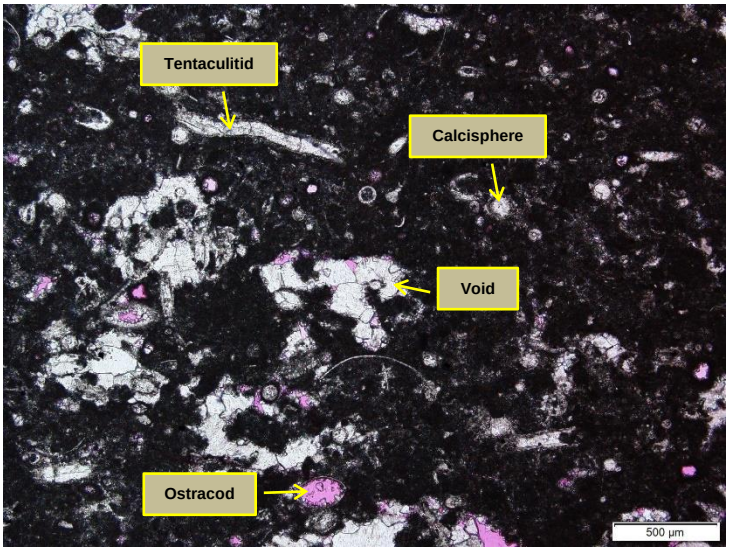


Fig. 8-89: Photomicrograph in PPL showing a representative overview of the bottom part of the thin section. This area of the sample is composed of a micritic matrix containing abundant smaller carbonate-filled dissolution voids, peloidal material and bioclast fragments (often partially dissolved, forming intraparticle pores). Bioclasts include calcispheres (up to 95 µm), ostracod carapaces (up to 500 µm), and tentaculitid/shell fragments (up to ~830 µm).

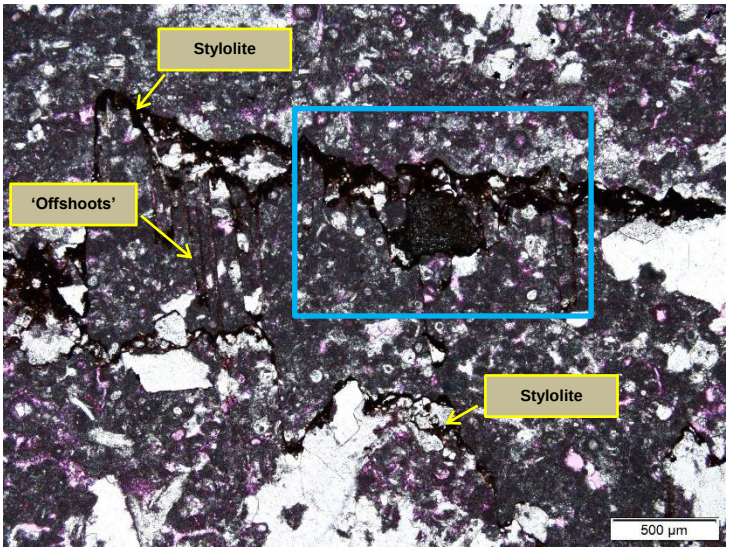


Fig. 8-90: Photomicrograph in overexposed PPL showing an opaque-rich stylolite (up to ~180 µm in width) that incorporates/wraps around sparry crystals (up to ~350 µm in size). The stylolite contains several diffuse offshoots, which connect to a finer stylolite (~35 µm) at the bottom of the image. The 'dirty' feature that borders the wider stylolite is examined in further detail in Figure 8-91.

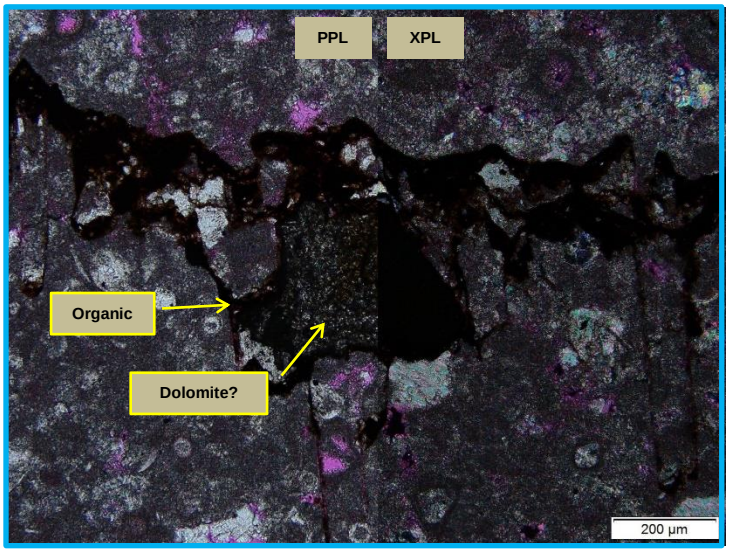


Fig. 8-91: Photomicrograph in PPL (left) and XPL (right) showing magnification of the 'dirty', angular feature imaged in Figure 8-90. The feature appears to be oil-stained and is lined by a thin layer (~15 µm) of organic-rich material. Lack of birefringence in XPL indicates that the feature likely represents an intraclast composed of microcrystalline dolomite.

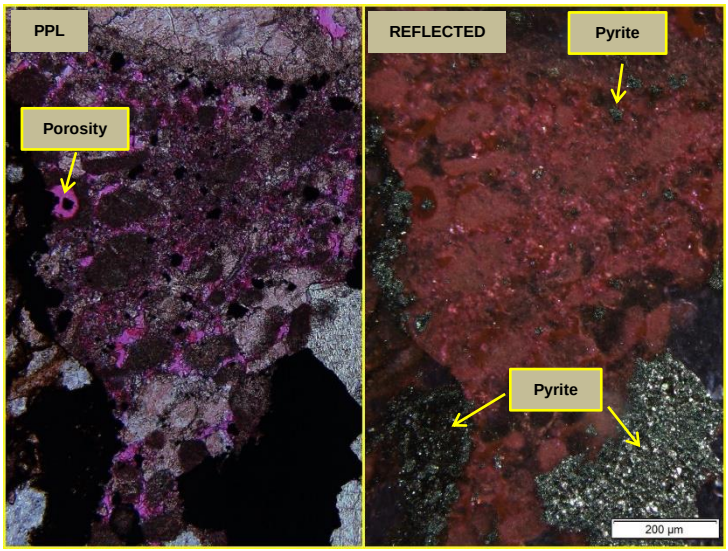


Fig. 8-92: Split-image photomicrograph in PPL (left) and reflected light (right) showing large cubic pyrite clusters (up to ~420 µm) that are abundant throughout the sample and commonly associated with sparry carbonate patches. Smaller disseminated pyrite crystals and clusters (up to 55 µm) are finely dispersed throughout the micritic matrix. Also note high porosity within this area of the sample (estimated to be ~10%).

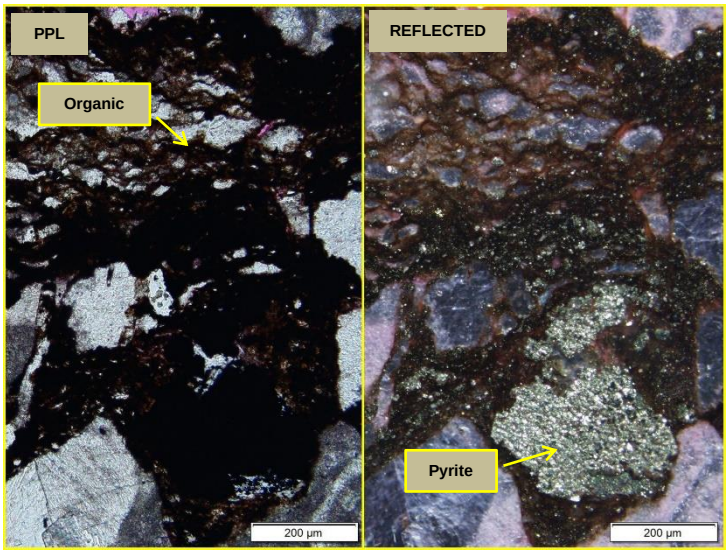


Fig. 8-93: Split-image photomicrograph in PPL (left) and reflected light (right) showing opaque-rich stylolites and/or mats (15-350 µm wide), which fill intercrystalline space and are often parallel (relative to each other). Reflected light shows that these opaque bands are composed of large cubic pyrite crystals and clusters (up to 375 µm), smaller disseminated pyrite crystals (generally <10 µm), clay and organic matter.

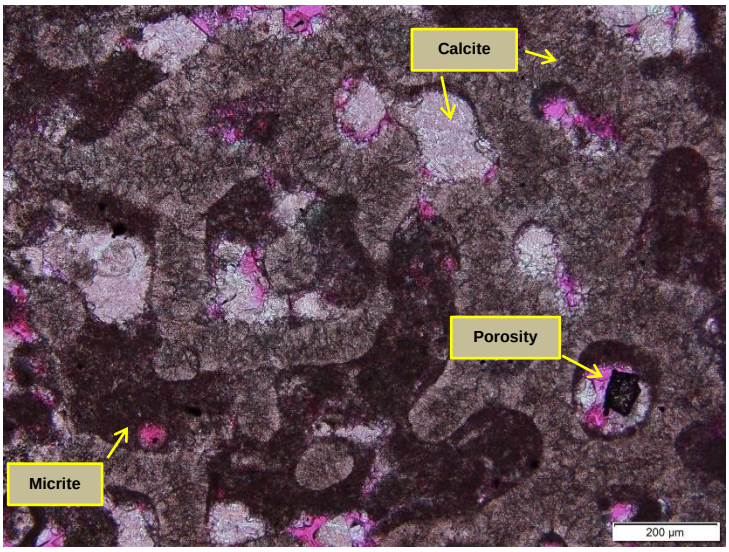


Fig. 8-94: Photomicrograph in PPL showing magnification of an apparent framework (possible stromatoporoid) that is predominantly composed of microcrystalline calcite and has elongate pores (up to 715 µm, generally ~200 µm) filled with micrite or calcite spar. Cementation of the framework pores is not always complete and thus shows some open framework porosity (~2-3% in this image).

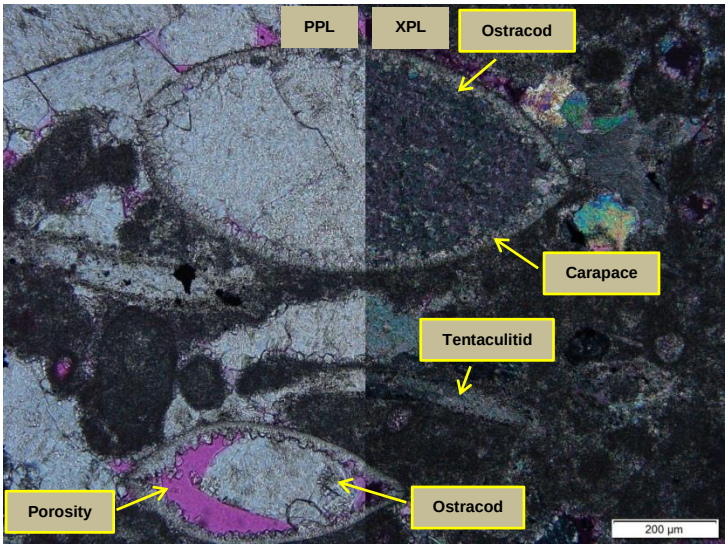


Fig. 8-95: Photomicrograph in PPL (left) and XPL (right) showing magnification of carbonate-replaced bioclast fragments present within the unstained part of the thin section. Two of the bioclasts represent ostracods (550-875 µm), which have clearly defined carapaces (~30 µm wide), and are often partially dissolved leaving open porosity (e.g. bottom of image). Other bioclast fragments represent poorly preserved tentaculitids (up to ~550 µm in this image). Some peloidal material (~80 µm) is also observed.

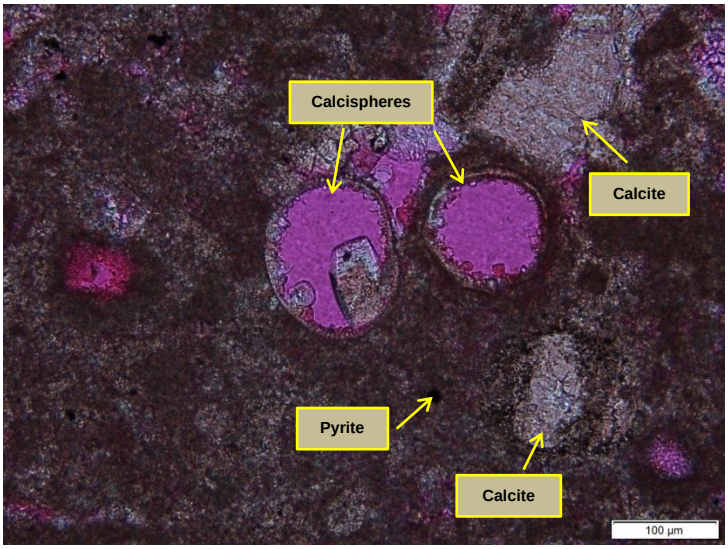


Fig. 8-96: Photomicrograph in PPL showing magnification of the matrix, which is predominantly composed of calcite-rich (pink-stained) micrite, containing finely dispersed pyrite crystals (up to 15 µm). Sparry calcite cements (up to 170 µm in this image) likely represent filled dissolution voids and/or replaced bioclast fragments. The two calcispheres (130-165 µm in diameter) towards the center of the image contain open pore space and small amounts of carbonate spar.

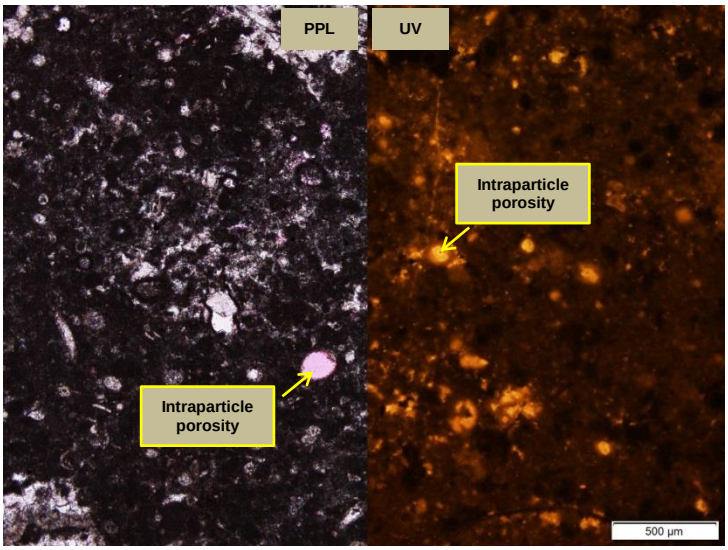


Fig. 8-97: Photomicrograph in PPL (left) and UV light (right) showing an overview of porosity within the bottom part of the sample. Most of the porosity in this image is related to the partial dissolution of bioclast fragments (especially ostracods). Overall, porosity in this area of the thin section is estimated to be ~5% (relatively low compared to other areas of the sample).

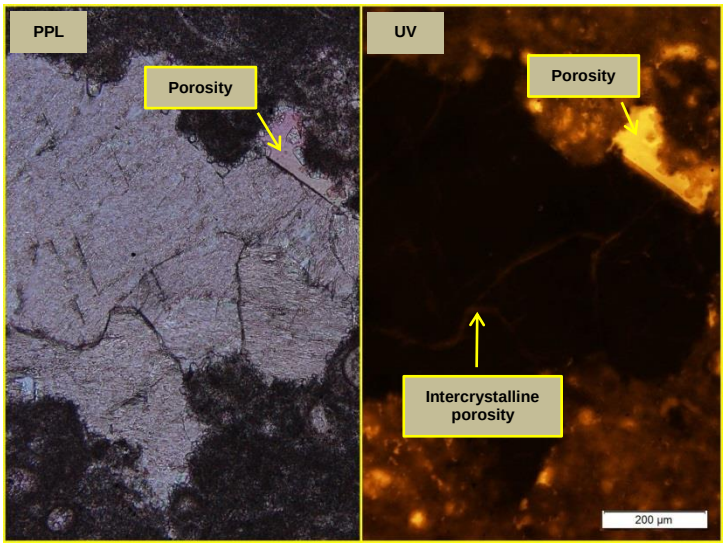


Fig. 8-98: Split-image photomicrograph in PPL (left) and UV light (right) showing very minor porosity associated with a sparry calcite patch. The top-right corner of the cement (~215 µm) is filled with pink epoxy, indicating that the calcite spar has been partially dissolved. Also note very fine (<5 µm wide) intercrystalline porosity between individual sparry calcite crystals.


TRICAN
Trican Geological Solutions